JOURNAL OF THE MECHANICS AND PHYSICS OF SOLIDS

EDITORIAL ADVISORY BOARD

J. F. BAKER—Cambridge W. M. BALDWIN—Cleveland
E. BRANDENBERGER—Zürich G. BUSCH—Zürich
A. H. COTTRELL—Harwell C. CRUSSARD—Paris M. J. DRUYVESTEYN—Delft
A. KOCHENDÖRFER—Düsseldorf N. F. MOTT—Cambridge
A. NADAI—Pittsburgh, Pa. G. SACHS—Syracuse, N.Y. E. SIEBEL—Stuttgart
V. V. SOKOLOVSKY—Moscow

EDITOR-IN-CHIEF

R. HILL
University of Nottingham

Voume 6
1957 — 58

PERGAMON PRESS · NEW YORK · LONDON · PARIS · LOS ANGELES

Contents of Volume 6

NUMBER 1

PAGE

R. HILL : Stability of rigid–plastic solids 1

W. E. BOYCE and W. PRAGER : On rigid workhardening solids with singular yield conditions 9

J. GEERTSMA : A remark on the analogy between thermoelasticity and the elasticity of saturated porous media 13

F. A. GAYDON and H. NUTTALL : On the combined bending and twisting of beams of various sections 17

G. N. RABOTNOV and S. A. SHESTERIKOV : Creep stability of columns and plates 27

K. TONG and G. SACHS : Roll-separating force and minimum thickness of cold-rolled strips 35

J. A. H. HULT : Fatigue crack propagation in torsion 47

J. D. CAMPBELL and C. J. MAIDEN : The effect of impact loading on the static yield strength of a medium-carbon steel 52

R. A. CLARK and E. REISSNER : On stresses and deformations of ellipsoidal shells subject to internal pressure 63

D. R. BLAND : The associated flow rule of plasticity 71

J. A. H. HULT : Elastic–plastic torsion of sharply notched bars .. 79

Book Review :

" Introduction to Solid State Physics," by C. KITTEL (reviewed by J. C. Woolley) 83

Books Received : 84

NUMBER 2

D. S. DUGDALE : Vickers hardness and compressive strength 85

N. E. FROST and D. S. DUGDALE : The propagation of fatigue cracks in sheet specimens 92

T. VREELAND, JR., D. S. WOOD and D. S. CLARK : The basal slip in zinc under static and dynamic loading 111

R. M. HAYTHORNTHWAITE and R. T. SHIELD : A note on the deformable region in a rigid–plastic structure 127

J. F. W. BISHOP : On the effect of friction on compression and indentation between flat dies 132

O. D. SHERBY and J. E. DORN : Anelastic creep of polymethyl methacrylate 145

B. VENKATRAMAN and P. G. HODGE, JR.: Creep behaviour of circular plates 163

NUMBER 3

D. S. BERRY : Stress propagation in visco-elastic bodies 177

P. S. SYMONDS and T. J. MENTEL : Impulsive loading of plastic beams with axial constraints 186

W. JOHNSON, P. B. MELLOR and D. M. WOO : Extrusion through single hole staggered and unequal multi-hole dies 203

P. CHADWICK and I. N. SNEDDON : Plane waves in an elastic solid conducting heat 223

G. EASON : Velocity fields for circular plates with the von Mises yield condition 231

R. HILL : A general theory of uniqueness and stability in elastic–plastic solids 236

Book Reviews :

" Solid State Physics " Edited by F. SEITZ and D. TURNBULL (reviewed by K. W. H. Stevens) 250

" Elasticity, Fracture and Flow " by J. C. JAEGER (reviewd by J. F. W. Bishop) .. 251

Books Received 252

Papers to be published in future issues 252

NUMBER 4 PAGE

E. I. GRIGOLJUK : Buckling of sandwich constructions beyond the elastic limit 253

J. E. ADKINS : A reciprocal property of the finite plane strain equations 267

J. P. ELLINGTON : An investigation of plastic stress-strain relationships using grooved tensile specimens 276

J. S. ELLIS : Plastic behaviour of compression members 282

R. L. FLEISCHER : Single crystal lattice rotation during compression .. 301

R. L. FLEISCHER and B. CHALMERS : Grip effects in the deformation of single crystals 307

H. PAYNE, S. J. CZYZAK, J. H. GREINER and T. H. LIN : A modification of Taylor's method for calculating the plastic stress-strain relation in face-centred cubic crystals 314

J. B. HUNT : Fracture mechanism of semi-brittle steels in torsion .. 321

Book Reviews :

" Deformation and Flow of Solids " Edited by R. GRAMMEL (reviewed by R. Hill) 327

" Elements of Partial Differential Equations. International Series in Pure and Applied Mathematics " by N. SNEDDON (reviewed by R. Hill) 327

" The Plastic Methods of Structural Analysis " by B. G. NEAL (reviewed by W. Merchant) 328

" Physical Properties of Crystals, their Representation by Tensors and Matrices " by J. F. NYE (reviewed by W. Boas) 328

" Surveys in Mechanics : the G.I. Taylor 70th Anniversary Volume " Edited by G. K. BATCHELOR and R. M. DAVIES (reviewed by I. N. Sneddon) 329

" Rheology " Edited by F. R. EIRICH (reviewed by J. F. W. Bishop) 330

" La Diffusion dans Les Metaux " Edited by J. D. FAST, H. G. VAN BUEREN and J. PHILIBERT (reviewed by A. H. Cottrell) 331

Some papers to be published in future issues 332

Author Index

(B) denotes a book review

BERRY, D. S. p. 177.
BISHOP, J. F. W. pp. 132, 251 (B), 330 (B).
BLAND, D. R. p. 71
BOAS, W. p. 328 (B).
BOYCE, W. E. p. 9.
CAMPBELL, J. D. p. 53.
CHADWICK, P. p. 223.
CHALMERS, B. p. 307.
CLARK, D. S. p. 111.
CLARK, R. A. p. 63.
COTTRELL, A. H. p. 331 (B).
CZYZAK, S. J. p. 314.
DORN, J. E. p. 145.
DUGDALE, D. S. pp. 85, 92.
EASON, G. p. 231.
ELLINGTON, J. P. p. 276.
ELLIS, J. S. p. 282.
FLEISCHER, R. L. pp. 301, 307.
FROST, N. E. p. 92.
GAYDON, F. A. p. 17.
GEERTSMA, J. p. 13.
GREINER, J. H. p. 314.
GRIGOLJUK, E. I. p. 253.
HAYTHORNTHWAITE, R. M. p. 127.
HILL, R. pp. 1, 236, 327 (B).
HODGE, JR., P. G. p. 163.
HULT, J. A. H. pp. 47, 79.
HUNT, J. B. p. 321.
JOHNSON, W. p. 203.
LIN, T. H. p. 314.
MAIDEN, C. J. p. 53.
MELLOR, P. B. p. 203.
MENTEL, T. J. p. 186.
MERCHANT, W. p. 328 (B).
NUTTALL, H. p. 17.
PAYNE, H. p. 314.
PRAGER, W. p. 9.
RABOTNOV, G. N. p. 27.
REISSNER, E. p. 63.
SACHS, G. p. 35.
SHERBY, O. D. p. 145.
SHESTERIKOV, S. A. p. 27.
SHIELD, R. T. p. 127.
SNEDDON, I. N. pp. 223, 329 (B).
STEVENS, K. W. H. p. 250 (B)
SYMONDS, P. S. p. 186.
TONG, K. p. 35.
VENKATRAMAN, B. p. 163.
VREELAND, B. p. 163.
WOO, D. M. p. 203.
WOOD, D. S. p. 111.
WOOLLEY, J. C. p. 83 (B).

Journal of the Mechanics and Physics of Solids, 1957, Vol. 6, pp. 1 to 8. Pergamon Press Ltd., London

STABILITY OF RIGID–PLASTIC SOLIDS

By R. Hill
Department of Mathematics, University of Nottingham

(*Received 29th August*, 1957)

Summary

The general problem of stability under dead loading is treated for a body of any shape, the material being workhardening and rigid–plastic. It is shown that when the plastic potential and yield function coincide it is only necessary to examine in detail those neighbouring positions which can be reached by strain paths beginning as virtual modes of the yield-point state under the given loading. The least energy dissipated in passing to any such position has to be determined in constructing a sufficient condition for stability. The functional concerned turns out to be identical with that in the uniqueness condition for the typical boundary-value problem. On the other hand, the classes of admissible functions are different, so that failures of uniqueness and stability need not coincide ; this is illustrated by the compression of a strut.

1. Reduction of the Problem

The term ' stability ' is used here in its classical dynamic context : a loaded body, initially at rest, is imagined to be set in motion by any kind of temporary disturbance and the magnitude of the resulting displacement is the feature isolated for study. There is an obvious requirement that the continuing geometric constraints and the subsequent variation of the existing loads with displacement should be specified. In this setting a state of equilibrium is said to be stable if the amplitude of the additional displacement is always vanishingly small when the disturbance itself is. If, on the other hand, the amplitude is finite for some one type of disturbance, *however small this might be*, the state is said to be unstable.

A sufficient condition for stability is that in *any* displacement from the position of equilibrium, within a definite (small) neighbourhood, the internal energy stored or dissipated should exceed the work done on the body by the external loads. For, by the principle of conservation of energy, the body can then move only as far as the point where this excess becomes equal to the kinetic energy communicated by the disturbance, and if this is vanishingly small so must be the movement.

In applying this test *every* geometrically-possible configuration infinitesimally near the initial one must be considered since all could presumably be reached by suitably starting the motion. In any such neighbouring configuration the stress field associated with the deformation need not be in equilibrium, nor need the corresponding stresses *arbitrarily near* the surface be statically consistent with the given tractions. For, if the disturbances are in no way restricted, we must envisage extremes involving arbitrarily large stress gradients. This possibility has now to be faced in an acute form by reason of the peculiar properties of a rigid–plastic solid.†

† In treatises on elastic stability the matter is never raised, so far as I can discover, no doubt because of the preoccupation with adjacent positions of equilibrium.

In a perfectly elastic solid the deformation produced by a first-order additional displacement is accompanied by a change in stress that is of *first-order* magnitude only. In a rigid-plastic solid the change of stress is generally *finite*,†† unless the pre-existing stress happens to be at the yield point and is compatible with the initial strain-rate compelled by the disturbance. In the phraseology of the usual 9-space representation, the stress vector at any point of the body instantaneously swings from $\boldsymbol{\sigma}$ initially to the position $\boldsymbol{\sigma}^*$ corresponding to the local strain-rate $\boldsymbol{\epsilon}^*$. Thus, a general infinitesimal disturbance entirely changes the distribution of stress, within the limits of the current yield condition; in particular, the stresses arbitrarily near the surface of the body can be totally (and not just infinitesimally) discordant with the given tractions $\mathbf{F}$.

This has an interesting consequence. The virtual work identity for the equilibrium state $\boldsymbol{\sigma}$ and the initial velocity field $\mathbf{v}^*$ is

$$\int \mathbf{F}\mathbf{v}^* \, dS = \int \boldsymbol{\sigma}\boldsymbol{\epsilon}^* \, dV.$$

The work of the given tractions in a small time δt is the left-hand side $\times \delta t$. In an elastic solid the right-hand side $\times \delta t$ is, to first order, the internal energy stored by the material; since the two sides are equal, an expression correct to second order has to be obtained in an examination of stability.‡‡ By contrast, in a rigid–plastic solid the right-hand side does not invariably have this interpretation: the rate at which energy is absorbed (and then dissipated as heat) is $\int \boldsymbol{\sigma}^* \boldsymbol{\epsilon}^* \, dV$ since the actual stress during the straining is $\boldsymbol{\sigma}^*$ and not $\boldsymbol{\sigma}$. Except when the deviators of $\boldsymbol{\sigma}^*$ and $\boldsymbol{\sigma}$ are identical, the first-order expressions for the external work done and the internal energy dissipated differ, and can themselves be compared in the condition for stability:

$$\left\{\int \boldsymbol{\sigma}^* \boldsymbol{\epsilon}^* \, dV - \int \mathbf{F}\mathbf{v}^* \, dS\right\} \delta t > 0 \qquad \text{or} \qquad \int (\boldsymbol{\sigma}^* - \boldsymbol{\sigma}) \boldsymbol{\epsilon}^* \, dV > 0.$$

But this is just the 'maximum work' inequality which holds when the strain-increment vector is in the direction of the outward normal to a convex yield surface at the stress point.** If the law is different, it is easy to see that the inequality is reversed for certain disturbances and initial states;* there is no guarantee of stability and a strong contrary presumption.

Here we adopt the conventional flow law. Only a vanishingly small motion is then produced by any infinitesimal disturbance that changes the initial stress (in particular, a completely non-plastic body is certainly stable). In a body partly or completely plastic we have still to examine disturbances producing strain paths that are initially compatible with the existing stress and compute the dissipation of energy to second order (Sections 2 and 3). Such a path *begins as one of the set of*

†† For the transitional behaviour of an elastic–plastic solid as the rigidity modulus is made large, see HILL (1950 pp. 58-9).

‡‡ See PEARSON (1956) and HILL (1957b) for a general treatment.

** For non-specialists it may be remarked that this is the conventionally assumed law for a rigid–plastic solid and is characteristic of metals that deform microscopically by slip. For an elementary account see HILL (1956).

* Even when no part of the body is plastic. On the other hand, an elastic–plastic solid with such a flow law for the plastic component of strain is always *stable* when stressed below the yield point, provided the rigidity modulus is sufficiently great. But the neighbourhood in which the stability functional is positive becomes vanishingly small as the modulus is increased indefinitely, the loads being given.

virtual modes defined by the rigid constraints, the given tractions, and the hardness distribution.

With the stability problem reduced to these terms we have a basis in common with the problem of uniqueness (HILL 1957a) and can compare the respective criteria. For an elastic solid the functionals and classes of admissible functions are identical (HILL 1957b), whereas for the rigid–plastic solid the functionals are the same but the classes are different (Section 4). Consequently, the ranges of certain stability and certain uniqueness need not coincide; this is illustrated in Section 5 for a strut in compression.

2. Method of Approach

In an elastic solid the energy absorbed in passing from one position to another depends only on the configurations, but in a plastic solid on the path itself (when the computation is made to second order or better). For any one final configuration the critical path is that in which the dissipation of energy is *least*, for if the sufficient condition for stability is satisfied on that path it is on all. The initial state is assuredly stable when the condition is satisfied for the critical path to every configuration within some definite neighbourhood.

Strictly, the optimum path has to be chosen from the dynamically-possible ones but it would generally be impracticable to determine these. We must therefore make the selection from *all* paths compatible with the constraints, though possibly at the expense of eventually obtaining a weakened stability criterion since the actual least energy will tend to be underestimated; i.e. the eventual condition may be over-sufficient. However, even this programme appears too formidable in general and a further simplification is necessary. It is proposed here to determine the least possible dissipation of energy if each element of the body could be brought *separately* to its final state of distortion; since the strain paths of adjacent elements would generally violate the continuity of the material, there will result a further underestimate of the actual least energy.

Each element being assumed isotropic, the ' state of distortion ' is unambiguously specified by the values of the principal extensions (i.e. the extensions of that triad of initially perpendicular directions which in the final configuration are once again mutually perpendicular), the rotation being irrelevant. Subject to certain light restrictions on the yield condition and workhardening law it is probable that the most efficient way to effect a given distortion is (a) to keep the principal axes of true strain-rate coincident with the same directions *in the element* throughout, and (b) to maintain constant ratios of the principal components of strain-rate. This is assumed here.

To lend plausibility to the general conjecture, (b) can easily be proved for a *nonhardening* material if (a) is granted. Let $(\lambda_1, \lambda_2, \lambda_3)$ be the total logarithmic strain components for the required distortion, i.e. the logarithms of the ratios of the final and initial lengths in the principal directions; for incompressibility, $\lambda_1 + \lambda_2 + \lambda_3 = 0$. These values could be produced by maintaining, at every stage, principal *true* strain-rates (based on the current configuration) in the constant ratios of the λ's. Denote by $(\sigma_1, \sigma_2, \sigma_3)$ the principal stresses corresponding to this strain-rate vector. Let (μ_1, μ_2, μ_3) be the (varying) logarithmic strains during any path leading to the same final λ's, and denote the current stress by (τ_1, τ_2, τ_3).

By the maximum work inequality, $\Sigma(\tau_r - \sigma_r)\, d\mu_r \geqslant 0$ since the yield condition is not affected by the path taken when there is no hardening. Integrating between the limits 0 and λ_r :

$$\Sigma \int \tau_r\, d\mu_r \geqslant \Sigma \sigma_r \int d\mu_r = \Sigma \sigma_r \lambda_r.$$

This proves the theorem since the left-hand side is the energy dissipated per unit volume in the possible path and the right-hand side is that dissipated in the optimum path. In particular, when the yield condition is that of Mises, the energy is proportional to the path length in the geometrical representation (HILL 1950, p. 39) and the inequality simply states that the optimum path is a straight line ; this is obviously also true when the material hardens in such a way that the energy dissipated is an increasing function of the path length alone.

Returning to the general case we have to derive a second-order expression for the energy dissipated in the optimum path, where the logarithmic strains are increased in constant ratio. Since the principal components of stress also increase in constant ratio we can apply the trapezoid rule for quadrature, giving the energy directly in the form

$$\Sigma\, (\sigma_r + \tfrac{1}{2}\, \delta\sigma_r)\, \lambda_r$$

per unit volume. Here $(\sigma_1, \sigma_2, \sigma_3)$ is the stress corresponding to a strain-rate in direction $(\lambda_1, \lambda_2, \lambda_3)$ in the initial state of hardness and $(\delta\sigma_1, \delta\sigma_2, \delta\sigma_3)$ is the overall change in stress ; the hydrostatic parts are arbitrary since $\Sigma\lambda_r = 0$. The requisite first-order relations between the $\delta\sigma$'s and λ's are supplied by the general relations between stress-rate $\dot{\boldsymbol{\sigma}}$ and strain-rate $\boldsymbol{\epsilon}$:

$$h\boldsymbol{\epsilon} = (\mathbf{n}\dot{\boldsymbol{\sigma}})\, \mathbf{n}$$

in a plastic element, where $\mathbf{n}$ is the unit outward normal to the yield surface and h is a measure of the rate of hardening. From this follows

$$\dot{\boldsymbol{\sigma}}\boldsymbol{\epsilon} = h\boldsymbol{\epsilon}^2, \qquad \text{or} \qquad \Sigma\lambda_r\, \delta\sigma_r = h\Sigma\lambda_r^2$$

correct to second order. The final formula is therefore

$$E = \Sigma(\sigma_r\, \lambda_r + \tfrac{1}{2}\, h\lambda_r^2). \tag{1}$$

In order to obtain an explicit stability criterion we have now to express this in terms of displacement gradients.

3. THE STABILITY FUNCTIONAL

It is convenient to introduce the Lagrangian strain tensor of the additional distortion :

$$e_{ij} = \tfrac{1}{2}\left(\frac{\partial u_i}{\partial x_j} + \frac{\partial u_j}{\partial x_i} + \frac{\partial u_k}{\partial x_i}\frac{\partial u_k}{\partial x_j}\right) \tag{2}$$

where u_i is the additional displacement and x_i the initial co-ordinates (see, for instance, SOKOLNIKOFF 1956, section 11). The principal axes of e_{ij} coincide with the initial positions of the material directions associated with the λ's, i.e. the so-called principal axes of strain. The principal components, e_r say, are such that

$$\lambda_r = \tfrac{1}{2}\log(1 + 2e_r)$$

or, to second order,

$$\lambda_r = e_r - e_r^2.$$

Hence

$$\Sigma\sigma_r \lambda_r = \Sigma\sigma_r (e_r - e_r^2) = \sigma_{ij}(e_{ji} - e_{jk}e_{ki}) \tag{3}$$

where the summation convention is adopted in the last expression. Here σ_{ij} denotes the tensor with principal values $(\sigma_1, \sigma_2, \sigma_3)$ and principal axes coinciding with those of e_{ij}; it is not (as yet) to be identified with $\boldsymbol{\sigma}$ in Section 1. From equation (2) the right-hand side of equation (3) becomes

$$\sigma_{ij}\left(\frac{\partial u_j}{\partial x_i} - \tfrac{1}{2}\frac{\partial u_i}{\partial x_k}\frac{\partial u_k}{\partial x_j}\right) + \tfrac{1}{4}\boldsymbol{\sigma}_{ij}\left(\frac{\partial u_k}{\partial x_i}\frac{\partial u_k}{\partial x_j} - \frac{\partial u_i}{\partial x_k}\frac{\partial u_j}{\partial x_k}\right).$$

But the last half of this vanishes to second order, as shown by HILL (1957c, Section 2). Substituting equation (3) in equation (1) now gives

$$E = \sigma_{ij}\left(\frac{\partial u_j}{\partial x_i} - \tfrac{1}{2}\frac{\partial u_i}{\partial x_k}\frac{\partial u_k}{\partial x_j}\right) + \tfrac{1}{2}he_{ij}^2.$$

The hydrostatic part of σ_{ij} is still arbitrary and without effect on E, the incompressibility condition being

$$\frac{\partial u_k}{\partial x_k} - \tfrac{1}{2}\frac{\partial u_i}{\partial x_j}\frac{\partial u_j}{\partial x_i} = 0 \tag{4}$$

to second order.

At this point it is convenient to introduce the symmetric tensor

$$\epsilon_{ij} = \tfrac{1}{2}\left(\frac{\partial u_i}{\partial x_j} + \frac{\partial u_j}{\partial x_i}\right),$$

whose hydrostatic part $\partial u_k/\partial x_k$ is of second order magnitude, by equation (4). At the moment ϵ_{ij} has a purely formal significance. The energy can be written

$$E = \boldsymbol{\sigma}\boldsymbol{\epsilon} + \tfrac{1}{2}\left(h\boldsymbol{\epsilon}^2 - \sigma_{ij}\frac{\partial u_i}{\partial x_k}\frac{\partial u_k}{\partial x_j}\right). \tag{5}$$

The functional in the sufficient condition for stability is

$$U(\mathbf{u}) = \int E\,dV - \int \mathbf{F}\mathbf{u}\,dS$$

$$= \left\{\int \boldsymbol{\sigma}\boldsymbol{\epsilon}\,dV - \int \mathbf{F}\mathbf{u}\,dS\right\} + \tfrac{1}{2}\int\left(h\boldsymbol{\epsilon}^2 - \sigma_{ij}\frac{\partial u_i}{\partial x_k}\frac{\partial u_k}{\partial x_j}\right)dV,$$

when part of the surface of the body is rigidly constrained and the remainder subject to *dead loading*. The only restrictions on the admissible fields $\mathbf{u}$ are that they should be continuous and differentiable, satisfy equation (4), and vanish at the constraints.

But, as we saw in Section 1, detailed consideration need be given only to those fields $\mathbf{u}$ which differ infinitesimally from one or other of the set of virtual modes. In the deforming zone of a mode the difference between the deviators of the given initial stress and $\boldsymbol{\sigma}$ (for any neighbouring field) is then a first-order stress in a direction tangential to the initial yield surface (by the assumed flow law) and has a

third-order scalar product with $\boldsymbol{\epsilon}$. From now on we can therefore let $\boldsymbol{\sigma}$ stand for the initial stress in the deforming zone (fixing the hydrostatic part of $\boldsymbol{\sigma}$, previously arbitrary), and also in the rigid zone where $\boldsymbol{\sigma}$ was hitherto undefined. For such fields the condition for stability reduces to

$$U(\mathbf{u}) = \tfrac{1}{2}\int\left(h\boldsymbol{\epsilon}^2 - \sigma_{ij}\frac{\partial u_i}{\partial x_k}\frac{\partial u_k}{\partial x_j}\right)dV > 0. \tag{6}$$

Moreover, since U is second order, we can *now* take the incompressibility condition to be $\partial u_k/\partial x_k = 0$ instead of equation (4) ,and the admissible fields to be *precisely* the virtual modes, with $\mathbf{u}$ replaced by velocity $\mathbf{v}$ and $\boldsymbol{\epsilon}$ denoting true strain-rate. Only continuous modes need be considered when $h \neq 0$ since U diverges positively on a velocity discontinuity.

4. Stability and Uniqueness

It has been shown that a body constrained on a part S_v of its surface is stable under dead loading on the remainder S_F if $U(\mathbf{v}) > 0$ for every (continuous) virtual mode $\mathbf{v}$ vanishing on S_v. But it is known (Hill 1957a, c) that the actual (continuous) mode is unique under given traction and nominal traction-rate on S_F if $U(\mathbf{w}) > 0$ for the difference $\mathbf{w}$ of any pair of virtual modes. The functionals in the two criteria are therefore identical, but not the classes of admissible functions since the difference of two modes is not itself generally a mode : the strain-rate vector $\boldsymbol{\eta}$ corresponding to $\mathbf{w}$ is normal to the yield surface at the stress point but not necessarily directed outward, as is $\boldsymbol{\epsilon}$ corresponding to $\mathbf{v}$. Moreover, since the boundary conditions and field equations satisfied by $\mathbf{v}$ are homogeneous, any mode can be multiplied by a constant positive factor to give a similar mode ; every mode can therefore be regarded as the difference of two similar ones and is accordingly contained in the class $\mathbf{w}$. The class of admissible functions in the condition for uniqueness is thus wider than in the condition for stability.

The import of this is most conveniently seen by regarding the rate of hardening as a variable parameter, the current shape and hardness of the body and the tractions being given.* We substitute μh for h, where μ is a *positive* parameter and the distribution of hardening-rate is given except in scale, and write

$$H(\mathbf{v}) = \int h\boldsymbol{\epsilon}^2\,dV, \qquad H(\mathbf{w}) = \int h\boldsymbol{\eta}^2\,dV,$$

$$\Sigma(\mathbf{v}) = \int \sigma_{ij}\frac{\partial v_i}{\partial x_k}\frac{\partial v_k}{\partial x_j}\,dV, \qquad \Sigma(\mathbf{w}) = \int \sigma_{ij}\frac{\partial w_i}{\partial x_k}\frac{\partial w_k}{\partial x_j}\,dV,$$

$$\alpha = \operatorname{Max}\frac{\Sigma(\mathbf{v})}{H(\mathbf{v})} \text{ in class } \mathbf{v}, \qquad \beta = \operatorname{Max}\frac{\Sigma(\mathbf{w})}{H(\mathbf{w})} \text{ in class } \mathbf{w}. \tag{7}$$

When $\mu > \beta$, $U(\mathbf{w})$ is always positive and the actual mode is unique ; when $\mu > \alpha$, $U(\mathbf{v})$ is always positive and the current state is stable. Furthermore, since β is obtained as a maximum in the wider class,

$$\beta \geqslant \alpha. \tag{8}$$

* In the elastic context this corresponds to taking the rigidity modulus as parameter, instead of the load, as is equally convenient and more usual when the pre-strain is negligible.

α and β can have either sign or vanish (along with Σ); in particular, they are both zero for torsion (HILL 1957a, Section 5). In the interesting case $\beta > \alpha > 0$, when the rate of hardening is progressively lowered, there is reached first the critical value β when uniqueness is no longer certain and afterwards a critical value α when stability is no longer certain. Since β itself, as defined in equation (7), does not depend on the specified traction-rate on S_F, it is to be expected that for certain distributions the range of uniqueness will extend to hardening rates less than β and even down to α (the condition $\mu > \beta$ then being sufficient but not necessary). For other loading programmes, however, a point of bifurcation (where more than one mode is possible) will be reached before a failure of stability. This is the situation originally made plausible by SHANLEY (1946, 1947) in his example of a compressed elastic–plastic strut (actually a severely idealized one). The explicit general formulation for rigid–plastic solids is contained in equations (7) and (8).

Further insight is afforded by the following interpretation of the stability functional. Since any virtual mode is actual for *some* distribution of traction-rate (it is only necessary to construct an equilibrium stress-rate field compatible with the hardening in that mode),

$$\int \dot{\mathbf{F}}\mathbf{v}\, dS = \int \left(\dot{\boldsymbol{\sigma}}\boldsymbol{\epsilon} - \sigma_{ij} \frac{\partial v_i}{\partial x_k} \frac{\partial v_k}{\partial x_j} \right) dV$$

$$= \int \left(\mu h \epsilon^2 - \sigma_{ij} \frac{\partial v_i}{\partial x_k} \frac{\partial v_k}{\partial x_j} \right) dV$$

as in HILL (1957a, Section 2), and so

$$U(\mathbf{v}) = \tfrac{1}{2} \int \dot{\mathbf{F}}\mathbf{v}\, dS \tag{9}$$

where $\dot{\mathbf{F}}$ is any nominal traction-rate that would operate the mode $\mathbf{v}$. It follows that at a bifurcation in the range $\beta > \mu > \alpha$, where $U(\mathbf{v})$ is positive, the loading cannot remain constant but must change with continuing deformation in either mode in such a way that the integral in equation (9) is positive (generalizing and making precise another part of SHANLEY's conception). On the other hand, there exist certain states and particular values of μ (eigenvalues) such that quasi-static deformation *can* proceed under temporarily constant loading. For these, $U(\mathbf{v})$ vanishes for the non-zero mode possible under dead loading, and so no eigenvalue can exceed the α corresponding to such a state. However, although the stability ' limit ' α is itself marked by the vanishing of $U(\mathbf{v})$ for a certain virtual mode, this need not be an actual mode under dead loading nor need α be an eigenvalue (as is the case when the solid is perfectly elastic, the stability functional being always one-signed until the varied parameter reaches the first eigenvalue – a restatement of Rayleigh's Principle).

5. Illustration : Compression of a Strut

A strut of uniform sectional area A is built in at one end and axially loaded at the other by a load P. Except in the immediate neighbourhood of the fixed end the stress is a uniform uniaxial compression of amount P/A. It seems safe to consider only those modes that produce no inflexions, which are (as in the investigation of uniqueness : HILL 1957a, Section 5)

$$v_1 = -\tfrac{1}{4}a(x_1^2 - x_2^2 + 2x_3^2) - \tfrac{1}{2}bx_1x_2 - 2cx_1x_3 - \tfrac{1}{2}dx_1,$$

$$v_2 = -\tfrac{1}{2}ax_1x_2 - \tfrac{1}{4}b(x_2^2 - x_1^2 + 2x_3^2) - 2cx_2x_3 - \tfrac{1}{2}dx_2,$$

$$v_3 = ax_1x_3 + bx_2x_3 + c(x_1^2 + x_2^2 + 2x_3^2) + dx_3.$$

Here the origin is at the centroid of the fixed end and the x_3 axis along the strut. a, b, c, d are not entirely arbitrary, as they were in the examination of uniqueness, but are subject to the condition for positive rate of work : $\epsilon_{33} \leqslant 0$ or

$$ax_1 + bx_2 + 4cx_3 + d \leqslant 0$$

everywhere in the body.

Suppose the strut is so slender that $(I_1 + I_2)/Al^2 << 1$, where l is the length and I_1, I_2 the second moments of sectional area about the x_1, x_2 axes respectively, and that h is uniform. The condition for stability, as for uniqueness, reduces to

$$\frac{3h}{2Pl^2} > \text{Max}\,\frac{\tfrac{1}{3}(a^2 + b^2 - c^2) - \dfrac{cd}{l} - \dfrac{d^2}{l^2}}{I_2a^2 + I_1b^2 + \tfrac{1}{3}Al^2c^2 + Ad^2}$$

but now the above restriction must be observed.

To be definite, let the section be a circle of radius r. The maximum is found to be

$$\frac{1}{3(I + Ar^2)}$$

and is obtained when $c = 0$, $d = -r\sqrt{(a^2 + b^2)}$, a and b arbitrary. The comparative value for uniqueness is $1/(3I)$. With $I = \frac{1}{4}Ar^2$ the critical hardening-rate for stability is $\frac{1}{6}$ of that for uniqueness. Similar small factors are obtained for other sections.

This is a remarkable result, but it cannot be seen in its true perspective until all aspects of this particular problem have been fully investigated. For this reason no comparison with experiment or with heuristic theories of the SHANLEY type is attempted here.

REFERENCES

HILL, R.	1950	*Mathematical Theory of Plasticity* (Clarendon Press, Oxford).
	1956	*Surveys in Mechanics* pp. 1-28. (Cambridge University Press).
	1957a	*J. Mech. Phys. Solids* **5**, 153.
	1957b	*Ibid.* **5**, 229.
	1957c	*Ibid.* **5**, 302.
PEARSON, C. E.	1956	*Quart. Appl. Math.* **14**, 133.
SHANLEY, F. R.	1946	*J. Aero. Sci.* **13**, 678.
	1947	*Ibid.* **14**, 261.
SOKOLNIKOFF, I. S.	1956	*Mathematical Theory of Elasticity* 2nd Ed. (McGraw-Hill, New York).

Journal of the Mechanics and Physics of Solids, 1957, Vol. 6, pp. 9 to 12. Pergamon Press Ltd., London

ON RIGID WORKHARDENING SOLIDS WITH SINGULAR YIELD CONDITIONS

By W. E. Boyce and W. Prager
Brown University

(*Received* 11*th June*, 1957)

1. Introduction and Summary

So many papers on the theory of plasticity have been concerned with uniqueness theorems and extremum principles that it would not have seemed likely some years ago that new significant results could be obtained. Yet the fundamental theorems of limit analysis constituted just such an addition to this field. More recently, Hill (1956) established important results concerning rigid workhardening solids with regular yield conditions. (The corresponding results for elastic workhardening solids had been available for some years : Hodge and Prager 1949, Hill 1950). In view of the increased use of singular yield conditions in recent work on plastic discs, plates, and shells, it seems worth while to extend Hill's results to rigid workhardening solids with singular yield conditions.

2. Stress-Strain Law

Consider a rigid workhardening material that is in a given state of hardening. The states of stress that the material can sustain without changing its state of hardening are classified as *plastic* or *rigid* according to whether plastic deformation can or cannot be produced by appropriate infinitesimal changes of stress. The yield condition for the considered state of hardening specifies the plastic states of stress.

For the discussion of yield conditions and flow rules, it is convenient to treat the components ϵ_{ij} and σ_{ij} of the tensors of strain rate and stress with respect to rectangular Cartesian co-ordinates x_i $(i = 1, 2, 3)$, as constituting the rectangular Cartesian components of the vectors $\boldsymbol{\epsilon}$ and $\boldsymbol{\sigma}$ in a nine-dimensional space. The state of stress σ_{ij} may then be represented by the point with the radius vector $\boldsymbol{\sigma}$. It will be assumed that, for a given state of hardening, the points representing rigid states of stress fill a *convex* domain (the *rigid range*) that contains the origin (the *stress-free state*). For a *regular* yield condition the bounding surface of the rigid range (the *yield locus*) has a continuously turning normal. If the unit vector along the outward normal is denoted by $\mathbf{n}$, the stress-strain law associated with a regular yield condition specifies that in a plastic state of stress the stress rate $\dot{\boldsymbol{\sigma}}$ produces the strain rate

$$\boldsymbol{\epsilon} = h^{-1} \left[\mathbf{n}\dot{\boldsymbol{\sigma}}\right] \mathbf{n}, \tag{1}$$

where h is a positive scalar function of stress and strain-history and $[\mathbf{n}\,\dot{\sigma}]$ stands for the scalar product of the vectors $\mathbf{n}$ and $\dot{\sigma}$, when this is positive, and for zero, when the scalar product is negative. The factor $\mathbf{n}$ in (1), which indicates the direction of the vector ϵ, is said to specify the yield mechanism associated with the considered plastic state of stress σ. A regular yield condition thus associates a unique yield mechanism with each plastic state of stress.

A singular yield condition, on the other hand, allows for the possibility that, for certain plastic states of stress, there may be two or more competing yield mechanisms each of which makes an independent contribution to the strain rate. Geometrically speaking, the yield locus consists of regular faces, each of which has a continuously turning normal $\mathbf{n}_\alpha$ ($\alpha = 1, 2, \ldots$). For a plastic state of stress that is represented by a point on an *edge* common to two or more faces, the stress-strain law (1) is replaced by (Koiter 1953)

$$\epsilon = \sum_\alpha \epsilon_\alpha = \sum_\alpha h_\alpha^{-1} [\mathbf{n}_\alpha\,\dot{\sigma}]\,\mathbf{n}_\alpha, \tag{2}$$

where the bracket has the same meaning as in (1), the summation includes the contributions ϵ_α from the yield mechanisms of all faces meeting in the considered edge, and h_α is a positive scalar function of the stress and the history of the contribution of the αth yield mechanism to the strain.

Note that, in a plastic state of stress, the scalar product of $\dot{\sigma}$ and ϵ is given by

$$\dot{\sigma}\,\epsilon = \begin{cases} \sum_\alpha h_\alpha^{-1} [\mathbf{n}_\alpha\,\dot{\sigma}]^2, \\ \sum_\alpha h_\alpha\,\epsilon_\alpha^2. \end{cases} \tag{3}$$

3. Statement of Problem. Uniqueness

Consider a body that consists of a rigid, workhardening material with a singular yield condition and is subjected to surface tractions or small surface displacements, which vary slowly with time. As a necessary step in analysing the time-dependent stresses, displacements, and strains in this body, we discuss the following boundary-value problem : given the strain history * and the instantaneous stress σ throughout the body, the rates of surface traction $\dot{\mathbf{F}}$ on the part S_F of its surface, and the surface velocity $\mathbf{v}$ on the remainder S_v of S, to find the stress rate $\dot{\sigma}$ and the velocity throughout the body.

The investigation of uniqueness starts as usual from the remark that the boundary conditions and the principle of virtual work show that

$$0 = \int (\dot{\mathbf{F}}' - \dot{\mathbf{F}}'')\,(\mathbf{v}' - \mathbf{v}'')\,dS = \int (\dot{\sigma}' - \dot{\sigma}'')\,(\epsilon' - \epsilon'')\,dV$$

$$= \int \sum_\alpha (\dot{\sigma}' - \dot{\sigma}'')\,(\epsilon_\alpha' - \epsilon_\alpha'')\,dV \tag{4}$$

where the primes and double primes are used to distinguish between two solutions, and dV is the volume element.

In discussing the sign of the last integrand in (4), we must keep in mind that both solutions correspond to the same strain history and instantaneous stress. At a

*More precisely, the history of the individual contributions of the various yield mechanisms to the strain.

generic point of the body, the summation over α in the stress-strain law therefore includes the same yield mechanisms and the function h_α has the same value for both solutions.

Let I_α denote the contribution made by the αth yield mechanism to the last integrand in (4). Where this yield mechanism is active in both solutions, $[\mathbf{n}_\alpha \dot{\boldsymbol{\sigma}}'] = \mathbf{n}_\alpha \dot{\boldsymbol{\sigma}}' > 0$ and $[\mathbf{n}_\alpha \dot{\boldsymbol{\sigma}}''] = \mathbf{n}_\alpha \dot{\boldsymbol{\sigma}}'' > 0$, and hence

$$I_\alpha = h_\alpha^{-1} \{\mathbf{n}_\alpha (\dot{\boldsymbol{\sigma}}' - \dot{\boldsymbol{\sigma}}'')\}^2 \geqslant 0, \tag{5}$$

with equality only if $\boldsymbol{\epsilon}_\alpha' = \boldsymbol{\epsilon}_\alpha''$. Where the αth yield mechanism is active for one solution, say the primed one, and inactive for the other, $[\mathbf{n}_\alpha \dot{\boldsymbol{\sigma}}'] = \mathbf{n}_\alpha \dot{\boldsymbol{\sigma}}' > 0$, $[\mathbf{n}_\alpha \dot{\boldsymbol{\sigma}}''] = 0$, and $\mathbf{n}_\alpha \dot{\boldsymbol{\sigma}}'' \leqslant 0$, and hence

$$I_\alpha = h_\alpha^{-1} \mathbf{n}_\alpha \dot{\boldsymbol{\sigma}}' \{\mathbf{n}_\alpha (\dot{\boldsymbol{\sigma}}' - \dot{\boldsymbol{\sigma}}'')\} > 0. \tag{6}$$

Finally, $I_\alpha = 0$ where the yield mechanism α is inactive for both solutions and hence $\boldsymbol{\epsilon}_\alpha' = \boldsymbol{\epsilon}_\alpha'' = 0$.

The contribution of the yield mechanism α to the last integrand in (4) is thus positive unless $\boldsymbol{\epsilon}_\alpha' = \boldsymbol{\epsilon}_\alpha''$. This shows that the strain-rate field $\boldsymbol{\epsilon} = \Sigma_\alpha \boldsymbol{\epsilon}_\alpha$ is unique, though the stress-rate field $\dot{\boldsymbol{\sigma}}$ is not necessarily unique. If we exclude the possibility that the area of S_v vanishes, the uniqueness of the strain-rate field $\boldsymbol{\epsilon}$ establishes the uniqueness of the velocity field $\mathbf{v}$. As in HILL's (1956) paper, it follows then that $\int \dot{\mathbf{F}} \mathbf{v}\, dS_v$ is unique, even though the rate of surface traction $\dot{\mathbf{F}}$ on S_v is not necessarily unique.

4. Extremum Principles

A strain-rate field $\boldsymbol{\epsilon}^*$ will be called *kinematically admissible* with respect to our boundary value problem if it is defined through the volume V of the considered body and fulfils the following conditions: (i) $\boldsymbol{\epsilon}^*$ is derivable from a continuous velocity field $\mathbf{v}^*$ that satisfies the boundary conditions on S_v; (ii) at a generic point P of V, the strain rate $\boldsymbol{\epsilon}^*$ is the sum of contributions $\boldsymbol{\epsilon}_\alpha^*$ that are compatible with the state of stress at P, i.e. if $\boldsymbol{\epsilon}_\alpha^* \neq 0$, then

$$\boldsymbol{\epsilon}_\alpha^* = \lambda_\alpha^* \mathbf{n}_\alpha, \qquad \text{where} \quad \lambda_\alpha^* > 0. \tag{7}$$

The unique strain-rate field $\boldsymbol{\epsilon}$ of the solutions is kinematically admissible. If the corresponding velocity field is denoted by $\mathbf{v}$, we have

$$\int \dot{\mathbf{F}} (\mathbf{v}^* - \mathbf{v})\, dS_F = \int \dot{\mathbf{F}} (\mathbf{v}^* - \mathbf{v})\, dS = \int \dot{\boldsymbol{\sigma}} (\boldsymbol{\epsilon}^* - \boldsymbol{\epsilon})\, dV$$
$$= \int \sum_\alpha \dot{\boldsymbol{\sigma}} (\boldsymbol{\epsilon}_\alpha^* - \boldsymbol{\epsilon}_\alpha)\, dV. \tag{8}$$

In (8), the summation over α again involves the same yield mechanisms for both strain-rate fields. The contribution I_α of the yield mechanism α to the last integrand in (8) is readily shown to be smaller than $\frac{1}{2} h_\alpha (\boldsymbol{\epsilon}_\alpha^{*2} - \boldsymbol{\epsilon}_\alpha^2)$ unless $\boldsymbol{\epsilon}_\alpha^* = \boldsymbol{\epsilon}_\alpha$. Thus,

$$\int \sum_\alpha h_\alpha \boldsymbol{\epsilon}_\alpha^{*2}\, dV - 2 \int \dot{\mathbf{F}} \mathbf{v}^*\, dS_F > \int \sum_\alpha h_\alpha \boldsymbol{\epsilon}_\alpha^2\, dV - 2 \int \dot{\mathbf{F}} \mathbf{v}\, dS_F$$
$$= \int \dot{\mathbf{F}} \mathbf{v}\, dS_v - \int \dot{\mathbf{F}} \mathbf{v}\, dS_F, \tag{9}$$

unless $\epsilon_\alpha^* = \epsilon_\alpha$. The inequality (9) gives a minimum characterization of the unique strain rate and velocity fields of the solutions. The steps establishing (9) follow those in Hill's (1956) paper so closely that they need not be detailed here.

A stress rate field $\dot{\sigma}^*$ will be called *statically admissible* with respect to our boundary-value problem if it is defined throughout V, satisfies the equation of equilibrium in V, and yields the prescribed rate of surface traction on S_F. The stress-rate field $\dot{\sigma}$ of a solution is statically admissible, and we have

$$\int (\dot{\mathbf{F}}^* - \dot{\mathbf{F}}) \cdot \mathbf{v}\, dS_v = \int (\dot{\mathbf{F}}^* - \dot{\mathbf{F}}) \cdot \mathbf{v}\, dS = \int (\dot{\sigma}^* - \dot{\sigma}) \cdot \epsilon\, dV$$

$$= \int \sum_\alpha (\dot{\sigma}^* - \dot{\sigma}) \cdot \epsilon_\alpha\, dV. \tag{10}$$

Wherever $\epsilon_\alpha \neq 0$, the contribution I_α of the αth yield mechanism to the last integrand in (10) is readily shown to be smaller than $\frac{1}{2} h_\alpha^{-1} \{(\mathbf{n}_\alpha \cdot \dot{\sigma}^*)^2 - (\mathbf{n}_\alpha \cdot \dot{\sigma})^2\}$, unless the stress rate field $\dot{\sigma}^*$ also corresponds to a solution of our boundary value problem. If this possibility is ruled out, we have the following maximum characterization of the stress rate fields of the solutions:

$$2 \int \dot{\mathbf{F}}^* \cdot \mathbf{v}\, dS_v - \int \sum_\alpha h_\alpha^{-1} (\mathbf{n}_\alpha \cdot \dot{\sigma}^*)^2\, dV < 2 \int \dot{\mathbf{F}} \cdot \mathbf{v}\, dS_v - \int \sum_\alpha h_\alpha^{-1} (\mathbf{n}_\alpha \cdot \dot{\sigma})\, dV$$

$$= \int \dot{\mathbf{F}} \cdot \mathbf{v}\, dS_v - \int \dot{\mathbf{F}} \cdot \mathbf{v}\, dS_F. \tag{11}$$

Acknowledgment

The results presented in this note were obtained in the course of research sponsored by the Office of Naval Research under Contract N-onr 562 (10).

References

Hill, R. 1950 *Mathematical Theory of Plasticity* Chap. III. (Clarendon Press, Oxford).
1956 *J. Mech. Phys. Solids* **4**, 247.
Hodge, P. G., Jr. and Prager, W. 1949 *J. Math. Phys.* **27**, 1.
Koiter, W. T. 1953 *Quart. Appl. Math.* **11**, 350.

Journal of the Mechanics and Physics of Solids, 1957, Vol. 6, pp. 13 to 16. Pergamon Press Ltd., London

A REMARK ON THE ANALOGY BETWEEN THERMOELASTICITY AND THE ELASTICITY OF SATURATED POROUS MEDIA

By J. GEERTSMA
Koninklijke/Shell-Laboratorium, Amsterdam

(*Received 17th May*, 1957)

SUMMARY

THE analogous behaviour of the temperature distribution in thermoelastic problems and the liquid pressure distribution in a saturated porous medium is worked out in detail and applied to the cases of plane strain and plane stress, the latter for thin plates only.

1. INTRODUCTION

LESSEN (1956) recently pointed out that in thermoelasticity in general the mechanical interaction term in the temperature-distribution equation is neglected, though the existence of such an interaction was pointed out long ago by DUHAMEL and later by NEUMANN. A detailed discussion of the complete temperature-distribution equation is given by BIOT (1956a). His equation can be written as*

$$\frac{\lambda}{\rho}\nabla^2(\Theta/T) = \bar{c}\,\frac{\partial(\Theta/T)}{\partial t} + \frac{a}{c_b}\frac{\partial e}{\partial t} \tag{1}$$

which equation is in structure identical with the equations derived by LESSEN. One purpose of this note is to discuss the analogous situation in the theory of elasticity of liquid saturated porous media.

That there is an analogy between both types of problems was e.g. demonstrated by LUBINSKY (1954) and afterwards by BIOT (1956a). Lubinsky in his theory of elasticity for porous bodies 'displaying a strong pore structure' neglects the influence of the compressibility of the pore volume on the pressure distribution in the pores. Consequently the dilatation e of the bulk volume of the porous medium does not occur in the differential equation for the pore pressure distribution. This equation turns out to be a Fourier-type equation if the fluid in the pores is a compressible liquid.

In this way an analogy was found with the common theory of thermoelasticity, in which the temperature-distribution is independent of the solid dilatation.

However, BIOT (1941) showed that the pore compressibility introduces an interaction term in the pore pressure-distribution equation in the same way as the dilatation of the solid introduces an interaction term in the temperature-distribution equation. The analogy was pointed out much later (BIOT 1956a).

*See list of symbols at end.

The equation for the complete pore pressure-distribution can according to BIOT (1941) be written as

$$\frac{k}{\eta}\nabla^2 p = \frac{1}{Q}\frac{\partial p}{\partial t} + \alpha\frac{\partial e}{\partial t}. \tag{2}$$

The constants Q and α are not simple measurable physical quantities as in the corresponding temperature-distribution equation (1). Later developments of (2) did not provide any improvement in this respect. The second purpose of this note therefore is to express these constants in measurable terms and to consider the results. This can be achieved by using the theory of pore and rock bulk volume variations for porous rocks, as developed by the writer (1956).

2. INTERPRETATION OF DEFORMATION CONSTANTS

If a porous medium is built up of an isotropic, homogeneous and continuous matrix material and the bulk has the same properties on a macroscopic scale, it was found that in the absence of a pore liquid

$$\frac{1}{Q} = c_r(1 - f - \beta) \tag{3}$$

and

$$\alpha = (1 - \beta). \tag{4}$$

For a compressible liquid in the pores α has the same value but now

$$\frac{1}{Q} = c_r(1 - f - \beta) + cf. \tag{3a}$$

Thus (2) can be expressed in the following way :

$$\frac{k}{\eta}\nabla^2 p = [c_r(1 - f - \beta) + cf]\frac{\partial p}{\partial t} + (1 - \beta)\frac{\partial e}{\partial t}. \tag{2a}*$$

A comparison of (1) and (2a) reveals that the heat conductivity $\lambda/\rho T$ replaces the liquid mobility k/η in the pores, the specific heat $\overline{c}/T$ replaces the compressibility $c_r(1 - f - \beta) + cf$, while the ratio of thermal expansion and compressibility a/c_b replaces the compressibility ratio $(1 - \beta)$.

3. APPLICATIONS

From a practical point of view the occurrence of the interaction term complicates the mathematical treatment considerably. However, in a number of cases the basic equations (1) or (2) still reduce to a Fourier type equation. An example of such a case is the thermal shock problem described by LESSEN (1956). Two other

*The second equation relating p and e is

$$\nabla^2 e - \tfrac{1}{3}\left(\frac{1+\nu}{1-\nu}\right) c_b(1-\beta)\nabla^2 p = 0$$

and the corresponding equation in the thermal stress problem is

$$\nabla^2 e - \tfrac{1}{3}\left(\frac{1+\nu}{1-\nu}\right)\alpha\nabla^2\Theta = 0.$$

specific examples will be given here, namely the radially symmetric case in plane stress and in plane strain. The latter is an example of zero rotation, for which BIOT (1956) showed in a general way that it leads to a Fourier type equation. The first case is a well-known problem of a different type and its occurrence shows that there are more of such special cases than are comprised in BIOT's group of problems.

The equation of equilibrium for both cases mentioned is

$$r\frac{\partial \sigma_r}{\partial r} + (\sigma_r - \sigma_\theta) = 0. \tag{5}$$

The stress-strain relations for a porous solid are

$$\left.\begin{aligned} \sigma_r &= 2G\epsilon_r - (1-\beta)p + \left(\frac{1}{c_b} - \tfrac{2}{3}G\right)e \\ \sigma_\theta &= 2G\epsilon_\theta - (1-\beta)p + \left(\frac{1}{c_b} - \tfrac{2}{3}G\right)e \\ \sigma_z &= 2G\epsilon_z - (1-\beta)p + \left(\frac{1}{c_b} - \tfrac{2}{3}G\right)e \end{aligned}\right\} \tag{6}$$

with $\epsilon_r = \partial u/\partial r$ and $\epsilon_\theta = u/r$. Substitution of the relations (6) and (5) leads to

$$2G\frac{\partial}{\partial r}(\epsilon_r + \epsilon_\theta) - (1-\beta)\frac{\partial p}{\partial r} + \left(\frac{1}{c_b} - \tfrac{2}{3}G\right)\frac{\partial e}{\partial r} = 0. \tag{7}$$

For *plane strain* $\epsilon_z = 0$ and thus $e = \epsilon_r + \epsilon_\theta$. Accordingly, we obtain

$$\left(\frac{1}{c_b} + \tfrac{4}{3}G\right)\frac{\partial e}{\partial r} - (1-\beta)\frac{\partial p}{\partial r} = 0$$

or, with

$$G = \tfrac{3}{2}\left(\frac{1-2\nu}{1+\nu}\right)\frac{1}{c_b},$$

$$\frac{3(1-\nu)}{(1+\nu)}\frac{1}{c_b}e - (1-\beta)p = \text{constant},$$

which relation in general (viz. for $\tau \to \infty$. $e = 0$ and $\beta = \text{const.}$) holds for any time t. By virtue of this fact (2a) reduces to a Fourier-type equation :

$$\frac{k}{\eta}\nabla^2 p = \left[c_r(1-f-\beta) + cf + \tfrac{1}{3}c_b(1-\beta)^2\left(\frac{1+\nu}{1-\nu}\right)\right]\frac{\partial p}{\partial t}. \tag{8}$$

The constant

$$c_r(1-f-\beta) + cf + \tfrac{1}{3}c_b(1-\beta)^2\left(\frac{1+\nu}{1-\nu}\right)$$

replaces the ratio f^2/K in (7a) of BIOT (1956b), this ratio now being given in terms of easily measurable quantities.

From the foregoing it will further be clear that the corresponding equation for the thermoelastic problem is

$$\frac{\lambda}{\rho}\nabla^2\Theta = \left[\bar{c} + \tfrac{1}{3}\frac{a^2}{c_b}\left(\frac{1+\nu}{1-\nu}\right)\right]\frac{\partial\Theta}{\partial t}. \tag{9}$$

In the case of *plane stress* $\sigma_z = 0$,* and consequently

*The case of thin plates is considered here.

$$2G\frac{\partial \epsilon_z}{\partial r} = (1-\beta)\frac{\partial p}{\partial r} - \left(\frac{1}{c_b} - \tfrac{2}{3}G\right)\frac{\partial e}{\partial r}.$$

If the latter is substituted in (7), after this has been brought into the form

$$2G\frac{\partial e}{\partial r} - 2G\frac{\partial \epsilon_z}{\partial r} - (1-\beta)\frac{\partial p}{\partial r} + \left(\frac{1}{c_b} - \tfrac{2}{3}G\right)\frac{\partial e}{\partial r} = 0,$$

we obtain

$$\tfrac{2}{3}\left(\frac{1}{1+\nu}\right)\frac{1}{c_b}e - (1-\beta)p = \text{constant},$$

which again holds for any time.

Equation (2a) now reduces to a Fourier-type equation with a different constant :

$$\frac{k}{\eta}\nabla^2 p = \left[c_r(1-f-\beta) + cf + \tfrac{2}{3}c_b(1-\beta)^2(1+\nu)\right]\frac{\partial p}{\partial t}. \tag{10}$$

The corresponding thermoelastic equation accordingly becomes

$$\frac{\lambda}{\rho}\nabla^2\Theta = \left[\overline{c} + \tfrac{2}{3}\frac{a^2}{c_b}(1+\nu)\right]\frac{\partial \Theta}{\partial t}. \tag{11}$$

List of Symbols

a = coefficient of thermal expansion (cubical)
$\beta = c_r/c_b$
c = liquid compressibility
$\overline{c}$ = specific heat
c_b = rock bulk compressibility
c_r = rock matrix compressibility
e = dilatation
η = viscosity
$\epsilon_r, \epsilon_\theta, \epsilon_z$ = strain in radial, tangential and axial directions
f = porosity
G = shear modulus
k = permeability
λ = heat conductivity
p = pore pressure
r = radial distance
ρ = density
$\sigma_r, \sigma_\theta, \sigma_z$ = stress in radial, tangential and axial directions
t = time
T = reference absolute temperature for the state of zero stress and strain
Θ = temperature variation
u = elongation
ν = Poisson's ratio

References

BIOT, M. A. 1941 *J. Appl. Phys.* **12**, 155.
1956a *J. Appl. Phys.* **27**, 240.
1956b *J. Appl. Mech.* **23**, 91.
GEERTSMA, J. 1956 *Preprint* 728-*G Fall Meeting AIME* (Petroleum Branch).
LESSEN, M. 1956 *J. Mech. Phys. Solids* **5**, 57.
LUBINSKY, A. 1954 *Proc. 2nd U.S. Cong. Appl. Mech.* 247.

Journal of the Mechanics and Physics of Solids, 1957, Vol. 6, pp. 17 to 26. Pergamon Press Ltd., London

ON THE COMBINED BENDING AND TWISTING OF BEAMS OF VARIOUS SECTIONS

By F. A. Gaydon and H. Nuttall
Department of Theoretical Mechanics, University of Bristol

(*Received 27th May*, 1957)

Summary

Upper and lower approximations are obtained to the interaction curve of the bending and twisting couples at yield for the combined bending and twisting of cylinders of ideally plastic-rigid material. Rectangular, I and box sections are dealt with in detail. For the box section a comparison is made with the 'thin' tube theory of Hill and Siebel (1951).

1. Introduction

The methods of plastic limit analysis are applied to the problem of the combined bending and twisting of cylinders of various cross-sections. It is assumed that the material is ideally plastic-rigid and non-hardening. The method used is ultimately based on a continued inequality due to Hill (1950a, p. 67 ; 1950b) but for the most part follows that of Hill and Siebel (1953). Approximations from above and below to the relation between the twisting and bending couples at yield are found. The method cited above has been extended to obtain good approximations by introducing a warping function into the assumed velocity mode which, in the case of the I section, has a discontinuity.

2. Method

For simplicity the discussion is restricted to the case of bending about a principal axis of the cross-section. Let Ox, Oy be principal axes of the cross-section, where Oy is the axis of bending, and let Oz be the axis of twist. Let T_0 and B_0 be the fully plastic yield torques for pure torsion and pure bending respectively. If T, B are the actual applied couples producing yield there will exist a certain relation, called an interaction relation, between T, B and the dimensions of the cross-section. This relation, if known, could be plotted for any given dimensions as a T-B curve. The aim of this paper is to sandwich this curve between one representing an approximation from above and one representing an approximation from below.

(a) *Approximation from below*

Following Hill and Siebel (1953), consider an assumed distribution of shearing stress $\tau(x, y)$ such that the shearing stress at every point of the cross-section is in

the same direction as the shearing stress k in pure torsion but is a constant fraction of k, say nk ($n < 1$). Then the torque T_L derived from this distribution is

$$T_L = n\, T_0.$$

A distribution of normal stress $\sigma = p\sqrt{3}k$, $x < 0$; $\sigma = -p\sqrt{3}k$, $x > 0$, where $p < 1$, is combined with the shear stress $\tau(x, y)$. Then the bending moment B_L obtained from this distribution is

$$B_L = p\, B_0.$$

Since the yield criterion $\sigma^2 + 3\tau^2 \leqslant 3k^2$ must not be violated at any point, the best approximation is obtained when

$$p^2 + n^2 = 1,$$

that is, when

$$\left(\frac{T_L}{T_0}\right)^2 + \left(\frac{B_L}{B_0}\right)^2 = 1 \tag{1}$$

This is the approximation from below and, with the appropriate B_0, T_0, is used for all the cross-sections considered in this paper.

(b) *Approximation from above*

An assumed velocity distribution representing a combination of bending and twisting at rates $\dot{\psi}$, $\dot{\theta}$ per unit length respectively, with associated warping but no volume change, is

$$\left.\begin{aligned} u &= \tfrac{1}{4}(x^2 - y^2 + 2z^2)\,\dot{\psi} - yz\dot{\theta} \\ v &= \tfrac{1}{2}xy\dot{\psi} + xz\dot{\theta} \\ w &= -xz\dot{\psi} + \phi(x, y)\,\dot{\theta} \end{aligned}\right\} \tag{2}$$

The maximum shear-strain rate γ is derived from these velocities and is substituted in HILL's inequality (1950a, p. 67 ; 1950b) whence

$$\begin{aligned} B\dot{\psi} + T\dot{\theta} &\leqslant 2k \int_A \gamma\, dA \\ &= k \int_A [3x^2\dot{\psi}^2 + \dot{\theta}^2(\phi_y + x)^2 + \dot{\theta}^2(\phi_x - y)^2]^{\frac{1}{2}}\, dA = W, \quad \text{say} \end{aligned} \tag{3}$$

where A is the cross-sectional area. For a given ratio B/T the best approximation to the magnitudes of B, T is given by (HILL and SIEBEL 1953)

$$B \leqslant B_u = \frac{\partial W}{\partial \dot{\psi}}, \qquad T \leqslant T_u = \frac{\partial W}{\partial \dot{\theta}}$$

provided that the assumed $\dot{\psi}$, $\dot{\theta}$ are chosen so that

$$B_u/T_u = B/T.$$

It then follows that

$$B_u = k \int\int \frac{3\lambda x^2\, dx\, dy}{[3x^2\lambda^2 + (\phi_y + x)^2 + (\phi_x - y)^2]^{\frac{1}{2}}} \tag{4}$$

and

$$T_u = k \int\int \frac{\{(\phi_y + x)^2 + (\phi_x - y)^2\}\, dx\, dy}{[3x^2 \lambda^2 + (\phi_y + x)^2 + (\phi_x - y)^2]^{\frac{1}{2}}} \tag{5}$$

where $\dot{\psi}/\dot{\theta} = \lambda$.

The simplest upper approximation is that in which the warping function is taken to be zero (HILL and SIEBEL 1953, STEELE 1955). However, this assumption does not give a reasonable upper approximation for the cross-sections considered here except for the square or nearly square cross-section, the former being dealt with in STEELE's paper. It is therefore necessary to consider a non-zero warping function of sufficient simplicity to allow the evaluation of the integrals (4) and (5) without too much complication.

3. Rectangular Section

(a) *Approximation from below*

For the rectangular cross-section with sides having the equations $x = \pm a$, $y = \pm b$, T_0 is given by

$$T_0/k = 4a^2 b - 4a^3/3, \qquad a \leqslant b,$$
$$= 4ab^2 - 4b^3/3, \qquad a \geqslant b.$$

The stress-state at yield for pure bending consists of stresses $\pm \sqrt{3}k$ on opposite sides of the plane $x = 0$, and B_0 is given by

$$B_0 = 2\sqrt{3}\, k\, a^2\, b.$$

The curve representing the approximation from below given by equation (1) is, of course, a quadrant of a circle of unit radius if B_L/B_0, T_L/T_0 are taken as the co-ordinates.

(b) *Approximation from above*

The warping function is taken to be $\phi(x, y) = Cxy$; the integrals (4) and (5) may now be evaluated analytically. Moreover such a function is the predominant term in the elastic warping function for many cross-sections. With this warping function the equations (4) and (5) lead to

$$\frac{B_u}{B_0} = \frac{\lambda}{\sqrt{3}} \left[\frac{(A\mu^2 + B)^{\frac{1}{2}}}{\mu A} + \frac{2\mu}{B^{\frac{1}{2}}} \ln \left\{ \frac{B^{\frac{1}{2}} + (A\mu^2 + B)^{\frac{1}{2}}}{\mu A^{\frac{1}{2}}} \right\} - \frac{B}{\mu^2 A^{3/2}} \ln \left\{ \frac{\mu A^{\frac{1}{2}} + (A\mu^2 + B)^{\frac{1}{2}}}{B^{\frac{1}{2}}} \right\} \right], \tag{6}$$

$$\frac{T_u}{T_0} = D \left[\frac{(A\mu^2 + B)^{\frac{1}{2}} (2A - 3\lambda^2)}{A} + \frac{\mu^2 (A - 6\lambda^2)}{B^{\frac{1}{2}}} \ln \left\{ \frac{B^{\frac{1}{2}} + (A\mu^2 + B)^{\frac{1}{2}}}{\mu A^{\frac{1}{2}}} \right\} + \frac{B(A + 3\lambda^2)}{\mu A^{3/2}} \ln \left\{ \frac{\mu A^{\frac{1}{2}} + (A\mu^2 + B)^{\frac{1}{2}}}{B^{\frac{1}{2}}} \right\} \right]$$

$$\text{with} \qquad D = \frac{\mu}{6\mu - 2}, \qquad \mu \geqslant 1, \tag{7}$$

$$\text{and} \qquad D = \frac{1}{6\mu - 2\mu^2}, \qquad \mu \leqslant 1, \tag{8}$$

where $a/b = \mu$, $A = (C+1)^2 + 3\lambda^2$ and $B = (C-1)^2$. Positive values for the square roots are to be understood.

For $a/b \leqslant \frac{1}{5}$, C is taken to be unity. It is interesting to note that the coefficient of xy in the warping function for the elastic torsion of a beam for which $a/b = \frac{1}{5}$ is 449/450. This latter value does, in fact, give a very slightly better upper approximation but the added complication in the numerical work makes it hardly worthwhile. When $C = 1$, equations (6) and (8) take the simpler form

$$\frac{B_u}{B_0} = \frac{\sqrt{3}\lambda}{(3\lambda^2 + 4)^{\frac{1}{2}}}$$

$$\frac{T_u}{T_0} = \frac{6}{(3-\mu)} \cdot \frac{1}{(3\lambda^2 + 4)^{\frac{1}{2}}}$$

and in this case

$$\left(\frac{T_u}{T_0}\right)^2 (1 - a/3b)^2 + \left(\frac{B_u}{B_0}\right)^2 = 1.$$

This equation represents the quadrant of an ellipse, centred at the origin of T_u/T_0, B_u/B_0, which tends to coincidence with the lower approximation given by (1) as a/b tends to zero. The maximum divergence occurs for pure torsion and is less than $7\frac{1}{2}$ per cent $a/b < \frac{1}{5}$. For $a/b > 5$ a good upper approximation is obtained from $C = -1$*; the formulae then become

$$\frac{B_u}{B_0} = \frac{\lambda}{\sqrt{3}} \left[\frac{(4 + 3\lambda^2\mu^2)^{\frac{1}{2}}}{3\lambda^2\mu} + \mu \ln \left\{ \frac{2 + (4 + 3\lambda^2\mu^2)^{\frac{1}{2}}}{\sqrt{3}\lambda\mu} \right\} \right.$$
$$\left. - \frac{4}{3\sqrt{3}\lambda^3\mu^2} \ln \left\{ \frac{\sqrt{3}\lambda\mu + (4 + 3\lambda^2\mu^2)^{\frac{1}{2}}}{2} \right\} \right], \tag{9}$$

$$\frac{T_u}{T_0} = \frac{\mu}{6\mu - 2} \left[(4 + 3\lambda^2\mu^2)^{\frac{1}{2}} - \frac{3\lambda^2\mu^2}{2} \ln \left\{ \frac{2 + (4 + 3\lambda^2\mu^2)^{\frac{1}{2}}}{\sqrt{3}\lambda\mu} \right\} \right.$$
$$\left. + \frac{8}{\sqrt{3}\lambda\mu} \ln \left\{ \frac{\sqrt{3}\lambda\mu + (4 + 3\lambda^2\mu^2)^{\frac{1}{2}}}{2} \right\} \right]. \tag{10}$$

For the range $\frac{1}{5} < a/b \leqslant 5$ C is taken as $(1-\mu^2)/(1+\mu^2)$,*

i.e. $$\phi(x, y) = \frac{b^2 - a^2}{b^2 + a^2} xy;$$

this is the elastic warping function for the inscribed ellipse.

For a/b less than about 3 the maximum divergence occurs for pure torsion, being greatest for the square†, in which case the upper approximation is 15 per cent above the lower approximation (STEELE 1955). For a/b greater than 3 the maximum divergence does not occur for pure torsion but for some B/T near unity, the actual value depending on a/b. The lower approximation (for all a/b) and the upper

*A slightly better approximation can, once again, be obtained by using the actual coefficient of xy in the elastic warping function.

†For the square, the coefficient of xy in the elastic warping function is zero. No doubt the upper approximation would be improved by taking $\phi(x, y)$ as the first non-zero term in this function. This, however, would mean that the integrals could not be evaluated analytically.

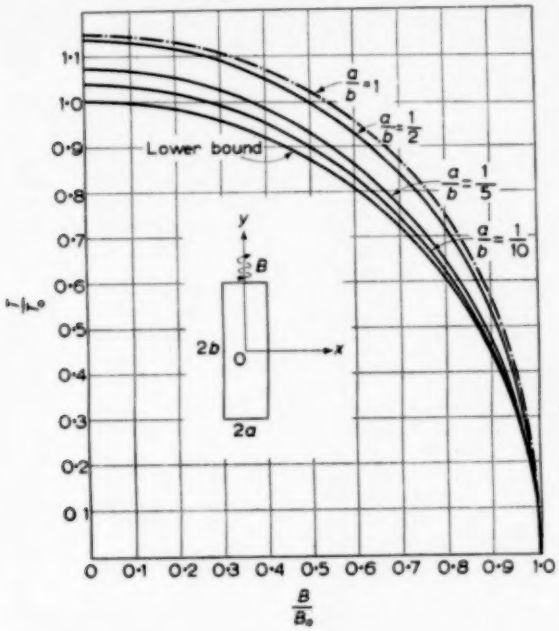
1·1
1·0
0·9
0·8
0·7
0·6
0·5
0·4
0·3
0·2
0·1
0
0·1 0·2 0·3 0·4 0·5 0·6 0·7 0·8 0·9 1·0
$\frac{a}{b}=1$
$\frac{a}{b}=\frac{1}{2}$
$\frac{a}{b}=\frac{1}{5}$
$\frac{a}{b}=\frac{1}{10}$
Lower bound
y
B
2b
O
x
2a
$\frac{B}{B_0}$

Fig. 1.

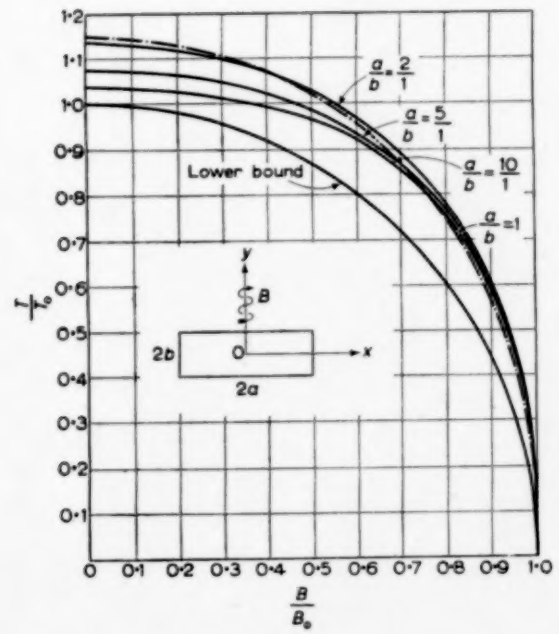
1·2
1·1
1·0
0·9
0·8
0·7
0·6
0·5
0·4
0·3
0·2
0·1
0
0·1 0·2 0·3 0·4 0·5 0·6 0·7 0·8 0·9 1·0
$\frac{a}{b}=\frac{2}{1}$
$\frac{a}{b}=\frac{5}{1}$
$\frac{a}{b}=\frac{10}{1}$
$\frac{a}{b}=1$
Lower bound
y
B
2b
O
x
2a
$\frac{B}{B_0}$

Fig. 2.

approximations for various a/b are shown in Figs. 1 and 2. Given any ratio of B to T at yield the upper and lower bounds to B and T may be taken from the appropriate curves.

4. I SECTION

(a) *Approximation from below*

For the I section depicted in Fig. 3 the yield couple in pure bending is

$$B_0 = 2\sqrt{3}\ k\,[b\,(a^2 - d^2) + cd^2].$$

The yield torque for pure torsion may be shown to be

$$T_0 = 4k\left[\frac{c^3}{3}\ln\frac{a-d}{c} + \frac{5c^3}{18} + \frac{b}{2}(a-d)^2 + dc^2 - \frac{(a-d)^3}{12}\right]$$

where it is assumed that $a - d > c$, which is generally the case for I sections.

(b) *Approximation from above*

It is stated in Section 3 that, for thin rectangles longer in the y direction, the warping function xy gives an excellent approximation. Likewise for a thin rectangle longer in the x direction, $-xy$ is a suitable warping function. In I sections used in practice $ABCD$, $EFGH$ (Fig. 3) can certainly be termed 'thin.' It would seem therefore that the warping function should be chosen as $-xy$ for $EFGH$ and as $\{x - \frac{1}{2}(a+d)\}\,y$ for $ABCD$. However, this does not give a good upper approximation. The integral (5) is minimized only if at the same time x in the v displacement for $ABCD$ is also replaced by $x - \frac{1}{2}(a+d)$ giving rise to a discontinuity in v which is inadmissible. A discontinuity in w, however, is admissible provided the necessary term is added to equation (3). If the warping function is taken to be $(x - h)\,y$ in $ABCD$ it is easy to show that the integral (5) is minimized when $h = a + d$. The assumed velocities in $ABCD$ are u and v as given in equations (2), and

$$w_1 = -xz\dot{\psi} + [x - (a+d)]\,y\dot{\theta}\ ;$$

and for $EFGH$, u and v as in equations (2), and

$$w_2 = -xy\dot{\psi} - xz\dot{\theta}.$$

The addition to W caused by the discontinuities in w across EH, FG is

$$2k\int_{-c}^{c}|w_1 - w_2|\,dy = 2k\,(a-d)\,c^2\,\dot{\theta}.$$

Equations (4) and (5) then become

$$B_u = k\int_{-d}^{d}\int_{-c}^{c}\frac{3\lambda x^2\,dx\,dy}{[3\lambda^2 x^2 + 4y^2]^{\frac{1}{2}}} + 2k\int_{d}^{a}\int_{-b}^{b}\frac{3\lambda x^2\,dx\,dy}{[3\lambda^2 x^2 + (2x - a - d)^2]^{\frac{1}{2}}},$$

$$T_u = k\int_{-d}^{d}\int_{-c}^{c}\frac{4y^2\,dx\,dy}{[3\lambda^2 x^2 + 4y^2]^{\frac{1}{2}}} + 2k\int_{d}^{a}\int_{-b}^{b}\frac{(2x-a-d)^2\,dx\,dy}{[3\lambda^2 x^2 + (2x-a-d)^2]^{\frac{1}{2}}} + 2k\,(a-d)\,c^2.$$

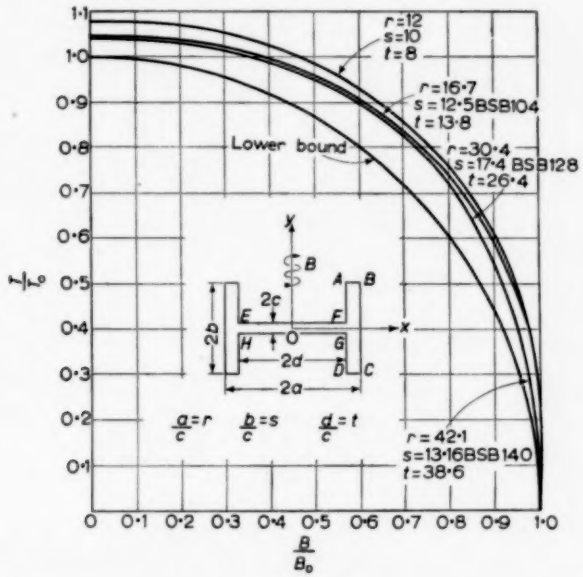

Fig. 3.

These integrals may be evaluated analytically to give

$$\frac{B_u}{kc^3} = \frac{2t\,(4+3\lambda^2 t^2)^{\frac{1}{2}}}{3\lambda} + 2\lambda t^3 \ln\left\{\frac{2+(4+3\lambda^2 t^2)^{\frac{1}{2}}}{\sqrt{3}\,\lambda t}\right\} - \frac{8}{3\sqrt{3}\,\lambda^2}\ln\left\{\frac{\sqrt{3}\,\lambda t + (4+3\lambda^2 t^2)^{\frac{1}{2}}}{2}\right\} + \frac{6s\lambda}{3\lambda^2+4}\left[r + \frac{6\,(r+t)}{3\lambda^2+4}\right]\{3\lambda^2 r^2 + (r-t)^2\}^{\frac{1}{2}} - \frac{6s\lambda}{3\lambda^2+4}\left[t + \frac{6\,(r+t)}{3\lambda^2+4}\right]\{3\lambda^2 t^2 + (r-t)^2\}^{\frac{1}{2}} + \frac{6s\lambda\,(8-3\lambda^2)\,(r+t)^2}{(3\lambda^2+4)^{5/2}}\ln\left\{\frac{3\lambda^2 r + 2\,(r-t) + (3\lambda^2+4)^{\frac{1}{2}}\,[3\lambda^2 r^2 + (r-t)^2]^{\frac{1}{2}}}{3\lambda^2 t - 2\,(r-t) + (3\lambda^2+4)^{\frac{1}{2}}\,[3\lambda^2 t^2 + (r-t)^2]^{\frac{1}{2}}}\right\},$$

$$\frac{T_u}{kc^3} = \frac{2t}{3}\,(4+3\lambda^2 t^2)^{\frac{1}{2}} - \lambda^2 t^3 \ln\left\{\frac{2+(4+3\lambda^2 t^2)^{\frac{1}{2}}}{\sqrt{3}\,\lambda t}\right\} + \frac{16}{3\sqrt{3}\,\lambda}\ln\left\{\frac{\sqrt{3}\,\lambda t + (4+3\lambda^2 t^2)^{\frac{1}{2}}}{2}\right\} + \{3\lambda^2 r^2 + (r-t)^2\}^{\frac{1}{2}}\left[\frac{4s\,(r-t)}{3\lambda^2+4} - \frac{36\lambda^2 s\,(r+t)}{(3\lambda^2+4)^2}\right] + \{3\lambda^2 t^2 + (r-t)^2\}^{\frac{1}{2}}\left[\frac{4s\,(r-t)}{3\lambda^2+4} + \frac{36\,\lambda^2\,s\,(r+t)}{(3\lambda^2+4)^2}\right] + \frac{6s\lambda^2\,(6\lambda^2-4)\,(r+t)^2}{(3\lambda^2+4)^{5/2}} \times \ln\left\{\frac{3\lambda^2 r + 2\,(r-t) + (3\lambda^2+4)^{\frac{1}{2}}\,[3\lambda^2 r^2 + (r-t)^2]^{\frac{1}{2}}}{3\lambda^2 t - 2\,(r-t) + (3\lambda^2+4)^{\frac{1}{2}}\,[3\lambda^2 t^2 + (r-t)^2]^{\frac{1}{2}}}\right\} + 2\,(r-t).$$

where $r = a/c$, $s = b/c$, $t = d/c$.

The upper approximations have been calculated for 3 I beams (*BSB* 104, 128, 140) taken from the Safe Load Tables (*Supplement to the Dorman Long Handbook for Constructional Engineers*). These beams have very different dimensions but their upper approximations are very close together; in fact, for *BSB* 128 and 140 they are indistinguishable on the scale of Fig. 3. The maximum divergence from the lower approximation occurs at about $B/T = 1$ and amounts to about 9 per cent.

All I sections given in the Safe Load Tables have dimensions satisfying the inequalities

$$1 \leqslant a/b \leqslant 3{\cdot}2, \qquad b/c > 10, \qquad a/c > 12,$$

with a flange web ratio between 1·15 and 2·1. After consideration of the effect variations in the dimensions have upon the upper approximations, it appears likely that all I sections in the Tables would have upper approximations below that of the beam with dimensions

$$b/c = 10, \qquad a/c = 12, \qquad d/c = 8.$$

The upper approximation for a section having these extreme proportions is also shown in Fig. 3.

5. Box-Beam

The box-beam is assumed to be of uniform* thickness $2c$ with external dimensions $2a$, $2b$ in the x, y directions respectively. The y-axis is the axis of bending, as before.

The pure couple B_0 for this section is given by

$$B_0 = 4\sqrt{3}\,kc\,[(a-2c)^2 + 2b\,(a-c)]$$

and the pure torsion couple T_0 by

$$T_0 = \frac{16}{3}\,kc^2\,[3a + 3b - 8c] + 16\,kc\,(a-2c)\,(b-2c).$$

The velocities are taken to be those of equations (2) with $\phi\,(x, y)$ again expressed as Cxy where $C = (b^2 - a^2)/(b^2 + a^2)$. The integrals for B_u, T_u are similar to those already obtained for the solid rectangular section and they may be written in the form

$$B_u/k = 3\lambda\,(I_1 - I_2)$$

and

$$T_u/k = (C+1)^2\,[I_1 - I_2] + (C-1)^2\,[I_3 - I_4]$$

where

$$I_1 = \frac{2ab}{3A}\,[Aa^2 + Bb^2]^{\frac{1}{2}} + \frac{4a^3}{3B^{\frac{1}{2}}}\ln\left\{\frac{bB^{\frac{1}{2}} + [Aa^2 + Bb^2]^{\frac{1}{2}}}{aA^{\frac{1}{2}}}\right\} - \frac{2Bb^3}{3A^{3/2}}\ln\left\{\frac{aA^{\frac{1}{2}} + [Aa^2 + Bb^2]^{\frac{1}{2}}}{bB^{\frac{1}{2}}}\right\}$$

and

$$I_3 = \frac{2ab}{3B}\,[Aa^2 + Bb^2]^{\frac{1}{2}} + \frac{4b^3}{3A^{\frac{1}{2}}}\ln\left\{\frac{aA^{\frac{1}{2}} + [Aa^2 + Bb^2]^{\frac{1}{2}}}{bB^{\frac{1}{2}}}\right\} - \frac{2Aa^3}{3B^{3/2}}\ln\left\{\frac{bB^{\frac{1}{2}} + [Aa^2 + Bb^2]^{\frac{1}{2}}}{aA^{\frac{1}{2}}}\right\}.$$

*This assumption is not necessary but leads to a simpler expression for T_0 and one variable the less in results for B_u, T_u.

I_2, I_4 are obtained from I_1, I_3 respectively by replacing a by $(a - 2c)$ and b by $(b - 2c)$, $A = (C + 1)^2 + 3\lambda^2$ and $B = (C - 1)^2$. The upper approximation for all dimensions are shown in Fig. 4.

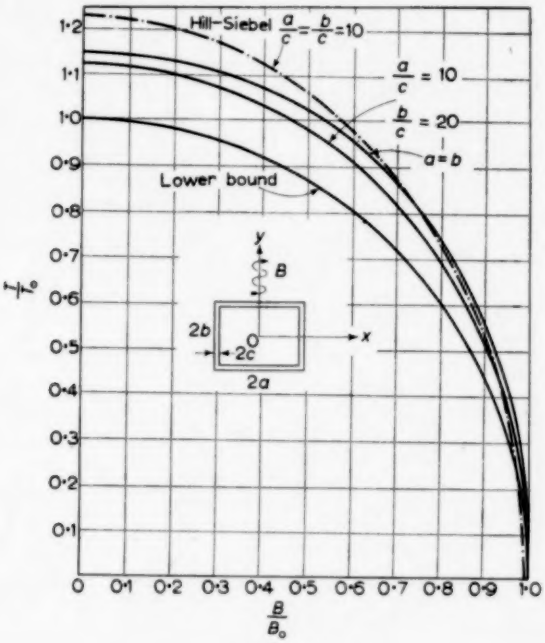

Fig. 4.

For a box-beam with square cross-section $a = b$, $C = 0$ and

$$\frac{B_u}{B_0} = \frac{\lambda}{\sqrt{3}}\left[\frac{(2+3\lambda^2)^{\frac{1}{2}}}{1+3\lambda^2} + 2\ln\left\{\frac{1+(2+3\lambda^2)^{\frac{1}{2}}}{(1+3\lambda^2)^{\frac{1}{2}}}\right\} - \frac{1}{(1+3\lambda^2)^{3/2}}\ln\left\{(1+3\lambda^2)^{\frac{1}{2}} + (2+3\lambda^2)^{\frac{1}{2}}\right\}\right],$$

$$\frac{T_u}{T_0} = \frac{1}{4}\left[\frac{(2+3\lambda^2)^{3/2}}{1+3\lambda^2} + (1-3\lambda^2)\ln\left\{\frac{1+(2+3\lambda^2)^{\frac{1}{2}}}{(1+3\lambda^2)^{\frac{1}{2}}}\right\} + \frac{1+6\lambda^2}{(1+3\lambda^2)^{3/2}}\ln\left\{(1+3\lambda^2)^{\frac{1}{2}} + (2+3\lambda^2)^{\frac{1}{2}}\right\}\right].$$

These expressions are independent of the dimensions and therefore the upper approximation is the same for all thicknesses and hence identical with that for the solid square section.

6. Comparison With Thin Tube Theory

Hill and Siebel (1951) have solved the problem of the combined bending and twisting of thin tubes of elastic–plastic material. In their paper the interaction curve for a thin tube of plastic-rigid material is deduced. It is interesting to

compare this curve with the approximations obtained here. HILL and SIEBEL's equation written in a more convenient form for this purpose is

$$\left(\frac{B}{B_0}\right)^2\left\{1+\frac{c^2}{a^2-4ac+2ab-2bc+3c^2}\right\}^2+\left(\frac{T}{T_0}\right)^2\left(1-\frac{c}{a}-\frac{c}{b}+\frac{4c^2}{3ab}\right)^2=1.$$

It is found that for a square section the HILL–SIEBEL curve is, for the most part, above the upper approximation when $c/a > 1/15$, and below it when $c/a < 1/15$. Since the exact solution is necessarily below the upper approximation obtained in Section 5 it would appear that the description ' thin ' in this connexion is justified for c/a less than about $1/15$. The maximum divergence occurs for pure torsion and the HILL–SIEBEL curve is at least 10 per cent above the exact solution for $c/a = 1/10$ and at least 15 per cent for $c/a = \frac{1}{8}$. For small ratios T/B all the curves are sufficiently close to the lower approximation for the divergence to be disregarded.

7. CONCLUSION

The method is directly applicable to any section, having an axis of symmetry, which can be built up from rectangular sections, in particular T and channel sections. Good upper approximations would be obtained provided that suitable warping functions were assumed on the lines indicated in this paper.

REFERENCES

HILL, R.	1950a	*Mathematical Theory of Plasticity* (Clarendon Press, Oxford).
	1950b	*J. Appl. Mech.* **17**, 64.
HILL, R. and SIEBEL, M. P. L.	1951	*Phil. Mag.* **42**, 722.
	1953	*J. Mech. Phys. Solids* **1**, 207.
STEELE, M. C.	1955	*J. Mech. Phys. Solids* **3**, 156.

Journal of the Mechanics and Physics of Solids, 1957, Vol. 6, pp. 27 to 34. Pergamon Press Ltd., London

CREEP STABILITY OF COLUMNS AND PLATES

By G. N. Rabotnov and S. A. Shesterikov
Moscow University

(*Received 11th April, 1957*)

Summary

A problem of creep stability of columns and plates is considered. In an analysis use is made of two forms of the creep theory based on the strain hardening hypothesis. For a uniformly compressed plate a comparison is made between the results according to the flow theory and strain theory.

Introduction

Recently the problem of creep stability of columns and thin-walled structural parts has drawn the attention of many investigators. However, in all the publications of which we are aware (Hoff 1954, 1956, Rozenblyum 1954) the subject of the analysis is the buckling of columns which are slightly curved in their natural state rather than the problem of stability in a direct sense. Most of these papers are based on the creep equations in which time is introduced explicitly. Such a description of the process cannot be recognized as accurate in principle; the application of this procedure is justified only by the simplicity of the calculations and by the possibility of a good approximation to creep curves used in the analysis.

In investigating the stability of columns and plates we shall proceed from a creep theory based on the strain hardening hypothesis (Rabotnov 1956). In this case the treatment of the stability problem in a direct sense is proved possible. If at a certain moment a deviation from straightness or plane form is given to the compressed column or plate under creep, the deflection will increase or decrease during a subsequent short interval of time. According to whether the deflection increases or decreases, the initial state is considered unstable or stable.

A quasi-static treatment of stability of motion under creep gives rise to certain difficulties, and therefore only in the case of a column is a dynamic treatment of the problem accepted. The result of this analysis makes possible a simplified method to be used further for plates.

1. Stability of a Compressed Column

According to the strain hardening theory, which will be accepted as a basic physical hypothesis, creep is described by an equation containing stress, plastic strain and plastic strain rate:

$$\Phi(\sigma, \rho, \dot{\rho}) = 0, \qquad \text{where} \qquad \rho = \epsilon - \frac{\sigma}{E}. \tag{1.1}$$

It is assumed that equation (1.1) has been integrated for the axial compression in question when σ is constant over the section and either the compressive load or strain is given as a function of time. It will also be assumed that the compressed column bends, deflection being sufficiently small. Stress, total strain, and plastic strain will receive small increments $\delta\sigma$, $\delta\epsilon$ and $\delta\rho$. For these increments one obtains from (1.1)

$$\lambda\delta\sigma + \mu\delta\rho + \nu\delta\dot{\rho} = 0. \tag{1.2}$$

Here

$$\lambda = \frac{\partial\Phi}{\partial\sigma}, \qquad \mu = \frac{\partial\Phi}{\partial\rho}, \qquad \nu = \frac{\partial\Phi}{\partial\dot{\rho}}.$$

Equation (1.2) can be written in the form

$$(E\lambda - \mu)\,\delta\sigma - \nu\delta\dot{\sigma} + E\,(\mu\delta\epsilon + \nu\delta\dot{\epsilon}) = 0. \tag{1.3}$$

The sections remaining plane, a relationship is obtained :

$$\delta\epsilon = \kappa z.$$

Therefore, from (1.3), the connexion between the bending moment m and curvature κ follows :

$$(E\lambda - \mu)\,m - \nu\dot{m} + EJ\,(\mu\kappa + \nu\dot{\kappa}) = 0. \tag{1.4}$$

It is assumed that a deviation from straightness, or an impulse, is given to a column. The equation of vibrations under condition (1.4) is

$$\left[-(E\lambda - \mu) + \nu\frac{\partial}{\partial t}\right]\left[P\frac{\partial^2 y}{\partial x^2} + \gamma F\frac{\partial^2 y}{\partial t^2}\right] + \\ + \frac{\partial^2}{\partial x^2}\left[EJ\left(\mu\frac{\partial^2 y}{\partial x^2} + \nu\frac{\partial^3 y}{\partial x^2\,\partial t}\right)\right] = 0. \tag{1.5}$$

We can satisfy this equation for a simply supported column having length a by assuming

$$y = \tau(t)\sin\frac{\pi x}{a}.$$

The following equation for $\tau(t)$ is obtained :

$$\dddot{\tau} + \frac{\mu - E\lambda}{\nu}\ddot{\tau} + \frac{\pi^2}{\gamma F}(P_e - P)\,\dot{\tau} + \\ + \frac{\pi^2}{\gamma F\nu}\left[E\lambda P + \mu(P_e - P) - \nu\dot{P}\right]\tau = 0. \tag{1.6}$$

Here P_e is the Euler critical load. As the coefficients of $\ddot{\tau}$ and $\dot{\tau}$ are positive, the function will be decreasing if the following condition is satisfied :

$$\frac{E\lambda P}{P_e - P} + \mu - \nu\frac{\dot{P}}{P_e - P} > 0. \tag{1.7}$$

The rate of load application being small, the last term in the above relationship can be omitted, so that

$$\frac{P}{P_e} = \frac{1}{1 - (E\lambda/\mu)}. \tag{1.8}$$

2. A Simplified Stability Criterion

An analysis of equation (1.5) in a general case is difficult. However, to know whether the column is stable or unstable, use can be made of the fact that if relationship (1.7) becomes an equality a characteristic equation, corresponding to (1.6), has a zero root. It is worth noting that (1.6) is actually an equation with variable coefficients but as the initial definition of stability relates to a sufficiently small interval of time this interval can always be chosen so small that the change of coefficients in (1.6) can be neglected. Now, in order to find the boundary of the range of stability, we search for conditions under which equation (1.5) has a time-independent solution $y = u(x)$. It is easy to see that such a solution exists if condition (1.7) is satisfied. Wishing to remain within the quasi-static treatment of the problem, we could obtain the equation of equilibrium of an axially compressed column on the basis of relationship (1.4). Assuming $y = u(x)\,\tau(t)$, one obtains

$$\frac{EJu''}{u} = \frac{(E\lambda - \mu)\,P\tau - \nu\dot{P}\tau - \nu P\dot{\tau}}{\mu\tau + \nu\dot{\tau}} = -P.$$

Hence the ratio $\dot{\tau}/\tau$ can be determined, the sign of this ratio indicating whether the deflection increases or decreases with time. It is evident that stability criterion (1.7) follows from this.

Consider special forms of the creep law.

(a)
$$\Phi \equiv \dot{\rho}\,\rho^{\alpha} - A\sigma^{n} = 0. \tag{2.1}$$

Equation (1.8) is reduced to

$$\bar{\epsilon} = \frac{\alpha}{n} + \bar{\sigma}\left(1 - \frac{\alpha}{n}\right). \tag{2.2}$$

Here

$$\bar{\sigma} = \frac{\sigma}{\sigma_s}, \qquad \bar{\epsilon} = \frac{E\epsilon}{\sigma_s}.$$

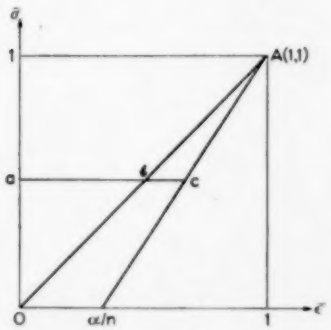

Fig. 1.

Equation (2.2) admits a simple graphic interpretation (Fig. 1). In the plane $\bar{\sigma} - \bar{\epsilon}$ the point A corresponds to elastic instability, the straight line (2.2) passes through this point and intersects the $\bar{\epsilon}$-axis at the point α/n. The elastic strain $\bar{\epsilon}$, corresponding to the stress $\bar{\sigma}$, is represented by the intercept ab. When the creep strain is equal to bc, a loss of stability occurs.

(b) $$\Phi \equiv \dot{\rho}\,\rho^{\alpha} - k \exp(\sigma/A). \tag{2.3}$$

In this case the critical value of the plastic strain is

$$\rho = \frac{A\alpha}{E}\left(\frac{\sigma_s}{\sigma} - 1\right). \tag{2.4}$$

3. Stability of plates

When treating two-dimensional problems we have first to fix a certain initial system of creep equations. The extension of the strain hardening hypothesis to the case of a three-dimensional stress state can be realized by various procedures. Consider the following variations of the theory.

(i) *Flow (or Incremental) Type Equations*

$$\dot{\rho}_{ij} = \tfrac{3}{2}\, g(\rho_i, \sigma_i)\, \sigma_{ij}^{*}. \tag{3.1}$$

Here σ_{ij}^{*} is the stress deviator and ρ_{ij} the plastic strain tensor. It will be assumed that the material is incompressible, and then

$$\rho_{ij} = \epsilon_{ij} - \frac{1}{2G}\sigma_{ij}^{*}.$$

The invariants σ_i and ρ_i are defined as

$$\sigma_i^{2} = \tfrac{3}{2}\,\sigma_{ij}^{*}\,\sigma_{ij}^{*}, \qquad \rho_i = \int_0^t (\tfrac{2}{3}\,\dot{\rho}_{ij}\,\dot{\rho}_{ij})^{\frac{1}{2}}\,d\tau,$$

$$\epsilon_i^{2} = \tfrac{2}{3}\,\epsilon_{ij}\,\epsilon_{ij}$$

(ii) *Strain (or Total) Type Equations*

$$\epsilon_{ij} = \frac{3\epsilon_i}{2\sigma_i}\,\sigma_{ij}^{*}. \tag{3.2}$$

The invariants σ_i and ρ_i satisfy the following differential relationship

$$\Phi(\sigma_i, \rho_i, \dot{\rho}_i) = 0.$$

Here the invariant ρ_i is defined as

$$\rho_i = \epsilon_i - \frac{\sigma_i}{E}.$$

To derive stability equations according to either of these theories it will be assumed that the basic stress state does not change with time. It will also be assumed that Kirchhoff–Love hypothesis holds, namely

$$\delta\epsilon_{11} = -z\,\frac{\partial^2 w}{\partial x^2}, \qquad \delta\epsilon_{22} = -z\,\frac{\partial^2 w}{\partial y^2}, \qquad \delta\epsilon_{12} = -z\,\frac{\partial^2 w}{\partial x\,\partial y}. \tag{3.3}$$

Here w is the deflection of the neutral surface. The additional strain of the neutral surface at the stability limit equals zero.

The moments of internal forces are expressed as

$$G_1 = \int_{-h}^{h} (2\delta\sigma_{11}^{*} + \delta\sigma_{22}^{*})\, z dz, \qquad G_2 = \int_{-h}^{h} (2\delta\sigma_{22}^{*} + \delta\sigma_{11}^{*})\, z dz,$$

$$H = \int_{-h}^{h} \delta\sigma_{12}\, z dz. \tag{3.4}$$

Introduce the following symbols :

$$\alpha_{ij} = \frac{\sigma_{ij}}{\sigma_i}, \qquad \alpha_{ij}^{*} = \frac{\sigma_{ij}^{*}}{\sigma_i}.$$

Further use will be made of a linear operator

$$P = \alpha_{11} \frac{\partial^2}{\partial x^2} + \alpha_{22} \frac{\partial^2}{\partial y^2} + 2\alpha_{12} \frac{\partial^2}{\partial x\, \partial y}.$$

The equilibrium equation of a buckling plate can be written with the aid of this operator in the form

$$\frac{\partial^2 G_1}{\partial x^2} + \frac{\partial^2 G_2}{\partial y^2} + 2 \frac{\partial^2 H}{\partial x\, \partial y} + 2h\sigma_i P(w) = 0. \tag{3.5}$$

4. Stability of Plates According to the Flow Theory

From (3.1) and the definition of the invariant ρ_i, it follows that

$$\dot{\rho}_i = g\sigma_i.$$

Giving small increments to ρ_i and σ_i and integrating the resulting equation, we obtain

$$\delta\rho_i = \int_0^t g\,(b+1)\, e^{a(t-\tau)}\, \delta\sigma_i\, d\tau = gL\, \delta\sigma_i. \tag{4.1}$$

Here

$$a = \sigma_i \frac{\partial g}{\partial \rho_i}, \qquad b = \frac{\sigma_i}{g} \frac{\partial g}{\partial \sigma_i}.$$

Having equation (3.1) rewritten for increments, and taking into account (4·1) and $\sigma_{33} = 0$, we have

$$\tfrac{2}{3}\, \delta\dot{\epsilon}_{ij} = \left(g + \frac{1}{E} \frac{\partial}{\partial t}\right) \delta\sigma_{ij}^{*} + \alpha_{ij}^{*}\, g\,(aL + b)\, \delta\sigma_i. \tag{4.2}$$

In order to eliminate $\delta\sigma_i$ one can multiply (4.2) by α_{ij}^{*} and sum. Then

$$\alpha_{ij}^{*}\, \delta\dot{\epsilon}_{ij} = M\delta\sigma_i. \tag{4.3}$$

Here M is the operator

$$M = g\,(b+1) + \frac{1}{E} \frac{\partial}{\partial t} + agL.$$

Introduce one more operator

$$N = g + \frac{1}{E} \frac{\partial}{\partial t}.$$

Then $\delta\sigma_i$ can be eliminated between equations (4.2) and (4.3) :

$$\delta\sigma_{ij}^{*} = \tfrac{2}{3}\, N^{-1}(\delta\dot{\epsilon}_{ij}) - \alpha_{ij}^{*}\, g\,(aL + b)\,(NM)^{-1}(\alpha_{ij}^{*}\, \delta\dot{\epsilon}_{ij}). \tag{4.4}$$

Substitution of (4.4) into equations (3.4) yields

$$G_1 = \frac{2h^3}{3}\left\{-N^{-1}\,\frac{4}{3}\left(\frac{\partial^2}{\partial x^2}+\frac{1}{2}\,\frac{\partial^2}{\partial y^2}\right)+\alpha_{11}\,g\,(aL+b)\,(MN)^{-1}P\right\}\dot{w} \qquad (4.5)$$

. . . . . .

Substitution of (4.5) into the equation of equilibrium (3.5) gives the following integro-differential equation of stability :

$$M\,(\Delta\Delta\dot{w})-\tfrac{3}{4}\,g\,(b+aL)\,PP\dot{w}-\frac{g\sigma_i}{(2h)^2}\,MNPw=0. \qquad (4.6)$$

Through differentiation the operator h can be eliminated and the following differential equation of stability results :

$$\left[\frac{\partial^2}{\partial t^2}+E\left(bg+g-\frac{a}{E}\right)\frac{\partial}{\partial t}\right]\Delta\Delta w-\tfrac{3}{4}\,gE\left(b\,\frac{\partial}{\partial t}+a\right)PPw-$$

$$-\frac{g\sigma_i}{E\,(2h)^2}\left[\frac{\partial^2}{\partial t^2}+E\left(bg+2g-\frac{a}{E}\right)\frac{\partial}{\partial t}+E^2\,g\left(bg+g-\frac{a}{E}\right)\right]Pw=0. \qquad (4.7)$$

5. Stability of Plates According to the Strain Theory

The relationship between the invariants ϵ_i and σ_i has the same form as relationship (1.1) for a one-dimensional case. Consequently, $\delta\epsilon_i$ and $\delta\sigma_i$ are connected by equation (1.3) or an equivalent relationship :

$$\delta\sigma_i = A\,\delta\epsilon_i. \qquad (5.1)$$

Here A designates a certain integral operator. Having (3.2) rewritten for increments $\delta\epsilon_{ij}$ and $\delta\sigma_{ij}{}^*$ in the case of a plane stress state, and using (5.1), we have

$$\delta\sigma_{ij}{}^* = \alpha_{ij}{}^*\left(A-\frac{\sigma_i}{\epsilon_i}\right)\delta\epsilon_i+\tfrac{2}{3}\,\delta\epsilon_{ij}.$$

Substitution of these expressions in (3.4) yields

$$G_1 = \frac{2h^3}{3}\left\{\frac{4}{3}\,\frac{\sigma_i}{\epsilon_i}\left(\frac{\partial^2}{\partial x^2}+\frac{1}{2}\,\frac{\partial^2}{\partial y^2}\right)+\alpha_{11}\left(A-\frac{\sigma_i}{\epsilon_i}\right)P\right\}w$$

. . . . . .

The equation of stability is obtained as

$$\tfrac{3}{4}\left(A-\frac{\sigma_i}{\epsilon_i}\right)PPw+\frac{\sigma_i}{\epsilon_i}\,\Delta\Delta w+\frac{g\sigma_i}{(2h)^2}\,Pw=0. \qquad (5.2)$$

6. Uniformly Compressed Plate

We will investigate here this simplest problem, having in mind comparison of analyses according to both theories. The power creep law of equation (2.1) is assumed. It is also assumed that

$$\sigma_{11}=\sigma_{22}=-q=-\sigma_i,\quad \sigma_{12}=0,\qquad P=-\Delta.$$

For an elastic plate the equation for deflection $u(x, y)$ follows both from (4.7) and from (5.2):

$$\Delta\Delta u + \frac{gq}{E(2h)^2}\Delta u = 0. \tag{6.1}$$

For $q = q_*$ a solution different from zero exists which satisfies the boundary conditions.

Flow theory. It is assumed that $w = u\tau(t)$. From (4.7) an equation for τ is obtained:

$$\left(1 - \frac{q}{q_*}\right)\ddot{\tau} + E\left[\left(bg + g - \frac{a}{E}\right)\left(1 - \frac{q}{q_*}\right) - g\frac{q}{q_*} - \tfrac{3}{4}bg\right]\dot{\tau} +$$
$$+ E\left[-\tfrac{3}{4}ag\left(1 - \tfrac{4}{3}\frac{q}{q_*}\right) - g^2E(b+1)\frac{q}{q_*}\right]\tau = 0.$$

The signs of the coefficients of $\dot{\tau}$ and τ are decisive for determining stability conditions. For a further analysis use will be made of a particular form of the creep law of equation (2.1). Then

$$g = A\sigma_i^{n-1}\rho_i^{-\alpha}, \qquad a = -\frac{\alpha\sigma_i g}{\rho_i}, \qquad b = n - 1.$$

Introduction of non-dimensional quantities gives

$$(1 - \bar{\sigma})\ddot{\tau} + Eg\left[\left(h + \frac{\bar{\sigma}\alpha}{\bar{\epsilon} - \bar{\sigma}}\right)(1 - \bar{\sigma}) - \bar{\sigma} - \tfrac{3}{4}(n-1)\right]\dot{\tau} +$$
$$+ E^2g^2\left[\tfrac{3}{4}\frac{\bar{\sigma}\alpha}{\bar{\epsilon} - \bar{\sigma}}(1 - \tfrac{4}{3}\bar{\sigma}) - n\bar{\sigma}\right]\tau = 0$$

where

$$\bar{\epsilon} = \frac{E\epsilon_i}{q_*}, \qquad \bar{\sigma} = \frac{q}{q_*}.$$

The boundary of the stability range in the plane $\bar{\sigma} - \bar{\epsilon}$ will be a broken line consisting of the straight line

$$\bar{\epsilon} = \bar{\sigma} + \frac{\alpha}{n}(\tfrac{3}{4} - \bar{\sigma}) \tag{6.2}$$

intersecting the $\bar{\epsilon}$-axis at the point $(\frac{3}{4})(\alpha/n)$, the bisector of the co-ordinate angle at the point $\bar{\epsilon} = \bar{\sigma} = \frac{3}{4}$, and of the intercept on this bisector from the point $(\frac{3}{4}, \frac{3}{4})$ to the point (1, 1).

Strain theory. Separating the variables in equation (5.2) in a similar way one obtains

$$A\tau = \left(\tfrac{4}{3}\frac{E\sigma_i}{q_*} - \tfrac{1}{3}\frac{\sigma_i}{\epsilon_i}\right)\tau.$$

This relationship indicates that τ and $\left(\frac{4}{3}\frac{E\sigma_i}{q_*} - \frac{1}{3}\frac{\sigma_i}{\epsilon_i}\right)\tau$ are connected by the same differential equation as (1.3) in which they substitute for $\delta\epsilon$ and $\delta\sigma$, respectively. Consequently, a differential equation of the first order is obtained for τ. The derivative $\dot{\tau}$ becomes equal to zero under the condition

$$\bar{\epsilon}^2 - \bar{\epsilon}\left[\left(1 - \frac{\alpha}{n}\right)\bar{\sigma} + \frac{1 + 3\,\alpha/n}{4}\right] + \frac{1 - \alpha/n}{4}\,\bar{\sigma} = 0. \qquad (6.3)$$

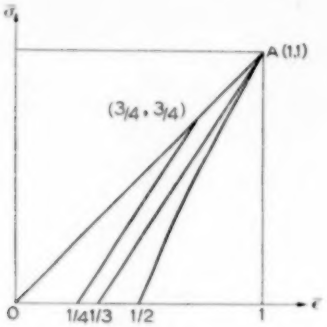

Fig. 2.

The ranges of stability according to equations (6.2) and (6.3) in the case of $\alpha/n = \frac{1}{3}$ are shown in Fig. 2, where the straight line (2.2) pertaining to the compressed column is also drawn.

REFERENCES

HOFF, N. J.	1954	*J. R. Aero. Soc.* **55**, 517.
	1956	*Aeronaut. Quart.* **7**, 1.
RABOTNOV, G. N.	1956	*Proc. 9th. Int. Congr. Appl. Mech.* **2**, 172.
ROZENBLYUM, V. I.	1954	*Inzh. sborn.* **18**, 99-104.

Journal of the Mechanics and Physics of Solids, 1957, Vol. 6, pp. 35 to 46. Pergamon Press Ltd., London.

ROLL-SEPARATING FORCE AND MINIMUM THICKNESS OF COLD-ROLLED STRIPS

By K. Tong* and G. Sachs†
Syracuse University, N.Y.

(*Received 3rd June*, 1957)

Summary

This paper describes a theory for the prediction of roll-separating forces in cold rolling of strips. The theory is based on the concept that the process of plastic deformation in rolling may be approximated by that of plane-strain compression between parallel plates. Computed results based on this theory agree well with published experimental data on cold rolling of copper strips. A method for determining the coefficient of friction and the flow stress of materials for use in this theory is included. Also included is an analysis of the limiting conditions in cold rolling.

1. Introduction

During recent years the forming of extended thin sections by rolling and forging has assumed great practical importance. The major problem encountered in the rolling and forging of such thin sections is the rapid increase in the pressure required for the operation due to the build-up of the frictional surface forces, if the ratio of section thickness to contact length between the tool and the work decreases to small values. A limit is eventually reached where further increase in pressure exerted by the tool merely increases the elastic deformation of the equipment without achieving further reduction in the thickness of the section.

This problem has been theoretically analysed for the process of cold-rolling thin strip, where it has been found that the most important contributing factor is the flattening of the rolls which occurs when the roll-separating force assumes high values (SKF 1930, Hitchcock 1935, Bland 1950). Several attempts have been made to determine the combinations of the rolling variables which lead to excessive flattening of the rolls and, therefore, to a limit in strip thickness that may be cold rolled to a given reduction (Keller 1937, Stone 1953, Hill and Longman 1952). This paper presents an additional contribution to this problem by correlating and evaluating some of the findings reported in these papers, and by devising methods for computing the roll-separating force and the minimum thickness in cold rolling.

Computation of the roll-separating force may be based on the original theory of von Karman (1925) of rolling in conjunction with Hitchcock's (1935) formula for roll distortion. The basic assumption of Karman's theory is that the metal is uniformly compressed in passing between the rolls. Although this theory was found to be adequate, the computation involved is a tedious affair (Orowan

*Department of Mechanical Engineering, Syracuse University.
†Syracuse University Research Institute.

1943, Hill 1950). Subsequent approximations made by Nadai (1939) and by Bland and Ford (1948) simplify the computation somewhat.

Recently, in studying the conditions which limit the use of a given mill to the rolling of thicknesses above a certain value, Keller, Stone, and Hill and Longman proposed that the calculation of roll-separating force may be based on simple concept of plane-strain compression of a strip between parallel dies (Siebel 1923). Keller, and later Stone, considered only the case of vanishingly small (zero) reductions where the concept of plane-strain compression is immediately applicable. Hill and Longman extended the analysis to the case of finite reductions by taking the average thickness of the metal between the tool gap as the equivalent strip thickness. In view of the simplification in the analysis resulting from this concept, and in view of the ever present uncertainties in the values of such physical constants as the coefficient of friction and the flow stress of material which have to be assumed in any analysis of the problem, it is felt that the approximation proposed by Hill and Longman may be used, without undue loss in accuracy, to compute the roll-separating force associated with rolling conditions other than that of the minimum thickness. From theoretical considerations it is estimated (Hill and Longman 1952) that this approximation gives the roll separating force to be within 5 per cent of von Karman's original theory at reductions up to 50 per cent. At greater reductions the increase in error is somewhat offset by the effect of sticking friction, the existence of which is generally neglected. The adequacy of this approximation, however, has not been verified experimentally to date for lack of sufficiently extensive test data.

Recently, Cook and Parker (1953) published measurements of roll-separating force for rolling copper under a wide range of rolling conditions. From these measurements which are illustrated in Fig. 1, they proposed a semi-empirical method of computation which does not utilize the consideration of roll flattening.

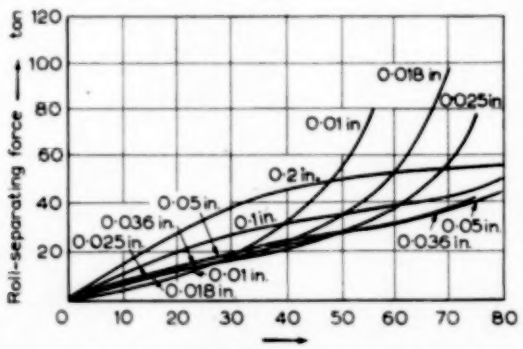

Fig. 1. Roll-separating force in rolling annealed copper strips on 8½ × 10 in. mill (Cook and Parker 1953). Strip width = 3 in. Strip thickness as indicated for each curve.

Since the analysis of Hill and Longman is more direct and easier to apply, an attempt is hereby made to ascertain if the results of this analysis agree with the test data. In order to do so a computation procedure was devised to carry out the analysis numerically. A more convenient method than that used by these authors for obtaining the values of the limiting thicknesses in cold rolling is also included.

2. Hill–Longman Theory of Roll-Separating Force

In plane-strain compression of a strip between two parallel dies, Siebel's formula gives the force required as follows :

$$P = \frac{kh}{f}\{\exp(fL/h) - 1\}$$

where

P = compressive force per unit width of strip
h = instantaneous thickness of the strip
f = coefficient of Coulomb friction
k = flow stress of the material in plane strain
L = contact length between strip and dies.

This formula is obtained by integrating the pressure distribution shown in Fig. 2. To adapt this formula to the determination of roll-separating force, these quantities have to be reinterpreted to represent the appropriate variables in strip rolling as follows (see Fig. 3) :

P = roll-separating force per unit strip width
$h = H(1 - r/2)$ = mean strip thickness
H = thickness of the strip at entry
r = reduction
k = average flow stress of the material under rolling conditions
f = average coefficient of friction under rolling conditions
L = contact length between strip and the rolls which are deformed by the roll-separating force
R = radius of the undeformed roll
$\theta = L/R$ = roll contact angle.

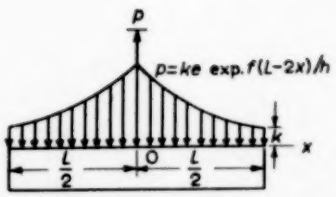

Fig. 2. Normal pressure distribution p in compression of strip with Coulomb friction.

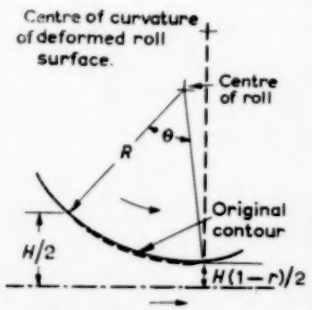

Fig. 3. Roll deformation according to Hitchcock.

Formula (1) now reads

$$P = \frac{k}{f}(1 - r/2)\,H\left[\exp\left\{\frac{fL}{(1 - r/2)\,H}\right\} - 1\right]. \qquad (2)$$

The contact length L is also related to P through Hitchcock's formula

$$P = c\,(L^2/R - rH)$$

where R is the radius of the undeformed roll and c is a rigidity constant of the roll given by

$$c = \frac{\pi E}{16\,(1 - \nu^2)}$$

with E and ν being the Young's modulus and Poisson's ratio of the roll material respectively. This formula is derived by replacing the actual pressure distribution at the roll surface with an elliptical (Hertz) pressure distribution.* The result is that at the contact the roll surface simply deforms into a cylindrical surface having a larger radius of curvature than the original.

Thus, for a given set of rolling conditions, P can be computed by eliminating L from (2) and (3). Because of the transcendental nature of the equations, this elimination process cannot be carried out explicitly. The following numerical procedure was therefore devised.

3. Computation Procedure for Roll-Separating Force

The equations (2) and (3) can be rewritten as

$$\frac{P}{H} = \frac{k\,(2 - r)}{2f}\left\{\exp\left(\frac{f\theta}{2r} - \frac{2R}{H}\right) - 1\right\}, \qquad (\theta = L/R) \tag{4}$$

$$\frac{P}{H} = \frac{c}{2}\left(\frac{2R}{H}\,\theta^2 - 2r\right). \tag{5}$$

Equating (4) and (5) yields

$$\theta^2 = \frac{k}{c}\frac{H}{2R} \cdot \frac{(2 - r)}{f} \cdot \left\{\exp\left(\frac{f\theta}{2 - r} \cdot \frac{2R}{H}\right) - 1\right\} + \frac{rH}{R}. \tag{6}$$

This is a non-dimensional equation with the parameters θ, $2Rf/H\,(2 - r)$, k/c and rH/R. For a given set of rolling conditions the contact angle θ can be computed by an iteration procedure. First, the values of all other parameters are computed. A tentative value of θ somewhat higher than the value for $\sqrt{(rH/R)}$ is then put into the right side of (6). The resulting value of θ, according to (6), if different from the initial assumed value, can be used as the assumed value for the next trial. This iteration process was found to converge to the solution of (6). The following tabulated form is found to be convenient :

θ^2	θ	$\frac{Bf}{2 - r} \cdot \frac{2R}{H}$	$e^C - 1$	$D\frac{k}{c} \Big/ \left(\frac{f}{2-r} \cdot \frac{2R}{H}\right)$	$E + \frac{rH}{R}$	*Error*
A	*B*	*C*	*D*	*E*	*F*	*F* − *A*

The iteration process is completed when the error is negligible. With some practice the solution yielding the value of θ for a particular set of rolling conditions can be obtained after a few trials. A set of such solutions is presented in Fig. 4, illustrating the dependence of θ upon reduction, r, and roll-diameter ratio, $2R/H$.

*The exact error introduced by assuming different pressure distributions on the roll and on the strip is not known. Bland has shown, however, that Hitchcock's approximation cannot be bettered by any useful or practical way.

With the value of θ known the roll-separating force, P, can now be obtained either from (4) or from (5). The left sides of both equations are the ratio of roll-separating force to cross-sectional area of the strip, P/H, which is a convenient quantity for evaluating rolling data. The set of P/H values, corresponding to the θ values in Fig. 4 is represented in Fig. 5.

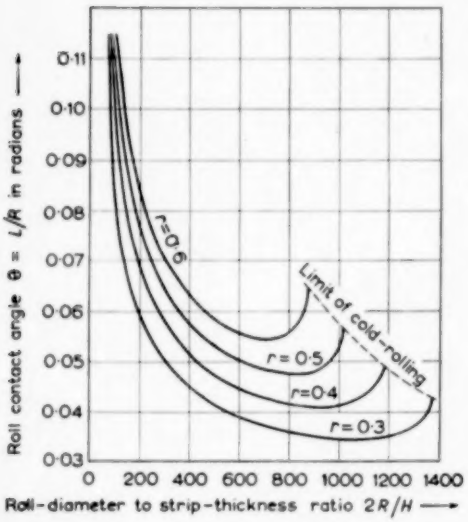

Fig. 4. Variation of roll-strip contact with strip thickness and reduction.
$K = 25$ ton/in^2. $f = 0{\cdot}07$.
$c = 3250$ ton/in^2 (steel rolls).

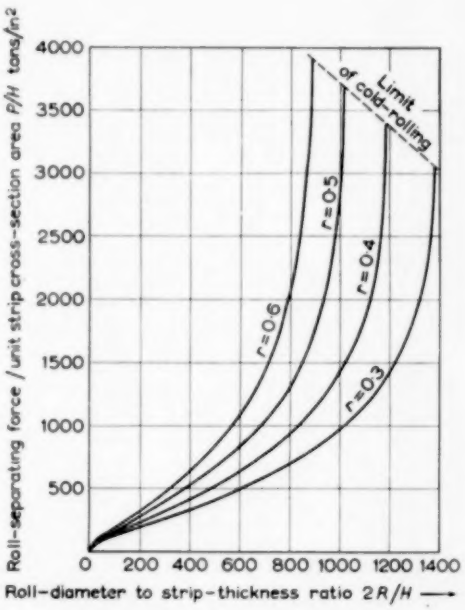

Fig. 5. Roll-separating force in cold-rolling strips of different thickness to different reductions.
$K = 25$ ton/in^2. $f = 0{\cdot}07$.
$c = 3250$ ton/in^2 (steel rolls).

4. Determination of Flow Stress k and Friction Coefficient f

In (1) k and f are the flow stress of the material and the coefficient of friction respectively, and they are assumed to be constant. In an actual rolling process, however, these quantities vary with the rolling conditions. An empirical approach therefore, requires that these constants be determined from actual measurements taken in the process. The 'constants' so determined can be interpreted as the apparent strength factor and the apparent friction factor of the material which will make an elementary theory of rolling applicable.

It is tentatively assumed that for a given mill, rolling a given material at a given speed, the values of k and f are determined by the reduction only. Thus these values can be experimentally determined from load (roll-separating force) measurements in rolling strips of different thicknesses by the same reduction. Let the two loads be $(P/H)_1$ corresponding to $(2R/H)_1$, and $(P/H)_2$ to $(2R/H)_2$. The corresponding θ_1 and θ_2 can be computed from (5). Substituting these values into (4) and eliminating k one obtains

$$\frac{(P/H)_1}{(P/H)_2} = \frac{\exp\left(\frac{f\theta_1}{2-r}\cdot\left(\frac{2R}{H}\right)_1\right)-1}{\exp\left(\frac{f\theta_2}{2-r}\cdot\left(\frac{2R}{H}\right)_2\right)-1}. \qquad (7)$$

From (7) the value for f can be found and, with f known, k can be found from (4).

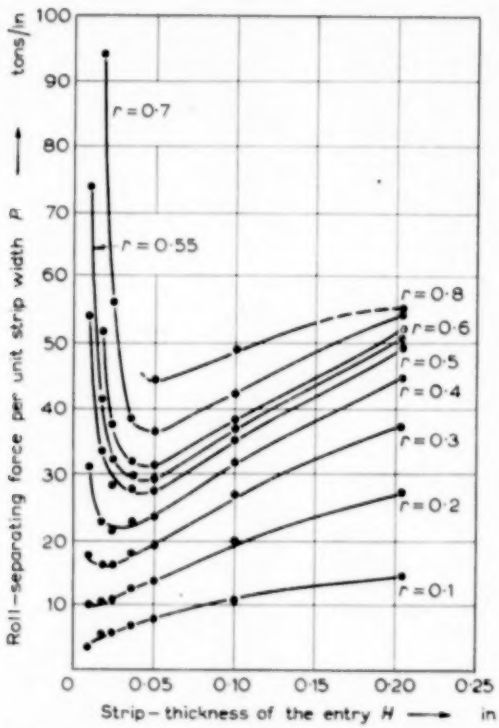

Fig. 6. Variation of roll-separating force with entering strip-thickness in cold-rolling of H.C. Copper (Data by Cook and Parker). Roll diameter = 8¼ in. Roll material = Steel. Rolling speed = 70-80 ft/min.

3. Analysis of the Data by Cook and Parker

Table 1 gives the values of P/H in tons (short) per square inch calculated directly from the measurements by Cook and Parker (Fig. 1). The measurements were taken in rolling high conductivity copper strip 3 in. in width of thicknesses ranging from 0·01 in. to 0·2 in. The mill used was of the two-high type with (steel) rolls having 8¼ in. diam. The rolling speed was constant at about 70-80 ft/min, and standard mineral rolling oil was used as lubricant. The graphical representation of the data originally given is shown in Fig. 1. A more lucid representation is obtained by plotting P vs. H for different reductions (Fig. 6). This graph clearly indicates that the roll-separating force for a given reduction and a given roll diameter first decreases slowly with decreasing thickness until a minimum is reached at a certain thickness ; with further decreasing thickness the force increases

sharply. The same data were replotted with the force per unit strip cross-section area, P/H, and roll-diameter ratio, $2R/H$, as the variables (Fig. 7). The general shape of these curves evidently resembles those in Fig. 5.

TABLE 1. *Roll separation force per unit cross-section area of strip* (P/H)
P/H ton/in^2

$2R/H = r$	40·5	82·5	165	230	344	470	860
0·10	23·4	35·1	52·2	*61·1*	76·1	98·0	*128*
0·20	44·0	66·0	90·2	*115·0*	149·	196	*341*
0·30	60·7	89·5	127	*163*	222	305	*613*
0·40	73·1	106	156	*211*	297	435	*1060*
0·50	80·4	117	181	*255*	390	637	*1884*
0·55	83·0	123	195	*274*	448	788	*2564*
0·60	85·5	128	208	295	520	989	
0·70	89·0	141	*243*	349	783	*1790*	

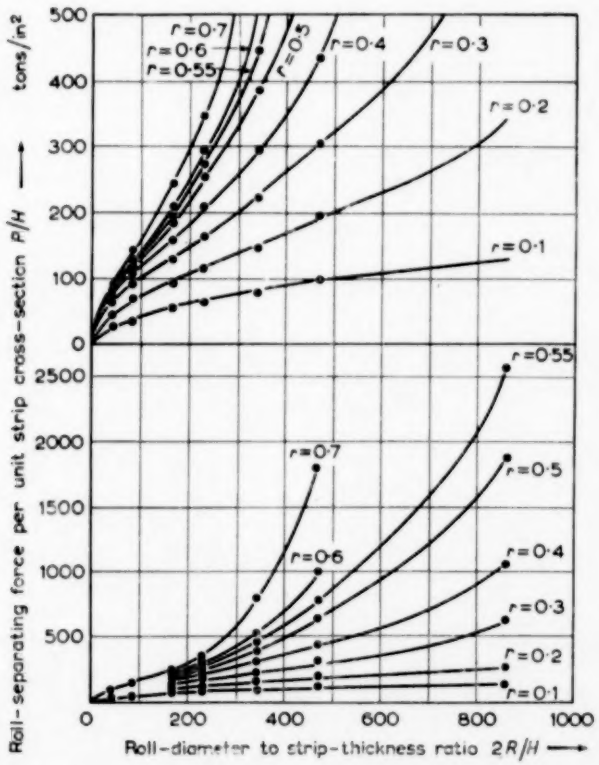

Fig. 7. Roll separating force per unit cross-section versus roll-diameter to strip-thickness in cold-rolling of H.C. copper to different reductions. (Data by COOK and PARKER).

To check the validity of the HILL–LONGMAN analysis, the values of k and f were computed for different reduction ratios by the procedure outlined above. Two values of roll-separating force (*italicized* in Table 1), one of them for the

thinnest strip, were used for this computation. The results are given in Table 2 and Fig. 8.

Based on the values of k and f in Table 2 the P/H vs. $2R/H$ curves were then calculated for reductions of 0·3, 0·4, 0·5 and 0·6. These curves are shown in Fig. 9, with the data by Cook and Parker plotted for comparison. It can be seen that the agreement between the analysis and experiment is very good.

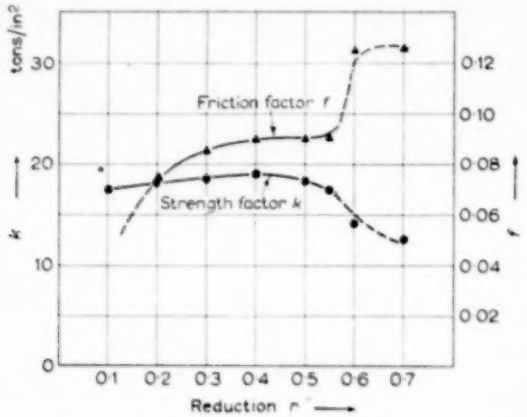

Fig. 8. Variation of f and k in cold-rolling of copper to different reductions. 8¼ in. steel roll. Rolling speed : 70-80 ft/min. ▲ Friction factor f. ● Strength factor k.

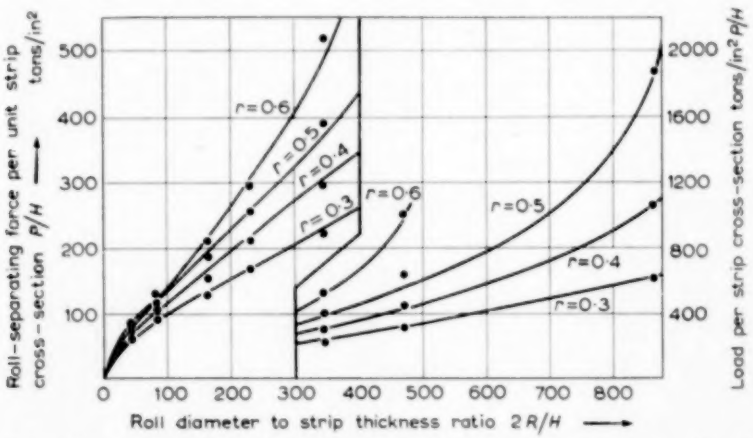

Fig. 9. Comparison of experimental results and calculated values of roll-separating force in cold-rolling of copper strips.
● Data by Cook and Parker (1953). —— Curves from calculated values.
(See Fig. 8 for k and f used).

The trends in the variation of the values of k and f with reduction apparent from Fig. 8 are as follows. There is the general trend for f to increase rapidly at first with reduction, then to maintain a relatively constant value, and to increase again to a certain value at high reduction. The sudden jump in the value of f between $r = 0{\cdot}55$ and $r = 0{\cdot}6$ is perhaps fictitious because there is a shift of the

reference measurements used in the computation (see the *italicized* items in Table 1). The value of k in the meantime shows a slight increase until a maximum value is reached. Thereafter, it decreases with increasing reduction perhaps

TABLE 2. *Values of f and k for different reductions*

r	k (ton/in^2)	f
0·1	17·5	*
0·2	18·0	0·075
0·3	18·5	0·085
0·4	19·0	0·09
0·5	18·5	0·09
0·55	17·5	0·09
0·6	14·0	0·125
0·7	12·5	0·125

because of the annealing effect due to the heat developed in rolling. The order of magnitude of the values of f given in Table 2 is in agreement with the measurement of NEKERVIS and EVANS (1948) for rolling steel at about the same speed. The values of k in Table 2 are perhaps slightly lower than those generally accepted.

6. ROLLING OF THICK STRIPS

The calculations presented above show that the tentative assumptions that k and f can be considered constant for a given reduction r offers a simple method of predicting roll-separating force. The largest difference between the experiments and the theory occurs at the lowest $2R/H$, amounting to 10–15 per cent. This difference quickly disappears as $2R/H$ increases beyond 100. The reason for this initial disparity is twofold. In the first place, the assumption of uniform compression of the strip is less satisfactory when the thickness of the strip is large. The usual limiting value of $2R/H$ for the validity of elementary rolling theories is of the order of 100-200 (HILL and LONGMAN). In the second place, it is possible that f decreases with decreasing $2R/H$ accompanied by a corresponding increase in k. Furthermore for small values of $2R/H$ the effect of f can be neglected. Thus, for the range of $2R/H < 200$, the following alternative analysis can be used.

In the range of small $2R/H$ the deformation of the rolls becomes negligible, and the geometry of rolling demands

$$\theta = (rH/R)^{\frac{1}{2}} \tag{8}$$

with a small error, of the order of $(L/R)^2$. For sufficiently small $2R/H$ and f the exponent in (2) is much less than unity, or

$$\frac{P}{H} = \frac{k}{f} \cdot \frac{(2-r)}{2} \cdot \frac{2fL}{(2-r)H} = \frac{kL}{H} = k\sqrt{(rR/H)}. \tag{9}$$

Fig. 10 shows the plot of P/H vs. $\sqrt{(R/H)}$ for different reductions in the range

*The data did not cover wide enough range for accurate computation of f. The value is, however, found to be below 0·05.

of $2R/H$ less than 200. For moderate reductions the curves are essentially straight lines at the lower end. From the slopes of these lines the values for k can also be determined. They are found to be 15-25 per cent higher than those determined previously, and are probably closer to the true values of the flow stress of the material, although their use in fitting the data to the Hill–Longman analysis for thinner strips will entail a lowering of f values from those chosen previously by amounts varying with $2R/H$. From a practical point of view this is not convenient.

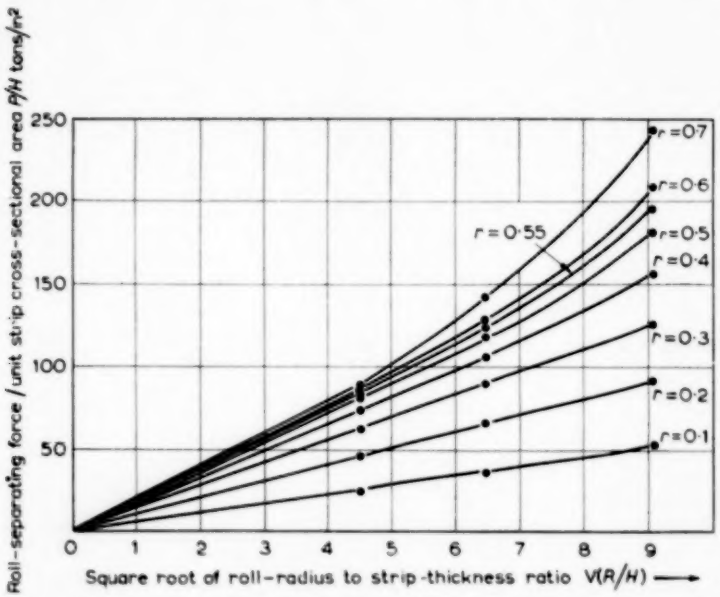

Fig. 10. Roll-separating force in cold-rolling thick copper strips.
Roll diameter $2R = 8{\cdot}25$ in. Roll material: Steel. Strip material: H. C. Copper
Data by Cook and Parker (1955)

7. Rolling of Thin Strips – Conditions of Minimum Thickness

From Figs. 4 and 5 it is seen that if $2R/H$ becomes large the values of θ and P/H increase rapidly, until a certain point is reached at which the slope of the curves becomes vertical. Physically this means, as H decreases further, screwing down the rolls merely produces additional deformation of the rolls without achieving the desired reduction. Mathematically, this condition corresponds to the following relation:

$$\frac{d}{d\theta}\left(\frac{2R}{H}\right) = 0. \tag{10}$$

To obtain the limiting condition which produces the above relation, (6) is rewritten as

$$\frac{2R}{H}(\theta^2 - 2r) = \frac{k}{c}\frac{(2-r)}{f}\left\{\exp\left(\frac{f\theta}{2-r}\cdot\frac{2R}{H}\right) - 1\right\}. \tag{11}$$

Differentiate with respect to θ and utilize (10) to obtain

$$\theta_m = \frac{k}{2c} \exp\left(\frac{f\theta_m}{2-r} \cdot \left(\frac{2R}{H}\right)_m\right)$$

or

$$\left(\frac{2R}{H}\right)_m \theta_m \frac{f}{(2-r)} = \ln\left(\frac{2c}{k}\theta_m\right). \tag{12}$$

where the subscript m stands for the values at minimum thickness condition. Elimination of $(2R/H)_m$ between (12) and (4) yields

$$\tfrac{1}{2}\ln\left(\frac{2c\theta}{k}\right)_m = 1 + \left(\frac{k}{2c\theta}\right)_m \left\{\frac{2rfc}{(2-r)\,k} - 1\right\}. \tag{13}$$

This is a transcendental equation in $(2c\theta/k)_m$, the solution of which for various values of $2rfc/(2-r)\,k$ is given graphically in Fig. 11. For a given set of rolling

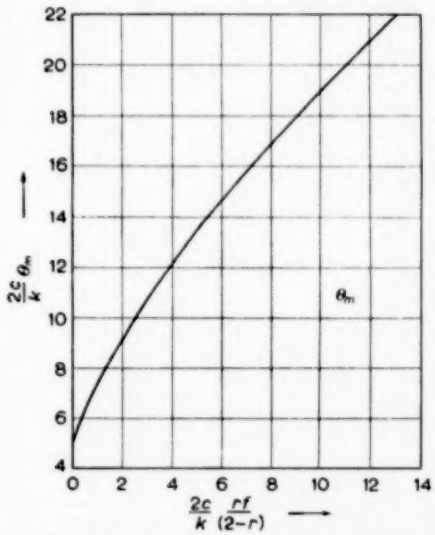

Fig. 11. Roll-contact angle for minimum strip thickness θ_m under various rolling conditions.

$$\frac{2c}{k} \cdot \frac{rf}{2-r} = 1 + \left[\tfrac{1}{2}\ln\left(\frac{2c}{k}\theta_m\right) - 1\right]\frac{2c}{k}\theta_m$$

conditions, the L/R ratio corresponding to the minimum thickness condition can readily be found, and subsequent use of (12) and (5) gives $(2R/H)_m$ and $(P/H)_m$.

An interesting feature of (13) is that it possesses a non-trivial solution for $r = 0$*:

$$\left(\frac{2c\theta}{k}\right)_m = 4{\cdot}92 \qquad \text{for} \qquad r = 0$$

and

$$H = 1{\cdot}56\,fRk/c. \tag{14}$$

Physically, this means that for a given pair of rolls there is an absolute minimum strip thickness given by (14) below which cold rolling is not possible even for very small reduction.

*The trivial solution $2c\theta_m/k = 1$ is not physical. It corresponds to $f = 0$ or $2R/H = 0$.

The above analysis was first made by Hill and Longman. The method of solution given here, however, is much simplified. The special case for vanishingly small reduction was first treated by Keller.

References

Bland, D. R.	1950	*Proc. Inst. Mech. Engrs.* **163**, 141.
Bland, D. R. and Ford, H.	1948	*Proc. Inst. Mech. Engrs.* **159**, 144.
Cook, M. and Parker, R. J.	1953	*J. Inst. Metals* **82**, 129.
Hill, R.	1950	*The Mathematical Theory of Plasticity* (Clarendon Press, Oxford).
Hill, R. and Longman, I. M.	1952	*Sheet Metal Indust.* **28**, 705.
Hitchcock, J. H.	1935	*Roll Neck Bearings, Special Research Communication.* p. 33 (American Society of Mechanical Engineers).
von Karman, T.	1925	*Z. Angew. Math. Mech.* **5**, 139.
Keller, J. D.	1937	*Blast Furnace* **25**, 1110.
Nadai, A.	1939	*J. Appl. Mech.* **6**, 54.
Nekervis, R. J. and Evans, R. M.	1948	*Iron Steel Engr.* **25**, 72.
Orowan, E.	1943	*Proc. Inst. Mech. Engrs.* **159**, 140.
Siebel, E.	1923	*Stahl. u. Eisen, Düsseldorf* **43**, 1295.
SKF	1939	*Cold Rolling Mills with SKF Roller Bearings.*
Stone, M. D.	1953	*Iron Steel Engr.* **30**, 61.

Journal of the Mechanics and Physics of Solids, 1957, Vol. 6, pp. 47 to 52. Pergamon Press Ltd., London

FATIGUE CRACK PROPAGATION IN TORSION*

By J. A. H. Hult
Department of Mechanical Engineering, Massachusetts Institute of Technology†

(*Received 27th June*, 1957)

Summary

The redistribution of stress and strain in front of a growing crack in a twisted bar is derived, assuming the material to be ideally plastic. The result is used in connexion with a simple fracture criterion to determine the initial rate of growth of a fatigue crack. Experiments with torsion members are reported.

1. Introduction

The formation and rate of growth of a crack are concepts of central importance in the fatigue problem. Two difficulties arise when this problem is studied as one in continuum mechanics. First, the stress and strain distribution in the vicinity of the growing crack has to be known. Second, a quantitative fracture criterion is needed that permits application to the case of cyclic loading.

Since a sharp crack acts as an infinite strain raiser, plastic flow occurs at the crack tip, and the crack all the time, penetrates into material that is plastically strained. Hence the methods of elasticity are insufficient in this problem, even though the bar at large might be in an elastic state of stress.

The crack growth is pictured as occurring in steps in the following fashion. First the bar is twisted reversedly, until the fracture criterion is satisfied. Then the crack grows a certain amount, while no further twisting is done. The bar is twisted again, until the fracture criterion is again satisfied, and so on.

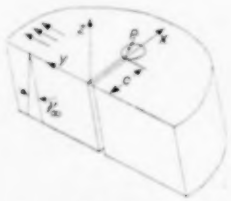

Fig. 1.

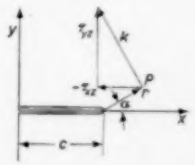

Fig. 2.

2. Stress and Strain Redistribution Due to Growth Under Constant Applied Strain

The state of stress and strain around the tip of a longitudinal crack in a twisted

*This research was supported by the United States Air Force through the Air Force Office of Scientific Research of the Air Research and Development Command under contract No. AF 18 (600)—937.
†Now at Royal Institute of Technology, Stockholm.

bar is equivalent to that around a similar crack in a body subject to pure shear (HULT 1957). Therefore the simpler case of pure shear (Fig. 1) is studied here.

Consider a point P, fixed in the body and located in the plastic region. If, under constant applied strain γ_∞, the crack grows by an amount dc, the shear strain at P changes by an amount $d\gamma$, consisting of an elastic part $d\gamma^e$ and a plastic part $d\gamma^p$.

In component form, then

$$d\gamma_{xz} = d\gamma^e{}_{xz} + d\gamma^p{}_{xz}, \qquad d\gamma_{yz} = d\gamma^e{}_{yz} + d\gamma^p{}_{yz},$$

or

$$\frac{d\gamma^p{}_{xz}}{d\gamma^p{}_{yz}} = \frac{d\gamma_{xz} - d\gamma^e{}_{xz}}{d\gamma_{yz} - d\gamma^e{}_{yz}}. \tag{1}$$

From the Reuss equations of plastic flow (see HILL 1950, p. 39) and Fig. 2,

$$\frac{d\gamma^p{}_{xz}}{d\gamma^p{}_{yz}} = \frac{\tau_{xz}}{\tau_{yz}} = -\tan\alpha. \tag{2}$$

The set of displacements

$$u = 0, \qquad v = \gamma_\infty z, \qquad w = w(x, y)$$

corresponds to the total strain increments

$$\left.\begin{aligned} d\gamma_{xz} &= d\left(\frac{\partial u}{\partial z} + \frac{\partial w}{\partial x}\right) = d\left(\frac{\partial w}{\partial x}\right) \\ d\gamma_{yz} &= d\left(\frac{\partial v}{\partial z} + \frac{\partial w}{\partial y}\right) = d\left(\gamma_\infty + \frac{\partial w}{\partial y}\right) = d\left(\frac{\partial w}{\partial y}\right) \end{aligned}\right\} \tag{3}$$

since γ_∞ is constant.

The elastic strain increments are obtained from Hooke's law

$$d\gamma^e{}_{xz} = \frac{1}{G}\, d\tau_{xz}, \qquad d\gamma^e{}_{yz} = \frac{1}{G}\, d\tau_{yz}. \tag{4}$$

In the plastic region equilibrium requires that the stress vector is perpendicular to the radius vector from the current crack tip. Hence, from Fig. 3, with k denoting the yield stress in shear,

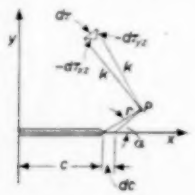

Fig. 3.

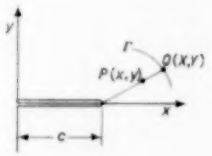

Fig. 4.

$$d\tau_{xz} = -k\,\frac{\sin\alpha\cos\alpha}{r}\,dc, \qquad d\tau_{yz} = -k\,\frac{\sin^2\alpha}{r}\,dc. \tag{5}$$

Insertion of (2)-(5) into (1) yields

$$\cos\alpha\, d\left(\frac{\partial w}{\partial x}\right) + \sin\alpha\, d\left(\frac{\partial w}{\partial y}\right) = -\frac{k}{G}\cdot\frac{\sin\alpha}{r}\cdot dc. \tag{6}$$

Since the polar co-ordinates (r, α) of the point P depend also on the crack length c, they will not be retained in the following analysis. With

$$\sin\alpha = y/r, \qquad \cos\alpha = (x-c)/r, \qquad r = \sqrt{(x-c)^2 + y^2}, \qquad \gamma_s = k/G,$$

(6) takes the form

$$(x-c)\cdot\frac{\partial}{\partial c}\left(\frac{\partial w}{\partial x}\right) + y\cdot\frac{\partial}{\partial c}\left(\frac{\partial w}{\partial y}\right) = -\gamma_s\cdot\frac{y}{\sqrt{(x-c)^2+y^2}}. \tag{7}$$

Here the order of differentiation is immaterial, and hence (7) can be written

$$(x-c)\cdot\frac{\partial}{\partial x}\left(\frac{\partial w}{\partial c}\right) + y\cdot\frac{\partial}{\partial y}\left(\frac{\partial w}{\partial c}\right) = -\gamma_s\cdot\frac{y}{\sqrt{(x-c)^2+y^2}}, \tag{8}$$

which is a partial differential equation for $\partial w/\partial c$.

The characteristics of (8) are straight lines radiating from the crack tip. Integration along QP of Fig. 4 yields

$$\left(\frac{\partial w}{\partial c}\right)_P = \left(\frac{\partial w}{\partial c}\right)_Q + \gamma_s\cdot\frac{y}{\sqrt{(x-c)^2+y^2}}\cdot\ln\frac{X-c}{x-c}. \tag{9}$$

Q being the intersection between the elastic–plastic boundary Γ and the characteristic through P.

If P is located on the x-axis, differentiation with respect to x and y respectively yields

$$\left.\begin{aligned}\left(\frac{\partial\gamma_{xz}}{\partial c}\right)_P &= \left(\frac{\partial\gamma_{xz}}{\partial c}\right)_Q \\ \left(\frac{\partial\gamma_{yz}}{\partial c}\right)_P &= \left(\frac{\partial\gamma_{yz}}{\partial c}\right)_Q + \gamma_s\cdot\frac{1}{x-c}\cdot\ln\frac{X-c}{x-c}\end{aligned}\right\} \tag{10}$$

By symmetry $\gamma_{xz} \equiv 0$ on the x-axis, and hence $\gamma = \gamma_{yz}$ so that (10) becomes

$$\left(\frac{\partial\gamma}{\partial c}\right)_P = \left(\frac{\partial\gamma}{\partial c}\right)_Q + \gamma_s\cdot\frac{1}{r}\cdot\ln\frac{R_0}{r}, \tag{11}$$

where $R_0 = X - c$ is the depth of the plastic region, and $r = x - c$ is the distance between P and the crack tip.

To determine $(\partial\gamma/\partial c)_Q$ the change of the elastic–plastic boundary with crack growth has to be known. In the following analysis of crack growth, however, only that case will be considered when P is located very close to the crack tip. For $r \ll R_0$ the last term in (11) becomes predominant, and hence

$$\left(\frac{\partial\gamma}{\partial c}\right)_P \simeq \gamma_s\cdot\frac{1}{r}\cdot\ln\frac{R_0}{r}. \tag{12}$$

3. Fracture Criterion

Recent experiments on crack propagation in fully plastic cyclic torsion (McClintock 1956) have shown that the direction of crack growth closely coincides with the direction of maximum shear strain. It would be natural, therefore, to use the maximum shear strain as a criterion quantity for crack growth. At the tip of a sharp crack, however,

$$\left.\begin{aligned} \gamma &= \frac{R}{r} \cdot \gamma_s \\ R &= R_0 \cos 2\alpha, \qquad R_0 = c\gamma_\infty^2/\gamma_s^2 \end{aligned}\right\} \tag{13}$$

(HULT 1957), i.e. the maximum shear strain is infinite for any applied strain, however small. A maximum shear strain criterion then would imply that all cracks were unstable.

Whereas the strain is infinite at the crack tip, the average strain in a region at the crack tip is a finite quantity. Within radius $\rho \ll R_0$ from the crack tip the average shear strain in the plastic region is, from (13),

$$\bar{\gamma} = \frac{\int_0^\rho \int_0^{\alpha(r)} \gamma r \, d\alpha \, dr}{\int_0^\rho \int_0^{\alpha(r)} r \, d\alpha \, dr} = \frac{2}{\pi} \cdot \frac{R_0}{\rho} \cdot \gamma_s. \tag{14}$$

Following early ideas by NEUBER (1937) the material will now be imagined to consist of 'blocks', within each of which the stress and strain are constant. The magnitude of stress and strain within a block are taken as the average stress

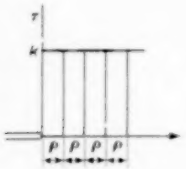

Fig. 5.

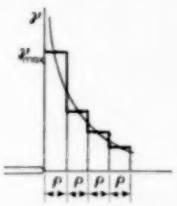

Fig. 6.

and strain within the block volume of the fully continuous material. In the plastic region the stress is then equal to the yield stress k in every block (Fig. 5), whereas the strain is largest in the block that is closest to the crack tip (Fig. 6). From (14), then,

$$\gamma_{max} \simeq \frac{R_0}{\rho} \cdot \gamma_s, \tag{15}$$

where the factor $2/\pi$ has been omitted to indicate the order of magnitude nature of this equation.

It is now assumed that if a block is strained beyond a certain fracture strain γ_f, the block will be destroyed, and the crack will penetrate through the block. However in carrying out the crack growth analysis it will be convenient to think again of the material as being homogeneous. From (13) and (15) it follows that

$$\gamma_{max,\,block} \simeq \gamma(\rho)_{homogeneous},$$

and therefore the fracture criterion can be stated in the following form:

When the shear strain at a distance ρ ahead of the crack tip reaches γ_f, the crack grows the distance ρ.

In this form the fracture criterion is applicable to the case of single loading. In cyclic loading the fracture strain is instead associated with the accumulated plastic strain, so that the fracture criterion reads

$$\Sigma \gamma_a{}^p(\rho) = \gamma_f, \tag{16}$$

where the plastic strain amplitude is

$$\gamma_a{}^p(\rho) \simeq \gamma_a(\rho) = \frac{c\gamma^2{}_{\infty a}}{\rho\gamma_s} \tag{17}$$

(HULT and MCCLINTOCK 1956), $\gamma_{\infty a}$ being the applied strain amplitude.

4. Rate of Crack Growth

Consider a virgin crack of length c_0 in a block subject to cyclic shear straining of constant amplitude $\gamma_{\infty a}$. After n cycles the accumulated plastic strain at P_0 (Fig. 7) is

$$4n \cdot \frac{c_0\,\gamma^2{}_{\infty a}}{\rho\gamma_s}$$

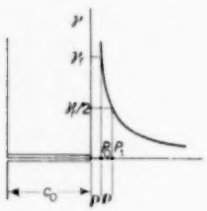

Fig. 7.

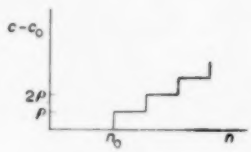

Fig. 8.

and hence the number of cycles required to initiate the crack growth is

$$n_0 = \tfrac{1}{4} \cdot \frac{\rho}{c_0} \cdot \frac{\gamma_s\,\gamma_f}{\gamma^2{}_{\infty a}}. \tag{18}$$

Just before n reaches n_0, the accumulated strain at P_1 (Fig. 7) is

$$4n_0 \cdot \frac{c_0\,\gamma^2{}_{\infty a}}{2\rho \cdot \gamma_s}$$

which, from (18), equals $\gamma_f/2$. The rise in strain at P_1 due to the crack growth is obtained from (12):

$$\Delta\gamma_{P_1} \simeq \left(\frac{\partial\gamma}{\partial c}\right)_{P_1} \cdot \rho \simeq \frac{\gamma_s}{2} \cdot \ln \frac{\gamma_f}{8n_0\,\gamma_s}.$$

Hence the accumulated strain at P_1 after the first step of growth is

$$\frac{\gamma_f}{2} + \frac{\gamma_s}{2} \cdot \ln \frac{\gamma_f}{8n_0\,\gamma_s}.$$

Here the first term is predominant, i.e. the strain at P_1 does not increase noticeably due to the crack growth. To make the crack growth continue, the accumulated strain at P_1 then has to be increased by almost $\gamma_f/2$, which requires $\Delta n = n_0/2$ more cycles. The crack then grows another distance ρ and so on (Fig. 8). The average initial rate of crack growth then is

$$\frac{\Delta c}{\Delta n} \simeq \frac{\rho}{n_0/2} \simeq 8c_0 \frac{\gamma^2{}_{\infty a}}{\gamma_s\,\gamma_f}. \tag{19}$$

If similarity were preserved all during the subsequent growth, so that $\Delta c/\Delta n \sim c$, the crack length would increase exponentially with the number of cycles. It has been shown, however, that for crack growth in fully plastic torsion the growth is accelerated also because the building up of strain ahead of the crack proceeds at an increasing rate (McCLINTOCK 1956). The above results, therefore, should be applicable only to the initial growth.

For two geometrically similar specimens (18) and (19) predict that in the larger one the crack growth will start earlier and proceed at a faster rate. A size effect of this kind is a well-known feature in fatigue testing.

5. EXPERIMENTS

A simple testing machine was designed, allowing torsion fatigue tests to be run at a constant angular amplitude. Sharp narrow longitudinal notches were pre-cut in 75S-T6 aluminium specimens, and a number of identical specimens were then run a different number of cycles. Finally the specimens were sectioned and polished, and in each specimen the crack length was measured. Another series was run, where the initial notch depth was twice as large. The results are shown in Fig. 9, where $c - c_0$ has been plotted versus $n \cdot c_0$. From (18) and (19) it follows that the curves corresponding to two different c_0 should then coincide.

An order of magnitude estimate from these results of the as-yet-undetermined material parameters ρ and γ_f yields

$$\rho \simeq 0{\cdot}01 \text{ in.}, \quad \gamma_f \simeq 10.$$

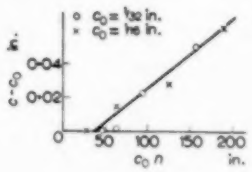

Fig. 9.

ACKNOWLEDGMENTS

The author wishes to acknowledge financial support from the Division of Sponsored Research at the Massachusetts Institute of Technology. This formed part of a dissertation at the Massachusetts Institute of Technology in January, 1957. Many discussions with Professor FRANK A. McCLINTOCK are deeply appreciated.

REFERENCES

HILL, R. 1950 *Mathematical Theory of Plasticity* (Clarendon Press).
HULT, J. A. H. 1957 *J. Mech. Phys. Solids.*
HULT, J. A. H. and McCLINTOCK, F. A. 1956 *Proc. IX Int. Cong. Appl. Mech.* (Brussels).
McCLINTOCK, F. A. 1956 *Int. Conf. on Fatigue of Metals* (London).
NEUBER, H. 1937 *Kerbspannungslehre* (Springer).

Journal of the Mechanics and Physics of Solids, 1957, Vol. 6, pp. 53 to 62. Pergamon Press Ltd., London

THE EFFECT OF IMPACT LOADING ON THE STATIC YIELD STRENGTH OF A MEDIUM-CARBON STEEL

By J. D. Campbell and C. J. Maiden
Department of Engineering Science, University of Oxford

(*Received 27th June*, 1957)

Summary

Experiments are described in which annealed medium-carbon steel specimens were subjected to rapidly-applied compressive loads maintained for times of the order of 10^{-4} sec. The applied stresses were between two and three times the static upper yield stress of the steel, and the permanent deformation varied from 1·2 per cent down to very small amounts.

Static stress–strain curves were obtained by reloading the specimens in compression immediately after impact. It appears that the upper yield stress can be considerably reduced by the application of an impact stress of insufficient magnitude and duration to cause appreciable permanent deformation. This reduction is related to the number of dislocations freed from their carbon atmospheres during the impact loading.

The reduction in the upper yield stress is found to be greatest after an impact causing about 1 per cent permanent strain. Tests at a temperature of − 84°C indicate that the effect of an impact depends mainly on the permanent strain caused, and not directly on the stress or duration of the load.

1. Introduction

Although many experimental investigations have been made of the behaviour of steel under rapid loading, the available information concerning the effect of such treatment on the mechanical properties of the steel is very limited and somewhat contradictory. Warnock and Pope (1947) found that moderate amounts of deformation due to tension impact did not alter the static yield stress appreciably; in general the tensile static stress–strain curves obtained after impact lay below that corresponding to static straining. Harris and White (1954), on the other hand, found that the micro-hardness of dynamically strained steel was greater than that of steel slowly strained an equal amount. Experiments by Campbell and Duby (1956) showed that mild steel specimens strained about 4 per cent in dynamic compression gave static stress–strain curves some 10 per cent lower than those of specimens strained the same amount statically. Duby (1956) also found that the static upper yield stress of mild steel was considerably reduced after the material had been loaded by a stress pulse of insufficient magnitude and duration to cause yielding.

It appears that no systematic investigation has previously been made of the static stress–strain behaviour of steel after it has been subjected to rapidly-applied loads of various magnitudes. In the tests described in the present paper, steel specimens were loaded by compressive stresses of order 10^5 lb/in^2, which were

maintained for about 100 microseconds. In some of these tests the specimen yielded, but in others no appreciable permanent deformation occurred. The specimens were tested statically within a few minutes of the dynamic stressing, in order to eliminate ageing effects. A few tests were also carried out at low temperatures, in order to determine the effect of increasing the magnitude and duration of the impact stress, while maintaining the permanent strain constant.

2. Details of Apparatus

(i) *Dynamic*

The impact apparatus (Fig. 1) used in the investigation was a modified form of that described in previous papers (Campbell 1954, Campbell and Duby 1956). The specimens were $\frac{3}{8}$ in. in diameter and $\frac{1}{2}$ in. in length. The stress, caused by the falling weight, was transmitted through a high-tensile steel weighbar which consisted of three lengths of different diameters. The changes of section were such that the stress propagated into the specimen was 2·10 times as large as that generated at the impact end by the falling weight. This stress magnification was required to obtain yield in the low-temperature tests. The lengths of the rods were such that the wave reflected from the change of section *A*, after travelling up to the impacting plate and back again, reached the specimen upper face after the unloading wave reflected from the free end of the anvil bar. Similarly the wave reflected from section *B*, after travelling up to section *A* and back again, also arrived at the upper specimen face after the unloading wave.

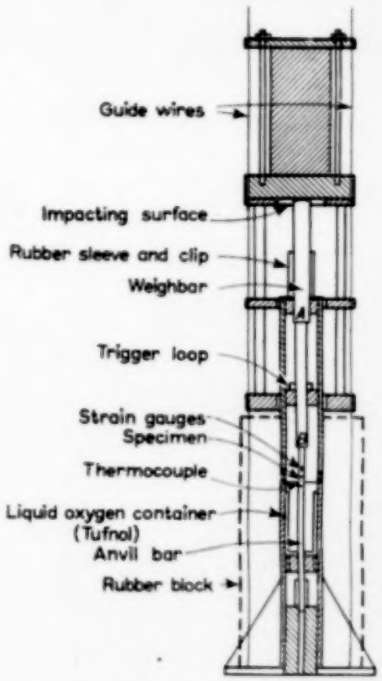

Fig. 1. Mechanical impact machine.

Three resistance strain gauges were mounted on the weighbar, as shown in Fig. 1. These gauges had a gauge length of $\frac{1}{4}$ in. and were centred $\frac{3}{8}$ in. from the upper face of the specimen. The anvil bar and the lowest section of the weighbar were of the same diameter as the specimen; thus no appreciable wave reflections occurred at the specimen faces until yielding was initiated. The amplified output of the gauges was applied to the Y plates of a high-speed cathode-ray oscilloscope. A single-sweep generator provided the horizontal deflection of the spot, and this was switched to full brightness by a pulse applied to the grid of the tube. The beam was interrupted every two microseconds by means of a 500 kc/s oscillation superimposed on the brightening pulse. From a coil surrounding the weighbar a magnetostrictive pulse was obtained; this pulse was fed through a

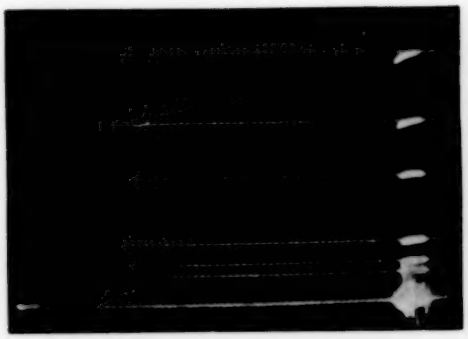

(a)

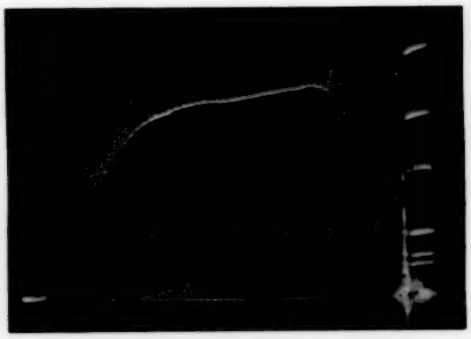

(b)

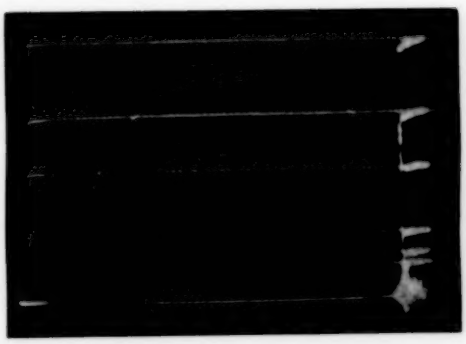

(c)

(d)

Fig 2 Stress-time oscillograms.

separate amplifier and triggered the sweep and brightener circuits. To calibrate the system, large non-inductive resistances were added in parallel to the gauges, thus simulating known strains. The calibration lines thus obtained, and the stress pulses, were recorded photographically.

To lower the specimen temperature a Tufnol container, shown in Fig. 1, was partially filled with liquid oxygen. The specimen was kept at a constant temperature by maintaining a slow feed of liquid oxygen into the container from a constant head reservoir. The temperature was measured by a copper–constantan thermocouple.

(ii) *Static*

The apparatus used for the static compression tests consisted of a lever-type testing machine fitted with a device to reduce eccentricity of loading. The strains were measured by a cylinder gauge reading to 10^{-4} in.

3. Specimens

The steel used was a medium-carbon steel (Park Gate M.2185) and had the following composition :

C	Si	Mn	S	P
0·32%	0·235%	0·62%	0·037%	0·025%

The bar supplied was $2\frac{1}{2}$ in. in diameter and was roughly machined into eight $\frac{1}{2}$ in. diameter rods, which were stress-relieved for one hour at 600°C. After cooling in the furnace, the rods were machined and ground to $\frac{3}{8}$ in. diameter before receiving a final vacuum anneal for thirty minutes at 850°C.

4. Experimental Results

(i) *Effect of impacting at room temperature*

A series of room-temperature impacts was carried out on the test specimens and on a high-tensile steel dummy, with impact velocities ranging from 277 in/sec to 365 in/sec. Static compression tests were performed on the specimens immediately after the impact tests.

Fig. 2 shows typical stress–time oscillograms, each of which has been superimposed, during enlarging, on the relevant recorded calibration lines. Records (a), (b) and (c) were obtained in tests on different annealed specimens ; record (d) was obtained using the high-tensile steel dummy.

Records (a) and (b) refer to tests at an impact velocity of 308 in/sec, in which no appreciable yielding of the specimens occurred. They show that the wave shape is accurately repeatable, the greatest difference between records (a) and (b) being about 2 per cent of the maximum stress. Neither of these records differs by more than this from the elastic wave shape, as recorded in a test on the high-tensile steel dummy at the same velocity of impact.

Records (c) and (d) refer to tests at an impact velocity of 340 in/sec. The difference in the two wave shapes is due to yielding of the specimen in the test which gave record (c).

Using the gauge factor quoted by the manufacturer, the value of Young's modulus obtained in a vibration test on the weighbar steel, and the known values of the gauge resistance and calibrating resistances, the stresses corresponding to the recorded calibration lines were evaluated. For the lines shown in Fig. 2, these stresses are 0, 14, 19, 28, 56, 80 and 112 $\times$ 10^3 lb/in^2. A calibration curve was drawn for each pulse, relating vertical deflection to stress at the gauge position. By means of these calibration curves, the pulses were converted to stress–time

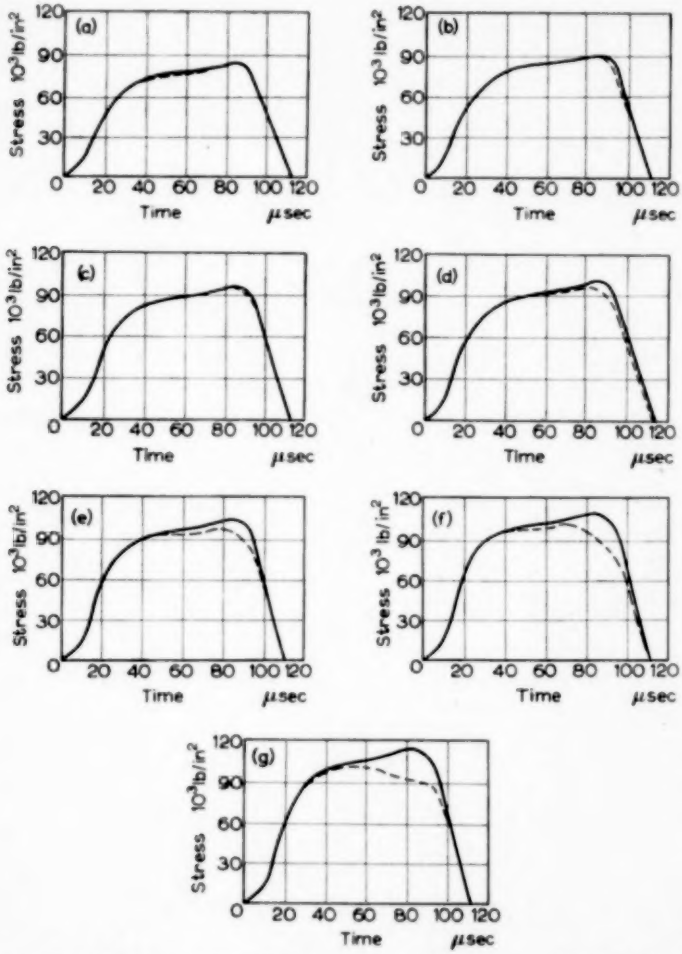

Fig. 3. Elastic and test stress–time curves obtained at various impact velocities.
(a) 277 in/sec ; (b) 293 in/sec ; (c) 308 in/sec ; (d) 326 in/sec ; (e) 340 in/sec ; (f) 352 in/sec ; (g) 365 in/sec.

curves. Fig. 3 shows the stress–time curves obtained at seven different impact velocities. It is to be observed that until an impact velocity of 326 in/sec is reached there is very little difference between the elastic curve and that obtained with a test specimen. It thus appears that no appreciable plastic deformation

occurred in the tests corresponding to impact velocities less than 326 in/sec. This was also indicated by micrometer measurements of the specimen dimensions before and after impact.

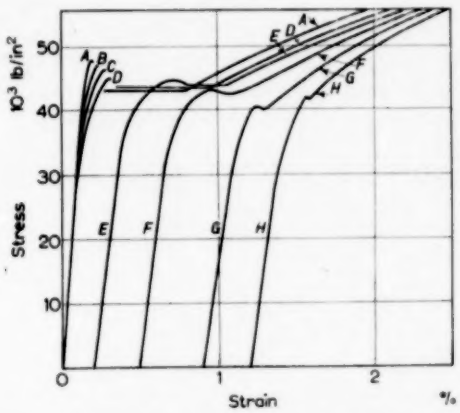

Fig. 4. Static stress–strain curves obtained after dynamic loading.
Curve *A* : annealed specimen (not pulsed). Curves *B*, *C*, *D* : specimens pulsed at 277, 293 and 308 in/sec, respectively. Curves *E*, *F*, *G*, *H* : specimens impacted at 326, 340, 352 and 365 in/sec, respectively.

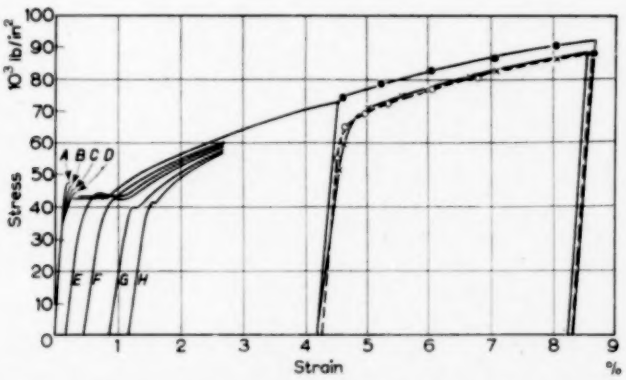

Fig. 5. Static stress–strain curves, showing the softening effect of a previous dynamic test.
●——● Static curve after statically straining 4·2 per cent at 15°C.
×——× Static curve after dynamically straining 4·2 per cent at 15°C (yielded dynamically at 108,000 lb/in^2 after 26 μsec).
○- - -○ Static curve after dynamically straining 4·2 per cent at − 84°C (yielded dynamically at 133,000 lb/in^2 after 47 μsec).

Fig. 4 shows the static stress–strain curves obtained immediately after impacting. The strain co-ordinate represents total (permanent dynamic plus static) strain. It is seen that the static upper yield stress is indeed reduced by pulsing without yielding ; however, the lowest value of the upper yield stress does not occur until the steel has been dynamically strained approximately 1 per cent. It is also to be observed that an upper yield point persists even after considerable dynamic straining has taken place.

(ii) *Effect of impacting at a low temperature*

To investigate the effect of increasing the magnitude and duration of the impact stress, a specimen was impacted twice at a temperature of − 84°C and a velocity of 503 in/sec. The resultant permanent strain was found to be 4·2 per cent, 2·6 per cent from the first impact and 1·6 per cent from the second. By varying the impact velocity, it was found that a specimen impacted at 460 in/sec and room temperature sustained the same permanent strain of 4·2 per cent. Analysis of the strain-gauge records for these tests showed that the stresses applied to the specimen deformed at − 84°C were some 30 per cent higher than those applied to the specimen deformed at room temperature; in addition the total duration of the stress was doubled at the low temperature.

The two specimens were tested statically within a few minutes of the impact tests, and Fig. 5 shows the stress–strain curves obtained. It is seen that there is little difference between the curves for the two impacted steels. These tests were repeated and the static stress–strain curves obtained were in each case found to agree with those shown in Fig. 5 to within 2 per cent.

From the above tests, the conclusion may be drawn that the shape of the static stress–strain curve obtained after impact is dependent mainly on the amount of dynamic deformation, and not on the temperature at which the steel was impacted.

5. DISCUSSION

For the purposes of this paper, yield is defined as that point where the strain rate increases suddenly as the stress rate falls to zero.

According to COTTRELL and BILBY's (1949) theory of yield, the dislocations in annealed ferritic steel are locked by carbon atoms. It has been suggested (CAMPBELL 1953) that yielding occurs when the density of released dislocations reaches a critical value. With certain assumptions, the density of released dislocations at time τ has been shown to be approximately proportional to

$$\int_0^{\tau} \sigma^{\alpha}\, dt, \qquad (1)$$

where σ is the applied stress at time t and α is a constant at any given temperature.

From previous dynamic tests (CAMPBELL and DUBY 1957) on steel of the same composition and heat treatment as that used in the present investigation, it was determined that at room temperature α was approximately thirteen. This value was therefore used in evaluating the integral (1).

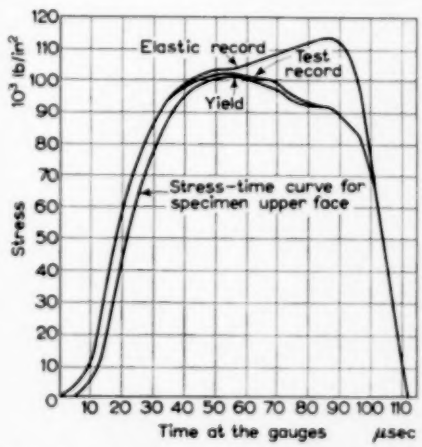

Fig. 6. Elastic record, test record and stress-time curve for the specimen upper face (impact velocity 365 in/sec).

Stress–time curves for the top face of the specimen were derived from thestra in-gauge records in the manner described in an earlier paper (CAMPBELL and DUBY

1956). Fig. 6 shows the gauge records obtained at an impact velocity of 365 in/sec using a high-tensile steel dummy and a steel specimen respectively ; it also shows the derived stress–time curve for the upper face of the specimen. The integral (1) was evaluated graphically up to the maximum of this curve, which was taken as giving the time at which yielding began. Fig. 7 shows the curves of σ^{13} obtained for seven different impact velocities. At the three lowest velocities there was no measurable permanent deformation of the specimen, and the integrals were evaluated for the complete duration of loading.

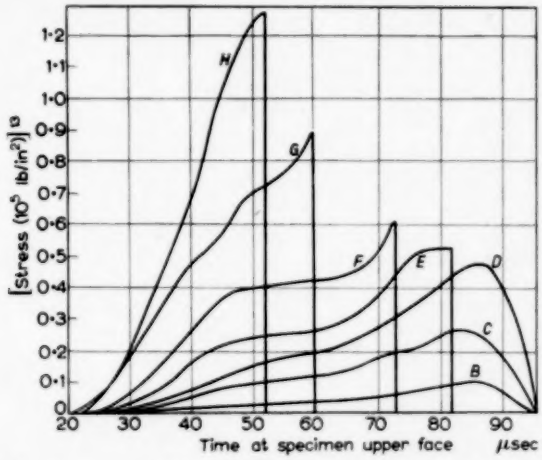

Fig. 7. Curves of (stress)^{13} against time, for dynamic tests.

Table 1 gives the results pertaining to tests in which yielding occurred. The variation in the values of the integral, from the average value of 16·1, is $\pm$ 10 per cent; this is within the experimental accuracy attainable, since the value of the integral is very sensitive to errors in the stress measurement.

TABLE 1.

Impact velocity (in/sec)	*Time to yield* (μsec)	*Yield stress* (10^3 lb/in^2)	$\int_0^{\tau}\left(\frac{\sigma}{10^5 \text{ lb/in}^2}\right)^{13} dt$ (μsec)	*Permanent axial deformation* (*per cent*)
326	82	95	14·1	0·2
340	73	96	15·1	0·5
352	60	99	17·7	0·9
365	52	102	17·3	1·2
		Average	16·1	

The average value obtained from the earlier tests (CAMPBELL and DUBY 1957) was 30·5. The discrepancy between these values corresponds to an error of about 5 per cent in the stress measurement. A possible cause of systematic error in this measurement is variation in the value of the gauge factor. In the earlier investiga-

tion, gauges of greater length (0·64 in.) were used. The manufacturers state that, for either type of gauge, the actual gauge factor should not differ by more than ± 2 per cent from the quoted value. It seems therefore that the observed discrepancy is somewhat greater than can be accounted for by errors in the gauge factors used. Another possible cause of systematic error is the change in specimen diameter: in the earlier tests this diameter was $\frac{1}{2}$ in., compared with $\frac{3}{8}$ in. used in the present tests. The smaller specimens might be expected to give lower yield stresses, for two reasons : (a) a given eccentricity of loading would cause a greater non-uniformity of stress across the section, and (b) the effect of transverse stresses due to the radial acceleration of the specimen material would be less. In addition to the factors already discussed, it is possible that the specimens used in the two investigations differed slightly in composition or structure.

The reduction in upper yield stress due to ' pulsing ', i.e. to dynamic loading insufficient to cause yield, may reasonably be postulated to depend on the ratio of the number of dislocations released to the number required to cause yield. This ratio is given by

$$R \equiv \frac{\int_0^{\tau_0} \sigma^2 \, dt}{\int_0^{\tau_y} \sigma^2 \, dt}, \tag{2}$$

where the integral in the numerator refers to a test in which yield does not occur, and that in the denominator to tests in which yield does occur. Table 2 shows

Table 2.

	Impact velocity (in/sec)	$\int_0^{\tau_0}\left(\frac{\sigma}{10^5 \text{ lb/in}^2}\right)^{18} dt$ (μsec)	R	r
First series of tests	Not pulsed	0	0	0·107
	277	2·8	0·17	0·087
	293	8·3	0·51	0·067
	308	14·4	0·89	0·036
Second series of tests	Not pulsed	0	0	0·095
	277	2·4	0·15	0·085
	293	7·3	0·45	0·060
	308	13·8	0·86	0·023

results obtained from tests in which yielding did not occur. The values of R were calculated by taking for the denominator the mean value of the integrals given in Table 1. As a check on the values obtained, the pulsing tests were repeated. The results of the repeat tests are also given in Table 2 and are in good agreement with the earlier results.

It was decided to use, as a measure of the reduction in the static upper yield stress caused by pulsing, the ratio

$$r \equiv (\sigma_{YU} - \sigma_{YL})/\sigma_{YL}, \tag{3}$$

where σ_{YU}, σ_{YL} are the static upper and lower yield stresses respectively. Table 2 gives the experimental values of r.

Fig. 8 shows R plotted against r, for the two series of pulsed specimens. It is seen that there is a reasonable correlation between the two quantities; it is, however, difficult to obtain either ratio accurately, and the straight line drawn in Fig. 8 only serves to indicate the general trend of the relationship.

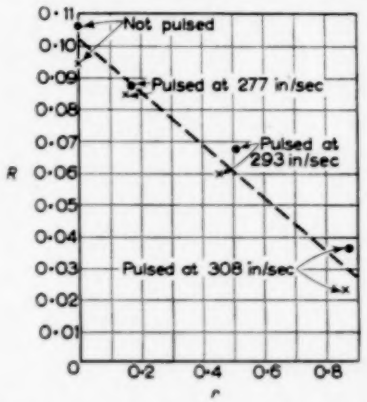

Fig. 8. Reduction of static upper yield stress caused by pulsing. (R and r are defined by equations (2) and (3) respectively.)
● First series × Second series

The static reloading curves of Fig. 5 show that the hardness of the dynamically deformed steel is very little affected by the temperature at which it is deformed, provided that the total amount of deformation is the same. According to the yielding criterion discussed above, the number of dislocations freed before yielding occurs is independent of the magnitude of the stress pulse causing yield. Assuming that it is also independent of temperature, the number of free dislocations at yield is the same in any dynamic test. During low-temperature yielding, the greater applied stress would tend to cause a larger number of Frank-Read sources to operate; however, this effect may be largely offset by the smaller energy available from thermal fluctuations. Two specimens which have been deformed dynamically to the same permanent strain may therefore be expected to contain approximately the same number of free dislocations similarly distributed, irrespective of the temture of testing. The two specimens should then give similar stress–strain curves when reloaded statically at room temperature.

Fig. 5 also shows that the static upper yield stress is a minimum when the steel has been strained about 1 per cent dynamically. After greater amounts of dynamic strain, the yield stress increases again; this is presumably caused by dislocations 'piling up' against obstacles such as grain boundaries and sessile dislocations, and thus causing increasingly high back stresses to act on the sources.

It is worthy of note that even after more than 1 per cent dynamic deformation the steel still exhibited a perceptible drop of stress at yield, though the increase of strain at the lower yield stress was greatly reduced.

6. Conclusions

1. The effect of 'pulsing' steel, i.e. subjecting it to a rapidly-applied compressive stress of insufficient magnitude and duration to cause yielding, is to reduce the upper yield stress obtained during static reloading in compression. It has been found that the reduction in the drop of stress at yield varies approximately linearly with the number of dislocations released in the pulsing test, though it does not appear to be possible to eliminate the drop altogether.

2. The effect of deforming a medium-carbon steel dynamically is to render it softer for subsequent static deformation of the same type. In particular, the static upper yield stress is reduced to a minimum after about 1 per cent permanent dynamic strain. However, a perceptible drop of stress during static yielding exists even after about 1·2 per cent permanent dynamic strain.

3. The static stress–strain curve obtained after impacting is little affected by lowering the temperature at which the impact occurs, provided that the magnitude and duration of the impact stress are increased so as to obtain the same permanent strain.

REFERENCES

CAMPBELL, J. D.	1953	*Acta Met.* **1**, 706.
	1954	*J. Mech. Phys. Solids* **3**, 54.
CAMPBELL, J. D. and DUBY, J.	1956	*Proc. Roy. Soc.* **A236**, 24.
	1957	*Proc. Inst. Mech. Engrs. Conf.* In press.
COTTRELL, A. H. and BILBY, B. A.	1949	*Proc. Phys. Soc.* **A62**, 49.
DUBY, J.	1956	*Dissertation* (Oxford).
HARRIS, D. B. and WHITE, M. P.	1954	*J. Appl. Mech.* **21**, 194.
WARNOCK, F. V. and POPE, J. A.	1947	*Proc. Inst. Mech. Engis.* **157**, 33.

Journal of the Mechanics and Physics of Solids, 1957, Vol. 6, pp. 68 to 70. Pergamon Press Ltd., London

ON STRESSES AND DEFORMATIONS OF ELLIPSOIDAL SHELLS SUBJECT TO INTERNAL PRESSURE*

By R. A. Clark and E. Reissner
Massachusetts Institute of Technology, Cambridge, Mass., U.S.A.

(*Received 24th April, 1957*)

Summary

For many problems of the theory of thin elastic shells, membrane theory is either applicable or not applicable depending on the type of loading involved and on the nature of the boundary or edge conditions. Here we consider a special problem where the applicability of membrane theory depends on the geometry of the shell. We establish the range of validity of the membrane solution and also determine quantitative corrections to this solution.

1. Introduction

In the following we consider a thin elastic ellipsoidal shell of revolution with the major axis of the elliptic cross section perpendicular to the axis of revolution. We assume that the only load is a uniform internal pressure (Fig. 1).

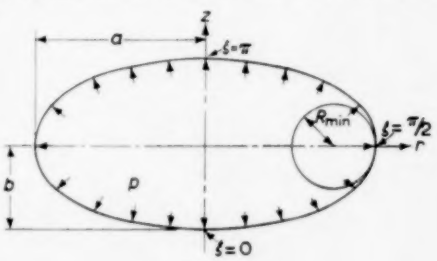

Fig. 1.

Existing solutions (Lorentz 1913; Timoshenko 1940) for the stresses are obtained using the membrane theory of shells which neglects effects due to bending. For the present problem membrane theory is general enough to allow one to satisfy all prescribed boundary conditions and, as there are no discontinuities either in the load function or in the radii of curvature of the shell, membrane theory yields a continuous stress distribution with no singularities.

A qualitative consideration of the problem indicates that some bending does occur and that effects due to bending become progressively more important as the elliptical cross section of the shell becomes flatter and flatter. Our object in the present note is to investigate this aspect of the problem quantitatively. We find that suitable results may be obtained if appropriate solutions of the differential equations of the bending theory of shells are represented by expansions in powers of a small parameter. In contrast to some problems of shell theory concerned with

*Sponsored by the Office of Naval Research under a contract with the Massachusetts Institute of Technology.

bending effects, we do not encounter any solutions of the boundary-layer type in the range of parameter values which we consider.

Our principal result of a qualitative nature may be described as follows. We know the range of validity of thin-shell theory is restricted by the basic assumption that $h/R_{\min} \ll 1$, where h is the wall thickness of the shell and $R_{\min}$ is the least value of the radii of curvature of the middle surface. For an ellipsoidal shell of revolution this order of magnitude relation is equivalent to the relation $h/b \ll b/a$, where a and b are the major and minor semi-axis of the elliptic cross section of the middle surface. Our result for the present problem is that bending effects are negligible, or membrane theory is valid, only if the more restrictive relation $h/b \ll (b/a)^3$ is satisfied.

2. Basic Equations

The middle surface of a closed ellipsoidal shell of revolution may be represented in cylindrical co-ordinates r, θ, z by parametric equations of the form

$$r = a \sin \xi, \qquad z = -b \cos \xi, \tag{1}$$

where $0 \leqslant \xi \leqslant \pi$.

Assuming that the thickness h of the shell is uniform and that a uniform internal pressure p is the only load, the basic differential equations of the linear bending theory may be written as follows (REISSNER 1949)

$$DL_1(\beta) + \frac{b}{a}\alpha\psi = \tfrac{1}{2} pa^2 \alpha \sin \xi \cos \xi, \tag{2}$$

$$L_2(\psi) - \frac{b}{a}\alpha C\beta = -\tfrac{1}{2} pab \left[(2-\nu)\frac{a^2}{\alpha^2} + 3\right] \sin \xi \cos \xi, \tag{3}$$

where the operators L are defined by

$$L_j(f) = f'' + \frac{a^2}{\alpha^2}\cot \xi f' - \left[\cot^2 \xi - (-1)^j \nu \frac{b^2}{\alpha^2}\right] f \tag{4}$$

and where

$$D = \frac{Eh^3}{12(1-\nu^2)}, \qquad C = Eh, \qquad \alpha^2 = a^2 \cos^2 \xi + b^2 \sin^2 \xi. \tag{5}$$

The quantity E is Young's modulus, ν is Poisson's ratio, β is the meridional angle of rotation due to deformation, ψ is a stress function, and primes indicate differentiation with respect to ξ.

Stress resultants and couples are given in terms of β and ψ by the following relations :

$$\begin{aligned}
\alpha N_\xi &= \psi \cot \xi + \tfrac{1}{2} pab \sin^2 \xi, \\
\alpha N_\theta &= \psi' + pab \sin^2 \xi, \\
\alpha Q &= -(b/a)\psi + \tfrac{1}{2} pa^2 \sin \xi \cos \xi, \\
\alpha M_\xi &= D(\beta' + \nu\beta \cot \xi), \\
\alpha M_\theta &= D(\beta \cot \xi + \nu\beta').
\end{aligned} \tag{6}$$

Displacements u and w in radial and axial directions are given by the formulas

$$u = (r/C)\,(N_\theta - \nu N_\xi),$$
$$w = \int [(z'/C)\,(N_\xi - \nu N_\theta) - r\,\beta]\,d\xi. \tag{7}$$

In order to determine stress and displacement quantities, as given by (6) and (7), it is necessary to solve the two simultaneous differential equations (2) and (3) in the interval $0 \leqslant \xi \leqslant \pi$ subject to suitable boundary conditions at the ends of this interval. Such boundary conditions are the symmetry conditions of vanishing angular deflection β and vanishing transverse shear force Q. In view of the form of Q as given by (6) the system of boundary conditions may be written as follows:

$$\xi = 0,\ \pi: \qquad \beta = 0, \qquad \psi = 0. \tag{8}$$

3. Membrane Solution

Membrane-theory formulation of the problem is obtained from the preceding equations by setting, in (2) and (6),

$$D = 0. \tag{9}$$

Indicating the corresponding expressions for ψ and β by a subscript M, we have

$$\psi_M = \tfrac{1}{2}\,p\,\frac{a^3}{b}\sin\xi\cos\xi, \tag{10}$$

$$\beta_M = \frac{a}{b\alpha C}\,L_2(\psi_M) + \tfrac{1}{2}\,p\,\frac{a^2}{\alpha C}\left[(2-\nu)\,\frac{a^2}{\alpha^2} + 3\right]\sin\xi\cos\xi, \tag{11}$$

and these expressions do in fact satisfy boundary conditions (8).

Introduction of (9) and (10) into expressions (6) for stress resultants shows that the couples and the transverse stress resultant Q are identically zero while the direct stress resultants N_ξ and N_θ are given by the known expressions

$$N_{\xi M} = \tfrac{1}{2}\,p\,\frac{a}{b}\,\alpha,$$
$$N_{\theta M} = p\,\frac{a}{b}\left(1 - \tfrac{1}{2}\,\frac{a^2}{\alpha^2}\right)\alpha. \tag{12}$$

Of particular interest is the fact that when $a/b > \sqrt{2}$ the circumferential stress resultant $N_{\theta M}$ changes sign as ξ varies from zero at the apex to the value $\frac{1}{2}\,\pi$ at points farthest removed from the axis of revolution of the shell.

4. Corrections to Membrane Solution

In order to obtain corrections to the membrane solution (10) and (11) which account for non-zero values of the bending stiffness factor D, we introduce non-dimensional variables and parameters, as follows:

$$\psi = \tfrac{1}{2}\,p\,\frac{a^3}{b}\,g(\xi), \tag{13}$$

$$\beta = \tfrac{1}{2} p \frac{a^3}{b} \frac{\sqrt{12\,(1-\nu^2)}}{Eh^2} f(\xi), \tag{14}$$

$$\mu = \sqrt{12\,(1-\nu^2)}\,\frac{R_{\min}}{h} = \sqrt{12\,(1-\nu^2)}\,\frac{b^2}{ah}. \tag{15}$$

The quantity $R_{\min}$ is the meridional radius of curvature for $\xi = \frac{1}{2}\pi$ and is the least value of the two principal radii of curvature when $b < a$. The basic equations being used here are meaningful only if the parameter μ is large compared to unity.

With (13) to (15) differential equations (2) and (3) assume the following more symmetrical form

$$L_1(f) + \mu \frac{\alpha}{b} g = \mu \frac{\alpha}{b} \sin\xi \cos\xi, \tag{16}$$

$$L_2(g) - \mu \frac{\alpha}{b} f = -\left(\frac{b}{a}\right)^2 \left[(2-\nu)\frac{a^2}{\alpha^2} + 3\right] \sin\xi \cos\xi. \tag{17}$$

Inspection of the system (16) and (17) suggests expansions of the form

$$g(\xi) = \sum_{n=0}^{\infty} g_n(\xi) \frac{1}{\mu^{2n}}, \tag{18}$$

$$f(\xi) = \sum_{n=0}^{\infty} f_n(\xi) \frac{1}{\mu^{2n+1}} \tag{19}$$

in terms of inverse powers of the large parameter μ. Equating coefficients of corresponding powers of μ on the right and on the left of (16) and (17), after introduction of (18) and (19) into these equations, leads to the following expressions for the coefficient functions g_n and f_n :

$$g_0(\xi) = \sin\xi \cos\xi, \tag{20}$$

$$f_0(\xi) = \frac{b}{\alpha}\left\{L_2(g_0) + \left(\frac{b}{a}\right)^2 \left[(2-\nu)\frac{a^2}{\alpha^2} + 3\right] \sin\xi \cos\xi\right\}, \tag{21}$$

$$g_n(\xi) = -\frac{b}{\alpha} L_1(f_{n-1}), \quad n = 1, 2, \ldots, \tag{22}$$

$$f_n(\xi) = \frac{b}{\alpha} L_2(g_n), \quad n = 1, 2, \ldots \tag{23}$$

It is readily seen that the leading terms of expansions (18) and (19) are identical with the corresponding membrane solutions (10) and (11). Accordingly, the remaining contributions to the series, beginning with g_1 and f_1, represent corrections to the membrane solution due to the finite bending stiffness of the shell wall.

The following observation is of importance. While the expansions (18) and (19), with g_n and f_n given by (20) to (23), represent particular solutions only of the system of differential equations (16) and (17), these expansions satisfy the boundary conditions (8) term by term. Accordingly, it is unnecessary to consider the general solution of the homogeneous system of differential equations.

For the purposes of this note we may limit outselves to the explicit evaluation of f_0 and g_1 in addition to g_0. We find, making use of the relation

$$\frac{\alpha'}{\alpha} = -\frac{a^2 - b^2}{\alpha^2} \sin\xi\cos\xi = \left(1 - \frac{a^2}{\alpha^2}\right)\cot\xi,$$

the following expressions

$$f_0 = -\left(1 - \frac{b^2}{a^2}\right)\frac{b}{\alpha}\left(\frac{a^2}{\alpha^2} + 3\right)\sin\xi\cos\xi, \tag{24}$$

$$g_1 = \left(1 - \frac{b^2}{a^2}\right)\frac{b^2}{\alpha^2}\left\{8\frac{a^4}{\alpha^4} - \frac{b^2}{\alpha^2}\left[18\frac{a^4}{\alpha^4} + (7+\nu)\frac{a^2}{\alpha^2} + 3 + 3\nu\right]\right\}\sin\xi\cos\xi. \tag{25}$$

5. Formulae for Stresses

From (6) and (13) we obtain for direct stresses $\sigma_{\xi D}$ and $\sigma_{\theta D}$,

$$\sigma_{\xi D} = \frac{N_\xi}{h} = \tfrac{1}{2}\frac{p}{h}\frac{a}{b}\alpha\left\{1 + \frac{a^2}{\alpha^2}\cot\xi\left[\frac{g_1}{\mu} + \ldots\right]\right\}, \tag{26}$$

$$\sigma_{\theta D} = \frac{N_\theta}{h} = \tfrac{1}{2}\frac{p}{h}\frac{a}{b}\alpha\left\{2 - \frac{a^2}{\alpha^2} + \frac{a^2}{\alpha^2}\left[\frac{g_1'}{\mu} + \ldots\right]\right\}. \tag{27}$$

From (6) and (14) we obtain for bending stresses $\sigma_{\xi B}$ and $\sigma_{\theta B}$,

$$\sigma_{\xi B} = \frac{6M_\xi}{h^2} = \frac{3}{\sqrt{12(1-\nu^2)}}\frac{p}{h}\frac{a^3}{b\alpha}\left\{\frac{f_0' + \nu f_0\cot\xi}{\mu} + \ldots\right\}, \tag{28}$$

$$\sigma_{\theta B} = \frac{6M_\theta}{h^2} = \frac{3}{\sqrt{12(1-\nu^2)}}\frac{p}{h}\frac{a^3}{b\alpha}\left\{\frac{f_0\cot\xi + \nu f_0'}{\mu} + \ldots\right\}. \tag{29}$$

We consider in particular the values of stresses at the apex $\xi = 0$ and at the points $\xi = \frac{1}{2}\pi$ farthest removed from the apex of the shell.

From equation (12) the direct stresses have the following values according to membrane theory

$$\sigma_{\xi M}(0) = \sigma_{\theta M}(0) = \tfrac{1}{2}p\frac{a^2}{bh}, \tag{30}$$

$$\sigma_{\xi M}(\tfrac{1}{2}\pi) = \tfrac{1}{2}p\frac{a}{h}, \tag{31}$$

$$\sigma_{\theta M}(\tfrac{1}{2}\pi) = -\tfrac{1}{2}p\left[\frac{a^2}{b^2} - 2\right]\frac{a}{h}. \tag{32}$$

From equations (26) to (29) we have according to bending theory

$$\sigma_{\xi D}(0) = \sigma_{\theta D}(0) = \tfrac{1}{2}p\frac{a^2}{bh}\left\{1 + \frac{8}{\mu^2}\frac{b^2}{a^2}\left(1 - \frac{b^2}{a^2}\right)\left(1 - \frac{7+\nu}{2}\frac{b^2}{a^2}\right) + \ldots\right\}, \tag{33}$$

$$\sigma_{\xi D}(\tfrac{1}{2}\pi) = \tfrac{1}{2}p\frac{a}{h}, \tag{34}$$

$$\sigma_{\theta D}(\tfrac{1}{2}\pi) = -\tfrac{1}{2}p\frac{a}{h}\left\{\frac{a^2}{b^2} - 2 - \frac{10}{\mu^2}\frac{a^6}{b^6}\left(1 - \frac{b^2}{a^2}\right)\left[1 + \frac{7+\nu}{10}\frac{b^2}{a^2} + \frac{3+3\nu}{10}\frac{b^4}{a^4}\right] + \ldots\right\}, \tag{35}$$

$$\sigma_{\xi B}(0) = \sigma_{\theta B}(0) = -\sqrt{12\,\frac{1+\nu}{1-\nu}}\,\frac{p}{\mu}\,\frac{a}{h}\left(1-\frac{b^2}{a^2}\right)\left[1+\frac{\cdots}{\mu^2}+\ldots\right], \tag{36}$$

$$\sigma_{\xi B}(\tfrac{1}{2}\pi) = \frac{3}{\sqrt{12\,(1-\nu^2)}}\,\frac{p}{\mu}\,\frac{a}{h}\,\frac{a^4}{b^4}\left(1-\frac{b^2}{a^2}\right)\left(1+3\,\frac{b^2}{a^2}\right)\left[1+\frac{\cdots}{\mu^2}+\ldots\right]. \tag{37}$$

We are mostly interested in shells for which a/b is reasonably large compared to unity. According to membrane theory the circumferential hoop stress $\sigma_{\theta D}(\frac{1}{2}\pi)$ is the critical stress provided $a/b \geqslant 2$ and we shall limit ourselves to this range in the following discussion. In order to compare the results of bending theory with those of membrane theory we consider the ratio of $\sigma_{\theta D}(\frac{1}{2}\pi)$ and $\sigma_{\xi B}(\frac{1}{2}\pi)$ to the membrane solution $\sigma_{\theta M}(\frac{1}{2}\pi)$. Dividing (35) and (37) by (32) and introducing μ from (15) we may write

$$\frac{\sigma_{\theta D}(\frac{1}{2}\pi)}{\sigma_{\theta M}(\frac{1}{2}\pi)} = 1 - A\left(\frac{a}{b}\right)^4\left(\frac{h}{R_{\min}}\right)^2+\ldots, \tag{38}$$

$$\frac{\sigma_{\xi B}(\frac{1}{2}\pi)}{\sigma_{\theta M}(\frac{1}{2}\pi)} = -B\left(\frac{a}{b}\right)^2\frac{h}{R_{\min}}+\ldots, \tag{39}$$

where

$$A = \frac{10}{12\,(1-\nu^2)}\left(\frac{1-\dfrac{b^2}{a^2}}{1-2\,\dfrac{b^2}{a^2}}\right)\left[1+\frac{7+\nu}{10}\,\frac{b^2}{a^2}+\frac{3+3\nu}{10}\,\frac{b^4}{a^4}\right], \tag{40}$$

$$B = \frac{1}{2\,(1-\nu^2)}\,\frac{\left(1-\dfrac{a^2}{b^2}\right)\left(1+3\,\dfrac{b^2}{a^2}\right)}{1-2\,\dfrac{b^2}{a^2}}. \tag{41}$$

For a/b greater than 3 or 4, coefficients A and B ,given by (40) and (41), vary relatively slowly as a/b increases. In particular, for $\nu = 0{\cdot}3$ we have the following Table :

a/b	2	3	4	5	6	∞
A	1·66	1·14	1·03	0·98	0·96	0·92
B	1·44	0·84	0·70	0·64	0·61	0·55

Using this Table we may easily draw curves, shown in Fig. 2, representing (38) and (39). Since we are limiting ourselves to the calculation of first-order corrections, we expect that the curves drawn are quantitatively reliable only as long as the corrections amount to no more than, say, 10 per cent of the critical membrane stress $\sigma_{\theta M}(\frac{1}{2}\pi)$, as is indicated by the solid portion of the curves in Fig. 2. The broken portions of the curves are probably qualitatively correct, but eventually the results become meaningless as the corrections, or the combination $(a/b)^2\,(h/R_{\min})$, increase.

The following observations may be made on the basis of equations (38) and (39) or Fig. 2. Membrane theory is valid or bending effects may be neglected only if

$$\frac{h}{R_{\min}} = \frac{ah}{b^2} \ll \left(\frac{b}{a}\right)^2, \tag{42}$$

which for $b/a \ll 1$ is a much more restrictive condition than the basic assumption of thin shell theory that $h/R_{\min} \ll 1$. Thus, for a shell with fixed dimensions a and b, there will always be a range of shell thickness h, satisfying (42), for which membrane theory is valid, but this may be only a small part of the range for which bending theory is valid. Also, for a fixed value of $h/R_{\min}$, no matter how small, there will always be shells or ratios a/b for which membrane theory is not valid.

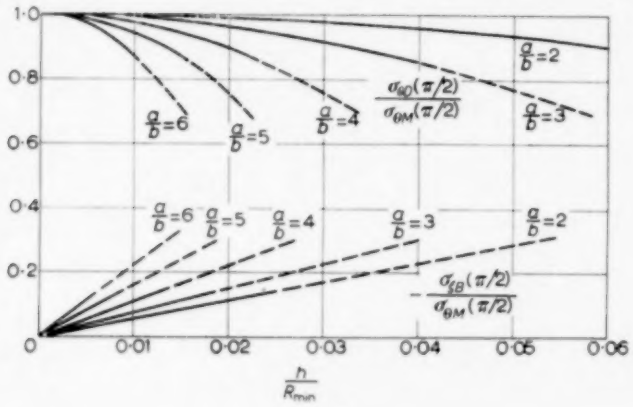

Fig. 2.

6. Formulae for Displacements

Combining relations (7), (13), (26) and (27) we obtain the following general expressions for the displacements :

$$u = \frac{pa^2}{Ehb}\,\alpha\left\{1 - \frac{\nu}{2} - \tfrac{1}{2}\frac{a^2}{\alpha^2} + \tfrac{1}{2}\frac{a^2}{\alpha^2}\left[\frac{g_1' - \nu g_1 \cot\xi}{\mu^2} + \ldots\right]\right\}\sin\xi, \tag{43}$$

$$w = \tfrac{1}{2}\frac{pa^2}{Eh}\int\left\{(1-2\nu)\frac{\alpha}{a} + \nu\frac{a}{\alpha} + \frac{a}{\alpha}\left[\frac{g_1\cot\xi - \nu g_1'}{\mu^2} + \ldots\right]\right\}\sin\xi\,d\xi$$
$$- \tfrac{1}{2}\frac{pa^2}{Eh}\left(\frac{a}{b}\right)^3\int\left\{f_0 + \frac{f_1}{\mu^2} + \ldots\right\}\cos\xi\,d\xi. \tag{44}$$

The axial displacement w is of greatest interest. The integrations involved may be carried out explicity in terms of elementary functions. Retaining only those terms which correspond to the membrane solutions (10) and (11), we find that the total axial expansion $\delta = w(\pi) - w(0)$ is given by

$$\delta_M = \tfrac{1}{2}\frac{pa^2}{Eh}\left\{\left(\frac{a}{b}\right)^2\left[1 - (1-3e^2)\frac{\tanh^{-1}e}{e}\right]\right.$$
$$\left. + 1 - 2\nu + (1 - e^2 + 2\nu e^2)\frac{\tanh^{-1}e}{e}\right\}, \tag{45}$$

where e is the eccentricity of the elliptic cross section given by

$$e^2 = 1 - \left(\frac{b}{a}\right)^2. \tag{46}$$

The first term in (45), involving the factor $(a/b)^2$, represents the contribution due to the angular rotation β and is seen to dominate for large values of a/b. Using (46) we may also write (45) in the somewhat more compact form

$$\delta_M = \tfrac{1}{2}\frac{pa^2}{Eh}\left(\frac{a}{b}\right)^2\left\{1 + (1-2\nu)\left(\frac{b}{a}\right)^2 + \left[2 - (1-2\nu)\left(\frac{b}{a}\right)^2\right] e \tanh^{-1} e\right\}. \tag{47}$$

For $a/b = 1$ and $e = 0$, expression (47) reduces to the value of the deflection for a spherical shell. But as a/b increases and $e \to 1$, the expression for δ eventually becomes meaningless, as does the membrane solution for stresses when the thickness h is held fixed.

REFERENCES

LORENTZ, H. 1913 *Technische Elastizitäts-lehre* p. 34. (Oldenbourg, München und Berlin).

REISSNER, E. 1949 *On the Theory of Thin Elastic Shells* Reissner Anniversary Volume, pp. 231-247. (Edwards).

TIMOSHENKO, S. 1940 *Theory of Plates and Shells* p. 265. (McGraw Hill, New York).

Journal of the Mechanics and Physics of Solids, 1957, Vol. 6, pp. 71 to 78. Pergamon Press Ltd., London

THE ASSOCIATED FLOW RULE OF PLASTICITY

By D. R. Bland
Department of Mathematics, University of Manchester

(*Received 27th March*, 1957)

Summary

The workhardening and linearity hypotheses introduced by Drucker are logically equivalent to the hypotheses of the existence of the plastic potential and of its identity with the yield function. Since neither of these sets of hypotheses is deducible from established physical laws, the author suggests that they are alternative statements of a new physical law.

The flow rule at singular points on a yield surface is found by considering the actual yield surface as the limit of a sequence of regular surfaces. This procedure has different consequences for workhardening and nonhardening materials.

1. Introduction

Although considerable work has been done on the theory of dislocations and on the deformation of a single crystal, the theory of plasticity at the present day rests on hypotheses concerning the macroscopic behaviour of the material. These hypotheses do not contradict the laws of mechanics and of thermodynamics and are in accord with experimental facts.

There are two basic hypotheses in the theory. They concern the yield criterion and the flow rule. The first hypothesis is now sufficiently well established to have the status of a physical law. The second hypothesis has been introduced in various ways. It is the purpose of this paper to show that two statements of this hypothesis are equivalent and to consider the modification of this hypothesis at singular points on the yield surface.

To state the first hypothesis we introduce the yield function f and the workhardening integral F, which depend on the current stress σ_{ij} and on the past history* of the material. Considered as a function of the σ_{ij}, f is convex. F is constant during an elastic deformation.

During deformation the components of stress and strain in general change in value. For an infinitesimal deformation, let the increments in stress and strain be denoted by $d\sigma_{ij}$ and $d\epsilon_{ij}$ respectively. The elastic part of the strain increment $d\epsilon_{ij}^{e}$ can be expressed in terms of $d\sigma_{ij}$ by the elastic stress–strain relation. The remainder of the strain increment is the plastic part,

$$d\epsilon_{ij}^{p} = d\epsilon_{ij} - d\epsilon_{ij}^{e}.$$

It is difficult to conceive that the increments df and dF can depend on increments

*It is necessary to be able to order a sequence of events in plasticity. Except in dynamic problems, it is not necessary to have a measure of time.

other that $d\sigma_{ij}$ and $d\epsilon_{ij}$, or $d\sigma_{ij}$ and $d\epsilon_{ij}^{\,p}$ in virtue of the above equation. Therefore it is assumed that

$$df = \partial f/\partial\sigma_{ij}\, d\sigma_{ij} + \partial f/\partial\epsilon_{ij}^{\,p}\, d\epsilon_{ij}^{\,p}, \qquad dF = A_{ij}\, d\sigma_{ij} + B_{ij}\, d\epsilon_{ij}^{\,p}.$$

However, in an elastic deformation $d\epsilon_{ij}^{\,p} = 0$ and $dF = 0$ for all $d\sigma_{ij}$.

Hence
$$A_{ij} = 0 \qquad \text{and} \qquad dF = B_{ij}\, d\epsilon_{ij}^{\,p}. \tag{1}$$

F depends only upon the past history of the material, not upon the current stress. For a workhardening material $dF \geqslant 0$, equality holding only when $d\epsilon_{ij}^{\,p} = 0$. For a nonhardening material $dF = 0$.

The first hypothesis for a workhardening material states that

$$\left.\begin{aligned} &d\epsilon_{ij}^{\,p} = 0 \quad \text{if} \quad f < F \quad \text{or} \quad f = F \quad \text{and} \quad df \leqslant 0, \\ \text{and} \quad &|d\epsilon_{ij}^{\,p}| > 0 \quad \text{if} \quad f = F \quad \text{and} \quad df > 0. \end{aligned}\right\} \tag{2}$$

For a nonhardening material it states that

$$\left.\begin{aligned} &d\epsilon_{ij}^{\,p} = 0 \quad \text{if} \quad f < F \quad \text{or} \quad f = F \quad \text{and} \quad df < 0, \\ \text{and} \quad &|d\epsilon_{ij}^{\,p}| \geqslant 0 \quad \text{if} \quad f = F \quad \text{and} \quad df = 0. \end{aligned}\right\} \tag{3}$$

In neither case can f exceed F. The equation $f = F$ is known as a yield criterion.

Consider, as an example, a material for which

$$f = \sqrt{\sigma'_{ij}\,\sigma'_{ij}} - c \tanh\left(\frac{1}{E}\,\epsilon_{ij}^{\,p}\,\sigma_{ij}\right)$$

and F is constant, where $\sigma'_{ij} = \sigma_{ij} - \frac{1}{3}\,\sigma_{kk}\,\delta_{ij}$. This material is initially isotropic but becomes anisotropic on plastic working. If it is subject to simple tension and if plastic flow occurs, the tensile stress will increase. This, however, is due not to workhardening but to anisotropy. If at some time the tensile stress has increased an amount δ above its initial value and if the tensile stress is then replaced by a compressive stress in the same direction, the material will begin to deform plastically again at a stress of magnitude δ less than its initial value. In this example f is a function of both σ_{ij} and $\epsilon_{ij}^{\,p}$.

It is interesting to consider two widely used forms of the workhardening integral F in the light of equation (1). The first is $F_1 = F_1(W_p)$ where $W_p = \int \sigma_{ij}\, d\epsilon_{ij}^{\,p}$; then

$$dF_1 = \frac{dF_1}{dW_p}\, dW_p = \frac{dF_1}{dW_p}\, \sigma_{ij}\, d\epsilon_{ij}^{\,p}.$$

The second is $F_2 = F_2(\bar{\epsilon}^{\,p})$ where $\bar{\epsilon}^{\,p} = \sqrt{\frac{2}{3}} \int (d\epsilon_{ij}^{\,p}\, d\epsilon_{ij}^{\,p})^{\frac{1}{2}}$. Then

$$dF_2 = \frac{dF_2}{d\bar{\epsilon}^{\,p}}\, d\bar{\epsilon}^{\,p} = \sqrt{\frac{2}{3}}\, \frac{dF_2}{d\bar{\epsilon}^{\,p}}\, (d\epsilon_{ij}^{\,p}\, d\epsilon_{ij}^{\,p})^{\frac{1}{2}}.$$

F_1 but not F_2 is expressible in the form of equation (1). If the arguments leading to equation (1) are valid, then W_p, but not $\bar{\epsilon}^{\,p}$, is admissible as a measure of workhardening. In certain cases a measure based on $\bar{\epsilon}^{\,p}$ leads to results identical to

those based on W_p (Bland 1957). It is sometimes algebraically convenient to use such a measure.

Subsequently in this paper consideration will be limited to yield functions that are independent of ϵ_{ij}^p; i.e. those for which

$$df = \frac{\partial f}{\partial \sigma_{ij}} d\sigma_{ij}. \tag{4}$$

Yield functions for which $\partial f/\partial \epsilon_{ij}^p \equiv 0$ have always been used in plasticity up to the present day. For many forms of the yield function this excludes changes in the isotropic nature of the material with progressive deformation. Yield functions for which $\partial f/\partial \epsilon_{ij}^p \neq 0$ await consideration.

2. The Associated Flow Rule

The first hypothesis states nothing about the irreversible strains that may occur when the yield criterion is satisfied. Various hypotheses have been put forward. In general it must be the increments of plastic strain, not the total plastic strain, which are related to the current stress tensor. Moreover, the ratios of the plastic strain increments must be independent of the stress increments; i.e.

$$d\epsilon_{ij}^p = a_{ij}\, d\lambda,$$

where the a_{ij} depend on σ_{ij} and on the past history of the material. The hypothesis of the existence of the plastic potential states that there exists a function $g(\sigma_{ij})$ such that the plastic strain increments are given by

$$d\epsilon_{ij}^p = \frac{\partial g}{\partial \sigma_{ij}} d\lambda,$$

where $d\lambda$ is a non-negative infinitesimal, which can depend only upon the space co-ordinates and the time. This equation for $d\epsilon_{ij}^p$ is called a 'flow rule'. If the dependence of g upon σ_{ij} is upon the invariants of σ_{ij}, then the principal axes of stress and plastic strain-increment coincide. The further hypothesis is made that the functions $f(\sigma_{ij})$ and $g(\sigma_{ij})$ are identical, in which case

$$d\epsilon_{ij}^p = \frac{\partial f}{\partial \sigma_{ij}} d\lambda. \tag{5}$$

The flow rule corresponding to a particular yield criterion is called the 'associated flow rule'. It is assumed, until further notice, that the partial derivatives $\partial f/\partial \sigma_{ij}$ are uniquely defined at each point on the yield surface.

Four considerations that lead to these hypotheses are:

(i) it is impossible to prove uniqueness theorems without these hypotheses for situations where experience leads one to believe that the solutions for stress and displacement are unique;

(ii) considerations of the microscopic basis of plasticity (Bishop and Hill 1951; Hill 1956);

(iii) if these hypotheses are valid, weak discontinuities of stress and velocity in two-dimensional problems occur across the same lines, i.e. the characteristics coincide in pairs;

(iv) experiment with materials satisfying the Mises criterion shows that they also satisfy the associated flow rule, i.e. the REUSS equations; see, for example, TAYLOR and QUINNEY (1931), MORRISON and SHEPHERD (1950). It is a consequence of these hypotheses that, if f is independent of the first invariant of stress, $d\epsilon_{ii}^{\,p} = 0$.

An alternative approach has been given by DRUCKER (1950). He considers a body about to yield under the stress distribution σ_{ij}. The body is then subject to a small additional stress $d\sigma_{ij}$, which is slowly applied and slowly removed. DRUCKER states that the net work done by the additional set of forces producing the stress $d\sigma_{ij}$, during their application and removal, is positive or zero for a workhardening material and zero for a nonhardening material. The work done by the original set of forces acting on the body during the application and removal of the additional forces is specifically excluded from this statement. His statement can be written

$$d\sigma_{ij}\, d\epsilon_{ij}^{\,p} > 0 \text{ if not all } d\epsilon_{ij}^{\,p} = 0 \text{ for a workhardening material,} \tag{6}$$

and $$d\sigma_{ij}\, d\epsilon_{ij}^{\,p} = 0 \text{ for a nonhardening material.} \tag{7}$$

This statement does not follow from purely thermodynamic considerations. If the application and removal of the additional forces produces only elastic strains the body will return to its initial condition and we can speak of a cycle, in the thermodynamic sense, having occurred. The net work done by all the forces during the cycle is zero. If the additional forces produce plastic strains, then the body does not return to its initial condition. Neither of the laws of thermodynamics would be violated if the forces originally acting on the body did sufficient work both to provide the necessary energy for the plastic deformation and to do work against the additional set of forces. In this case the net work done by the additional set of forces would be negative. If follows that, from the thermodynamical viewpoint, DRUCKER's statement is a hypothesis.*

DRUCKER states that the work done by the additional set of forces during their application is positive. This inequality is not required below and it will not be considered further. He also makes the hypothesis, called in the remainder of this paper 'DRUCKER's second hypothesis', that, for a workhardening material only, the increments of plastic strain are linear homogeneous functions of the increments of stress for any set of values of stress increments which do not produce unloading.

It will be shown in the next section that DRUCKER's two hypotheses are logically equivalent to the hypotheses of the existence of the plastic potential and of its identity with the yield criterion.

3. PROOF OF EQUIVALENCE OF THE TWO SETS OF HYPOTHESES

DRUCKER (*loc. cit.*, Sections 4–6) has shown that equation (5) can be deduced from his two hypotheses. To prove equivalence, his hypotheses must be deduced from equation (5). If the material is workhardening and if irreversible or plastic flow occurs, then from equations (2) and (4)

$$\frac{\partial f}{\partial \sigma_{ij}}\, d\sigma_{ij} > 0. \tag{8}$$

*See also a review by R. HILL *Applied Mechanics Reviews*, 9, No. 3243, October 1956.

Since $d\lambda > 0$ when plastic flow occurs, one can substitute from equation (5) into the inequality (8) for $\partial f/\partial\sigma_{ij}$. This gives

$$d\epsilon_{ij}^{\,p}\, d\sigma_{ij} > 0,$$

which is DRUCKER's first hypothesis.

If the material is nonhardening, the inequality sign in (8) is replaced by an equality and substitution for $\partial f/\partial\sigma_{ij}$ again yields DRUCKER's first hypothesis. This was shown by DRUCKER, GREENBERG and PRAGER (1952, lemma 1).

To derive DRUCKER's second hypothesis the increment in the workhardening integral F must be considered. From equations (1) and (5),

$$dF = B_{ij}\, d\epsilon_{ij}^{\,p} = B_{ij}\frac{\partial f}{\partial\sigma_{ij}}\, d\lambda$$

and, from equation (4),

$$df = \frac{\partial f}{\partial\sigma_{ij}}\, d\sigma_{ij}.$$

Since $dF = df$ whenever unloading does not occur,

$$\partial\lambda = \frac{df}{\partial\sigma_{ij}}\, d\sigma_{ij}\left(B_{kl}\frac{\partial f}{\partial\sigma_{kl}}\right)^{-1}.$$

Therefore

$$\begin{aligned} d\epsilon_{ij}^{\,p} &= \frac{\partial f}{\partial\sigma_{ij}}\, d\lambda \\ &= \frac{\partial f}{\partial\sigma_{ij}}\left(B_{kl}\frac{\partial f}{\partial\sigma_{kl}}\right)^{-1}\frac{\partial f}{\partial\sigma_{mn}}\, d\sigma_{mn} \end{aligned}$$

which is DRUCKER's second hypothesis.

4. Singular Points on the Yield Surface

The assumption that the partial derivatives $\partial f/\partial\sigma_{ij}$ are uniquely defined at all points on the convex yield surface (henceforth called a regular surface) is now dropped. A point where $\partial f/\partial\sigma_{ij}$ is not uniquely defined is called a singular point. It is assumed that the yield surface in the neighbourhood of a singular point in the join of a number of surfaces S_r such that on the interior of each of these surface $\partial f/\partial\sigma_{ij}$ is uniquely defined. The limit of $\partial f/\partial\sigma_{ij}$ as the singular point is approached along any line on the surface S_r exists and will be written $\partial f_r/\partial\sigma_{ij}$.

The plastic strain increment has frequently been written

$$d\epsilon_{ij}^{\,p} = \sum_r \frac{\partial f_r}{\partial\sigma_{ij}}\, d\lambda_r \tag{9}$$

where the $d\lambda_r$ are non-negative infinitesimals and the sum is over all the surfaces S_r whose join forms the yield surface in the neighbourhood of the singular point. Until further notice only workhardening materials are considered. Many authors restrict the application of equation (9) only by the remark that all $d\lambda_r$ are zero if the stress increment $d\sigma_{ij}$, considered as a vector (based on the singular point) in stress 9-space lies inside or on the yield surface. However, KOITER (1953) introduces the stronger restriction that $d\lambda_r$ is zero if

$$\frac{\partial f_r}{\partial \sigma_{ij}} d\sigma_{ij} \leqslant 0. \tag{10}$$

If the yield surface with singular points is considered as a limit of a sequence of regular convex surfaces, it will be shown that a restriction is required on equation (9) but that of KOITER's is too strong.

Consider neighbourhoods of the singular points in stress 9-space such that l is a typical length of all the neighbourhoods. (Neighbourhoods may overlap). Then it is possible to find regular convex surfaces for any non-zero l however small such that the distance between each surface and the yield surface is less than l in the neighbourhoods of the singular points and zero elsewhere. These are called 'l-surfaces'. On a regular yield surface the plastic strain increment vector has the direction and sense of the outward normal to the surface at σ_{ij} and it satisfies DRUCKER's first hypothesis. Since the limiting surface as $l \to 0$ is the yield surface, the author makes the following hypothesis about the plastic strain increment for a given stress increment when the stress is at a singular point on the yield surface: namely, that it has the direction and sense that it would have if the stress point lying on the yield surface were replaced by any point in the neighbourhood of the singular point lying on an l-surface provided that l is sufficiently small.

If $d\sigma_{ij}$ satisfies $\partial f_r/\partial \sigma_{ij}\, d\sigma_{ij} > 0$ for all r, the $d\epsilon_{ij}^{\,p}$ are given by equation (9) because sets of quantities not included in this equation are excluded from being sets of values of $d\epsilon_{ij}^{\,p}$ by the convexity of the l-surfaces and no sets of quantities included in the equation can be excluded from $d\epsilon_{ij}^{\,p}$ since l can be made arbitrarily small. However, the fact that DRUCKER's first hypothesis holds when any l-surface replaces the actual yield surface imposes a limitation on possible $d\epsilon_{ij}^{\,p}$ when $d\sigma_{ij}$ does not satisfy $\partial f_r/\partial \sigma_{ij}\, d\sigma_{ij} > 0$ for all r. This limitation is

$$d\epsilon_{ij}^{\,p}\, d\sigma_{ij} > 0 \quad \text{when } |d\epsilon_{ij}^{\,p}| > 0 \text{ for a workhardening material.} \tag{11}$$

It is clear that when the inequality (10) is satisfied so is (11), but that the converse is not true. The inequality proposed by KOITER is therefore stronger than the consequence of the author's hypothesis. The differences between the three formulae for $d\epsilon_{ij}^{\,p}$, namely that given by equation (9) unmodified, modified by the inequality (10), and modified by the inequality (11), are illustrated by a normal projection of the Tresca hexagonal cylinder in principal stress 3-space (Fig. 1).

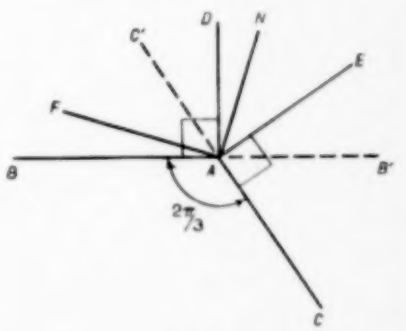

Fig. 1.

BAC is a corner of the projection. BA is produced to B', CA to C'. DA is normal to BA, EA to CA. If $d\sigma_{ij}$ is any vector (based on A) lying in $< B'\,A'\,C'$, then $d\epsilon_{ij}^{\,p}$ can lie anywhere in $< DAE$. However, if $d\sigma_{ij}$ is any vector AF lying in $< BAC'$, equation (9) unmodified allows $d\epsilon_{ij}^{\,p}$ to lie anywhere in the $< DAE$; if equation (9) is modified by KOITER's inequality (10), then $d\epsilon_{ij}^{\,p}$ lies along AD; if equation (9) is modified by the DRUCKER inequality (11), then $d\epsilon_{ij}^{\,p}$ lies in $< DAN$ where AN is normal to AF.

Now consider a nonhardening material when the stress is at a singular point. A normal at any point in the neighbourhood on an l-surface is a possible direction for $d\epsilon_{ij}^{p}$, subject to DRUCKER's first hypothesis for a nonhardening material, namely $d\sigma_{ij}\, d\epsilon_{ij}^{p} = 0$. This is satisfied identically when $d\sigma_{ij} = 0$. Therefore in this case $d\epsilon_{ij}^{p}$ is given by equation (9) without limitations.

When $d\sigma_{ij} \neq 0$, $d\sigma_{ij}$ must lie in one or more of the surfaces f_r. Denote this sub-group of the f_r by a subscript s. Denote the sub-group of the surfaces f_r, in which $d\sigma_{ij}$ does not lie, by a subscript t. For each value of s,

$$d\sigma_{ij} \frac{\partial f_s}{\partial \sigma_{ij}} = 0;$$

and, since the complete yield surface is convex, for each value of t,

$$d\sigma_{ij} \frac{\partial f_t}{\partial \sigma_{ij}} < 0.$$

Using DRUCKER's hypothesis and equation (9),

$$0 = d\sigma_{ij}\, d\epsilon_{ij}^{p} = \sum_{t} \frac{\partial f_t}{\partial \sigma_{ij}}\, d\sigma_{ij}\, d\lambda_t.$$

Since $d\lambda_r \geqslant 0$, this equation can only be satisfied if $d\lambda_t = 0$ for all t. It follows that

$$d\epsilon_{ij}^{p} = \sum_{s} \frac{\partial f_s}{\partial \sigma_{ij}}\, d\lambda_s;$$

i.e. the summation in equation (9) is taken only over the normals to those surfaces in which $d\sigma_{ij}$ lies.

5. CONCLUSIONS

In this paper the equivalence of two sets of hypotheses have been proved. Neither of them is deducible from established physical laws. This situation indicates the presence of a new physical law. The author suggests that this law should be called 'the second law of plasticity'. Its statement is either of the two sets of hypotheses or any other equivalent set. The position is analogous to that of the second law of thermodynamics which can be stated in many ways, all logically equivalent.

It is interesting to note that the limitations, imposed on the plastic strain increment at a singular point on the yield surface, for a workhardening material are different from those imposed when the material is nonhardening. This is further evidence that it is not possible to consider the properties of a nonhardening material to be the same as those of a workhardening material as the rate of workhardening tends to zero.

WARNER and HANDELMAN (1956) have attempted to generalize the flow rule that can be deduced from DRUCKER's hypotheses for a workhardening material. They introduce loading conditions to replace the inequality (8). Since the inequality (8) is a direct consequence of the existence of a yield criterion, one can only assume that the materials considered by these two authors possess no yield criterion. There is no *a priori* reason why a theory should not be built on the existence of loading conditions rather than on the existence of a yield criterion. But such a

theory can hardly be considered as part of the theory of plasticity where the existence of a yield criterion is a fundamental postulate.

Acknowledgments

This paper was written while the author was the holder of an I.C.I. Research Fellowship at King's College, London. He wishes to thank Mr. H. G. Hopkins and Mr. S. J. Tupper for their advice.

References

Eishop, J. F. W. and Hill, R. 1951 *Phil. Mag.* **42**, 414.

Bland, D. R. 1957 *Proc. 9th International Congress of Appl. Mech.* (to be published).

Drucker, D. C. 1950 *Qu. Appl. Math.* **7**, 411.

Drucker, D. C., Prager, W. and Greenberg, H. J. 1952 *Qu. Appl. Math.* **9**, 381.

Hill, R. 1950 *Mathematical Theory of Plasticity* (Clarendon Press).

1956 *Mechanics of Quasi-static Plastic Deformation in Metals.* Surveys in Mechanics, G. I. Taylor Anniversary Volume (C.U.P.), 7–31.

Koiter, W. T. 1953 *Qu. Appl. Math.* **11**, 350.

Morrison, J. L. and Shepherd, W. M. 1950 *Proc. Instn. Mech. Engrs., Lond.* **163**, 1.

Taylor, G. I. and Quinney, H. 1931 *Phil. Trans. Roy. Soc.* A. **230**, 323.

Warner, W. H. and Handelman, G. H. 1956 *Qu. J. Mech. Appl. Math.* **9**, 279.

Journal of the Mechanics and Physics of Solids, 1957, Vol. 6, pp. 79 to 82. Pergamon Press Ltd., London

ELASTIC–PLASTIC TORSION OF SHARPLY NOTCHED BARS*

By J. A. H. Hult
Department of Mechanical Engineering, Massachusetts Institute of Technology†

(*Received* 21*st March*, 1957)

Summary

The shape of the incipient plastic region at the tip of a sharp notch in a twisted bar is derived, assuming the material to be ideally plastic. The result is used to determine the strain in the plastic region.

1. Introduction

Torsion of a bar with a sharp longitudinal notch produces plastic yielding at the tip of the notch for any magnitude of the applied torque, however small. It is shown below that the shape of the region of incipient plastic yielding can be found for any shape of the cross section, provided the solution of the corresponding elastic problem is known.

The elastic stress field near the tip of a sharp notch in pure shear is found to be similar to the elastic stress field near a similar longitudinal notch in torsion. Since the shape of the plastic region produced at the notch in pure shear is known, the corresponding region in the torsion case can be derived by analogy.

2. Sharp Notch in Shear, Elastic Material

The analysis follows closely that of the torsion problem in elasticity. With the notation of Hill (1950), one obtains (writing τ_x for τ_{xz} and τ_y for τ_{yz})

$$\tau_x = \frac{\partial \phi}{\partial y}, \qquad \tau_y = -\frac{\partial \phi}{\partial x}; \qquad \frac{\partial^2 \phi}{\partial x^2} + \frac{\partial^2 \phi}{\partial y^2} = 0.$$

Along the free boundary $\phi = 0$ and at infinity $\phi = \tau_\infty y$.

This boundary value problem is readily solved by means of conformal mapping. The Schwarz-Christoffel integral

$$z - ic = \int_0^w \frac{t^{2m}\, dt}{(t^2 - d^2)^m}, \tag{1}$$

where

$$m = \tfrac{1}{2} - \frac{\omega}{2\pi}, \qquad d = c\,\frac{2\pi - \omega}{\sqrt{\pi\,(\pi - \omega)}} \cdot \frac{\Gamma\left(\frac{3}{2} - \frac{\omega}{2\pi}\right)}{\Gamma\left(2 - \frac{\omega}{2\pi}\right)}, \tag{2}$$

*This research was supported by the United States Air Force through the Office of Scientific Research of the Air Research and Development Command, under contract No. AF 18 (600) - 957.

†Now at Royal Institute of Technology, Stockholm.

transforms the boundary in the z-plane to the real axis in the w-plane, as shown by Fig. 1. The complex stress function in the w-plane then is $\phi = \tau_\infty \cdot w$. Since the integral (1) cannot be evaluated except for points in the vicinity of the singular point $z = ic$, the solution in the z-plane can be explicitly stated only in that region. For $|w| \ll d$ (1) takes the form

$$z - ic \simeq \frac{1}{(-d^2)^m} \cdot \frac{w^{2m+1}}{2m+1}. \tag{3}$$

Furthermore,

$$\tau_x - i\tau_y = \frac{d\phi}{dz} = \tau_\infty \frac{dw}{dz} = \tau_\infty \frac{(w^2 - d^2)^m}{w^{2m}}$$

or, for $|w| \ll d$,

$$\tau_x - i\tau_y \simeq \tau_\infty \frac{(-d^2)^m}{w^{2m}}.$$

Inserting here m and d from (2) and w from (3), one obtains for the stress in the vicinity of the notch tip, with the notation of Fig. 1,

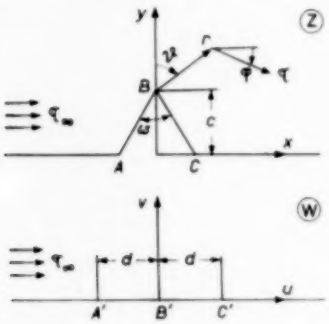

Fig. 1.

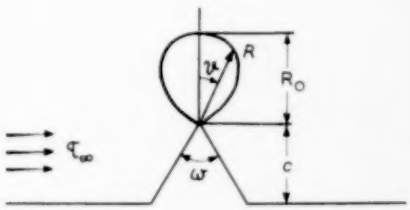

Fig. 2.

$$\left.\begin{aligned} \tau &= H \cdot r^{-\frac{\pi-\omega}{2\pi-\omega}}, \\ H &= \tau_\infty \cdot \left[\frac{c\sqrt{\pi}}{\pi-\omega} \cdot \frac{\Gamma\left(\frac{3}{2} - \frac{\omega}{2\pi}\right)}{\Gamma\left(2 - \frac{\omega}{2\pi}\right)}\right]^{\frac{\pi-\omega}{2\pi-\omega}}, \\ \phi &= \frac{\pi-\omega}{2\pi-\omega} \cdot \vartheta. \end{aligned}\right\} \tag{4}$$

3. Sharp Notch in Shear, Ideally Plastic Material

For an ideally plastic material the shape of the plastic region developed at the tip of a sharp notch in shear was determined by HULT and MCCLINTOCK (1956). With the notation of Fig. 2 the polar co-ordinate representation of the elastic–plastic boundary is

$$R = R_0 \cos\frac{\pi\vartheta}{\pi-\omega}, \qquad R_0 = 2\left(\frac{H}{k}\right)^{\frac{2\pi-\omega}{\pi-\omega}} \tag{5}$$

where H is defined by (4) and k is the yield stress in shear. The result (5) is valid only for small values of τ_∞/k, i.e. for the incipient yielding.

4. Sharp Notch in Torsion, Elastic material

The stress distribution near a re-entrant corner in torsion was studied by De Schwarz (1953). It was found that close to the notch tip, with the notation of Fig. 3,

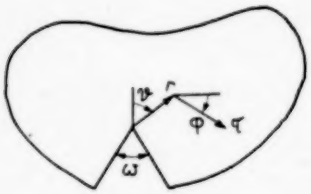

Fig. 3.

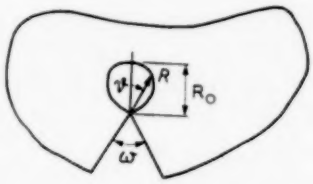

Fig. 4.

$$\tau = K \cdot r^{\frac{\pi-\omega}{2\pi-\omega}}, \qquad \phi = \frac{\pi-\omega}{2\pi-\omega}\cdot\vartheta, \tag{6}$$

where K depends on the applied torque and on the cross sectional geometry, but not on r or ϑ.

5. Sharp Notch in Torsion, Ideally Plastic Material

The similarity between (4) and (6) suggests that for a sharp notch in torsion the incipient plastic region can be obtained from (5) by analogy, i.e. that the elastic–plastic boundary takes the form, with the notation of Fig. 4,

$$R = R_0 \cos\frac{\pi\vartheta}{\pi-\omega}, \qquad R_0 = 2\left(\frac{K}{k}\right)^{\frac{2\pi-\omega}{\pi-\omega}}. \tag{7}$$

This conclusion is justified by the following argument: For every given sharp notch in torsion can be found a corresponding sharp notch in shear, with the same notch angle ω, such that the elastic stress field, within a certain sufficiently small distance from the notch tip, is identical in the two cases. This is accomplished by choosing c or τ_∞ such that $H = K$. Since the elastic stress fields are identical, the embedded plastic regions will then also be identical, and (7) follows from (5).

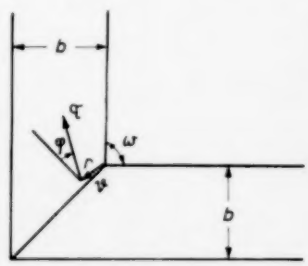

Fig. 5.

Equation (7) implies that the plastic region around a sharp notch in torsion can be found directly from the corresponding elastic solution. As an illustration might serve the L-beam, studied by Trefftz (1921, 1925*).

In the elastic case the stress vector was found to be, with the notation of Fig. 5,

*A few misprints in the 1925 paper should be observed.

$$\tau = G\theta b \cdot \sqrt[3]{0{\cdot}1737} \cdot \sqrt[3]{\frac{b}{r}}, \qquad \phi = \tfrac{1}{3} \cdot \vartheta ;$$

i.e., with the notation of (6),

$$K = G\theta b \cdot \sqrt[3]{0{\cdot}1737 \cdot b}.$$

Hence, from (7), the plastic region at the re-entrant corner of the L-beam has the form

$$R = R_0 \cos 2\vartheta, \qquad R_0 = 0{\cdot}1737 \cdot \left(\frac{G\theta b}{k}\right)^3 2b.$$

This coincides with the result obtained by TREFFTZ (1925).

The above result can be applied to finding the strain distribution around sharp notches or cracks in torsion. As shown by HULT and MCCLINTOCK (1956) the strain in the plastic region near a sharp notch or crack in shear is

$$\gamma = \frac{R}{r} \cdot \frac{k}{G}. \tag{8}$$

By the same reasoning as above it is clear that this relation holds also for a sharp notch or crack in torsion, so that the strain will be given by (7) and (8).

Application of this result to a study of the stress and strain distribution around a growing fatigue crack in torsion will be shown in a subsequent paper.

ACKNOWLEDGMENTS

The author wishes to acknowledge financial support from the Division of Sponsored Research at the Massachusetts Institute of Technology. This is part of a Dissertation submitted to the Massachusetts Institute of Technology in January 1957, in partial fulfilment of the requirements for the degree of Doctor of Science.

REFERENCES

DE SCHWARZ, M. J.	1953	*Öst. Ing. Arch.* **7**, 88.
HILL, R.	1950	*Mathematical Theory of Plasticity* pp. 84-88 (Clarendon Press).
HULT, J. A. H. and MCCLINTOCK, F. A.	1956	*Proc. IX Int. Cong. Appl. Mech.* Brussels.
TREFFTZ, E.	1921	*Math. Ann.* **82**, 97.
TREFFTZ, E.	1925	*Z. Angew. Math. Mech.* **5**, 64.

BOOK REVIEW

C. Kittel : Introduction to Solid State Physics. 2nd Edition. Chapman and Hall, 1956. 617 pp., 96*s*.

This second edition, appearing three years after the first edition, represents a considerable increase in the size of the book, a change from approximately 400 to 600 pages. As the author indicates, " half of the increase in length is brought about by fuller explanations of the basic concepts, particularly in the areas of crystal symmetry and energy band theory. The other half represents the addition of new material on alloys, semiconductors, photoconductivity, luminescence and imperfections in solids." The sections on elastic and thermal properties of solids, dielectric, ferroelectric and magnetic properties, and superconductivity have not been greatly changed from the first edition.

Much of the new material added on semiconductors, imperfections, etc. is concerned with work carried out in the last three years and one of the attractive features of the book is the account given of recent work on a number of topics of which cyclotron resonance, exciton spectra, and photoconductivity in semiconductors are typical examples. Here the author presents results on modern research work in solid state, so as to enable the reader both to see its correlation with basic theory, and also the trend of present research. This is very well supported by the addition of recent references, of the order of two hundred dated between 1953 and 1956 having been added.

On the side of fundamental theory, the section on band theory has been considerably expanded and the extra space has been well used in discussing the more difficult concepts involved. However, the relatively large increase in the sections on crystal symmetry and X-ray diffraction in crystals, while concerned with basic concepts, represents to a considerable extent the introduction of new concepts not considered in the first edition. As a result, even with the large expansion in the space allocated to it, this section is still highly condensed, more so than any others of the book, and may represent very hard going for a reader relatively unversed in crystallography.

The above considerations are perhaps particularly relevant as the book is intended as an introductory textbook to students in solid state physics. So far as the undergraduate student is concerned, in most cases the new material in this second edition will concern him but little, and it is the post-graduate student who will find the book most useful. The raising of the average academic level of the text is further illustrated by the inclusion in the text of some material which previously occurred in appendices.

So far as the beginning post-graduate student is concerned, the author has achieved his purpose very satisfactorily. Any such student will find a thorough knowledge of the book very rewarding, while the more advanced worker can also gain much from it. It is regrettable that perhaps only the latter will feel that the price does not place the book beyond his reach.

J. C. Woolley

BOOKS RECEIVED

Revue de Mécanique Appliquée Tome I, No. 2, pp. 206 (Éditions de L'Académie de la République Populaire Roumane, 1956).

Studii si cercetari de Mecanica Applicata 1, anul VIII. pp. 300 (Academiei Republicci populare Romine, 1956).

D. McLean, Edited by W. Jackson, H. Fröhlich, N. F. Mott : *Grain Boundaries in Metals.* pp. 346 (Oxford University Press, 1957) 50s.

Edited by J. E. Goldman : *The Science of Engineering Materials.* pp. 258 (J. Wiley & Son, 1957) 96s.

Edited by Fred. Seitz and David Turnbull : Vol. 4, *Research and Applications.* pp. 540 (Academic Press N. York, 1957) $12.00.

W. A. Wooster : *Experimental Crystal Physics.* pp. 115 (Oxford, 1957) 18s.

René Dugas : *A History of Mechanics.* pp. 771 (Routledge & Kegan Paul, 1957) 100s.

Journal of the Mechanics and Physics of Solids, 1958, Vol. 6, pp. 85 to 91. Pergamon Press Ltd., London

VICKERS HARDNESS AND COMPRESSIVE STRENGTH

By D. S. DUGDALE
Engineering Department, University College of Swansea

(*Received 25th July*, 1957)

SUMMARY

HARDNESS and compression tests are reported for a wide variety of materials. A simple empirical method for relating hardness number to the stress–strain curve is suggested. The correlation obtained leads to the conclusion that the Vickers test is not at all sensitive to yield stresses corresponding to compressive strains greater than 0·15.

1. INTRODUCTION

INDENTATION hardness evidently represents some kind of average of yield stress taken over a certain range of strain. For an ideal rigid-plastic material there is only a single value of yield stress at all values of strain, so the hardness found with a particular kind of indenter must be a certain multiple of this stress. For a perfectly elastic material one might expect the hardness to be defined by the elastic constants (e.g. SNEDDON 1951, p. 466). However, most materials strain-harden in a more or less irregular manner after the initial breakdown of elasticity, so any proposed method of calculating hardness must take account of the whole stress–strain curve. This has been realized for some time, due to the failure of special methods involving elastic constants, initial yield stress, ultimate tensile stress, etc. to give any generally valid indication of the hardness value (HANKINS 1929).

It is an everyday experience in hardness testing that the material displaced by the indenter flows upwards around the indenter only for relatively few materials, chiefly those that have been cold-worked. Usually, the indenter appears to push material in front of it into the interior of the body, and clearly this feature must be kept in mind in any attempt to calculate hardness from results of tensile and compression tests. This deformation has been investigated many times in the past. Recently, WILLIAMS and O'NEILL (1956) plotted hardness contours over sections of indentations, and SAMUELS and MULHEARN (1957) carried out quantitative strain-etching tests. These investigations suggested that the deformation consists largely of the expansion of hemispherical shells of material beneath the indenter. If this is so, the pressure required to form an impression must be such as to overcome the resistance to expansion of all these shells, which will be strained more or less severely according to their radial distance from the centre of the impression. The idea of a purely radial expansion will be utilized later in an attempt to correlate hardness with compressive strength.

2. Compression Tests

Cylinders of diameter 1 in. and length 2 in. were tested in a 100 tons capacity Amsler testing machine. Strains up to 1 per cent were measured with diametrically opposite Huggenburger extensometers of 1 in. gauge length. During this part of the test a ball joint was interposed between the specimen and the machine platen to ensure coaxial loading. After this stage, the extensometers and ball joint were removed and the strain was calculated from diameter measurements taken with a micrometer. The ends of the specimen were lubricated about five times during the test with calcium oleate. Each load was maintained for a few seconds only, while readings were taken. The logarithmic strain ϵ, defined as the natural logarithm of the ratio (initial height/final height) was calculated, and the true stress was plotted against the decimal logarithm of this strain. Typical curves are shown in Fig. 1. Selected values of compressive yield stress (tons/in^2) are given in Table 1.

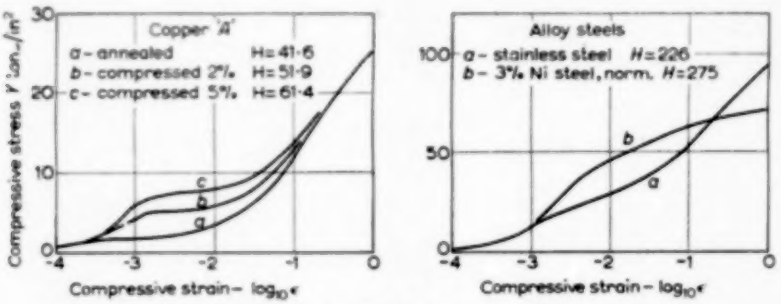

Fig. 1. Compression test results.

For tests on lead, the specimens were periodically cooled in ice to delay recovery, but nevertheless the precise values of yield stresses for strains beyond 0·1 cannot be quoted with confidence. Cast iron fractured at a strain of 0·1 and cold-drawn brass at a strain of 0·5 (all strains are logarithmic). Nylon deformed almost linearly up to a well-marked yield point. However, Perspex was found not to have a distinct yield stress ; creep occurred at an accelerating rate at high stresses, and the results were of such doubtful value that they were discarded. Copper A and Copper B had slightly different annealing treatments.

Materials giving pronounced raised lips around the impression, with a high convexity ratio, are not discussed at present. It is thought that the hardness of such materials is better compared with results of torsion tests. Materials containing internal stress and having marked anisotropy were avoided.

3. Hardness Tests

A standard Vickers hardness testing machine was used, with a pyramidal diamond indenter. The test load was such as to give the largest measurable impression, normally 100 kg. Special care was taken to avoid errors due to hard surface layers. After machining the specimens were progressively polished on emery paper until a constant value of hardness was obtained. No special measures were taken

either to clean the polished surface of the specimen or to lubricate it. About fifteen impressions were made on either end of the cylinder which was later tested in compression. In addition to the diagonals, the lateral dimensions of the impression were measured, by means of the Vickers microscope. From these measurements the convexity ratio b/s was calculated (Fig. 2). For obtaining lateral dimensions of the surface of contact, the usual vertical illumination of the impression was occasionally supplemented with extra oblique illumination. About 3000 Vickers tests were carried out. Average values are shown in Table 1.

TABLE 1

	Vickers hardness H	*Convexity ratio* b/s	*Area* $A_{0.15}$	*Yield stresses* $Y_{0.15}$	$Y_{0.30}$
Steel, 0·1% C normalized	130	− 0·004	51·6	35·0	39·0
Steel, 0·1% C annealed	107	− 0·014	42·5	31·6	37·0
Steel compressed 2%, aged	143	+ 0·024	59·9	37·2	41·5
Steel, 0·4% C normalized	185	− 0·017	74·0	51·2	55·0
Steel, 0·4% C annealed	161	− 0·031	61·1	45·9	50·0
Steel, 13% Mn	205	− 0·036	65·2	53·6	82·7
Steel, stainless	226	− 0·026	77·2	61·3	74·0
Steel, 3% Ni normalized	275	+ 0·032	103	65·0	68·0
Steel 3% Ni annealed	227	+ 0·022	87·5	56·0	59·2
Copper A, annealed	41·6	− 0·115	13·4	14·3	19·2
Copper compressed 2%	51·9	− 0·027	18·2	15·1	19·4
Copper compressed 4%	56·8	− 0·004	21·4	15·6	19·6
Copper compressed 5%	61·5	+ 0·016	22·4	15·8	19·7
Copper B, annealed	45·2	− 0·078	14·4	14·8	19·3
Copper compressed 3%	64·7	+ 0·027	25·1	16·8	19·9
Brass, 60 : 40 cold-drawn	126	+ 0·005	45·0	30·4	37·8
Brass, 60 : 40 annealed	90·0	− 0·025	29·4	22·5	27·2
Brass, 70 : 30 annealed	56·6	− 0·055	18·0	15·1	23·4
Aluminium, 11% Si.	55·0	+ 0·013	19·7	13·5	13·8
Lead, annealed	4·95	+ 0·046	1·59	—	—
Cast iron	220	− 0·036	71·3	—	—
Nylon	18·2	− 0·054	7·05	5·90	5·90

4. DEFORMATION AROUND IMPRESSION

In the Vickers test a pyramid of 136° included angle is pressed into the surface under a known load. To obtain the hardness number H, the load (kg) is divided by the area of the sloping surface (mm^2) calculated from the average of the diagonals. The problem considered here is that of finding an empirical relation between hardness and compressive strength valid for materials having any kind of stress–strain curve. A fairly simple and essentially correct model of the deformation is required for indicating magnitudes of strains in the material beneath the indenter. SAMUELS and MULHEARN worked with annealed brass (which gives an impression of the sinking-in type) and showed that, at a short distance from the tip of the indenter, surfaces of equal strain were hemispherical. This suggests that hardness may be usefully compared with the radial pressure required to produce a purely

radial expansion of a spherical cavity in an infinite mass of material. Let the radius of the cavity be a (Fig. 2). The radial pressure p_1 at radius r_1 is obtained by integrating the equilibrium equation :

$$p_1 = 2\int_{r_1}^{\infty} \frac{Y}{r}\, dr \qquad (1)$$

where Y is the compressive yield stress at radius r.

In order to calculate strains, the material is assumed to be incompressible. BISHOP, HILL and MOTT (1945) found the following expression for the logarithmic compressive strain ϵ at radius r :

$$\epsilon = \tfrac{2}{3} \ln \left(\frac{r^3}{r^3 - a^3} \right). \qquad (2)$$

For values of r that are fairly large in comparison with a, we may expand and differentiate (2) to obtain

$$d\epsilon/\epsilon = -3\, dr/r. \qquad (3)$$

Substituting for dr/r in (1), the integral for the radial pressure becomes

$$p_1 = \tfrac{2}{3}\int_0^{\epsilon_1} Y\, d(\ln \epsilon). \qquad (4)$$

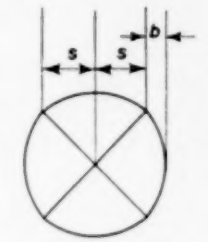

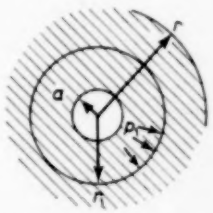

Fig. 2. Dimensions of impression.

This means that when the compressive yield stress Y is plotted against the logarithm of strain, the radial pressure at any radius r_1 is proportional to the area under the curve taken up to the appropriate value of ϵ_1. BISHOP, HILL and MOTT used equations (1) and (2) to evaluate the pressure acting on the surface of the expanding cavity, i.e. at radius $r = a$, and compared this value with the pressure required for deep punching. Here the pressure is almost twice as great as that required for producing a shallow indentation.

There are various reasons for this difference. The radial pressure required to expand a hemispherical shell will not be exactly the same as that required to expand a whole spherical shell, due to the presence of a free surface. However, previous work (DUGDALE 1955) showed that an indenter of 70° included angle required a pressure equal to about 0·9 of the pressure to expand a spherical cavity, so the presence of the free surface does not satisfactorily explain the discrepancy. The most important reason for it seems to be suggested by the experimental result that (for the materials considered here) indentation pressure falls rapidly with increasing indenter angle. This is interpreted as meaning that as the indentation becomes shallower, the pressure required is predominantly governed by yield stresses at smaller and smaller strains. So it might be expected that the calculated pressure required to expand a spherical cavity would depend to an excessive degree on yield stresses at large strains, and would not give a suitable value for comparison with the pressure required for the relatively shallow Vickers indentation. Calculations, which can be readily carried out with the experimental data given, showed that this was so, and suggested the need for a modified method which would take less account of yield stresses at large strains.

No exact method of calculating the strains produced around a shallow indentation

is known to the writer. However, the object of the present work was simply to derive a single numerical value from the stress–strain curve for comparison with the hardness value, using a method that takes account of the gradually decreasing strain values at increasing distances from the centre of the impression. A possible way of modifying the calculation would be to set a finite upper limit to the integral for radial pressure (4) in place of the theoretically infinite strain value for an expanding spherical cavity. This excludes altogether the contribution made by yield stresses at strains larger than some arbitrarily chosen value. The resulting pressure may be thought of as the radial pressure acting on a hemisphere of material having a radius comparable to half the impression diagonal, but it does not seem to be necessary for the purpose of the present work to relate it in any precise way to the geometry of the pyramidal impression. The usefulness of such a hypothetical pressure may be judged from another standpoint, i.e. whether it bears a constant ratio to the hardness value.

5. Analysis of Results

When the sides of the impression are not too convex, material displaced by the indenter is to a large extent forced downwards into the body being indented. It is thought that, when this happens, the hardness number is governed primarily by the pressure required to cause a radial expansion within the material. It has been shown that at any radius the radial pressure required to cause a purely radial expansion is proportionate to the area under the stress–strain curve drawn on a logarithmic base (Fig. 3). If the precise radius at which the radial pressure is

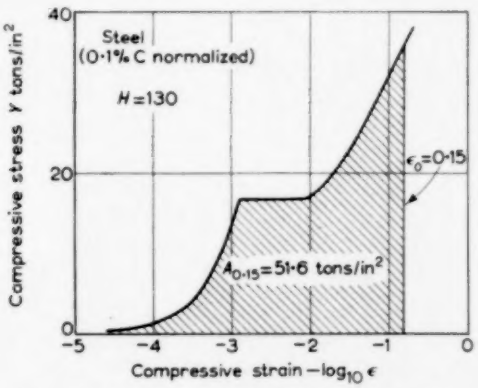

Fig. 3. Analysis of compression test results.

measured is left unspecified, the upper limit of strain is available as a variable parameter for obtaining the most favourable set of values for comparison with values of hardness. It was found that a value of compressive strain $\epsilon_1 = 0{\cdot}15$ gave the best correlation for the materials examined. Ratios of hardness H divided by area $A_{0{\cdot}15}$ (given in Table 1) are plotted against convexity ratio b/s in Fig. 4. Quite a small variation in the chosen limit of strain was found to be sufficient to impair this correlation. The information given in Table 1 is thought to be sufficient

to allow this result to be checked. It is of interest to note that TABOR (1951, p. 106) found that hardness bore an almost constant ratio to *yield stress* if this is selected at a compressive strain of 8 per cent. The curve shown in Fig. 4 tends to fall slightly for convexity ratios greater than $-0{\cdot}02$. This might be expected, as flow upwards to the surface then provides a slightly easier path of escape for some of the displaced material than the purely radial mode of flow.

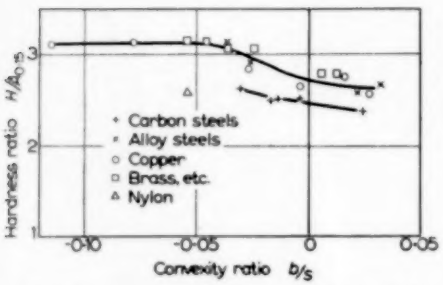

Fig. 4. Correlation between hardness and compressive strength.

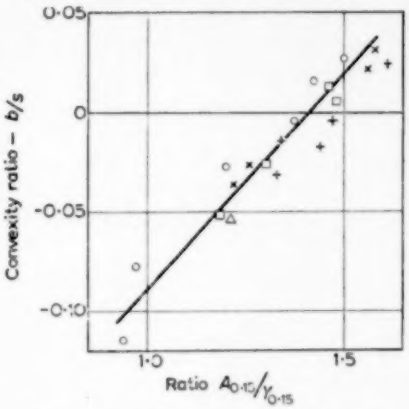

Fig. 5. Shape of impression related to stress–strain curve.

It is of considerable interest to attempt to estimate the convexity ratio from the stress–strain curve. It may be conjectured that upward flow would occur more easily as the pressure beneath the indenter increased in relation to the yield strength of material lying on the periphery of the impression. It may be argued that the area $A_{0\cdot15}$ representing radial pressure, when divided by the yield stress at a particular value of strain, should provide a ratio for correlating with convexity ratio. This strain may be varied so as to obtain the best correlation. The best value was found to be 0·15. These ratios are plotted in Fig. 5. It should perhaps be pointed out that the convexity ratio depends on the difference in elevation of the centre of the lateral lip and the corner of the impression. Factors influencing the elevation of the corner have not been specifically studied.

6. Discussion and Conclusions

The reasonable correlation between hardness values and the proposed quantity derived from the stress–strain curve (Fig. 4) is thought to justify the method used. If this is accepted, it follows that the Vickers hardness value depends critically on yield stresses corresponding to strains up to 0·15, but very little on stresses corresponding to larger strains. This can be well appreciated by inspection of the columns of yield stress in Table 1. For some materials the yield stress increases very rapidly for strains greater than 0·15 and for some materials it hardly increases at all, but this does not seem to influence the hardness. The fact that conventional Vickers and Brinell tests give no indication of strain-hardening at large strains has been keenly appreciated in the past, and has given rise to methods such as the MEYER analysis for obtaining this further information.

The hardnesses of the plain carbon steels appear to be distinctly lower than the values predicted from the stress–strain curves (Fig. 4). It appears that for steels which have a marked yield point, the constant stress required to maintain flow after initial yielding is not applicable to the type of deformation that occurs beneath an indenter, for some geometrical reason. Strain-etching of sectioned impressions usually reveals a very irregular system of LUDERS bands enclosing areas that have not yet yielded (DUGDALE 1956).

The ratio for nylon (Fig. 3) is lower than those for the metals. This is attributed to the low value of the elastic modulus in relation to hardness ($E = 250$ tons/in^2).

ACKNOWLEDGMENTS

The author is grateful for encouragement received from Professor H. O'NEILL and helpful criticism received from Professor R. HILL. The plastics were kindly supplied by British Nylon Spinners, Ltd.

REFERENCES

BISHOP, R. F., HILL, R. and MOTT, N. F.	1945	*Proc. Phys. Soc.* **57**, 147.
DUGDALE, D. S.	1955	*J. Mech. Phys. Solids* **3**, 206.
	1956	*J. Iron St. Inst.* **184**, 22.
HANKINS, G. A.	1929	*Proc. Instn. Mech. Engrs., Lond.* **1**, 317.
SAMUELS, L. E. and MULHEARN, T. O.	1957	*J. Mech. Phys. Solids* **5**, 125.
SNEDDON, I. N.	1951	*Fourier Transforms* (McGraw-Hill, New York).
TABOR, D.	1951	*Hardness of Metals* (Clarendon Press, Oxford).
WILLIAMS, G. H. and O'NEILL, H.	1956	*J. Iron St. Inst.* **182**, 266.

Journal of the Mechanics and Physics of Solids, 1958, Vol. 6, pp. 92 to 110. Pergamon Press Ltd., London

THE PROPAGATION OF FATIGUE CRACKS IN SHEET SPECIMENS

By N. E. Frost and D. S. Dugdale*
Mechanical Engineering Research Laboratory, East Kilbride

(*Received 19th July*, 1957)

Summary

Fatigue tests have been carried out on mild steel, aluminium alloy and copper sheet specimens containing a small central slit. Measurements of the growth of the fatigue cracks initiated by the slit were made as the test proceeded. In some of the mild steel specimens a plastic zone was visible around the growing crack. Measurements of the plastic zone were made whenever possible and these showed that a state of geometrical similarity existed between the crack length and plastic zone dimensions.

For low stresses the crack growth was sometimes erratic, but while the growth was steady and the overall crack length less than about one eighth of the specimen width it was found that the rate of growth was proportional to the current crack length. The effect of mean stress is discussed.

1. Introduction

Although a vast quantity of information on the fatigue properties of materials has been accumulated during the last fifty years, the study of the laws governing the rate of growth of a fatigue crack has received little attention until recently. This has been mainly due to two reasons. First, in the laboratory testing of fatigue specimens, by far the greater part of the work has been carried out on cylindrical specimens, the geometry of which makes it very difficult to obtain accurate quantitative data on crack growth. This difficulty is especially serious for notched specimens in which it is possible for a crack to form early in the life. Secondly, trends in the design of high performance equipment, such as aircraft engine components, have been towards the use of polished components of high strength steel in which cracks are on no account permissible. For such components, working stresses are governed by consideration of fatigue crack initiation rather than crack propagation. At the present time, however, interest has revived for a number of reasons. It is desirable to rationalize design in many departments of engineering so as to economize in material. In railway rolling-stock, components often work under conditions where a combination of corrosion and fretting makes it inevitable that small fatigue cracks form, and a safe design is one in which these cracks are not allowed to spread. In aircraft structures the 'fail-safe' design philosophy requires the structure to be constructed in such a way that fatigue cracks do not cause catastrophic failure before corrective measures can be taken. Again, in bridges or ship structures a disastrous failure may occur if a crack should

* Now at University College, Swansea.

grow to a length sufficient to set off brittle fracture. The initiation of the crack is usually due to some kind of stress raiser, such as a sharp corner, a rivet hole, a notch or slit, or an inclusion in a welded joint.

In order to obtain information on the propagation of fatigue cracks under idealized laboratory conditions, fatigue tests have been carried out on thin sheet panels of various materials. Cracks were grown from a central slit in the panel and growth measurements taken continuously.

2. Survey of Previous Work

There is little published information on the growth of fatigue cracks which can be considered relevant to the work of the present paper. Some work has been carried out using plain and circumferentially notched cylindrical specimens (Moore 1927, Lessels and Jacques 1950, Hyler *et al.* 1956) tested under conditions of rotating bending. However, for the plain specimens, only the circumferential length of the crack can be estimated, while for the notched ones sectioning of the specimen is necessary to obtain the depth of crack (which of course allows only one measurement per specimen to be made). Also, with such specimens a complex three-dimensional stress distribution is present which makes the test results difficult to interpret. Again, where cracks are formed in plain specimens at stresses above the intrinsic fatigue limit and then reloaded (Moore 1927, Frost and Phillips 1956) the conditioning of the material ahead of the crack due to the initial crack formation profoundly influences the subsequent behaviour of the crack.

The ideal experiment calls for a wide sheet with a small internal slit. Weibull (1954, 1956) has carried out such tests although unfortunately his sheets were not particularly wide. In the analysis of the results Weibull (1954) attempted to apply a correction to the applied nominal stresses to allow for the reduction of cross section as the crack grew. In the work described in his later paper (1956) the applied loads were progressively reduced throughout the test so that nominal stresses calculated on the remaining cross section remained constant. From these tests Weibull concluded that the length of crack was proportional to the number of cycles of applied load, or alternatively that the rate of crack growth was constant and independent of the current crack length. Two controversial points arise from Weibull's work. First, the length of the crack was measured from the end of the internal slit and not from the centre of the specimen. This does not conform with present-day methods of analysis as discussed by Wells (1955). It has, however, no serious consequences since Weibull's graphs employ a linear length scale. The second point is concerned with the validity of correction made to the applied loads in order to keep a constant stress value across the remaining section. This matter is discussed in detail in the next section.

A mathematical study of the question of crack propagation has been made by Head (1953). The following expression was derived :

$$dl/dN = l^{3/2}/a^{1/2} f(\sigma)$$

where $f(\sigma)$ is a function of the nominal applied stress, N the number of cycles, l the half crack length and a the thickness of plastic zone ahead of the crack. Head

assumes that this thickness remains constant, and independent of crack length, but the experimental work described in the present paper suggests that this assumption is not correct. If a is considered constant it follows that $l^{-\frac{1}{2}}$ varies linearly with N, the number of cycles. To verify his theoretical relationship Head used the experimental results of Moore (1927), De Forrest (1936) and Bennet (1946) and showed that the results gave a linear relation between $l^{-\frac{1}{2}}$ and N. Although the measurements appeared to agree with the above expression, replotting shows that they also conform with a variety of other expressions relating rate of growth and crack length. However, experiments of the type carried out by these authors cannot be considered to furnish reliable measurements of crack length and the use of them in support of a basic theory of crack propagation is most unsatisfactory.

3. Effect of Finite Width of Sheet

When the sheet is very wide the stresses in the vicinity of a central internal crack are defined by the mean external stress applied to the sheet, irrespective of the precise width. As the length of the crack becomes an appreciable fraction of the width of the sheet, the stresses around the tip of the crack will increase even though the mean stress calculated on the gross section of the sheet is the same as before. One possible assumption is that the stresses near the end of the crack increase so as to bear a constant relation to the average stress over the reduced section of the sheet. As mentioned earlier, this is the assumption made by Weibull (1954, 1956) and is one of a kind familiar to engineers. However it is quite arbitrary and can be shown, in specific examples, to be incorrect. For instance, Timoshenko and Goodier (1951, p. 81) state that the solution for the stresses around a circular hole in an infinite plate can be applied to a plate of finite width. When the width of the plate is as small as four diameters of the hole, the error in the infinite plate solution for calculating the maximum stress is only 6 per cent if the stress is considered as the load divided by the gross area of the plate, and not $33\frac{1}{3}$ per cent, as the use of the net area would suggest.

For the hole in a plate of finite width Howland (1930) evaluated the maximum stress concentration for various ratios of hole radius c to half plate width b. His tabulated values of stress concentration factor can be represented quite well by the series

$$3\left\{1+\left(\frac{c}{b}\right)^2+4\left(\frac{c}{b}\right)^4-4\left(\frac{c}{b}\right)^6\ldots\ldots\right\}; \qquad 0<\frac{c}{b}<0{\cdot}5.$$

It should be noted that the first term of the correction occurs as the square of the ratio. So far as the authors are aware, the corresponding solution for an internal slit has not yet been evaluated. However, the above feature is likely to be found again, since it appears to follow from the condition of symmetry about the longitudinal centre-line. Suppose that the stress function may be expressed, in terms of x and y, as

$$\sum_{m=-\infty}^{\infty}\sum_{n=-\infty}^{\infty} a_{mn}\left(\frac{x}{l}\right)^m\left(\frac{y}{l}\right)^n$$

where the crack of length $2l$ lies along the x-axis, with its centre at the origin. The condition that σ_y should remain unaltered when the sign of x is changed ex-

cludes odd values of m. Then the boundary condition $\sigma_x = 0$ along $x = b$ gives only even powers of b/l for determining the constants a_{mn}.

For the purpose of obtaining an estimate of this effect some experiments were carried out on mild steel sheets containing internal slits, tested under static tension. The specimen was similar to those used for the fatigue tests described later and is shown in Fig. 2. Each sheet contained a central slit of different length and was loaded in increments up to a nominal stress of 3 tons/in^2 based on the gross area. Two Johannson extensometers of $\frac{1}{16}$in. gauge length were fitted centrally on either side of the specimen in such a way as to measure the amount of opening of the slit as load was applied. As it was found that this movement was reversible it was assumed that the amount of opening was proportionate to the stresses in the elastic material surrounding the slit. If the amount of opening is $2u$, the length of slit $2l$ and p the nominal stress acting on the gross area of the sheet, then the theoretical value of the function $uE/2pl$ is unity for an infinite sheet. The experimental values obtained for sheets of finite width $2b$ are shown in Fig. 1,

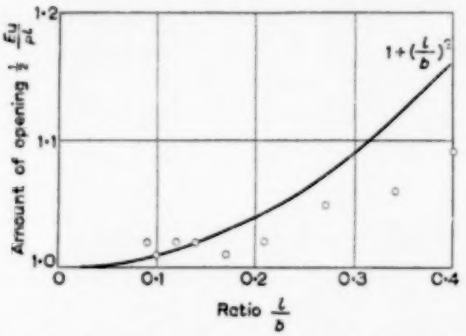

Fig. 1. Experimental values of amount of opening of slit in mild steel sheet.

from which it may be concluded that the stresses in the vicinity of the slit increase according to a factor $1 + A\,(l/b)^2$ where A is a coefficient whose value is somewhat less than unity. The procedure of obtaining a corrected stress by dividing the applied force by the reduced area does not seem appropriate. It would appear for investigating basic laws of crack propagation it is best to avoid as far as possible any correction for the finite width of the sheet. This correction involves both the fractional error in the stresses near the crack and also the response of rate of growth to stress. The first of these factors is not accurately known and the second cannot be defined with certainty without a knowledge of the basic laws which it is the purpose of the experiment to determine.

In the following experimental work the internal slits used were made small in relation to the width of the sheet so that errors due to finite length were negligible. The nominal stresses considered are all obtained by dividing the applied loads by the gross area of the sheet and not by the reduced area.

4. Experimental Details

The materials tested were mild steel, aluminium alloy (BS.L71), and commercially pure copper, these materials being in the form of sheets measuring 6 ft by 3 ft. The mild steel sheet of thick-

ness 10 SWG (0·128 in.) was supplied in two batches, hot rolled and normalized. The first, marked MBLV, had an analysis 0·12 per cent carbon, 0·46 per cent manganese, 0·052 per cent sulphur. This material was stress-relieved at 650°C and gave a tensile strength of 20·5 tons/in^2 with 26 per cent elongation. The second, marked MBPQ, had an analysis 0·05 per cent carbon, 0·28 per cent manganese, 0·016 per cent sulphur. This material was annealed by heating to 800°C and furnace cooling, resulting in a tensile strength of 19 tons/in^2 with 48 per cent elongation. The aluminium alloy (4·45 per cent copper) was supplied rolled to 14 SWG (0·080 in.) and was in the fully solution treated and aged condition. It was not subjected to any further heat treatment and gave a tensile strength of 30·5 tons/in^2 with an elongation of 10 per cent. The copper (10 SWG) was annealed at 600°C and gave a tensile strength of 15·5 tons/in^2 with an elongation of 50 per cent. The micro-structures of all the materials were quite normal.

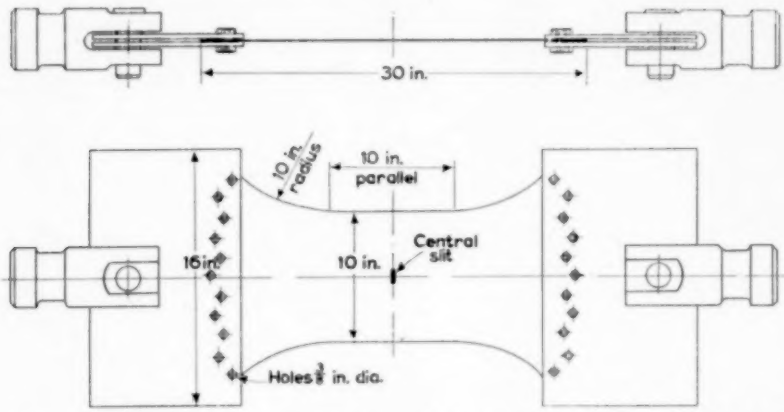

Fig. 2. Test specimen and method of clamping in 60 ton Schenck fatigue machine.

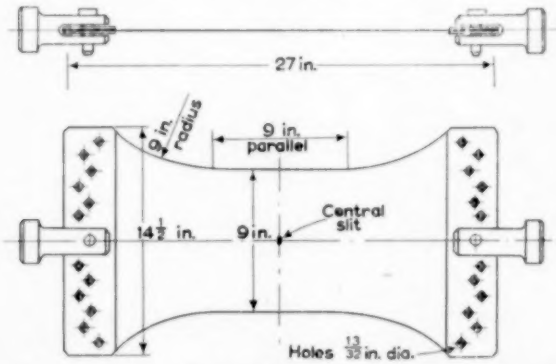

Fig. 3. Test specimen and method of clamping in 6 ton Schenck fatigue machine.

Specimens of the form shown in Figs. 2 and 3 were cut from the sheets with their longitudinal direction coinciding with the direction of rolling. No machining was carried out on the surface of the specimens. The ends of the specimens were drilled for clamping in Schenck-type fatigue machines. Specimens of the type shown in Fig. 2 were tested in a 60 ton capacity machine while the type shown in Fig. 3 were tested in a 6 ton capacity machine. The grips were fitted in the fatigue machine so that the specimen lay in the vertical plane although some of the earlier tests were carried out with the specimen in the horizontal plane. The grips were carefully aligned to ensure that no bending stresses were introduced into the specimen. The stress distribution across the test section was checked by means of Huggenberger extensometers, a series of statie

loads being applied. It was found that the stress did not vary more than 2 per cent from the average across the central section.

To initiate fatigue cracks, a central slit was made in the specimen. This was done by first drilling a central hole 0·040 in. diameter and then cutting diametrically opposite slits 0·15 to 0·5 in. long, perpendicular to the longitudinal direction of the specimen, by means of a fine steel fret-saw blade. Thin steel razor blades which had had saw teeth ground in the cutting edge were then used to extend the slit a further 0·01 in. approximately, the extremity of the slit thus formed being about 0·002 in. wide and 0·001 in. root radius. A typical profile can be seen from the photomicrograph shown in Fig. 9. After this operation the specimens were given the respective heat-treatments mentioned earlier.

To facilitate measurement of the fatigue cracks both sides of the specimen were polished across the central section. Light scribe-marks were then made at intervals of 0·1 in. from the centre of the sheet. The specimens were strongly illuminated and a small hand microscope with a magnification of $\times$ 10 was used for estimating the crack length. For specimens tested in the vertical plane the crack lengths were read on both sides of the specimen. It is important to note that all crack lengths and other related measurements are measured from the centre of the sheet and not from the end of the initial slit. The crack lengths were measured at regular intervals while the machine was running, and it was considered that they could be measured to an accuracy of 0·005 in. Specimens in which no cracks could be seen, or those in which a crack formed but did not propagate, were cut up and the section containing the central slit metallurgically mounted. These sections were polished and etched and examined under magnifications up to $\times$ 500.

The specimens were tested in the appropriate Schenck fatigue machine, which ran at about 2000 cycles/min, the specimens being subject to direct stress. Fatigue tests were carried out with various tensile mean loads, these being such that the loading was never compressive.

It may be reiterated here that nominal stresses are based on the gross cross-sectional area of the specimen, taking no account of the presence of the crack. The symbols l and N respectively represent the average half-length of the crack in inches measured from the centre line of the sheet and the number of stress cycles in millions.

5. Tests on Plain Specimens

To obtain the intrinsic fatigue strength of the sheet materials, conventional fatigue tests were carried out with mean loads comparable to those used for the sheets containing central slits. The value of the mean load was limited by the fact that it was necessary to keep the sheet specimen always in tension to prevent buckling. The specimens were given the same heat treatment as the sheets containing central slits. The estimated limiting fatigue strengths, based on an endurance of 10^7 cycles, were found to be: Mild steel (both batches) $10 \pm 5\frac{1}{2}$ tons/in^2, Aluminium alloy $8 \pm 5\frac{1}{2}$ tons/in^2, Copper $6 \pm 2\frac{1}{2}$ and 4 ± 3 tons/in^2.

6. Tests on Sheet Specimens Containing Central Slits

The length of the fatigue crack was measured at regular intervals throughout the test. In the earlier tests, where the sheet was tested in the horizontal plane, only two measurements were possible but in the later tests, where the sheet was tested in the vertical plane, four measurements were obtained, two on either side of the specimen. On any one specimen, at a given instant during the test, the individual readings varied only slightly one from another and for the purpose of plotting curves the average value was used. In the earlier tests slits of half-length 0·5 in. were used, but as the technique for producing the slits was improved, later tests were done with slits of half-length 0·15–0·2 in.

The mild steel specimens were tested with mean stresses of 10, 7, 5 and 2 tons/in^2,

Table 1. *Details of fatigue tests on sheets containing central slits*

Specimen mark	*Average half length of initial slit* (in.)	*Stress* (tons/in^2.)	*Endurance* (millions of cycles)	*Remarks*
Mild steel				
MBLV 4	0·50	10 ± 6	0·0146	Crack growth
MBPQ 21	0·153	10 ± 4	0·3935	Crack growth
MBPQ 8	0·16	10 ± 3	0·4111	Crack growth
MBPQ 19	0·159	10 ± 2½	2·7292	Crack growth
MBLV 19	0·51	10 ± 2½	1·2000	Crack growth
MBLV 22	0·375	10 ± 2	2·1590	Crack growth
MBPQ 14	0·16	10 ± 1½	13·3439	Crack growth
MBLV 7	0·50	10 ± 1	3·4115	Crack growth
MBLV 8	0·50	10 ± ½	16·6142	Non-propagating crack
MBPQ 1	0·193	7 ± 5	0·1009	Crack growth
MBPQ 10	0·166	7 ± 4	0·2737	Crack growth
MBPQ 3	0·16	7 ± 3½	0·5637	Crack growth
MBPQ 4	0·163	7 ± 3	0·8603	Crack growth
MBPQ 5	0·159	7 ± 2½	1·3082	Crack growth
MBPQ 6	0·166	7 ± 2	2·2086	Crack growth
MBPQ 7	0·15	7 ± 1½	10·5321	Crack growth
MBPQ 9	0·15	7 ± 1	23·5766	Non-propagating crack
MBPQ 20	0·165	5 ± 4	0·3523	Crack growth
MBPQ 16	0·163	5 ± 3	0·7897	Crack growth
MBLV 11	0·50	5 ± 3	0·3223	Crack growth
MBPQ 17	0·143	5 ± 2½	1·7456	Crack growth
MBPQ 11A	0·171	5 ± 2	3·3303	Crack growth
MBLV 10	0·48	5 ± 2	1·3358	Crack growth
MBPQ 18	0·155	5 ± 1¾	4·9697	Crack growth
MBPQ 15	0·148	5 ± 1½	10·4522	Crack growth
MBLV 26	0·55	5 ± 1½	12·7328	Non-propagating crack
MBLV 23	0·50	5 ± 1	14·4171	Non-propagating crack
MBPQ 14	0·16	5 ± 1	10·2364	No crack formed
MBLV 12	0·50	5 ± ½	10·0943	Non-propagating crack
MBPQ 13	0·131	2 ± 1½	8·4467	Crack growth
MBLV 17	0·50	2 ± 1½	13·0306	Non-propagating crack
MBLV 18	0·50	2 ± 1¼	12·0781	Non-propagating crack
MBLV 19	0·50	2 ± 1¼	12·0849	Non-propagating crack
MBLV 13	0·50	2 ± 1	9·9076	Crack growth
Aluminium alloy				
MBNQ 11	0·375	4 ± 3	0·0169	Crack growth
MBNQ 12	0·375	4 ± 1½	0·1005	Crack growth
MBNQ 21	0·158	4 ± 1	0·5031	Crack growth
MBNQ 13	0·375	4 ± ¾	0·6212	Crack growth
MBNQ 20	0·184	4 ± ½	11·7789	Crack growth
MBNQ 14	0·375	4 ± ¼	15·3023	Crack growth
MBNQ 15	0·20*	2 ± 1	1·0639	Crack growth
MBNQ 18	0·285	2 ± ¾	1·3703	Crack growth
MBNQ 23	0·18	2 ± ¾	2·4104	Crack growth
MBNQ 19	0·28	2 ± ½	2·3051	Crack growth
MBNQ 22	0·244	2 ± ½	10·2047	Crack growth
MBNQ 17	0·25	2 ± ¼	12·9345	No crack formed
MBNQ 16	0·20	2 ± ¼	10·3635	No crack formed

*Crack cut at 45° through sheet thickness.

TABLE 1 (*continued*)

Specimen mark	*Average half length of initial slit* (in.)	*Stress* (tons/in^2)	*Endurance* (millions of cycles)	*Remarks*
Copper				
MBNK 11	0·27	$2 \pm 1\frac{1}{2}$	1·1333	Crack growth
MBNK 14	0·265	$2 \pm 1\frac{1}{4}$	3·0611	Crack growth
MBNK 13	0·32	2 ± 1	6·0941	Crack growth
MBNK 15	0·275	$2 \pm \frac{3}{4}$	26·8323	Non-propagating crack
MBNK 12	0·30	$2 \pm \frac{1}{2}$	15·8193	No crack formed

the aluminium alloy at mean stresses of 4 and 2 tons/in^2 and the copper at a mean stress of 2 tons/in^2. The details of the tests carried out are given in Table 1. As these tests involved some thousands of measurements of crack length it is only possible to present the final analysis of the experimental data here. Tabulations and plots of the data are given in extenso in the unpublished report (FROST and DUGDALE 1957b).

It was noted that non-propagating cracks were present for some of the lower alternating stress values. Where the crack could be seen with the low-power microscope, the measurements showed clearly that such cracks were non-propagating. In other cases, although no crack could be detected during the test, subsequent microscopic examination revealed small cracks.

On final examination of the fractured specimens, two modes of fracture were apparent. At first the cracks had grown from the initial slit at 90° to the plane of the specimen. After growing in this manner for a certain length, fracture subsequently occurred on a plane inclined at roughly 45° to the plane of the sheet. For some of the aluminium alloy specimens, fracture occurred as a double shear instead of the usual single shear. No distinct change in the rate of growth was observed when the transition from 90° to 45° growth occurred.

For one aluminium alloy specimen, the slit was cut at an angle of 45° to the plane of the sheet to see if this would induce the crack to grow immediately along a 45° plane. However, the crack behaved exactly as if the slit had been cut in the normal manner, and started off on a 90° plane.

With the second batch of mild steel (MBPQ), it was found that, by heating to 800°C for 1 hr and furnace cooling, strain markings were apparent on the surface of the sheet around the tip of the growing crack. Measurements of the plastic zone revealed by these markings were made whenever possible. Although there was never any doubt about the length of the plastic zone it was difficult to obtain accurate measurements of the width. Photographs of the growing crack and plastic zone were taken throughout some of the tests.

7. PROPAGATION OF FATIGUE CRACKS

Consider first a small idealized slit in a perfectly elastic sheet of infinite extent subject to plane stress. The theory of elasticity shows that the configurations of stress and strain around the slit remain geometrically similar as the slit extends.

In other words if a unit diagram is prepared in which dimensions are so scaled as to represent the length of the slit by unity then at any point defined by a vector drawn from the origin, the stress or displacement is the same regardless of the actual length of slit. The same answer can be arrived at by a dimensional analysis of all the parameters that have a bearing on the problem. If the sheet width is large in comparison with the slit length it will have only an infinitesimal effect on the stresses in the vicinity of the slit. Also, if the sheet is thin in comparison with the length of slit, it can be assumed that stresses through the thickness are zero and so the precise value of sheet thickness in relation to slit length cannot be of any consequence. If it is assumed that the structural dimensions of the material are small enough to allow it to be considered as homogeneous, then no other lengths are involved and all other parameters are stresses. It then appears reasonable to say that during a single loading up to a certain nominal stress a configuration will be attained in the vicinity of the slit which can be reduced to a unit diagram regardless of the slit length. This must be so whether or not part or the whole of the sheet deforms plastically.

It is assumed in the previous argument that two or more sheets in an initially identical and uniform condition but with different lengths of slit are deformed with a single application of load. If, however, load is applied to a single sheet with a slit of a certain length and later re-applied when the slit has elongated, the configurations will only be similar if the sheet suffers no permanent change due to loading and unloading. If, for instance, internal stresses are introduced, or work-hardening occurs during the first loading, then the second configuration for the increased slit length may not be the same as the first because two values of length are now involved.

A further step is to regard fracture under fatigue loading as if it were a continuous process. Suppose that a crack has grown continuously from an initial length of either zero or a value small in relation to the current length. As it has not been arrested at any stage, there is only one independent variable of length to which the configuration of stress and strain can be referred, namely, the current length of crack. It follows that the rate of propagation must be proportionate to the current length of crack.

This argument does not take into account independent dimensions of length associated with any plastic zone adjacent to the tip of the crack. If there is an independent length parameter of this kind then there can be no geometrical similarity of strain distribution and the above arguments are invalidated.

8. Measurements of Plastic Zone Ahead of Crack

The development of the plastic zone ahead of the growing crack appears to be of importance with regard to the above argument. The measurements of the half-length of the plastic zone were plotted against the half-length of crack for each of the appropriate mild steel (MBPQ) tests. In the cases where measurements of the width of the plastic zone were available, similar plots were also made. It was found that the results were well represented by straight lines passing through the origin. Hence it is reasonable to assume that both the length and width of the plastic zone were directly proportional to the current crack length. Two

typical curves are shown in Fig. 4. It should be noted that the half-length of both the crack and the plastic zone are measured from the centre-line of the specimen. The ratio of these lengths is shown plotted against the maximum nominal tensile stress of the cycle in Fig. 5. A reasonably smooth curve is obtained showing that, as expected, there is some functional relationship.

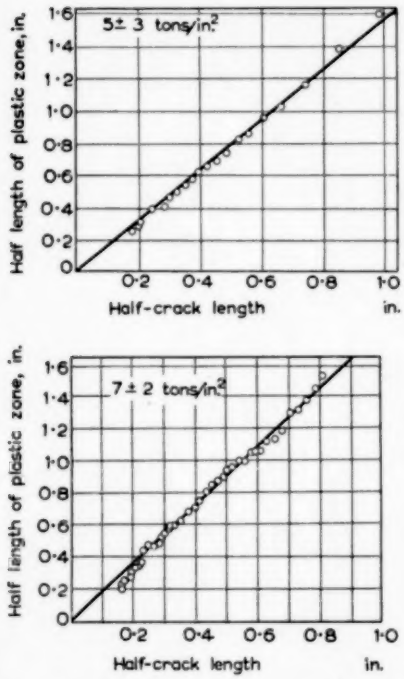

Fig. 4. Length of plastic zone *v* crack length for mild steel sheet (MBPQ).

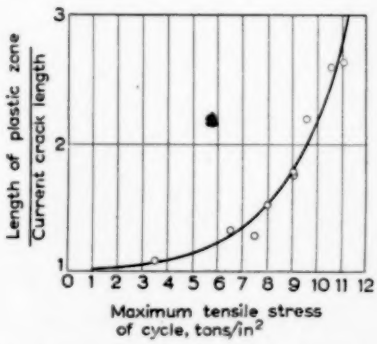

Fig. 5. Ratio of length of plastic zone to crack length for mild steel sheet (MBPQ).

With the tests at 10 tons/in² mean stress a plastic zone and small dimples in the surface around the tip of the initial slit were observed as soon as the load was applied. The plastic zone spread rapidly across the sheet as the crack grew, presumably due to the fact that the whole sheet was on the point of yielding. It appears, however, to be firmly established that for the cases where the remaining area remains sensibly elastic the plastic zone dimensions are directly proportional to the current crack length. Thus the plastic zone does not introduce an independent length parameter, and the hypothesis that geometrical similarity is maintained receives the strongest support from the experimental observations.

It is interesting to re-examine the equation obtained by HEAD (1953) referred to in Section 2. If the parameter a, representing the width of the plastic layer adjacent to the growing crack, is taken to be proportionate to the crack length then it is immediately obvious that the rate of growth is also proportionate to the crack length.

9. Analysis of Crack Growth Curves

From the preceding sections the geometrical similarity hypothesis leads directly to the relations

$$\left.\begin{aligned} dl/dN &= kl \\ \ln (l/l_0) &= kN \end{aligned}\right\} \qquad (1)$$

where N is in millions of cycles, and l_0 is the initial half crack length. Hence a linear relation should be obtained between $\log l$ and N. However, until the stress dependence of the growth has been obtained experimentally, it is not possible to

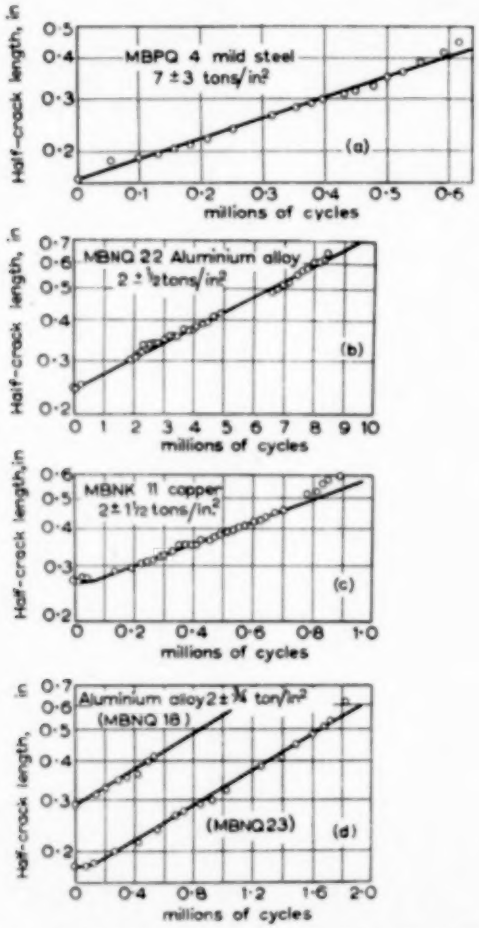

Fig. 6. Curves of crack growth (a), (b) and (c) examples of steady growth, (d) example of growth at same stress for different initial lengths.

determine how long the crack can grow before any stress increase due to the reduction in area of the specimen affects the results. This problem is one of the generic type in which a plastic deformation is contained within surrounding elastic material

of finite extent. The experimental approach was to take careful observations over a range of crack lengths to determine the point at which the presence of the boundaries first began to affect the rate of growth. It was found that, while the total length of crack was less than about one eighth of the sheet width, the disturbing effect due to the finite width was quite small. This agrees well with the simplified analysis given later. With this restriction, the half-crack length measured from the sheet centre-line gave straight lines when plotted against number of cycles. Typical curves are shown in Figs. 6 and 7.

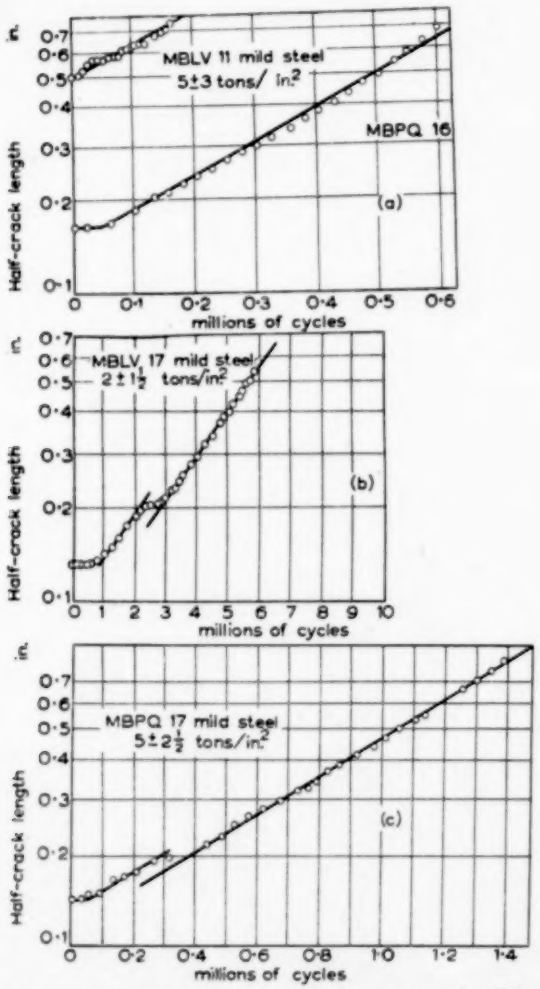

Fig. 7. Curves of crack growth : (a) example of growth at same stress for different initial lengths, (b) and (c) examples of ' dormant ' period in growth curve.

These curves clearly show an important feature which tends to be masked on the orthodox growth curves. Periods occur in the life during which the rate of growth decreases, sometimes quite abruptly and in some cases ceasing altogether,

after which the growth continues at its original rate as though the 'dormant' period had never existed. This is exemplified by the parallel lines which have been drawn through the plotted experimental points. The number of dormant periods and their duration in any one test appears to be absolutely random except that they are more prevalent and prolonged at the lower stresses (as would be expected). In the extreme case this leads to the formation of non-propagating cracks, which are discussed later in Section 10. Clearly, any law of continuous growth deduced from data obtained during this phase would not give a satisfactory representation of the process. These dormant periods explain the apparently paradoxical results of some of the tests. For example, a test at $10 \pm 2\frac{1}{2}$ tons/in^2 had a longer life than the test at $5 \pm 2\frac{1}{2}$ tons/in^2 due to the long dormant period that existed in the former test. This slowing down or stopping of the crack during these periods cannot be due to the fortuitous occurrence of some hard constituent in the material just ahead of the crack as both cracks on any one specimen tend to exhibit the same behaviour at the same time. Both metallurgical examination and micro-hardness tests have failed to reveal anything peculiar about the material just ahead of a non-propagating crack.

Table 2. *Values of coefficient k*

Stress (tons/in^2)	*k*	*Stress* (tons/in^2)	*k*
Mild steel		10 ± 3	3·961
		10 ± 4	5·296
2 ± 1	0·127		
$2 \pm 1\frac{1}{2}$	0·325		
$5 \pm 1\frac{1}{2}$	0·410	*Aluminium alloy*	
$5 \pm 1\frac{3}{4}$	0·447	$2 \pm \frac{1}{2}$	0·114
5 ± 2	0·548	$2 \pm \frac{5}{8}$	0·363
$5 \pm 2\frac{1}{2}$	1·379	$2 \pm \frac{3}{4}$	0·670
5 ± 3	2·409	2 ± 1	1·204
5 ± 4	4·732	$4 \pm \frac{1}{4}$	0·079
$7 \pm 1\frac{1}{2}$	0·152	$4 \pm \frac{1}{2}$	0·184
7 ± 2	0·951	$4 \pm \frac{3}{4}$	1·711
$7 \pm 2\frac{1}{2}$	1·232	4 ± 1	2·141
7 ± 3	1·488	$4 \pm 1\frac{1}{2}$	10·085
$7 \pm 3\frac{1}{2}$	2·240	4 ± 3	90·262
7 ± 4	5·929		
7 ± 5	9·164		
10 ± 1	0·385	*Copper*	
$10 \pm 1\frac{1}{2}$	0·145	2 ± 1	0·543
10 ± 2	0·587	$2 \pm 1\frac{1}{4}$	0·599
$10 \pm 2\frac{1}{2}$	1·877	$2 \pm 1\frac{1}{2}$	0·843

However, apart from these dormant periods, Figs. 6 and 7 clearly show that a linear relation exists between the logarithm of the crack length and the number of cycles for the initial portion of the growth. For tests carried out at the same applied stresses, but with differing initial slit lengths, parallel lines are obtained with different intercepts on the ordinate axis. Of the three materials tested,

the results for the mild steel and annealed copper are particularly affected by the dormant periods. Future work is directed towards obtaining and subsequently testing materials which do not exhibit this phenomenon. Such materials should give $\log l$ vs. N curves free from any discontinuities.

From the foregoing remarks it will be appreciated that only one definite numerical value can be derived from a test of this kind, namely, the gradient k of the straight line relation (note that this constant assumes natural logarithms). This fact suggests a concise and, at the same time, comprehensive way of presenting the test results. The values of the coefficient k are given in Table 2. When these values were plotted against alternating stress they were found to increase sharply with stress, suggesting a power law. Therefore, $\log k$ was plotted against log (alternating stress). Straight line relations were obtained as shown in Fig. 8. For the mild steel, it appears that all the points lie scattered about a single line, showing that for this material the mean stress has little influence on the rate of growth. For the aluminium alloy there appears to be a fairly distinct response to mean stress as two parallel lines are obtained. These graphs suggest that the coefficient k can be related to the alternating stress σ by

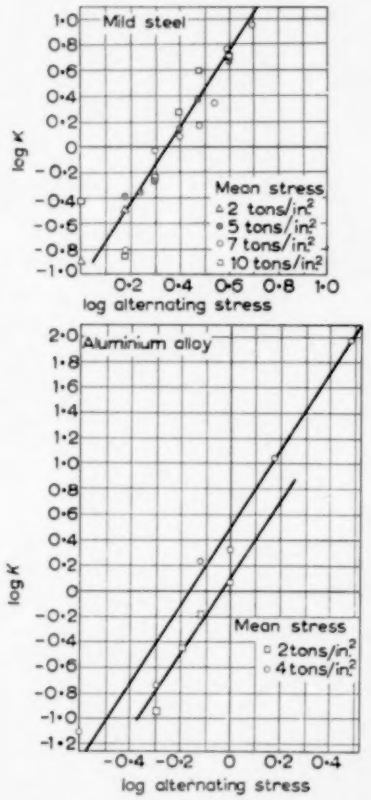

Fig. 8. Values of rate of growth coefficient k plotted against alternating stress.

$$k = \frac{\sigma^n}{N_s}, \tag{2}$$

where n and N_s are constants. The physical meaning of the constant N_s is apparent from equation (1). It is the number of cycles (millions) required to cause the crack to grow to 2·718 times its original length when an alternating stress of 1 ton/in^2 is applied to the sheet.

For mild steel (all values of mean stress)

$$k = \frac{\sigma^3}{11{\cdot}6}.$$

For aluminium alloy (2 tons/in^2 mean stress)

$$k = \frac{\sigma^3}{0{\cdot}775}.$$

For aluminium alloy (4 tons/in^2 mean stress)

$$k = \frac{\sigma^3}{0{\cdot}331}.$$

It is interesting to note that the index n is equal to 3 for both materials. Whether or not it is the same for other materials will have to await further experimental work. It must be noted that the relations are of course based on a steady rate of growth and are not applicable when there are dormant periods. The use of such formulae will therefore give lives that are on the safe side in estimates of endurance.

The presence of a distinct effect of mean stress for aluminium alloy, and the apparent absence of such an effect for mild steel, is very interesting both from a practical and a theoretical point of view. At the moment, two explanations based on different properties of these materials seem to be quite plausible. The stress–strain curve for normalized mild steel shows a definite yield point and, when this is passed, the material flows for a little while at constant stress. When the mean stress on a cracked mild steel specimen is increased, the plastic zone increases in size by an amount governed by the straining of the surrounding elastic material. However, as the stress within this zone is equal to the yield stress, the increase in the externally applied stress is not transmitted directly to the tip of the crack. Another explanation is based on strain hysteresis. It is possible that in a small region around the tip of a crack, considerable inelastic strain occurs, otherwise extremely high stresses would exist. This material is constrained to follow a certain cycle of strain imposed upon it by the straining of the surrounding elastic material. Therefore, when a mean stress is externally applied to the sheet, it may be possible for the material within this inelastic zone to relax under the influence of cyclic straining until the mean stress acting throughout the zone is greatly diminished. Mild steel shows a pronounced hysteresis effect while age-hardened aluminium alloy shows relatively little (Forrest 1956). These suggestions are only tentative, and it is hoped that further comparative tests with various selected materials will throw more light on the matter.

10. Non-Propagating Cracks

As already stated, it is possible at the lower stresses for a crack to grow a short distance and then stop. In a few tests no crack was observed while the specimen was in the testing machine but on subsequent microscopic examination of the polished and etched surface, at magnification of up to $\times$ 500, small cracks were observed. Non-propagating cracks were found in both steel and copper specimens but not in any of the aluminium alloy specimens. A typical photomicrograph is shown in Fig. 9.

It is interesting to note that the non-propagating cracks ended in a fork. The formation of non-propagating cracks in 0·3 in. thick mild steel plate specimens containing edge notches has been discussed by Frost and Dugdale (1957a). For that type of specimen there was no indication that the non-propagating crack ended in a fork. Earlier work on round bar specimens with circumferential grooves (Frost 1955, 1957) again showed no sign of non-propagating cracks ending in a fork. Further experimental work is necessary, however, before it can be decided

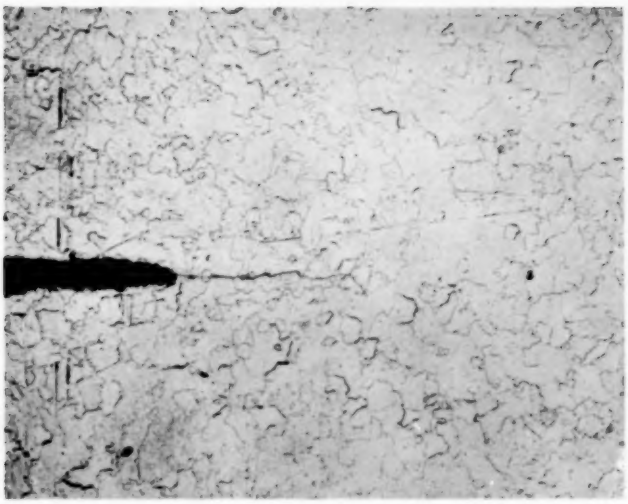

(a)

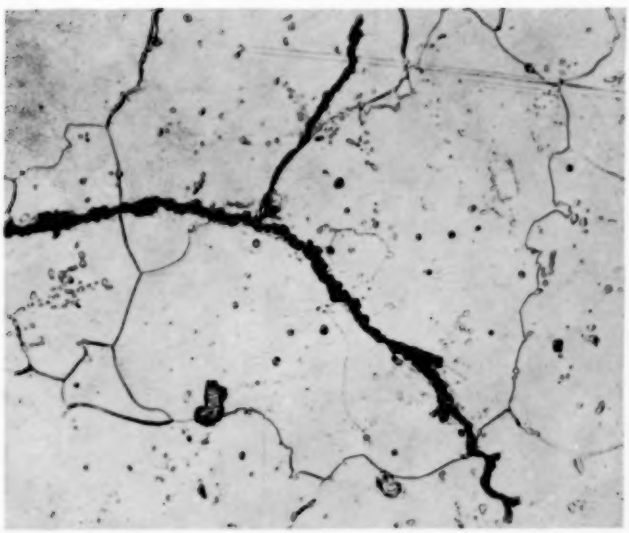

(b)

Fig. 9. Photomicrographs of non-propagating crack in mild steel specimen (MBLV) after 12×10^6 cycles at $2 \pm 1\frac{1}{4}$ tons/in^2. (a) $\times$ 50 ; (b) enlarged view of end of crack $\times$ 500.

whether the non-propagating cracks in the sheet specimens necessarily end in a fork. FROST and DUGALE (1957) also stated that cracks would spread in mild steel if the maximum tensile stress in the cycle exceeded $3\frac{1}{4}$ tons/in^2 over a range of mean stress from 2 tons/in^2 tension to 2 tons/in^2 compression. The present work shows that in thin mild steel sheet specimens it is certainly possible to have a non-propagating crack at $5 \pm \frac{1}{2}$ tons/in^2, i.e. at a maximum tensile stress of $5\frac{1}{2}$ tons/in^2.

11. MISCELLANEOUS REMARKS

For the reasons stated, rigorous analysis has been restricted to overall crack lengths of the order of one eighth of the sheet width. However, previous workers have attempted to analyse the whole of the crack growth data up to complete fracture of the specimen. This has been done either by a purely empirical approach or by attempting to correct the applied nominal stresses to allow for the reduction

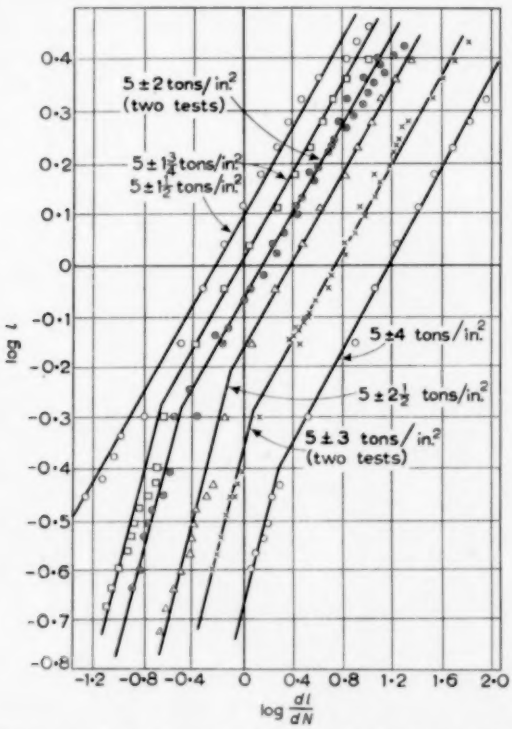

Fig. 10. Log (rate of growth) plotted against log (half-crack length) for mild steel.

in area of the specimen as the crack grows. The work of WEIBULL (1954, 1956) mentioned in Section 2 is an example of the latter type. WEIBULL concluded that if the nominal stress across the remaining section was kept constant the rate of growth was independent of crack length. It is possible to make a rough analysis for these conditions. Taking $A = 1$ (Section 3), equation (1) transforms to

$dN/dx = (1 + x)^n/x$ where x = crack length/sheet width, provided powers of x higher than 3 are neglected. From Section 9, n may be taken equal to 3; on integrating this equation, noting that $x = 0{\cdot}12$ when $N = 0$ (Weibull's initial condition), N plotted against x was found to give a curve with a long straight portion. The inference is that these lines happen to be straight because of the particular test conditions.

A typical example of the empirical approach for the present tests is shown on Fig. 10. This shows $\log(dl/dN)$ plotted against $\log l$, dl/dN being obtained geometrically from the growth curves. Reasonably straight lines are obtained up to crack lengths of well over half the sheet width. There is a discontinuity in the lower part of the curves where the slope of the line becomes equal to unity corresponding to equation (1). Such methods are of course only approximate and, it must be emphasized, have no general application, as they are completely dependent on the particular test conditions.

It is hoped that, when more work has been done on the stress dependence of the coefficient k in (2), it may then be possible to predict the whole of the crack growth curve although theoretical difficulties appear formidable.

The suggestion is sometimes made that the process of fatigue of a plain specimen can be thought of as the spreading of a very small crack which either forms almost immediately the test starts or previously existed in the virgin material. Consider the mild steel and aluminium alloy plain specimen tests mentioned in Section 5 and select a stress range above the fatigue limit; then, for the mild steel at a stress of 10 ± 6 tons/in^2, the endurance was 3×10^6 cycles while for the aluminium alloy at 8 ± 6 tons/in^2 the endurance was 1×10^6 cycles. From (2) the coefficient k has the values 18·6 and 650 respectively. If failure is considered to have occurred in the plain specimen when $l = 1$ in. then the life can be calculated from (1). For the crack to be propagating for 100 per cent of the life the initial lengths would need to be 10^{-24} and 10^{-280} in. for the mild steel and aluminium alloy, respectively. These values must be considered most improbable. It is more realistic to note that about 12 per cent and 1 per cent of the respective mild steel and aluminium alloy endurances would be spent in propagating a crack from an initial size of 10^{-3} in.

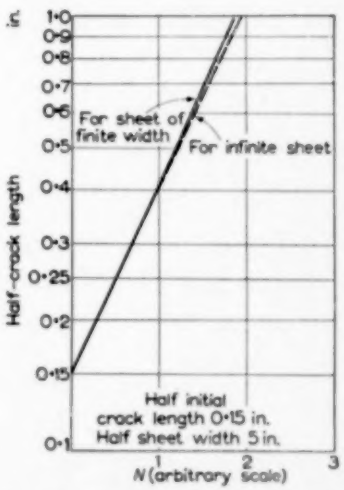

Fig. 11. Theoretical curves of crack growth.

It is interesting to consider the strength reduction factors of the sheets containing central slits. Although the definition of the strength reduction factor is ambiguous when mean stresses are involved, comparison with the plain specimen values given in Section 5 shows that apparently large reductions in strengths are obtained. As the mean stress values were not the same for both plain and slitted specimens the values must be considered approximate. The values of the fatigue limit and strength

reduction factors are given in Table 3. The strength reduction obtained with the aluminium alloy is particularly severe.

TABLE 3

Material	*Mean stress* (ton/in^2)	*Fatigue limit* (tons/in^2)	*Strength reduction factor*
Mild steel	10	$\pm \frac{1}{2}$	5 – 11
	7	± 1	
	5	± 1	
	2	± 1	
Aluminium alloy	4	$< \pm \frac{1}{4}$	10 – 25
	2	$\pm \frac{1}{2}$	
Copper	2	$\pm \frac{3}{4}$	4

Finally, the foregoing methods of analysing crack growth offer a means of predicting the length of crack at which effects of the sheet width become noticeable. If the local stresses near the tip of the crack are increased by a factor $1 + A\,(l/b)^2$, and the growth is accelerated according to stress raised to the power n, then (1) gives $dl/dN = l\left[1 + nA\,(l/b)^2\right]$ when constants are omitted. Hence $N = \ln\,(l/l_0) - nA\,(l^2 - l_0^2)/2b^2$, where l_0 is the length of crack when $N = 0$. This function is plotted in Fig. 11, for $A = 1$, $n = 3$, $l_0 = 0{\cdot}15$ in., $b = 5$ in. It can be seen that the error is negligible if the part of the curve $l < 0{\cdot}6$ in. is considered. This agrees with the experimental observations.

12. Conclusions

(1) The experimental results suggest that, up to overall crack lengths of about one eighth of the specimen width, the rate of growth is proportional to the current crack length.

(2) Crack growth may be erratic and dormant periods can exist ; at the lowest stresses non-propagating cracks may be obtained. This leads to difficulties in the formulation of any single law of continuous growth over the entire range of crack length.

(3) In the suggested basic equations of steady crack growth, $dl/dN = kl$ and $\ln l/l_0 = kN$, the coefficient k can be expressed as $k = \sigma^n/N_s$ where σ is the alternating stress and N_s a constant depending on material and mean stress. If was found that $n = 3$ for both the mild steel and the aluminium alloy irrespective of the mean stress. The value of N_s was not affected by mean stress for the mild steel but a dependence upon the mean stress was found for the aluminium alloy.

(4) Where measurements of the length of the plastic zone ahead of the crack were made these showed that geometric similarity of the crack length and plastic zone dimensions was maintained up to the point where the latter extended almost across the sheet.

Acknowledgments

The authors acknowledge the help of Mr. K. Denton and Miss M. McCallum with the experimental work and also the interest of Mr. C. E. Phillips (Head of the Mechanics and Materials Division). The work has been carried out as part of the research programme of the Mechanical Engineering Research Board of the Department of Scientific and Industrial Research. The paper is published by permission of the Director of Mechanical Engineering Research.

References

Bennet, J. A.	1946	*Proc. Amer. Soc. Test. Mater.* **46**, 693.
De Forrest, A. V.	1936	*J. Appl. Mech.* **58**, A23.
Forrest, P. G.	1956	*Int. Conference on Fatigue of Metals.* Institute of Mechanical Engineers.
Frost, N. E.	1955	*Engineer, Lond.* **200**, 464 and 501.
	1957	*Aeronaut. Quart.* **8**, 1.
Frost, N. E. and Dugdale, D. S.	1957a	*J. Mech. Phys. Solids* **5**, 182.
	1957b	*D.S.I.R., M.E.R.L. Report* PM 218.
Frost, N. E. and Phillips, C. E.	1956	*Proc. Instn. Mech. Engrs., Lond.* **170**, 713.
Head, A. K.	1953	*Phil. Mag.* **44**, 925.
Howland, R. C. J.	1930	*Phil. Trans.* A **229**, 49.
Hyler, W. S., Abraham, E. D. and Grover, H. J.	1956	*N.A.C.A. Tech. Note* 3685.
Lessels, J. M. and Jacques, H. E.	1950	*Weld. J., Lond. (Research Supplement)* **15**, 75s.
Moore, H. F.	1927	*Univ. of Illinois Eng. Exp. Station, Bulletin* No. 165.
Timoshenko, S. and Goodier, J. N.	1951	*Theory of Elasticity* (McGraw-Hill, New York).
Weibull, W.	1954	*Saab Aircraft Co., Tech. Note* 25.
	1956	*Aero. Res. Inst. Sweden, FFA Report* 65.
Wells, A. A.	1955	*B.W.R.A Eng. Research Station.*

Journal of the Mechanics and Physics of Solids, 1958, Vol. 6, pp. 111 to 126. Pergamon Press Ltd., London

THE BASAL SLIP IN ZINC UNDER STATIC AND DYNAMIC LOADING

By T. Vreeland, Jr., D. S. Wood and D. S. Clark
Division of Engineering, California Institute of Technology

(*Received 2nd August*, 1957)

Summary

This paper presents the results of an investigation of static and dynamic shear behaviour of two purities of zinc single crystals. All the crystals tested were in the form of cylindrical rods with the [0001] crystallographic direction parallel to the rod axis. The static tests were performed by applying simple transverse shear loading in one of the slip directions to one end of the crystals with the other end of the crystals rigidly clamped. The static shear stress vs. shear strain relations are obtained from these tests. The dynamic tests were conducted by suddenly stopping (within a period of about 25×10^{-6} sec) one end of the crystals which were moving in the slip direction with various velocities. The resulting waves of plastic shear deformation which propagate from the stopped ends of the crystals toward the free ends are analysed. The analysis is based upon the assumption that elastic strains may be neglected in comparison with the plastic strains. The use of the results of this analysis in conjunction with measurements of the permanent lateral deflections of the crystals resulting from the dynamic tests leads to the determination of dynamic shear stress vs. shear strain relations.

The results of this study show that the stress required to produce a given permanent basal shear strain in single crystals of zinc is considerably greater under the dynamic conditions employed than under static conditions. This stress decreases with increasing temperature.

1. Introduction

The behaviour of metals and alloys under dynamic loading conditions has received considerable attention in recent years. Many of these investigations have shown that, for a polycrystalline material, the stress for a given strain in a dynamic test is somewhat greater than the static stress for the same strain. The stress–strain behaviour of the material could be determined in only a few of these investigations. Careful attention must be given to the shape of the specimen, the boundary constraints, and the method of loading in order that the stress–strain behaviour may be deduced from the results of a dynamic test.

Taylor (1948) devised a method of determining the dynamic yield stress of a flat-ended projectile by the use of a theory of wave propagation in a rigid–plastic solid. Lee and Tupper (1954) applied the theory of von Kármán (1950) to obtain the deformation a flat-ended projectile composed of a material for which the dynamic stress–strain curve was known. An analysis based on a rigid–plastic approximation of the stress–strain relation was also employed. The results obtained with both theories were shown to predict the experimentally determined deformations satisfactorily. The propagation of strain in a rigid–plastic solid is relatively simple to describe because elastic strain waves in such a material travel with an infinite velocity and the interaction between elastic and plastic strain waves may be treated as a continuous process.

The propagation of plastic strain under dynamic conditions in single crystals has received relatively little attention. KRAMER and MADDIN (1952) investigated the initiation of slip in short duration impact tests on single crystals. A delay time for the initiation of slip was observed at temperatures below room temperature in β-brass, but none was observed in α-brass and aluminium. LIU *et al.* (1956) determined the critical resolved shear stress in short duration impact tests on copper, zinc, and β-brass. Crystals of zinc and β-brass were found to exhibit a definite increase of critical resolved shear stress at temperatures below room temperature when the stress duration was decreased below 10^{-3} sec. This phenomenon was not observed in the tests on single crystals of copper.

The difference between the static and dynamic stress–strain relations of a material may be attributable to several mechanisms. If the deformation process requires or is aided by thermal activation, the deformation process would be time dependent and this would give rise to different static and dynamic behaviour. If there is some limiting speed at which the deformation process can proceed, different static and dynamic behaviour could result. The limiting speed of dislocation travel through a crystal lattice, which is theoretically less than the shear wave velocity in the lattice, is one example of a mechanism by which the speed of the slip process may be limited.

A careful analysis of the factors involved in the dynamic testing of single crystals has indicated that it is desirable to use a stress system that is oriented properly with respect to the deformations produced in the crystal. If this proper orientation is not maintained, the deformation produced by the stress system may cause a considerable change in the stress and thereby complicate an analysis of the stress history of the crystal. Hence it is important to obtain crystals for the dynamic tests in which the desired deformations may be oriented properly with respect to the applied stress.

In view of these considerations an investigation has been made of static and dynamic slip in zinc single crystals. Zinc was chosen because it was anticipated that suitable single crystals could be prepared with relative ease and because plastic deformation may be limited to the one set of [0001] crystallographic planes which have a relatively low critical shear stress for slip. Furthermore, the work of LIU *et al.* indicates that zinc exhibits a definite difference in static and dynamic slip behaviour.

The purpose of this paper is to present the results of an experimental investigation of the static and dynamic slip behaviour of zinc single crystals with specific reference to the stress–strain relations.

2. MATERIAL

Two purities of electrolytic zinc were purchased from the New Jersey Zinc Company which are reported to have the following typical impurity content in percentages :

Impurity	99·99 + *purity*	99·999 + *purity*
Iron	0·003	0·0003
Lead	0·0007	0·0007
Cadmium	0·003	0·00005
Copper	0·001	0·00005
Arsenic	—	0·000004
Tin	0·001	0·00005
Total impurities	0·01	0·001

The single crystals were grown from the melt in precision bore Pyrex tubes, $\frac{1}{2}$ in. in diameter (VREELAND *et al.* 1955). The completed zinc crystals are rods $\frac{1}{2}$ in. in diameter and approximately 20 in. long with the basal, [0001], plane perpendicular to the rod axis [$\pm 1°$]. The 99·99 + per cent purity zinc was in contact with air during melting and growth of the single crystal rods while the 99·999 + per cent purity zinc was protected by a helium atmosphere. The specimens employed in the tests of this investigation were all taken from one of two original single crystal rods, one rod of each of the two grades of zinc used.

Some zone refining of the zinc takes place in the crystal growing process. Specimens taken from the middle portion of single crystal rods exhibit comparable mechanical properties, while the bottom and top portions may have different properties due to the differing impurity content produced by the zone refining. Specimens taken from the middle portion of the single crystal rods were used for the tests in this investigation.

Both of the crystal rods contained a substructure consisting of a network of small angle dislocation boundaries. The crystallographic orientation of the lattice on opposite sides of these boundaries differed by a maximum angle of 10^{-2} radian. There was a slight variation of the distribution of the substructure along the length of each crystal rod, but this variation was less than that observed by comparing the two crystal rods.

3. Static Tests

Test specimens

The single crystal rods were cleaved or acid-sawed into segments approximately $\frac{3}{8}$ in. long. These segments were annealed at a temperature of 750°F (400°C) for one hour in a protective atmosphere. Pure dry hydrogen was used as the atmosphere for the 99·99 + per cent purity zinc, and helium was used for the 99·999 + per cent purity zinc. Two copper pieces, 1 and 2 in. long and $\frac{1}{2}$ in. in diameter, were cemented with Epon VI to the ends of the segment forming the test specimen. The coefficient of thermal expansion of the copper is nearly the same as that of the zinc single crystal in the radial direction, therefore only negligible radial thermal stresses are produced when the temperature of the assembly is varied. Cementing the segment to copper is preferable to clamping the segment in a fixture because clamping stresses may induce undesirable deformations of the crystal.

A slip direction of the crystal was located, either by observing the direction, $[11\bar{2}0]$, of a twin trace on a basal plane, or by observation of the cylindrical surface of the crystal after etching. The etchant preferentially attacks the different crystallographic planes thus revealing the sixfold symmetry of the hexagonal crystal. All specimens were polished and etched prior to testing. The etchant consisted of equal parts of hydrochloric acid and water. The crystals were polished chemically with a mixture of 200g CrO_3, 15 g Na_2SO_4 10 H_2O, and 1000 ml H_2O.

Static testing

The static tests on the crystal specimens were made by clamping the copper piece on one end of the crystal and applying a transverse load to the copper piece on the other end in a direction parallel to a slip direction of the crystal. Thus a shear stress was produced on the slip plane and in the slip direction. This method of loading also produced bending stresses which act normal to the slip plane. However, these bending stresses are not sufficiently large to cause twinning and hence did not affect the results of the static tests.

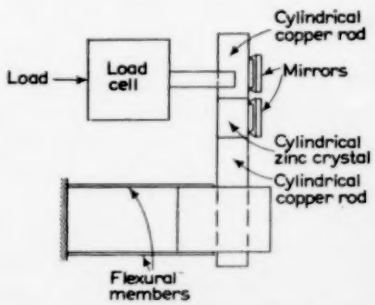

Fig. 1. Schematic diagram of static testing assembly.

The longer copper end of the specimen is clamped in the assembly shown in Fig. 1. The clamp in which the specimen is held is mounted on flexural members which assures that the axial load will be negligible. The load is applied to the shorter copper end of the specimen. This load is applied through a load-cell by means of a screw mechanism. The sensitivity of the load-cell is approximately $\pm$ 0·01 lb over the range of 0 to 50 lb that may be applied. This loading system

is relatively stiff. Thus it is suitable for detecting a definite yield point when and if it occurs, whereas the use of a dead weight or other 'soft' loading system could prevent the detection of a yield point.

The shear strain occurring in the specimens during static tests was determined by measuring the deflections of the image of a line filament reflected from a small mirror attached to the specimen. A strain sensitivity of approximately 3×10^{-5} was obtained by employing an optical lever arm of 147·4 in. and measuring the image deflections to within $\pm$ 0·005 in. The elasticity of the crystal gripping system and of the specimen produces a change in slope of the crystal surface when a load is applied. This change in slope is determined and subtracted from the total change in slope to give the plastic shear strain in the crystal. A second mirror is mounted on the copper rod above the crystal as shown in Fig. 1. Slip on the basal planes of the crystal does not produce any deflection of the image of the filament reflected by this mirror, but if twinning or slip in a direction not lying in the basal plane occurs, a deflection will be produced. Thus a means is provided for detecting the presence of undesired deformation processes, should they occur.

The static tests were made by a step-wise loading procedure in which one pound increments of load were applied at equal time intervals of 4 min. The output voltage of the load-cell bridge circuit and the lamp image deflection were determined at the end of each time interval. Static tests were made only at room temperature. Tests at higher temperatures were unsatisfactory because of creep in the cement between the specimens and the copper end pieces. Reproducable results could be obtained from repeated static tests on a given specimen by annealing the specimen at a temperature of 750°F (400°C) between tests.

Static test results

The results of the static tests are presented as shear stress–shear strain curves in Figs. 2 and 3. The degree of reproducibility of the static shear stress–shear strain behaviour of a single specimen tested twice with an intermediate anneal is shown

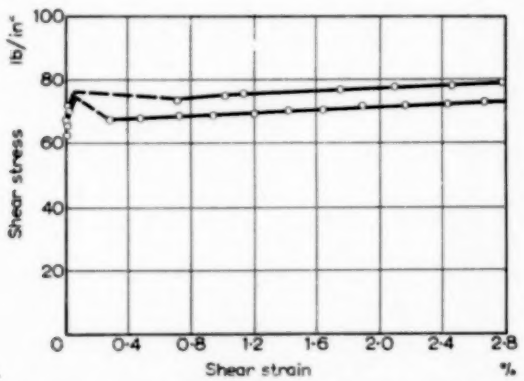

Fig. 2. Static shear stress vs. shear strain, 76°F 99·99 + per cent zinc single crystal, grown in air. (Annealed in pure, dry H_2 at 750°F (420°C) between tests, lower curve, first test.)

in Fig. 2. The elastic portions of the static stress–strain relation could not be determined in these tests because the maximum elastic shear strain in the crystals (of the order of 10^{-5}) was less than the minimum strain that can be detected in the tests. The deflection of the image reflected by the mirror mounted on the copper rod above the crystal was observed to be directly proportional to the load in all of the static tests. This result indicates that only elastic deformation and basal slip took place in the zinc single crystals. Slip steps were not detected when observations were made at a magnification of approximately 600 $\times$ on polished surfaces of crystals after permanent straining in the static tests.

A crystal of 99·99 + per cent purity zinc prepared by acid-sawing from the original crystal rod exhibited an upper yield point in the stress–strain relation. The maximum stress level attained before the occurrence of relatively rapid strain

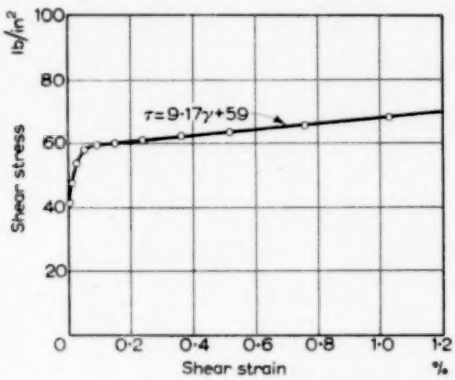

Fig. 3. Static shear stress vs. shear strain, 80°F 99·999 + per cent zinc single crystal, grown in helium.

is indicated by the junction between the solid and dashed lines in Fig. 2. The screw of the loading mechanism was turned in an attempt to apply additional load after the onset of rapid strain in these tests so that the first stress after the upper yield point does not represent the lower yield stress.

An upper yield point was not observed in a test of a specimen from the same original crystal when the ends of the specimen had been cleaved instead of acid-sawed. The strain produced by cleaving and the effect of small twin bands that are formed in cleaving are probably responsible for the suppression of the static upper yield point in the cleaved specimens. The static tests on a crystal of 99·999 + per cent purity zinc with acid-sawed ends did not exhibit an upper yield point. The minimum stress at which plastic deformation could be detected, for convenience called the ' elastic limit ' stress in this paper, was determined to be approximately 40 lb/in^2 and 60 lb/in^2 for the 99·999 + per cent purity zinc and the 99·99 + per cent purity zinc crystals respectively.

4. Dynamic Tests

Method of testing

The dynamic loading for this investigation was accomplished by means of impact in which the loading is produced by the inertia of the test specimen. Initially, the specimen is moving with a uniform velocity of translation in a direction perpendicular to its cylindrical axis (*c* axis of the hexagonal crystal lattice) and parallel to one of the slip directions in the basal plane. One end of the specimen is suddenly brought to rest (ideally in zero time, but in practice within about 25 $\times$ 10^{-6} sec) in such a way that the end is prevented from attaining any rotational motion. The other end of the specimen is free at all times.

The resultant dynamic loading of the crystal specimen consists of both shear and bending waves propagating away from the fixed end. The normal stresses acting on the basal planes of the crystal which are associated with the bending waves do not produce basal slip since they do not produce a shear stress in the crystallographic slip direction. These bending stresses may produce twinning deformation since they produce a resultant shear stress in the twinning direction.

However, in the present experiments the lengths of the specimens were chosen short enough in relation to the impact velocities employed that negligible amounts of twinning, if any, were produced.

The shear wave produced by the impact consists of both elastic and plastic strains. The elastic shear strains are very small in comparison with the plastic shear strains. Therefore the process of dynamic shear deformation of the specimens can be analysed to a good approximation by neglecting the elastic strains. That is, a rigid–plastic approximation of the shear stress vs. shear strain relation is employed in the analysis which follows along lines similar to those employed by TAYLOR (1948).

The details of the analysis of the dynamic shear deformation process pertaining to the present experiments are given in the next section. The results of the analysis provide a means for predicting the amount and distribution of permanent shear deformations along the crystal specimens if the shear stress vs. shear strain relation for the crystals is known. The results of the analysis may also be used in inverted form to deduce the dynamic shear stress vs. shear strain relations for the crystals from experimental measurements of the permanent shear deformations resulting from the tests. The latter process involves the additional assumption that all elements along the length of a given crystal followed the same shear stress vs. shear strain relation during the dynamic deformation process. This implies that the dynamic shear stress vs. shear strain relation is independent of time or strain rate. Although this cannot be exactly correct if the dynamic stress–strain relation differs from the static relation, the dynamic stress–strain relation obtained with the aid of the analysis should provide a good first approximation, valid for total times of loading of the order of those existing in the experiments, namely, the times of the order of 10^{-4} sec.

Analysis of dynamic shear deformation

The deformation of a material with a single set of parallel active slip planes will be considered. The material will be assumed to behave as a rigid–plastic solid, that is, the material exhibits no elastic strain under load, but may exhibit plastic shear strain on the one set of active slip planes. The shear stress vs. shear strain relation for the active slip planes may be termed rigid–plastic. The minimum shear stress which produces plastic deformation in a specimen not previously deformed will be designated as τ_e, and will be called the 'elastic limit'. It will be assumed that τ_e is independent of time (no load-rate or strain-rate effects), and is the same for each slip plane in the material. The slip planes are assumed to be sufficiently close together so that the strain may be taken as continuously distributed along a specimen. The material may exhibit workhardening.

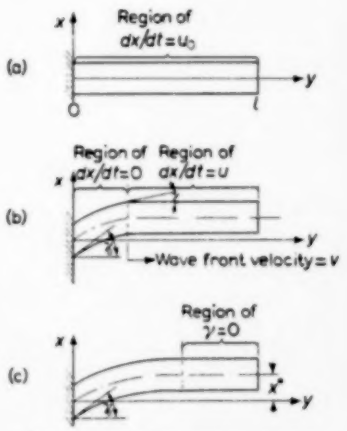

Fig. 4. Dynamic test geometry. (a) Initial conditions : $\dot{x} = 0$ at $y = 0$, $\dot{x} = u_0$ for $0 < y < l$. (b) Propagation of wave front. (c) Final specimen geometry.

Consider a cylindrical specimen with all slip planes perdendicular to the cylindrical axis of the specimen, as shown in Fig. 4(a). This axis will be designated the y axis. The specimen is initially travelling with a uniform velocity u_0 in the x-direction which is perpendicular to the y-axis. The slip plane at $y = 0$ is suddenly brought to rest at time $t = 0$. This will cause a wave of plastic shear strain to be initiated at $y = 0$, which will propagate along the specimen in the y-direction. At any stage during the period of wave propagation the material

behind the wave front is at rest, the shear stress immediately ahead of the wave front is τ_e and the material ahead of the wave front has suffered no deformation. It is assumed that the stress is distributed uniformly over each slip plane. As the wave front propagates along the specimen, the particle velocity of the rigid section ahead of the wave is progressively decreased due to the action of the stress τ_e. Finally the remaining rigid section ahead of the wave is brought to rest, at which time the amplitude of the wave has decreased to zero, and no further motion or deformation takes place.

The magnitude of the shear strain, γ, immediately behind the wave front at any instant during the period of wave propagation may be obtained from the equation of continuity written for a longitudinal element of the specimen while the wave front traverses it. The result is

$$\gamma = \frac{dx}{dy} = \frac{u}{v}, \tag{1}$$

where u is the lateral velocity of the rigid material ahead of the wave front, and v is the velocity of propagation of the wave front along the specimen, as shown in Fig. 4 (b).

The shear stress, τ, immediately behind the wave front may be obtained from the momentum equation for the element as the wave front passes over it. This momentum equation may be written as

$$\rho u \, dy = (\tau - \tau_e) \, dt$$

or

$$\rho u v = \tau - \tau_e, \tag{2}$$

where ρ is the mass density of the material, and t is the time.

Equations (1) and (2) may be combined to give

$$v = \sqrt{\frac{\tau - \tau_e}{\rho \gamma}}, \tag{3}$$

and

$$\rho u^2 = (\tau - \tau_e) \, \gamma. \tag{4}$$

When u is set equal to the impact velocity, u_0, τ and γ take the values $\tau(\gamma_0)$ and γ_0 respectively, which are the values pertaining to the impacted end of the specimen at $y = 0$.

An expression relating the particle velocity of the rigid section, u, to the time, t, and the instantaneous position of the wave front, y, may be obtained from the equation of motion of the rigid section. This equation may be written as

$$\rho (l - y) \frac{du}{dt} = - \tau_e, \tag{5}$$

where l is the total length of the specimen. Since

$$\frac{du}{dt} = u \frac{du}{dx} = \tfrac{1}{2} \frac{d}{dx} (u^2),$$

(5) may be written in the form

$$\rho d (u^2) = - 2 \tau_e \cdot \frac{dx}{l - y}. \tag{6}$$

Using (1) and (4) to eliminate u^2 and dx from (6), the following relation is obtained:

$$\frac{d\{(\tau - \tau_e)\gamma\}}{\tau_e \gamma} = -2\frac{dy}{l-y}. \tag{7}$$

When the right-hand side of this relation is integrated over the range from $y = 0$ to the instantaneous position of the wave front at $y = y_1$, the left-hand side must be integrated over the range of plastic strains from γ_0, the value of strain at $y = 0$, to γ_1, the value of strain at the position y_1. Therefore

$$\int_{\gamma_0}^{\gamma_1} \frac{d\left\{\left(\frac{\tau}{\tau_e} - 1\right)\gamma\right\}}{\gamma} = 2\ln\left(\frac{l-y_1}{l}\right), \tag{8}$$

where γ_0 may be found from (4) with $u = u_0$. The distribution of plastic shear deformation along the crystal may be found by use of (8).

The solution of the plastic wave propagation problem developed above may be put into a form which will facilitate the determination of the dynamic stress–strain relation followed by the material from measurements of the permanent deflections of the specimen after the impact test. Equation (6) may be integrated directly:

$$\tfrac{1}{2}\rho\int_{u=u_0}^{u=u_1} d(u^2) = -\tau_e\int_0^{x_1}\frac{dx}{l-y}, \tag{9}$$

where u_1 is the transverse particle velocity of the undeformed portion of the specimen adjacent to the free end at the instant when the lateral deflection of that portion of the specimen is x_1. Performing the integration indicated on the left-hand side of (9) gives

$$\tfrac{1}{2}\rho(u_0^2 - u_1^2) = \tau_e\int_0^{x_1}\frac{dx}{l-y}. \tag{10}$$

The velocity u_1 may be eliminated from (10) by using (4) for the particular case $u = u_1$, $\tau = \tau_1$, and $\gamma = \gamma_1$, where τ_1 and γ_1 are the maximum values of the shear stress and the permanent strain respectively which are produced during the impact test at the section of the specimen at which the deflection is x_1. Thus

$$\begin{aligned} &\tfrac{1}{2}\rho u_0^2 - \tfrac{1}{2}(\tau_1 - \tau_e)\gamma_1 = \tau_e\int_0^{x_1}\frac{dx}{l-y}, \\ \text{or}\quad &\tau_1 = \tau_e\left[1 + \frac{1}{\gamma_1}\left\{\frac{\rho u_0^2}{\tau_e} - 2\int_0^{x_1}\frac{dx}{l-y}\right\}\right]. \end{aligned} \tag{11}$$

Considering (10) further, if u_1 is set equal to zero, the corresponding value of x_1 to be used in the equation is x^*, the lateral displacement of that portion of the specimen which remains undeformed throughout the test, as shown in Fig. 4(c). Therefore

$$\tfrac{1}{2}\rho u_0^2 = \tau_e\int_0^{x^*}\frac{dx}{l-y}, \qquad \tau_e = \frac{\tfrac{1}{2}\rho u_0^2}{\displaystyle\int_0^{x^*}\frac{dx}{l-y}}. \tag{12}$$

Experimentally determined curves of lateral deflection vs. distance from the clamped end may be used together with (11) and (12) to determine the stress–strain curve followed by the crystals. It is interesting to note that the determina-

tion of the elastic limit stress involves an integration of experimentally determined quantities.

Equipment

The equipment employed to produce the type of dynamic loading of the crystal specimen discussed above consists primarily of two hard steel bars of equal dimensions (1 in^2 cross section by 24 in. long). One end of the specimen is rigidly mounted at a position $\frac{1}{2}$ in. from the end of one of these bars with the specimen axis perpendicular to the bar axis. This bar with specimen attached is suspended as a bifilar pendulum with the bar axis horizontal. Thus any desired longitudinal velocity can be imparted smoothly by displacing the bar from equilibrium, parallel to itself, and releasing it from an appropriate position.

The second or anvil bar is placed at rest parallel to the pendulum bar in such a position that the pendulum bar impacts the anvil bar centrally and longitudinally when the pendulum bar reached the lowest position of its arc of travel. The anvil bar rests on rollers so that it is free to move off after the impact, leaving the pendulum bar at rest at its equilibrium position. A dummy specimen is mounted on the anvil bar at the end remote from the impact end in order to ensure nearly perfect symmetry of the two bars and hence nearly perfect transfer of momentum during the impact. The arrangement of the two bars is shown in Fig. 5. The multiple wire type of suspension system shown supporting the pendulum bar is such that all five of the undesired degrees of freedom of the pendulum bar are suppressed.

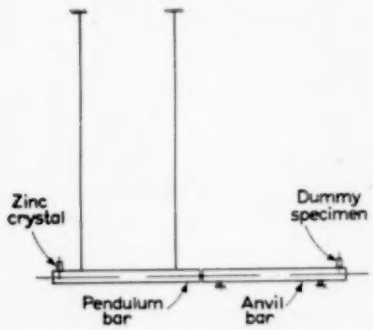

Fig. 5. Schematic diagram of dynamic test assembly.

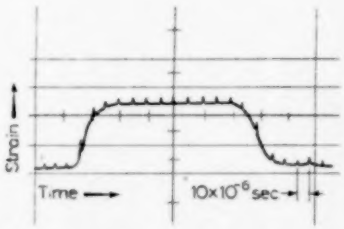

Fig. 6. Tracing of a record of longitudinal strain vs. time at the mid-point of the pendulum bar during a typical impact.

The impact between the pendulum and anvil bars produces equal longitudinal elastic strain wave fronts in each bar. These fronts propagate away from the impact surface toward the free ends of the bars at a velocity of propagation of about 2×10^{-5} in/sec (velocity of sound in long steel bars). At the free ends they are reflected as unloading wave fronts and then return to the impact surface. Following this, both bars are unstressed and no further wave fronts pass through them, but all the initial momentum of the pendulum bar has been transferred to the anvil bar.

The form of the elastic wave front in the pendulum bar is governed by the relative shapes of the impact surfaces of the pendulum and anvil bars. The impact end of the pendulum bar is lapped to a spherical radius of 5 ft, while the impact end of the anvil bar is lapped flat. This arrangement is employed for two reasons. First, it makes it possible to achieve a central impact of the two bars so that no yawing or pitching moments or bending waves are produced by the impact. Second, the relative curvature of the two impacting surfaces insures that the longitudinal impact force in the bar rises from zero to its final value in a finite time of sufficient duration that the radial modes of vibration of the bars are not excited. If such modes were to be excited, the longitudinal strain waves in the bars would exhibit an oscillatory component which might disturb the behaviour of the crystal specimen.

The form of the elastic wave front in the pendulum bar was checked experimentally by measuring the longitudinal strain-time relation at the mid-point of the pendulum bar for several different impact velocities by means of SR-4 wire resistance strain gauges and a suitable oscilloscope system. A tracing of a typical record is shown in Fig. 6. A time base is provided by superimposing a 10^5 c/s signal on the strain signal. The rise time of the strain wave is approximately 20×10^{-6} sec. No significant oscillatory strains are observed in the record. The decrease of strain to zero in Fig. 6 occurs when the wave reflected from the free end of the pendulum bar reaches the strain gauges.

The time required for the velocity of the clamped end of the specimen to decrease to zero is the time required for the strain wave to pass the specimen (20×10^{-6}) plus the time required for the wave to reach the free end of the bar and reflect past the specimen (5×10^{-6} sec). Thus, this arrangement accomplishes the desired sudden change of velocity of one end of the specimen within a period of approximately 25×10^{-6} sec. The method of mounting the specimen is designed to minimize any possible disturbances of the elastic wave front in the pendulum bar. The pendulum bar contains a tapered hole $\frac{1}{2}$ in. from its free end. A tapered copper piece to which the specimen is cemented fits this hole tightly.

The permanent lateral displacements of the crystal specimens after impact are determined by means of a cathetometer and a special fixture. The fixture holds the pendulum bar with specimen attached in a reproducible position with respect to a fixed vertical scale. The horizontal distance between the fixed vertical scale and a number of positions along a fine vertical scratch on the specimen are measured before and after the test. Lateral displacements of the specimen may be determined with this system to within $\pm 8 \times 10^{-4}$ cm. The lateral displacements of some specimens were determined to within $\pm 2 \times 10^{-4}$ cm with a microscope fitted with a filareye piece and a travelling stage for traversing the specimen.

The fixture mentioned above also incorporates an optical system which is used to detect any deformations that produce a change of the angle between the top surface of the crystal and the axis of the pendulum bar, i.e. any deformations other than basal slip. This system consists of a line filament and a lens, and mirrors. One of the mirrors rests on the top or free end of the specimens. The position of the image of the line filament reflected from this mirror and mirrors on the fixture is noted before and after test. A shift of the position of the filament image indicates the presence of deformation other than basal slip. A change of angle of 6×10^{-5} radian may be detected with this arrangement.

Dynamic test specimens

Sections of the single crystal rods were cut by acid machining into specimens of different lengths ranging from approximately 1 to 2·3 cm. The specimens were made long enough to secure measurable permanent deflection in the impact tests and at the same time short enough to prevent appreciable twinning deformation. This necessary compromise gives rise to the principal limitations upon the accuracy of results obtained and the maximum amount of basal slip which can be produced by this method of dynamic testing. This condition was found to be more severe than had been anticipated because of the relatively very large increase in shear strength of the crystals observed in the tests. One end of each specimen was attached to a tapered copper piece with Epon VI cement. The crystals were etched and polished with the same solutions used for the static specimens.

Dynamic test procedure

The pendulum and anvil bars are carefully aligned before each test to ensure central impact. The impacting surfaces are cleaned with acetone and cotton before each test in order to achieve the desired form of the elastic wave front in the pendulum bar. The copper piece cemented to the test specimen is inserted into the tapered hole in the pendulum bar with the slip direction of the crystal aligned with the axis of the bar. The copper end is then drawn into the taper by screwing a nut to a thread attached to the copper taper pin thus assuring metal to metal contact between the pin and the pendulum bar. This operation places the bottom surface of the zinc crystal level with or slightly above (1/32 in. maximum) the top surface of the pendulum bar. The pendulum bar is drawn back to a position that will give the desired impact velocity when it strikes the anvil bar. The pendulum is held in this position by a cotton string which is then burned with

a match to release the pendulum without introducing undesirable disturbances into its motion. The impact velocity is determined from a measurement of the chord of the arc through which the pendulum bar will swing and the known length of the pendulum suspension (150·25 ± 0·1 in.).

Dynamic tests were made at impact velocities of 40, 60, 80 and 114 in/sec and at temperatures of 150°, 200° and 250°F as well as at room temperature. Attempts were made to conduct tests at a temperature as high as 500°F, but the tests above a temperature of 250°F were unreliable because of deformation of the cement between the specimen and the copper piece and oxidation of the surface of the specimen. The specimens were heated by a battery of infra-red heat lamps for tests at temperatures above room temperature. Special precautions must be taken in these tests to avoid thermal stresses which might result from the expansion of the copper holding piece in the steel pendulum bar. The copper pin is placed in the pendulum bar when the bar has reached the test temperature and the copper pin is approximately 50°F cooler than the bar. The expansion of the copper pin brings the tapered surfaces into positive contact. Temperatures were maintained to within ± 2°F during the tests.

Experimental results

Curves representing measurements of permanent deflection vs. distance from the clamped end of three typical specimens tested at different impact velocities are presented in Fig. 7. The influence of temperature on the permanent deflection

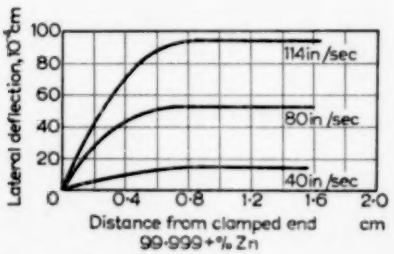

Fig. 7. Permanent deflection vs. distance from the clamped end of three specimens tested at different impact velocities, 76° F.

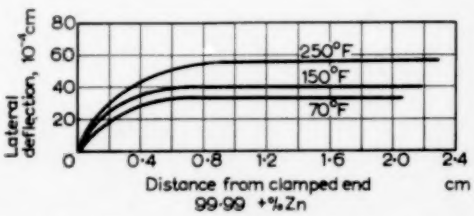

Fig. 8. Permanent deflection vs. distance from the clamped end of three specimens tested at different temperatures, 60 in/sec.

for one impact velocity is shown in Fig. 8. The permanent deflection increases with increasing temperature and with increasing impact velocity. The permanent shear strain at any point along the crystal is given by the slope of the deflection vs. distance curve at that point. The maximum strain occurs at the fixed end and the strain decreases smoothly to zero at some position between the fixed and free ends of the specimen. The data determined for the deflection vs. distance curves by means of the microscopic technique were sufficiently accurate to permit the determination of the slope of the curves with reasonable precision. Slip steps were not observed on the surface of strained crystals at a magnification of approximately 600 ×.

Measurements of the angular change between the top surface of the crystal and the axis of the pendulum bar revealed a maximum change of approximately 2×10^{-3} radian. This change of angle could be attributed to a permanent deformation of the crystal by processes other than basal slip, such as twinning, or to deformation of the copper taper pin or the cement by which the crystal was attached to the copper pin. Etching of the crystals after testing revealed small twin bands at the base of some of the specimens. These twin bands appeared on

the side of the specimen subjected to compression stresses. Twinning could not be detected on the specimen that was tested at the lowest impact velocity, namely 40 in/sec.

5. DISCUSSION

The results of the dynamic loading tests may be compared with the measured static properties of the crystals in two ways, by employing the methods of analysis of the dynamic tests previously indicated. First, the permanent lateral deflections as a function of position along the dynamically loaded crystals may be predicted on the assumption that the statically determined shear stress vs. shear strain relation applies during the dynamic tests. This may be done by employing the static stress–strain relation, $\tau = \tau_s(\gamma)$ in (4) and (8). The integration indicated in (8) is made numerically. Thus the expected distribution of permanent shear strains along the crystals are found. A simple numerical integration of these shear strain distributions then gives the predicted curves of permanent lateral deflection vs. position along the crystals.

The static stress–strain relation of Fig. 3 has been used to calculate the expected deflection vs. distance curve of a specimen of 99·999 + per cent purity zinc tested at an impact velocity of 80 in/sec. This curve is presented in Fig. 8 in dimensionless form where the values of displacement and distance are divided by the specimen length. A linear stress–strain relation, coincident with the linear portion of the static stress–strain relation was also used to calculate a deflection vs. distance curve for the same impact velocity. The effect of the difference in the low strain portion of the two stress–strain relations used to calculate the deflection vs. distance curves may be seen in Fig. 9. As would be expected, the major difference is in the portion of the deflection curve where the slope (strain) is small, and an increase in elastic limit decreases the maximum lateral deflection. An experimental deflection vs. distance curve for the 99·999 + per cent purity zinc tested at an impact velocity of 80 in/sec and at a temperature of 76°F is also shown in Fig. 9. The experimental values of deflection are considerably less than the values predicted by the analysis using the static stress–strain relation. However, the general shape of predicted curves and the qualitative dependence on impact velocity is in agreement with the experimental results.

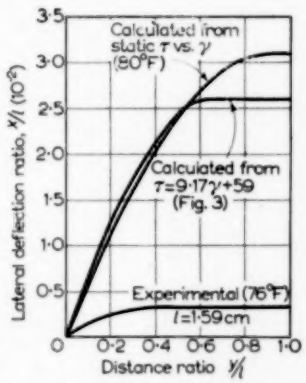

Fig. 9. Calculated and experimental lateral deflection ratio vs. distance ratio for $u_0 = 80$ in./sec., 99·999 + per cent zinc.

The duration of loading in the dynamic test, estimated by the use of the static stress–strain relation, is approximately 300×10^{-6} sec. Thus, the time required to stop the base of the specimen in the dynamic test is approximately one twelfth of the duration of loading. Therefore the implicit assumption, made in the analysis, that the velocity change of the base of the specimen takes place instantaneously, is a reasonable approximation.

These results clearly indicate that it would be necessary to use a stress–strain diagram that lies considerably above the static stress–strain relation in the analysis in order to give a deflection vs. distance curve the same as the experimental curve.

The second way in which the results of the dynamic tests may be compared with the static stress–strain relations is to calculate dynamic stress–strain relations based upon the measured permanent deflection curves by means of (11) and (12). Dynamic shear stress vs. shear strain relations caculated in this manner for the 99·999 + per cent pure zinc crystals tested at temperatures of 76° and 200°F and at impact velocities of 80 and 60 in/sec respectively are shown in Fig. 10. The static stress–strain relation for crystals of this material tested at 80°F is also shown in the figure for comparison. These results show clearly that the dynamic stress–strain relations are very much higher than the static relation. Elevated dynamic stress–strain relations have been found previously for polycrystalline metals such as aluminium by Johnson *et al.* (1953) and King *et al.* (1955). However, in the latter cases the degree of elevation of the dynamic relation above the static is much less than for the zinc single crystals of the present investigation.

Values of the apparent elastic limit stress under dynamic loading have been computed from the results of the dynamic tests by means of (12). The results of these computations for the zinc crystals of the two purities employed and for the various temperatures and impact velocities at which the tests were conducted are given in Table 1.

Table 1. *Calculated values of the elastic limit for dynamic loading tests*

Test temperature (°F)	*Impact velocity* (in/sec)	*Crystal length* (cm)	*Elastic limit* (lb/in^2)
99·99 + *purity*			
70	60	2·07	660 ± 10%
76	114	1·77	640 ± 10%
150	60	2·18	592 ± 20%
200	80	1·13	580 ± 10%
250	60	2·29	442 ± 10%
99·999 + *purity*			
76	40	1·55	430 ± 10%
76	60	1·55	395 ± 20%
76	80	1·59	547 ± 10%
200	60	1·55	200 ± 10%
200	60	2·56	358 ± 10%

The probable errors assigned to the values of elastic limit stress in Table 1 are based upon estimates of the uncertainties in the experimental measurements of lateral deflections. These uncertainties were estimated independently for each test.

These results show that there is no definite relation between the apparent dynamic elastic limit and the impact velocity in the range of 40 to 114 in/sec. However, the elastic limit stress decreases with increasing temperature. The zinc of higher purity exhibits a lower elastic limit stress than the lower purity material and the decrease with increasing temperature is greater for the higher purity material up to a temperature of 200°F.

While these values of 'elastic limit' stress are only approximate, they give definite evidence that the material does not have a unique 'elastic limit' stress since the apparent values of the dynamic elastic limit are so large in comparison with the static elastic limits. In view of this fact, the assumption used in the analysis that the material has a unique 'elastic limit' stress and stress–strain relation must be examined. The average strain rates produced by the dynamic loading are many orders of magnitude greater than the strain rates in the static tests. For example, it may be reasonably estimated that a strain of 0·1 per cent in the dynamic test occurred in a time of about 25×10^{-6} sec, i.e. the time for the change in velocity of the base of the specimen. Hence the strain rate was of the order of 40 sec^{-1}. An equal strain in the static test would be associated with a strain rate of approximately 10^{-5} sec^{-1}. Thus it may be seen that a change in the strain rate by a factor of the order of 4×10^6 produces a change in the stress level for a given strain by approximately a factor of ten. The differences in strain rate occurring at different positions along a specimen in a given dynamic test and the differences between the various dynamic tests are considerably less than the differences in strain rates between the static and dynamic tests. The actual variation in the stress–strain relation followed by different portions of a specimen in a dynamic test should therefore be relatively small compared to the variation in the stress–strain relation of the material between the static and dynamic tests.

The durations of loading in the dynamic tests from which the stress–strain relations were deduced (Fig. 10) are approximately 60×10^{-6} sec and 140×10^{-6} sec for the 76°F test and 200°F test of the 99·999+ per cent purity zinc respectively. Thus the duration of loading in these tests was approximately 2·5 and 5·5 times as long as the time required to stop the base of the specimen. The assumption of an instantaneous change in velocity which was used in the analysis is therefore not as reasonable an approximation of the actual specimen base velocity vs. time relation as would be expected if the material followed the static stress–strain relation.

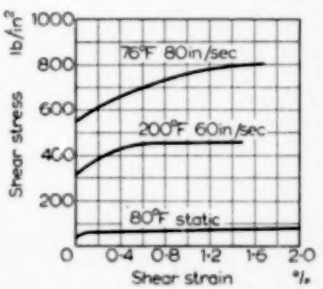

Fig. 10. Static and calculated dynamic shear stress vs. shear strain.

The assumptions involved in the analysis of the dynamic tests give rise to overestimates of the stress under dynamic loading for the crystals of zinc. Furthermore, the insensitivity of the deflection measuring system to small strains of the order of elastic strain contributes to an overestimation of dynamic stresses. Nevertheless, the experimental results clearly indicate that, for a given strain, the stress under dynamic loading is several times as great as under static loading. The results are sufficiently accurate, however, to establish definite trends in the effects of purity of the zinc and the test temperature upon the elastic limit under conditions of dynamic loading.

The temperature dependence of the dynamic elastic limit stress indicates that thermal activation plays a relatively important role in the slip process in zinc single crystals. Thermal activation may aid the generation of new dislocations

in the crystal. Some of the energy needed to release a dislocation from a Cottrell atmosphere may be supplied by thermal energy. Thermal activation may aid dislocations to pass obstacles such as small angle boundaries, intersecting dislocations, and inclusions.

The effect of a substructure of small angle dislocation boundaries on the dynamic slip properties of a crystal has not been determined. WASHBURN (1955) has shown that the effect of boundaries of approximately 2×10^{-2} radian in angle is to raise the static yield stress in zinc single crystals approximately 50 per cent. The effect of these boundaries in dynamic loading may be considerably greater than in static loading as a consequence of the role of thermal activation discussed above. The differences between the elastic limit stress found for several crystals of the same purity at a given temperature might therefore be attributable to differences in the substructure of those crystals.

The differences of static and dynamic elastic limit stresses of the crystals of different purity may be due to the difference in purity and to a difference of the substructure of the crystals. The impurity content of all of the crystals tested in this investigation was sufficient to form Cottrell atmospheres around all of the dislocations in the annealed crystal. An interesting investigation would be to make static and dynamic tests on crystals containing controlled amounts of substructure and of the same purity. Crystals having this substructure variation are not available at the present time.

The relatively greater decrease of elastic limit stress with increasing temperature for the purer material may be explained by a change in the Cottrell atmosphere around the dislocations when the temperature is increased. The atmosphere in a material of higher purity would ' boil off ' to a greater degree as the temperature is increased according to WEBB (1957). Thus, the strength of the more pure material would decrease more with increasing temperature until a temperature is reached which causes the loss of the atmospheres in both materials.

The effect of the small twinning deformation observed in the tests at velocities of 60 in/sec and greater on the results of these tests appears to be negligible. Twinning deformation gives rise to lateral displacement of the specimen which is approximately equal to or less than the minimum reading possible with the deflection measuring system. The consistent results obtained in the determination of the elastic limit stress over the range of impact velocities, including velocities which did not produce observable twinning, indicates that the small amount of twinning did not substantially influence the stress system or the propagation of plastic strain in the specimens.

ACKNOWLEDGMENTS

The authors wish to express their appreciation to the Office of Scientific Research of the Air Research and Development Command for sponsoring this research. The assistance of Mr. ROBERT T. HERZOG and Mr. REX B. PETERS in the construction of equipment and testing is gratefully recognized.

REFERENCES

JOHNSON, J. E., WOOD, D. S. and CLARK, D. S. 1953 *J. Appl. Mech.* **20**, 523.

VON KARMAN, T. and DUWEZ, P.	1950	*J. Appl. Phys.* **21**, 987.
KING, K. R., WOOD, D. S. and CLARK, D. S.	1955	*ONR Research Report NR* 031-285.
KRAMER, I. R. and MADDIN, R.	1952	*J. Metals* **4**, 197.
LEE, E. H. and TUPPER, S. J.	1954	*J. Appl. Mech.* **21**, 63.
LIU, T. S., KRAMER, I. R. and STEINBERG, M. A.	1956	*Acta Met.* **4**, 364.
TAYLOR, G. I.	1948	*Proc. Roy. Soc.* A **194**, 289.
VREELAND, T., WOOD, D. S. and CLARK, D. S.	1955	*OSR Research Report R*-335-10-6.
WASHBURN, J.	1955	*Trans. Amer. Inst. Min. (Metall.) Engrs.* **203**, 675.
WEBB, W. W.	1957	*Acta Met.* **5**, 89.

Journal of the Mechanics and Physics of Solids, 1958, Vol. 6, pp. 127 to 131. Pergamon Press Ltd., London

A NOTE ON THE DEFORMABLE REGION IN A RIGID–PLASTIC STRUCTURE*

R. M. Haythornthwaite and R. T. Shield
Brown University, Providence, R.I.

(*Received 2nd September*, 1957)

Summary

A theorem due to Bishop *et al.* (1956) which leads to a method for determining the extent of the deformable region in a rigid–plastic body at yield is shown to be applicable to structures. As an example the extent of the deformable region is determined for the bending of a clamped thin plate of arbitrary shape under a concentrated transverse load.

1. Introduction

In a recent note Bishop *et al.* (1956) have presented a procedure for finding the greatest extent of the deformable region in a rigid–plastic body yielding under given boundary conditions. The procedure was established for an ideal work-hardening rigid–plastic material whose yield function and plastic potential are identical. The method can be extended without difficulty to rigid–plastic structures, the yielding of which is characterized by generalized stresses and strain rates, as introduced by Prager (1955). Approximate plasticity theories for beams, frames, plates and shells are then brought within its scope.

The method of Bishop *et al.* is based on a theorem due to Hill (1951), which states that in a region of deformation the state of stress is uniquely defined. A theorem and a corollary which follow from this uniqueness theorem provide the general basis for determining the deformable region and are re-stated here.

Theorem. A deformation mode associated with the stress field in one complete solution is compatible with the stress field in any other complete solution.

Corollary. Any region of the stress field in a known complete solution which is shown to be necessarily rigid for *that* field (i.e. by arguments based solely on the geometrical and other properties of that field) must be rigid in all complete solutions.

The corollary is of immediate use in limiting the extent of the deformable region when the velocity equations are hyperbolic, and examples have been given by Bishop *et al.*

The yield surface in nine-dimensional stress space is necessarily convex (Drucker, 1951), but the uniqueness theorem of Hill (1951) requires a *strictly* convex yield surface. As mentioned by Hill (1956) this theorem requires modification when the yield surface is not strictly convex but contains a flat, consisting of a family

*The results presented in this paper were obtained in the course of research conducted under Contract Nonr 562 (10) by the Office of Naval Research and Brown University.

of points lying in a tangent plane to the surface or consisting of a family of singular points lying in a supporting plane of the surface. By a singular point is meant a point where the yield surface does not have a continuously turning tangent plane. At a point of the material where deformation is occurring with a strain-rate vector associated with a flat, the stress state is not necessarily uniquely defined but must be represented by a stress point on the flat in question. However, each alternative stress state is compatible with the deformation and it follows that the theorem and corollary stated above are still valid.

In a particular case in which the strain-rate vector is associated with a flat over a finite region of the material, equilibrium conditions may impose further restrictions that enforce uniqueness of the stress field in that region.

2. STRUCTURES

In the analysis of structures, an exact three-dimensional analysis is usually either too difficult to carry out or too unwieldy to be of practical use. Important information on the plastic behaviour of structures such as beams, frames and shells can be obtained from an approximate theory formulated in terms of generalized stresses such as the moments and force resultants across a section of the structure. The state of stress at a point of the structure is specified by generalized stresses $Q_1, Q_2, \ldots, Q_N$. During deformation of the structure the corresponding generalized strain rates $q_1, q_2, \ldots, q_N$ are chosen so that the rate at which energy is dissipated is given by

$$D = Q_1 q_1 + Q_2 q_2 + \ldots + Q_N q_N. \tag{1}$$

In the bending of a thin plate, for instance, the generalized stresses are two bending moments and one twisting moment and the corresponding generalized strain-rates two rates of bending and a rate of twist. Shear forces, which enter into the equations of equilibrium of the plate, are in the nature of reactions as they do no work during bending of the plate.

The extension of the theory of limit analysis (DRUCKER *et al.* 1952) to structures of rigid–plastic material has been carried out by PRAGER (1955) in a general manner. The structure yields when the stresses Q_n ($n = 1, 2, \ldots, N$) are such that the point Q_n lies on the yield surface

$$F(Q_n) = K^2 \tag{2}$$

in a generalized stress space of N dimensions. The strain-rate vector with components proportional to q_n is normal to the yield surface (2) at a regular point and at singular points lies in the fan bounded by the normals to adjacent points. For a convex yield surface it then follows that

$$(Q_n - Q_n^*)\, q_n \geqslant 0 \tag{3}$$

where Q_n^* is any other state of stress within or on the yield surface.

The uniqueness of the generalized stresses Q_n in a plastically deforming region can now be examined as for conventional stresses and parallel results can be obtained. The Q_n must satisfy equilibrium conditions and it is assumed that the velocity field describing the deformation of the structure is such that the principle of virtual work may be applied. The corresponding theorem and corollary on

the extent of the deformable region also apply. As for conventional stresses the corollary can be applied directly to delineate the deformable region when the velocity equations are hyperbolic. An example follows.

3. Example

Within the framework of thin-shell theory, there are a number of complete solutions in the literature to problems involving cylindrical shells and circular plates. The statements on the uniqueness of the generalized stress distribution and the extent of the deformable region apply to such complete solutions. In this Section a complete solution is derived for the problem of a plate of arbitrary shape clamped along its edge and loaded by a concentrated lateral force, and the extent of the deformable region is found.

A complete solution is obtained by assuming rotational symmetry about the point of application of the load. The material of the plate is assumed to be a rigid–plastic material which obeys the yield condition of Tresca. For a rotationally symmetric moment distribution involving two bending moments M_r, M_θ, limiting combinations of these moments are represented by the points on the hexagon of Fig. 1 (see for example Hopkins and Prager 1953).

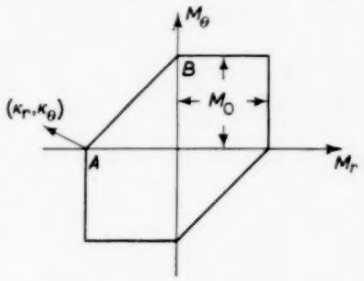

Fig. 1.

M_0 is the magnitude of the maximum moment which the plate can carry and has the value $\sigma_0 h^2/4$ for a homogeneous plate of (constant) thickness h, σ_0 being the yield stress of the material. For equilibrium

$$d(rQ)/dr + rp = 0, \tag{4}$$

$$d(r M_r)/dr - M_\theta - rQ = 0, \tag{5}$$

where r measures distance from the point of application of the load, Q is the transverse shear force per unit length in the circumferential direction and p is the surface pressure. For a concentrated load P at the origin, p is zero except at $r = 0$ and integration of (4) gives

$$Q = -P/2\pi r. \tag{6}$$

Taking the moment field

$$M_r = -M_0, \qquad M_\theta = 0, \tag{7}$$

for which all elements of the plate are at the moment state represented by the point A of Fig. 1, equilibrium equation (5) now gives

$$P = 2\pi M_0. \tag{8}$$

The moment field (7) is not the only moment field which satisfies yield and the equilibrium condition (5) when $P = 2\pi M_0$. Any constant value of M_r between $-M_0$ and zero and

$$M_r - M_\theta = -M_0 \tag{9}$$

represented by a point on the side AB of the yield hexagon, will satisfy (5). However, in order to complete the solution an associated pattern of deformation must be found and this enforces the moment state A of Fig. 1. The generalized strain-rates corresponding to the generalized stresses M_r, M_θ are the curvature rates κ_r, κ_θ. The rate of twist $\kappa_{r\theta}$ is zero in this case as κ_r, κ_θ are principal curvature rates. For the moment state A of Fig. 1, the curvature rates must be such that

$$0 \leqslant \kappa_\theta \leqslant -\kappa_r. \tag{10}$$

For a rotationally symmetric deformation pattern, the normal rate of deflection w of the middle surface of the plate is a function of r only and

$$\kappa_r = -\frac{d^2 w}{dr^2}, \qquad \kappa_\theta = -\frac{1}{r}\cdot\frac{dw}{dr}. \tag{11}$$

Many functions $w(r)$ can be chosen such that conditions (10) and the boundary conditions of zero deflection and slope at the edge of the plate are satisfied. The deflection rate w must be continuous but discontinuities in dw/dr implying an infinite (negative) value of κ_r are permissible. One deflection pattern is given by

$$w = \begin{cases} w_0\left(1 - \dfrac{a}{r}\right), & r \leqslant a \\ 0, & r \geqslant a \end{cases} \tag{12}$$

where w_0 is a positive constant and the circle $r = a$ lies wholly within the plate. With the exception of the hinge circle $r = a$, where deformation takes place, κ_r is equal to $-2\kappa_\theta$ for this collapse mode. A common feature of all the possible deformation patterns is that they involve a deflection rate at the point of application of the load which is indefinitely high compared with that at all other points.

A possible deformation pattern has now been associated with the moment field (7), so the value (8) is the limit load and the solution is now a complete one. The limit load value, $2\pi M_0$ has been obtained previously by SCHUMANN (1957) by using limit analysis to bound the limit load from above and below. A complete solution for the special case of the centrally-loaded circular plate was given previously by HOPKINS and PRAGER (1953).

Point loading is not met in practice but the result obtained here may be regarded as the limiting case which will be approached as the area of the loaded region is reduced.

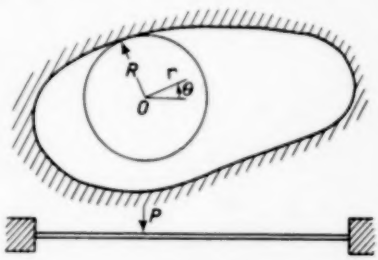

Fig. 2.

The largest value of the radius a which can be taken in (12) is the radius R of the circle centred at the load and passing through the point on the clamped edge nearest to the load (Fig. 2). Thus, deformation can take place in this circular area of radius R. It follows that the moment field (7) is the unique plastic moment field in this region, because the strain rate vector $(\kappa_r, \kappa_\theta)$ with $\kappa_r = -2\kappa_\theta$ is compatible only with the moment state A of Fig. 1. Further, the remainder of the plate outside this circular region is necessarily rigid for the moment distribution (7). The condition $\kappa_{r\theta} = 0$, which follows from isotropy of the material, requires

$$\frac{\partial^2 (w/r)}{\partial r \, \partial \theta} = 0. \tag{13}$$

The characteristics of the hyperbolic equation (13) for w/r are the circles $r =$ constant and the radial lines $\theta =$ constant, and so the boundary conditions of zero deflection and slope at the clamped edge enforce w to be zero throughout the region outside the circle of radius R. It follows from the corollary that the plate must be rigid in this outer region in all complete solutions.

References

Bishop, J. W., Green, A. P. and Hill, R.	1956	*J. Mech. Phys. Solids* **4**, 256.
Drucker, D. C.	1951	*Proc. 1st U.S. Nat. Cong. Appl. Mech.* (ASME) 487.
Drucker, D. C., Greenberg, H. J. and Prager, W.	1952	*Quart. Appl. Math.* **9**, 381.
Hill, R.	1951	*Phil. Mag.* **42**, 868.
	1956	*J. Mech. Phys. Solids* **4**, 247.
Hopkins, H. G. and Prager, W.	1953	*J. Mech. Phys. Solids* **2**, 1.
Prager, W.	1955	*Proc. 8th Int. Cong. Appl. Mech., Istanbul*, 1952, 65.
Schumann, W.	1957	*Brown Univ. Tech. Rep. No. DA–798/29.* (To appear in *Quart. Appl. Math.*).

Journal of the Mechanics and Physics of Solids, 1958, Vol., 6 pp. 132 to 144. Pergamon Press Ltd., London

ON THE EFFECT OF FRICTION ON COMPRESSION AND INDENTATION BETWEEN FLAT DIES

By J. F. W. Bishop
Mechanical Engineering Research Laboratory, East Kilbride

(*Received* 1st *April*, 1957)

Summary

The relevant theoretical work under plane-strain conditions with both overhanging and indenting smooth and rough dies for various geometrical configurations is reviewed. The frictional conditions under which certain postulated solutions are valid are established. The known exact solutions are examined in relation to an approximate solution of the compression of a rectangular slab between rough dies for small values of the coefficient of friction μ. It is demonstrated both by exemplification and deduction that the modified approximate solution gives reasonably good results for all relevant coefficients of friction. The approximate solution (Siebel) for the axially symmetric problem is examined in the light of these results and it is suggested that it can be expected to give reasonable results for all μ. An approximate solution for the compression of a square slab between rough dies is given. The plane-strain, axially symmetric and square slab deformation results are presented graphically with mean pressure plotted as a function of μ and the relevant geometrical shape factors.

1. Introduction

In two typical forging operations material is compressed between overlapping dies as in upsetting, or indented between narrow platens as in edging and fullering. The simplest idealization of the former process is the compression of a circular cylinder. An approximation to the second process is the plane-strain indentation between narrow parallel-sided dies of a flat slab with overhang (see Fig. 1).

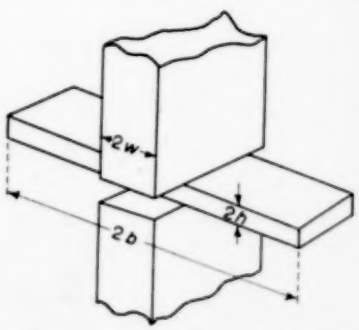

Fig. 1. Plane strain indentation.

The compression of a circular cylinder constitutes a problem with axial symmetry. Very few non-trivial exact solutions of problems of this kind are available. Shield (1955) has considered the indentation of a semi-infinite slab by a smooth circular cylindrical punch for a material obeying Tresca's yield criterion and with a Tresca plastic-potential. A solution along similar lines could be obtained for the compression of a circular cylinder between rough dies provided the coefficient of friction between the dies and the specimen were sufficiently small. As in the solution obtained by Shield, this would involve lengthy iterative numerical computation. Siebel

(1923) has given an approximate solution to the problem of the compression of a circular disc with small friction at the die-disc interface. A modification of this theory due to SCHROEDER and WEBSTER (1949) extends it to the range in which the maximum stress in shear occurs at the die-disc interface.

Since these approximate theories are the only ones available for examining the effect of friction on forging loads, it is desirable to determine how valid they are. It is suggested that this can be done by considering the situation under plane-strain conditions. The plane-strain compression of a slab both by indenting and by overhanging dies has received considerable attention. Theoretical work by PRANDTL (1923), HILL, LEE and TUPPER (1951) and GREEN (1951) has covered variations in friction and height/width ratio of the block. An approximate solution for small coefficients of friction analogous to that of SIEBEL has been given by HILL (1950*a*, p. 236). This enables the accuracy of this approximate solution to be determined.

Strictly speaking an analysis of the forging process should take into account the effect of details of change of shape, e.g. barrelling, and of non-uniform hardening on loads. This topic is only just coming under consideration and involves considerable difficulty (see HILL 1956). For the purpose of this paper simplifying assumptions will be made about change of shape. In the compression of a cylinder, for example, it will be assumed that the specimen remains cylindrical and that the only geometrical variable is the height to radius ratio. Thus the problem of finding the forging load in upsetting a cylinder is reduced to that of finding the yield point loads for cylinders of different height/radius ratio. Recourse must be made to the limit theorems to examine the significance of these loads in relation to the yield point loads of actual deformed bodies. The results will be more or less in error depending on how good the assumptions are. At the moment the only available method for checking this in the majority of cases is by comparison with experiment.

2. PLANE DEFORMATION

For a comprehensive discussion of this topic up to the date of publication, the reader is referred to HILL (1950*a*, pp. 226–236). A brief summary only is given here.

The theory for plane strain is relevant when one principal axis of strain is fixed in space and the corresponding strain component is zero. This condition may be brought about in a variety of ways, e.g. constraint of non-plastic material, edge constraint, frictional restraint. Throughout this note it will be assumed that the material is rigid-plastic and non-hardening. In this section the compression of rectangular slabs under plane-strain conditions with varying height to width ratios is considered, and the following notation is adopted.

When the dies overlap the specimen (Case I, Fig. 12) the specimen dimensions are taken as height $2h$, width $2w$. When the dies indent the specimen (Case II, Fig. 12) the specimen height is $2h$ and the *die* width $2w$: the specimen width, where specified, is $2b$ (Fig. 1).

Smooth flat dies

When the dies overlap the specimen the compressive pressure is $2k$, where k is the yield stress in shear. This result is independent of height/width ratio of

the specimen. A geometrically possible deformation mode, compatible with the stress state, preserves the rectangular shape of the specimen.

When the dies are narrower than the specimen ($w < b$) the problem is considerably more complex. Three types of deformation must be distinguished. When $b \geqslant w$ the deformation occurs by material being forced out at the surface adjacent to the dies for $h/w > 8{\cdot}73$; when $0 \leqslant h/w < 8{\cdot}73$ the two ends of the slab move apart as rigid masses with a simultaneous deformation of the material between the dies. With narrower blocks and depending on the h/w, h/b ratios, deformation will extend to the sides of the block. Thus Hill (1950*b*) has shown that for large h/w the dies cause the corners of the bar to rotate when $b/w < 8{\cdot}6$ rather than force material out at the surface. When $w/h \geqslant 1$ Green (1951) has shown that the indentation pressure oscillates with increasing w/h, being equal to $2k$ for integer values of w/h. The results due to Hill and Green are shown graphically in Fig. 2. The indentation pressure divided by $2k$ is plotted against the height/

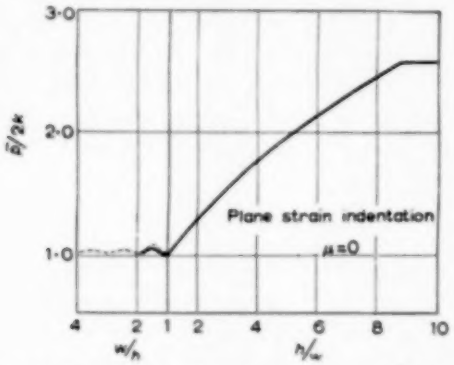

Fig. 2. Mean indentation pressure for smooth dies.

width ratio. The dotted line for $w/h \geqslant 1$ is due to Hill and gives an upper bound to $\bar{p}/2k$. Experimental investigations in the regime $w/h \geqslant 1$ by Watts and Ford (1952) strikingly confirm the theoretical work of Green.

Rough flat dies

In the following discussion the coefficient of friction μ is regarded as the value that would be obtained from a slider and plate test using the relevant materials. A solution of a problem of plastic deformation will be regarded as valid if the conditions at constraints are

(1) Ratio of tangential to normal force, λ, less than or equal to μ, the coefficient of friction, where no *sliding* motion occurs in a suggested deformation mode.

(2) $\lambda = \mu$ where sliding occurs.

It is assumed that where the maximum stress in shear is reached at the constraint, this corresponds to *not* sliding. It is presupposed that the solution is satisfactory in all other respects.

Consider first the compression of a slab between overhanging dies. For $h/w \geqslant 1$ the compressive stress is $2k$ for all μ. A geometrically-possible yield point mode

compatible with the stress for a typical case is shown in Fig. 3. The regions AOB, $A'O'B'$ move rigidly with no relative motion at the interfaces AB, $A'B'$. It is clear that this mode would result in a type of ' barrelling '.

When $1 \geqslant w/h \geqslant 3{\cdot}64$ a solution has been proposed by HILL (1950*a*, p. 230). A typical slip-line field is shown in Fig. 4. The material in AOB, $A'O'B'$, APA', BQB', remains rigid. The range of validity of the solutions is not specified and

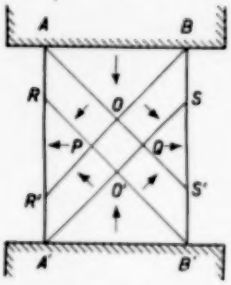

Fig. 3. Deformation mode for plane strain compression between rough dies.

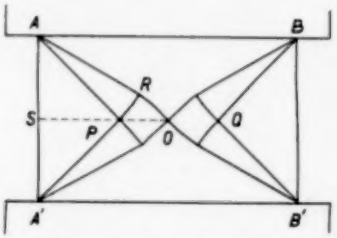

Fig. 4. Slip-line field ; compression between rough dies.

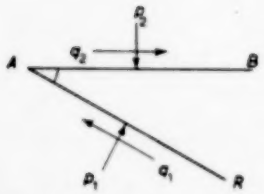

Fig. 5. Stress state in an angle.

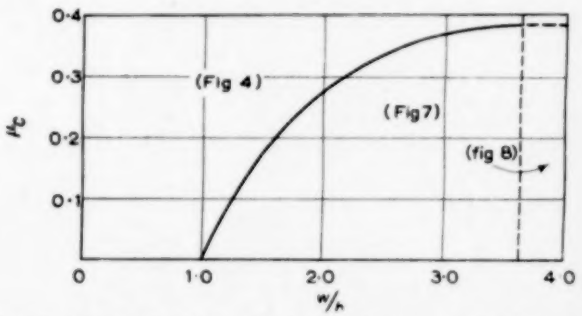

Fig. 6. Range of validity of solutions for compression between rough dies : $w/h \geqslant 1$. (Figure numbers in parentheses indicate type of solution valid.)

may be determined as follows. Consider the configuration of Fig. 5. HILL (1954) has shown that considerations of yield and stress equilibrium enable bounds to be placed on the possible variations of $(p_1 - p_2)$, q_1, q_2 and α. This configuration exists at A in Fig. 4 with p_1, q_1 and α given. An examination of the inequalities given by HILL enables the least possible ratio of q_2/p_2 to be found. This is plotted as μ_c in Fig. 6 as a function of w/h. At this stage it can be stated that for a given w/h ratio the solution of Fig. 4 is *not* valid for all $\mu < \mu_c$. To determine whether a solution exists for values of μ as small as μ_c it is necessary to construct a stress solution in the rigid regions AOB, $A'OB'$ which has $\lambda = \mu_c$ at A, B, A' and B' and such that $\lambda \leqslant \mu_c$ on AB and $A'B'$. A stress state corresponding to $\lambda = \mu_c$ at A can be obtained from the fully plastic continuation of the slip-line field into AOB based on the slip-lines AO, BO. It is simple to demonstrate that the values of λ obtained from this solution are such that $\lambda \leqslant \mu_c$ on AB. Hence the values of μ_c gives the *least* value of the coefficient of friction for which the relevant solution

is valid. The solution is acceptable for all larger values of μ. The largest value of μ_c is obtained when one family of slip-lines coincides with AB at A. All values of μ larger than this correspond to what are called 'perfectly rough' dies in the literature. For values of $\mu < \mu_c$ for a given w/h in the range under consideration, there is a region of slipping at the die face with a slip-line field determined by μ (Fig. 7).

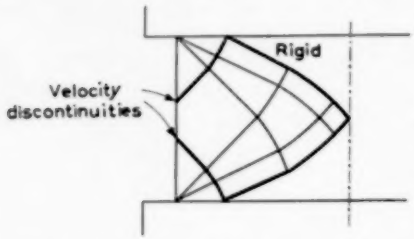

Fig. 7. Slip-line field; compression between rough dies, $\mu < \mu_c$, $w/h < 3{\cdot}64$.

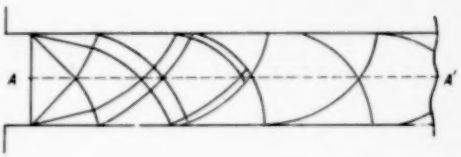

Fig. 8. Slip-line field; compression between rough dies, $w/h > 3{\cdot}64$.

For $w/h > 3{\cdot}64$ Hill (1950a, p. 231) has indicated the general nature of the solution. The slip-lines are ultimately normal and tangential to the die face for all $\mu > 0$ as typified in Fig. 8.

Computations covering various values of μ for varying w/h have been made from the relevant slip-line fields. The results are conveniently shown in Fig. 9 where the normal pressure acting across AA' in Fig. 8 is plotted as a function of x/h, where x is the distance from the edge of the block and $x \leqslant w$. The mean die pressures can, therefore, be obtained by integration from this diagram.

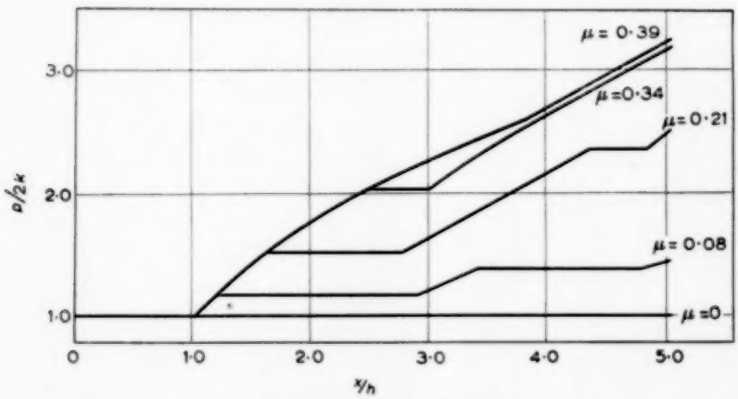

Fig. 9. Plane-strain compression.

When w/h is very large a solution proposed by Prandtl becomes valid. It is for the limiting state in which the maximum stress in shear is achieved at the die faces and neglects the edge conditions. Hill, Lee and Tupper (1951) have pointed out that their solution for perfectly rough plates rapidly asymptotes to this solution. All the slip-line fields for non-zero μ will eventually asymptote to

it for large enough x/h. This implies that ultimately the die or centre-line pressure will increase linearly with x/h.

When the slab extends beyond the dies, again the position is modified. In the range $h/w > 1$, the identation pressures are the same for all values of μ as for smooth dies. It is interesting to note that the PRANDTL deformation mode as opposed to that due to HILL is taken in the range $h/w > 8{\cdot}75$ (see HILL 1950*a*, p. 254). When $1 < w/h < 3{\cdot}64$, i.e. in the range corresponding to Fig. 4, the solution is as for overhanging dies if $\mu > \mu_c$. For other values of μ the solution differs from that with over hanging dies since velocity discontinuities emerge at the edge as in Fig. 7. When $w/h > 3{\cdot}64$ and $\mu = 0{\cdot}39$ the solution is as for overhanging dies. For smaller values of μ the solutions are similar to those for overhanging dies when the velocity discontinuities terminate at the corners of the die. For other values of w/h the slip-line field must be modified in an analogous manner to that given by GREEN (1951) for $\mu = 0$. It can be inferred from his work that the indentation pressures will differ by only a few per cent at most from those for overhanging dies.

Approximate solution

Of considerable interest in the current analysis is an approximate solution due to HILL (1950*a*, p. 236). This theory was formulated for *small* values of μ and $w > h$. It is valid for indenting or overlapping dies. It is proposed to examine the solution in some detail because of its importance in assessing the validity of approximate solutions.

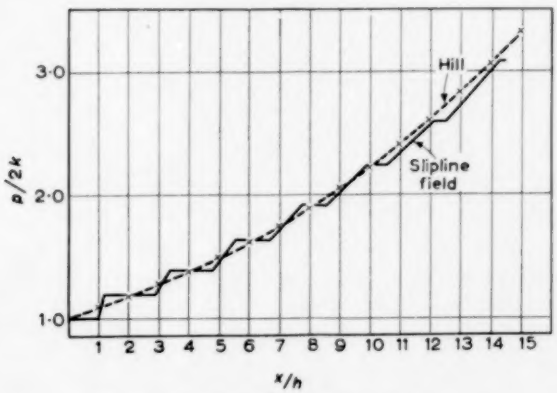

Fig. 10. Plane-strain compression $\mu = 0{\cdot}08$.

Let p be the normal compressive stress at a distance x from the edge of a block of thickness $2h$, and q the mean transverse compressive stress in the x direction. From equilibrium considerations

$$\frac{dq}{dx} = \frac{\mu p}{h}, \qquad (\mu p < k). \tag{2.1}$$

If μ is small, the yield criterion is expressible as

$$p - q = 2k. \tag{2·2}$$

Since $q = 0$ at $x = 0$,

$$p = 2ke^{\mu x/h}. \tag{2·3}$$

In Fig. 10 the pressure given by (2·3) is compared with the centre-line pressure derived from slip-line field calculations for $\mu = 0{\cdot}08$. The agreement is very good. In Fig. 11 the comparison is made for $\mu = 0{\cdot}21$. It is seen that initially the agreement is good but at $w/h \simeq 4$ the approximate curve diverges from the slip-line field results. This is because equation (2·1) should be replaced by

$$\frac{dq}{dx} = \frac{k}{h}. \tag{2.4}$$

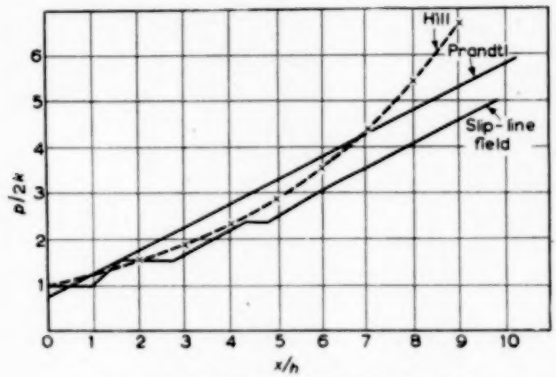

Fig. 11. Plane-strain compression $\mu = 0{\cdot}21$.

for values of x greater than x_0 where

$$\mu p = k = 2\mu k e^{\mu x_0/h},$$

otherwise shearing stresses larger than the maximum stress in shear of the material will be assumed to be occurring at the die face. Surprisingly the slope of the (p, x) curve derived from (2.2) and (2.4) is identical to that obtained from the Prandtl solution although (2.2) itself is certainly not true. The reason for this is that in deriving (2.3) or the analogous result from (2.4), strictly speaking it is not equation (2.2) which is used, but the equation $dp/dx = dq/dx$. Reference to the Prandtl solution shows that this holds for the limiting value of μ ($= 0{\cdot}39$). Hence a composite expression for p given by

$$p = 2ke^{\mu x/h}, \qquad 0 \leqslant x \leqslant x_0,$$

$$p = k\left[\frac{1}{\mu} + \frac{1}{h}(x - x_0)\right], \qquad x_0 \leqslant x,$$

where

$$x_0 = \frac{h}{\mu}\log\frac{1}{2\mu},$$

is a reasonably good approximation for *all* μ.

Summary of plane-strain results

For all *practical* purposes the results in plane strain may be summarized as

follows (w/h is taken to refer to the *die* width to material thickness for indenting dies and to the *block* dimensions for overhanging dies).

(1) $\dfrac{h}{w} > 1.$

(i) Overhanging dies. $p = 2k$ for all μ. (ii) Indenting dies. Pressure as for smooth dies for all μ.

(2) $w/h > 1.$

Overhanging and indenting dies similar. Pressure given by

$$p = 2ke^{\mu x/h}, \qquad 0 \leqslant x \leqslant x_0,$$

$$p = k\left[\frac{1}{\mu} + \frac{1}{h}(x - x_0)\right],$$

$$x_0 = \frac{h}{\mu}\log\frac{1}{2\mu}.$$

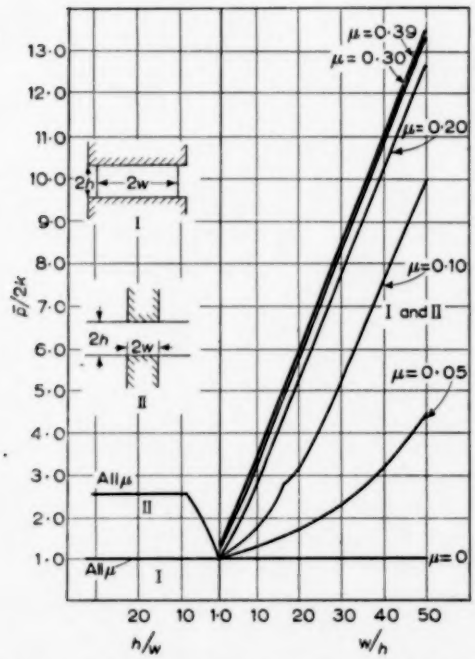

Fig. 12. Mean pressures for indentation and compression in plane strain.

From these the *mean* pressure is

$$\bar{p} = \frac{2kh}{\mu w}(e^{\mu w/h} - 1), \qquad w \leqslant x_0,$$

$$\bar{p} = \frac{2kh}{\mu w}\left(\frac{1}{2\mu} - 1\right) + \frac{k}{\mu w}(w - x_0) + \frac{w - x_0}{2h}, \qquad w \geqslant x_0.$$

The results are summarized graphically in Fig. 12.

3. Axial Symmetry

The only exact non-trivial solutions of problems of axial symmetry which are relevant here are due to Shield (1955). These are based on the Tresca yield and potential functions, which are singular and lack physical reality ; the importance of the solutions lies partly in the fact that the Haar–Kármán hypothesis (viz., that the circumferential stress and one of the other principal stresses should be equal) can be justified a *posteriori* by reference to the velocity solution.

In this Section the compression of circular cylinders between overlapping parallel dies is considered. It can be inferred from the work of Shield that, when the height/radius ratio h/r is greater than two, the compressive stress is $2k$ ($= Y$, the uniaxial yield stress) for all values of μ ; k is the maximum stress in shear. This is because Shield has obtained deformation modes which allow cones of material making contact with the dies to remain rigid.

For $r/h > \frac{1}{2}$, an approximate solution has been given by Siebel which is analogous to that due to Hill. This solution is based on

(a) Small values of μ.

(b) The assumption that the radial and circumferential stress components are equal.

Schroeder and Webster (1949) have used the same analysis to deal with large values of μ. The analysis is very similar to that given in Section 2 for plane strain.

When μ is small the hypothesis that the radial and circumferential stress components are equal is not very different from the Haar–Kármán hypothesis, which can be justified in certain circumstances as stated above. When μ is large, in particular when the maximum stress in shear occurs at the die face, the term which is neglected by assuming that the circumferential and radial stress components are equal is not important unless r is small. Hence although, as Hill (1950*a*, p. 277) remarks, the assumption that the two stress components are equal introduces an unknown error, the considerations given here suggest it will not be serious.

The theory uses a yield criterion in the form $p + \sigma_r = 2k$, where p is the die pressure and σ_r the radial stress, to derive the relation $dp/dr = -d\sigma_r/dr$. Since this form of the criterion breaks down at the die face for large μ, the question arises as to whether it is still reasonable to use the theory when μ is not small.

Let θ, r and z be circumferential, radial and axial co-ordinates. Consider a disc of thickness h and radius a. Let the maximum stress in shear occur at the die faces, i.e. $|\tau_{rz}| = k$ at $z = \pm h/2$. Then, at $z = \pm h/2$, $\partial\sigma_r/\partial r = \partial\sigma_z/\partial r$. At the midsection $z = 0$, $\sigma_\theta = \sigma_r$ at $r = 0$ and $\sigma_z > \sigma_\theta \geqslant \sigma_r$ at $r = a$. It is reasonable to take the Tresca criterion as $\sigma_z - \sigma_r = 2k$, $z = 0$, and hence $\partial\sigma_z/\partial r = \partial\sigma_r/\partial r$ $z = 0$. It cannot be too erroneous to take $\partial\sigma_r/\partial r = \partial\sigma_z/\partial r$ for all z. In any event the maximum range of $\sigma_z - \sigma_r$ is $2k$ and hence for large r the value of $\partial\sigma_r/\partial r$ cannot be largely different from $\partial\sigma_z/\partial r$ for most r. It follows from equilibrium considerations that the normal pressure at the die face is

$$p = 2ke^{2\mu(a-r)/h}.$$

This relation must be modified when the maximum stress in shear occurs at the die face. Schroeder and Webster give the maximum possible value of μ as 0·577. This is based on the conditions at the edge of the disc in the approximate

solution. A more realistic estimate can be obtained from the analysis using the Haar–Kármán hypothesis, giving the value $\mu \leqslant 0{\cdot}39$.

The results for axial symmetry may be summarized as follows :—

(1) $h/a > 2$. Compressive stress $2k$ for all μ.

(2) $a/h > \frac{1}{2}$. $p = 2ke^{2\mu(a-r)/h}, \qquad r_0 \leqslant r \leqslant a,$

$$p = \frac{k}{\mu} + \frac{2k}{h}(r_0 - r), \qquad 0 \leqslant r \leqslant r_0.$$

The mean pressure $\bar{p}$ is

$$\bar{p} = \frac{4k}{\alpha^2}\{e^{\alpha} - 1 - \alpha\}, \qquad r_0 < 0,$$

$$\bar{p} = \frac{4k}{\alpha^2}\left\{\frac{1}{2\mu}(1+\beta) - 1 - \alpha\right\} + \frac{k\beta^2}{\alpha^2}\left(\frac{1}{\mu} + \frac{2}{3}\frac{r_0}{h}\right), \qquad r_0 > 0,$$

where $$\alpha = \frac{2\mu a}{h}, \qquad \beta = \frac{2\mu r_0}{h}, \qquad r_0 = a - \frac{h}{2\mu}\log\frac{1}{2\mu}.$$

These results are shown graphically in Fig. 13.

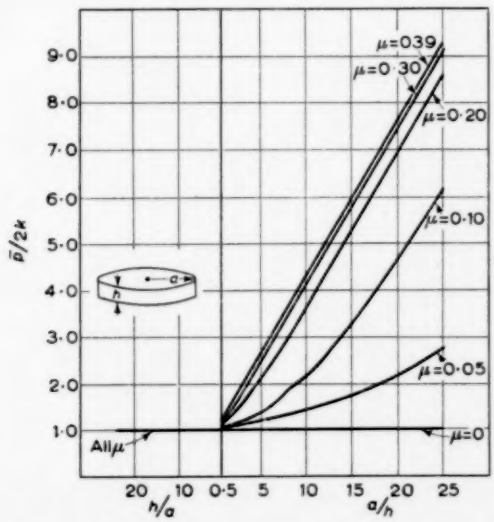

Fig. 13. Mean pressures for compression of circular cylinders.

4. General Deformation

So far two important types of deformation have been considered, namely plane and axisymmetric. In practice a large number of forging operations can be reasonably approximated by one or other of these types. A further common type of deformation which does not fall into either of the above categories occurs in which a blank is compressed between overhanging parallel dies. Hill (1950*c*) has discussed the general theory in some detail, and has given an approximate solution of the

compression of a rectangular strip of large length/breadth ratio between rough parallel dies. The semi-breadth is assumed to be of the same order as the thickness. In this solution both the mean pressure and the change of shape are evaluated. With $2b$ as the breadth, $2a$ the length and h the height, the mean pressure p was found to be

$$\bar{p} \simeq \left(1 + \frac{\mu b}{2h}\right) Y, \qquad \frac{\mu b}{h} \leqslant 0{\cdot}288,$$

$$\bar{p} \simeq \tfrac{4}{3} - 0{\cdot}051 \frac{h}{\mu b} mY, \qquad \frac{\mu b}{h} \geqslant 0{\cdot}288.$$

$$\frac{\sqrt{3}}{2} \leqslant m \leqslant 1\,; \qquad m = 1 \text{ for } \frac{\mu b}{h} = 0{\cdot}288, \qquad m \to \frac{\sqrt{3}}{2} \text{ as } \mu b \to \infty.$$

In the latter case the central portion of the strip deforms in the breadth of the strip under plane-strain conditions.

The compression of a rectangular slab of breadth/length ratio of order unity and with thickness small compared with the other dimensions does not appear to have been considered. Consider a square block of side $2a$ and thickness h. For $2a \leqslant h$ it is reasonable to suppose that the compressive stress is $2k$ for all μ having regard to the results given previously. For $2a \geqslant h$, the following approximate analysis is suggested. Let the yielding be governed by Tresca's criterion, i.e.,

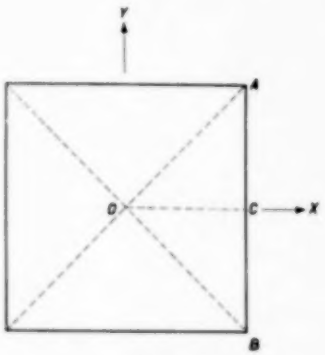

Fig. 14.

$$\sigma_1 - \sigma_3 = 2k\,; \qquad \sigma_1 \geqslant \sigma_2 \geqslant \sigma_3.$$

Let p be the compressive stress normal to the slab and q and r the mean compressive stresses in the x and y directions (Fig. 14).

On OC, $q = r$ at O by symmetry and at C $p > r \geqslant q$. Hence on OC the yield criterion can be taken as

$$p - q = 2k \tag{4.1}$$

Let τ_{xy} be the mean shear stress averaged over the thickness. From equilibrium considerations :—

$$h \frac{\partial q}{\partial x} = -2\mu p + h \frac{\partial \tau_{xy}}{\partial y}.$$

For large x or μ the deformation near $y = 0$ is sensibly independent of y and the term in $\partial \tau_{xy}/\partial y$ may be neglected. For small x and μ the equation for axial symmetry, namely

$$\frac{\partial q}{\partial r} = -\frac{2\mu p}{h}$$

will not be largely in error on OC. Hence on OC the equilibrium equation may be reasonably approximated by

$$h \frac{\partial q}{\partial x} = -2\mu p.$$

From (4.1) and bearing in mind the arguments of Section 2 (iii) when μ is not small :—

$$\frac{\partial p}{\partial x} = -2\mu p/h, \qquad p = 2ke^{2\mu(a-x)/h}; \qquad \mu p \leqslant k.$$

Now along AB, $q = 0$ and $p > r \geqslant q$. Hence on AB $p = 2k$. A functional relation which satisfies the conditions on AB and the value of p on OC is

$$p = 2ke^{2\mu(a-x)/h}; \qquad \mu p \leqslant k, \qquad 0 \leqslant x \leqslant a, \qquad x \geqslant |y|. \tag{4.2}$$

For this relation it is seen that the contours of equal pressure are squares. It is not difficult to establish that for large a/h these contours are more nearly circular for small x. However, it hardly seems worthwhile to refine (4.2) for practical purposes at the moment.

If $\mu p = k$ at $x = x_0$,

$$x_0 = a - \frac{h}{2\mu}\log\frac{1}{2\mu}$$

and

$$p = \frac{k}{\mu} + \frac{2k}{h}(x_0 - x), \qquad 0 \leqslant x \leqslant x_0. \tag{4.3}$$

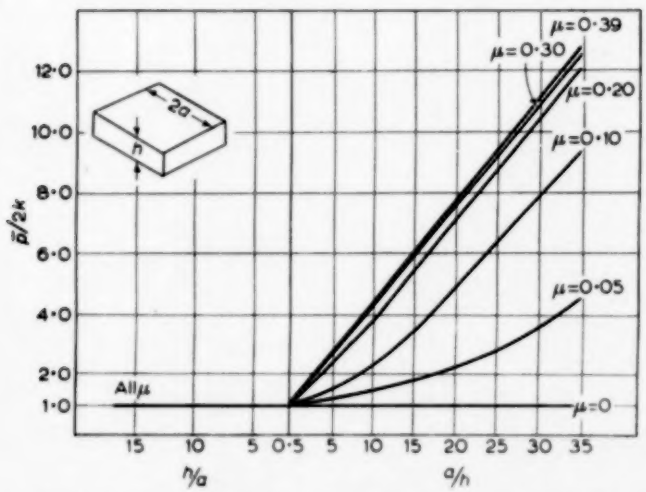

Fig. 15. Mean pressures for compression of a square specimen.

The values of the mean pressure derived from (4.2) and (4.3) are

(a) $x_0 < 0$; $\qquad \bar{p} = \dfrac{kh^2}{a^2\mu^2}\left[e^{2\mu a/h} - 1 - \dfrac{2\mu a}{h}\right]$

(b) $x_0 > 0$; $\qquad \bar{p} = \dfrac{kx_0^2}{a^2}\left(\dfrac{1}{\mu} + \dfrac{2}{3}\dfrac{x_0}{h}\right) + \dfrac{kh^2}{a^2\mu^2}\left[\dfrac{1}{2\mu}\left(1 + \dfrac{2\mu x_0}{h}\right) - 1 - \dfrac{2\mu a}{h}\right]$.

It is suggested that the best available estimate for the maximum value of μ is 0·39.

The results are presented graphically in Fig. 15.

5. Discussion

The summarized results of Figs. 12, 13 and 15 give what are believed to be reasonably accurate figures for the mean die pressures for different geometrical shapes and for varying constraint, friction and ratios of geometric parameters. It is of course well known that, qualitatively, friction considerably raises the mean pressure in forging operations such as disc-forging. How important friction is can be deduced from Fig. 13. Bearing in mind that the volume of material remains constant, it is seen that the *load* ultimately varies as the fifth power of the radius.

Under impact conditions two inferences can be drawn from the results. In the first place the energy necessary to effect a desired reduction can be computed from the data given. Secondly, the elastic energy stored in the specimen will be related to the current mean pressure. The analysis leading to the above results ignores elastic deformation. Nevertheless the strain-energy calculated from the stresses would probably be a good approximation to the actual energy. In practice the energy lost will depend very much on the characteristics of the forge. It cannot, however, be less than the elastic strain-energy of the specimen and hence drop forging will become increasingly inefficient with reduction in the presence of friction until finally no reduction occurs under a blow of given energy. All the results given relate the mean die pressure to the yield stress either through the uniaxial yield stress Y or the maximum stress in shear k. These values must be interpreted as the mean values for the current state of hardening and will depend on the conditions of working and on the total work of plastic deformation.

Acknowledgments

The author wishes to acknowledge his indebtedness to his colleague, M. T. Watkins, for helpful suggestions. The work described forms part of the research programme of the Mechanical Engineering Research Board of the Department of Scientific and Industrial Research. It was carried out in the Plasticity Division of the Mechanical Engineering Research Laboratory and is published by permission of the Director.

References

Green, A. P.	1951	*Phil. Mag.* **42**, 900.
Hill, R.	1950*a*	*The Mathematical Theory of Plasticity* (Clarendon Press, Oxford).
	1950*b*	*Phil. Mag.* **41**, 745.
	1950*c*	*Phil. Mag.* **41**, 733.
	1954	*J. Mech. Phys. Solids* **2**, 278.
	1956	*J. Mech. Phys. Solids* **4**, 247.
Hill, R., Lee, E. H. and Tupper, S. J.	1951	*J. Appl. Mech.* **18**, 46.
Prandtl, L.	1923	*Z. Angew. Math. Mech.* **3**, 401.
Schroeder, W. and Webster, D. A.	1949	*J. Appl. Mech.* **16**, 289.
Shield, R. T.	1955	*Proc. Roy. Soc.* A **233**, 267.
Siebel, E.	1923	*Stahl und Eisen* **43**, 1295.
Watts, A. B. and Ford, H.	1952	*Proc. Inst. Mech. Engrs.* **1B**, 448.

Journal of the Mechanics and Physics of Solids, 1958, Vol. 6, pp. 145 to 162. Pergamon Press Ltd., London

ANELASTIC CREEP OF POLYMETHYL METHACRYLATE

By O. D. Sherby* and J. E. Dorn†
University of California, Berkeley

(*Received* 11*th September*, 1957)

Summary

The deformation of polymethyl methacrylate over the temperature range 263° K to at least 410° K is entirely anelastic. That is, removal of the stress causes the material to return completely to its original length, provided sufficient time is allowed to permit complete recovery to take place. In the temperature range 263° K to 320° K it is shown that the activation energy for creep is independent of the strain but decreases linearly with an increase in the applied creep stress. These results are strikingly dissimilar from the results obtained for metals where the activation energy for creep is known to be insensitive to the applied creep stress. Above 320° K, the activation energy for creep increases rapidly with increasing temperature. In this range, transients are observed in the creep curves when sudden changes in temperature are made. These transients are best explained by a second order phase change occurring over a range of temperature.

1. Introduction

Creep is generally defined as the time-dependent deformation of a material under constant load or stress which occurs as a result of some thermal activation process. Most theories of creep (Becker 1926, Kauzmann 1941, Seitz and Read 1941, Nowick and Machlin 1947, Mott 1954) can be formulated to appear as follows :

$$\dot{\epsilon} = A \exp(-Q/RT) \text{ when } \sigma = \text{constant}, \tag{1}$$

where $\dot{\epsilon}$ = creep rate at specified state, A = constant, Q = experimental (or observed) activation energy for creep, R = gas constant, T = absolute temperature and σ = applied creep stress. Generally, these theories postulate that the applied creep stress decreases the thermal energy fluctuation necessary to cause flow. Kauzmann (1941), Seitz and Read (1941) and Mott (1954) suggest that Q varies with the stress according to

$$Q = \Delta H^* - B\sigma, \tag{2}$$

where ΔH^* = activation energy for unit flow process in the absence of stress and B = constant associated with the volume of the flow unit. Thus, according to (2), the observed activation energy should be linearly dependent on the applied stress σ, and the true value of ΔH^* can be obtained by an extrapolation of the $Q - \sigma$ relationship to zero stress.

* Scientific Liaison Officer, Office of Naval Research, London Branch, formerly Research Engineer, Institute of Engineering Research, University of California, Berkeley.
† Professor of Physical Metallurgy, University of California, Berkeley.

Application of these theories to creep of metals has not been rewarding (SHERBY *et al.* 1954, 1957, TIETZ and DORN 1956, HUANG *et al.* 1956, WEERTMAN and SHAHINIAN 1956). A large discrepancy arises from the experimental fact that the observed activation energy for creep, Q, appears to be insensitive to the stress. An example of this discrepancy is shown in Fig. 1 for creep of pure aluminium at

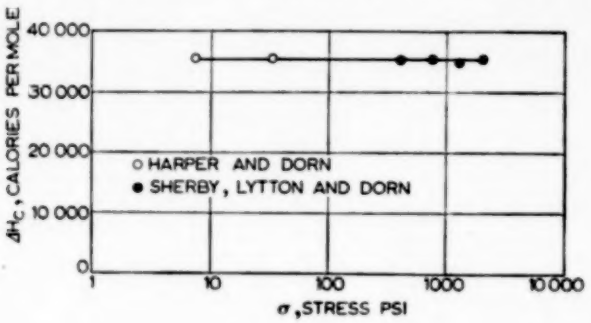

Fig. 1.

elevated temperatures. This suggests a separation of the stress and temperature terms into two separate parameters, namely

$$\dot{\epsilon} = A \exp(-\Delta H_c/RT) f(\sigma) \tag{3}$$

where ΔH_c = activation energy for creep and $f(\sigma)$ is some function of stress which does not include a temperature term. This discrepancy undoubtedly arises from the type of deformation occurring in creep of metals at high temperatures. It is now an established fact that ΔH_c for most pure polycrystalline cubic and hexagonal metals equals the respective activation energies for self-diffusion, (SHERBY *et al.* 1954, DORN 1954, FRENKEL *et al.* 1955, WEERTMAN and SHAHINIAN 1956). These results suggest that high temperature creep in metals is thermally controlled by dislocation climb where dislocations are imagined to surmount barriers by climbing away from their original slip plane through an atom-vacancy exchange process. WEERTMAN (1955) has presented a detailed model for creep in metals based on dislocation climb and has obtained a theoretical expression equivalent to (3).

High polymeric materials are structurally quite different from metals. Deformation of such materials is believed to occur by a motion of large chain segments one past another rather than by motion of dislocations as in metals. No known data on high polymers are believed to be currently available to suggest whether the observed activation energy for creep is dependent on the applied stress or whether the situation is similar to that for metals. The current investigation was initiated to check these two alternative possibilities for the creep mechanisms of a typical high polymeric material.

2. MATERIAL, EQUIPMENT AND EXPERIMENTAL TECHNIQUES

The material chosen for investigation was a polymethyl methacrylate commercially available under the name 'Plexiglas' (Rohm and Haas). Several reasons

prompted the use of this material for the current investigation : (1) Polymethyl methacrylate is a typical thermoplastic material. (2) It does not absorb water, and therefore the mechanical properties will not change with changes in atmospheric humidity. Furthermore, it is unattacked by most inorganic reagents and some of the more common organic solvents. (3) Commerical polymethyl methacrylate contains little, if any, plasticizing agents. (4) The mechanical properties of this material are known to be strongly affected by temperature, thus permitting a wide range of investigation. (5) The material has been extensively investigated for its tensile and creep properties and such data might be useful in cross-correlations with the data of the present investigation.

Specimens were prepared from 0·125 in. thick sheet, with gauge dimensions of 0·25 in. in width and length of 1·80 in. Extensions were obtained by means of extensometers which were sensitive to 10^{-4} in., thus permitting a strain sensitivity of about $5{\cdot}10^{-5}$ in. per in. Creep testing was conducted in machines having specially contoured Andrade–Chalmers type lever arms (Andrade and Chalmers 1932) served to maintain the stress constant within $\pm$ 1 per cent of the indicated value. A check on the constancy of the true stress during a creep test was made by means of a specially calibrated proving ring placed in series with the specimen. Constant temperatures above room temperature were obtained with silicone oil baths controlled by mercury thermoregulators. The temperatures used below room temperature, namely, 263° K and 273° K, were conducted in silicone oil baths

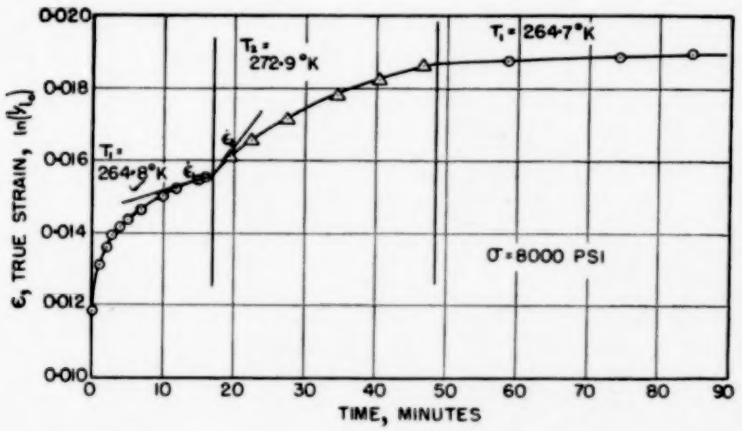

Fig. 2.

surrounded by baths containing a eutectic mixture of ice and potassium chloride solution for the 263° K bath, and an ice-water mixture for the 273° K bath. Specimen temperatures were maintained constant to within $\pm$ 0·2° C at any given temperature. All strains recorded in this investigation are reported as true strain ϵ, name $\epsilon = \ln (l/l_0)$, where ln is the natural logarithm, l is the total length of the specimen at any time during creep (including elastic strain), and l_0 is the original length. This appears to be a common procedure in reporting tensile and creep data on plastics (Marin *et al.* 1951).

A natural difficulty arises in the determination of activation energies for creep of materials from the fact that in the usual creep tests under constant stress the creep rate is constantly changing as a function of time. This change in creep resistance of the material is a result of structural changes that occur during creep deformation. It is therefore necessary to isolate the structure in order to determine activation energies that are free from possible errors arising from neglect of structural differences. A simple and direct technique was recently utilized in the determination of activation energies for creep of pure copper (TIETZ and DORN 1956) and pure aluminium (HUANG *et al.* 1956, SHERBY *et al.* 1957). This technique involves rapid changes in temperature during creep under constant stress. A typical example of such a test for polymethyl methacrylate is shown in Fig. 2.

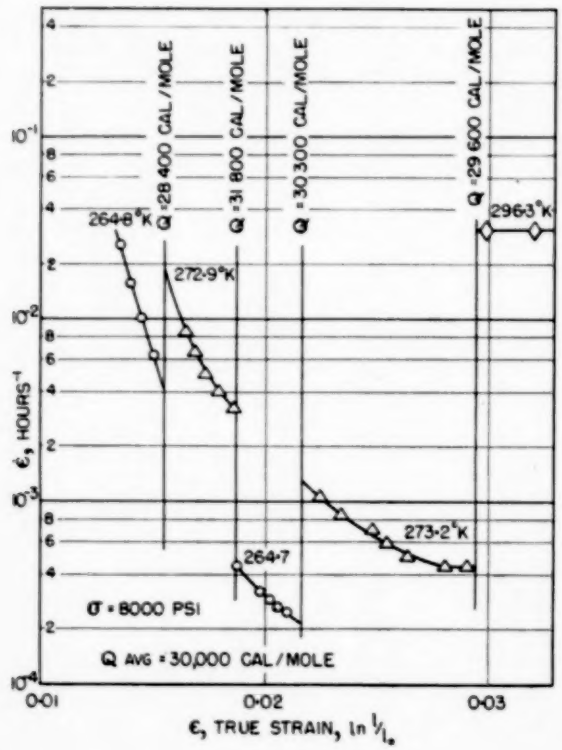

Fig. 3.

The material is allowed to creep under a constant stress of 8000 psi at $T_1 = 264{\cdot}8°\text{K}$ to a strain of about $\epsilon = 0{\cdot}0155$, whereupon the temperature is rapidly changed to a new higher temperature $T_2 = 272{\cdot}9°\text{ K}$. After further creep at the new temperature T_2, the temperature is again rapidly changed to the previous low temperature T_1, etc. It is readily appreciated that the rates of creep immediately preceding and immediately after a change in temperature, $\dot{\epsilon}_1$, and $\dot{\epsilon}_2$ respectively, refer to the creep rates at the two temperatures for the same prescribed strained

state ϵ_1 and the same creep stress σ. Thus, the activation energy is readily determinable from (1), namely

$$\dot{\epsilon}_1 \exp(Q/RT_1) = \dot{\epsilon}_2 \exp(Q/RT_2). \tag{4}$$

Actually, activation energies for creep were obtained from a graphical differentiation of curves such as those in Fig. 2, the resulting creep rates being plotted as a function of the true strain (Fig. 3). Extrapolations of the creep rate – true strain curves to the strain where the temperature change is made permits an unambiguous and reliable method of determining activation energies.

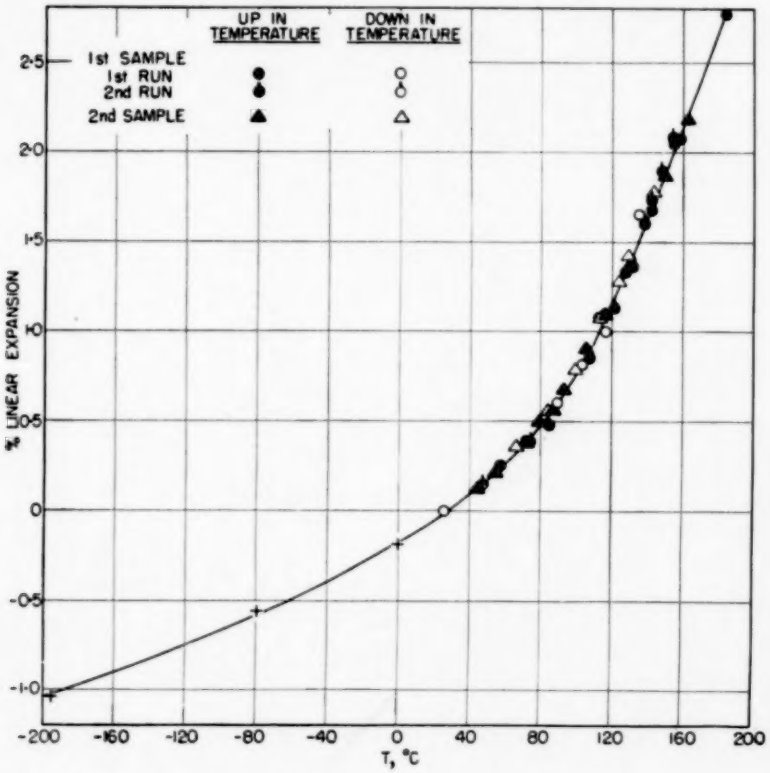

Fig. 4.

Because high polymeric materials are known to expand considerably with temperature, it was necessary to correct for this change in length when a rapid change in temperature was made. For this reason the linear thermal expansion of commercial polymethyl methacrylate was determined and is recorded in Fig. 4. Measurements at low temperatures were made by the use of a 10^{-4} in. sensitivity dial gauge on a six inch long specimen, whereas measurements above room were made by means of a travelling stage microscope on a three inch long specimen which was heated in a silicone oil bath. Each temperature at which a measurement

was made was kept constant for 12 hr before a change was made to the next higher or lower temperature. The data in Figs. 2 and 3 and all similar data recorded in subsequent figures reveal creep strains that are corrected for thermal expansion following temperature changes.

3. PRELIMINARY TESTS

In order to determine the nature of creep of commercial polymethyl methacrylate many preliminary creep tests were performed.

Anelastic creep. Materials deformed under constant stress exhibit three types of deformation : elastic, anelastic and plastic. Elastic deformation refers to the strain occurring on application of a stress which is completely recovered immediately on removal of the load. Anelastic deformation (ZENER 1948) is also recoverable after removal of the load but is time-dependent. On the other hand plastic deformation refers to permanent deformation which does not recover after removal of the load. Metals normally exhibit elastic and plastic deformation with very little anelastic behaviour. Plastics on the other hand are known to exhibit large elastic and anelastic components of creep. A few preliminary tests performed on polymethyl methacrylate revealed that over the temperature range – 10° C to + 140° C (263° K to 413° K) and up to creep strains of at least 200 per cent the material exhibited only elastic and anelastic behaviour always returning to its original shape and dimensions after removal of the creep stress provided sufficient time was given for complete recovery to occur. A typical example of this behaviour is shown in Fig. 5 where after creep at 365° K to a true creep strain of 0·42 the temperature was decreased to a

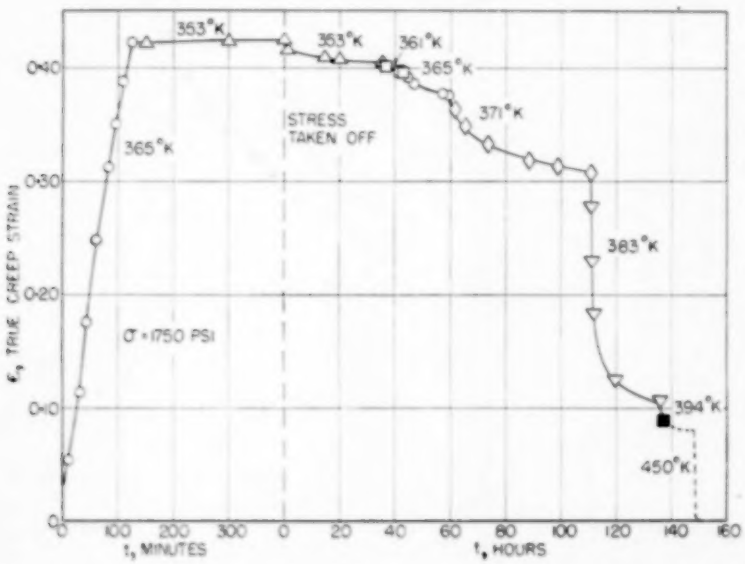

Fig. 5.

lower creep test temperature of 353° K. This was done in order to study the anelastic recovery properties over as wide a temperature range as was reasonably possible. At a strain of 0·425 the load was removed and the creep strain recovery was observed as a function of time. Because the recovery rate was observed to decay rapidly with the recovered strain it was decided to speed up the process by increasing the temperature in abrupt increments. It can be seen that by the time a temperature of 394° K was reached approximately 70 per cent of the original deformation had been recovered. It was not possible to measure additional recovery of the specimen at this point because the weight of the extensometer was sufficiently large to impose a stress on the

material preventing further recovery. However after removal of the extensometer the specimen was immersed into a 450° K bath for 2 hours and complete recovery of the material was observed to take place as measured by precision micrometers.

This result, together with many additional tests up to 410° K clearly revealed that only one time-dependent mode of deformation occurs during creep of polymethyl methacrylate, namely, anelastic creep. The common report made by many investigators on creep of high polymeric materials that constant rate creep is due to a 'viscous' component of deformation which is not anelastic but plastic must be subject to question. Moreover, recovery tests performed at the same temperature as the creep test do not reveal the amount of creep due to a viscous component (as assumed by many investigators, e.g. Robinson *et al.* 1944, Alfrey 1948) since the rate of creep recovery decreases so rapidly with time. For example, a rough estimate from a knowledge of the effect of temperature on the creep recovery rate as shown in Fig. 5 reveals that it would have taken about 25×10^6 hr or about 3000 years to recover the material from 0·425 to 0·11 at a temperature of 353° K. Thus, creep recovery of polymethyl methacrylate would appear to have ceased for all practical purposes after the first few hours but in reality it would be contracting at a monotonically decreasing rate.

Heat treating procedure. In order to assure the best possible reproducibility of the creep data many tests were performed to determine the effect of previous heat treatment on the subsequent creep properties. The importance of this factor is clearly revealed in Figs. 6 and 7.

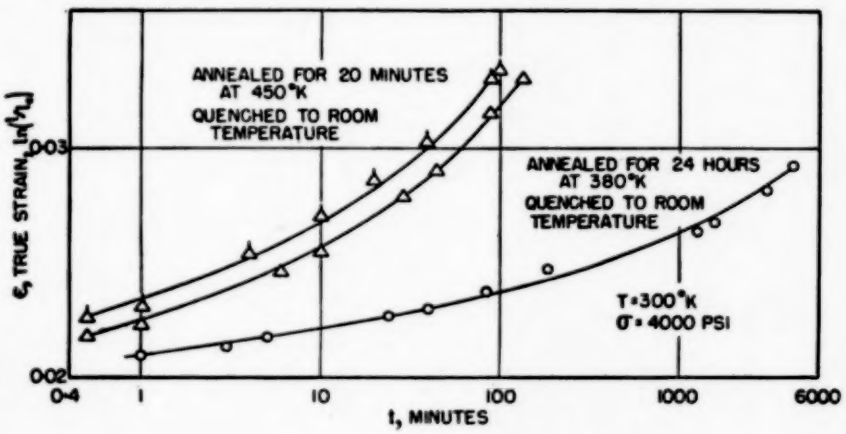

Fig. 6.

The data of Fig. 6 reveal that retention of the high temperature structure by air quenching from 450° K results in a vastly less creep resistant structure than a similar material quenched from 380° K. Apparently the structure of commercial polymethyl methacrylate is strongly dependent on temperature in the range of high annealing temperatures used here. This effect of quenching is discussed in greater detail later.

The data in Fig. 7 reveal three pertinent and interesting facts:

(1) The results on Specimens *A* reveal the effect of a re-annealing cycle on the creep properties of commercial polymethyl methacrylate. Since it has already been established that this material exhibits only anelastic creep, it would be expected that the structure after complete recovery would be identical to the initial state of the material. That this is reasonably so is shown by the series of experiments on specimen *A* shown in Fig. 7. This specimen was initially annealed at 450° K for 20 min then air cooled. It was then creep tested under the variable stress conditions documented in the Figure until a total true strain of $\epsilon = 0{\cdot}18$ was achieved, at which point the test was terminated and the specimen annealed at 450° K for 20 min and air cooled; measurements on the specimen revealed complete recovery of the elongation. The same cycle of stressing was then repeated on the same specimen. It will be seen that the two tests revealed about the same creep properties, although some scatter is evident in the resulting creep curves. The scatter,

however, is approximately the same as that achieved in creep of identically treated specimens which can be seen from the individually tested specimens as quenched from 380° K shown in the same Fig. 7.

(2) The tests on specimen *A* also suggest that there is no apparent effect from the silcone oil on the creep properties of polymethyl methacrylate.

(3) Although the creep resistance is increased by a low temperature anneal, the elongation properties are adversely effected. The specimens annealed at 380° K all began to craze at about a strain of 0·04 and failed soon thereafter.

In order to minimize the presence of crazing it was decided to adopt a standard heat treatment at 450° K for 20 min followed by an air quench.

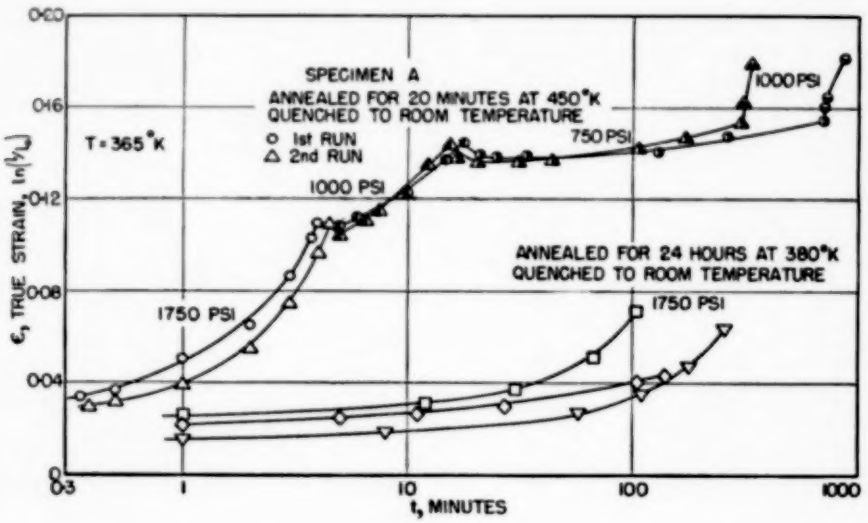

Fig. 7.

4. Results and Discussion

Tensile creep of polymethyl methacrylate in the temperature range 260° K *to* 320° K.

Activation energies for creep of polymethyl methacrylate were obtained over a stress range from 10000 psi to 1000 psi. It was observed that the activation energy for creep did not vary with the creep strain for any one given creep stress. An example of this strain insensitivity of Q can be seen in Fig. 3. On the other hand, the observed activation energy appears to be strongly affected by the applied creep stress. The higher the applied stress the lower the observed activation energy. This point is clearly revealed by the data in Fig. 8 where the average observed activation energy for each stress is plotted as a function of the creep stress. In fact, an excellent linear relationship between Q and σ is apparent showing that the applied stress lowers the activation energy for creep in complete harmony with those theories of creep (Kauzmann 1941, Seitz and Read 1941, Mott 1954) which suggest that the stress linearly decreases the thermal energy fluctuation for activation of the flow process. Extrapolation of the $Q - \sigma$ curve to zero stress suggests that the true activation energy for the process is equal to about 48,000 cal/mole. Kauzmann (1941), using Eyring's reaction rate theory

(GLASSTONE *et al.* 1941), has shown that B in equation (2) can be related to a volume of a flow unit by $B = Nq\,A\lambda/2\sqrt{3}$, where N = Avogadro's number, q = stress concentration factor usually assumed equal to unity, and $A\lambda$ = volume of flow unit. B is equal to the slope of the curve in Fig. 8, and simple calculations reveal that $A\lambda = (20{\cdot}3\ \text{Å})^3$. This appears to be a reasonable value for the average volume of the flow unit in a high polymeric material and suggests that each unit of activation involves the motion of only a segment of a molecule. Unfortunately,

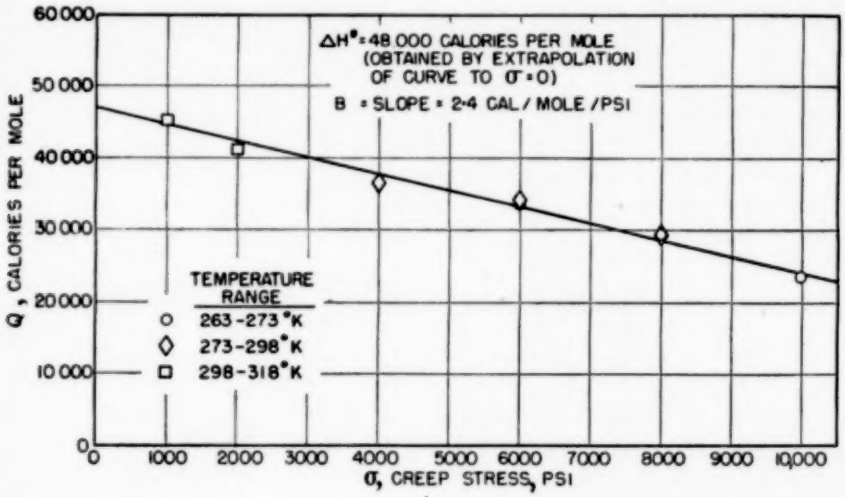

Fig. 8.

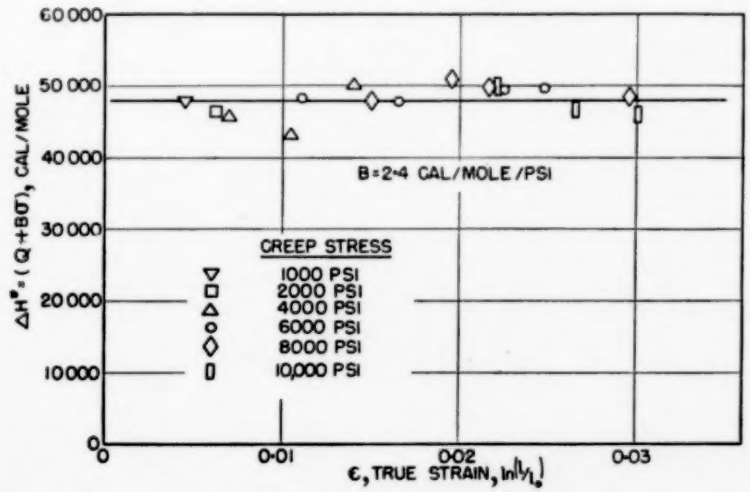

Fig. 9.

there is nothing available in the literature on other properties of polymethyl methacrylate to suggest what segment of the polymer might be involved nor is there any hint as to the significance of 48,000 cal/mole that was obtained for the

activation energy for anelastic creep. It is interesting to note that this value of ΔH^* is a rather high value when compared with the activation energies for high temperature creep of pure metals where a comparable melting metal ($T_m = 600°$ K) would possess an activation energy of about 20,000 cal/mole (Dorn 1954). It is entirely possible that the high activation energy for polymethal methacrylate is associated with its rather large flow unit. In certain respects it is not clear why the activation energy is insensitive to the creep strain although this fact is readily apparent from the composite graph of ΔH^* values versus the creep strain, shown in Fig. 9, where $\Delta H^* = Q + B\sigma$. Since creep of polymethyl methacrylate is anelastic and therefore refers to simply an uncurling process of the large intertangled molecules, it might be thought that creep might occur by a spectrum of activation energies. The easier ones might take place early in the creep process and the more difficult processes might take place later, and this would account for the diminishing creep rate. Since this is not the case, however, it must be concluded that even though ΔH^* remains constant other structural changes take place during

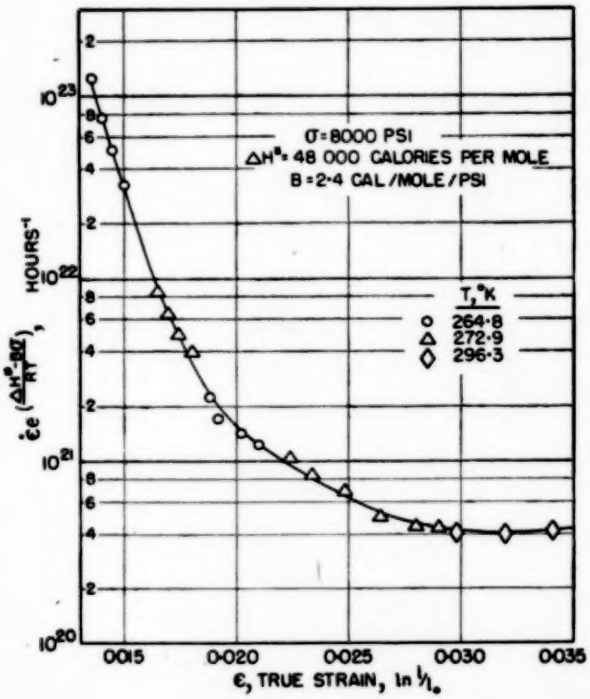

Fig. 10.

creep which account for the diminishing creep rate characteristics of polymethyl methacrylate. In terms of the Kauzmann–Eyring theory this would mean changes in the unit jump distance or in the entropy of activation for the flow process, which is incorporated in the constant A of (1).

The most significant conclusion of the results however, is that the stress appears to lower the free energy of activation as would be anticipated from the Kauzmann–

EYRING types of creep theories. This fact is in sharp contrast to the results obtained for metals and suggests a fundamental difference in the creep behaviour of metals and high polymeric materials.

The validity of (1) and (2) suggests that, for a constant stress creep test, the following creep expression might be valid for creep of polymethyl methacrylate at low temperatures :

$$\dot{\epsilon} \exp\left[(\Delta H^* - B\,\sigma)/RT\right] = F(\epsilon) \text{ when } \sigma = \text{constant}, \tag{5}$$

based on the reasonable assumption that A is some function of the creep strain ϵ. Here $\Delta H^* = 48{,}000$ cal/mole and $B = 2{\cdot}4$ cal/mole/psi. The validity of (5) is readily revealed for creep of polymethyl methacrylate at $\sigma = 8000$ psi (Fig. 10).

In terms of creep strain-time data it might be suggested that, since $\dot{\epsilon} \sim 1/t$, a similar expression to (5) is applicable for correlation of such data under constant stress, namely

$$t \exp\left[-(\Delta H^* - B\,\sigma/RT\right] = F(\epsilon) \text{ when } \sigma = \text{constant} \tag{6}$$

An example of the validity of (6) is clearly revealed for creep of polymethyl methacrylate in Fig. 11.

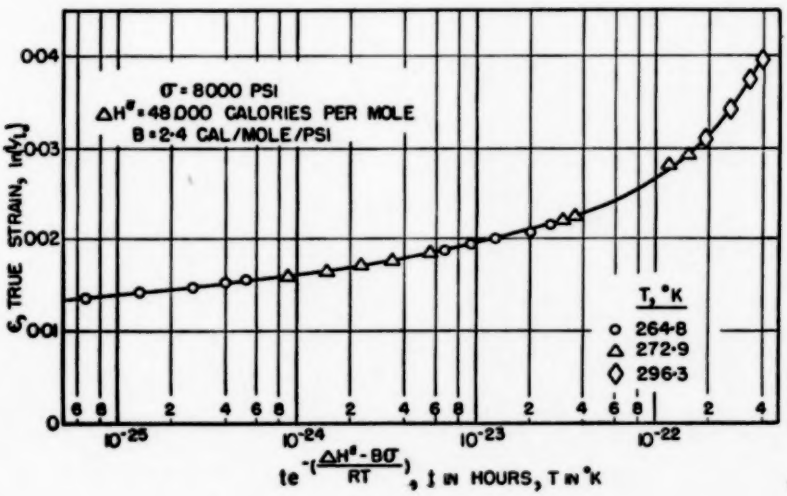

Fig. 11.

In a report (SHERBY 1956) on which this paper is based it was shown that data on creep of polymethyl methacrylate obtained by other investigators can be satisfactorily correlated with (5) and (6). Such correlations again suggest that the creep stress appears to decrease the thermal activation energy necessary for anelastic flow.

Tensile creep of polymethyl methacrylate in the temperature range 320° K *to* 380° K

Evaluation of ΔH^* *and* $A\lambda$. A typical example of the effect of temperature on the creep rate of polymethyl methacrylate in this temperature range is revealed

by the data recorded in Fig. 12. The results of this test are not immediately apparent although, for any one test covering a small temperature interval, it appears that the creep strain again does not affect the observed activation energy for creep. Fig. 13 reveals the effect of stress on the observed activation energy for creep, where each line refers to the values obtained over the indicated temperature interval.

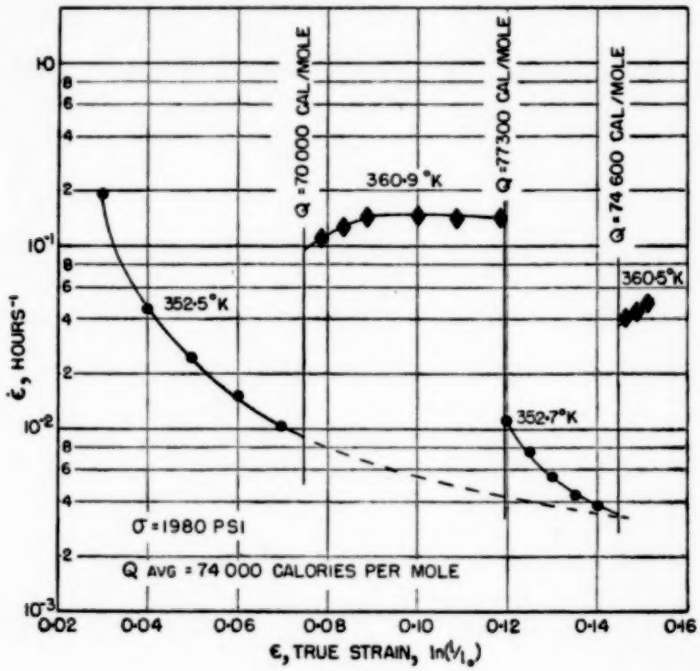

Fig. 12.

It will be noted that two new trends are evident. Firstly, the activation energy ΔH^* appears to be increasing rapidly with temperature and, secondly, the slope of the $Q - \sigma$ curve increases with increasing temperature, suggesting that the volume of the flow unit increases with temperature.

The rapid change of ΔH^* and $A\lambda$ with temperature above 320° K is not easily understood, although it is reasonable to assume that a larger activation energy would be related to a larger flow unit size. These results might be associated with certain important changes in other properties that take place in polymethyl methacrylate above 320° K. For example, CARSWELL and NASON (1944) reveal that the ductility of polymethyl methacrylate increases abruptly above 320° K, and the thermal expansion characteristics are known to change rather sharply above 320° K to yield a much higher coefficient of thermal expansion (Fig. 4). A plot of ΔH^* and $A\lambda$ as affected by temperature from 263° K to 370° K is shown in Fig. 14. To be sure, increased thermal vibration occurs at higher temperatures, and the so-called transition temperature (about 320–340° K for polymethyl methacrylate) is ascribed to the initiation of free rotation about carbon–carbon bonds

(Boyer and Spencer 1945). If one considers that the energy for flow is associated with the breaking of the van der Waals' bonds between adjacent segments, then it is difficult to conceive why the thermal energy for this process should increase so drastically with temperature. Obviously, other processes with higher activation energies begin to predominate. One possibility for such an occurrence would

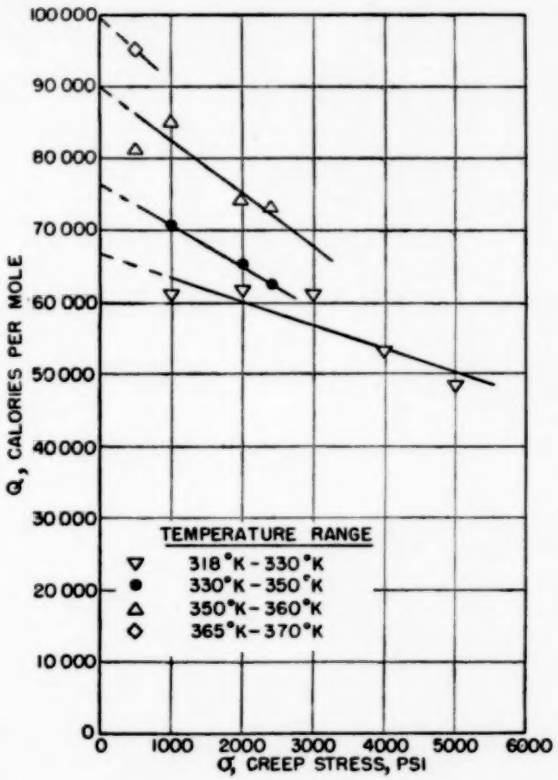

Fig. 13.

arise if the weight factor (frequency of occurrence) for such a higher activation process were sufficiently greater than the weight factor for the lower activation energy process. It was shown that such considerations permitted a correlation of the observed activation energies for creep of pure aluminium at low temperatures (Sherby *et al.* 1957) where ΔH_c is no longer a constant. Thus, if creep were to take place by the mutual interaction of several thermal activation processes acting additively, the creep rate would be given by

$$\dot{\epsilon} = F\,\Sigma\left[W_i \exp\left(-\Delta H_i^*/RT\right)\right], \qquad \sigma \text{ and } \epsilon \text{ constant}, \tag{7}$$

where W_i = weight factor for ith process, ΔH_i = activation energy for ith process, σ = stress, and ϵ = specified strained state. Since the observed activation energy is derived from the relation

$$Q = -R\frac{d\left(\ln \dot{\epsilon}\right)}{d\left(1/T\right)},$$

it is readily seen from a differentiation of (7) with respect to $1/T$ that the observed activation energy should be related to the various actual activation energies ΔH_i^* by

$$Q = \frac{\Sigma W_i \Delta H_i^* \exp(-\Delta H_i^*/RT)}{\Sigma W_i \exp(-\Delta H_i^*/RT)}. \tag{8}$$

It was shown that the assumption of four activation energies in the temperature range 78° K to 250° K yielded perfect agreement with the experimentally observed activation energies which decreased linearly with a decrease in temperature for high purity aluminium (SHERBY *et al.* 1957). The current results do not suggest whether anelastic creep of polymethyl methacrylate above 320° K occurs by the

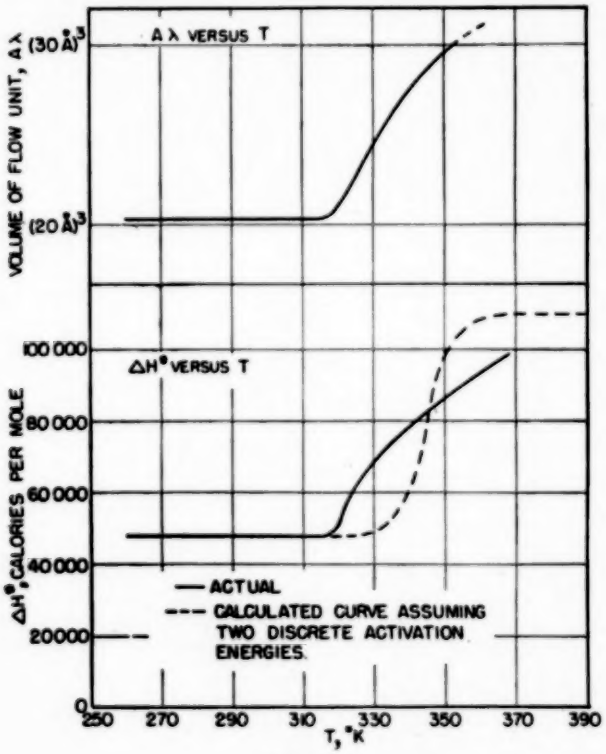

Fig. 14.

presence of a spectrum of activation energies or by the co-operative interaction of several (at least two) characteristic activation energies. One characteristic activation energy appears to have been obtained below 320° K equal to $\Delta H^* = 48{,}000$ cal/mole. It is possible that at yet higher temperatures, above 370° K, another constant activation energy would have been obtained over another temperature interval. Unfortunately, the creep resistance of polymethyl methacrylate was so small above 370° K that it was not possible to accurately determine the effect of temperature on creep with the presently designed equipment. It can be readily shown that the results obtained cannot be accounted for on the assump-

tion that only two activation energy processes exist, one equal to 48,000 cal/mole and one high activation energy, say equal to 110,000 cal/mole which might predominate above 370° K. On the basis of such an assumption the weight factors can be readily calculated. Arbitrarily assigning $W_1 = 1$ for $\Delta H_1^* = 48{,}000$ cal/mole, W_2 can be calculated by the use of (8) from a knowledge of the observed activation energy in the intermediate temperature range such as $T = 345°$ K where $Q = 82{,}000$ cal/mole. By such a procedure, W_2 was found to be extremely large, equal to about $9{\cdot}6 \times 10^{38}$. The activation energy for creep can now be solved for at any temperature from a knowledge of the constants W_1, W_2, ΔH_1^*, and ΔH_2^*. The curve predicted by such an analysis is revealed by the dotted line in Fig. 14. It can be readily seen that in no way is there a correlation between the predicted and the actual curve. This analysis strongly suggests that, if several characteristic activation energies exist that are co-operating additively, then there must be several closely spaced ones. Indeed it is entirely possible that a spectrum of activation energies and weight factors exist which control the creep process of polymethyl methacrylate in the temperature range 320° K to 370° K.

Transients observed upon sudden temperature changes

In addition to the trends of ΔH^* and $A\lambda$ with temperature, it was also observed that transients were obtained in the creep behaviour of the material after a rapid decrease or increase in temperature above about 340° K. A typical example illustrating the type of transient obtained at high temperature can be seen in Fig. 12. It will be observed that after the temperature was increased from 352·5° K to 360·9° K (and the new temperature was attained) the creep rate continued to increase with creep straining until a certain maximum rate was attained and then the creep rate began to decrease as creep continued. On the other hand, when the temperature was decreased the rate would appear to be much more rapid than the rate as predicted from an extrapolation of the creep curve at the original low temperature. But with subsequent creep straining the rate of creep appears to decrease very rapidly and soon coincides with an extrapolation of the previous creep curve at the same temperature. These results are highly suggestive of a second-order phase change occurring within the plastic as a function of temperature. The reason for considering it a second order phase change is based on the fact that the transient phenomenon persists over a wide range of temperature. Perhaps polymethyl methacrylate can be considered as a crystalline polymer where there are regions of high order and regions of disorder (Alfrey 1948). A single polymer molecule would probably extend through several zones of order and disorder. Such a material does not have a sharp melting point but gradually loses its crystallinity as the temperature is increased. Of course, such a disordering of the polymer with increase in temperature would be time dependent, perhaps requiring the diffusion of holes from the surface to the crystalline region in order to permit accommodation for the larger volume of the amorphous phase. Such processes would be reversible with temperature. However, there are several experimental facts for polymethyl methacrylate which reveal that, if such a second order phase change is present, complicated controlling mechanisms occur. If it were a true order-disorder phenomenon then it might be suspected that the thermal expansion curve for a specified temperature at high temperatures (Fig. 4) represents the coefficient of

thermal expansion for the specified thermodynamically stable disordered state. Therefore, if a polymethyl methacrylate sample were quenched from a high temperature, the coefficient of thermal expansion at low temperatures should be approximately equal to the coefficient of expansion at high temperatures if the high temperature structure were retained. This does not appear to be the case

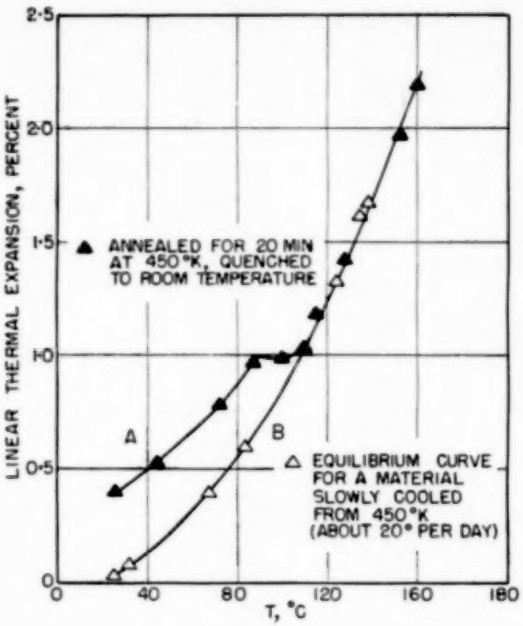

Fig. 15.

as revealed by such an experiment recorded in Fig. 15. Apparently, the high temperature quenched state exhibits the same coefficient of thermal expansion as a slowly cooled sample. It must therefore be concluded that the high temperature coefficients of thermal expansion are not real but reflect a change in volume due to other changes in structure. Such results suggest the strong probability that holes diffuse into the structure as a function of increased temperature (ALFREY *et al.* 1943), perhaps, as mentioned previously, in order to attain the thermodynamically stable disordered state. Therefore, if the temperature is increased rapidly, the specimen will contract according to its normal low temperature expansion curve but because no time is permitted for diffusion the specimen is larger than the equilibrium length.

The quenching experiments described earlier in the paper are in complete harmony with the suggested structural changes occurring in polymethyl methacrylate as a function of temperature. Thus, the high temperature quenched state represents a disordered open sturcture which would be expected to cause creep to occur at a more rapid rate than a more ordered compact structure. The results in Figs. 6 and 7 bear out this suggestion.

Conclusions

(1) The deformation of polymethyl methacrylate at constant stress over the temperature range 263° K to at least 410° K is entirely anelastic. That is, removal of stress causes the material to return completely to its original shape, provided sufficient time is allowed to permit complete recovery to take place.

(2) The experimental activation energy for anelastic creep of polymethyl methacrylate, Q, was determined by rapidly changing the temperature during creep under constant stress. In the temperature range 263° K to 320° K it was shown that the activation energy for creep remains constant as a function of strain but decreases linearly with an increase in the applied creep stress. These results give strong support to the Kauzmann–Eyring types of creep theories which suggest that the applied creep stress linearly decreases the energy of activation for the flow process. The true activation energy for anelastic creep, obtained by extrapolation of the observed activation energy-creep stress relation to zero stress, is $\Delta H^* = 48{,}000$ cal/mole. The flow unit size, calculated by means of the Kauzmann–Eyring theory, was determined to be $(20{\cdot}3\text{Å})^3$.

(3) Creep strain-time data at various temperatures in the low temperature range of creep for polymethyl methacrylate can be correlated by the relation

$$\epsilon = F\{t \exp[-(\Delta H^* - B\sigma)/RT]\}$$

when σ is constant, where ϵ = strain, t = time under constant stress σ, R = gas constant, T = absolute temperature, $\Delta H^* = 48{,}000$ cal/mole and $B = 2{\cdot}4$ cal/mole/psi.

(4) Above 320° K the activation energy for the unit flow process, as well as the volume of the flow unit, increases rapidly with increasing temperature. It is believed that the factors responsible for these results are the same factors involved in the rapid increase in the coefficient of thermal expansion above 320° K.

(5) Transients were observed in the creep curves above 320° K when sudden changes in temperature were made. These transients are best explained by a second-order phase change occurring over a range of temperatures. The results of low temperature creep tests on specimens quenched from various high temperatures are in harmony with the observed transients.

Acknowledgments

It is a pleasure to acknowledge stimulating discussions with W. Elkington, J. Lytton, J. Harper, T. Trozera and L. Shepard.

References

Alfrey, T. 1948 *Mechanical Behaviour of High Polymers* (Interscience Publishers Inc.)

Alfrey, T., Goldfinger, G. and Mark, H. 1943 *J. Appl.* **14**, 700.

Andrade, E. N. da C. and Chalmers, B. 1932 *Proc. Roy. Soc.* **138**, 348.

BECKER, R.	1926	*Z. Tech. Phys.* **7**, 547.
BOYER, R. F. and SPENCER, R. S.	1945	*J. Appl. Phys.* **16**, 594.
CARSWELL, T. S. and NASON, N. K.	1944	*Symposium on Plastics* (A.S.T.M.).
DORN, J. E.	1954	*J. Mech. Phys. Solids* **3**, 85.
FRENKEL, R. E., SHERBY, O. D. and DORN, J. E.	1955	*Acta Met.* **3**, 470.
GLASSTONE, S., LAIDLER, K. J. and EYRING, H.	1941	*The Theory of Rate Processes* (McGraw-Hill, New York).
HARPER, J. and DORN, J. E.	1957	*Acta Met.* **5**, 654.
HUANG, H. I.-LIEH, SHERBY, O. D. and DORN, J. E.	1956	*Trans. Amer. Inst. Min. (Metall.) Engrs.*, **206**, 1385.
KAUZMANN, W.	1941	*Trans. Amer. Inst. Min. (Metall.) Engrs.* **143**, 57.
MARIN, J., PAO, YOH-HAN and CUFF, G.	1951	*Trans. Amer. Soc. Mech. Engrs.* **73**, 705.
MOTT, N. F.	1954	*Creep and Fracture of Metals at Elevated Temperature* (H.M.S.O.).
NOWICK, A. S. and MACHLIN, E. S.	1947	*J Appl. Phys.* **18**, 79.
ROBINSON, M. A., RUGGY, R. and SLANTZ, E.	1944	*J. Appl. Phys.* **15**, 343.
SEITZ, F. and READ, T. A.	1941	*J. Appl. Phys.* **12**, 538.
SHERBY, O. D.	1956	*Anelastic Creep of Polymethyl Methacrylate.* Ph.D. Thesis of Univ. of California, Berkeley.
SHERBY, O. D., ORR, R. L. and DORN, J. E.	1954	*Trans. Amer. Inst. Min. (Metall.) Engrs.* **200**, 71.
SHERBY, O. D., FRENKEL, R., NADEAU, J. and DORN, J. E.	1954	*Trans. Amer. Inst. Min. (Metall.) Engrs.* **200**, 275.
SHERBY, O. D., LYTTON, J. L. and DORN, J. E.	1957	*Acta Met.* **5**, 219.
TIETZ, T. E. and DORN, J. E.	1956	*Trans. Amer. Inst. Min. (Metall.) Engrs.* **206**, 156.
WEERTMAN, J.	1955	*J. Appl. Phys.* **26**, 1213.
WEERTMAN, J. and SHAHINIAN, P.	1956	*Trans. Amer. Inst. Min. (Metall.) Engrs.* **206**, 1223.
ZENER, C.	1948	*Elasticity and Anelasticity of Metals* (Chicago Univ. Press).

Journal of the Mechanics and Physics of Solids, 1958, Vol. 6, pp. 163 to 176. Pergamon Press Ltd., London

CREEP BEHAVIOUR OF CIRCULAR PLATES*

By B. VENKATRAMAN and P. G. HODGE, JR.
Polytechnic Institute of Brooklyn

(*Received 3rd June, 1957*)

SUMMARY

AN analysis of creep in circular plates under the action of uniformly distributed lateral loads is presented. The creep law used is based upon a flow rule associated with a condition of maximum shearing stress. It is assumed that steady creep conditions prevail and that the creep rate is equal to a function of moment multiplied by a function of time. The method is applied to plates with simply supported and clamped edges. Closed form solutions for moments and creep deformations are presented.

1. INTRODUCTION

MOST engineering theories of creep are based on assumed empirical relations between stress and creep rate. A great number of these relations have been obtained from experiments in which the stresses were essentially one-dimensional. Various attempts at generalizing these relations have been made for the analysis of creep in a multi-dimensional state of stress. To this end, theories which have proved successful in plasticity theory may provide a reasonable basis.

The essential ingredients of a theory of plasticity are a yield condition for initiation of plastic flow, and a flow rule for its continuation. The yield condition is generally regarded as the plastic potential for the flow rule. The two most commonly used yield conditions are Tresca's condition, based upon the maximum shearing stress, and Mises' condition, based upon the octahedral shearing stress.

BAILEY (1935) in his paper on the design use of creep test data was one of the first to adapt plasticity theory for use in creep problems. SODERBERG (1936) and ODQVIST (1934) based their theories of creep on the octahedral shearing stress criterion. POPOV (1947) and MILLENSON and MANSON (1948) used this criterion for the determination of stresses in turbine disks under creep conditions. In the calculation of creep deformations in rotating disks, WAHL and his co-authors (1954) made use of both the Mises and the Tresca criteria and the flow rule associated with the Mises criterion.

For stresses in a plastic solid, use of Tresca's yield condition frequently leads to a simpler system of equations than the use of Mises' yield condition. PRAGER (1953) and KOITER (1953) have discussed the further simplification obtained by using the Tresca criterion and the associated flow rule for certain types of problems

*The results presented in this paper were obtained in the course of research sponsored by the Air Force Office of Scientific Research of The Air Research and Development Command. The paper is part of a thesis submitted by one of the authors (B.V.) in partial fulfilment of the requirements for the degree of Doctor of Philosophy in Applied Mechanics at the Polytechnic Institute of Brooklyn.

involving plastic flow. WAHL (1956) showed that the use of this procedure considerably simplified the analysis of creep in rotating disks. The present paper is concerned with the application of the Tresca criterion and the associated flow rule to problems of calculating creep deformations and moments in circular plates.

A brief review of the Tresca criterion, the associated flow rule, and the equilibrium equations in problems relating to bending of circular plates is presented in Section 2. The discussion is restricted to rotationally symmetric types of loading and edge support. In particular, simply supported and built-in plates are considered, and the load is assumed to be uniformly distributed over the entire plate.

Next, the assumption is made that the elastic deformations are negligibly small in comparison with deformations due to creep. Further, steady-state creep conditions are assumed to prevail, i.e., the transient change in stress has already occurred, and creep takes place under essentially constant stress. Finally, the creep rate is considered equal to a function of moment times a function of time (BAILEY 1951, JOHNSON 1951).

With the above assumptions the simply supported plate under normal pressure is analysed in Section 3. Solutions for moments and creep deformations are pesented for both a power-function moment-creep-rate law and an exponential moment-creep-rate law. Section 4 outlines the use of the method for a built-in circular plate under the same conditions. The conclusions are briefly summarized in Section 5.

2. BASIC EQUATIONS

In plasticity theory it is convenient to represent the yield condition geometrically in a stress space whose coordinates are the stress variables. The plastic flow laws can then be formulated in terms of a vector whose components are the corresponding strain rate variables. Such a representation may be made in terms of the three dimensional stress and strain rate components or in terms of suitably chosen stress and velocity resultants.

The stress state in a rotationally symmetrically loaded circular plate is fully specified by the principal bending moments M_r and M_θ. It can be shown (HOPKINS and PRAGER 1953, PAUL and HODGE 1956) that the yield condition has the same form in terms of M_r and M_θ as in terms of the plane stress components σ_r and σ_θ, provided the tensile yield stress σ_0 is replaced by the maximum bending moment M_0. The corresponding strain rate variables are the middle surface curvature rates $\dot{\kappa}_r$ and $\dot{\kappa}_\theta$. In terms of these quantities the plasticity flow law states that the curvature rate with components $\dot{\kappa}_r$, $\dot{\kappa}_\theta$ must be normal to the yield curve.

For the particular case of Tresca's yield condition, the yield curve is the hexagon defined by

$$M = M_0, \tag{1a}$$

where

$$M = \max\left[|M_r|, \quad |M_\theta|, \quad |M_r - M_\theta|\right]. \tag{1b}$$

On each side of the hexagon, the curvature-rate vector must be normal to the side; at the corners it may take on any value between the limiting normals (Fig. 1). For a perfectly plastic material the length of the curvature-rate vector is undetermined. For strain-hardening plastic materials an additional relation between the curvature-rate vector and the stress intensity must be provided.

A creep flow law can be formulated in quite similar terms. The essential difference is that creep is assumed to be present at any stress intensity so that, effectively, the " yield moment " M_0 is zero. However, although the yield curve as such is thus reduced to a point, various domains in stress space are distinguished by

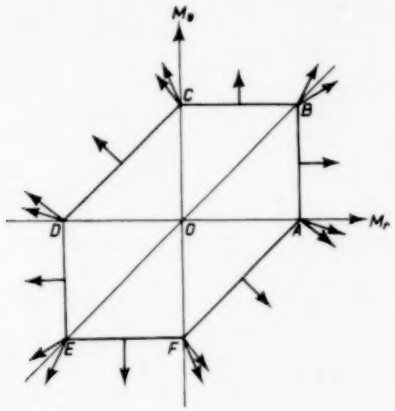

Fig. 1. Curvature-rate vectors.

different forms for the flow law, as indicated in Fig. 1. For example, in the octant defined by

$$0 < M_r < M_\theta \tag{2}$$

the curvature -rate vector must be vertical, so that

$$\dot{\kappa}_r = 0, \qquad \dot{\kappa}_\theta \geqslant 0. \tag{3}$$

Similarly, the relations

$$0 < M_\theta < M_r, \qquad \dot{\kappa}_\theta = 0, \qquad \dot{\kappa}_r \geqslant 0, \tag{4}$$

and

$$M_r < 0 < M_\theta, \qquad \dot{\kappa}_r + \dot{\kappa}_\theta = 0, \qquad \dot{\kappa}_\theta - \dot{\kappa}_r \geqslant 0 \tag{5}$$

go together. On the other hand, at a moment point on the line

$$0 < M_r = M_\theta \tag{6}$$

the curvature-rate vector has arbitrary direction, subject only to the inequalities

$$\dot{\kappa}_r \geqslant 0, \qquad \dot{\kappa}_\theta \geqslant 0. \tag{7}$$

Similar results hold for the other regimes, as indicated in Table 1.

The magnitude of the strain-rate vector is assumed to be expressible as a product of a function of the stress intensity and a function of time. Thus, in regime *BOC* (Fig. 1),

$$\dot{\kappa}_\theta = F(M)\, G(t) = F(M_\theta)\, G(t). \tag{8}$$

Equation (8) is generalized to the other regimes by requiring that the dissipation function

$$U = M_r \dot{\kappa}_r + M_\theta \dot{\kappa}_\theta, \tag{9}$$

be an invariant function of the stress intensity. It follows from (3) and (8) that in regime *BOC*

$$U = M_\theta \dot{\kappa}_\theta = M F(M) G(t). \tag{10}$$

Equation (10) is to be valid in all regimes. In *COD*, for example,

$$U = M_r(-\dot{\kappa}_\theta) + M_\theta \dot{\kappa}_\theta = M\dot{\kappa}_\theta = MF(M) Gt); \tag{11}$$

so that (8) holds in this case also. However, in regime *OB*,

$$U = M \dot{\kappa}_r + M \dot{\kappa}_\theta = M F(M) G(t); \tag{12a}$$

so that

$$\dot{\kappa}_r + \dot{\kappa}_\theta = F(M) G(t). \tag{12b}$$

Similar results are available for all twelve regimes; they are summarized in Table 1.

TABLE 1. *Creep flow laws for Tresca condition*

Regime	*Moments*	*Curvature rates*	*Creep law*
AOB	$M = M_r > M_\theta > 0$	$\dot{\kappa}_\theta = 0, \dot{\kappa}_r \geqslant 0$	$\dot{\kappa}_r = F(M) G(t)$
OB	$M = M_r = M_\theta > 0$	$\dot{\kappa}_r \geqslant 0, \dot{\kappa}_\theta \geqslant 0$	$\dot{\kappa}_r + \dot{\kappa}_\theta = F(M) G(t)$
BOC	$M = M_\theta > M_r > 0$	$\dot{\kappa}_r = 0, \dot{\kappa}_\theta \geqslant 0$	$\dot{\kappa}_\theta = F(M) G(t)$
OC	$M = M_\theta > M_r = 0$	$\dot{\kappa}_r \leqslant 0, \dot{\kappa}_r + \dot{\kappa}_\theta \geqslant 0$	$\dot{\kappa}_\theta = F(M) G(t)$
COD	$M_\theta > 0 > M_r, M = M_\theta - M_r$	$\dot{\kappa}_r + \dot{\kappa}_\theta = O, \dot{\kappa}_\theta - \dot{\kappa}_r \geqslant 0$	$\dot{\kappa}_\theta = F(M) G(t)$
OD	$-M = M_r < M_\theta = 0$	$\dot{\kappa}_\theta \geqslant 0, \dot{\kappa}_\theta + \dot{\kappa}_r \leqslant 0$	$\dot{\kappa}_r = -F(M) G(t)$
DOE	$-M = M_r < M_\theta < 0$	$\dot{\kappa}_\theta = 0, \dot{\kappa}_r \leqslant 0$	$\dot{\kappa}_r = -F(M) G(t)$
OE	$-M = M_r = M_\theta < 0$	$\dot{\kappa}_r \leqslant 0, \dot{\kappa}_\theta \leqslant 0$	$\dot{\kappa}_r + \dot{\kappa}_\theta = -F(M) G(t)$
EOF	$-M = M_\theta < M_r < 0$	$\dot{\kappa}_r = 0, \dot{\kappa}_\theta \leqslant 0$	$\dot{\kappa}_\theta = -F(M) G(t)$
OF	$-M = M_\theta < M_r = 0$	$\dot{\kappa}_r \geqslant 0, \dot{\kappa}_\theta + \dot{\kappa}_r \leqslant 0$	$\dot{\kappa}_\theta = -F(M) G(t)$
FOA	$M_\theta < 0 < M_r, M = M_r - M_\theta$	$\dot{\kappa}_r + \dot{\kappa}_\theta = O, \dot{\kappa}_r - \dot{\kappa}_\theta \geqslant 0$	$\dot{\kappa}_r = F(M) G(t)$
OA	$M = M_r > M_\theta = 0$	$\dot{\kappa}_\theta \leqslant 0, \dot{\kappa}_r + \dot{\kappa}_\theta \geqslant 0$	$\dot{\kappa}_r = F(M) G(t)$

In addition to satisfying the appropriate entry in Table 1, the bending moments must be in equilibrium, and the curvature rates must be derivable from a displacement field. These conditions are expressed mathematically by

$$\frac{d}{dr}(rM_r) - M_\theta + \frac{pr^2}{2} = 0, \tag{13a}$$

and

$$\dot{\kappa}_r = -\frac{d^2\dot{w}}{dr^2}, \qquad \dot{\kappa}_\theta = -\frac{1}{r}\frac{d\dot{w}}{dr}. \tag{13b}$$

Here the z axis is vertical downward and the r coordinate is measured from the plate centre. Bending moments and curvatures are positive if they correspond to tension on the lower plate surface.

Equations (13), together with any row of Table 1, provide three equations for the determination of M_r, M_θ, and $\dot{w}$. Therefore, each row of Table 1 can provide a 'solution' and the problem is to determine which such 'solution' is correct. In order to be acceptable, not only the appropriate equations, but also the corresponding inequalities must be satisfied. The general method of attack is to assume a stress profile in relation to the stress space (Fig. 1). Points on the plate may be

represented by points on this curve. For instance, regimes CF and AD would correspond, respectively, to points on the plate where $M_\theta = 0$ and $M_r = 0$; similarly regime BE corresponds to points on the plate where $M_r = M_\theta$. On the other hand, if $0 < M_r < M_\theta$, the corresponding stress point will be in the interior of regime BOC.

If the entire plate corresponds to only one of the twelve regimes, then the appropriate row in Table 1 and equations (13) provide the necessary three equations and the solution of the problem is relatively simple. However, in general, a central circular region and surrounding annular regions correspond to different regimes. Then, the continuity of M_r, M_θ, w, and dw/dr at each circle separating two such regions provide the additional equations for the solution of the problem. How an incorrect hypothesis with regard to the stress profile manifests itself will be illustrated in the next section.

With the equations (13) and Table 1 as basis, examples of the creep behaviour of circular plates will be discussed in the remaining sections of this paper. The analysis will be carried out on the assumption that $F(M)$ is either a power function or an exponential function of the moment :

$$F(M) = (M/\mu)^n, \tag{14a}$$

or

$$F(M) = \lambda e^{M/\mu}, \tag{14b}$$

where μ, n, and λ are creep constants depending on the material and the temperature.

3. Simply Supported Edge

In the case of a plate on simple edge support $0 < M_r = M_\theta = M$ at the centre. Thus, the centre of the plate must be represented by point B in regime BE (Fig. 2). For $r > 0$ the point representing a state of stress can not be in regime AOB, since here $0 < M_\theta < M_r = M$ and with p positive this is not compatible with (13a). Hence, points near $r = 0$ must be in either regime BE or BOC. At the simply supported edge $M_r = 0$. Therefore, the point corresponding to the edge of the plate must be in regime OC.

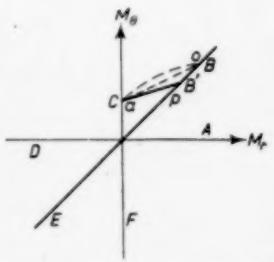

Fig. 2. Stress profiles-simple support.

As a first choice let it be asumed that the entire plate $0 < r < a$ is in regime BOC. It follows from Table 1 that

$$\dot{\kappa}_r = -\frac{d^2\dot{w}}{dr^2} = 0, \qquad 0 \leqslant r \leqslant a, \tag{15a}$$

so that

$$\dot{w} = B(a - r), \qquad 0 \leqslant r \leqslant a \tag{15b}$$

This violates the condition that the slope be zero at $r = 0$. Therefore, line BC is unacceptable as hypothesis for the stress profile. Since the proposed solution was unacceptable at $r = 0$, it appears reasonable to modify the hypothesis near

the centre of the plate. Since the only alternative to regime *BOC* is regime *BC*, it will be assumed that a finite circular region $0 \leqslant r \leqslant \rho$ of the plate is on *BB'* in regime *BE* and an annular region $\rho \leqslant r \leqslant a$ is on *B' C* in regime *BOC* (Fig. 2).

These considerations, together with Table 1 and equations (13), may now be formulated as the following mathematical problem.

$$\left.\begin{aligned} &\frac{dM}{dr} + \frac{pr}{2} = 0 \\ &\dot{\kappa}_r + \dot{\kappa}_\theta = -\frac{1}{r}\frac{d}{dr}\left(r\frac{d\dot{w}}{dr}\right) = G(t)\,F(M) \end{aligned}\right\} 0 \leqslant r \leqslant \rho, \qquad \text{(16a, b)}$$

$$\left.\begin{aligned} &\frac{d(rM_r)}{dr} - M_\theta + \frac{pr^2}{2} = 0 \\ &\dot{\kappa}_r = -\frac{d^2\dot{w}}{dr^2} = 0, \qquad \dot{\kappa}_\theta = -\frac{d\dot{w}}{rdr} = G(t)\,F(M) \end{aligned}\right\} \rho \leqslant r \leqslant a. \qquad \text{(17a, b, c)}$$

The boundary conditions are

$$\frac{dw}{dr}(0) = 0, \qquad w(a) = 0, \qquad M_r(a) = 0, \qquad \text{(18a, b, c)}$$

and it is further required that M_r, M_θ, w, and dw/dr be continuous at $r = \rho$.

A. Power-function moment-curvature-rate law

The case where F is the power function given by (14a) is considered first. A trivial integration of (16a) yields the stress solution

$$M_r = M_\theta = -\tfrac{1}{4}pr^2 + A, \qquad 0 \leqslant r \leqslant \rho. \qquad (19)$$

The constant A will be determined by the moment continuity condition. Substitution of (19) into (14a) and use of (16b) yields the creep deformation equation

$$\frac{1}{r}\frac{d}{dr}\left(r\frac{d\dot{w}}{dr}\right) = G\left[(\tfrac{1}{4}pr^2 - A)/\mu\right]^n, \qquad 0 \leqslant r \leqslant \rho \qquad (20)$$

Integration and use of boundary condition (18a) yields

$$\frac{rd\dot{w}}{dr} = \frac{2G}{p\mu^n(n+1)}\left[(\tfrac{1}{4}pr^2 - A)^{n+1} - A^{n+1}\right], \qquad 0 \leqslant r \leqslant \rho. \qquad (21)$$

Now, (17b) may be solved and boundary condition (18b) used to obtain

$$\left.\begin{aligned} &\frac{d\dot{w}}{dr} = -B \\ &\dot{w} = B(a - r) \end{aligned}\right\} \rho \leqslant r \leqslant a. \qquad \text{(22a, b)}$$

Hence, by virtue of (14a) and (17c) the equilibrium equation (16a) reduces to

$$\frac{d(rM_r)}{dr} = \mu(B/Gr)^{1/n} - \tfrac{1}{2}pr^2, \qquad \rho \leqslant r \leqslant a. \qquad (23)$$

Integration and use of boundary condition (18c) yields the stress solution

$$\left.\begin{aligned} M_r &= \frac{pa^2}{6}(a/r - r^2/a^2) - \frac{\mu n}{n-1}(B/Ga)^{1/n}\left[(a/r) - (a/r)^{1/n}\right] \\ M_\theta &= \mu(B/Gr)^{1/n} \end{aligned}\right\} \rho \leqslant r \leqslant a. \qquad \text{(24a, b)}$$

The requirement that M_r and M_θ be continuous at $r = \rho$ may be now enforced to yield the following values for A and B in terms of ρ :

$$A = (p\alpha^2 \alpha^2/4) + (p\alpha^2/6)(n-1)(1-\alpha^3)/(n\alpha^{1/n} - \alpha),$$
$$B = G\left[(p\alpha^{2+1/n}/6\mu)(n-1)(1-\alpha^3)/(n-\alpha^{1-1/n})\right]^n, \tag{25}$$

where $\alpha = \rho/a$. These values together with the condition that dw/dr be continuous at $r = \rho$, lead to the following equation for the evaluation of α :

$$(3\beta/2 + 1)^{n+1} - 3(n+1)\beta - 1 = 0, \tag{26a}$$

where

$$\beta = \alpha^2(n\alpha^{1/n} - \alpha)/(n-1)(1-\alpha^3). \tag{26b}$$

These equations may be solved for α by a numerical procedure for known values of n.

For the creep deflection rates near the centre of the plate (21) may be integrated and used with the condition that $\dot{w}(\rho)$ be continuous, to yield the expression

$$\dot{w} = B(a-\rho) - \frac{2G}{p\mu^n(n+1)}\int_r^\rho \left[\left(\frac{pr^2}{4} - A\right)^{n+1} - A^{n+1}\right]\frac{dr}{r}, \qquad 0 \leqslant r \leqslant \rho. \tag{27}$$

The values of ρ are known for given values of n from equations (26), and the integral may be evaluated numerically for various values of r in the region $0 \leqslant r \leqslant \rho$.

Finally, incorporation of the values of B and A from (25) into (19), (22b), (24), and (27) and simplification lead to the following expressions for the moments and deformation rates :

$0 \leqslant \xi \leqslant \alpha$:

$$\left.\begin{aligned} &M_r = M_\theta = (p\alpha^2 \alpha^2/6\beta)(1 + 3\beta/2 - 3\beta\xi^2/2\alpha^2), \\ &\dot{w} = G\alpha^2\left(\frac{p\alpha^2\alpha^2}{6\mu\beta}\right)^n \left\{\alpha(1-\alpha) + \frac{(\alpha^2/\beta)}{3(n+1)}\int_\xi^\alpha \frac{1}{\xi}\left[\left(1+\frac{3\beta}{2}\right)^{n+1} - \left(1 + \frac{3\beta}{2} - \frac{3\beta\xi^2}{2\alpha^2}\right)^{n+1}\right]d\xi\right\} \end{aligned}\right\} \tag{28}$$

$\alpha \leqslant \xi \leqslant 1$:

$$\left.\begin{aligned} &M_r = (p\alpha^2\alpha^2/6\beta)\left[(\beta/\alpha^2)(1-\xi^3)/\xi - n\alpha^{1/n}(1/\xi - 1/\xi^{1/n})/(n-1)\right], \\ &M_\theta = (p\alpha^2\alpha^2/6\beta)(\alpha/\xi)^{1/n}, \\ &\dot{w} = G\alpha^2(p\alpha^2\alpha^2/6\mu\beta)^n\alpha(1-\xi), \end{aligned}\right\} \tag{29}$$

where $\xi = r/a$ and α and β are obtained from (26).

B. Exponential moment-curvature-rate law

The exponential moment-curvature-rate law of (14b) is used next. The stress solution in the region $0 \leqslant r \leqslant \rho$ is again given by (19). The creep deformation equation in the region now becomes

$$\frac{1}{r}\frac{d}{dr}\left(r\frac{d\dot{w}}{dr}\right) = G\lambda \exp\left[(A - \tfrac{1}{4}pr^2)/\mu\right], \qquad 0 \leqslant r \leqslant \rho, \tag{30}$$

so that

$$r\frac{d\dot{w}}{dr} = (2G\lambda\mu/p)\left\{\exp\left[(A - \tfrac{1}{4}pr^2/\mu\right] - \exp(A/\mu)\right\}, \qquad 0 \leqslant r \leqslant \rho. \tag{31}$$

The creep deformation solution in the region $\rho \leqslant r \leqslant a$ is still given by (22). The equilibrium equation in this region is reduced to

$$\frac{d(rM_r)}{dr} = \mu \ln(G\lambda r) - \tfrac{1}{4}pr^2, \qquad \rho \leqslant r \leqslant a. \tag{32}$$

Hence, the stress solutions are

$$\left.\begin{aligned} &M_r = (p\alpha^2/6)(a/r - r^2/a^2) + \mu\left\{\ln(a/r) - \left[\ln(B/G\lambda a) + 1\right](a/r - 1)\right\}, \\ &M_\theta = \mu \ln(B/G\lambda r), \qquad\qquad \rho \leqslant r \leqslant a. \end{aligned}\right\} \tag{33a, b}$$

The constants A and B may be found by the continuity of M_r and M_θ which yield, in terms of $\alpha = \rho/a$, the expressions

$$\left.\begin{aligned} A &= (pa^2/6)(1 + 3\alpha^2/2 - \alpha^3) - \mu(1 - \alpha + \ln\alpha), \\ B &= G\lambda a \exp\left[(pa^2/6\mu)(1 - \alpha^3) - (1 - \alpha)\right]. \end{aligned}\right\} \tag{34}$$

The equation for the evaluation of α is obtained by the continuity of dw/dr and may be written

$$1 + 2k\alpha^2 - \exp(k\alpha^2) = 0 \tag{35}$$

where

$$k = pa^2/4\mu. \tag{36}$$

For a given value of load p, (35) may be solved for α by a numerical procedure.

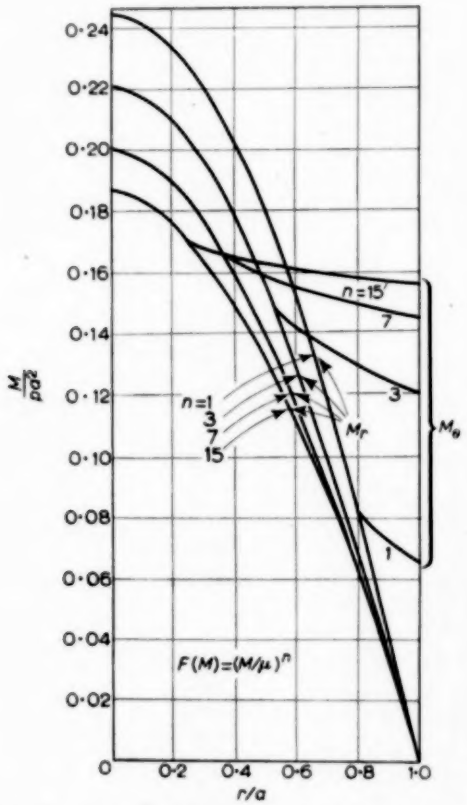

Fig. 3. Moment distribution-simple support.

Finally, it follows from a procedure similar to that of the power-function case that the expressions for the moments and deformation rate are

$0 \leqslant \xi \leqslant a$:

$$\left.\begin{aligned} M_r = M_\theta &= (pa^2/6)\left[1 - \alpha^3 + 3(\alpha^2 - \xi^2)/2\right] - \mu(1 - \alpha + \ln\alpha), \\ \dot{w} &= (G\lambda a^2/2k)\left\{\exp\left[2k(1-\alpha^3)/3 - (1-\alpha)\right]\right\}\left\{2k(1-\alpha) + \left[\exp(k^2 - \ln\alpha)\right]\int_\xi^\alpha (1 - \exp(-k\xi^2))\frac{d\xi}{\xi}\right\} \end{aligned}\right\} \tag{37}$$

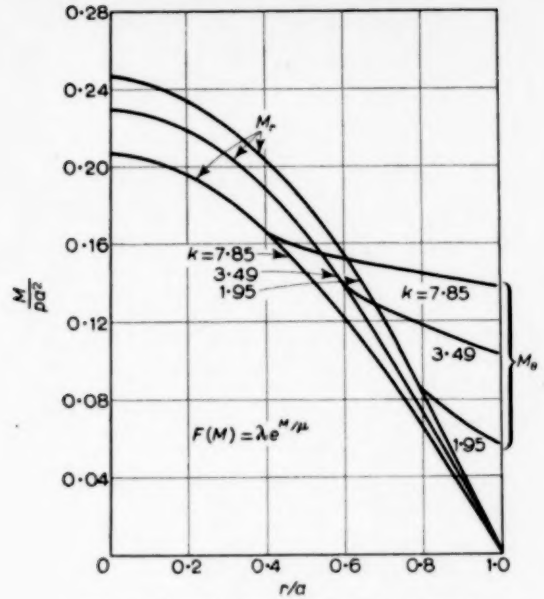

Fig. 4. Moment distribution-simple support.

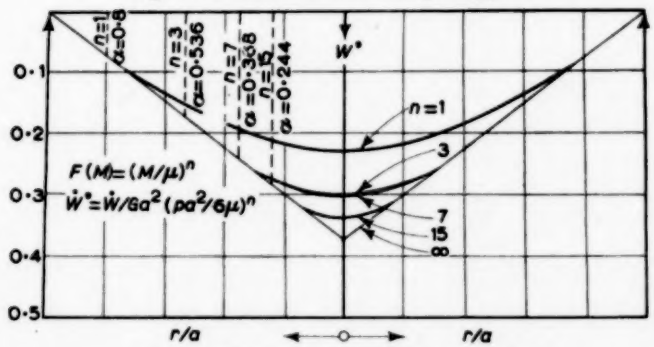

Fig. 5. Deformation rates-simple support.

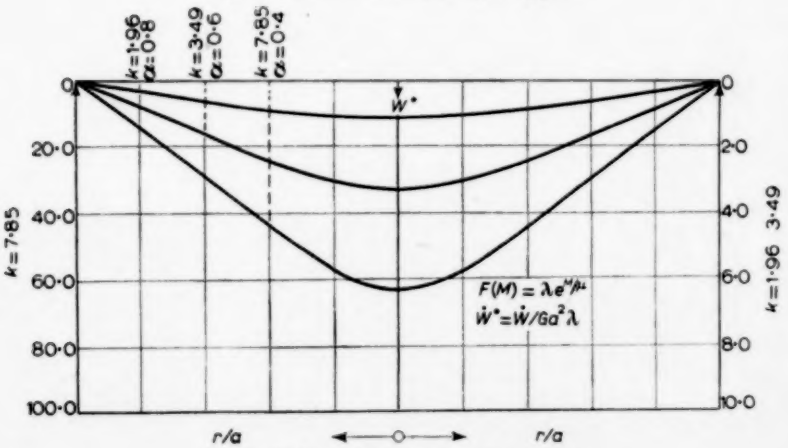

Fig. 6. Deformation rates-simple support.

$\alpha \leqslant \xi \leqslant 1$:

$$\left.\begin{aligned} M_r &= (pa^2/6)\,[\alpha^3 - \xi^2 + (1-\alpha^3)\,\xi]/\xi - \mu\,[\alpha\,(1-\xi)/\xi + \ln \xi], \\ M_\theta &= (pa^2/6)\,(1-\alpha^3) - \mu\,(1 - \alpha + \ln \xi), \\ \dot{w} &= G\lambda a^2\,(1-\xi)\exp\,[2k\,(1-\alpha^3)/3 - (1-\alpha)], \end{aligned}\right\} \qquad (38)$$

where $\xi = r/a$ and α is obtained from (35) for given values of k.

The radial and tangential moment distribution along the radius is shown in Figs. 3, 4, and plots of the deformation rates along the radius are shown in Figs. 5, 6. For the power-function case plots are given for four different values of n, and for the exponential case for three different values of the load.

4. Built-in Edge

The analysis presented in the previous section may now be extended to the corresponding problem of the circular plate with built-in edge support. Again $0 < M_r = M_\theta = M$ at the centre and, as in the case of simple support, the stress profile cannot be in region BOA (Fig. 7). The centre corresponds to the point B. At the built-in edge $M_r < 0$ and the portion near the edge of the plate may be represented by any one of the profiles indicated in Fig. 7. It is readily verified that all except one may be eliminated as incorrect.

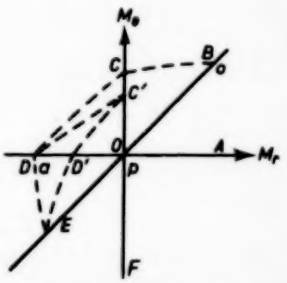

Fig. 7. Stress profiles-built-in edge.

The assumption that appears acceptable is that B, BO and OD apply, respectively, to the centre of the plate, the circular region $0 \leqslant r \leqslant \rho$, and the annular region $\rho \leqslant r \leqslant a$. The choice of D to correspond to the edge of the plate seems reasonable, since $\dot{\kappa}_\theta = 0$ at the edge and so M_θ may be assumed to be zero there. A similar argument to that presented for the case of simple supports leads to the formulation of the following mathematical problem.

$$\left.\begin{aligned} &\frac{dM}{dr} + \frac{pr}{2} = 0 \\ &\dot{\kappa}_r + \dot{\kappa}_\theta = \frac{1}{r}\frac{d}{dr}\left(r\frac{d\dot{w}}{dr}\right) = G\,(t)\,F\,(M) \end{aligned}\right\} \quad 0 \leqslant r \leqslant \rho, \qquad (39a, b)$$

$$\left.\begin{aligned} &\frac{d}{dr}\,(rM_r) + \tfrac{1}{2}\,pr^2 = 0 \\ &\dot{\kappa}_r = -\frac{d^2\,\dot{w}}{dr^2} = -\,G\,(t)\,F\,(-M_r) \end{aligned}\right\} \quad \rho \leqslant r \leqslant a. \qquad (40a, b)$$

The boundary conditions are

$$\frac{d\dot{w}}{dr}\,(0) = 0, \qquad \frac{d\dot{w}}{dr}\,(a) = 0, \qquad \dot{w}\,(a) = 0, \qquad (41a, b, c)$$

and the continuity of M_r, M_θ, $\dot{w}$, and $d\dot{w}/dr$ at ρ must be satisfied.

A. Power-function law

The solution of the equations is first carried out for the power-function of (14a). Equation (39a together with the condition $M(\rho) = 0$ yields the stress solution

$$M_r = M_\theta = \tfrac{1}{4} p(\rho^2 - r^2), \qquad 0 \leqslant r \leqslant \rho. \tag{42}$$

Thus, (39b) with the use of (14a) and (42) may be written

$$\frac{1}{r}\frac{d}{dr}\left(r\frac{d\dot{w}}{dr}\right) = G(p/4\mu)^n (r^2 - \rho^2)^n, \qquad 0 \leqslant r \leqslant \rho. \tag{43}$$

Integration and use of boundary condition (41a) yields

$$r\frac{d\dot{w}}{dr} = \frac{G(p/4\mu)^n}{2(n+1)}\left[(\rho^2 - r^2)^{n+1} - \rho^{2(n+1)}\right], \qquad 0 \leqslant r \leqslant \rho. \tag{44}$$

Now, (40a) may be solved for M_r and with the use of the condition $M_r(\rho) = 0$ yields the solution

$$M_r = (p/6r)(\rho^3 - r^3), \qquad \rho \leqslant r \leqslant a. \tag{45}$$

By simple substitution it follows from (40b), (14a) and (45) that

$$\frac{d^2\dot{w}}{dr^2} = G(p/6\mu)^n\left[(r^3 - \rho^3)/r\right]^n, \qquad \rho \leqslant r \leqslant a. \tag{46}$$

Integration and use of boundary condition (41b) yields

$$\frac{d\dot{w}}{dr} = G(p/6\mu)^n \int_r^a \left[\frac{\rho^3 - r^3}{r}\right]^n dr, \qquad \rho \leqslant r \leqslant a. \tag{47}$$

The condition that $d\dot{w}/dr$ be continuous at $r = \rho$ yields the following equation for the evaluation of $\alpha = \rho/a$:

$$\left(\frac{3}{2}\right)^n \frac{\alpha^{2n+1}}{2(n+1)} - \int_\alpha^1 \left[\frac{\xi^3 - \alpha^3}{\xi}\right]^n d\xi = 0 \tag{48}$$

This equation may be solved for α by a graphical procedure for given values of n.

The deformation rates may be obtained by respective integrations of (44) and (47) and use of the conditions that $w(a) = O$ and $w(\rho)$ be continuous. Thus, the final expressions for the moments and deformation rates are

$$\left.\begin{aligned} &0 \leqslant \xi \leqslant \alpha: \\ &M_r = M_\theta = (pa^2/4)(\alpha^2 - \xi^2), \\ &\dot{w} = Ga^2(pa^2/6\mu)^n \left\{\int_\alpha^1 \left[\int_\xi^1 \frac{(\xi^3 - \alpha^3)^n}{\xi^n} d\xi\right] d\xi + \frac{(3/2)^n}{2(n+1)} \int_\xi^\alpha \left[\alpha^{2(n+1)} - (\alpha^2 - \xi^2)^{n+1}\right] \frac{d\xi}{\xi}\right\} \end{aligned}\right\} \tag{49}$$

$$\left.\begin{aligned} &\alpha \leqslant \xi \leqslant 1: \\ &M_r = (pa^2/6)(\alpha^3 - \xi^3)/\xi, \\ &M_\theta = 0, \\ &\dot{w} = Ga^2(pa^2/6\mu)^n \int_\xi^1 \left[\int_\xi^1 \frac{(\xi^3 - \alpha^3)^n}{\xi^n} d\xi\right] d\xi, \end{aligned}\right\} \tag{50}$$

where $\xi = r/a$, and the integrals may be evaluated by graphical procedure once the value of α is known from (84).

B. Exponential law

With the exponential-function assumption of (14b) and a procedure similar to the one outlined in Section 4*A*, the following solutions are obtained for the moments and creep deformation rates.

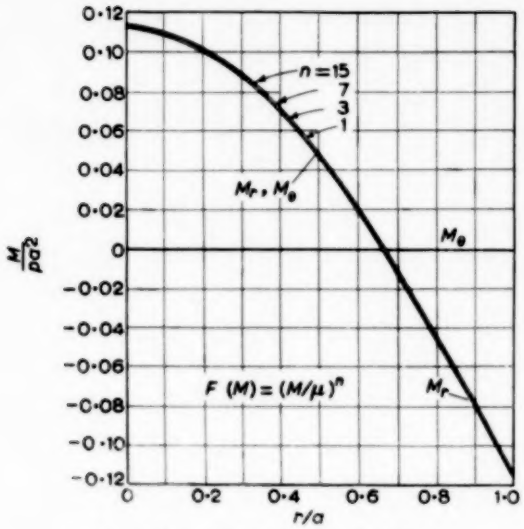

Fig. 8. Moment distribution-built-in edge.

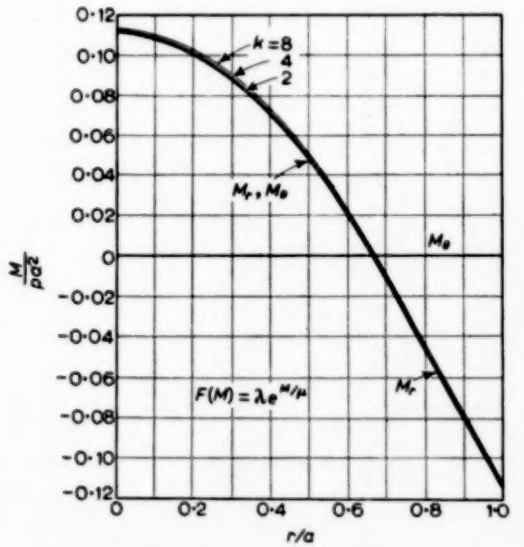

Fig. 9. Moment distribution-built-in edge.

$0 \leqslant \xi \leqslant \alpha$:

$$M_r = M_\theta = (pa^2/4)(\alpha^2 - \xi^2),$$

$$\dot{w} = G\lambda a^2 \left(\int_\alpha^1 \left\{ \int_\xi^1 \exp\left[\frac{2k}{3} \left(\frac{\xi^3 - \alpha^3}{\xi} \right) \right] d\xi \right\} d\xi + \frac{\exp(k\alpha^2)}{2k} \int_\xi^\alpha (1 - \exp(-k\xi^2)) \frac{d\xi}{\xi} \right). \tag{51}$$

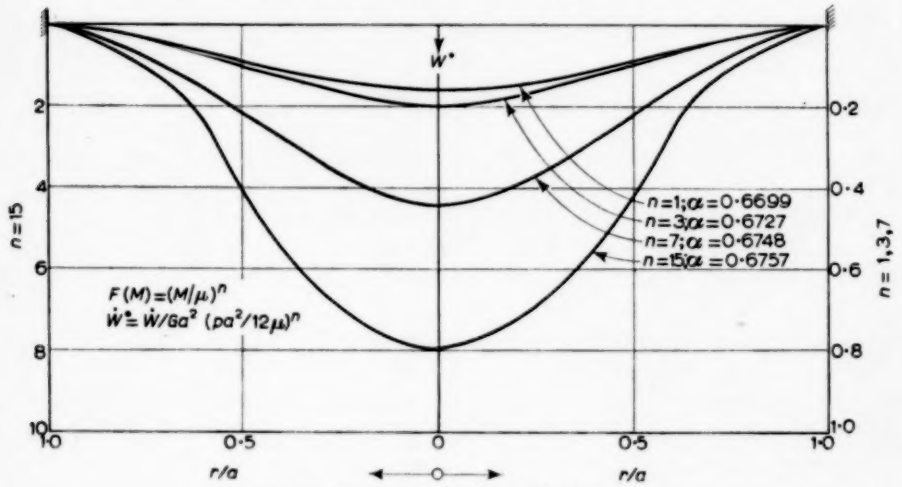

Fig. 10. Deformation rates – built-in edge.

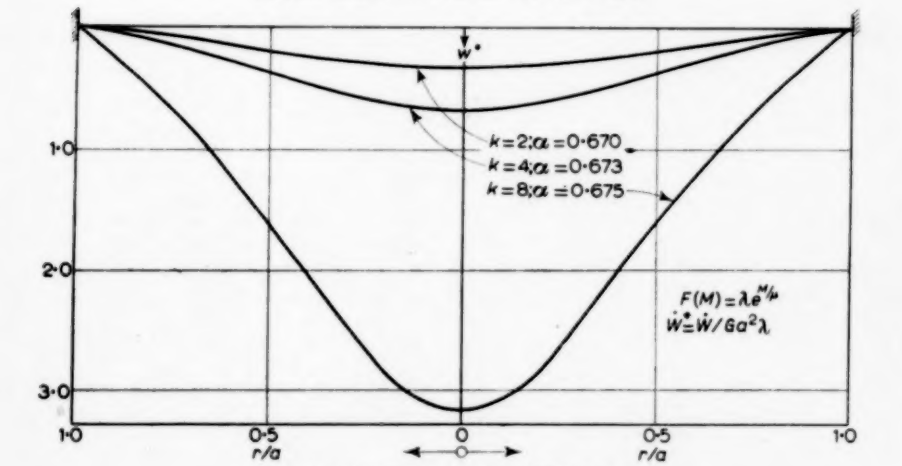

Fig. 11. Deformation rates – built-in edge.

$\alpha \leqslant \xi \leqslant 1$:

$$M_r = (pa^2/6)(\alpha^3 - \xi^3)/\xi, \qquad M_\theta = 0,$$

$$\dot{w} = G\lambda a^2 \int_\xi^1 \left\{ \int_\xi^1 \exp\left[\frac{2k}{3} \left(\frac{\xi^3 - \alpha^3}{\xi} \right) \right] d\xi \right\} d\xi, \tag{52}$$

where k is given by (36) and the equation for the evaluation of α is

$$1 - \exp(k\alpha^2) + 2k\alpha \int_\alpha^1 \exp\left[\frac{2k}{3} \left(\frac{\xi^3 - \alpha^3}{\xi} \right) \right] d\xi = 0. \tag{53}$$

Plots similar to those for the simply supported plate are shown in Figs. 8, 9, 10, and 11 for both the power-function law and the exponential law.

5. CONCLUSION

The creep deformations and stress distributions in circular plates subject to normal pressure have been analysed in the present paper with the use of a creep law based upon a flow rule associated with a maximum shearing stress. Steady-state conditions are assumed, and it is shown that solutions may be obtained in relatively simple forms.

In the case of the simple supported plate it is seen from Figs. 5 and 6 that the value of α decreases as the values of the power n and the load p increase. This may have been expected from the plastic flow behaviour of a rigid plastic plate. On the other hand, in the case of the clamped plate the value of α remains approximately constant for all values of n and p. However, it is seen from Figs. 10 and 11 that for larger values of n and p the curves approximate to the plastic flow behaviour of a rigid-plastic plate.

It should be mentioned in conclusion that the basis for the theory presented here is of a comparatively recent origin and adequate test results are not available to test its relationship to real physical materials. A similar basis was used by WAHL (1954) in the analysis of creep in rotating disks, and the theoretical predictions there show reasonably good agreement with experimental results. Additional such evidence is necessary before the theory is confirmed. However, the analysis is mathematically consistent and comparatively simple to apply. Therefore, it appears to be a reasonable method for solving creep problems, at least in our present state of limited knowledge concerning the creep phenomenon.

REFERENCES

BAILEY, R. W.	1935	*Proc. Inst. Mech. Engrs.* **131**, 260.
	1951	*Proc. Inst. Mech. Engrs.* **164**, 425.
HOPKINS, H. G. and PRAGER, W.	1953	*J. Mech. Phys. Solids* **2**, 1.
JOHNSON, A. E.	1951	*Proc. Inst. Mech. Engrs.* **164**, 433.
KOITER, W. T.	1953	*Biezeno Anniversary Volume* p. 232.
MILLENSON, M. B. and MANSON, S. S.	1948	*NACA Report* 906.
ODQVIST, F. K. G.	1934	*Proc. 4th Int. Cong. Appl. Mech.* p. 228.
PAUL, B. and HODGE, P. G.	1956	*Poly. Inst. Brooklyn, Aero. Lab. Report* 348.
POPOV, E. P.	1947	*J. Franklin Inst.* **243**, 365.
PRAGER, W.	1953	*J. Appl. Mech.* **75**, 317.
SODERBERG, C. R.	1936	*Trans. Amer. Soc. Mech. Engrs.* **58**, 733.
WAHL, A. M.	1956	*J. Appl. Mech.* **23**, 231.
WAHL, A. M., SANKEY, G. O., MANJOINE, M. J. and SHOEMAKER, E.	1954	*J. Appl. Mech.* **21**, 225.

Journal of the Mechanics and Physics of Solids, 1958, Vol. 6, pp. 177 to 185. Pergamon Press Ltd., London

STRESS PROPAGATION IN VISCO-ELASTIC BODIES

By D. S. Berry
Research Association of British Rubber Manufacturers, Shawbury, Shrewsbury

(*Received 2nd September*, 1957)

Summary

The correspondence between the wave propagation problems of isotropic elastic and visco-elastic solids is discussed. The visco-elastic materials are supposed to satisfy linear stress-strain relations of the form

$$\sigma_{ij} = \delta_{ij} \int_0^t \lambda (t - \tau) \frac{\partial}{\partial \tau} \Delta (\tau)\, d\tau + 2 \int_0^t \mu (t - \tau) \frac{\partial}{\partial \tau} \epsilon_{ij} (\tau)\, d\tau.$$

Two problems are solved. The first, that of forced torsional vibrations in a finite cylinder, leads to a simple method of deriving the "complex shear modulus" of the material from experimental measurements at high frequencies. The second, that of stress waves due to an impulsive pressure acting on the surface of a spherical cavity in an infinite solid, is solved by Laplace transform methods, which yield a solution for the displacement in the form of a real integral in the particular case of a kind of Maxwell solid.

1. Introduction

This paper is concerned with the application of three-dimensional visco-elastic theory to problems of wave propagation. It is assumed that the components of strain are infinitesimal, so that the general linear theory of visco-elasticity is valid. The two well-known general stress-strain relations for one dimension, one involving a relaxation function and the other a creep function, were originally based on Boltzmann's principle of superposition (Leadermann 1943, Gross 1953). The first of these relations has also been derived by the use of non-equilibrium thermodynamics by Staverman and Schwarzl (1952), whose treatment shows that the relaxation function must correspond to an assembly of Maxwell elements or to a continuous relaxation spectrum if the number of notional elements is very large. The three-dimensional stress-strain relations for an isotropic solid are obtained by a simple extension of the phenomenological method, while a derivation from thermodynamical considerations is given by Biot (1954).

Laplace transform methods bring out a close correspondence between visco-elastic and elastic problems (Sips 1951, Mandel 1955, 1956), while their use in the one-dimensional case enables a formal solution of the equation of motion to be obtained under any type of boundary condition (Berry and Hunter 1956, Berry 1956)*. In fact, any problem of wave propagation in a visco-elastic medium can be reduced to a Laplace inversion problem, so long as a solution can

*Previous solutions to particular problems of uniaxial stress propagation in simple visco-elastic models were obtained by Laplace transform methods by Lee and Kanter (1953) and by Glauz and Lee (1954).

be found for an elastic solid subject to the same boundary conditions. Moreover, explicit steady state solutions are always possible if they can be found in the elastic case.

2. The Stress-Strain Relations

Referred to rectangular Cartesian axes Ox_i $(i = 1, 2, 3)$ the stress-strain relations may be written

$$\sigma_{ij}(t) = \delta_{ij} \int_0^t \lambda(t-\tau) \frac{\partial}{\partial \tau} \Delta(\tau)\, d\tau + 2 \int_0^t \mu(t-\tau) \frac{\partial}{\partial \tau} \epsilon_{ij}(\tau)\, d\tau, \qquad (2.1)$$

where δ_{ij} is the Kronecker delta and $\Delta(t)$ the dilatation, so long as the strain components ϵ_{ij} are zero for $t < 0$. The stress and strain tensors, $\sigma_{ij}(t)$, $\epsilon_{ij}(t)$, are understood to depend on the coordinates, x_i, as well as on the time t. The functions $\lambda(t)$, $\mu(t)$ are analogous to the relaxation functions of the one-dimensional theory, except that they include the ultimate values reached after relaxation of a set of constant strains has run its full course. The classical stress-strain relations may be regarded as a special case of (2.1) where $\lambda(t)$, $\mu(t)$ are independent of t and reduce to Lamé's constants. A formulation of the stress-strain relations in terms of creep functions is possible but will not be presented here.

A difficulty arises when we have to consider finite instantaneous increases in the strain components $\epsilon_{ij}(t)$. Sips (1951) overcomes this problem by writing the stress-strain relations as Stieltjes integrals, while Mandel (1955, 1956) allows for discontinuities at $t = 0$ by explicitly including terms due to the initial values of the ϵ_{ij}. Here we account for discontinuities in the ϵ_{ij} by means of the convention that their derivatives are represented there by the Dirac delta function, which can be regarded as the derivative of the Heaviside unit function (Sneddon 1955). Thus, if

$$\epsilon_{12}(t) = \epsilon_0 H(t)$$

then

$$\epsilon'_{12}(t) = \epsilon_0 \delta(t)$$

and substitution in (2.1) gives

$$\sigma_{12} = 2 \int_0^t \mu(t-\tau)\, \epsilon_0\, \delta(\tau)\, d\tau = 2\, \epsilon_0\, \mu(t).$$

If the components of strain vary sinusoidally with time we write

$$\epsilon_{ij}(t) = \epsilon_{ij}^*\, e^{i\omega t}$$

where the ϵ_{ij}^* are functions of the spatial coordinates alone. Substituting in (2.1) we have

$$\sigma_{ij}(t) = i\omega e^{i\omega t} \left[\delta_{ij}\, \Delta^* \int_0^t \lambda(\tau)\, e^{-i\omega\tau}\, d\tau + 2\epsilon_{ij}^* \int_0^t \mu(\tau)\, e^{-i\omega\tau}\, d\tau \right].$$

Letting the upper limits of the integrals tend to infinity we find the steady state relations

$$\sigma_{ij}^* = i\omega \left[\delta_{ij}\, \Delta^*\, \bar{\lambda}(i\omega) + 2\epsilon_{ij}^*\, \bar{\mu}(i\omega) \right], \qquad (2.2)$$

where

$$\sigma_{ij}(t) = \dot{\sigma}_{ij}^{*} e^{i\omega t}$$

and $\bar{\lambda}(s)$, $\bar{\mu}(s)$ are the Laplace transforms of $\lambda(t)$, $\mu(t)$.

In tensor notation the equations of motion are

$$\frac{\partial \sigma_{ij}}{\partial x_j} + X_i = \rho \frac{\partial^2 u_i}{\partial t^2} \tag{2.3}$$

where X_i are the body force components, while the components of the strain tensor are given by

$$\epsilon_{ij} = \tfrac{1}{2}\left(\frac{\partial u_i}{\partial x_j} + \frac{\partial u_j}{\partial x_i}\right). \tag{2.4}$$

3. Correspondence with Classical Elasticity

We assume that the components of displacement are continuous and the components of stress and strain sectionally continuous, while the components of displacement and velocity are zero at $t = 0$. In practice the latter restrictions are unimportant, since they can only apply at the point of initiation of the disturbance. They are required to enable a general theory to be established but it is usually found that, by systematic use of the Heaviside unit function and the Dirac delta function, all types of discontinuity can be allowed.

We denote the Laplace transform of a function $f(t)$ by $\bar{f}(s)$, so that

$$\bar{f}(s) = \int_0^\infty f(t)\, e^{-st}\, dt.$$

Then from (2.1), (2.3) and (2.4) we have

$$\bar{\sigma}_{ij} = \delta_{ij}\, s\bar{\lambda}\bar{\Delta} + 2s\bar{\mu}\bar{\epsilon}_{ij}, \tag{3.1}$$

$$\frac{\partial \bar{\sigma}_{ij}}{\partial x_j} + \bar{X}_i = \rho s^2 \bar{u}_i, \tag{3.2}$$

$$\bar{\epsilon}_{ij} = \tfrac{1}{2}\left(\frac{\partial \bar{u}_i}{\partial x_j} + \frac{\partial \bar{u}_j}{\partial x_i}\right), \tag{3.3}$$

where the $\bar{\sigma}_{ij}$, $\bar{\epsilon}_{ij}$, $\bar{u}_i$ are functions of the x_i as well as of s. Equations (3.1) to (3.3) form a system of fifteen equations in the Laplace transforms of fifteen components of stress, strain and displacement, which, with sufficient boundary conditions, will have a unique solution.

In the purely elastic case, $\lambda(t)$, $\mu(t)$ are constants, λ_e, μ_e, say, and

$$\bar{\lambda} = \lambda_e/s, \qquad \bar{\mu} = \mu_e/s.$$

It follows that the Laplace transforms of any elastic problem will immediately yield those of the visco-elastic problem with the same boundary conditions if λ_e and μ_e are replaced by $s\bar{\lambda}(s)$ and $s\bar{\mu}(s)$.

A similar result holds under steady state conditions. We suppose that after a sufficiently long period of sinusoidal excitation all the dependent variables have reached the steady state. The sinusoidal stimulus may be a body force, but

otherwise we must assume all body forces zero. In the latter case we have from equations (2.2) to (2.4)

$$\sigma_{ij}^* = \delta_{ij}\,\Delta^*\,\Lambda(\omega) + 2\epsilon_{ij}^*\,M(\omega), \tag{3.4}$$

$$\frac{\partial \sigma_{ij}^*}{\partial x_j} = -\rho\omega^2\,u_i^*, \tag{3.5}$$

$$\epsilon_{ij}^* = \tfrac{1}{2}\left(\frac{\partial u_i^*}{\partial x_j} + \frac{\partial u_j^*}{\partial x_i}\right), \tag{3.6}$$

where, as before, the starred quantities are the amplitudes of oscillation, and

$$\Lambda(\omega) = i\omega\bar{\lambda}(i\omega), \qquad M(\omega) = i\omega\bar{\mu}(i\omega).$$

In the elastic case, $\Lambda(\omega) = \lambda_e$, $M(\omega) = \mu_e$, so that the solution to a visco-elastic problem is obtained from that of the corresponding elastic problem by the substitution of the complex quantities Λ, M for Lamé's constants λ_e, μ_e. $M(\omega)$ is usually known as the complex shear modulus.

4. Torsional Oscillations in a Circular Cylinder

So far as the author is aware, the solution of the problem of forced torsional vibrations in an elastic cylinder does not appear in the literature, although *free* vibrations are considered by Love (1952). The generalization to visco-elastic materials may have important practical applications, the more so since it leads to a simple method of deriving the complex shear modulus, as a function of frequency, from experimental measurements at high frequencies.

Referred to cylindrical coordinates (r, θ, z), the cylinder is bounded by the surfaces $r = a$, $z = 0$, h. The end $z = 0$ is fixed, while the other, $z = h$, oscillates sinusoidally in its own plane about the centre point, $r = 0$, with a small angular amplitude α and frequency $\omega/2\pi$. The cylindrical surface is free of external stress.

In this coordinate system the stress-strain relations (3.4) take the form

$$\left.\begin{aligned} \sigma_r^* &= (\Lambda + 2M)\,\epsilon_r^* + \Lambda(\epsilon_\theta^* + \epsilon_z^*) \\ &\cdots\cdots\cdots \\ \tau_{r\theta}^* &= 2M\gamma_{r\theta}^* \\ &\cdots\cdots\cdots \end{aligned}\right\} \tag{4.1}$$

using an obvious notation, while the equations of motion become

$$\left.\begin{aligned} &\frac{\partial \sigma_r^*}{\partial r} + \frac{1}{r}\frac{\partial \tau_{r\theta}^*}{\partial \theta} + \frac{\partial \tau_{rz}^*}{\partial z} + \frac{\sigma_r^* - \sigma_\theta^*}{r} + \rho\omega^2 u_r^* = 0, \\ &\frac{\partial \tau_{r\theta}^*}{\partial r} + \frac{1}{r}\frac{\partial \sigma_\theta^*}{\partial \theta} + \frac{\partial \tau_{\theta z}^*}{\partial z} + \frac{2}{r}\tau_{r\theta}^* + \rho\omega^2 u_\theta^* = 0, \\ &\frac{\partial \tau_{rz}^*}{\partial r} + \frac{1}{r}\frac{\partial \tau_{\theta z}^*}{\partial \theta} + \frac{\partial \sigma_z^*}{\partial z} + \frac{1}{r}\tau_{rz}^* + \rho\omega^2 u_z^* = 0. \end{aligned}\right\} \tag{4.2}$$

The components of strain are given by the equations

$$\left.\begin{aligned}
\epsilon_r^* &= \frac{\partial u_r^*}{\partial r}, & \gamma_{r\theta}^* &= \tfrac{1}{2}\left(\frac{1}{r}\frac{\partial u_r^*}{\partial \theta} + \frac{\partial u_\theta^*}{\partial r} - \frac{u_\theta^*}{r}\right),\\
\epsilon_\theta^* &= \frac{1}{r}\frac{\partial u_\theta^*}{\partial \theta} + \frac{u_r^*}{r}, & \gamma_{rz}^* &= \tfrac{1}{2}\left(\frac{\partial u_z^*}{\partial r} + \frac{\partial u_r^*}{\partial z}\right),\\
\epsilon_z^* &= \frac{\partial u_z^*}{\partial z}, & \gamma_{\theta z}^* &= \tfrac{1}{2}\left(\frac{\partial u_\theta^*}{\partial z} + \frac{1}{r}\frac{\partial u_z^*}{\partial \theta}\right).
\end{aligned}\right\} \tag{4.3}$$

The boundary conditions are

$$\begin{aligned}
&\sigma_r^* = \tau_{r\theta}^* = \tau_{rz}^* = 0 && \text{on} \quad r = a,\\
&u_r^* = u_\theta^* = u_z^* = 0 && \text{on} \quad z = 0,\\
&u_r^* = u_z^* = 0, \quad u_\theta^* = \alpha r && \text{on} \quad z = h.
\end{aligned}$$

It is clear that all the physical quantities must be independent of θ. Using this condition and eliminating the components of stress and strain between equations (4.1) to (4.3) we find that the components of displacement must satisfy the equations

$$\left.\begin{aligned}
&(\Lambda + 2M)\left(\frac{\partial^2 u_r^*}{\partial r^2} + \frac{1}{r}\frac{\partial u_r^*}{\partial r} - \frac{u_r^*}{r^2}\right)\\
&\qquad + (\Lambda + M)\frac{\partial^2 u_z^*}{\partial r\,\partial z} + M\frac{\partial^2 u_r^*}{\partial z^2} + \rho\omega^2 u_r^* = 0,\\
&\frac{\partial^2 u_\theta^*}{\partial r^2} + \frac{1}{r}\frac{\partial u_\theta^*}{\partial r} - \frac{u^*}{r^2} + \frac{\partial^2 u_\theta^*}{\partial z^2} + \frac{\rho\omega^2}{M} u_\theta^* = 0,\\
&(\Lambda + M)\left(\frac{\partial}{\partial r} + \frac{1}{r}\right)\frac{\partial u_r^*}{\partial z} + (\Lambda + 2M)\frac{\partial^2 u_z^*}{\partial z^2}\\
&\qquad + M\frac{\partial^2 u_z^*}{\partial r^2} + \frac{M}{r}\frac{\partial u_r^*}{\partial r} + \rho\omega^2 u_z^* = 0.
\end{aligned}\right\} \tag{4.4}$$

The second of these equations describes the propagation of torsional waves, while the other two are satisfied identically if $u_r^* = u_z^* = 0$ everywhere. If we seek a solution for u_θ^* with separable variables, it is clear from the boundary conditions that it must be proportional to r. Making the substitution $u_\theta^* = rf(z)$ in the second equation we obtain the ordinary equation

$$f''(z) + q^2 f(z) = 0 \tag{4.5}$$

where

$$q^2 = \frac{\rho\omega^2}{M(\omega)}. \tag{4.6}$$

The solution of (4.5) which is zero at $z = 0$ is

$$f(z) = A \sin qz, \qquad A \text{ a const.}$$

Then, using the boundary condition at $z = h$, we obtain the solution

$$u_\theta = \frac{\alpha r \sin qz}{\sin qh} e^{i\omega t}. \tag{4.7}$$

The non-zero components of strain and stress are then found to be

$$\gamma_{\theta z} = \frac{\alpha\, rq \cos qz}{2 \sin qh}\, e^{i\omega t}, \tag{4.8}$$

$$\tau_{\theta z} = \frac{\alpha r\, Mq \cos qz}{\sin qh}\, e^{i\omega t}. \tag{4.9}$$

From equation (4.9) we find that the total forces acting on the ends of the cylinder are equivalent to the couples

$$\left.\begin{aligned} G_0 &= \frac{\pi\alpha\, a^4\, Mq}{2 \sin qh}\, e^{i\omega t}, \quad \text{at} \quad z = 0, \\ G_h &= \frac{\pi\alpha\, a^4\, Mq}{2 \tan qh}\, e^{i\omega t}, \quad \text{at} \quad z = h. \end{aligned}\right\} \tag{4.10}$$

We write

$$G_0 = A_0 \exp\left[i\,(\omega t + \delta_0)\right], \qquad G_h = A_h \exp\left[i\,(\omega t + \delta_h)\right],$$

where A_0, A_h, δ_0, δ_h are real. Then, eliminating the circular functions between equations (4.10) and remembering the definition (4.6), we have

$$M(\omega) = 4\, \frac{A_0^{\,2}\, e^{2i\delta_0} - A_h^{\,2}\, e^{2i\delta_h}}{\pi^2\, \alpha^2\, \rho a^8\, \omega^2}. \tag{4.11}$$

If the amplitudes, A_0, A_h, and phase angles, δ_0, δ_h, are known experimentally for a sequence of values of ω, (4.11) provides a simple means of determining the complex shear modulus, $M(\omega)$, over that range of frequency.

Knowledge of the visco-elastic properties in the specified frequency range is complete if the complex Young's modulus can be determined also, either by a similar analysis of *longitudinal* waves in a thin rod (BERRY and HUNTER 1956) or by a vibrating reed method (BLAND and LEE 1955).

5. SPHERICAL WAVES IN AN INFINITE SOLID

We consider here an infinite visco-elastic solid in which stress waves are initiated by a uniform time-dependent pressure $f(t)$ acting on the surface of a spherical cavity in the solid, assuming the displacement to be zero at infinity. We use a spherical coordinate system (r, θ, ϕ) in which the surface of the sphere is given by $r = b$.

Because of the spherical symmetry of the problem, all derivatives with respect to θ, ϕ are zero, and the only non-zero components of displacement, stress and strain are u_r, σ_r, σ_θ, σ_ϕ, ϵ_r, ϵ_θ, ϵ_ϕ. The Laplace transforms of the non-zero strain components are then given by the equations

$$\bar{\epsilon}_r = \frac{\partial \bar{u}_r}{\partial r}, \qquad \bar{\epsilon}_\theta = \bar{\epsilon}_\phi = \frac{\bar{u}_r}{r}, \tag{5.1}$$

and hence the transformed stress-strain relations corresponding to (3.1) can be written

$$\left.\begin{aligned} \bar{\sigma}_r &= s\bar{\lambda}\left(\frac{\partial \bar{u}_r}{\partial r} + 2\,\frac{\bar{u}_r}{r}\right) + 2s\bar{\mu}\,\frac{\partial \bar{u}_r}{\partial r}, \\ \bar{\sigma}_\theta &= \bar{\sigma}_\phi = s\bar{\lambda}\left(\frac{\partial \bar{u}_r}{\partial r} + 2\,\frac{\bar{u}_r}{r}\right) + 2s\bar{\mu}\,\frac{\bar{u}_r}{r}, \end{aligned}\right\} \tag{5.2}$$

the others being identically zero. Two of the equations of motion are identically satisfied : the remaining equation, in the radial direction, yields upon transformation

$$\frac{\partial \bar{\sigma}_r}{\partial r} + \frac{1}{r}\,(2\bar{\sigma}_r - \bar{\sigma}_\theta - \bar{\sigma}_\phi) + \bar{X}_r = \rho s^2\,\bar{u}_r \tag{5.3}$$

in the case of spherical symmetry, provided $u_r = \partial u_r/\partial t = 0$ at $t = 0$. These conditions will be satisfied in the present problem except possibly at $r = b$. When the body force component X_r is zero, we find by substituting from (5.2) into (5.3) that $\bar{u}_r$ satisfies the equation

$$\frac{\partial^2 \bar{u}_r}{\partial r^2} + \frac{2}{r}\,\frac{\partial \bar{u}_r}{\partial r} - \left(\frac{2}{r^2} + p^2\right)\bar{u}_r = 0 \tag{5.4}$$

where

$$1/p^2 = \frac{\bar{\lambda}\,(s) + 2\bar{\mu}\,(s)}{\rho s}. \tag{5.5}$$

Under the Laplace transform the boundary conditions become

$$\left.\begin{aligned} \bar{\sigma}_r = s\,(\bar{\lambda} + 2\bar{\mu})\,\frac{\partial \bar{u}_r}{\partial r} + 2s\bar{\lambda}\,\frac{\bar{u}_r}{r} &= -\,\bar{f}\,(s), \qquad r = b, \\ \bar{u}_r &= 0, \qquad r = \infty. \end{aligned}\right\} \tag{5.6}$$

The general solution of equation (5.4) is

$$\bar{u}_r = r^{-\frac{1}{2}}\left[AI_{3/2}\,(pr) + BK_{3/2}\,(pr)\right] \tag{5.7}$$

where A, B are functions of s alone to be determined by the boundary conditions. Since $|I_{3/2}\,(z)| \to \infty$ as $|z| \to \infty$, A must be zero in this problem. Putting the other Bessel function into exponential form and using the first of conditions (5.6) the function $B\,(s)$ can be determined, and we find that

$$\bar{u}_r = \frac{\bar{f}\,(s)\,b^3\,e^{-p(r-b)}\,(1 + pr)}{r^2\,s\left[(\bar{\lambda} + 2\bar{\mu})\,p^2\,b^2 + 4\bar{\mu}\,(1 + pb)\right]} \tag{5.8}$$

provided p is determined from equation (5.5) so that $|arg\ p| \leqslant \frac{1}{2}\pi$ when s is in the half-plane of convergence of $\bar{u}_r$. The Laplace transforms of the components of strain and stress can now be obtained by means of (5.1) and (5.2), but here we shall confine our attention to the displacement.

If the pressure at $r = b$ is impulsive we represent it by a Dirac delta function, putting $f\,(t) = P\delta\,(t)$, so that

$$\bar{f}\,(s) = P. \tag{5.9}$$

Under the boundary condition the solution of the problem can be expressed as a real integral for a material analogous to the Maxwell solid of one-dimensional visco-elasticity. If the Poisson's ratio of the material is independent of time under

constant stress, the relaxation functions have a common relaxation time, α^{-1}, say, and we can write

$$\lambda(t) = \lambda_0 e^{-\alpha t}, \qquad \mu(t) = \mu_0 e^{-\alpha t}.$$

Then

$$\bar{\lambda}(s) + 2\bar{\mu}(s) = \frac{\lambda_0 + 2\mu_0}{s + \alpha}$$

and, by substitution in (5.5),

$$p^2 = \kappa^2 s(s + \alpha) \tag{5.10}$$

where

$$\kappa^2 = \frac{\rho}{\lambda_0 + 2\mu_0}$$

from which p is determined so that it is positive when s is positive. By substitution from (5.9) and (5.10), equation (5.8) becomes

$$\bar{u}_r = \frac{Pp}{\rho r^2}\left(1 + \frac{\alpha}{s}\right)\phi\left(r, \sqrt{s(s+\alpha)}\right), \tag{5.11}$$

where

$$\phi(r, s) = \frac{e^{-\kappa s(r-b)}(1 + \kappa r s)}{(s + c)^2 + \gamma^2}, \tag{5.12}$$

$$\left.\begin{aligned} c &= \frac{2\mu_0 \kappa}{\rho} \cdot \frac{1}{b}, \\ \gamma^2 &= \frac{4\mu_0(\lambda_0 + \mu_0)}{\rho(\lambda_0 + 2\mu_0)} \cdot \frac{1}{b^2}. \end{aligned}\right\} \tag{5.13}$$

The Laplace inversion of (5.11) can be found by using some results by ERDÉLYI *et al.* (1954) and some wellknown properties of the Laplace transform : notably, the inversion of the function (5.12) is given by

$$\mathcal{L}^{-1}\{\phi(r, s)\} = \psi(r, t)\, H[t - \kappa(r - b)]$$

where

$$\psi(r, t) = e^{-c[t-\kappa(r-b)]}\left\{\kappa r \cos\gamma[t - \kappa(r-b)] + \frac{1 - c\kappa r}{\gamma}\sin\gamma[t - \kappa(r-b)]\right\}, \tag{5.14}$$

to which can be applied the results

$$\mathcal{L}^{-1}\left\{\bar{f}\left(\sqrt{s(s+\alpha)}\right)\right\} = e^{-\frac{\alpha}{2}t}\left[f(t) + \frac{\alpha}{2}\int_0^t f\left(\sqrt{t^2 - u^2}\right) I_1\left(\frac{\alpha}{2}u\right) du\right],$$

$$\mathcal{L}^{-1}\left\{\frac{\bar{f}\left(\sqrt{s(s+\alpha)}\right)}{\sqrt{s(s+\alpha)}}\right\} = e^{-\frac{\alpha}{2}t}\int_0^t f(u)\, I_0\left(\frac{\alpha}{2}\sqrt{t^2 - u^2}\right) du.$$

We put equation (5.11) into the form

$$\bar{u}_r = \frac{Pb}{\rho r^2}\left[\phi\left(r, \sqrt{s(s+\alpha)}\right) + (\alpha s + s^2)\frac{\phi\left(r, \sqrt{s(s+\alpha)}\right)}{s(s+\alpha)}\right]$$

and after some calculation find that the radial displacement is given by

$$u_r = \frac{Pb}{\rho r^2} e^{-\frac{\alpha}{2}t} \left\{ \psi(r,t) + \alpha\Psi(r,t) + \frac{\alpha^2}{2} \int_{\kappa(r-b)}^{t} \Psi(r,u)\, I_0\left(\frac{\alpha}{2}\sqrt{t^2-u^2}\right) du \right.$$

$$\left. + \frac{\alpha}{2} \int_{\kappa(r-b)}^{t} \left[u\psi(r,u) + \alpha t\Psi(r,u)\right] \frac{I_1\left(\frac{\alpha}{2}\sqrt{t^2-u^2}\right)}{\sqrt{t^2-u^2}}\, du \right\} H\left[t - \kappa(r-b)\right] \qquad (5.15)$$

where $\psi(r,t)$ is given by (5.14) and

$$\Psi(r,t) = \int_{\kappa(r-b)}^{t} \psi(r,\tau)\, d\tau$$

$$= \frac{1 - e^{-c[t-\kappa(r-b)]} \cos\gamma\left[t - \kappa(r-b)\right]}{c^2+\gamma^2}$$

$$+ \frac{1}{\gamma}\left(\kappa r - \frac{c}{c^2+\gamma^2}\right) e^{-c[t-\kappa(r-b)]} \sin\gamma\left[t - \kappa(r-b)\right]. \qquad (5.16)$$

By putting $\alpha = 0$ in (5.15) we easily obtain the solution for a purely elastic solid:

$$u_r = \frac{Pb}{\rho r^2}\, \psi(r,t)\, H\left[t - \kappa(r-b)\right]. \qquad (5.17)$$

The velocity of propagation of the wave front, $\kappa^{-1} = \left[\lambda_0 + 2\mu_0)/\rho\right]^{\frac{1}{2}}$, is independent of the relaxation time, α^{-1}, and is that of a dilatational or *P*-wave.

Acknowledgments

The author is indebted to the Council of the Research Association of British Rubber Manufacturers for permission to publish this paper and to Professor I. N. Sneddon for directing his attention to the problems considered.

References

Berry, D. S.	1956	*Thesis of University of London.*
Berry, D. S. and Hunter, S. C.	1956	*J. Mech. Phys. Solids* **4**, 72.
Biot, M. A.	1954	*J. Appl. Phys.* **25**, 1385.
Bland, D. R. and Lee, E. H.	1955	*J. Appl. Phys.* **26**, 1497.
Erdélyi, A., Magnus, W., Oberhettinger, F. and Tricomi, F. G.	1954	*Tables of Integral Transforms* (New York, McGraw-Hill Book Co. Ltd.).
Glauz, R. D. and Lee, E. H.	1954	*J. Appl. Phys.* **25**, 947.
Gross, B.	1953	*Mathematical Structure of the Theories of Visco-elasticity* (Paris, Hermann et Cie).
Leadermann, H.	1943	*Elastic and Creep Properties of Filamentous Materials and other Hight Polymers* (Washington, Textile Foundation).
Lee, E. H. and Kanter, T.	1953	*J. Appl. Phys.* **24**, 1115.
Love, A. E. H.	1952	*A Treatise on the Mathematical Theory of Elasticity*, 4th edition (C.U.P.).
Mandel, J.	1953	*C.R. Acad. Sci.* **241**, 1910.
	1956	*Ibid.* **242**, 2803.
Sips, R.	1951	*J. Polymer Sci.* **7**, 191.
Sneddon, I. N.	1955	*Functional Analysis*, in *Handbuch der Physik* pp. 198-348 (Berlin, Springer).
Staverman, A. J. and Schwarzl, F.	1952	*Proc. K. Ned. Akad. Wetensch.* **55**, 486.

Journal of the Mechanic and Physics of Solids, 1958, Vol. 6, pp. 186 to 202. Pergamon Press Ltd., London

IMPULSIVE LOADING OF PLASTIC BEAMS WITH AXIAL CONSTRAINTS*

By P. S. Symonds† and T. J. Mentel‡

(*Received 16th September*, 1957)

Summary

This paper concerns the plastic deformations of simply supported and clamped beams whose ends are prevented from displacing axially, and which are subjected to transverse impulsive pressure loading. Finite axial forces arise as soon as the beam acquires a finite deflection, and the paper describes the transition from the initial simple beam behaviour to the final stage in which deformations are governed primarily by catenary effects. It is shown that when loads are such that deflections are of the order of the beam thickness, or greater, the treatment as a simple beam becomes unrealistic, the deflections being greatly reduced by the action of the axial force. For example, in a problem of a continuous beam on many supports where full axial constraint would be realized, the deflection may be a small fraction of that predicted by the treatment where axial forces are disregarded. Curves are presented showing how the reduction depends on the span-depth ratio of the beam and on the intensity of loading.

1. Introduction

The solutions presented in this paper for problems of impulsive loading of a beam with axial constraints are based on a rigid-plastic type of analysis, elastic deformations being disregarded as negligible by comparison with plastic ones. This approach is held to be appropriate if the energy absorbed in plastic deformation is very large compared to the maximum strain energy the structure could absorb in an elastic manner. We assume also that the properties governing the plastic behaviour are those measured in static tests, strain rate effects being ignored. In the present analysis shape changes are taken into account, but it is assumed that deflections are so small that the length of a segment does not differ appreciably from its projection on the axis passing through the support points. This requires the square of the slope of the deflection curve to be small compared with unity. With this assumption the normal force N on a cross-section is taken as constant along the beam. Finally, the closing phase of the motion, in which the beam behaves like a plastic string, is treated by an approximate method that is believed to give reasonably close bounds on the final deformations. The present paper supplements earlier reports which were concerned primarily with the treatment as a simple beam (Symonds 1955) and with the transition from behaviour as a

* The results presented in this paper were obtained in the course of research sponsored by Norfolk Naval Shipyard under Contract N189-15164A with Brown University.

† Brown University.

‡ University of Minnesota.

simple beam to that in which both bending moments and axial forces occur (MENTEL and SYMONDS 1955)*.

2. FLEXURAL RESPONSE

The problems considered are indicated in Figs. 1 (a) and 1 (b), which refer to pinned and clamped end conditions, respectively. In both cases the end sections are constrained against both axial and transverse displacements. The loading is taken as a very short pulse of uniform pressure that imparts a uniform velocity V to the beam, with zero initial displacement. The span of the beam is $2l$ and its mass per unit length is m.

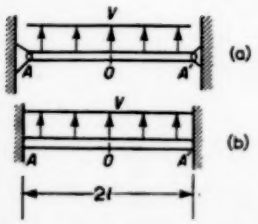

Fig. 1. Problems treated: (a) simply supported (pin-ended) beam; (b) built-in (clamped) beam, both with ends constrained against axial motion, with uniform initial velocity V.

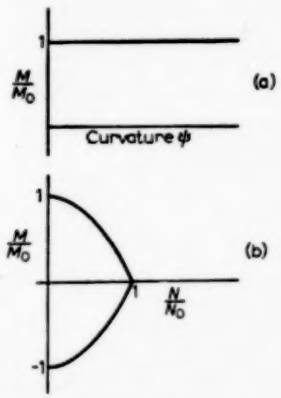

Fig. 2. (a) Moment–curvature relation for rigid–plastic beam; (b) interaction curve between bending moment M and axial force N in fully-plastic state.

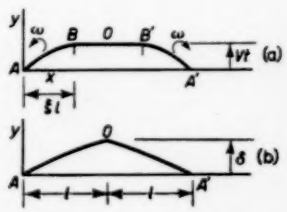

Fig. 3. Patterns of deformation: (a) first phase, (b) second phase.

If effects of axial constraints are ignored the plastic-rigid solution is obtainable very simply (SYMONDS 1955). In this case the plasticity condition is that indicated by Fig. 2 (a). No curvature change occurs if the moment is less than the limit moment M_0, while if this is maintained at a cross-section unlimited plastic flow can occur there. The pattern of deformation in the first phase of motion is found to be as indicated in Fig. 3 (a). The central portion moves with the original velocity V while segments at the ends rotate as rigid bars about the support points. It is verified *a posteriori* that the bending moment in the end segments decreases monotonically from M_0 to zero at the supports in the case of pinned ends, and from M_0 to $-M_0$ at the supports in the clamped end case. The motion in either case will be determined if the length ξl and angular velocity ω of the end segments are found. The required equations are that expressing continuity of velocity at the junction of the rigid segment AB with the central region BB', namely

* HAYTHORNTHWAITE (1957) has described analytical and experimental work showing large effects of end constraints in static loading of beams.

$$\omega \xi l = V, \tag{1}$$

and that for moment of momentum with respect to A. For the simply supported beam this equation is

$$\int_0^{\xi l} \omega x^2 m \, dx + \int_{\xi l}^{l} Vxm \, dx - \int_0^{l} Vxm \, dx = -M_0 t. \tag{2}$$

From these it is found that

$$\xi^2 = \frac{6M_0}{ml^2 V} t, \qquad \omega^2 = \frac{mV^3}{6M_0 t}. \tag{3}$$

The type of configuration shown in Fig. 3 (a) holds until the time t_1 when $\xi = 1$, i.e. when the rigid segments have increased in length to l. After this time the two halves rotate with a central plastic hinge joining them, motion continuing until the kinetic energy at time t_1 is absorbed in work at the plastic hinge. For the simply supported beam the final central deflection δ_f and slope angles θ_0 at the centre and θ_s at the support are easily found to be

$$\delta_f = \tfrac{1}{3} \frac{ml^2 V^2}{M_0}, \qquad \theta_0 = \tfrac{1}{6} \frac{mlV^2}{M_0}, \qquad \theta_s = \tfrac{1}{2} \frac{mlV^2}{M_0}. \tag{4}$$

For the beam with clamped ends the patterns of deformation are the same as with simple support, and the only change in the analysis is the replacement of M_0 by $2M_0$ in (2) and hence in all the results of (3) and (4).

3. Effects of End Constraints

We now consider the effects of preventing motion at the ends. At any section there is now an axial force N as well as a bending moment M. In order for plastic deformation to occur M and N must satisfy a plasticity condition, which we take as

$$f(M/M_0, N/N_0) = M/M_0 + N^2/N_0^2 - 1 = 0 \tag{5}$$

where M_0 is the limit moment in pure bending, as before, and N_0 is the axial force at yield in simple tension or compression. The formula applies strictly to a rectangular section. If the width is b, depth h, and yield stress σ_y, then $M_0 = \frac{1}{4} \sigma_y bh^2$, $N_0 = \sigma_y bh$. Whenever (5) is satisfied plastic deformation consisting of both curvature change and extension (or contraction) of the middle surface takes place. These two types of plastic deformation take place in definite proportions governed by the value of M and N. The flow rule appropriate to the present problem was discussed by Onat and Prager (1953) who showed that it takes the form

$$\frac{N_0 \dot{\epsilon}}{M_0 \dot{\psi}} = 2 \frac{N}{N_0}, \tag{6}$$

where ϵ is the strain at the beam centre-line and ψ is the curvature; dots indicate time rates. The flow rule of (6) expresses the general fact that the direction of the strain rate vector is that of the normal to the yield curve. When the yield curve is plotted as in Fig. 2 (b) the appropriate strain-rate vector has components $M_0 \dot{\psi}$, $N_0 \dot{\epsilon}$.

In deriving the equations it is again assumed that successive stages of deformation occur as indicated in Figs. (3a) and (3b), the difference now being that an axial force N occurs together with axial deformations as well as curvature changes. Consider the first stage in Fig. (3a) in which the central plastic region BOB' moves with velocity V and the outer segments AB and $A'B'$ rotate as rigid bodies with angular velocity ω. If the axial force in the central region BOB' is N, that at any point x is $N' = N/\cos\phi$ where ϕ is the slope angle. We assume that ϕ is so small that N' can be taken as equal to N everywhere; this requires that the slope dy/dx be so small that $(dy/dx)^2 \ll 1$.

Consider first the *simply supported* beam (Fig. 4) when a segment AB of length ξl is rotating about the support point A with angular velocity ω. The bending moment in AB varies from zero at A to M at B. The segment BO has constant

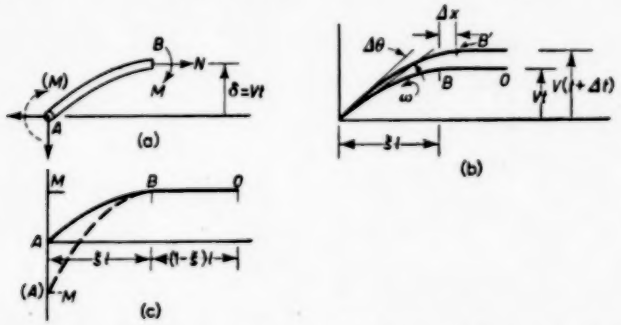

Fig. 4. (a) Free body diagram for segment AB in first phase ; (b) diagram for deriving constraint relation ; (c) bending moment diagrams for supported and built-in ends (dashed curve).

moment M throughout its length. Since shear force is zero in this segment all elements in it move with the initial velocity V. The axial force is N at this instant. The unknowns in this phase of the problem are M, N, ω, and ξ. To find these we have to solve simultaneously four equations, two of which are the equation (1) expressing continuity of velocity at the plastic-rigid junction, and the plasticity condition (5) relating M and N in the plastic zone. The equation of angular acceleration of segment AB about the fixed point A is

$$\tfrac{1}{3}\, ml^3\, \xi^3\, \dot{\omega} = -\,M - N\delta \tag{7}$$

where the central deflection δ is equal to Vt in this phase. The fourth equation needed is that expressing the condition of axial constraint. Referring to Fig. 4 (b), in a small time interval Δt the segment AB rotates through an angle $\Delta\theta$ while the length of the segment increases by an amount Δx, the interface between rigid and plastic zones moving to B'. The average strain ϵ and the curvature change ψ occurring in the segment Δx are as follows :

$$\epsilon\Delta x = (\Delta\theta)\,\delta, \qquad \psi = \Delta\theta/\Delta x. \tag{8}$$

The relation between linear strain and curvature change required by the flow rule (6) therefore furnishes the equation

$$\frac{N}{N_0} = \frac{N_0\,\delta}{2M_0}. \tag{9}$$

In this phase $\delta = Vt$, so that (9) gives N/N_0 directly in terms of known quantities. The determination of M, N, ω, ξ in this phase are found by simultaneous solution of (1), (5), (7) and (9). These may be combined to give

$$-\frac{mV^3}{3M_0}\frac{\dot{\omega}}{\omega^3} = \frac{mV^3}{6M_0}\frac{d}{dt}(\omega^{-2}) = 1 + \frac{N_0^2 V^2 t^2}{4M_0^2}. \tag{10}$$

The solution of this is

$$\frac{6M_0\omega^2}{mV^3} = \frac{1}{t}\left(1 + \frac{N_0^2 V^2 t^2}{12M_0^2}\right)^{-1}. \tag{11}$$

This phase of the motion ends at time t_1 when $\xi = 1$, $l\omega = V$. From (11) t_1 is given by

$$t_1\left(1 + \frac{N_0^2 V^2 t_1^2}{12M_0^2}\right) = \frac{mVl^2}{6M_0}. \tag{12}$$

It is convenient to use dimensionless parameters as follows :

$$\eta \equiv \frac{Vt}{l}, \qquad \beta \equiv \frac{N_0 l}{\sqrt{12}\, M_0}, \qquad \alpha \equiv \frac{ml V^2}{6M_0}. \tag{13}*$$

In terms of these (11) and (13) are

$$\left(\frac{d\theta}{d\eta}\right)^2 = \frac{\alpha}{\eta(1 + \beta^2\eta^2)}, \tag{14}$$

$$\eta_1(1 + \beta^2\eta_1^2) = \alpha, \tag{15}$$

where $\eta_1 = Vt_1/l$. The angle θ_1 attained at the end of the first phase is given by

$$\theta_1 = \sqrt{\alpha}\int_0^{\eta_1} \frac{d\eta}{\sqrt{\{\eta(1 + \beta^2\eta^2)\}}}. \tag{16}$$

With substitutions

$$z^2 = \beta\eta, \qquad \sin\psi = 2z/(1 + z^2), \tag{17a}$$

$$\theta_1 = \sqrt{\frac{\alpha}{\beta}}\int_0^{z_1} \frac{2\,dz}{\sqrt{(1 + z^4)}} = \frac{\alpha}{\beta}\int_0^{\psi_1} \frac{d\psi}{\sqrt{(1 - \tfrac{1}{2}\sin^2\psi)}} \tag{17b}$$

where $z_1^2 = \beta\eta_1$ is the solution of

$$z_1^2(1 + z_1^4) = \beta\alpha \tag{18}$$

and furnishes ψ_1 by (17a). The angle θ_1 is given by

$$\theta_1 = \sqrt{\frac{\alpha}{\beta}}\, F(1/\sqrt{2}, \psi_1) \tag{19}$$

where $F(1/\sqrt{2}, \psi_1)$ is the elliptic integral of the first kind with modulus $1/\sqrt{2}$,

*The parameter β determines the importance of axial constraints. Note that $\beta = \sigma_y A l/\sqrt{12}\,\sigma_y kZ = lh/2\sqrt{12}\,ki^2$, where A is cross-section area, Z is section modulus and k is the shape factor of plastic beam theory i.e. ratio of limit moment to yield moment. For a rectangular section $k = 1{\cdot}5$. For I-sections $Z = 2I/h = 2Ai^2/h$, where i is the radius of gyration, and for many commercial sections $i \simeq 0{\cdot}4h$. Hence we have

$$\underset{\beta = 1{\cdot}15\, l/h}{\text{Rectangle}} \qquad \underset{0{\cdot}8\, l/h}{\text{I-section}} \tag{13a}$$

For these sections therefore β can roughly be identified with the length-depth ratio l/h.

amplitude ψ_1. The central deflection δ_1 at the end of this phase is

$$\delta_1 = Vt_1 = l\eta_1. \tag{20}$$

In the second phase of the deformation the two halves of the beam rotate as rigid bars pivoted at the supports and attached at the central plastic hinge, where permanent curvature change and axial extension occur. The unknown quantities are M, N, $\omega = \dot{\theta}$ and δ. These are found by simultaneous solution of (1), (5), (7) and (9) after placing $\xi = 1$. Equation (1) then furnishes at once

$$\delta = Vt_1 + (\theta - \theta_1)\, l. \tag{21}$$

In terms of η, β, and α as defined in (13), we obtain the following differential equation for θ:

$$2\alpha \frac{d^2\theta}{d\eta^2} = -1 - 3\beta^2 (\eta_1 + \theta - \theta_1)^2. \tag{22}$$

This has the first integral

$$\alpha \left(\frac{d\theta}{d\eta}\right)^2 = -\theta - \beta^2 (\theta - \theta_1 + \eta_1)^3 + C. \tag{23}$$

The integration constant C is found from the conditions at $\eta = \eta_1 : \theta = \theta_1$, $d\theta/d\eta = 1$,

$$C = \alpha + \theta_1 + \beta^2 \eta_1{}^3. \tag{23a}$$

Deformation ends at time $t_f = \eta_f\, l/V$ when $d\theta/d\eta = 0$, $\theta = \theta_f$.

From (23), therefore,

$$\theta_f - \theta_1 + \beta^2 (\theta_f - \theta_1 + \eta_1)^3 = \alpha + \beta^2 \eta_1{}^3. \tag{24}$$

The final deflection δ_f is given by solving the equation

$$\frac{\delta_f}{l} + \beta^2 \left(\frac{\delta_f}{l}\right)^3 = 2\alpha \tag{25}$$

where (15) giving η_1 has been used. It is seen that δ_f is obtainable directly from knowledge of the parameters α and β; however, the determination of the final deflection curve and strain and curvature functions require numerical integration based on (14).

Equation (25) satisfies the requirement that for $\delta_f/l \to 0$ or for $\beta \to 0$ the solution becomes that found above neglecting axial forces, given in equation (4).

We next show that the corresponding results for a beam with *built-in* ends may be solved by a simple modification in the results obtained above for simple support conditions. Of the previous governing equations, (1) and (5) remain unchanged. The equation of angular acceleration of segment AB becomes (from the free-body diagram, Fig. 4 (a))

$$\tfrac{1}{3} ml^3 \xi^3 \dot{\omega} = -2M - N\delta, \tag{26}$$

where the bending moment at the built-in end A is taken as equal to that at B; this follows from the assumption that the deflections are so small that the axial force is N throughout the segment. In this case both axial strain ϵ_A and curvature change ψ_A take place at the built-in end A as well as at B, where axial strain ϵ_B

and curvature change ψ_B are not necessarily equal to the respective quantities at A. Suppose that in a small time interval Δt a rotation $\Delta\theta$ of segment AB occurs, with the rigid–plastic interface at A moving Δx_A while that at B moves Δx_B. Then, replacing (8), we have

$$\epsilon_A \Delta x_A + \epsilon_B \Delta x_B = (\Delta\theta)\,\delta, \tag{27}$$

$$\psi_A = \frac{\Delta\theta}{\Delta x_A}, \qquad \psi_B = \frac{\Delta\theta}{\Delta x_B}, \qquad \delta = \frac{\epsilon_A}{\psi_A} + \frac{\epsilon_B}{\psi_B}. \tag{28}$$

But the flow rule (6) shows that ϵ_A/ψ_A and ϵ_B/ψ_B are both equal to $2M_0 N/N_0^2$, (again assuming deflections small so that the axial force is N at both hinges). Hence we obtain, replacing (9),

$$\frac{N}{N_0} = \frac{N_0\,\delta}{4M_0}. \tag{29}$$

In the first phase in which $\delta = Vt$ the result of combining (1), (5), (26) and (29) is

$$-\frac{mV^3t^3}{6M_0}\frac{\dot\omega}{\omega^3} = 1 + \frac{N_0^2\,V^2t^2}{16M_0^2}. \tag{30}$$

It is seen that this equation could have been obtained from the corresponding equation for the supported beam, (10), by substitution of $2M_0$ for M_0 in that equation.

The same result is found to hold for the second phase of motion ; (22) furnishes the correct equation for the built-in beam if M_0 is replaced by $2\,M_0$ in (22). Thus the expressions (24) and (25) for final deformations of supported beams give correct results for clamped beams when M_0 is replaced by $2\,M_0$.

This analysis, which is surprisingly simple, furnishes results for the influence of axial constraints on flexural behaviour of beams under the rigid–plastic assumption. It is subject to important limitations as discussed in the following Section. Comparisons between the deflections of a simple beam (no axial constraints) according to (4) and those of the beam fully constrained against axial motions are given by curves A and B in Figs. 10-12, which are for $\beta = 5,\ 15,\ 30$. (As pointed out above in footnote equation (13a), $\beta \simeq l/h$).

4. Transition to Plastic String

Reference is now made to the case of a supported beam, results for which were given in detail in the foregoing Section. Results for beams with clamped ends are immediately obtained by replacement of M_0 by $2M_0$; thus $\alpha = ml\,V^2/6M_0$ is replaced by $\alpha/2$ and $\beta \equiv N_0\,l/\sqrt{12}\,M_0$ is replaced by $\beta/2$.

The foregoing treatment provides N/N_0 in terms of the central deflection, and is valid only so long as $N/N_0 \leqslant 1$. From (7) in the first phase we must have

$$\frac{N_0\,Vt}{2M_0} = \frac{N}{N_0} \leqslant 1. \tag{31}$$

Since $N_0\,l/M_0 \equiv \sqrt{12}\,\beta$, the requirement for validity of the results obtained for the first phase is

$$\sqrt{3}\,\beta\,\eta_1 \leqslant 1. \tag{32}$$

But η_1 is the solution of (15), and combination of the inequality (32) with (15) gives the result that the first phase is valid if

$$\alpha\beta \leqslant \frac{4}{3\sqrt{3}}. \tag{33}$$

A similar result expresses the necessary condition for the complete solution obtained above to be valid, rather than merely the first phase. The basic condition is

$$\frac{N}{N_0} = \frac{N_0\,\delta_f}{2M_0} = \sqrt{3}\,\beta\,\frac{\delta_f}{l} \leqslant 1. \tag{34}$$

Combining this with (25), we obtain the following condition for validity of the complete solution :

$$\alpha\beta \leqslant \frac{2}{3\sqrt{3}}. \tag{35}$$

It can be seen from (34) that the beam solution is valid only for deflections smaller than the depth of the beam, since $\beta \simeq l/h$.

Suppose that, at time $\eta^* = Vt^*/l$,

$$\frac{N(t^*)}{N_0} = 1. \tag{36}$$

In a succeeding interval of time it is surmised that the axial force remains constant and equal to N_0 while the bending moment is zero throughout the beam. If the assumption of small deflections is retained the equation of motion is

$$\frac{\partial^2 y}{\partial x^2} = \frac{m}{N_0}\frac{\partial^2 y}{\partial t^2}. \tag{37}$$

Thus the beam now behaves as a plastic string with tension N_0, whose motion is governed by the velocity and displacement functions at time t^*. Behaviour as a string, however, can continue only so long as the deformation at each point satisfies conditions set by the flow rule. If the structure behaved strictly like a plastic string the only condition on the deformation would be that the centre-line should undergo extension, rather than contraction. The fact that the beam has finite thickness means that the ratio of curvature to centre-line strain must lie within a certain range. All points of the cross-section are assumed to be at the yield stress in tension. This requires all strains likewise to be tensile strains. If the strain varies linearly across the depth of the beam then the minimum strain is

$$\epsilon_{min} = \epsilon - c_1\,\psi \tag{38}$$

where ϵ is the strain at the centre-line, ψ is the curvature, and c_1 is the distance from the centre-line to the extreme fibre on the concave side. To have all strains positive we must therefore have

$$\frac{\epsilon}{\psi} \geqslant c_1. \tag{39}$$

For curvature in the opposite sense the analogous expression is

$$\frac{\epsilon}{\psi} \geqslant c_2. \tag{40}$$

If the curvature and centre-line strain are expressed in terms of the centre-line deflection $y(x)$, the two requirements can be written as

$$-\frac{1}{c_2} \leqslant \frac{\partial^2 y}{\partial x_2} \Big/ \tfrac{1}{2}\left(\frac{\partial y}{\partial x}\right)^2 \leqslant \frac{1}{c_1}. \tag{41}$$

For a rectangular section, to which (5) strictly applies, the limiting conditions are

$$-\frac{2}{h} \leqslant \frac{\partial^2 y}{\partial x^2} \Big/ \tfrac{1}{2}\left(\frac{\partial y}{\partial x}\right)^2 \leqslant \frac{2}{h}. \tag{42a}$$

These conditions may also be derived by using the fact that the plastic strain-rate vector $(M_0\,\dot{\psi},\ N_0\,\dot{\epsilon})$ is normal to the loading surface $f(M/M_0,\ N/N_0) = 0$ wherever the latter has a continuously turning normal ; at a corner the strain-rate vector may have any direction between the normals defined at opposite sides of the corner. At the point $N/N_0 = 1$ of the interaction curve Fig. 2 (b) the strain-rate vector must lie between the outward normals to the two branches of the curve above and below the N/N_0 axis, respectively. Since from (5) the normal to the curve for a rectangular section has components $(2N/N_0,\ 1)$ we have at the point $N/N_0 = 1$

$$-\tfrac{1}{2} \leqslant \frac{M_0\,\dot{\psi}}{N_0\,\dot{\epsilon}} \leqslant \tfrac{1}{2}. \tag{42b}$$

But for a rectangular section $M_0/N_0 = h/4$, and this substitution yields conditions (42a).

Continuing now with the solution beyond time t^*, the string equation (37) is to be satisfied subject to the special conditions (42) and corresponding to given functions of velocity and displacement at time t^*. The general solution can be written in the form

$$y = F_1(x - ct) + F_2(x + ct), \qquad \text{where} \qquad c = \sqrt{N_0/m}. \tag{43}$$

We take a new time origin corresponding to the instant t^*, and specify initial conditions

$$y(x, 0) = Y(x), \qquad y_t(x, 0) = v(x). \tag{44}$$

The end conditions are

$$y(0, t) = y(2l, t) = 0. \tag{45}$$

These will be satisfied if the travelling waves $F_1(x - ct)$ and $F_2(x + ct)$ satisfy the following relations :

$$\left.\begin{aligned} F_2(z) &= -F_1(-z) \\ F_1(z) &= F_1(z \pm 4l \\ F_2(z) &= F_2(z \pm 4l) \end{aligned}\right\} \tag{46}$$

where $z = x \pm ct$. Finally, the initial conditions require that the complete solution take the form

$$y(x, t) = \tfrac{1}{2}\,Y(x - ct) + \tfrac{1}{2}\,Y(x + ct) - \tfrac{1}{2}\,S(x - ct) + \tfrac{1}{2}\,S(x + ct) \tag{47}$$

where

$$S(z) = \frac{1}{c}\int_c^z v(s)\,ds. \tag{48}$$

The initial velocity and displacement functions have the shapes shown in Fig. 5 if $t^* < t_1$, i.e. if the transition from beam to string behaviour occurs during the first phase of the beam motion. Then the function $S(z)$ is shown in Fig. 6 and

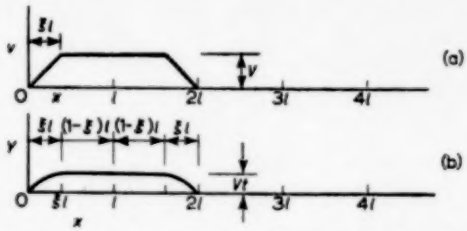

Fig. 5. Initial displacement and velocity functions for plastic string phase of motion.

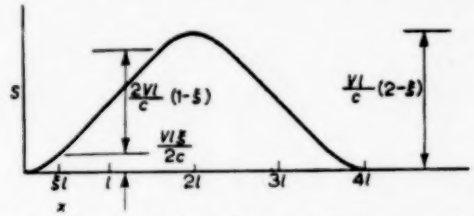

Fig. 6. Function $S(z)$ used in travelling wave solution.

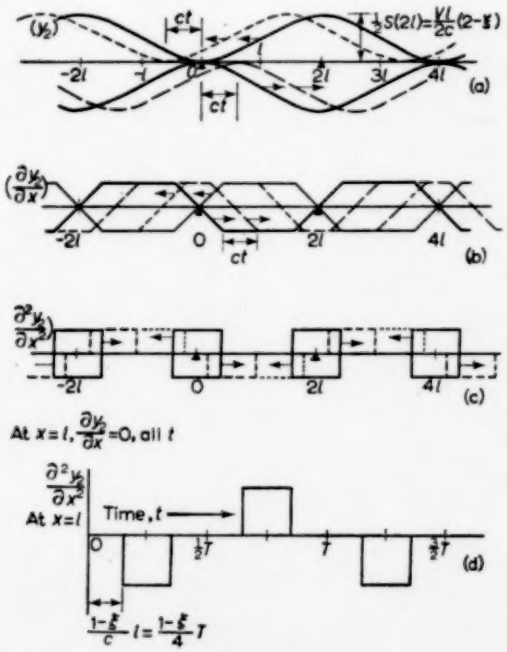

Fig. 7. " Plastic string " phase : travelling wave contributions to displacement, slope, and other functions arising from initial velocity distribution.

by the solid curves in Fig. 7 (a) which show $-\frac{1}{2}S(x-ct)$ and $\frac{1}{2}S(x+ct)$ at $t = 0$. The dashed curves in Fig. 7 (a) indicate the positions of the two travelling

waves after a small time has elapsed. The corresponding curves in Figs. 7 (b) and 7 (c) show the contributions to the slope and to the curvature, respectively, from the two travelling waves. Finally, Fig. 7 (d) shows the variation of curvature

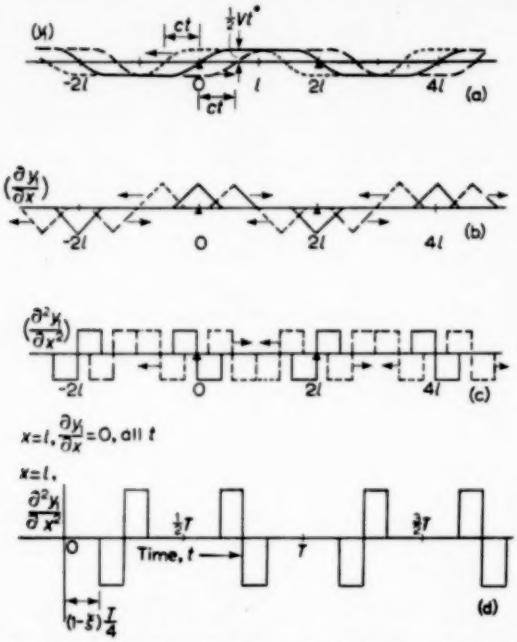

Fig. 8. "Plastic string" phase: travelling wave contributions to displacement, slope, and other functions arising from initial displacement configuration.

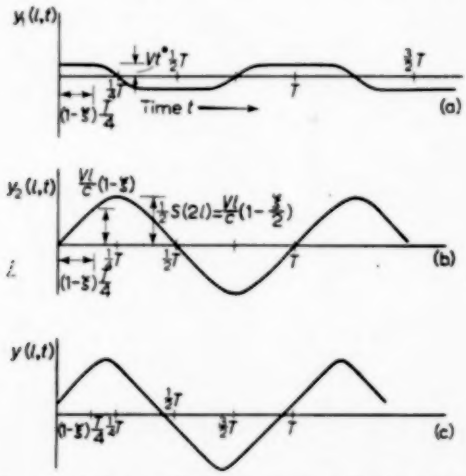

Fig. 9. Time variation of displacement contributions at midpoint.

at the beam midpoint as a function of time; this is the contribution arising from the initial velocity distribution. The curves of Fig. 8 (a) show the travelling waves $\frac{1}{2}\,Y\,(x - ct)$ and $\frac{1}{2}\,Y\,(x + ct)$ that express the contributions to the motion

arising from the initial displacement configuration. The shape of the curve $Y(x)$ in the range $0 \leqslant x \leqslant \xi l$ is approximately parabolic; the derived travelling waves expressing the slope and curvature are shown in Figs. 8 (b) and 8 (c) as they would be if the corresponding arc of $Y(x)$ were a parabola. Fig. 8 (d) shows the time variation of curvature at the beam centre resulting from the initial displacement configuration.

In order to determine strictly when behaviour as a string ceases, the time variations of both $\frac{\partial y}{\partial x}$ and $\frac{\partial^2 y}{\partial x^2}$ would have to be plotted for a series of closely spaced stations along the beam. For each station the quantity $\frac{\partial^2 y}{\partial x^2} \Big/ \frac{1}{2}\left(\frac{\partial y}{\partial x}\right)^2$ could then be plotted and the instant when one of the equalities (42) is first satisfied could be found from these plots. At subsequent times the behaviour of the beam would apparently be extremely complicated. Presumably the axial force would remain constant (approximately) at N_0. In certain regions of the beam one of the equations (42) (rather than inequalities) would be satisfied, so that in these regions the deflection would be such that $N_0 \epsilon = 2 M_0 \psi$. Outside these regions all of the inequalities (42) would be satisfied, and motion would continue to be governed by (37). The problem of matching solutions at the various moving boundaries is obviously a difficult one. This problem is not attacked in the present paper; instead, we present an approximate solution which may nevertheless show the main effects of the end constraints in this type of problem.

The approximation consists in disregarding altogether the limiting conditions on the string solution set by inequalities (42). Thus, for all times $t > t^*$, the governing equation is taken to be (37) subject to the appropriate initial conditions. This neglect of constraints actually present will lead to an overestimate of final deflections. Therefore the actual final deflection would lie between the curve obtained in the present paper and that obtained in the previous Section.

According to the present approximation the travelling waves of Figs. 7 (a) and 8 (a) are combined to determine the maximum displacement. The midpoint displacements $y_1(l, t)$ and $y_2(l, t)$, corresponding to the initial displacement and the initial velocity, respectively, are shown in Figs. 9 (a), (b). These add to give the curve Fig. 9 (c). It is easily seen that the maximum displacement occurs roughly midway between the times $\frac{1}{4}(1 - \xi)\, T$ and $\frac{1}{4}\, T$, since the values at these times are equal. This is shown as follows. At the time $\frac{1}{4}(1 - \xi)\, T$ the total displacement is, from Figs. 7 (a) and 8 (a),

$$y\left(l, \tfrac{1}{4}(1 - \xi)\, T\right) = Vt^* + \frac{Vl}{c}(1 - \xi). \tag{49}$$

At time $\frac{1}{4}\, T$ the total displacement is, from Fig. 7 (a),

$$y\left(l, \tfrac{1}{4}\, T\right) = \frac{Vl}{c}\left(1 - \frac{\xi}{2}\right). \tag{50}$$

These can be evaluated easily. We have first from (31) that

$$Vt^* = \frac{2M_0}{N_0}. \tag{51}$$

To evaluate ξ in terms of the basic parameters of the problem, we use the result

(11) that, during the first phase,

$$\frac{6M_0}{mV^3}\dot{\theta}^2 = t\left(1 + \frac{N_0^2\,V^2}{12M_0^2}\,t^2\right)^{-1}. \tag{52}$$

Putting in t^* from (51), and simplifying, we obtain

$$\dot{\theta}\,(t^*) = \tfrac{1}{4}\sqrt{\frac{m}{N_0}}\,\frac{N_0\,V^2}{M_0}. \tag{53}$$

Then we find

$$\xi = \frac{V}{l\dot{\theta}} = \frac{4M_0}{lN_0\,V}\sqrt{\frac{N_0}{m}} = \frac{4M_0\,c}{lN_0\,V}. \tag{54}$$

Using these results and $c = \sqrt{N_0/m}$, we obtain

$$y\,(l, \tfrac{1}{4}\,(1-\xi)\,T) = \frac{2M_0}{N_0} + Vl\sqrt{\frac{m}{N_0}} - \frac{4M_0}{lN_0} = Vl\sqrt{\frac{m}{N_0}} - \frac{2M_0}{lN_0}, \tag{55}$$

$$y\,(l, \tfrac{1}{4}\,T) = Vl\sqrt{\frac{m}{N_0}} - \frac{2M_0}{lN_0}. \tag{56}$$

To obtain an approximation for the maximum value of $y\,(l, t)$ we assume the displacement configuration at time t^* is a parabolic curve between $x = 0$ and $x = \xi l$. Then the curve for the displacement–time function is also parabolic in the range $\frac{1}{4}\,(1-\xi)\,T \leqslant t \leqslant \frac{1}{4}\,T$, and the maximum value of the displacement occurs midway between the instants $\frac{1}{4}\,(1-\xi)\,T$ and $\frac{1}{4}\,T$. Its value is

$$y\,(l, \tfrac{1}{4}\,(1-\xi/2)\,T) = \frac{Vl}{c}\,(1-\xi) + \tfrac{3}{4}\,\frac{Vl\xi}{2c} + \tfrac{3}{4}\,Vt^* = Vl\sqrt{\frac{m}{N_0}} - \frac{M_0}{N_0}. \tag{57}$$

We may take this as an approximation to the final deflection δ_f of the beam, and thus have

$$\frac{\delta_f}{l} \cong V\sqrt{\frac{m}{N_0}} - \frac{M_0}{lN_0} \tag{58a}$$

or

$$\frac{\delta_f}{l} = 3^{\frac{1}{2}}\sqrt{\frac{\alpha}{\beta}} - \frac{1}{2\sqrt{3}\,\beta}. \tag{58b}$$

Use of the dimensionless variables $\alpha = ml\,V^2/6M_0$ and $\beta = N_0\,l/\sqrt{12}\,M_0 \pm l/h$ facilitates comparison with previous results.

The result expressed by (58) involves approximations which would make its errors positive ; the actual deflection would be less than that computed from (58). This is so because (58) ignores the constraints which would be imposed on the beam when the equations included in inequalities (42) become satisfied. On the other hand, the actual deflection is probably *greater* than that which would be computed from (55). This equation gives the value at time $t = \frac{1}{4}\,(1-\xi)\,T$, which is the instant when one of the inequalities (42) would just cease to be satisfied at the beam centre. Thus we can probably bound the final deflection as follows :

$$Vl\sqrt{\frac{m}{N_0}} - \frac{2M_0}{N_0 l} < \frac{\delta_f}{l} < Vl\sqrt{\frac{m}{N_0}} - \frac{M_0}{N_0\,l} \tag{59a}$$

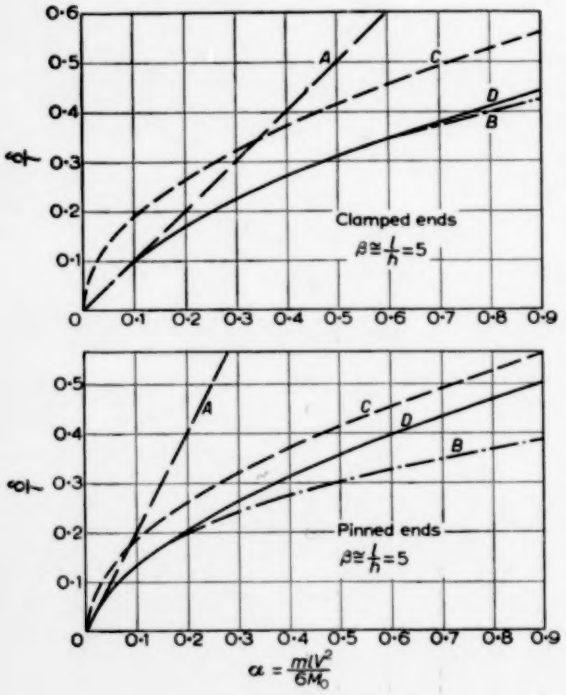

Fig. 10.

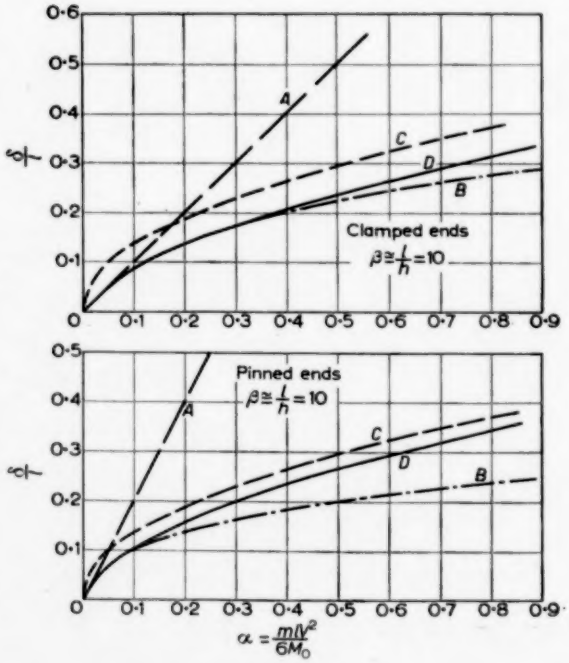

Fig. 11.

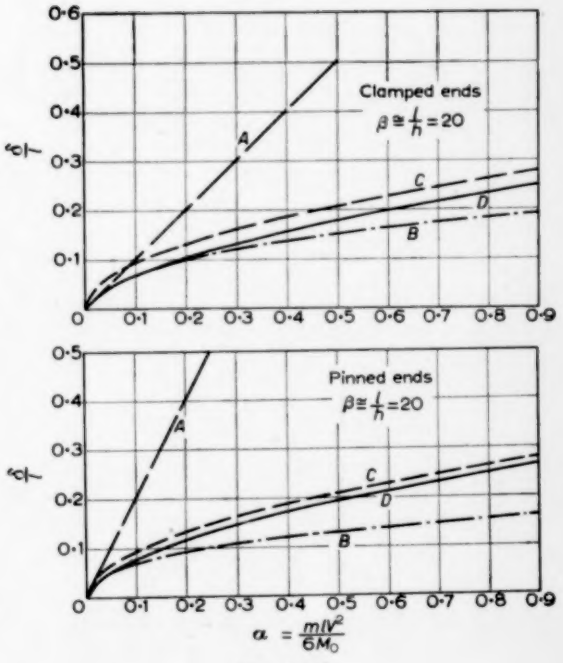

Fig. 12.

Figs. 10, 11 and 12. Final deflection at midpoint as functions of parameter $\alpha = mlV^2/6M_0$. *A* is curve for simple beam solution (no axial constraint) ; *B* is curve for solution taking account of axial constraint but neglecting plastic string phase ; *C* is solution for " plastic string " behaviour during entire motion ; *D* is complete (approximate) solution of this paper.

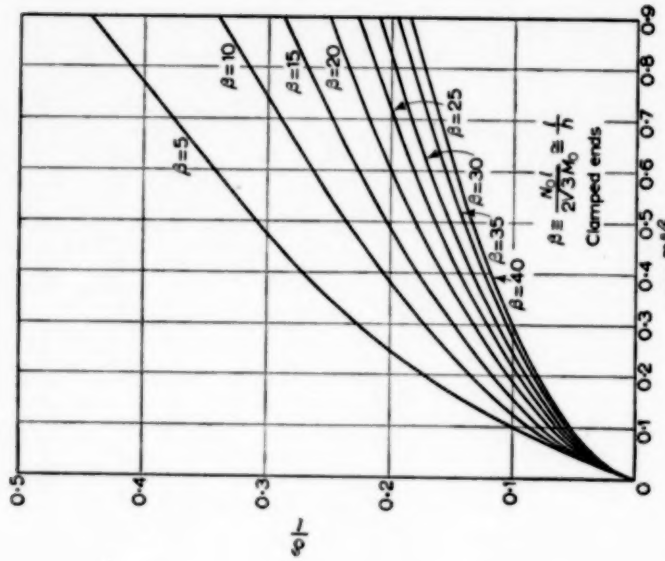

Fig. 14.

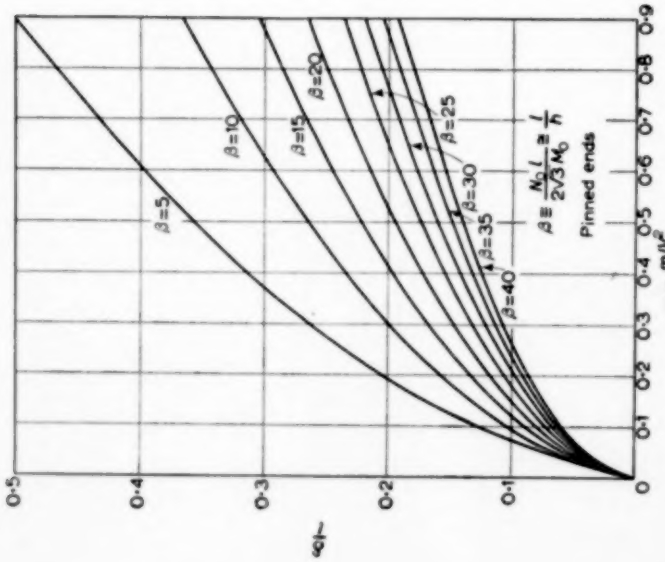

Fig. 13.

Figs. 13 and 14. Curves showing variation of final deflection (complete solution of this paper) for various values of $\beta = N_0 l/\sqrt{12}\, M_0 \simeq l/h$.

or, equivalently,

$$3^{\frac{1}{4}}\sqrt{\frac{\alpha}{\beta}}-\frac{1}{\sqrt{3}\,\beta}<\frac{\delta_f}{l}<3^{\frac{1}{4}}\sqrt{\frac{\alpha}{\beta}}-\frac{1}{2\sqrt{3}\,\beta}. \tag{59b}$$

All of the above discussion and results pertain to simply-supported beams whose supports are fixed against axial motion. However, the corresponding solutions for *built-in beams* may be easily obtained. It was shown that the governing equations for the part of the motion governed by beam theory may be derived from those applicable to simple support conditions by replacing M_0 everywhere by $2M_0$. Thus the bounding deflections for *built-in beams* are as follows :

$$Vl\sqrt{\frac{m}{N_0}}-\frac{4M_0}{N_0 l}<\frac{\delta_f}{l}<Vl\sqrt{\frac{m}{N_0}}-\frac{2M_0}{N_0 l} \tag{60a}$$

or, equivalently,

$$3^{\frac{1}{4}}\sqrt{\frac{\alpha}{\beta}}-\frac{\sqrt{3}\,\beta}{2}<\frac{\delta_f}{l}<3^{\frac{1}{4}}\sqrt{\frac{\alpha}{\beta}}-\frac{1}{\sqrt{3}\,\beta}. \tag{60b}$$

In Figs. 10-12 are shown curves of the final deflection ratio δ_f/l as function of $\alpha = mlV^2/6M_0$, for three values of the parameter $\beta = N_0 l/\sqrt{12}\,M_0 \simeq l/h$. In each case the *upper bound*, according to (59) and (60), respectively, is plotted as curve D. Curve C in each case shows the final deflection that would occur if the beam behaved like a plastic string throughout the motion. This is $Vl/c = Vl\sqrt{m/N_0} = 3^{\frac{1}{4}}\sqrt{\alpha/\beta}$. Curves A and B are respectively the deflections according to simple beam theory and to the beam theory with axial constraint effects of Section 3.

The curves of Figs. 13 and 14 show final deflections according to the complete theory of this paper, equations (59) and (60), using the upper bound as an approximate value.

5. Conclusions

The present analysis is approximate, within the framework of rigid–plastic theory. Nevertheless it is believed to represent the behaviour of beams with constrained ends closely enough for many practical purposes. The curves of Figs. 10–12 show that in any case where there is full constraint against axial motion, as would happen for example in an interior span of a beam on many supports, the deflections suggested by a simple beam treatment will be much greater than the actual ones. A major role in the reduction would be played by the tensile forces arising from the constraints against axial motion, as indicated by the deflection response curves, Figs. 13 and 14.

It should be kept in mind that the whole analysis has assumed ideally plastic behaviour, and thus has neglected both strain hardening and strain–rate effects. Both these effects tend to reduce deflections. In addition, elastic vibrations would be expected to decrease final deflections, since their influence is partly to spread out plastic deformations which appear concentrated in the rigid–plastic analysis. No simple estimates of the magnitude of these effects or of their mutual interaction can be given.

References

Haythornthwaite, R. M.	1957	*Engineering* **183**, 110.
Mentel, T. J. and Symonds, P. S.	1955	*Brown University Report* NNS–7.
Onat, E. T. and Prager, W.	1953	*J. Mech. Phys. Solids* **1**, 77.
Symonds, P. S.	1955	*Brown University Report* UERD–3.

Journal of the Mechanics and Physics of Solids, 1958, Vol. 6, pp. 203 to 222. Pergamon Press Ltd., London

EXTRUSION THROUGH SINGLE HOLE STAGGERED AND UNEQUAL MULTI-HOLE DIES

By W. JOHNSON*, P. B. MELLOR† and D. M. WOO‡

(*Received 16th September*, 1957)

SUMMARY

METHODS and the results of calculations for the pressure to cause end extrusion through perfectly smooth and rough wedge-shaped dies of small unequal angles are given and an examination is made of the effects on the pressure and obliquity of the emergent sheet of inclining the die orifice to the direction of the punch travel, using approximate methods.

End extrusion through three holes of unequal size is considered for two different hypotheses and some calculated results are presented.

Some cases of side extrusion through single and then two oppositely situated orifices are examined. Finally, a case of combined end and two side extrusions is considered.

1. INTRODUCTION

THE extrusion process is undoubtedly one of the fastest growing metal-working methods and the variety of shapes that can be achieved by it using variously shaped dies makes it an econonomically attractive process. The increase in complexity of extruded product shapes attainable through the ingenious use of dies and die-changes, and the continued upward trend in section sizes is apparent from many articles in the trade press (e.g. WICK 1957). For these reasons it is worthwhile exploring the cases to which the theoretical mechanics of the process can be extended for use as a guide in press design. The mechanics is examinable, however, only as a two-dimensional or plane-strain process, mainly by use of the theory of slip-line fields**, but it may usefully be coupled with experimental work on common axisymmetric products (JOHNSON 1954 and 1957a, DODEJA and JOHNSON 1957a and THOMSEN 1954). Further, results obtained for extrusion may well be adapted to other forming processes such as closed-die coining (e.g. JOHNSON 1957b, WANG 1957, PRAGER and HODGE 1951) and indenting and forging (HILL 1950 and JOHNSON 1957c).

This paper examines four main types of extrusion problem : end extrusion through wedge-shaped dies and extrusion through unequal multi-hole dies of large total reduction ; side extrusion ; combined end and side extrusion. In the first Section computational methods and some results are given for pressure variation with reduction for end extrusion through perfectly rough small-angle dies, for die

* Department of Mechanical Engineering, University of Manchester.
† Department of Mechanical Engineering, University of Liverpool.
‡ Department of Mechanical Engineering, University of Sheffield.

** For an account of the theory of plane plastic strain see R. HILL, *The Mathematical Theory of Plasticity*, ch. VI (Clarendon Press, 1950).

combinations in which the wedge angles are unequal and such that orifice eccentricity becomes a factor. There follows a brief reference to analytical methods and an example of a graphical construction dealing with unequal semi-angle dies positioned so that the orifice is not at right-angles to the punch travel direction. The latter example is included since it provides a simple and approximate, but effective approach which should commend itself particularly to engineers.

Secondly, there is presented an extension of an earlier paper giving the theoretical and experimental results of an investigation into the end extrusion of equal thickness sheets (DODEJA and JOHNSON 1957 b). The extension examines the consequences of using orifices of unequal size. Since the amount of computation is large, results are given only for a restricted range of total reductions.

Thirdly, some cases of full sideways extrusion are examined; in particular, a novel solution is encountered in the problem of sideways extrusion through an orifice which is more than twice as wide as the sheet is thick. This solution together with those given by HILL (1948) and GREEN (1955) makes clear the mechanics of sideways extrusion for the full range of reductions in this particular case. A brief reference is also made to the possible use of more than one ram, either for side extrusion or the commonly employed combined direct and reverse end extrusion. In addition, two instances of multi-hole side extrusion are obtained by compounding the earlier solutions.

Fourthly, and in conclusion, a single example of combined direct and side extrusion is presented to illustrate how many of the slip-line fields hitherto presented may be combined to yield solutions for circumstances which superficially appear rather complex.

2. END EXTRUSIONS

(i) *Unstaggered symmetrical dies*

In a previous paper (JOHNSON 1955) methods of calculation and results were given for $p/2k$ versus r for extrusion through smooth wedge-shaped dies using the kind of slip-line field shown in Fig. 1 (a). These results can well be summarized by an empirical equation of the form

$$p/2k = a + b \ln \{1/(1 - r)\} \tag{1}$$

TABLE 1.

Die angle	90°	80°	70°	60°	50°	40°	30°	20°
a	0·62	0·62	0·514	0·43	0·41	0·31	0·24	0·17
b	0·988	0·892	0·907	0·91	0·825	0·848	0·817	0·74
r_L	0·667	0·52	0·5	0·4	0·35	0·35	0·35	
r_U	0·97	0·90	0·9	0·9	0·80	0·75	0·70	

where p is the extrusion pressure, k the yield shear stress in plane strain, r the total fractional reduction and a and b empirical constants whose values for the various wedge-angles are given in Table 1. r_L and r_U denote the lower and upper values to the range of reductions for which the constants apply.

For dies which are so rough that the slip-lines meet them tangentially and orthogonally, as in Fig. 1 (b), the calculated values of $p/2k$ versus r for certain wedge angles are as given in Fig. 2.

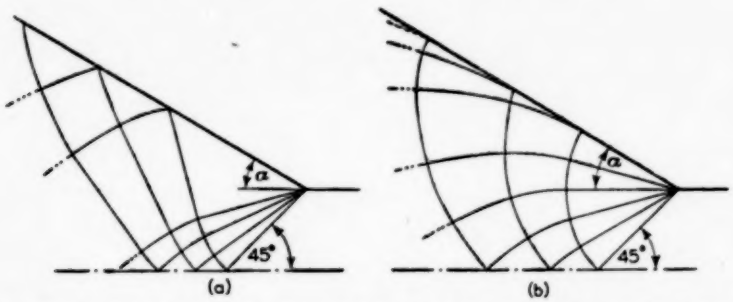

Fig. 1. Slip-line field for extrusion through (a) smooth symmetrical wedge-shaped die for $r > 2 \sin \alpha/(1 + 2 \sin \alpha)$; (b) perfectly rough symmetrical wedge-shaped die.

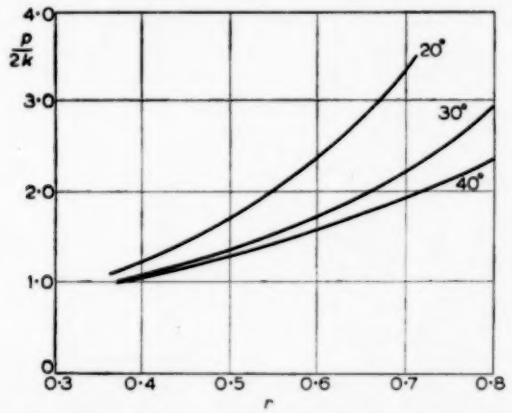

Fig. 2. Variation of $p/2k$ with r for various wedge-angles for rough dies.

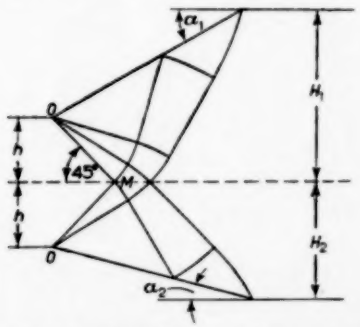

Fig. 3. Slip-line field for extrusion through a smooth unsymmetrical wedge-shaped die.

(ii) *Unstaggered dies of unequal wedge angles*

The analysis here is a simple extension of the method referred to in the previous Section. Two earlier papers concerned with dies which are unsymmetrically dis-

posed are GREEN (1955) and JOHNSON (1957d). Attention here is restricted to instances in which the reduction is so large that the slip-line field is drawn by starting from the assumption that the radial slip-lines OM from the singular points O are equally inclined to the orifice OO (Fig. 3).

Following Fig. 3 the eccentricity e is defined by

$$e = (1 - x)/(1 + x) \qquad \text{where} \qquad x = H_2/H_1. \tag{2}$$

The total nominal reduction r is

$$r = 1 - 2h/(H_1 + H_2). \tag{3}$$

Also,

$$\left.\begin{aligned} 1/(1 - r_1) &= (1 + e)/(1 - r) \\ \text{and} \quad 1/(1 - r_2) &= (1 - e)/(1 - r). \end{aligned}\right\} \tag{4}$$

The extrusion pressure assumed to be exerted uniformly by the punch is easily shown to be

$$p = \tfrac{1}{2} p_1 (1 + e) + \tfrac{1}{2} p_2 (1 - e) \tag{5}$$

in which p_1 and p_2 are the pressures to cause extrusion through wedge-shaped dies of angle α_1 and α_2 respectively. $p/2k$ can easily be evaluated for given values of r and e by using (4) in conjuction with (1) and Table 1, and then substituting for $p_1/2k$ and $p_2/2k$ in (5).

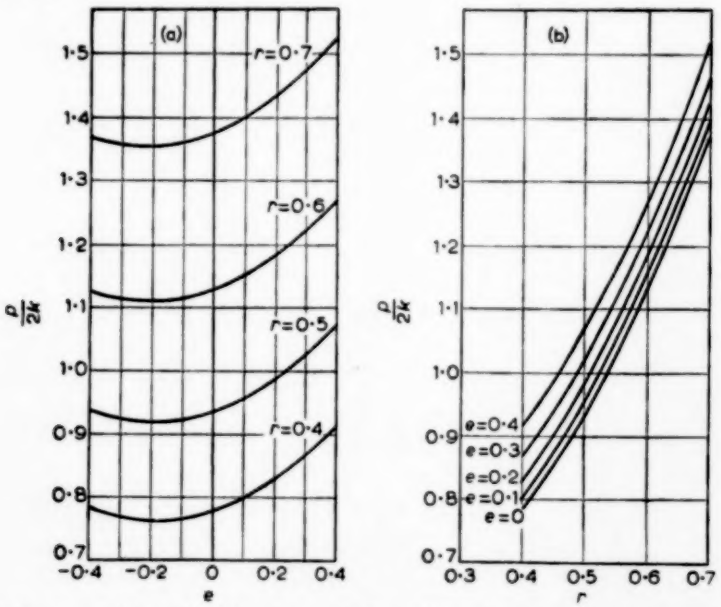

Fig. 4. Variation of (a) $p/2k$ with e for particular values of r; (b) $p/2k$ with r for particular values of e, for smooth die having wedge-angles of 60° and 30°.

Corresponding velocity fields for these particular stress fields can be drawn and a simple particular case is given in Fig. 8 (b). The range of applicability for these compound asymmetrical dies may be derived by reference to Table 1. It is em-

phasized, however, that the reductions are nominal ones, since the extruded product will not in general emerge at right angles to the line of the orifice.

Fig. 4 (a) shows the effect of eccentricity on the extrusion pressure for given values of r for a smooth die, one side having a wedge-angle of 30° and the other 60°. Fig. 4 (b) shows the variation of $p/2k$ with r for given values of e for the same 30° – 60° die. Since the accuracy of the initial empirical formula is only correct to about 2½ per cent, the curves in Figs. 4 and 5 are similarly correct to about the same amount. Figs. 5 and 6 again show how $p/2k$ varies with e for a die combination of wedge-angles 20° and 40°, for both smooth and rough dies, for values of r between 0·4 and 0·7.

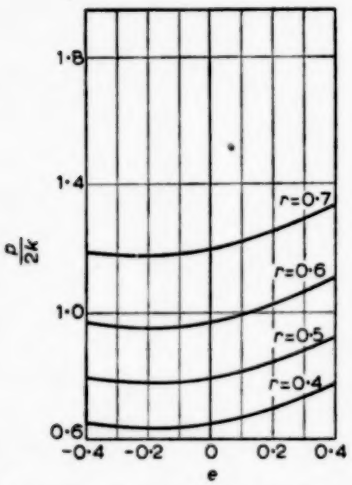

Fig. 5. Variation of $p/2k$ with e for particular values of r for a smooth die having wedge-angles of 40° and 20°.

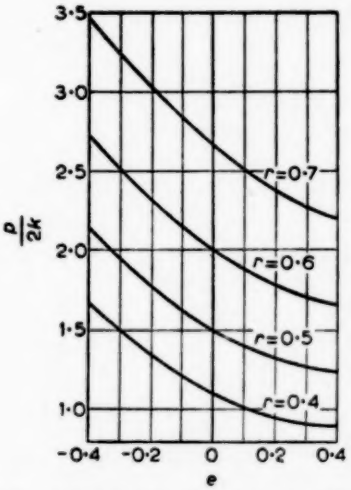

Fig. 6. Variation of $p/2k$ with e for particular values of r for perfectly rough wedge-shaped dies of angles 40° and 20°.

(iii) *Staggered dies*

Fig. 7 shows the slip-line field for extrusion through a staggered die whose wedge-angles are α and β, and whose orifice is at angle γ to the direction of punch travel, when the reduction is large. This case presents no difficulty as regards calculating pressures or angle of emission since it is essentially composed of two dies of unequal angles $\alpha' = (\alpha + \gamma)$ and $\beta' = (\beta - \gamma)$. α' and β' once known, the appropriate coefficients a and b may be selected for use in expression (1) which can then be adapted to give the total force on the die faces; thereafter it is easy, though tedious, to derive the extrusion pressure.

The simplest field of the type in Fig. 7 is shown in Fig. 8 (a) and is amenable to easy analytical treatment; Fig. 8 (b) is the velocity field corresponding to Fig. 8 (a). It may be shown that

$$\frac{p}{2k} = \frac{(1 + \alpha + \gamma)\sin\alpha + (1 + \beta - \gamma)\sin\beta}{\sin\alpha + \sin\beta + \sin\gamma} \qquad (6)$$

and

$$t = 2h \sin(\eta - \gamma) \text{ or}$$

$$r' = 1 - \sin(\eta + \gamma)/(\sin\alpha + \sin\beta + \cos\gamma) \tag{7}$$

r' being the true reduction ; the meaning of the symbols will be obvious by reference to Fig. 8.

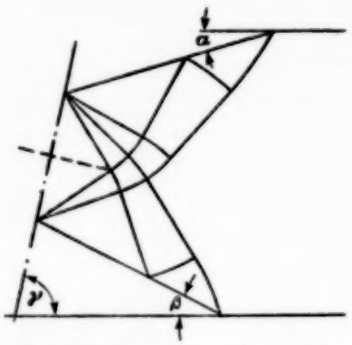

Fig. 7. Slip-line field for extrusion though a smooth unsymmetrical unequal wedge angle staggered die.

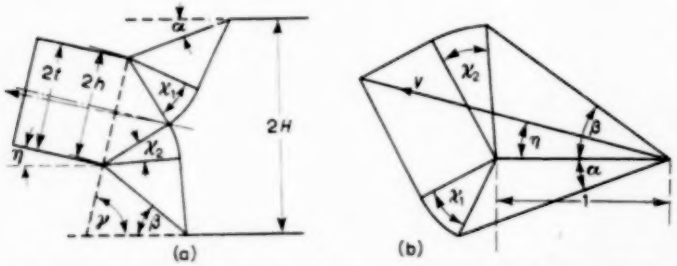

Fig. 8. (a) Simple slip-line field for a smooth staggered unequal angle die. (b) Hodograph corresponding to the slip-line field of (a).

An alternative to computing pressures by amalgamating slip-line fields as above is to obtain an upper bound for p by following the example given by HILL (1951) in connexion with sheet drawing and which was based on his principle of maximum work (1950).

Fig. 9 (a) shows a possible adaptation of the field of Fig. 7, for a perfectly smooth die, the lines along which the velocity discontinuities occur being OB, OD, OC and OA, V^* denoting the absolute discontinuity magnitude across these lines. (This configuration should be adequate for moderate reductions, but for much larger reductions more than the two triangles AOB and COD would be required). The corresponding hodograph is shown in Fig. 9 (b). The upper bound for $p/2k$ is then given by

$$p/k = V_1^* OB + V_2^* OD + V_3^* OA + V_4^* OC, \tag{8}$$

and the value of $p/2k$ finally selected is that for which the right-hand side of (8) is a minimum. It is possible to obtain an analytical expression for (8) as applied to this case and then to minimize it, but this results in long and cumbersome equations.

Accordingly, a graphical trial and error method may be adopted, which is quite suitable for investigating particular reductions; to exemplify the procedure the effect on pressure and direction of emission of moving forward the lower die CD in Fig. 9 (a) is presented. Angles α and β remain 40° and 20° and the die face lengths also remain the same. The case for $e = 1/6$ and nominal reduction $r = 0{\cdot}5$ when $\gamma = 90°$ was drawn, assuming $AO = CO$ and giving angle $AOC = 2\theta$ values at 10° increments between 60° and 120°. The various hodographs obtained for each particular value of θ were used to ascertain the V^* values which, with the triangle lengths in Fig. 9 (a), enabled $p/2k$ versus θ to be calculated (Fig. 10). The minimum value of $p/2k$ occurs for $45° < \theta < 40°$ and is about 0·80.

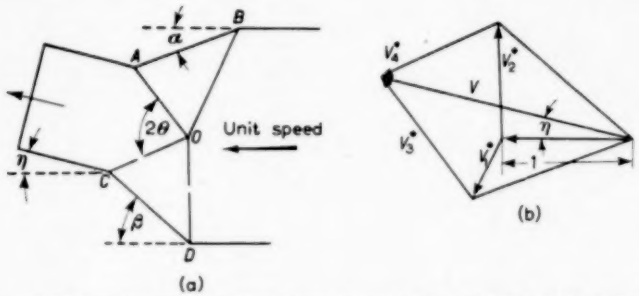

Fig. 9. (a) Discontinuous velocity pattern to replace the slip-line field of Fig. 8 (a).
(b) Hodograph corresponding to the pattern in (a).

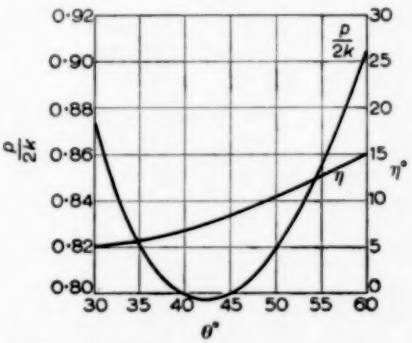

Fig. 10. Showing the variation in $p/2k$ and η with θ.

Also shown is the variation of the predicted angle of emergence, η, with θ. The value of η corresponding to the least value of $p/2k$ is 8°. If the results for the simple slip-line field of Fig. 8 (a) with $\gamma = 90°$ are compared with the results of the graphical method above, using (6) and calculating η, the exact values are $p/2k = 0{\cdot}775$ and $\eta = 9°$ for $r = 0{\cdot}496$, with $e = 0{\cdot}152$. It is clear that the graphical method is capable of giving a very close approximation to the slip-line field solution.

Returning to the initial problem, two positions were selected in which $\gamma = 73\frac{1}{2}°$ and 60°, the lower die being simply moved to a position in advance of the upper die. The results of applying the approximate graphical approach are given in Fig. 11, constructed from the three minimum values obtained for each of $\gamma = 90°$, $73\frac{1}{2}°$

and 60°. It will be observed that, as η decreases, the nominal reduction decreases while the true reduction and pressure increase and the angle of emission changes from being about 9° below the container axis to about 7° above it.

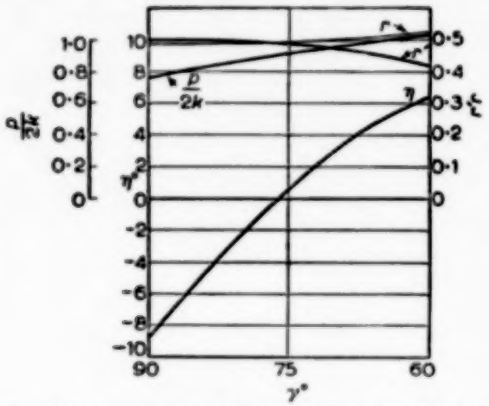

Fig. 11. Showing the variation in r, r', $p/2k$, and η with γ.

Numerous examples of how slip-line fields may be rationalized for use as discontinuous velocity field solutions, easily adapted for graphical use, will be found elsewhere (Johnson 1957c and 1957e).

3. Extrusion of Sheets of Various Thicknesses Through Three-Hole Dies

Plane strain solutions for the problem of extrusion through three-hole dies can be obtained in certain cases by the building-up of the requisite slip-line field from the known slip-line fields for single hole extrusion. The type of basic slip-line field adopted depends on the total reduction required, the individual size and relative disposition of the holes in the die and on the frictional conditions between metal and die and between metal and container wall.

In the following work the three holes of the die are in line, with the middle hole centred along, and the two outer holes situated symmetrically about the container axis. The two outer holes are of equal thickness, not necessarily equal to the thickness of the centre hole. The application of two different types of slip-line fields to this situation is discussed, the essential difference between the two basic fields being that in the first it is assumed there are no dead metal zones whereas in the second it is assumed that a dead metal zone covers the whole, or very nearly the whole of the die face, in the case of very large reductions. It is also assumed in both cases that there is no friction between the metal and the container wall.

(i) *Smooth die and smooth container wall*

The type of slip-line field when the die face and container wall are both smooth is shown in Fig. 12. In this case the basic slip-line field can be considered to be that covered by the distance y_1, with thickness of extrudeed sheet h_1. This slip-line field was given by Hill (1950) in connexion with sheet drawing through dies of small angle and applied to extrusion through a square die by Johnson

(1956). $O_1C_1A_1$ is a circular arc with angle $A_1O_1C_1$ equal to 90°, O_1C_1 being inclined at 45° to the centre-line of the extruding sheet, and A_1B_1 at 45° to the die face. This simple pattern is easily extended outwards from $O_1A_1C_1$, the slip-lines continuing to meet the centre-line and the die face at 45°. This satisfies the assumption of no friction between the metal and the die or the container wall. The initial pattern applies for a reduction of 0·667 and the extended fields to reductions larger than this. It should therefore be noted that the solution for the three-hole die will be only for reductions of 0·667 or greater.

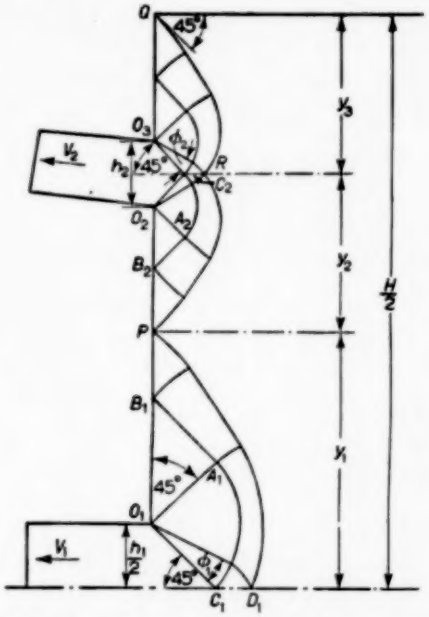

Fig. 12. Half slip-line field when die face and container wall are both smooth.

In Fig. 12 H is the original sheet thickness and h_2 the distance directly across one of the outer orifices. The slip-line fields covered by the distances y_1 and y_2 meet on the die face at P. Making the reasonable assumption that there are no stress or pressure discontinuities across this intermediate portion of the die face, then, for the two fields to be compatible, the pressure at P must be the same whether it is calculated from the central or the outer orifice. This requires that $\phi_1 = \phi_2$ and the slip-line fields over distances y_1 and y_2 are geometrically similar. In other words $h_1/h_2 = y_1/y_2$ and in particular when $h_1 = h_2$ then $y_1 = y_2$. The outer field covered by the distance y_3 is such that its particular reduction is greater than 0·667 and all slip-lines meet the die face, and container wall up to Q, at 45°.

In order to calculate the extrusion pressure, the extrusion force for each of the fields covered by y_1, y_2 and y_3 was first obtained using the values of extrusion pressure against fractional reduction for a single such field which had been obtained previously by Johnson (1956).

If $p_1/2k$ is the extrusion pressure for the innermost field, y_1, then the extrusion force for this particular field is

$$F_1 = (p_1/2k)\, 2k\, y_1 \tag{9}$$

and the extrusion force for the field covered by the distance y_2 is

$$F_2 = F_1\, d_2/d_1. \tag{10}$$

The extrusion pressure for the outermost field, $p_3/2k$, is found as for single hole extrusion, and the extrusion force for this field is

$$F_3 = (p_3/2k)\, 2k\, y_3. \tag{11}$$

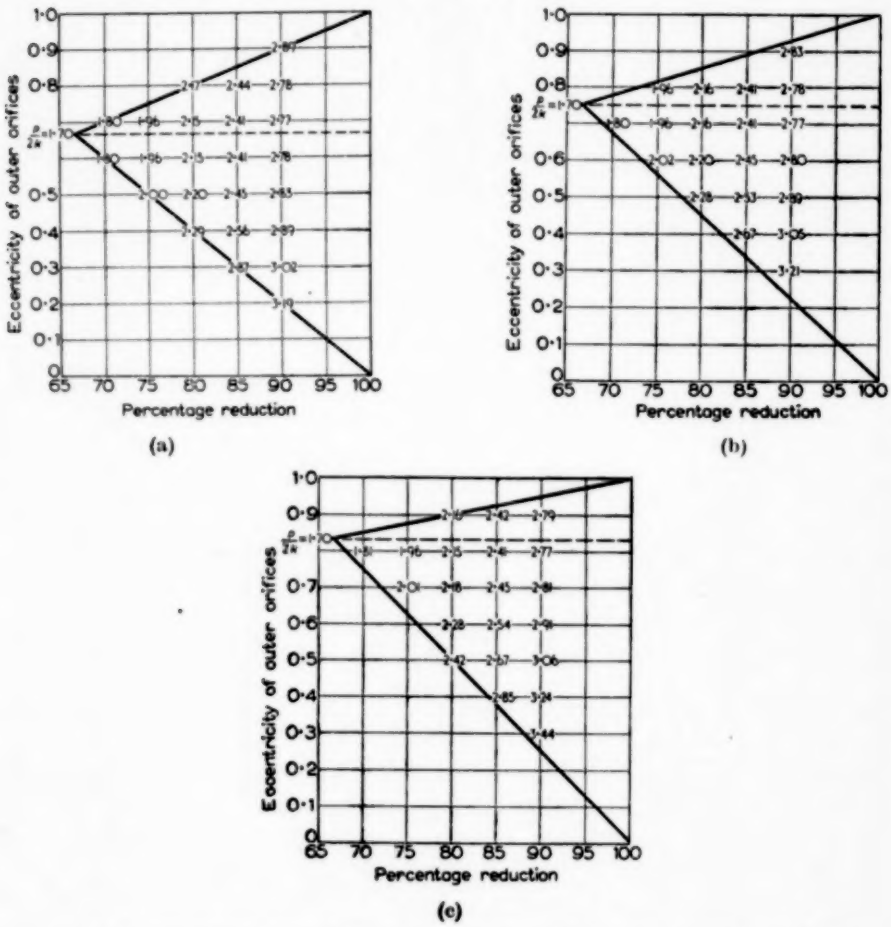

Fig. 13. Extrusion pressure for various values of eccentricity and percentage reduction : (a) $h_1/h_2 = 1$, (b) $h_1/h_2 = 2$, (c) $h_1/h_2 = 4$.

Thus, the final extrusion pressure is

$$p/2k = (F_1 + F_2 + F_3)/kH. \tag{12}$$

For a given slip-line field the extrusion pressure varies with the reduction, with the eccentricity of the outer orifices, and with the ratio h_1/h_2.

The total reduction, r, is defined as

$$r = 1 - (h_1 + 2h_2)/H$$

neglecting any difference between the thickness of the sheet emerging from the outer orifices and the width h_2, of the outer orifices, which there will be when the sheet emerges obliquely.

The eccentricity, e, of the outer orifices will be defined as

$$e = (y_1 + y_2)/(H/2). \tag{14}$$

Values of extrusion pressure for given values of eccentricity and reduction, when the ratio h_1/h_2 is constant, are given in Figs. 13 (a) (b) and (c). In Fig. 13 (a) $h_1/h_2 = 1$ and when $e = 0{\cdot}667$, $r = 0{\cdot}667$ and the pressure $p/2k = 1{\cdot}70$ as for single hole extrusion; the straight lines drawn from this point to $e = 1$, $r = 1$, and $e = 0$, $r = 1$, denote the limits of the above solution. The broken line through $e = 0{\cdot}667$ parallel to the abscissa denotes the lines of minimum extrusion pressure, corresponding to single hole extrusion of the same fractional reduction; as the value of e varies above or below this line so the extrusion pressure increases. The figures at the intersection of the coordinate lines for r and e are the appropriate values of $p/2k$.

Figs. 13 (b) and (c) show similar relations for $h_1/h_2 = 2$ and $h_1/h_2 = 4$ respectively. The minimum pressures are, of course, as before but the value of e for these pressures increases as the ratio h_1/h_2 increases.

If v_1 is the velocity of the extrusion from h_1 and v_2 the velocity of extrusion from h_2 then

$$v_2/v_1 = (y_2 + y_3)(h_1/y_1)\, 2h_2. \tag{15}$$

The variation of v_2/v_1 with e is given in Fig. 14 for constant values of h_1/h_2. For a given value of h_1/h_2 the ratio of the velocities is independent of the fractional reduction. It will be seen that the ratio v_2/v_1 becomes less than unity only at high values of eccentricity.

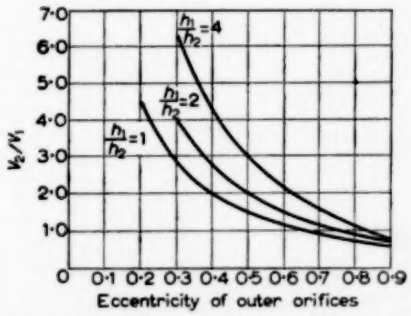

Fig. 14. Ratio of extrusion velocities v_2/v_1 with eccentricity for various values of h_1/h_2.

(ii) *Dead metal zone over die face and smooth container wall*

Hill (1948) calculated the plane strain extrusion pressure for reductions between 0·12 and 0·88 assuming dead metal zones to cover the whole of the die face and no friction between the metal and the container wall. Johnson (1955) calculated

extrusion pressure for the cases where there are various amounts of friction between the metal and the container wall. It is from a 5° equiangular net used in this latter work that the present calculations have been made. The field investigated and the results of which are presented applies where the reduction is greater than 0·5 for each particular portion of the synthesized field.

The assumed slip-line field is shown in Fig. 15 (a). The dead metal zones are bounded by the slip lines $O_1 A_1 P$, $O_2 A_2 P$ and $O_3 A_3 Q$, and since the container wall is assumed smooth the slip-line $O_2 RQ$ meets it at 45°. The slip-lines of the two fields covered by distances y_1 and y_2 must intersect orthogonally at point P. Also, the pressure at P as determined by the Hencky equations must be the same whether arrived at by working from the top sheet or the centre one. For these orthogonal and pressure equality conditions to be fulfilled, the following angular relations must hold :

$$\theta_1 + \phi_1 = \theta_2 + \phi_2 \tag{16}$$

and

$$(\theta_1 - \phi_1) + (\theta_2 - \phi_2) = 180^\circ \tag{17}$$

which together give $\theta_2 = 90^\circ + \phi_1$.

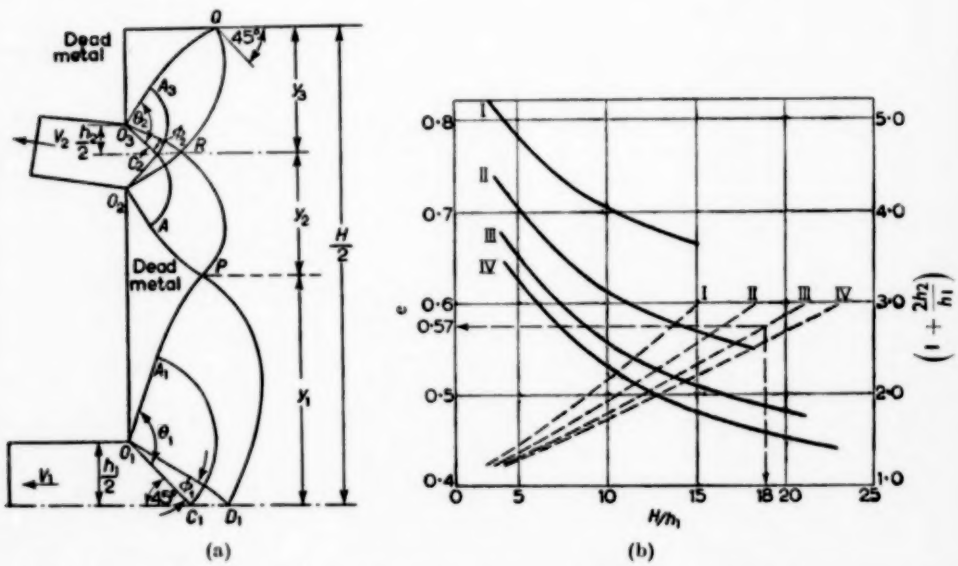

(a) (b)

Fig. 15. (a) Half slip-line field assuming dead metal zones to cover the whole of the die face and no friction between metal and container wall. (b) Graphical summary of the die proportions appertaining to (a). ———— e . — — — — — $(1 + 2h_2/h_1)$.

To determine the position of P pairs of points were selected in an orderly manner from the 5° net to satisfy the above equations and the extrusion force was calculated in the normal way for the field covered by y_1. The second field covered by y_2 was so scaled from the original net that, when joined to field y_1, not only were equations (16) and (17) satisfied, but P was the same distance from the die face in both cases ; thus the two fields met in the common point P and the correspond-

ing extrusion force was calculated. (The orifice size was, of course, reduced in the same proportion). Finally the third field, y_3, was scaled in the same proportion and the extrusion force again calculated. Then, knowing the individual extrusion forces and the initial sheet thickness H, the extrusion pressure $p/2k$ could be finally determined.

A general solution to this problem would be extremely laborous to obtain but, in order to exemplify the method of approach, a set of results covering as wide a range of conditions as possible has been obtained. Seven pairs of points P, forming a family, were considered and four different sizes of fields y_3. The geometry of the die is summarized in Fig. 15 (b) where the curves I to IV refer to the different outermost fields used, y_3. Selecting any ratio of initial sheet thickness to height of centre orifice H/h, the ratio h_2/h_1 and the eccentricity of the outer orifices, $2(y_1 + y_2)/H$, can be found. The reduction, $r = 1 - (h_1 + 2h_2)/H$, can also be readily obtained.

In Fig. 16 extrusion pressure and total reduction are plotted against H/h_1. For any value of H/h_1 the extrusion pressure and the corresponding reduction can be read off. Thus, if $H/h_1 = 18$, then from its intersection with curves III, the reduction is 0·85, $p/2k$ is 2·86 and, from Fig. 15 (b) the eccentricity is 0·57. Examining Figs. 15 (b) and 16 together, it is seen that the extrusion pressure for given size orifices increases as the eccentricity of the outer orifices decreases.

Also plotted in Fig. 16 is the extrusion pressure assuming that *no* extrusion takes place through the outer orifices. The reduction in this case will be $(1 - h_1/H)$. This curve intersects curves III and IV of the extrusion pressure for all three orifices. Considering curve IV this means that for values of $H/h_1 > 5{\cdot}2$ *extrusion will take place through the centre orifice only*, since less pressure is required for this mode of flow. Taking the limiting case $H/h_1 = 5{\cdot}2$ for which the corresponding reduction is 0·748, $p/2k$ is 2·75, the eccentricity is 0·617 and $h_2/h_1 = 0{\cdot}15$.

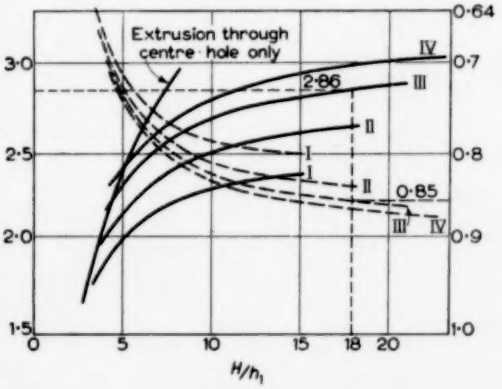

Fig. 16. Extrusion pressure and reduction versus H/h_1, orifice eccentricity neglected.
——— $p/2k$. — — — — — — — r.

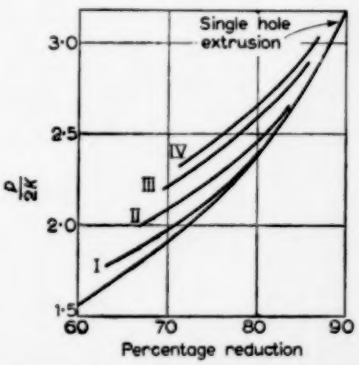

Fig. 17. Extrusion pressure versus reduction.

It is worth noting that cases are encountered industrially in which extrusion does not occur through all the orifices provided. Further, as DODEJA and JOHNSON's plane strain experiments showed (1957a), the extrusion pressures

required for multi-sheet extrusion generally exceed those anticipated on purely theoretical grounds. It seems likely, therefore, that the phenomenon of material emerging from one hole only, and ignoring the other two, may occur for conditions less extreme than those predicted here. It would also be expected that the change over from three to one hole extrusion would not occur suddenly but only more or less rapidly over a range of values.

The variation of extrusion pressure with reduction for the four cases is shown in Fig. 17. These results are compared with the extrusion pressure through a single orifice giving the same total reduction. It is seen that the extrusion pressure for the three hole die is always greater than, or equal to, that for the symmetrically situated single hole die of the same *total* reduction. Hodographs for the various cases considered may easily be assembled by reference to previous work (JOHNSON 1957b and d, DODEJA and JOHNSON 1957a, and WANG 1957).

It must be noted that the solution offered in this particular instance assumes that the die face is so rough that the dead metal zone situated on the intermediate portion between the orifices, cannot be displaced due to any inequality in the total transverse forces acting over surfaces $O_1 A_1 P$ and $O_2 A_2 P$ in Fig. 15 (a). To examine this point in detail would require a prohibitive amount of calculation, but from experimental evidence it does appear to be the case that dead metal zones are deposited over the face of the die in almost all instances (DODEJA and JOHNSON 1957a).

4. SIDE EXTRUSIONS

(i) *Single hole*

Side extrusions are practised principally and traditionally in connexion with lead tube squirting and cable covering. It is not obvious to the authors, however, why the potential advantage of the area over which orifices may be placed, e.g. round the circumference of the container as opposed to the lesser end area of the container, has not been exploited for production purposes in multi-hole extrusion; it could well be that tooling difficulties are greatly increased. Despite the comparatively small industrial interest in side extrusion, interesting features in the associated mechanics do present themselves and some of these will now be examined.

The slip-line field for side extrusion through a single hole from a rough container when $H > a$, using a single punch, has been given by GREEN (1955); this is illustrated by the full line curves in Fig. 18 (a), with Fig. 18 (c) as the corresponding hodograph. For a perfectly smooth container wall, with two punches moving in opposite directions with speeds u and v (i.e. Fig. 18 (a) having $\phi = 45°$ so that the full and dotted line fields are superimposed) the hodograph is shown in Fig. 18 (e). When the container is perfectly rough, one ram only being used, the slip-lines meet the wall tangentially and orthogonally, so that one of the set of circular arcs of the hodograph degenerates to a point and the velocity field then appears as in Fig. 18 (d). In Fig. 18 (f) $p/2k$ and η, the angle made by the emergent rod and the punch axis, are plotted against h/a for two instances in which the bottom container wall was rough and smooth, the upper wall being perfectly smooth.

Considering next the case in Fig. 18 (b), in which the orifice is rotated through angle θ and in which two rams (moving at speeds u and v) are employed, the slip-line field must be modified to include a dead metal zone if the container is in

any degree rough. The ability to vary either the orifice inclination or the ratio of the punch speeds would enable control to be kept of the directions of the emergent sheet. (Certain types of domestic traps are made by a side extrusion process which employs two rams moving at different and variable speeds). When cal-

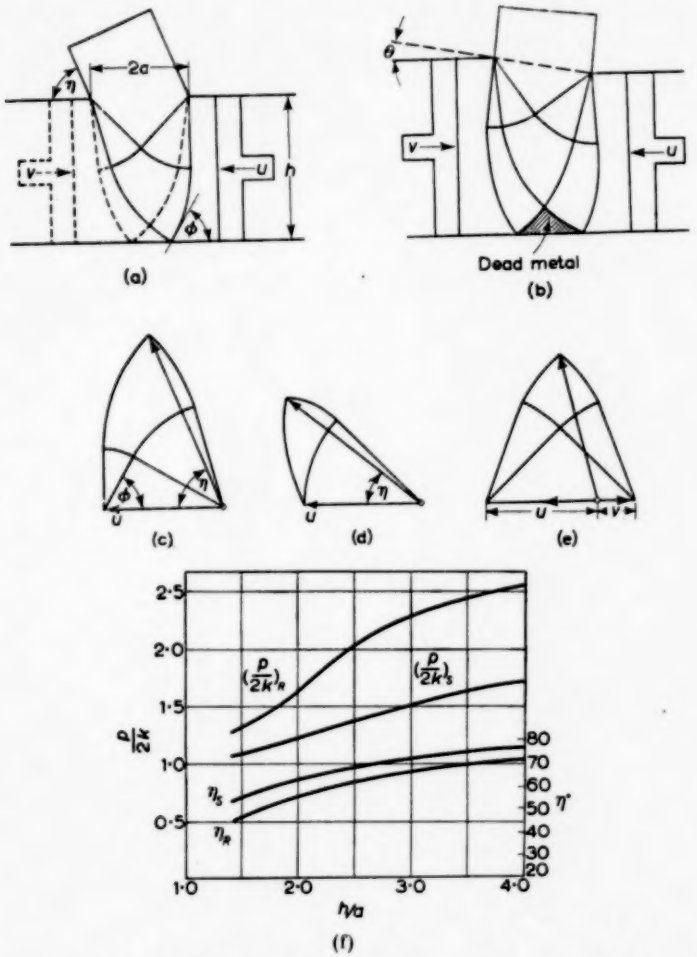

Fig. 18. (a) Slip-line field for side extrusion from a rough container when $h \geqslant a$. (c) Hodograph for field in (a). (e) Hodograph as for (a) but $\phi = 45°$ and using two rams. (d) Hodograph for the degenerate case of (c) obtained when container wall is perfectly rough. (f) Variation of $p/2k$ and η with h/a; (S) smooth container walls, (R) perfectly rough container walls. (b) Side extrusion through an inclined orifice, using two rams and with a rough container wall which induces a dead metal zone.

culating $p/2k$ and η versus h/a, with angle $\theta = 0°$, $\phi = 90°$ and $u/v = 1$, use can be made of some of the calculations for the *formally* similar instance of a punch indenting material resting on a perfectly rough foundation (Johnson and Woo 1957).

For solving the case of extrusion from a smooth container when $h' < a'$, the slip-line field given in Fig. 19 (a) appears to be acceptable. The associated hodograph occurs as Fig. 19 (b), and can only be completed when the direction and speed of the final product have been decided. Assuming the product moves in a straight line, the velocity magnitude easily follows once the actual direction is determined and this is given by the direction of line AC. Material emerging across line CDE is rigid; some of it, however, approximately that moving across CD, will be

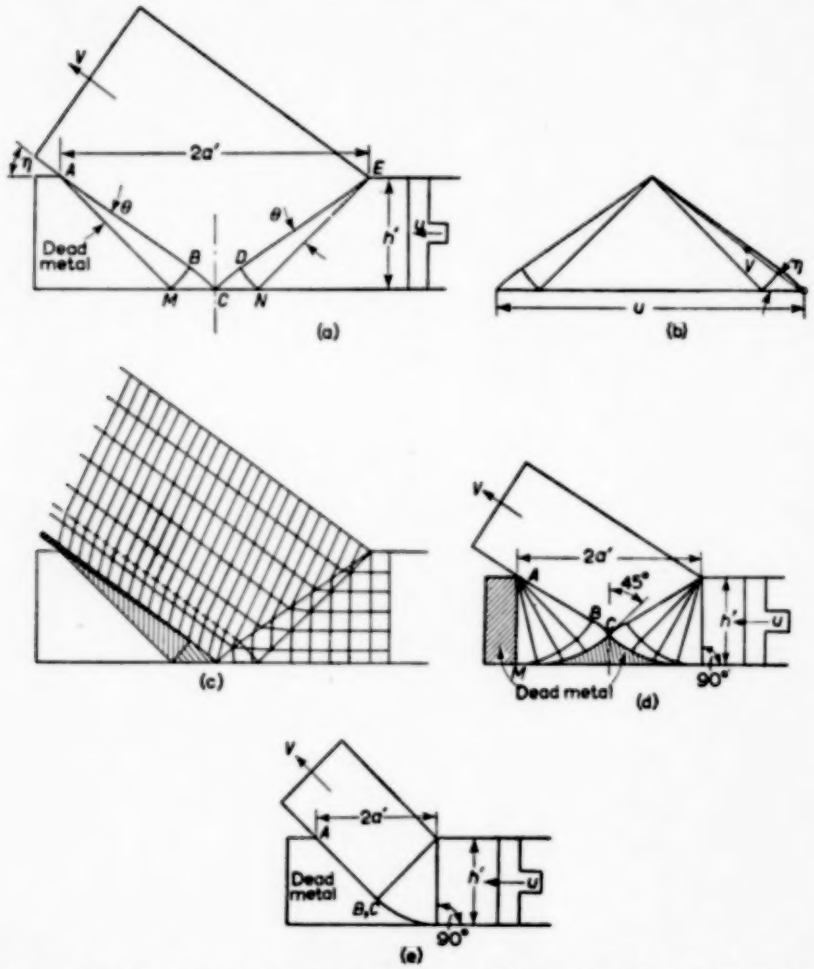

Fig. 19. (a) Slip-line field for side extrusion from a smooth container, $h' \leqslant a'$. (b) Hodograph corresponding to (a). (c) Showing the calculated deformation undergone by a square grid when side extruded, $h/2a \simeq 4$. (d) Slip-line field for side extrusion from a perfectly rough container, $h' < 2a'$. (e) Slip-line field for side extrusion from a perfectly rough container, $2a'/h' = \sqrt{2}$.

emerging so obliquely as to encounter line BC and will be deformed a second time in the portion of the field to the left of the orifice centre-line. Unless the proposed direction AC is assumed, the volume of material entering this latter portion of

the field will not equal that leaving it. Material leaving region $ABCM$ has the same velocity as that entering it.

The extrusion pressure required for this latter case is identical with that for the smooth case of Fig. 18 (a), given in Fig. 18 (f), the place of h/a there being taken by a'/h'.

In an effort to facilitate the calculation of the deformation imposed on an initially square grid by its passage through a relatively wide orifice of this kind, rigid blocks separated by lines of velocity discontinuity have been substituted for the various curvilinear sectors and triangles of Figs. 19 (a) and (b). The calculated square grid then appears as in Fig. 19 (c). The most interesting feature is the slowness of the metal movement in region $ABCM$ and the immense amount of distortion occurring at exit over AB.

When the container is perfectly rough the appropriate slip-line field would appear to be that of Fig. 19 (d), it being necessary to assume the deposition of a zone of dead metal on the bottom container wall. The emergent sheet direction becomes CA, C now being the apex of the dead metal zone; this is justified exactly as is the direction associated with the smooth container. This case is interesting in that at first sight it would appear to conflict with a limit of Fig. 18 (a), shown here as Fig. 19 (e), i.e. when $a' = h'/\sqrt{2}$. The latter shows a dead metal zone occupying the sector to the left of the centre-line, while working from Fig. 19 (d) one is led to suppose that the region is plastic. In fact, there is such a small amount of material entering the comparatively large region $ABCM$ that, as is foreshadowed by the distorted grid of Fig. 19 (c), movement or distortion in this zone must be extremely slow or small. Ultimately the amount of distortion becomes vanishingly small as B approaches C (i.e. $a' \to h'/\sqrt{2}$) and in the limit, sector ABM can be thought of as rigid and the two types of slip-line field are thus not contradictory.

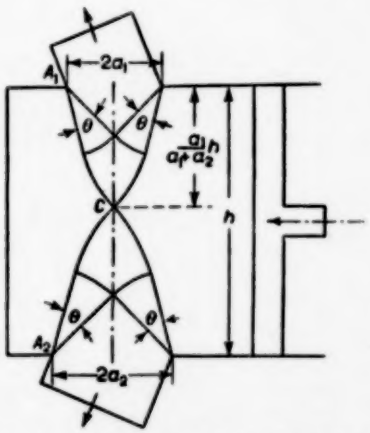

Fig. 20. Side extrusion through oppositely situated holes, $h \geqslant (a_1 + a_2)$.

(ii) *Holes on opposite sides of the container*

The case considered is shown in Fig. 20, the centre lines of the two unequal orifices being collateral and such that $h \geqslant (a_1 + a_2)$. The slip-line fields on either

side of point C are chosen similar in shape and so that the pressure at C is the same whether approached from the top or the bottom orifice, i.e. $\theta_1 = \theta_2 = \theta_3 = \theta_4$. The extrusion pressure and the emergent velocity of the sheet are thus the same as that appropriate to a simple side extrusion through one hole for a thickness–orifice ratio of $h/(a_1 + a_2)$.

It is not difficult to see that, when the orifice centre-lines are not collateral, a similar kind of field still prevails. The θ's would no longer all be equal but would have to be chosen so that the orthogonality and pressure equality conditions described in Section 3 (ii) hold at a single common point such as C.

The analysis of the similar situation when $h \leqslant (a_1 + a_2)$ is not so straightforward that it can be built up in the same manner as that described above for $h \geqslant (a_1 + a_2)$.

5. Simultaneous End and Side Extrusion

Fig. 21 (a) shows material being extruded sideways through two holes and endwise through one hole and in the particular case shown the orifice widths are all of the same size. The problem has been investigated only in relation to holes

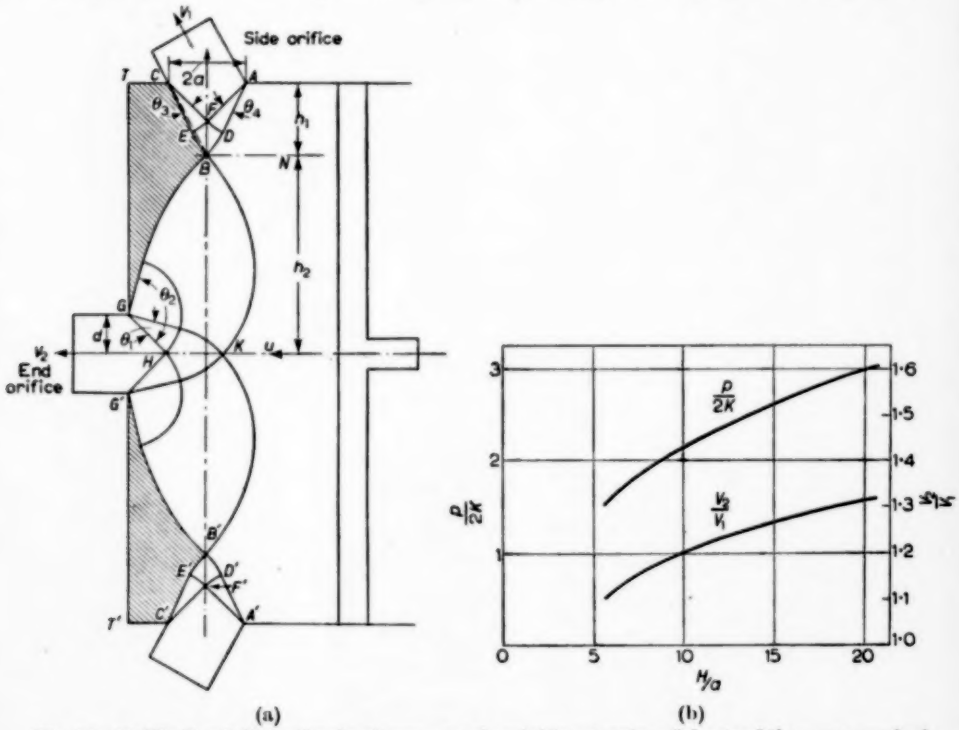

(a) (b)

Fig. 21. (a) Slip-line field for the simultaneous end and side extrusion of sheets of the same nominal thickness. (b) Variation of $p/2k$ and v_2/v_1 with H/a.

of equal sizes but the solution seems easily adaptable for holes of unequal size. An interesting feature of the slip-line field is that it is independent of container wall friction so long as AD is inclined at more than 45° to the wall. To draw

the slip-line field, circular arcs centred on singular points, C, A, G and G' are drawn and the remainder of the field is developed in the usual way from both orifices until the fields have points in common such as B; essentially a side extrusion slip-line field is added to one for end extrusion. The centre-line of the side orifice on which B is located was selected for the purpose of making some typical calculations from readily obtainable previous work.

At B the slip-lines are orthogonal and thus it is required that

$$\theta_2 + \theta_3 = \theta_1 + \theta_2 + \tfrac{1}{2}\pi. \tag{19}$$

Taking $\theta_3 = \theta_4$ in this particular case,

$$\theta_2 - \theta_1 = \tfrac{1}{2}\pi. \tag{20}$$

Also, the position of B is uniquely determined by the fact that the value of p must be the same whether it is determined by starting from a side orifice or an end orifice. Using the Hencky equations this requires that

$$\theta_1 + \theta_2 = \theta_3 + \theta_4, \tag{21}$$

and for this particular instance

$$\theta_1 + \theta_2 = 2\theta_3. \tag{22}$$

Regions $TCEBG$ and $T'\,C'\,E'\,B'\,G'$ are dead metal zones which are assumed to remain fixed in the container corners. In regions $AFCEBDA$, $M'\,F'\,C'\,E'\,B'\,D'\,A'$ and $GBKB'\,G'\,H$, the material is being plastically deformed, and outside them is considered to be rigid. In effect, and for the particular case chosen, the field is seen to be composed of two fields of depth h_1 which control the side extrusions and one end extrusion of depth $2\,h_2$. The pressure and hence the force required over length $2\,h_2$ to cause extrusion through the end orifice is readily calculable and also that required to cause side extrusion, applied over lengths h_1. The total force required to cause simultaneous extrusion through all three orifices may thus be determined and hence the uniform extrusion pressure, p, exerted by the ram. For equal size orifices of width $2a$ Fig. 21 b shows the variation of $p/2k$ and ratio v_2/v_1 with H/a, H being the total initial sheet thickness $= 2\,(h_1 + h_2)$. The sheet proceeding through the end orifice moves at speed v_2 perpendicularly to the gap $G\,G'$ while that leaving the side orifices moves at speed v_1 and is inclined to the gap CA at angle CBN.

This last simple problem is sufficient to illustrate how some different dispositions, of many holes mutually inclined, may easily be added together.

References

Dodeja, L. C. and Johnson, W.	1957a	*J. Mech. Phys. Solids* **5**, 267.
	1957b	*J. Mech. Phys. Solids* **5**, 281.
Green, A. P.	1955	*J. Mech. Phys. Solids* **3**, 189.
Hill, R.	1948	*J. Iron Steel Inst.* **158**, 177.
	1950	*Mathematical Theory of Plasticity* (Clarendon Press).
	1951	*Phil. Mag.* **42**, 868.
Johnson, W.	1954	*B.I.S.R.A. Report MW/E/55/54.*
	1955	*J. Mech. Phys. Solids* **3**, 218.
	1956	*J. Mech. Phys. Solids* **4**, 191.

	1957a	*J. Inst. Metals* **85**, 403.
	1957b	*J. Mech. Phys. Solids* **5**, 202.
	1957c	(To be published, *A.S.M.E.*).
	1957d	*J. Mech. Phys. Solids* **5**, 193.
	1957e	(To be published, *Inst. Mech. Engrs.*).
JOHNSON, W. and WOO, D. M.	1957	*J. Appl. Mech.*, in press.
PRAGER, W. and HODGE, P. G.	1951	*Theory of Perfectly Plastic Solids* (John Wiley and Co. Limited).
THOMSEN, E. G.	1954	*Univ. Calif. Pub. Eng.* **5**, 89.
WANG, A. J.	1957	*Chinese J. Mech.* **1**, 95.
WICK, C. H.	1957	*Machinery (New York)* **63**, 143 and 166.

Journal of the Mechanics and Physics of Solids, 1958, Vol. 6, pp. 223 to 230. Pergamon Press Ltd., London

PLANE WAVES IN AN ELASTIC SOLID CONDUCTING HEAT

By P. CHADWICK* and I. N. SNEDDON†

(*Received* 18*th September*, 1957)

SUMMARY

THIS paper is concerned with the propagation of waves in an isotropic thermoelastic solid. It is shown that the shear waves are uninfluenced by thermal effects but that two distinct dilatational waves exist, one being similar in nature to a purely elastic longitudinal wave, but dispersed and attenuated by the medium, and the other similar to a purely thermal wave. Plane harmonic waves are selected for detailed examination. It is found that if the frequency ω is small compared with $\omega^* = \rho c v_P^2/k$ then the phase velocity of the modified elastic wave is, to a close approximation, given by $(1 + \frac{1}{2}\epsilon)\, v_P$, where $\epsilon = \alpha^2 v_P^2\, T\,(1 + \nu)^2/c\,(1 - \nu)^2$, and the attenuation coefficient of this mode is, to the same degree of accuracy, $\frac{1}{4}\,(2 - 5\epsilon)\,\epsilon\omega^2/\omega^* v_P$. In these expressions ρ denotes the density, c the specific heat at constant strain, k the thermal conductivity, ν Poisson's ratio, α the coefficient of linear expansion and v_P the velocity of purely elastic longitudinal waves in the solid. T is the absolute temperature of the medium in its reference state of uniformly zero stress and strain. Numerical calculations have been performed on a high-speed digital computer for aluminium, copper, iron and lead and it is shown that the values of the phase velocity and the attenuation coefficient of the modified elastic wave in these metals deviate sharply from the above approximations at frequencies in the neighbourhood of ω^*.

1. INTRODUCTION

WHEN the heat content of a body changes, the dimensions of volume elements of the body are altered. In elastic media these changes in dimension produce strains which in turn set up a distribution of stress throughout the solid. Conversely, some of the mechanical energy expended in changing the volume of an elastic solid during straining is converted into heat. This paper is concerned with the effect of these interlinked changes on the form of plane waves travelling in the solid.

The study of thermoelastic phenomena has recently been stimulated by the work of BIOT (1956) and LESSEN (1956) on the basic equations of thermoelasticity. These equations were first established by VOIGT (1910) and JEFFREYS (1930) and postulated much earlier by DUHAMEL (1837).

In Section 2 the equations governing the propagation of small amplitude thermoelastic disturbances in a homogeneous solid are written in a dimensionless form using as the unit of time the reciprocal of a frequency ω^* which is characteristic of the medium being considered. The unit of length is taken to be v_P/ω^*, where v_P is the velocity of longitudinal elastic waves (P–waves) in the solid. The units

* Atomic Weapons Research Establishment, Aldermaston, Berks.
† Department of Mathematics, The University of Glasgow.

of temperature and stress are taken to be the reference temperature (at which the solid is initially in a state of zero stress and strain) and the rigidity modulus respectively. The choice of these units throws the equations into a form suitable for numerical work, but it emerges that the characteristic frequency ω^* has a physical significance beyond its purely mathematical utility.

In Section 3 it is shown that the rotation vector satisfies the usual wave equation for transverse elastic waves (*S*–waves), but that the dilatation and temperature, instead of satisfying the *P*–wave equation and the diffusion equation respectively, satisfy the pair of interlinked equations (2.10) and (3.3). It follows from these results that the dilatation and the temperature both satisfy the equation

$$\left(\nabla^2 - \frac{\partial^2}{\partial t^2}\right)\left(\nabla^2 f - \frac{\partial f}{\partial t}\right) = \epsilon \frac{\partial}{\partial t}(\nabla^2 f), \qquad *(1.1)$$

where the constant ϵ is defined by equation (3.8). Harmonic plane wave solutions of this equation are then considered.

Approximate expressions for the phase velocities and attenuation coefficients of the two thermoelastic waves are obtained in Section 4 and their accuracy is confirmed in Section 5 by direct computation. The calculations described in this section refer to four metals and cover a very wide frequency range. They show that the phase velocity of the modified elastic mode is virtually constant for frequencies up to ω^* when it changes abruptly to v_P, the value appropriate to a pure *P*–wave. The attenuation coefficient varies as ω^2 up to frequencies of the order of ω^* when it changes over to a constant value. It appears, therefore, that in some sense ω^* is a characteristic frequency of the medium. For the metals adopted in the calculations ω^* is well beyond the range attainable in the laboratory and is indeed not very far short of the cut–off frequency of the Debye spectrum.

A preliminary study of this problem has been made by DERESIEWICZ (1957), but the central equation (3.7) is derived here by a different method. DERESIEWICZ gives practically no numerical values and the significance of the frequency ω^* does not emerge from his analysis. These remarks also apply to a very brief treatment of plane thermoelastic waves by LESSEN (1957).

2. THE THERMOELASTIC EQUATIONS

The basic equations of thermoelasticity are the equation of motion (SOKOLNIKOFF 1956, p. 367),

$$\tau_{ij,j} = \rho \ddot{u}_i, \qquad (i, j = 1, 2, 3) \qquad (2.1)$$

the DUHAMEL-NEUMANN equation (DUHAMEL, 1837 ; NEUMANN, 1885)

$$\tau_{ij} = (\lambda\Delta - \gamma\theta)\,\delta_{ij} + 2\mu\gamma_{ij}, \qquad (i, j = 1, 2, 3) \qquad (2.2)$$

and the diffusion equation (JEFFREYS, 1930 ; BIOT 1956)

$$k\nabla^2\theta = \rho c\dot{\theta} + \gamma T\dot{\Delta}. \qquad (2.3)$$

Of these equations, (2.1) and (2.3) express conservation of linear momentum and energy respectively and (2.2) is essentially an equation of state. The usual suffix notation is used, u_i being the displacement vector of a point referred to cartesian axis $O(x_1, x_2, x_3)$. $\tau_{ij,j}$ denotes $\partial\tau_{ij}/\partial x_j$ and a superposed dot represents

the time derivative $\partial/\partial t$. The stress and strain tensors are respectively τ_{ij} and γ_{ij} and θ is the temperature change measured from T, the absolute temperature of the solid in its reference state of uniformly zero stress and strain. λ and μ are the Lamé elastic constants of the solid, ρ is its density, c is its specific heat at constant strain, k is its thermal conductivity and

$$\gamma = \alpha(3\lambda + 2\mu), \tag{2.4}$$

where α is the coefficient of linear expansion of the solid.

Since the present analysis is restricted to small amplitude disturbances products of deviations from the reference state and their derivatives are systematically neglected. The strain tensor is thus given by

$$\gamma_{ij} = \tfrac{1}{2}(u_{i,j} + u_{j,i}) \tag{2.5}$$

and the dilatation is

$$\Delta = u_{j,j}. \tag{2.6}$$

It is convenient to recast the basic equations in dimensionless form (SNEDDON and BERRY 1958, p .124). Defining the frequency

$$\omega^* = \rho c v_P^2/k, \tag{2.7}$$

we take as our unit of time ω^{*-1} and as our unit of length v_P/ω^*, the unit of velocity thus being $v_P = [(\lambda + 2\mu)/\rho]^{\frac{1}{2}}$. We choose the reference temperature T as the unit of temperature and the rigidity modulus μ as the unit of stress. Equations (2.1) to (2.3) can now be written in the form

$$\tau_{ij,j} = \beta^2 \ddot{u}_i, \tag{*2.8}$$

$$\tau_{ij} = [(\beta^2 - 2)\Delta - b\theta]\,\delta_{ij} + 2\gamma_{ij}, \tag{*2.9}$$

$$\nabla^2 \theta = \dot{\theta} + g\dot{\Delta}, \tag{*2.10}$$

where

$$\beta = \left(\frac{\lambda + 2\mu}{\mu}\right)^{\frac{1}{2}} = \frac{v_P}{v_S},\ b = \frac{\gamma T}{\mu},\ g = \frac{\gamma}{\rho c}, \tag{2.11}$$

$v_S = (\mu/\rho)^{\frac{1}{2}}$ being the velocity of pure S–waves.

To avoid confusion between the variables τ_{ij}, u_i, θ; x_i, t and their dimensionless counterparts (for which the same notation is used), an asterisk is placed before the number of each equation expressed in dimensionless form.

3. PLANE WAVES

Substituting from equations (2.5) and (2.9) into equation (2.8) and writing the result in vector form we have

$$(\beta^2 - 1)\,\mathrm{grad}\,\Delta + \nabla^2 \mathbf{u} - b\,\mathrm{grad}\,\theta = \beta^2 \frac{\partial^2 \mathbf{u}}{\partial t^2}, \tag{*3.1}$$

On applying the vector operator curl to both sides of equation (3.1) we obtain the wave equation

$$\nabla^2 \boldsymbol{\omega} = \beta^2 \frac{\partial^2 \boldsymbol{\omega}}{\partial t^2} \tag{*3.2}$$

for the rotation vector $\boldsymbol{\omega} = \operatorname{curl} \mathbf{u}$. This shows that $\boldsymbol{\omega}$ is propagated with velocity β^{-1} in our units, which is v_S in conventional units. In other words the transverse modes of oscillation undergo no thermal modification. This is to be expected since the propagation of S-waves causes no volume changes and the mechanical coupling term is then absent from the diffusion equation (2.3).

Applying the operator div to both sides of equation (3.1) we find

$$\beta^2 \nabla^2 \Delta - b\nabla^2 \theta = \beta^2 \frac{\partial^2 \Delta}{\partial t^2}. \qquad *(3.3)$$

We therefore have a pair of coupled equations, (2.10) and (3.3), for the determination of the scalar quantities θ and Δ. It may readily be verified that both these variables satisfy equation (1.1).

We now specialize the analysis to harmonic plane waves and seek solutions of the basic equations in the form

$$\Delta = \Delta^\circ \exp\left[i\omega t + p\,(\mathbf{a}\cdot\mathbf{r})\right], \qquad \theta = \theta^\circ \exp\left[i\omega t + p\,(\mathbf{a}\cdot\mathbf{r})\right], \qquad *(3.4)$$

where $\mathbf{r} = (x, y, z)$ and $\mathbf{a}$ is a constant unit vector. It is assumed that ω is a real constant. The phase velocity of the plane waves represented by (3.4) is

$$v = \frac{\omega}{\mathcal{I}(p)} \qquad *(3.5)$$

and

$$q = \mathcal{R}(p) \qquad *(3.6)$$

is the attenuation coefficient, so that we must choose in (3.4) values of p which have a negative real part.

Substituting the expression (3.4) into equations (2.10) and (3.3) and eliminating the ratio $\theta^\circ/\Delta^\circ$ from the resulting pair of linear equations there follows the relation

$$p^4 + p^2\left\{\omega^2 - i\omega\,(1+\epsilon)\right\} - i\omega^3 = 0 \qquad *(3.7)$$

with

$$\epsilon = \frac{bg}{\beta^2} = \frac{\alpha^2 T v_p^{\,2}}{c}\left(\frac{1+\nu}{1-\nu}\right)^2 \qquad (3.8)$$

for the determination of the possible values of p. ν is the Poisson's ratio of the solid.

4. Approximate Results

The roots of equation (3.7) are $\pm p_1, \pm p_2$ where

$$p_1^{\,2} = \tfrac{1}{2}\left[-\omega^2 + i\omega\,(1+\epsilon) + \mathcal{D}\right], \qquad p_2^{\,2} = \tfrac{1}{2}\left[-\omega^2 + i\omega\,(1+\epsilon) - \mathcal{D}\right],$$

and $\mathcal{D}$ is the discriminant

$$\mathcal{D} = +\left[\omega^4 + 2i\omega^3\,(1-\epsilon) - \omega^2\,(1+\epsilon)^2\right]^{\frac{1}{2}}.$$

By expanding these expressions in powers of ω^{-1} and ω, approximations to p_1 and p_2 can be found for the extreme cases $\omega \gg 1$, $\omega \ll 1$ respectively.

For high frequencies we obtain

$$p_1 = \pm (\tfrac{1}{2}\omega)^{\frac{1}{2}} \left\{ \left(1 - \frac{\epsilon}{2\omega}\right) + i \left(1 + \frac{\epsilon}{2\omega}\right) \right\}, \qquad *(4.1)$$

$$p_2 = \pm (\tfrac{1}{2}\epsilon + i\omega). \qquad *(4.2)$$

Examining the effect of putting $\epsilon = 0$ in these results we see that the root p_1 corresponds to a modification of the purely thermal wave and that the root p_2 corresponds to a modification of the purely elastic P–wave. Both modified waves are dispersed and attenuated by the medium. Reference to equations (3.5) and (3.6) shows that when $\omega \gg 1$ the modified P–wave is transmitted with phase velocity v_P but has a coefficient of attenuation

$$q_\infty = \tfrac{1}{2}\epsilon, \qquad *(4.3)$$

which, in conventional units, is

$$q_\infty = \tfrac{1}{2}\epsilon \, (\omega^*/v_P). \qquad (4.4)$$

For low frequencies the roots of equation (3.7) are approximately

$$p_1 = \pm \left[\tfrac{1}{2}(1+\epsilon)\,\omega\right]^{\frac{1}{2}} \left[\left\{ 1 - \frac{\omega\epsilon}{2(1+\epsilon)^2} \right\} + i \left\{ 1 + \frac{\omega\epsilon}{2(1+\epsilon)^2} \right\} \right], \qquad *(4.5)$$

$$p_2 = \pm \left\{ \frac{\omega^2 \epsilon}{2(1+\epsilon)^{5/2}} + \frac{i\omega}{(1+\epsilon)^{1/2}} \right\}. \qquad *(4.6)$$

Thus, when $\omega \ll 1$, the phase velocity and attenuation coefficient of the modified P–wave are given by

$$v = (1+\epsilon)^{\frac{1}{2}}, \qquad q = \tfrac{1}{2}\,\epsilon\,(1+\epsilon)^{-5/2}\,\omega^2.$$

For most materials ϵ is small at normal temperatures (see Table 1). Thus, for $\omega \ll 1$, we have, in conventional units,

$$v = (1 + \tfrac{1}{2}\epsilon)\, v_P, \qquad q = \tfrac{1}{2}(2 - 5\epsilon)\, q_\infty \, (\omega/\omega^*)^2. \qquad (4.7)$$

Putting $\omega = 1$ in equation (3.7) we find that, for small ϵ, $p_2 = \pm\left[\tfrac{1}{4}\epsilon + i(1 - \tfrac{1}{4}\epsilon)\right]$. Thus when $\omega = \omega^*$ the attenuation coefficient is

$$q = \tfrac{1}{2}\, q_\infty. \qquad (4.8)$$

Equations (4.4), (4.7) and (4.8) indicate that the attenuation coefficient of thermally modified P–waves is an increasing function of the frequency ω, varying like ω^2 at low frequencies and approaching the value q_∞ asymptotically as $\omega \to \infty$. The range of attainable frequencies is actually limited above by the cut–off frequency ω_c of the Debye spectrum. For longitudinal vibrations

$$\omega_c = 2\pi v_P \left(\frac{3\rho}{4\pi M}\right)^{\frac{1}{3}}, \qquad (4.9)$$

(Brillouin 1938, p. 324), M being the mass of an atom of the material forming the elastic body. Some values of q_∞ are given in Table 1 and it is clear from the above results that, in all cases, longitudinal elastic waves are strongly attenuated in the frequency range $\omega^* < \omega < \omega_c$.

From equations (3.4), (3.6) it follows that a wave of frequency ω has its amplitude reduced by a factor of one–half over a distance $L = \ln(2/q)$. When $\omega \ll \omega^*$ we have, from equation (4.7),

$$L_0 = \frac{\ln 2}{2q_\infty}\left(\frac{\omega^*}{\omega}\right)^2(2 + 5\epsilon). \tag{4.10}$$

TABLE 1. *Values of the Fundamental Constants for Four Metals* ($T = 293°K$)

	Aluminium	*Copper*	*Iron*	*Lead*
v_P (km sec^{-1})	6·32	4·36	5·80	2·14
ω_c (sec^{-1})	$9{\cdot}80 \times 10^{13}$	$7{\cdot}55 \times 10^{13}$	$9{\cdot}95 \times 10^{13}$	$3{\cdot}69 \times 10^{13}$
ω^* (sec^{-1})	$4{\cdot}66 \times 10^{11}$	$1{\cdot}73 \times 10^{11}$	$1{\cdot}75 \times 10^{12}$	$1{\cdot}91 \times 10^{11}$
q_∞ (cm^{-1})	$1{\cdot}31 \times 10^{4}$	$3{\cdot}29 \times 10^{3}$	$4{\cdot}48 \times 10^{2}$	$3{\cdot}27 \times 10^{4}$
ϵ	$3{\cdot}56 \times 10^{-2}$	$1{\cdot}68 \times 10^{-2}$	$2{\cdot}97 \times 10^{-4}$	$7{\cdot}33 \times 10^{-2}$
$L_0\,\omega^2$ (km sec^{-1})	$1{\cdot}17 \times 10^{14}$	$6{\cdot}19 \times 10^{13}$	$7{\cdot}55 \times 10^{15}$	$4{\cdot}00 \times 10^{12}$

Values of ω^*, v_P, ϵ, q_∞ and $L_0\,\omega^2$ for four typical metals are given in Table 1. It will be observed that in each case the characteristic frequency ω^* is very much greater than the frequencies attainable even in experiments employing ultrasonic pulses and is of the order of one-hundredth of the cut-off frequency of the Debye spectrum. In other words, in all the physical experiments so far conducted to measure the velocity of longitudinal waves in a solid we may assume that $\omega \ll \omega^*$ and make use of the appropriate approximations given above. In particular we would expect the measured velocity of longitudinal elastic waves to be $(1 + \frac{1}{2}\epsilon)\left[(\lambda + 2\mu)/\rho\right]^{\frac{1}{2}}$.

TABLE 2. *The Variation of the Phase Velocity v with Frequency ω* ($T = 293°K$)

ω/ω^*	v/v_P			
	Aluminium	*Copper*	*Iron*	*Lead*
10^{-2}	1·0177	1·0084	1·0002	1·0360
10^{-1}	1·0175	1·0083	1·0002	1·0358
1	1·0091	1·0043	1·0001	1·0194
10	1·0002	1·0001	1·0000	1·0004
10^{2}	1·0000	1·0000	1·0000	1·0000
$1 + \frac{1}{2}\epsilon$	1·0178	1·0084	1·0001	1·0367

5. NUMERICAL RESULTS

In order to test the validity of the arguments advanced in Section 4 the characteristics of the modified P-wave have been computed directly from equations (3.5) to (3.7) in a number of special cases. The results refer to the four metals listed in Table 1 and span the frequency range $10^{-11} \leqslant \omega/\omega^* \leqslant 10^{3}$. A programme for performing these calculations on DEUCE, the high-speed electronic computer installed at the National Physical Laboratory, Teddington, was devised by Mr. J. H. Wilkinson of the Mathematics Division of that laboratory.

Some of the results provided by DEUCE are set out in Tables 2 and 3. In Table 2 we see that for each metal the phase velocity v is very nearly equal to $(1 + \frac{1}{2}\epsilon)\,v_P$ when $\omega/\omega^* = 10^{-2}$. Further results (not included here) confirm that over the range $10^{-11} \leqslant \omega/\omega^* \leqslant 10^{-2}$, v remains extremely close to this constant value.

When $\omega/\omega^* = 1$, v is approximately equal to $(1 + \frac{1}{4}\epsilon)\, v_P$ and when $\omega/\omega^* > 10$ it falls to the constant value v_P. Table 3 contains values of q/q_∞ in the range $10^{-2} \leqslant \omega/\omega^* \leqslant 10^2$. At higher frequencies it was found that $q = q_\infty$ and for $\omega/\omega^* < 10^{-2}$ the attenuation coefficient was found to be given accurately by equation (4.7).

TABLE 3. *The Variation of the Attenuation Coefficient q with Frequency* ω ($T = 293°K$)

ω/ω^*	q/q_∞			
	Aluminium	*Copper*	*Iron*	*Lead*
10^{-2}	$0{\cdot}9162 \times 10^{-4}$	$0{\cdot}9520 \times 10^{-4}$	$0{\cdot}9801 \times 10^{-4}$	$0{\cdot}8364 \times 10^{-4}$
10^{-1}	$0{\cdot}9195 \times 10^{-2}$	$0{\cdot}9523 \times 10^{-2}$	$0{\cdot}9895 \times 10^{-2}$	$0{\cdot}8391 \times 10^{-2}$
1	0·4953	0·4987	0·4999	0·4903
10	0·9906	0·9921	0·9901	0·9999
10^2	1·0000	1·0000	0·9999	1·0000
$1 - 2{\cdot}5\,\epsilon$	0·9110	0·9580	0·9993	0·8168

TABLE 4. *The Variation of* v/v_P *and* q/q_∞ *for Copper in the Neighbourhood of* ω^* ($T = 293°K$)

ω/ω^*	0·1	0·3	0·7	1·0	3·0	5·0	7·0	10·0
v/v_P	1·00830	1·0077	1·0057	1·0043	1·0009	1·0003	1·0002	1·0000
q/q_∞	$0{\cdot}9523 \times 10^{-2}$	0·07999	0·3250	0·4987	0·9033	0·9641	0·9822	0·9921

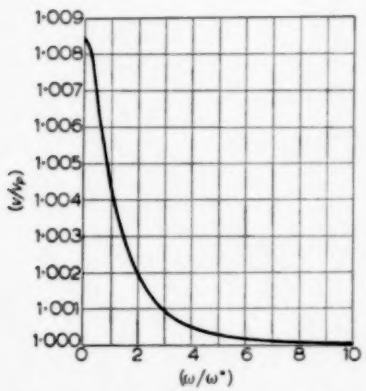

Fig. 1. The variation with frequency of the phase velocity of longitudinal elastic waves in copper.

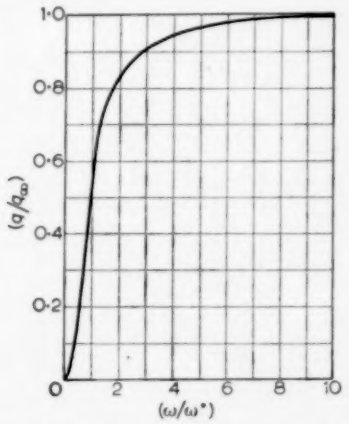

Fig. 2. The variation with frequency of the attenuation coefficient of longitudinal elastic waves in copper.

From Tables 2 and 3 it is clear that in each medium v and q change sharply in the neighbourhood of the frequency ω^*. In order to examine this behaviour in more detail the calculations were repeated for a number of frequencies lying between 0·1 ω^* and 10 ω^*. The results obtained for copper are summarized in Table 4 and represented graphically in Figures 1 and 2; those for the other metals

follow the same pattern and are omitted. Fig. 1 shows the variation of v with ω in the neighbourhood of the frequency ω^*. We see that v falls sharply from the value $1{\cdot}008\, v_p$ when $\omega/\omega^* = 0{\cdot}3$ to the value $1{\cdot}001\, v_p$ when $\omega/\omega^* = 3{\cdot}0$. It would appear, then, that in the mechanics of thermoelastic disturbances the frequency ω^* is critical to the transmitting medium. A similar conclusion may be drawn from Fig. 2 which shows the frequency dependence of q in the neighbourhood of ω^*.

The fact that, for $\omega \ll \omega^*$,

$$v = (1 + \tfrac{1}{2}\epsilon)\, v_p \tag{5.1}$$

has an interesting physical significance. In any experiment which uses the accurate measurement of the phase velocity of longitudinal elastic waves to determine the value of an elastic constant (*cf.* MARKHAM 1957), the dynamical value of $\lambda + 2\mu$ would be given by the equation

$$(\lambda + 2\mu)_d = \rho v^2 = (1 + \epsilon)\, \rho v_p{}^2$$

so that the relation between the dynamical value of $\lambda + 2\mu$ and the statical value, $(\lambda + 2\mu)_s$, is

$$\frac{(\lambda + 2\mu)_d}{(\lambda + 2\mu)_s} = 1 + \epsilon. \tag{5.2}$$

This result is independent of the frequency used provided that it is less than 1000 Mc/s. From the values given in Table 1 we see that in the case of aluminium the dynamical value will be $3\frac{1}{2}$ per cent higher than the statical value, for copper it will be $1\frac{1}{2}$ per cent higher and for lead nearly $7\frac{1}{2}$ per cent higher; there is no significant difference in the case of iron. Except in the case of iron the effect of the thermal properties is therefore significant; certainly it is greater than the experimental error of measurements made by the ultrasonic pulse technique.

ACKNOWLEDGMENTS

We are indebted to MR. J. H. WILKINSON of the Mathematics Division, the National Physical Laboratory, for his assistance with the numerical work, and to the Director of the Atomic Weapons Research Establishment for permission to publish this paper.

REFERENCES

BIOT, M. A.	1956	*J. Appl. Phys.* **27**, 240.
BRILLOUIN, L.	1938	*Tenseurs en Mécanique et en Élasticité* (Masson et Cie, Paris).
DERESIEWICZ, H.	1957	*J. Acoust. Soc. America* **29**, 204.
DUHAMEL, J. M. C.	1837	*J. de l'École Polytechn.* **15**, 1.
JEFFREYS, H.	1930	*Proc. Cambridge Phil. Soc.* **26**, 101.
LESSEN, M.	1956	*J. Mech. Phys. Solids* **5**, 57.
	1957	*Quart. Appl. Math.* **15**, 105.
MARKHAM, M. F.	1957	*Brit. J. Appl. Physics.* Supp. No. **6**, pp. S56-S63.
NEUMANN, F. E.	1885	*Vorlesung über die Theorie der Elasticität der Festen Körper* (Leipzig).
SNEDDON, I. N. and BERRY, D. S.	1958	*Handbuch der Physik* **6**, 1-126 (Berlin, Springer-Verlag).
SOKOLNIKOFF, I. S.	1956	*Mathematical Theory of Elasticity*, 2nd edn. (McGraw-Hill, New York).
VOIGT, W.	1910	*Lehrbuch der Kristallphysik* (Teubner-Verlag, Berlin).

Journal of the Mechanics and Physics of Solids, 1958, Vol. 6, pp. 231 to 235. Pergamon Press Ltd., London

VELOCITY FIELDS FOR CIRCULAR PLATES WITH THE VON MISES YIELD CONDITION

By G. Eason
King's College, Newcastle-upon-Tyne

(*Received* 31*st October*, 1957)

Summary

In this paper stress fields and associated velocity fields are obtained for circular plates of perfectly–plastic material obeying the von Mises yield condition. Attention is given to the cases in which the plate is loaded over a central circular area and either simply supported or built–in at its edge.

1. Introduction

A complete discussion has been given by Hopkins and Prager (1953) to the problem of the loading of circular plates of perfectly–plastic material obeying the Tresca yield condition and the associated flow rule. Hopkins and Wang (1954)* discussed the load carrying capacities of circular plates with the von Mises yield condition. Stress fields were obtained, but no attempt was made to obtain velocity fields. In this paper velocity fields are obtained which are associated with the stress fields of *A*. The method of analysis differs from that used in *A* and is based upon a substitution due to Hill (1950).

In Section 2 the basic equations are discussed. In Section 3 stress fields are obtained for a plate subjected to constant applied load over a central circular area and either simply supported or built–in at its edge. Velocity fields associated with these stress fields are determined in Section 4. The resulting equations are put into a form suitable for numerical integration and numerical results, in the form of graphs, are given in certain cases.

2. The Basic Equations

Let r, ϕ, z be cylindrical coordinates with the z–axis directed vertically downwards. Let the plate have radius R and thickness $2h$. The equations of equilibrium when the applied load has axial symmetry are then

$$\frac{d}{dr}(rQ) + rp = 0, \tag{1}$$

$$\frac{d}{dr}(rM) - N = rQ, \tag{2}$$

*Subsequently referred to as *A*.

where M is the radial bending moment, N the circumferential bending moment, Q the vertical shear force, and p the applied load, considered positive when it acts downwards.

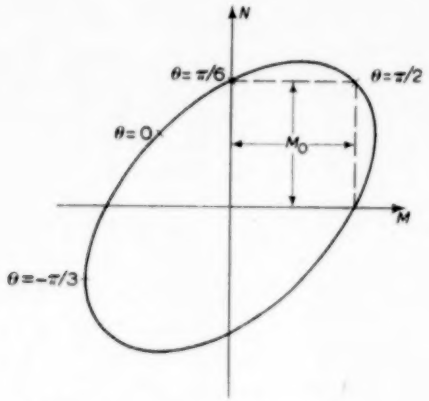

Fig. 1. von Mises yield condition.

The von Mises yield condition for plates, shown in Fig. 1, has the form

$$f = M^2 - MN + N^2 - M_0^2 = 0, \tag{3}$$

where M_0 is the fully plastic bending moment. Associated with the bending moments M, N are the curvature rates κ, λ which must be such that

$$\kappa = -\frac{d^2 w}{dr^2} = \mu \frac{\partial f}{\partial M} = \mu (2M - N), \tag{4}$$

$$\lambda = -\frac{1}{r}\frac{dw}{dr} = \mu \frac{\partial f}{\partial N} = \mu (2N - M), \tag{5}$$

where μ is a non-negative parameter, and w is the downward velocity of the plate. Equations (4), (5) combine to give

$$\frac{d^2 w}{dr^2}(2N - M) = \frac{1}{r}\frac{dw}{dr}(2M - N). \tag{6}$$

Equation (3) is satisfied by the relations (see HILL 1950, p. 308)

$$M = -\frac{2}{\sqrt{3}} M_0 \sin(\tfrac{1}{6}\pi - \theta), \qquad N = \frac{2}{\sqrt{3}} M_0 \sin(\tfrac{1}{6}\pi + \theta), \tag{7}$$

where the parameter θ is taken to have the value $\frac{1}{2}\pi$ when $M = N = M_0$. Equations (1), (2) and (6) now become

$$r\cos(\tfrac{1}{6}\pi - \theta)\frac{d\theta}{dr} - \cos\theta = -\frac{\sqrt{3}}{2M_0}\int_0^r rp\,dr, \tag{8}$$

$$\frac{d^2 w}{dr^2}\cos(\tfrac{1}{6}\pi - \theta) + \frac{1}{r}\frac{dw}{dr}\cos(\tfrac{1}{6}\pi + \theta) = 0. \tag{9}$$

We shall now consider the integration of (8) and (9) for the case in which p is constant.

3. The Stress Field

In this Section the integration of (8) will be considered for the case in which p, the applied load, is constant over a central area of the plate of radius a, and zero elsewhere. At the plate–centre $M = N = M_0$ and $\theta = \frac{1}{2}\pi$. When the plate is simply supported $M = 0$, $\theta = \frac{1}{6}\pi$ at the plate–edge. At the plate–edge in the case of built–in support $M = -2M_0/\sqrt{3}$, the algebraically smallest value of the radial bending moment, so that $\theta = -\frac{1}{3}\pi$, and the ratio λ/κ is zero. The problems of simply supported and built–in plates will be discussed simultaneously.

Let $\theta = \theta_1$ at the plate–edge, $r = R$, and $\theta = \theta_2$ when $r = a$. Taking p constant in (8) gives

$$\left.\begin{aligned} 2s\cos(\tfrac{1}{6}\pi - \theta)\frac{d\theta}{ds} - \cos\theta &= -Fs, \qquad \theta_2 \leqslant \theta \leqslant \tfrac{1}{2}\pi, \\ 2s\cos(\tfrac{1}{6}\pi - \theta)\frac{d\theta}{ds} - \cos\theta &= -F, \qquad \theta_1 \leqslant \theta \leqslant \theta_2, \end{aligned}\right\} \tag{10}$$

where $s = r^2/a^2$, $F = pa^2\sqrt{3}/4M_0$. Writing $Fs = t$ in the first of equations (10) it may be put in the form

$$(\cos\theta - t)\frac{dt}{d\theta} = 2t\cos(\tfrac{1}{6}\pi - \theta), \qquad \theta_2 \leqslant \theta \leqslant \tfrac{1}{2}\pi. \tag{11}$$

The second of equations (10) may be partially integrated to give

$$\frac{sa^2}{R^2} = \frac{r^2}{R^2} = \frac{F - \cos\theta_1}{F - \cos\theta}\exp\left\{-\sqrt{3}\int_{\theta_1}^{\theta}\frac{\cos\theta\,d\theta}{F - \cos\theta}\right\}, \qquad \theta_1 \leqslant \theta \leqslant \theta_2. \tag{12}$$

The integral may be integrated formally by the substitution $t = \tan(\frac{1}{2}\theta)$, but it is simpler to carry out the integration numerically in a particular case.

The integrated form of (12) shows that, for a point force, $a \to 0$, $\pi pa^2 \to P$; $F = \sqrt{3}/2$, $P = 2\pi M_0$ for simple support; and $F = 1$, $P = 4\pi M_0/\sqrt{3}$ for built–in support, in agreement with *A*. In both cases $\theta =$ constant over the plate, so that $\cos\theta = F$ over the plate. There is a discontinuity in θ at the plate–centre and, in the case of built–in support, one at the plate–edge also.

The single numerical integration of (11) over the range $-\frac{1}{3}\pi \leqslant \theta \leqslant \frac{1}{2}\pi$ covers all possible cases. The method of integration used was that due to Moulton (see Milne 1953, p. 58). The value of a corresponding to a particular value of F may be obtained from (12) with $r = a$, $\theta = \theta_2$. The results for uniform loading were found to be $pR^2/M_0 = 6{\cdot}51$ for simple support, and $pR^2/M_0 = 12{\cdot}55$ for built-in support, in substantial agreement with *A*.

4. The Velocity Field

In this Section a velocity field compatible with the stress field of the previous Section will be obtained by integrating (9). This may be put into the form

$$2s\cos(\tfrac{1}{6}\pi - \theta)\frac{d^2w}{ds^2} + \sqrt{3}\cos\theta\frac{dw}{ds} = 0, \tag{13}$$

where s is defined as in the previous Section, and is to be integrated with the conditions $w = 0$, $dw/dr = -\eta$ at the plate edge, $\theta = \theta_1$. The second of these

conditions is taken for convenience, but it may easily be converted into one concerning the velocity at the plate-centre. At $r = a$, $\theta = \theta_2$; w, dw/dr must be continuous.

Equation (13) may be integrated to give

$$\left.\begin{aligned} w &= \eta R (F - \cos\theta_1) \int_{\theta_1}^{\theta} \frac{\cos(\tfrac{1}{6}\pi - \theta)\, d\theta}{(F - \cos\theta)^2}, \qquad \theta_1 \leqslant \theta \leqslant \theta_2, \\ w &= \eta R (F - \cos\theta_1) \int_{\theta_1}^{\theta_2} \frac{\cos(\tfrac{1}{6}\pi - \theta)\, d\theta}{(F - \cos\theta)^2} \\ &\quad - \frac{\eta R (F - \cos\theta_1)}{2F(F - \cos\theta_2)} \exp\left\{-\sqrt{3}\int_{-\pi/3}^{\theta_2} \frac{\cos\theta\, d\theta}{t - \cos\theta}\right\} \\ &\quad \int_{\theta_2}^{\theta} \frac{dt}{d\theta} \exp\left\{\sqrt{3}\int_{-\pi/3}^{\theta} \frac{\cos\theta\, d\theta}{t - \cos\theta}\right\} d\theta, \qquad \theta_2 \leqslant \theta \leqslant \tfrac{1}{2}\pi, \end{aligned}\right\} \tag{14}$$

where t is defined as in the previous Section. The integral occuring in the first of these equations may be integrated formally, but it is simpler to carry out the integration numerically in a particular case. A relation between the velocity at the plate-centre, w_0, and η is given by the second of equations (14) with $\theta = \frac{1}{2}\pi$.

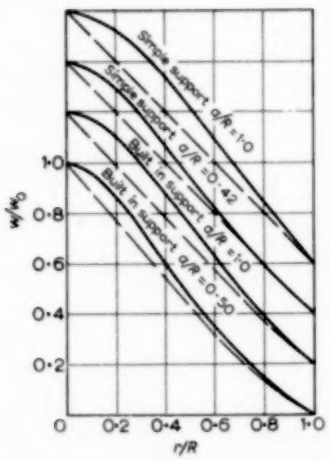

Fig. 2. Variation of deflection with radial distance.
——————— von Mises yield condition.
– – – – – – – Tresca yield condition.
(For convenience some of the curves have been raised).

In the case of a point force the velocity field may be obtained directly from (9). For simple support $\cos\theta = \sqrt{3}/2$, $\theta = \frac{1}{6}\pi$ everywhere except at the plate-centre, so that

$$w = w_0 \{1 - (r/R)^2\}. \tag{15}$$

For built-in support $\cos\theta = 1$, $\theta = 0$ everywhere except the plate-centre and edge, so that

$$w \propto \ln(R/r). \tag{16}$$

The double integral occuring in the second of equations (14) was evaluated numerically over the range $-\frac{1}{3}\pi \leqslant \theta \leqslant \frac{1}{2}\pi$; these results cover all possible loadings. Velocity fields have been calculated for uniform loading and one other case for a built-in or simply supported plate. The results of these calculations are shown graphically in Fig. 2. In all cases the full line shows the deflection with the von Mises yield criterion and the broken line shows the deflection with the Tresca yield criterion for the same loaded area, but different applied pressure. The curves for the two yield conditions differ most strikingly at the origin, where the circumferential curvature–rate is always finite, except for point loading with the von Mises yield condition, but always infinite with the Tresca yield condition.

Acknowledgments

The author would like to thank Mr. H. G. Hopkins who originally suggested this problem to him, and Miss W. D. Ashton for assistance with the computation.

References

Hill, R. 1950 The Mathematical Theory of Plasticity (Clarendon Press, Oxford).

Hopkins, H. G. and Prager, W. 1953 *J. Mech. Phys. Solids* **2**, 1.

Hopkins, H. G. and Wang, A. J. 1954 *J. Mech. Phys. Solids* **3**, 117.

Milne, W. E. 1953 *Numerical Solution of Differential Equations* (John Wiley, New York).

Journal of the Mechanics and Physics of Solids, 1958, Vol. 6, pp. 236 to 249. Pergamon Press Ltd., London

A GENERAL THEORY OF UNIQUENESS AND STABILITY IN ELASTIC–PLASTIC SOLIDS

By R. Hill
Department of Mathematics, University of Nottingham

(*Received 27th February*, 1958)

Summary

A sufficient condition is established for uniqueness of the boundary-value problem set by given velocities on a part of the surface of a body and given nominal traction-rates on the remainder. No restriction is placed on changes in geometry either in the boundary-value problem itself or in the postulated material properties, which are a generalization of those conventionally assumed for workhardening elastic–plastic solids. The solution, when it is unique, is characterized by an extremum principle.

Stability under dead loading is also examined, and a criterion is proposed. This has a formal resemblance to the uniqueness criterion, but differs from it in a significant respect when the body is partly plastic, so that stability and uniqueness need not be parallel properties.

Finally, the present theorems are compared with those previously proved for rigid-plastic solids (Hill 1957a, b, d).

1. Scope of Paper

The theory of partly plastic solids is especially concerned with the following boundary-value problem. At a generic stage in a process of quasi-static distortion the current shape of the body and the internal distribution of stress are supposed to have been determined already, together with the existing state of hardening and mechanical properties generally. The incremental changes in all these variables have now to be calculated for a further infinitesimal variation of the surface loads and geometrical constraints. When the total strain remains small, and the positional changes and rotations of material elements are neglected, the boundary-value problem always has a unique solution when the workhardening is monotonic and the yield function and plastic potential are identical (Melan 1938; a somewhat more rigorous and general proof can be found in Hill 1950, pp. 55-6).

However, the really typical plastic problems involve changes in geometry that cannot be disregarded, and here the question of uniqueness has remained open until very recently, when an answer was given for rigid–plastic solids (Hill 1957a). Broadly speaking, it is found that a unique solution is certain only when the rate of hardening exceeds a determinable critical value, depending on the particular situation. In the present paper a similar result is proved for an extensive class of elastic–plastic solids, including metals, with mechanical properties wider in important respects than those usually contemplated. Moreover, the solution, when it is unique, is characterized by an extremum principle, analogous to that for rigid–plastic solids (Hill 1957b).

In elastic solids the problem of instability is closely related to that of uniqueness (HILL 1957c); in plastic solids the connexion is looser, but still significant. For this reason we also investigate the question of stability here, and treat it from the most general standpoint, namely via the energy criterion. Previous work is unsatisfactory in that either the mechanical properties, the field equations, or the boundary conditions, are often not properly formulated for a situation where rotations of material elements are large compared with the strains. Furthermore, the occurrence of instability has invariably been taken as synonymous with the existence of infinitesimally near positions of equilibrium; this may be quite unjustified when the system is non-linear or non-conservative. For these reasons alone it is hardly surprising that theoretical predictions of the onset of instability should often have disagreed markedly with each other and with experiment. It is not, however, the present intention to review a confused literature nor to attempt any correlation with experiment but to make a fresh start and establish a broad basic theory free at least from the objections mentioned.

2. Basis for Analysis of Stress

The typical traction boundary-condition considered here is that the change in the *load* vector on an infinitesimal surface element is assigned, irrespective of changes in its area and orientation. Thus, at any stage t during a quasi-static process of deformation there is given, not the rate of change of the 'true' traction, but the rate of change of the 'nominal' traction based on the configuration at that instant. To formulate this boundary condition we introduce the unsymmetrical 'nominal stress' tensor $s_{ij}(t)$ associated with certain fixed rectangular axes. At any stage $t + \delta t$ subsequent to t, $(s_{ij} + \delta s_{ij})\,dS$ is the jth component of the force on the plane element which at t was perpendicular to the ith axis and of infinitesimal area dS. Correspondingly, the force at $t + \delta t$ on a plane area whose vectorial area was $l_i\,dS$ at t has components $(F_j + \delta F_j)\,dS$ where

$$F_j = l_i\,s_{ij}, \qquad \delta F_j = l_i\,\delta s_{ij}.$$

F_j is the 'nominal traction' based on the configuration at t. The boundary condition is then that

$$\dot{F}_j = l_i\,\dot{s}_{ij} \tag{1}$$

is prescribed.

In equilibrium and in the absence of body forces,

$$\frac{\partial \dot{s}_{ij}}{\partial x_i} = 0 \tag{2}$$

where x_i marks the position of elements at stage t. The angular equations of equilibrium are satisfied through the association of s_{ij} with the symmetric 'true stress' tensor σ_{ij} referred to the same axes. If $\dot{\sigma}_{ij}^{\circ}$ denotes its rate of change following the same element,

$$\dot{s}_{ij} - \dot{\sigma}_{ij}^{\circ} = \sigma_{ij}\frac{\partial v_k}{\partial x_k} - \sigma_{jk}\frac{\partial v_i}{\partial x_k}$$

where v_i is the velocity. This is an immediate specialization of Murnaghan's well-known formula connecting the true and nominal stress tensors.

Now the material properties found by experiment are given, in the first instance, in terms of the true stress tensor σ_{ij} associated with rectangular axes rotating with the element and so having spin $\frac{1}{2}$ curl $\mathbf{v}$. From the transformation rule for tensors it is easily shown that

$$\dot{\sigma}_{ij} - \dot{\sigma}_{ij}^{\circ} = \sigma_{ik}\,\alpha_{kj} + \sigma_{jk}\,\alpha_{ki}$$

where

$$\alpha_{ij} = \tfrac{1}{2}\left(\frac{\partial v_i}{\partial x_j} - \frac{\partial v_j}{\partial x_i}\right)$$

is the antisymmetric part of the velocity gradient tensor. (It is worth noting that $\dot{\sigma}_{ij}$ and $\dot{\sigma}_{ij}^{\circ}$ have the same scalar product with any tensor whose principal axes coincide with those of σ_{ij}.) On combining the last two equations :

$$\dot{s}_{ij} - \left(\dot{\sigma}_{ij} + \sigma_{ij}\frac{\partial v_k}{\partial x_k}\right) = \sigma_{ik}\frac{\partial v_j}{\partial x_k} - (\sigma_{ik}\,\epsilon_{jk} + \sigma_{jk}\,\epsilon_{ik}). \tag{3}$$

3. Material Properties

In an element whose response to any further infinitesimal change of stress is purely elastic (i.e. an element that has either never yielded or is now partly unloaded after being plastic), the isothermal relations between stress-rate and strain-rate are taken to be homogeneous and linear, and are written as

$$\dot{\sigma}_{ij} + \sigma_{ij}\frac{\partial v_k}{\partial x_k} = g_{ijkl}\,\epsilon_{kl} \tag{4}$$

where the moduli g_{ijkl} depend on the current stress and orientation of the axes of anisotropy, and possibly also on the entire strain-history if the element has previously been plastic. Moreover, and this is of paramount importance for what follows, it is stipulated that

$$g_{ijkl} = g_{klij} \tag{5}$$

in addition to the necessary symmetry with respect to interchange of i and j, and the arbitrarily arranged symmetry with regard to interchange of k and l. Equation (4), with (5), is certainly justifiable when the element behaves as a perfectly elastic solid during *complete* unloading from the current stress : it follows directly from a formula of Cauchy's in the theory of finite elastic strain*.

To simplify the notation (4) is written as

$$\dot{\boldsymbol{\sigma}} + \theta\boldsymbol{\sigma} = \boldsymbol{K}\boldsymbol{\epsilon} \tag{6}$$

where tensor elements are regarded as constituting vectors in a 9-space. $\boldsymbol{K}$ is a symmetric 9×9 matrix and θ is the fractional rate of volume increase. If the total strain recoverable by complete unloading is infinitesimal, $\boldsymbol{K}$ would be positive-definite for any actual solid, according to the familiar thermodynamic argument in classical elasticity. On the other hand, $\boldsymbol{K}$ need not be positive-definite when the

*See, for example, equation (18) of HILL (1957c) ; note that there the stress-rate symbol refers to components associated with fixed axes and differs from the present one.

recoverable strain is finite, and indeed there is no need so to restrict K in the subsequent analysis*.

For a plastic element the simplest hypothesis is

$$\dot{\boldsymbol{\sigma}} + \theta\boldsymbol{\sigma} = K(\boldsymbol{\epsilon} - \boldsymbol{\epsilon}_p) \tag{7}$$

where $\boldsymbol{\epsilon}_p$ is the plastic part of the strain-rate, and K is a symmetric matrix depending only on strain-history. Suppose that

$$\boldsymbol{\epsilon}_p = \begin{cases} h^{-1}\left[\mathbf{n}(\dot{\boldsymbol{\sigma}} + \theta\boldsymbol{\sigma})\right]\mathbf{n} & \text{when} \quad \mathbf{n}(\dot{\boldsymbol{\sigma}} + \theta\boldsymbol{\sigma}) \geqslant 0 \\ 0 & \ldots\ldots\ldots\ldots\ldots \leqslant 0 \end{cases} \tag{8}$$

where h is a positive scalar measure of the current rate of workhardening and depends on $\boldsymbol{\sigma}$ as well as the strain-history. The ' direction ' of the plastic strain-rate is specified by the unit vector $\mathbf{n}$, which also depends on $\boldsymbol{\sigma}$ and strain-history; $\mathbf{n}$ is stipulated to be deviatoric so that there is no permanent volume change. Since θ is directly expressible in terms of stress-rate through the elastic moduli, the equation

$$\mathbf{n}(\dot{\boldsymbol{\sigma}} + \theta\boldsymbol{\sigma}) = 0$$

effectively defines those stress-rate vectors that are tangential to the yield surface at the current stress point, and thereby the surface element. This does not have $\mathbf{n}$ as its normal and so yielding is affected by the hydrostatic part of the true stress. For present purposes no restrictions need be placed on the shape of the surface, and in particular we do not make the customary assumption of convexity.

Note that, in view of the definition of $\dot{\boldsymbol{\sigma}}$, equation (8) conforms to the minimum requirement that it is satisfied identically by a rigid-body spin of the element together with the stress state.

To invert the relations (7), with (8), we first remark that

$$\mathbf{n}K\boldsymbol{\epsilon} = \mathbf{n}(\dot{\boldsymbol{\sigma}} + \theta\boldsymbol{\sigma}).\begin{cases} (1 + h^{-1}\,\mathbf{n}K\mathbf{n}) & \text{when} \quad \mathbf{n}(\dot{\boldsymbol{\sigma}} + \theta\boldsymbol{\sigma}) \geqslant 0 \\ 1 & \ldots\ldots\ldots\ldots\ldots \leqslant 0 \end{cases}$$

provided $1 + h^{-1}\,\mathbf{n}K\mathbf{n} > 0$. This inequality we satisfy *a fortiori* for any $h > 0$ by requiring

$$\mathbf{n}K\mathbf{n} > 0 \text{ in a plastic element.} \tag{9}$$

That is, the K quadratic form is positive for *deviatoric* vectors; this has the interpretation that a strain-rate in direction $\mathbf{n}$ constitutes loading. Then, in a plastic element,

$$\dot{\boldsymbol{\sigma}} + \theta\boldsymbol{\sigma} = K\boldsymbol{\epsilon} - \begin{cases} \dfrac{\mathbf{n}K\boldsymbol{\epsilon}}{(\mathbf{n}K\mathbf{n} + h)}K\mathbf{n} & \text{when} \quad \mathbf{n}K\boldsymbol{\epsilon} \geqslant 0 \\ 0 & \ldots\ldots\ldots\ldots \leqslant 0. \end{cases} \tag{10}$$

If the rate of hardening is zero (8) is replaced by

$$\boldsymbol{\epsilon}_p = \begin{cases} \gamma\mathbf{n}, & \text{where} \quad \gamma \geqslant 0, \quad \text{when} \quad \mathbf{n}(\dot{\boldsymbol{\sigma}} + \theta\boldsymbol{\sigma}) = 0 \\ 0 & \ldots\ldots\ldots\ldots\ldots\ldots < 0 \end{cases} \tag{8'}$$

*It is of more than academic interest that the eventual uniqueness theorem and extremum principle then apply also to some ' unreal ' materials. For it can happen that a boundary-value problem is solvable in the first instance more easily for some special kind of unreal material; this solution can then be of use in finding that for the real material.

while (10) still holds, with $h = 0$.

Now in fact the only elastic-plastic solids that have been studied experimentally are the common metals. These have elastic moduli so great compared with any stress supportable by the material that there is perhaps no point in retaining the $\theta\boldsymbol{\sigma}$ term nor in postulating any particular stress-dependence of $\boldsymbol{K}$ itself in the elastic range, though we may still envisage measurable changes in $\boldsymbol{K}$ due to *plastic* straining, especially through changes in the state of anisotropy. Equations (7), (8) and (10) then reduce to the generally accepted relations*, with $\mathbf{n}$ as the unit normal to the yield surface (now independent of hydrostatic stress).

4. Fundamental Identities and Inequalities

We shall later need to refer to the quantity

$$E(\mathbf{v}) = \tfrac{1}{2}(\dot{\boldsymbol{\sigma}} + \theta\boldsymbol{\sigma})\,\boldsymbol{\epsilon} - \tfrac{1}{2}\,\sigma_{ik}\left(2\epsilon_{ij}\,\epsilon_{jk} - \frac{\partial v_j}{\partial x_i}\frac{\partial v_j}{\partial x_k}\right) \tag{11}$$

which is a function of velocity gradient, equal to $\frac{1}{2}\,\dot{s}_{ij}\,\partial v_j/\partial x_i$ by (3). Moreover, in view of (6) and (10),

$$\dot{s}_{ij}\,d\left(\frac{\partial v_j}{\partial x_i}\right) = dE, \qquad \dot{s}_{ij} = \frac{\partial E}{\partial\,(\partial v_j/\partial x_i)}.$$

That the left-hand differential is perfect could also be recognised in advance from the symmetry, with respect to interchange of ij and kl, of the matrix of coefficients in the relations between $\dot{s}_{ij}$ and $\partial v_i/\partial x_i$.

Now let $\boldsymbol{\epsilon}^*$, $\boldsymbol{\epsilon}$ denote distinct strain-rates and $\dot{\boldsymbol{\sigma}}^*$, $\dot{\boldsymbol{\sigma}}$ the corresponding stress-rates in an element in a given condition and state of stress. We write $\Delta\boldsymbol{\epsilon} = \boldsymbol{\epsilon}^* - \boldsymbol{\epsilon}$ and similarly for the differences of other starred and unstarred quantities. Note that when the element is plastic $\Delta\,\dot{\boldsymbol{\sigma}}$ and $\Delta\,\boldsymbol{\epsilon}$, regarded as single vectors, do not necessarily correspond in the sense of being related by (10).

Lemma I. In an elastic element there is the immediate identity

$$\Delta(\dot{\boldsymbol{\sigma}} + \theta\boldsymbol{\sigma})\,\Delta\,\boldsymbol{\epsilon} = \Delta\boldsymbol{\epsilon}\,\boldsymbol{K}\,\Delta\boldsymbol{\epsilon}. \tag{12}$$

In a plastic element, for $h \geqslant 0$,

$$\Delta(\dot{\boldsymbol{\sigma}} + \theta\boldsymbol{\sigma})\,\Delta\boldsymbol{\epsilon} \geqslant \Delta\boldsymbol{\epsilon}\,\boldsymbol{K}\,\Delta\boldsymbol{\epsilon} - \frac{(\mathbf{n}\boldsymbol{K}\,\Delta\boldsymbol{\epsilon})^2}{\mathbf{n}\boldsymbol{K}\mathbf{n} + h}. \tag{13}$$

This lemma is used in deriving the uniqueness criterion (Section 5).

Proof. The equality in (13) holds when both strain-rates call for additional loading, from (11) and the symmetry of $\boldsymbol{K}$. The inequality holds when $\mathbf{n}\,\boldsymbol{K}\,\boldsymbol{\epsilon}^* \geqslant 0$ and $\mathbf{n}\boldsymbol{K}\boldsymbol{\epsilon} < 0$. For then the left side of (13) is

$$\Delta\boldsymbol{\epsilon}\,\boldsymbol{K}\Delta\boldsymbol{\epsilon} - \frac{(\mathbf{n}\boldsymbol{K}\boldsymbol{\epsilon}^*)(\mathbf{n}\boldsymbol{K}\Delta\boldsymbol{\epsilon})}{\mathbf{n}\boldsymbol{K}\mathbf{n} + h}$$

and this exceeds the right side. Finally, if both strain-rates produce unloading, their difference satisfies (12) and hence (13) *a fortiori* (with equality only when $\mathbf{n}\boldsymbol{K}\,\Delta\boldsymbol{\epsilon} = 0$).

*Though the form of (10), and the modification of the loading criterion through the inclusion of elastic anisotropy, is perhaps a new generalization.

Lemma II. In an elastic element there is the easily verified identity

$$2\,(\dot{\boldsymbol{\sigma}} + \theta\boldsymbol{\sigma})\,\Delta\boldsymbol{\epsilon} + \Delta\boldsymbol{\epsilon}\,\boldsymbol{K}\,\Delta\boldsymbol{\epsilon} = \Delta\left[(\dot{\boldsymbol{\sigma}} + \theta\boldsymbol{\sigma})\,\boldsymbol{\epsilon}\right]. \tag{14}$$

In a plastic element, for $h \geqslant 0$,

$$2\,(\dot{\boldsymbol{\sigma}} + \theta\boldsymbol{\sigma})\,\Delta\boldsymbol{\epsilon} + \left[\Delta\boldsymbol{\epsilon}\,\boldsymbol{K}\,\Delta\boldsymbol{\epsilon} - \frac{(\mathbf{n}\boldsymbol{K}\,\Delta\boldsymbol{\epsilon})^2}{\mathbf{n}\boldsymbol{K}\mathbf{n} + h}\right] \leqslant \Delta\left[(\dot{\boldsymbol{\sigma}} + \theta\boldsymbol{\sigma})\,\boldsymbol{\epsilon}\right]. \tag{15}$$

This lemma is used in obtaining the extremum principle (Section 6). A weaker inequality sufficed in the existing proof of this principle when geometry changes are neglected ($\boldsymbol{K}$ being positive-definite) : in that event the square bracket, which is positive by Cauchy's inequality, is omitted from the left side of (15).

Proof. When $\mathbf{n}\boldsymbol{K}\boldsymbol{\epsilon} \geqslant 0$ the left side of (15) is equal to

$$\Delta\left[\boldsymbol{\epsilon}\boldsymbol{K}\boldsymbol{\epsilon} - \frac{(\mathbf{n}\boldsymbol{K}\boldsymbol{\epsilon})^2}{\mathbf{n}\boldsymbol{K}\mathbf{n} + h}\right]$$

by (10) and the symmetry of $\boldsymbol{K}$. If $\mathbf{n}\,\boldsymbol{K}\,\boldsymbol{\epsilon}^* \geqslant 0$ this is just the right side of (15) which is therefore an equality. If, however, $\mathbf{n}\,\boldsymbol{K}\,\boldsymbol{\epsilon}^* < 0$ the right side exceeds the left by $(\mathbf{n}\boldsymbol{K}\boldsymbol{\epsilon}^*)^2/(\mathbf{n}\boldsymbol{K}\mathbf{n} + h)$.

When $\mathbf{n}\boldsymbol{K}\boldsymbol{\epsilon} < 0$ the left side of (15) is equal to

$$\Delta\,(\boldsymbol{\epsilon}\boldsymbol{K}\boldsymbol{\epsilon}) - \frac{(\mathbf{n}\boldsymbol{K}\,\Delta\boldsymbol{\epsilon})^2}{\mathbf{n}\boldsymbol{K}\mathbf{n} + h}.$$

If $\mathbf{n}\boldsymbol{K}\boldsymbol{\epsilon}^* \geqslant 0$ the right side of (15) is

$$\Delta\,(\boldsymbol{\epsilon}\boldsymbol{K}\boldsymbol{\epsilon}) - \frac{(\mathbf{n}\boldsymbol{K}\boldsymbol{\epsilon}^*)^2}{\mathbf{n}\boldsymbol{K}\mathbf{n} + h}$$

which exceeds the left since $(\mathbf{n}\,\boldsymbol{K}\,\Delta\,\boldsymbol{\epsilon})^2 > (\mathbf{n}\,\boldsymbol{K}\,\boldsymbol{\epsilon}^*)^2$. If $\mathbf{n}\,\boldsymbol{K}\,\boldsymbol{\epsilon} < 0$ the right side of (15) is just $\Delta\,(\boldsymbol{\epsilon}\,\boldsymbol{K}\,\boldsymbol{\epsilon})$ and is not less than the left (being equal when $\mathbf{n}\,\boldsymbol{K}\,\Delta\,\boldsymbol{\epsilon} = 0$).

5. Uniqueness Criterion

We regard the current distribution of stress in a body as given, together with the material properties at every point. For simplicity body forces are omitted since their mode of inclusion is sufficiently obvious. The nominal traction-rate $\dot{\mathbf{F}}$ is specified on a part S_F of the current surface and the velocity $\mathbf{v}$ on the remainder S_v. These conditions and the field equations (2), (3), (6) and (10) set a boundary-value problem for the internal velocity field.

Suppose that there could be two distinct solutions (not differing merely by a rigid-body motion when $S_v = 0$) and denote their difference by $\Delta\,\mathbf{v}$. Then, from (1) and (2), with S and V as the present surface and volume,

$$0 = \int \Delta\dot{\mathbf{F}}\,\Delta\mathbf{v}\,dS = \int \Delta\dot{\boldsymbol{s}}_{ij}\,\Delta\left(\frac{\partial v_j}{\partial x_i}\right)dV$$

$$= \int \Delta\,(\dot{\boldsymbol{\sigma}} + \theta\boldsymbol{\sigma})\,\Delta\boldsymbol{\epsilon}\,dV - \boldsymbol{\Sigma}\,(\Delta\mathbf{v})$$

where

$$\boldsymbol{\Sigma}\,(\mathbf{v}) = \int \sigma_{ik}\left(2\epsilon_{ij}\,\epsilon_{jk} - \frac{\partial v_j}{\partial x_i}\frac{\partial v_j}{\partial x_k}\right)dV.$$

A sufficient condition for uniqueness is therefore that

$$\int \Delta(\dot{\boldsymbol{\sigma}} + \theta\boldsymbol{\sigma})\,\Delta\boldsymbol{\epsilon}\,dV - \Sigma(\Delta\mathbf{v}) > 0$$

for the differences $\Delta\mathbf{v}$ of every distinct pair of continuous velocity fields taking the given values on S_v.

For applications it is preferable to replace this condition by a slightly weaker (over-sufficient) criterion which is a functional only of the single vector $\Delta\mathbf{v}$. From lemma I, when $h \geqslant 0$,

$$\int \Delta(\dot{\boldsymbol{\sigma}} + \theta\boldsymbol{\sigma})\,\Delta\boldsymbol{\epsilon}\,dV \geqslant H(\Delta\mathbf{v})$$

where

$$H(\mathbf{v}) = \int \boldsymbol{\epsilon}\boldsymbol{K}\boldsymbol{\epsilon}\,dV - \int \frac{(\mathbf{n}\boldsymbol{K}\boldsymbol{\epsilon})^2}{\mathbf{n}\boldsymbol{K}\mathbf{n} + h}\,dV_p,$$

V_p being the *whole* of the plastically stressed zone. We thereby obtain the sufficient condition

$$H(\mathbf{w}) - \Sigma(\mathbf{w}) > 0 \tag{16}$$

for all continuous velocity fields $\mathbf{w}$ vanishing on S_v but not identically zero in V.

That the condition may well be often *over-sufficient* (i.e. not necessary) can be surmised from its being entirely independent of the particular boundary values of velocity and traction-rate.

H_0 will henceforward be written for H when $h = 0$ in V_p, corresponding to a non-hardening solid. Similarly H_∞ will be written for $\int \boldsymbol{\epsilon}\boldsymbol{K}\boldsymbol{\epsilon}\,dV$, the value of H when $h \to \infty$ in V_p, corresponding to a solid which has not previously been plastically strained. Note that $H_0 \leqslant H \leqslant H_\infty$.

The following situations may be distinguished :

(i) $\Sigma < H_\infty$ for all $\mathbf{w}$ fields. The problem is unique for purely elastic behaviour, as has been shown elsewhere (HILL 1957c).

(ii) $\Sigma < H_0$ for all $\mathbf{w}$ fields. The problem is unique for all $h \geqslant 0$, since $H \geqslant H_0$ and $\Sigma < H$ always.

(iii) $\Sigma \leqslant H_0$ for all $\mathbf{w}$ fields, with equality for at least one. The problem is unique whenever $h > 0$ (workhardening solid) since $\Sigma \leqslant H_0 < H$. But nothing can be concluded when $h = 0$ everywhere in V_p (non-hardening solid) since $\Sigma = H_0 = H$ for at least one field.

(iv) $\Sigma > H_0$ for at least one field and $\Sigma < H_\infty$ for all. The problem is unique with certainty only for sufficiently great rates of hardening.

To clarify and give precision to (iv) consider an elastically-isotropic solid, for which $\mathbf{n}\boldsymbol{K}\mathbf{n} = 2\mu$ where μ is the rigidity modulus. Then

$$H_\infty(\mathbf{w}) = \int (\lambda\phi^2 + 2\mu\eta^2)\,dV, \qquad H_0(\mathbf{w}) = H_\infty(\mathbf{w}) - \int 2\mu\,(\mathbf{n}\boldsymbol{\eta})^2\,dV_p, \tag{17}$$

where λ is the other Lamé constant, and $\boldsymbol{\eta}$ is the strain-rate and ϕ the fractional rate of volume increase corresponding to $\mathbf{w}$. If h/μ has the same value throughout

V_p, the uniqueness condition can be rearranged to give explicitly

$$\frac{h}{2\mu} > \beta \qquad \text{where} \qquad \beta = \text{Max}\left(\frac{\Sigma - H_0}{H_\infty - \Sigma}\right) \text{ in class } \mathbf{w}, \tag{18}$$

the *algebraic* maximum being implied.

6. Extremum Principle

When the criterion (16) is satisfied, the unique solution is characterized by the following extremum property. In the class of continuous velocity fields taking the given values on S_v the functional

$$\int E(\mathbf{v})\, dV - \int \dot{\mathbf{F}}\mathbf{v}\, dS_F \tag{19}$$

has an absolute minimum when $\mathbf{v}$ is the actual solution, E being as in (11). The least value is $\frac{1}{2}\left(\int \dot{\mathbf{F}}\mathbf{v}\, dS_v - \int \dot{\mathbf{F}}\mathbf{v}\, dS_F\right)$ from (3) and the usual transformation.

With $\Delta\mathbf{v} = \mathbf{v}^* - \mathbf{v}$, where $\mathbf{v}^*$ is any distinct field of the class,

$$\Delta \int \dot{\mathbf{F}}\mathbf{v}\, dS_F = \int \dot{\mathbf{F}}\Delta\mathbf{v}\, dS,$$

$\dot{\mathbf{F}}$ being given in the left-hand integral. From (3) this becomes

$$\int (\dot{\boldsymbol{\sigma}} + \theta\boldsymbol{\sigma})\, \Delta\boldsymbol{\epsilon}\, dV - \int \sigma_{ik}\left[2\epsilon_{jk}\, \Delta\epsilon_{ij} - \frac{\partial v_j}{\partial x_k}\, \Delta\left(\frac{\partial v_j}{\partial x_i}\right)\right] dV.$$

Now by (14) and (15)

$$2\int (\dot{\boldsymbol{\sigma}} + \theta\boldsymbol{\sigma})\, \Delta\boldsymbol{\epsilon}\, dV + H(\Delta\mathbf{v}) \leqslant \Delta \int (\dot{\boldsymbol{\sigma}} + \theta\boldsymbol{\sigma})\, \boldsymbol{\epsilon}\, dV.$$

There is also the identity

$$2\int \sigma_{ik}\left[2\epsilon_{jk}\, \Delta\epsilon_{ij} - \frac{\partial v_j}{\partial x_k}\, \Delta\left(\frac{\partial v_j}{\partial x_i}\right)\right] dV + \Sigma(\Delta\mathbf{v}) = \Delta\, \Sigma(\mathbf{v}).$$

Combining the last three equations and using (16), which holds for $\mathbf{w} = \Delta\mathbf{v}$ by hypothesis,

$$\Delta\left[\int (\dot{\boldsymbol{\sigma}} + \theta\boldsymbol{\sigma})\, \boldsymbol{\epsilon}\, dV - \Sigma(\mathbf{v}) - 2\int \dot{\mathbf{F}}\mathbf{v}\, dS_F\right] > 0.$$

This proves the extremum principle. When geometry changes are negligible (Σ and θ terms discarded, true and nominal stress-rates not distinguished) it reduces to a known result (Hill 1950, pp. 65-6).

The minimum is also analytic, as well as absolute, in the sense that, for any infinitesimal variation $\delta\mathbf{v}$, the first variation of (19) vanishes when $\mathbf{v}$ is the actual solution. For the inequality rests on the second-order term $H(\delta\mathbf{v}) - \Sigma(\delta\mathbf{v})$ and (by inspection of the proof of lemma II) on the integral of $(\mathbf{n}K\,\delta\boldsymbol{\epsilon})^2/(\mathbf{n}K\mathbf{n} + h)$ over that part of the plastic zone where neither of the actual and varied fields produce loading.

For the same reasons, even when the solution is not unique and (16) is not

satisfied, the variation principle exists in respect of each solution, though the extremum principle may not.

It is essential to keep in mind the distinction between the functionals in (16) and (19). In the elastic zone and in the part of the plastic zone where $\mathbf{n}\,K\,\dot{\boldsymbol{\epsilon}} \leqslant 0$, $(\dot{\boldsymbol{\sigma}} + \theta\,\boldsymbol{\sigma})\,\dot{\boldsymbol{\epsilon}}$ is equal to $\dot{\boldsymbol{\epsilon}}\,K\,\dot{\boldsymbol{\epsilon}}$. Only in the loading part of the plastic zone, where $\mathbf{n}\,K\,\dot{\boldsymbol{\epsilon}} > 0$, is it equal to

$$\dot{\boldsymbol{\epsilon}}K\dot{\boldsymbol{\epsilon}} - \frac{(\mathbf{n}K\dot{\boldsymbol{\epsilon}})^2}{\mathbf{n}K\mathbf{n} + h}.$$

By contrast, in the uniqueness functional the term containing h has to be included *everywhere* in the plastic zone, irrespective of the sign of $\mathbf{n}K\boldsymbol{\eta}$.

Further insight into the connexion between the extremum principle and uniqueness criterion can be gained by studying the matter for a still more general class of solids. We describe the basic idea here only in outline. Let the (non-linear) relations between nominal stress-rate and velocity gradient be

$$\dot{s}_{ij} = \frac{\partial E}{\partial\,(\partial v_j/\partial x_i)}$$

where E is a function of the velocity gradient, depending also on strain history, with continuous first derivatives and sectionally continuous second derivatives. Supposing there could be two distinct solutions to the boundary-value problem,

$$\int \Delta\dot{s}_{ij}\,\Delta\left(\frac{\partial v_j}{\partial x_i}\right) dV = 0.$$

A sufficient condition for uniqueness is therefore that

$$\int \Delta\left\{\frac{\partial E}{\partial\,(\partial v_j/\partial x_i)}\right\}\Delta\left(\frac{\partial v_j}{\partial x_i}\right) dV > 0 \tag{20}$$

for all pairs of continuous velocity fields taking the prescribed values on S_v. By specializing (20) for pairs differing only infinitesimally, we see that it implies

$$\int c_{ijkl}\,\xi_{ij}\,\xi_{kl}\,dV > 0 \tag{21}$$

for arbitrary ξ_{ij} and for

$$c_{ijkl} = \frac{\partial^2 E}{\partial\,(\partial v_j/\partial x_i)\,\partial\,(\partial v_l/\partial x_k)}$$

corresponding to *any* velocity field.

Now, by the mean value theorem of the second order, when c_{ijkl} is a continuous function of velocity gradient,

$$\int\left[\Delta E - \frac{\partial E}{\partial\,(\partial v_j/\partial x_i)}\,\Delta\left(\frac{\partial v_j}{\partial x_i}\right)\right] dV = \tfrac{1}{2}\int \bar{c}_{ijkl}\,\Delta\left(\frac{\partial v_j}{\partial x_i}\right)\Delta\left(\frac{\partial v_l}{\partial x_k}\right) dV \tag{22}$$

where $\Delta\,\mathbf{v}$ is now the difference of *any* two fields, and the bar denotes a value for some velocity gradient on the 'join' of those for the two fields. From (21) and (23), with $\xi_{ij} = \Delta\,(\partial v_j/\partial x_i)$,

$$\int\left[\Delta E - \frac{\partial E}{\partial\,(\partial v_j/\partial x_i)}\,\Delta\left(\frac{\partial v_j}{\partial x_i}\right)\right] dV > 0.$$

(When c_{ijkl} is discontinuous an extension of the conventional mean-value theorem has to be invoked, and a corresponding interpretation placed on (21)). If, now, $\mathbf{v}$ is the actual unique solution a transformation of the last equation gives the extremum principle

$$\Delta\left[\int E\,dV - \int \dot{\mathbf{F}}\mathbf{v}\,dS_F\right] > 0, \tag{23}$$

which has thereby been derived as a consequence of (20).

This is an extension of the systematic procedure of Hill (1956a) for 'convex' functions E, in that (20) can be satisfied without the integrand itself being always positive. This extension was given in essence by Hill (1957c, pp. 233-4) in connexion with rubber-like solids for which E is a quadratic form whose second derivatives are the elastic moduli. For elastic–plastic solids E is given by (11) in conjunction with (6) and (10); its second derivatives are discontinuous for velocity gradients such that $\mathbf{n}\,K\,\boldsymbol{\epsilon} = 0$.

7. Stability Criterion

Suppose that a part of the surface of the body is rigidly constrained and that constant nominal tractions (dead loading) are maintained on the remainder throughout any movement from the position of equilibrium at stage t. Let $\mathbf{u}$ be an arbitrary virtual displacement, during the course of which the nominal stress changes from s_{ij} to $s_{ij} + \delta s_{ij}$ (still referred to stage t). In a further infinitesimal displacement $d\mathbf{u}$ the increase in internal energy exceeds the work of the external forces by the amount

$$\int\left\{(s_{ij} + \delta s_{ij})\,d\left(\frac{\partial u_j}{\partial x_i}\right)\right\}dV - \int(\mathbf{F}\,d\mathbf{u})\,dS = \int\left\{\delta s_{ij}\,d\left(\frac{\partial u_j}{\partial x_i}\right)\right\}dV,$$

where S, V and x_i are the surface, volume and position at stage t. The total excess in reaching the position $\mathbf{u}$ is the integral of this over the whole 'path.' A sufficient condition for stability at stage t is therefore that

$$\int\left\{\int \delta s_{ij}\,d\left(\frac{\partial u_j}{\partial x_i}\right)\right\}dV > 0, \tag{24}$$

where the inner integral is taken along any path leading to each geometrically possible configuration infinitesimally near the initial one. These configurations need not of course be positions of equilibrium since they are envisaged as being attained (if at all) by free motion following a transitory dynamical disturbance. However, it may happen that there is a certain path that can be traversed quasi-statically under the dead loads; in this event the integral vanishes, as may be shown by direct transformation or equivalently from the virtual work principle. Of course the integral can vanish in other circumstances also.

In a plastic solid the change in stress is not a single-valued function of the total displacement gradient, and so (and if only for this reason) the integral in (24) is strongly path-dependent. Among the paths leading to any one final position the most critical for stability is that which calls for the smallest increase in internal energy in the body as a whole. In attempting to determine this it seems desirable, at the outset, to approach the problem by calculating the least increase in energy

in bringing each element of the body *separately* to its final state of distortion; since this would generally violate the continuity of the material, the actual least value may be underestimated and the resulting stability criterion be over-sufficient. However, we shall later give a reason why this is not the case here.

In an element after a finite distortion there is a unique triad of mutually perpendicular directions which were also perpendicular initially, though not necessarily so during the straining. These are the 'principal directions' in the element. Let λ_r $(r = 1, 2, 3)$ be the natural logarithms of the ratios of the final and initial lengths in these directions. The final distortion could be reached along a path at every stage of which the *true* strain-rate (based on the configuration at that stage) has principal axes coinciding with the principal directions and principal components proportional to the λ_r's. It seems very probable that this is actually the optimum path (at all events to *neighbouring* states), but a rigorous proof has not been found. We adopt it here as a hypothesis.

The calculation need only be correct to second order in the additional displacements, which are now taken to be infinitesimal. Let the true stress initially have normal (*not* principal) components σ_r along the strain-rate axes and suppose they finally become $\sigma_r + \delta\sigma_r$. At any intermediate stage on the optimum path the changes in the normal components are in proportion to the respective $\delta\sigma_r$'s, to first order, since the strain-rate components are maintained in fixed ratio; moreover, to this order, the relations between the $\delta\sigma_r$'s and the λ_r's are exactly those between the true stress-rates and the strain-rates (10). The total work of distortion, per unit *initial* volume, is then easily shown to be

$$\Sigma\left[\sigma_r + \tfrac{1}{2}\left(\delta\sigma_r - \sigma_r\,\delta\rho/\rho\right)\right]\lambda_r$$

to second order, where ρ is the density. In terms of components referred to the x_i axes this is

$$\left[\sigma_{ij} + \tfrac{1}{2}\left(\delta\sigma_{ij} - \sigma_{ij}\,\delta\rho/\rho\right)\right]\lambda_{ij}$$

where, to second order,

$$\lambda_{ij} = e_{ij} - e_{ik}\,e_{jk}$$

and

$$e_{ij} = \tfrac{1}{2}\left(\frac{\partial u_i}{\partial x_j} + \frac{\partial u_j}{\partial x_i} + \frac{\partial u_k}{\partial x_i}\frac{\partial u_k}{\partial x_j}\right)$$

is the Lagrangian strain tensor. $\delta\sigma_{ij}$ denotes the change in the stress components along axes rotating with the element and initially coincident with the x_i axes.

With the help of the differential form of (3) we finally obtain the compact second-order formula

$$(s_{ij} + \tfrac{1}{2}\,\delta s_{ij})\,\frac{\partial u_j}{\partial x_i}$$

for the work of distortion per unit initial volume on the optimum path. In this it is to be understood that δs_{ij} and $\partial u_j/\partial x_i$ are related in the same way as $\dot{s}_{ij}$ and $\partial v_j/\partial x_i$, namely through (3) and (10) if the element is plastic, and through (6) if it is elastic. This expression for the work is evidently obtained also from a path in which the displacement field throughout the body is increased proportionately and continuously (possible if the material is compressible). It follows that we have certainly not *under*estimated the least work.

Equation (24) can now be replaced by

$$\int \delta s_{ij} \frac{\partial u_j}{\partial x_i} \, dV > 0 \qquad \text{or} \qquad \int \dot{s}_{ij} \frac{\partial v_j}{\partial x_i} \, dV > 0, \tag{25}$$

since the admissible fields can *now* be regarded indifferently as either displacement or velocity. Equivalently, by (3) and (11), the criterion is

$$2 \int E(\mathbf{v}) \, dV \equiv \int (\dot{\boldsymbol{\sigma}} + \theta \boldsymbol{\sigma}) \, \boldsymbol{\epsilon} \, dV - \Sigma(\mathbf{v}) > 0 \tag{26}$$

for all fields $\mathbf{v}$ vanishing at the constraints. Now it was shown that the boundary-value problem set by rigid constraints on S_v and given nominal traction-rates on S_F has a unique solution when

$$\int \Delta(\dot{\boldsymbol{\sigma}} + \theta \boldsymbol{\sigma}) \, \Delta \boldsymbol{\epsilon} \, dV - \Sigma(\Delta \mathbf{v}) > 0 \tag{27}$$

where $\Delta \mathbf{v}$ is the difference of any pair of fields vanishing at the constraints. $\Delta \dot{\boldsymbol{\sigma}}$, $\Delta \boldsymbol{\epsilon}$ are the differences of the corresponding stress-rates and strain-rates, but are not necessarily related by (10) in the plastic zone, on account of the non-linearity inherent in the different behaviour in loading and unloading. Consequently (26) and (27) are distinct criteria. Nevertheless, there is a definite connexion in that (26) is always satisfied when (27) is (but not vice versa); for (27) reduces to (26) when one field of a pair vanishes identically. A partly plastic state in which the boundary-value problem has a unique solution is therefore *certainly* stable; and even when the solution is not unique the state *may* still be stable. This is the general statement and proof of a conjecture by SHANLEY (1946, 1947).

The situation can be seen more clearly when the solid is elastically isotropic and h/μ has the same value everywhere in the plastic zone. With the notation of Section 5, and supposing that $\Sigma < H_\infty$, (26) becomes

$$\frac{h}{2\mu} > \alpha \qquad \text{where} \qquad \alpha = \operatorname{Max} \left(\frac{\Sigma - H_0'}{H_\infty - \Sigma} \right) \qquad \text{in class } \mathbf{w}, \tag{28}$$

$$H_0'(\mathbf{w}) = H_\infty(\mathbf{w}) - \int 2\mu \, (\mathbf{n}\boldsymbol{\eta})^2 \, dV_p',$$

where V_p' is that part of the plastic zone where $\mathbf{n}\boldsymbol{\eta} > 0$. This formula differs from (17) in that H_0' replaces H_0. Since $H_0' \geqslant H_0$ for any one field, $\beta \geqslant \alpha$. The critical values α and β can have either sign or vanish.

In the case $\beta > \alpha > 0$, if the rate of hardening is progressively lowered, keeping everything else fixed, there is reached first the value β when uniqueness is no longer certain and afterwards the value α when instability first occurs. Thus, for certain processes of distortion, a point of bifurcation can be reached at an earlier stage than a failure of stability (supposing, naturally, that the rate of hardening diminishes with continued strain). Moreover, at such a stable bifurcation the loading must change with further deformation in such a way that

$$\int \dot{\mathbf{F}} \mathbf{v} \, dS = 2 \int E(\mathbf{v}) \, dV > 0$$

where $\mathbf{v}$ here denotes the velocity in any of the possible actual modes.

The given state may be such that there are special values of $h/2\mu$ (eigenvalues) for which deformation can proceed under temporarily constant loading (i.e. loosely speaking, through adjacent positions of equilibrium). Since $\int E\,dV$ then vanishes for the actual velocity field, no eigenvalue can exceed the stability limit α corresponding to the given state. On the other hand, although the stability limit is itself marked by the vanishing of $\int E\,dV$ for *some* field, there seems no reason why this should necessarily be an actual field under dead loading nor α an eigenvalue. This does not appear to have been envisaged in previous work, which has been concerned almost exclusively with determining neighbouring positions of equilibrium. We may contrast this possibility sharply with the behaviour of an elastic solid (at least in the classical linear theory) where, according to Rayleigh's Principle, the stability functional remains positive as the varied parameter ranges right up to the first eigenvalue.

8. Comparison with Rigid–Plastic Theory

Consider the limiting form of the previous theorems when the elastic moduli are indefinitely increased, the current stresses and rate of hardening being held fixed. $\boldsymbol{K}$ is now taken to be positive-definite.

In the uniqueness criterion (16) the functional Σ is independent of the moduli while the asymptotic form of H is

$$H(\mathbf{w}) \simeq H_0(\mathbf{w}) + \int h \left(\frac{\mathbf{n}K\boldsymbol{\eta}}{\mathbf{n}K\mathbf{n}}\right)^2 dV_p$$

since $\mathbf{n}\,K\,\mathbf{n}$ never vanishes. H_0 is never negative, by the Schwarz inequality, and vanishes only for incompressible $\mathbf{w}$ fields such that $\boldsymbol{\eta} = 0$ in the elastic zone and $\boldsymbol{\eta} \propto \mathbf{n}$ in the plastic zone (the proportionality factor being *arbtirary in sign* and magnitude). For these special fields

$$H(\mathbf{w}) \simeq \int h\eta^2\,dV$$

while for all others H_0 and H can be made arbitrarily large and positive by increasing the moduli. Consequently the sufficient condition for uniqueness approaches the requirement that

$$\int h\eta^2\,dV - \Sigma(\mathbf{w}) > 0$$

for all *special* $\mathbf{w}$ fields vanishing on S_v. In particular, when the solid is plastically isotropic, the principal axes of $\mathbf{n}$, $\boldsymbol{\sigma}$ and the special $\boldsymbol{\eta}$ coincide and Σ can be written more concisely as

$$\int \sigma_{ik} \frac{\partial w_j}{\partial x_i} \frac{\partial w_k}{\partial x_j}\,dV.$$

These are exactly the results obtained for a rigid–plastic solid, when it is treated purely on its own merits and not as a limiting case (HILL 1957a*); that is, from

*The restriction there to convex yield surfaces is in no way essential to the proof and could be dropped forthwith (other considerations apart). A slight modification would arise since the stress in the deformable zone need not then be determined uniquely by the current tractions on S_F and velocities on S_v. Similarly, in an elastic-plastic solid the state of stress approached asymptotically under constant surface traction and velocity need not be unique anywhere (contrast HILL 1956a, p. 72) but would depend on the initial stresses.

the outset ϵ is put zero in the elastic zone while (8) is replaced by $h\,\epsilon = (\mathbf{n}\,\dot{\sigma})\,\mathbf{n}$ in the plastic zone. There are no inverse relations such as (10), for which reason the boundary value problem uniquely determines the strain-rate only and not the stress-rate, unless $S_v = 0$ (cf. HILL 1956b, p. 248).

The general connexion could not indeed be regarded in advance as automatic, if only on the ground that a property possessed by all members of a limiting sequence need not be a property of the limit itself. Not only that, but the setting of the boundary-value problem itself for a rigid–plastic solid is different in that, if the existing stresses are regarded as given, the velocity can not be prescribed arbitrarily on S_v. Conversely, if we choose to regard the velocity on S_v as arbitrarily prescribed, the associated stress in the deformable zone is decided, at least when the yield surface is convex (HILL 1951); if the pre-existing stress were different it would change instantaneously to become consistent with the imposed velocities (cf. HILL 1950, pp. 58-9).

Consider, next, the functional (19) in the extremum principle. As the elastic moduli are increased, the value of the functional is unbounded except for incompressible fields $\mathbf{v}$ such that $\epsilon = 0$ in the elastic zone and $\epsilon \propto \mathbf{n}$ in the plastic zone, with a *non-negative* factor of proportionality, when its limiting value is

$$\int h\epsilon^2\,dV - \Sigma(\mathbf{v}) - 2\int \dot{\mathbf{F}}\mathbf{v}\,dS_F.$$

Only such special $\mathbf{v}$ fields satisfying the velocity boundary-conditions need be considered in the principle. These fields exist and are just the set of virtual modes for a rigid–plastic solid under the given surface tractions and velocities, provided the latter are consistent with the given internal stress. Just such a principle was proved by HILL (1957b) for a rigid–plastic solid treated on its merits. But the minimum is only analytic when the actual solution involves no unloading (*op. cit.*, p. 304); this is therefore an example of a property *not* shared by the two solids.

Consider, finally, the stability criterion (26). In the limit, as before, we need only consider the set of virtual modes for a rigid–plastic solid under the given loads and constraints, the functional becoming

$$\int h\epsilon^2\,dV - \Sigma(\mathbf{v}).$$

This agrees with the results obtained for a rigid–plastic solid treated on its merits (HILL 1957d). However, for an elastic–plastic solid the uniqueness and stability functionals differ but the classes of admissible fields are identical, while for a rigid-plastic solid the functionals are the same but the admissible classes differ.

REFERENCES

HILL, R.	1950	*Mathematical Theory of Plasticity* (Clarendon Press, Oxford).
	1951	*Phil. Mag.* **42**, 868.
	1956	*J. Mech. Phys. Solids* (a) **5**, 66; (b) **4**, 247.
	1957	*J. Mech. Phys. Solids* (a) **5**, 153; (b) **5**, 302; (c) **5**, 229; (d) **6**, 1.
MELAN, E.	1938	*Ing.-Archiv* **9**, 116.
SHANLEY, F. R.	1946	*J. Aero. Sci.* **13**, 678.
	1947	*J. Aero. Sci.* **14**, 261.

BOOK REVIEWS

Solid State Physics. Edited by F. SEITZ and D. TURNBULL. Vol. IV. Academic Books, London, 1957. 540 pp. 96s.

THE fourth volume in this valuable series follows the same pattern as its three predecessors, and contains five review articles on relatively unrelated topics in solid state physics. Two of these, *Ferroelectrics and Antiferroelectrics* by W. KÄNZER, and *Theory of Mobility of Electrons in Solids* by F. J. BLATT, are of considerable length, and might well have formed books on these important topics. In fact had they done so we would probably have had indexes – as it is, it is far from easy to refer back to topics touched upon in these reviews. Of the three remaining, two, *The Orthogonalised Plane-Wave Method* by T. O. WOODRUFF and *Techniques of Zone Melting and Crystal Growing* by W. G. PFANN, are of average length while the third, by R. S. KNOX, is a *Bibliography of Atomic Wave Functions* and is very short, being essentially a table, similar to that given earlier by PROFESSOR HARTREE, of references to all the computed atomic wave functions published before March, 1957.

The article on ferroelectrics and antiferroelectrics is a mine of information about the various properties of these substances, and will be invaluable. The method of presentation is to take each type of physical measurement separately, make a few general remarks and then describe in detail how the different types of ferro- and antiferroelectrics behave. This reader was fairly rapidly saturated with the wealth of information recorded, and would have welcomed some systematization within the framework of a fairly simple theory, though nothing along these lines seems to be available. The author indicates a number of directions in which further studies would be valuable, and one cannot help but feel that here is a wonderful field for the right theoretician.

The article on electrons in solids is mainly theoretical and is concerned with the use of the Boltzmann equation in transport problems in metals and semiconductors. The approach is to deal with the simplest cases first. This leads to a certain amount of duplication, since these can usually be studied as special cases of more complicated systems. Nevertheless the step-by-step treatment makes for easy assimilation and would seem on balance to be the best way of presenting this subject.

The description of the orthogonalized plane-wave method forms a very specialized article. This is a method which has been used by a number of workers to obtain information about the wave functions and energies of electrons in solids. However, when the accounts are published in the literature there is usually so much abbreviation that, although the general outline of the method is clear enough, it is often difficult to appreciate exactly what has had to be done. This article sets out to remedy this by describing in detail the various steps needed to use the method for silicon, so that apart from its general interest it should enable anyone contemplating such a calculation to see what is involved.

In the article on zone melting and crystal growing the attempt is made to describe in words what must surely be regarded as an art. However, it is an art that is widely practised and such a clear and interesting account of it will be most welcome, particularly as a number of valuable curves, such as those giving solute concentration against distance in zone length for different numbers of passes, are given. The article also contains descriptions of new methods, a particularly ingenious scheme being that devised for continuous zone refining.

This fourth volume entirely lives up to the standard set by the earlier volumes, both in the value of the subject matter reviewed and in its standard of presentation. Originally it was proposed that after the first few volumes the rate of production should drop to one volume per year. From the list of projected articles it might seem that so far little impression has been made on reviewing the whole field, for there are still forty-five articles to come. The editors have decided to continue publishing two volumes a year for some time longer !

K. W. H. STEVENS

J. C. JAEGER : **Elasticity, Fracture and Flow.** Methuen's Monographs on Physical Subjects, London, 1956. 152 + viii pp. 10s. 6d.

MANY books have appeared in recent years in the field covered by the title of this volume. It is relevant to enquire, therefore, whether the book fills a real need, either in the sense of presenting a new approach, or in covering in a significantly more satisfactory manner ground covered in other books. The author justifies his volumes as a presentation of the basic mathematics of the theories of elasticity, plasticity, viscosity and rheology, together with a discussion of the properties of the materials involved and the way in which they are idealized to form a basis for the mathematical theory. It is his intention that the book should not only be regarded as an introduction to more comprehensive mathematical works, but should help a larger class of readers who wish to gain an understanding of the basic mathematics and assumptions of the theories and their relation to actual materials, without themselves acquiring facility in the solution of specific problems.

The volume is divided into three chapters. The first, of 48 pages, gives a conventional analysis of stress and strain in two and three dimensions. Finite as well as infinitesimal strain is introduced. The second chapter of 58 pages discusses the behaviour of both real and idealized substances, noting the assumptions involved in the models used. A large variety of topics ranging from the elasticity of anisotropic substances to MOHR's theory of fracture and GRIFFITH cracks are treated in this chapter. The final 43 pages deals with equations of motion and equilibrium and contains illustrative examples.

Of the space specifically dealing with one of the theories discussed, rather more than a half is devoted to elasticity, with viscous flow and rheology having the least. It would be very easy and quite unfair to critize a volume of this kind for what it does not do. Clearly the author cannot be expected to compress the contents of several volumes into one of 152 pages and the selection of, and emphasis on material is partly a matter of individual interest. The reviewer feels that both in conception and execution the book is a worthwhile addition to the available literature and fully meets the objectives set out by the author. As a matter of personal preference the reviewer would have shifted the emphasis a little away from elasticity towards plasticity, since the former topic is much more fully covered in the literature than the latter.

The author is to be congratulated on the writing of this useful volume which will undoubtedly be of value and interest to students, teachers and research workers. The standards of printing and binding are high and the publishers deserve commendation for producing the volume at a price which should be well within the reach of the intended reader.

J. F. W. BISHOP

BOOKS RECEIVED

R. H. Griffith and J. D. F. Marsh : *Contact Catalysis.* (Clarendon Press : Oxford University Press, 1957). 299 pp., 50s.

P. Delahay : *Intrumental Analysis.* (MacMillan & Co., New York and London, 1957). 384 pp. 55s. 6d.

W. A. Wooster : *Experimental Crystal Physics.* (Oxford University Press, 1957). 115 pp., 18s.

R. Dugas : *History of Mechanics.* (Routledge and Kegan Paul, 1957). 771 pp., 100s.

F. Seitz and D. Turnbull (*Eds.*) : *Solid State Physics* - v. *Advances in Research and Applications.* (Academic Press Inc., 1957). 455 pp., $11.00.

PAPERS TO BE PUBLISHED IN FUTURE ISSUES

J. E. Adkins : *A reciprocal property of the finite plainstrain equations.*

J. B. Hunt : *Fracture mechanism of semi-brittle steels in torsion.*

L. Fleischer : *Single crystal lattice rotation during compression.*

L. Fleischer and B. Chalmers : *Grip effects in the deformation of single crystals.*

J. P. Ellington : *An investigation of plastic stress-strain relationships using grooved tensile specimens.*

J. S. Ellis : *Plastic behaviour of compression members.*

H. Payne, S. J. Czyzak, J. H. Greiner and T. H. Lin : *A modification of Taylor's method for calculating the plastic stress-strain relation in face-centred cubic crystals.*

E. I. Grijoljuk : *Buckling of sandwich constructions beyond the elastic limit.*

W. Johnson : *Experiments in the cold extrusion of rods of non-circular section.*

Journal of the Mechanics and Physics of Solids, 1958, Vol. 6, pp. 253 to 266. Pergamon Press Ltd., London

BUCKLING OF SANDWICH CONSTRUCTIONS BEYOND THE ELASTIC LIMIT

By E. I. Grigoljuk
Institute of Mechanics, Academy of Sciences of U.S.S.R.

(*Received* 10*th January*, 1958)

Summary

The stability of elastic–plastic sandwich shells of an arbitrary shape is investigated on the assumption that, at the moment of buckling, the load-carrying faces are in a fully plastic state and the core remains elastic. The equations are obtained on the basis of both the deformation theory and the plastic flow theory. The flexural stiffness of the faces is taken into account. The equations obtained permit the prediction of the critical loads of columns, plates, and shells of arbitrary form.

1. Previous Investigations

An analysis of the stability of sandwich structural elements has been presented only in a limited number of papers, which are primarily related to the analysis of rectangular plates.

Columns. The first attempt to analyse the stability of sandwich columns under centrally axial compression is contained in the paper by Troxell and Engel (1947). For determining the critical load of a simply supported column with a core resisting only transverse shear, and faces whose own bending rigidity can be neglected, use is made of the Engesser formula (1891) which evaluates the effect of transverse shear on the critical stress of the column :

$$P_{cr} = \frac{P_E}{1 + P_E/G_c F}$$

where

$$P_E = \frac{\pi^2 EI}{l^2}, \qquad P_{cr} = 2\sigma bt, \qquad I = \tfrac{1}{2} t (c + t)^2, \qquad F = bc$$

E is the Young's modulus of the load-carrying face material ; G_c the shear modulus of the core material ; b, l the column width and length, respectively ; t, c the face sheet thickness and core thickness, respectively.

At stresses above the elastic limit the authors recommended replacing E by the tangent modulus E', the relation of slenderness ratio and stress being assumed to be linear :

$$E' = \frac{27}{4} \frac{\sigma (\sigma_0 - \sigma)^2}{\sigma_0^3} E$$

where σ_0 is the failing stress.

NORRIS and KOMMERS (1950) have presented curves of critical stress as a function of the ratio of face and core thickness (honeycomb core, dural faces).

Unnecessary simplification of the plastic buckling analysis is contained in the paper by FLÜGGE (1952), who for determining the optimum column dimensions assumes stress to be constant.

Plates. The author is aware of only those publications which are related to the analysis of rectangular plates. In the first of these, NORRIS (1948) investigated the stability of a rectangular plate in compression and introduced a double or reduced modulus

$$E_{red} = \frac{2EE'}{E + E'},$$

obtained for an ideal I section with an infinitely thin web and identical flanges, the cross-sectional areas being concentrated in the centroid.

All the subsequent papers that will be discussed here are based on the assumption that strains are fully plastic at the moment of buckling. It is usually supposed that faces and core are orthotropic, the flexural stiffness of the faces is negligibly small, the core is always elastic and resists only transverse shear, shearing deformations are distributed uniformly across the thickness of the core, and the core is attached to the middle surfaces of the faces.

SEIDE and STOWELL (1950) treated the stability of a rectangular plate under compression in one direction by using the LIBOVE and BATDORF (1948) relationships, where the bending curvatures κ_1, κ_2 and twisting curvature κ_{12} are defined on the assumption that plane sections remain plane under transverse shear:

$$\kappa_1 = \left(w_x - \frac{Q_1}{d_{13}}\right)_x, \qquad \kappa_2 = \left(w_y - \frac{Q_2}{d_{23}}\right)_y, \qquad \kappa_{12} = \tfrac{1}{2}\left[\left(w_x - \frac{Q_1}{d_{13}}\right)_y + \left(w_y - \frac{Q_2}{d_{23}}\right)_x\right]$$

where w is the deflection, Q_1, Q_2 are the transverse forces, d_{13}, d_{23} are the core shear stiffnesses, and x, y are the orthogonal coordinates.

The relationship between bending δM_1, δM_2 and twisting δH moments and curvatures is accepted as

$$\delta M_1 = -d_{11}\kappa_1 - d_{12}\kappa_2, \qquad \delta M_2 = -d_{21}\kappa_1 - d_{22}\kappa_2, \qquad \delta H = -d_{33}\kappa_{12}.$$

Here d_{11}, $d_{12} = d_{21}$, d_{22}, d_{33} are stiffnesses that can be obtained either experimentally from flexural and torsion tests or from the schematised representation of the deformation of a plate. Under the foregoing assumptions in the elastic buckling problem (with ν = Poisson's ratio for the face material, and G_c = shear modulus of the core material),

$$d_{11} = d_{22} = D = \frac{Et\,(c+t)^2}{2\,(1-\nu^2)}, \qquad d_{12} = d_{21} = \nu D,$$

$$d_{13} = d_{23} = cG_c, \qquad d_{33} = (1-\nu)\,D,$$

whereas for a fully plastic state of the incompressible face material under uniaxial compression the following expressions are obtained either in the elastic or in the plastic range, by use of the deformation (total strain) theory:

$$d_{11} = \tfrac{1}{6}E_s t\,(c+t)^2\,(1 + 3\,E'/E_s), \qquad d_{12} = d_{21} = d_{33} = \tfrac{1}{2}\,d_{22} = \tfrac{1}{3}E_s t\,(c+t)^2,$$

where E_s is the secant modulus. The core shear stiffness remains unchanged since stresses in the core are assumed not to exceed the elastic limit.

By adding to the foregoing relations the equations of neutral equilibrium (with N_1, N_2 and T as the middle surface forces)

$$(\delta M_1)_{xx} + 2(\delta H)_{xy} + (\delta M_2)_{yy} - N_1 w_{xx} - N_2 w_{yy} - 2T w_{xy} = 0$$

$$\delta Q_1 - (\delta H)_y - (\delta M_1)_x = 0, \qquad \delta Q_2 - (\delta H)_x - (\delta M_2)_y = 0,$$

one can obtain three equations for w, δQ_1, δQ_2, which in the case of simply supported edges are satisfied by the following expressions :

$$w = w_0 \sin \frac{m\pi x}{a} \sin \frac{n\pi y}{b}, \qquad \delta Q_1 = \delta Q_{10} \cos \frac{m\pi x}{a} \sin \frac{n\pi y}{b},$$

$$\delta Q_2 = \delta Q_{20} \sin \frac{m\pi x}{a} \cos \frac{n\pi y}{b}.$$

Here w_0, δQ_{10}, δQ_{20} are constant ; a, b are the plate dimensions in the plane ; m and n are the numbers of halfwaves in the buckled plate in the direction of the x- and y axes.

In treating the elastic stability problem the authors used essentially Reissner's equations (1948), to which the equations of Libove and Batdorf (1948) can be shown to reduce under the foregoing hypotheses.

It should be pointed out that the form of the relationships between moments and curvatures similar to that accepted in elastic problems cannot be regarded as reasonable for investigating the buckling of elastic-plastic plates, since in this case both the bending and twisting moments are defined by the bending curvatures as well as the twisting curvature of the plate surface.

Elastic compressibility may be taken into account as follows. The ratio of the elastic buckling stresses and stresses at the moment of buckling in the elastic–plastic range is assumed to be independent of Poisson's ratio. Then the buckling stress beyond the elastic limit, corrected for elastic compressibility, is equal to the buckling stress computed for a given Poisson's ratio by the use of the elastic stability formula, multiplied by a constant factor. The latter equals the ratio of the inelastic buckling stress to the elastic buckling stress calculated for $\nu = \frac{1}{2}$.

The computed buckling stresses of Seide and Stowell (1950) are found to be in satisfactory agreement with the experimental results reported by Boller (1947) (dural faces, cork-tree core).

Further, Seide (1949a) treated the shear buckling of an infinitely-long simply-supported rectangular plate, and also of a rectangular plate with two opposite edges clamped and two others simply supported under uniform compression in one direction (1949b, 1952). A comparison of Seide's theory and experimental data for plates having dural faces and a cellular cellulose acetate core (1949b, 1952) indicates considerably better agreement than in the case of end-grain-balsa cores.

Bijlaard (1949, 1950, 1951) gave an approximate method (called by him ' method of split rigidities ') for determining the critical loads of sandwich plates

supported along the loaded edges. By assuming that the deflection surfaces of homogeneous and sandwich plates are geometrically similar, the elastic buckling load of sandwich plates may be expressed as

$$P_{cr} = P_0 + P_1 P_2/(P_1 + P_2)$$

where P_0 is the buckling load of faces working independently, P_1 is the buckling load of a sandwich plate having infinite core shear rigidity and, P_2 is the buckling load of a sandwich plate when core shear rigidity is taken into account and the faces are inextensible and have zero flexural rigidity. Beyond the elastic limit the forces P_0 and P_1 are multiplied by a certain factor.

The method of split rigidities, though not universal, permits consideration of a number of special problems. Solutions for these are presented by BIJLAARD (1950, 1951). As a rule, this method gives buckling loads lower than those computed exactly, though in some cases, as follows from a comparison with the solution presented by SEIDE (1949) for the problem of the compressive buckling of a rectangular plate with two simply supported loaded edges and clamped unloaded edges, in a certain range it gives higher buckling loads than the theoretical ones.

KUENZI and ERICKSEN (1951) investigated the shear stability of simply supported and clamped sandwich plates beyond the elastic limit.

Cylindrical shell. ERINGEN (1956) using formulae of his previous paper (1951) plotted the curves of the buckling stresses of sandwich cylinders under uniform axial compressive load for ripple type of buckling with both faces deformed in the same direction, and also in the opposite direction (dural faces, cellular cellulose acetate core). The stresses are corrected for the effects of plasticity by replacing the Young's modulus by the reduced modulus, on the assumption that the material is incompressible and a part of the shell unloads across its thickness during buckling and assuming a fictitious idea about the work of the face material.

2. FORMULATION OF THE PROBLEM

Let us consider the inelastic stability of a shallow shell type of sandwich construction with a lightweight core. The faces and core are assumed to be isotropic and homogeneous. Suppose that the Kirchhoff–Love hypotheses hold for the faces and that the variation of displacements across the thickness of the core is linear. The core has ability to resist only transverse shear. The thicknesses of the face sheets are constant and equal; the mechanical properties of the upper and lower faces are also identical. A small-deflection theory of buckling will be considered.

Assume that any element of the faces is in a fully plastic state. With regard to the plastic stress–strain relations we proceed both from the deformation (total strain) theory and the flow (incremental strain) theory. The relationships derived are equally valid for both theories.

In the present paper use is made of some results previously obtained by the author (1957a, b).

3. Relations Between Variations of Stresses and Strains Beyond the Elastic Limit

It was shown by the author (1957b) that the variations of the stresses $\delta\sigma_x$, $\delta\sigma_y$, $\delta\tau_{xy}$ and strains $\delta\epsilon_x$, $\delta\epsilon_y$, $\delta\gamma_{xy}$ in any surface of a shell are related by

$$\left.\begin{aligned} t\delta\sigma_x &= b_{11}\,\delta\epsilon_x + b_{12}\,\delta\epsilon_y - b_{13}\,\delta\gamma_{xy} \\ t\delta\sigma_y &= b_{21}\,\delta\epsilon_x + b_{22}\,\delta\epsilon_y - b_{23}\,\delta\gamma_{xy} \\ t\delta\tau_{xy} &= -\,b_{31}\,\delta\epsilon_x - b_{32}\,\delta\epsilon_y + b_{33}\,\delta\gamma_{xy} \end{aligned}\right\} \tag{3.1}$$

where the coefficients b_{11}, $b_{12} = b_{21}$, b_{22}, $b_{13} = b_{31}$, $b_{23} = b_{32}$, b_{33} depend on the mechanical properties of the material, on the state of stress before buckling and on the kind of theory of plasticity used.

According to the Prandtl–Reuss (flow) theory,

$$\left.\begin{aligned} b_{11} &= A\left[2(1+\nu) + \tfrac{1}{2}\phi\,\frac{(1+\nu)(\sigma_y-\sigma_x)^2 + 18\tau^2_{xy}}{\sigma_i^2}\right] \\ b_{12} = b_{21} &= A\left[2\nu(1+\nu) + \tfrac{1}{2}\phi\,\frac{(1+\nu)(2\sigma_y-\sigma_x)(\sigma_y-2\sigma_x) + 18\nu\tau^2_{xy}}{\sigma_i^2}\right] \\ b_{13} = b_{31} &= \tfrac{3}{2}A\phi\,\frac{(2-\nu)\sigma_x - (1-2\nu)\sigma_y}{\sigma_i^2}\,\tau_{xy} \\ b_{22} &= A\left[2(1+\nu) + \tfrac{1}{2}\phi\,\frac{(1+\nu)(2\sigma_x-\sigma_y)^2 + 18\tau^2_{xy}}{\sigma_i^2}\right] \\ b_{23} = b_{32} &= \tfrac{3}{2}A\phi\,\frac{(2-\nu)\sigma_y - (1-2\nu)\sigma_x}{\sigma_i^2}\,\tau_{xy} \\ b_{33} &= A\left[1-\nu^2 + \tfrac{1}{4}\phi\,\frac{(5-4\nu)(\sigma^2_x+\sigma^2_y) - 2(4-5\nu)\sigma_x\sigma_y}{\sigma_i^2}\right] \end{aligned}\right\} \tag{3.2}$$

where

$$\left.\begin{aligned} &\sigma_i = \sqrt{\sigma^2_x - \sigma_x\sigma_y + \sigma^2_y + 3\tau^2_{xy}}, \qquad \phi = \frac{E}{E'} - 1, \\ &A = \tfrac{1}{2}\frac{Et}{1+\nu}\left[1-\nu^2 + \right. \\ &\qquad \left. \tfrac{1}{4}\phi\,\frac{(5-4\nu)(\sigma^2_x+\sigma^2_y) - 2(4-5\nu)\sigma_x\sigma_y + 18(1-\nu)\tau^2_{xy}}{\sigma_i^2}\right]. \end{aligned}\right\} \tag{3.3}$$

Here σ_x, σ_y, τ_{xy} are the membrane stresses before buckling.

According to the Hencky (deformation) theory,

$$\left.\begin{aligned} b_{11} = A\Bigg\{ &3\frac{E'}{E_s} - (1-2\nu)\frac{E'}{E} \\ &+ \frac{1}{\sigma_i^2}\left(1-\frac{E'}{E_s}\right)\left[\left(3 - \frac{1-2\nu}{E}E_s\right)(\sigma_y - \tfrac{1}{2}\sigma_x)^2 + 9\tau^2_{xy}\right]\Bigg\} \end{aligned}\right.$$

$$
\left.\begin{aligned}
b_{12} = b_{21} &= A\left\{\tfrac{1}{2}\left(3\frac{E'}{E_s} - \frac{1-2\nu}{E}E'\right)\left(1 - \frac{1-2\nu}{E}E_s\right) - \frac{1}{\sigma^2_i}\left(1 - \frac{E'}{E_s}\right)\times\right. \\
&\left.\times\left[\left(3 - \frac{1-2\nu}{E}E_s\right)(\sigma_y - \tfrac{1}{2}\sigma_x)(\sigma_x - \tfrac{1}{2}\sigma_y) - \tfrac{9}{2}\left(1 - \frac{1-2\nu}{E}E_s\right)\tau^2_{xy}\right]\right\} \\
b_{13} = b_{31} &= \tfrac{3}{2}A\frac{1}{\sigma^2_i}\left(1 - \frac{E'}{E_s}\right)\left[\tfrac{3}{2}\sigma_x - \frac{1-2\nu}{E}E_s(\sigma_y - \tfrac{1}{2}\sigma_x)\right]\tau_{xy} \\
b_{22} &= A\left\{3\frac{E'}{E_s} - \frac{1-2\nu}{E}E'\right. \\
&\left.+ \frac{1}{\sigma^2_i}\left(1 - \frac{E'}{E_s}\right)\left[\left(3 - \frac{1-2\nu}{E}E_s\right)(\sigma_x - \tfrac{1}{2}\sigma_y)^2 + 9\tau^2_{xy}\right]\right\} \\
b_{23} = b_{32} &= \tfrac{3}{2}A\frac{1}{\sigma^2_i}\left(1 - \frac{E'}{E_s}\right)\left[\tfrac{3}{2}\sigma_y - \frac{1-2\nu}{E}E_s(\sigma_x - \tfrac{1}{2}\sigma_y)\right]\tau_{xy} \\
b_{33} &= A\left\{\tfrac{1}{4}\left[3 + 2\frac{1-2\nu}{E}E' - \frac{(1-2\nu)^2}{E^2}E'E_s\right] -\right. \\
&\left.-\frac{1}{\sigma^2_i}\left(1 - \frac{E'}{E_s}\right)\left[\frac{1-2\nu}{E}E_s(\sigma_x - \tfrac{1}{2}\sigma_y)(\sigma_y - \tfrac{1}{2}\sigma_x) + \tfrac{9}{4}\tau^2_{xy}\right]\right\}
\end{aligned}\right\} \quad (3.4)
$$

where

$$
A = Et\left(3 - \frac{1-2\nu}{E}E_s\right)^{-1}\left\{\tfrac{1}{4}\left[3\frac{E}{E_s} + 2\frac{1-2\nu}{E_s}E' - \frac{(1-2\nu)^2}{E}E'\right] -\right.
$$
$$
\left.- \frac{1-2\nu}{\sigma^2_i}\left(1 - \frac{E'}{E_s}\right)\left[(\sigma_x - \tfrac{1}{2}\sigma_y)(\sigma_y - \tfrac{1}{2}\sigma_x) - \tfrac{9}{4}\tau^2_{xy}\right]\right\} \quad (3.5)
$$

For $\nu = \frac{1}{2}$ expressions (3.2) and (3.4) give the values of the coefficients for incompressible material.

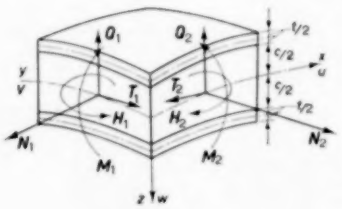

Fig. 1.

4. Relations Between Variations of Forces and Moments in the Shell and Displacements Due to Buckling

Introduce forces and moments per unit length of the middle line of the corresponding shell cross section. The forces and moments in the faces are indicated in Fig. 1. For the entire cross section

$$
\left.\begin{aligned}
\delta N_1 &= \delta N_{11} + \delta N_{12}, & \delta N_2 &= \delta N_{21} + \delta N_{22}, \\
\delta M_1 &= \delta M_{11} + \delta M_{12}, & \delta M_2 &= \delta M_{21} + \delta M_{22}, \\
\delta T &= \delta T_1 + \delta T_2, & \delta H &= \delta H_1 + \delta H_2,
\end{aligned}\right\} \quad (4.1)
$$

where

$$\left.\begin{aligned}
\delta N_{11} &= \int_{\frac{1}{2}c}^{\frac{1}{2}c+t} \delta\sigma_x\,dz, \qquad \delta N_{12} = \int_{-\frac{1}{2}c-t}^{-\frac{1}{2}c} \delta\sigma_x\,dz,\\
\delta N_{21} &= \int_{\frac{1}{2}c}^{\frac{1}{2}c+t} \delta\sigma_y\,dz, \qquad \delta N_{22} = \int_{-\frac{1}{2}c-t}^{-\frac{1}{2}c} \delta\sigma_y\,dz,\\
\delta M_{11} &= -\int_{\frac{1}{2}c}^{\frac{1}{2}c+t} \delta\sigma_x\,z\,dz, \qquad \delta M_{12} = -\int_{-\frac{1}{2}c-t}^{-\frac{1}{2}c} \delta\sigma_x\,z\,dz,\\
\delta M_{21} &= -\int_{\frac{1}{2}c}^{\frac{1}{2}c+t} \delta\sigma_y\,z\,dz, \qquad \delta M_{22} = -\int_{-\frac{1}{2}c-t}^{-\frac{1}{2}c} \delta\sigma_y\,z\,dz,\\
\delta T_1 &= \int_{\frac{1}{2}c}^{\frac{1}{2}c+t} \delta\tau_{xy}\,dz, \qquad \delta T_2 = \int_{-\frac{1}{2}c-t}^{-\frac{1}{2}c} \delta\tau_{xy}\,dz,\\
\delta H_1 &= -\int_{\frac{1}{2}c}^{\frac{1}{2}c+t} \delta\tau_{xy}\,z\,dz, \qquad \delta H_2 = -\int_{-\frac{1}{2}c-t}^{-\frac{1}{2}c} \delta\tau_{xy}\,z\,dz.
\end{aligned}\right\} \tag{4.2}$$

By means of the assumptions that any line in the faces that is initially straight and normal to the middle line of the faces will remain straight after deformation and normal to the deformed middle line, and that the variation of displacements across the thickness of the core is linear, the following expressions are derived for the displacements u and v due to buckling, in the directions parallel to the x- and y axes, in a surface that is at a distance z from the middle surface of the entire shell (Fig. 2).

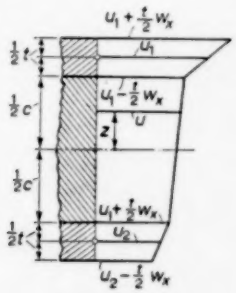

Fig. 2.

(a) Upper face sheet ($\frac{1}{2}c \leqslant z \leqslant \frac{1}{2}c + t$):

$$u = u_1 + (z - \tfrac{1}{2}(c + t))\,w_x, \qquad v = v_1 + (z - \tfrac{1}{2}(c + t))\,w_y. \tag{4.3}$$

(b) Core ($-\frac{1}{2}c \leqslant z \leqslant \frac{1}{2}c$):

$$u = \frac{u_1 + u_2}{2} + \frac{z}{c}(u_1 - u_2 - tw_x), \qquad v = \frac{v_1 + v_2}{2} + \frac{z}{c}(v_1 - v_2 - tw_y) \tag{4.4}$$

(c) **Lower face sheet** $(-\frac{1}{2}c - t \leqslant z \leqslant -\frac{1}{2}c)$:

$$u = u_2 + (z + \tfrac{1}{2}(c + t))\, w_x, \qquad v = v_2 + (z + \tfrac{1}{2}(c + t))\, w_y. \tag{4.5}$$

Here u_1 and v_1, u_2 and v_2 are the middle-surface displacements in the upper and lower faces, respectively, w is the deflection due to buckling, and z is the coordinate across the thickness of the shell.

The variations of strains are

(a) **Faces**:

$$\delta\epsilon_x = u_x - \frac{w}{R_1}, \qquad \delta\epsilon_y = v_y - \frac{w}{R_2}, \qquad \delta\gamma_{xy} = v_x + u_y, \tag{4.6}$$

where R_1, R_2 are the principal radii of the middle surface of the shell.

(b) **Core**:

$$\delta\gamma_{xz} = u_z - w_x, \qquad \delta\gamma_{yz} = v_z - w_y \tag{4.7}$$

Add Hooke's law to the last two relations:

$$\delta\tau_{xz} = G_c\, \delta\gamma_{xz}, \qquad \delta\tau_{yz} = G_c\, \delta\gamma_{yz}. \tag{4.8}$$

The substitution of (3.1) into (4.2) with consideration of (4.3), (4.5) and (4.6), yields

$$\left.\begin{aligned}
\delta N_{11} &= b_{11}\, u_{1x} - b_{13}\, u_{1y} + b_{12}\, v_{1y} - b_{13}\, v_{1x} - \left(\frac{b_{11}}{R_1} + \frac{b_{12}}{R_2}\right) w,\\
\delta N_{12} &= b_{11}\, u_{2x} - b_{13}\, u_{2y} + b_{12}\, v_{1y} - b_{13}\, v_{1x} - \left(\frac{b_{11}}{R_1} + \frac{b_{22}}{R_2}\right) w,\\
\delta N_{21} &= b_{21}\, u_{1x} - b_{23}\, u_{1y} + b_{22}\, v_{1y} - b_{13}\, v_{1x} - \left(\frac{b_{21}}{R_1} + \frac{b_{22}}{R_2}\right) w,\\
\delta N_{22} &= b_{21}\, u_{2x} - b_{23}\, u_{2y} + b_{22}\, v_{2y} - b_{23}\, v_{2x} - \left(\frac{b_{21}}{R_1} + \frac{b_{22}}{R_2}\right) w,\\
\delta T_1 &= -b_{31}\, u_{1x} + b_{33}\, u_{1y} - b_{32}\, v_{1y} + b_{33}\, v_{1x} + \left(\frac{b_{31}}{R_1} + \frac{b_{32}}{R_2}\right) w,\\
\delta T_2 &= -b_{31}\, u_{2x} + b_{33}\, u_{2y} - b_{32}\, v_{2y} + b_{33}\, v_{2x} + \left(\frac{b_{31}}{R_1} + \frac{b_{32}}{R_2}\right) w,\\
\delta M_{11} &= -\frac{c + t}{2}\left[b_{11}\, u_{1x} - b_{13}\, u_{1y} + b_{12}\, v_{1y} - b_{13}\, v_{1x} - \left(\frac{b_{11}}{R_1} + \frac{b_{12}}{R_2}\right) w\right] -\\
&\quad - \frac{t^2}{12}\,(b_{11}\, w_{xx} + b_{12}\, w_{yy} - 2b_{13}\, w_{xy})\\
\delta M_{12} &= \frac{c + t}{2}\left[b_{11}\, u_{2x} - b_{13}\, u_{2y} + b_{12}\, v_{2y} - b_{13}\, v_{2x} - \left(\frac{b_{11}}{R_1} + \frac{b_{12}}{R_2}\right) w\right] -\\
&\quad - \frac{t^2}{12}\,(b_{11}\, w_{xx} + b_{12}\, w_{yy} - 2b_{13}\, w_{xy})\\
\delta M_{21} &= -\frac{c + t}{2}\left[b_{21}\, u_{1x} - b_{23}\, u_{1y} + b_{22}\, v_{1y} - b_{23}\, v_{1x} - \left(\frac{b_{21}}{R_1} + \frac{b_{22}}{R_2}\right) w\right] -\\
&\quad - \frac{t^2}{12}\,(b_{21}\, w_{xx} + b_{22}\, w_{yy} - 2b_{23}\, w_{xy})
\end{aligned}\right\} \tag{4.9}$$

$$\delta M_{22} = \frac{c+t}{2}\left[b_{21}\,u_{2x} - b_{23}\,u_{2y} + b_{22}\,v_{2y} - b_{23}\,v_{2x} - \left(\frac{b_{21}}{R_1} + \frac{b_{22}}{R_2}\right) w\right] -$$

$$- \frac{t^2}{12}\,(b_{21}\,w_{xx} + b_{22}\,w_{yy} - 2b_{23}\,w_{xy})$$

$$\delta H_1 = -\frac{c+t}{2}\left[-b_{31}\,u_{1x} + b_{33}\,u_{1y} - b_{32}\,v_{1y} + b_{33}\,v_{1x} + \left(\frac{b_{31}}{R_1} + \frac{b_{32}}{R_2}\right) w\right] +$$

$$+ \frac{t^2}{12}\,(b_{31}\,w_{xx} + b_{32}\,w_{yy} - 2b_{33}\,w_{xy})$$

$$\delta H_2 = \frac{c+t}{2}\left[-b_{31}\,u_{2x} + b_{33}\,u_{2y} - b_{32}\,v_{2y} + b_{33}\,v_{2x} + \left(\frac{b_{31}}{R_1} + \frac{b_{32}}{R_2}\right) w\right] +$$

$$+ \frac{t^2}{12}\,(b_{31}\,w_{xx} + b_{32}\,w_{yy} - 2b_{33}\,w_{xy})$$

Introduce new variables (Reissner 1950):

$$U = \frac{u_1 + u_2}{2}, \qquad V = \frac{v_1 + v_2}{2}, \qquad \alpha = \frac{u_1 - u_2}{c+t}, \qquad \beta = \frac{v_1 - v_2}{c+t}. \tag{4.10}$$

From (4.1) and (4.9) it follows that

$$\begin{aligned}
\delta N_1 &= 2b_{11}\,U_x + 2b_{12}\,V_y - 2b_{13}\,(U_y + V_x) - 2\left(\frac{b_{11}}{R_1} + \frac{b_{12}}{R_2}\right) w \\
\delta N_2 &= 2b_{21}\,U_x + 2b_{22}\,V_y - 2b_{23}\,(U_y + V_x) - 2\left(\frac{b_{21}}{R_1} + \frac{b_{22}}{R_2}\right) w \\
\delta T &= -2b_{31}\,U_x - 2b_{32}\,V_y + 2b_{33}\,(U_y + V_x) + 2\left(\frac{b_{31}}{R_1} + \frac{b_{32}}{R_2}\right) w \\
\delta M_1 &= -\frac{(c+t)^2}{2}\,[b_{11}\,\alpha_x + b_{12}\,\beta_y - b_{13}\,(\alpha_y + \beta_x)] - \frac{t^2}{6}\,(b_{11}\,w_{xx} + b_{12}\,w_{yy} - 2b_{13}\,w_{xy}) \\
\delta M_2 &= -\frac{(c+t)^2}{2}\,[b_{21}\,\alpha_x + b_{22}\,\beta_y - b_{23}\,(\alpha_y + \beta_x)] - \frac{t^2}{6}\,(b_{21}\,w_{xx} + b_{22}\,w_{yy} - 2b_{23}\,w_{xy}) \\
\delta H &= -\frac{(c+t)^2}{2}\,[-b_{31}\,\alpha_x - b_{32}\,\beta_y + b_{33}\,(\alpha_y + \beta_x)] + \frac{t^2}{6}\,(b_{31}\,w_{xx} + b_{32} w_{yy} - 2b_{33}\,w_{xy})
\end{aligned} \tag{4.11}$$

Let us introduce the following notations:

$$\delta m^*_1 = (\delta N_{11} - \delta N_{12})\,\frac{c+t}{2}, \qquad \delta m^*_2 = (\delta N_{21} - \delta N_{22})\,\frac{c+t}{2},$$

$$\delta m^*_{12} = (\delta T_1 - \delta T_2)\,\frac{c+t}{2}. \tag{4.12}$$

By substituting the first six equations of (4.9) into (4.12):

$$\delta m^*_1 = \frac{(c+t)^2}{2}\,[b_{11}\,\alpha_x + b_{12}\,\beta_y - b_{13}\,(\alpha_y + \beta_x)]$$

$$\left.\begin{aligned}\delta m^*_2 &= \frac{(c+t)^2}{2}\left[b_{21}\,\varkappa_x + b_{22}\,\beta_y - b_{23}\,(\varkappa_y + \beta_x)\right]\\ \delta m^*_{12} &= \frac{(c+t)^2}{2}\left[-b_{31}\,\varkappa_x - b_{32}\,\beta_y + b_{33}\,(\varkappa_y + \beta_x)\right].\end{aligned}\right\} \tag{4.13}$$

For the core

$$\delta\tau_{xz} = \frac{c+t}{c}\,G_c\,(\varkappa - w_x), \qquad \delta\tau_{yz} = \frac{c+t}{c}\,G_c\,(\beta - w_y). \tag{4.14}$$

5. Equations of Neutral Equilibrium and of Compatibility

By use of the results obtained by the author (1957a) the equations of neutral equilibrium may be written as

$$\left.\begin{aligned}&(\delta N_1)_x + (\delta T)_y = 0, \qquad (\delta N_2)_y + (\delta T)_x = 0,\\ &(\delta m^*_1)_x + (\delta m^*_{12})_y - \frac{(c+t)^2}{c}\,G_c\,(\varkappa - w_x) = 0,\\ &(\delta m^*_2)_y + (\delta m^*_{12})_x - \frac{(c+t)^2}{c}\,G_c\,(\beta - w_y) = 0,\\ &(\delta M_1)_{xx} + 2\,(\delta H)_{xy} + (\delta M_2)_{yy} + \frac{\delta N_1}{R_1} + \frac{\delta N_2}{R_2} +\\ &\qquad + N_1\,w_{xx} + N_2\,w_{yy} + 2T w_{xy} = 0,\end{aligned}\right\} \tag{5.1}$$

where $N_1 = 2\sigma_x t$, $N_2 = 2\sigma_y t$, $T = 2\tau_{xy} t$ are the forces in a sandwich shell, corresponding to its membrane state.

The compatibility equation is derived by eliminating displacements u and v from (4.6):

$$\left(\frac{\delta\epsilon_{x1} + \delta\epsilon_{x2}}{2}\right)_{yy} + \left(\frac{\delta\epsilon_{y1} + \delta\epsilon_{y2}}{2}\right)_{xx} - \left(\frac{\delta\gamma_{xy1} + \delta\gamma_{xy2}}{2}\right)_{xy} + \frac{w_{yy}}{R_1} + \frac{w_{xx}}{R_2} = 0. \tag{5.2}$$

The subscripts 1 and 2 refer to the middle surface of the upper and lower faces, respectively.

The first two equations of (5.1) are satisfied by the force function F

$$\delta N_1 = F_{yy}, \qquad \delta N_2 = F_{xx}, \qquad \delta T = -F_{xy}. \tag{5.3}$$

From the first three equations of (4.11)

$$\delta\epsilon_{x1} + \delta\epsilon_{x2}, \qquad \delta\epsilon_{y1} + \delta\epsilon_{y2}, \qquad \delta\gamma_{xy1} + \delta\gamma_{xy2}$$

may be expressed in terms of the force function F:

$$\left.\begin{aligned}\delta\epsilon_{x1} + \delta\epsilon_{x2} &= A_{11}\,F_{yy} + A_{12}\,F_{xx} + A_{13}\,F_{xy}\\ \delta\epsilon_{y1} + \delta\epsilon_{y2} &= A_{21}\,F_{yy} + A_{22}\,F_{xx} + A_{23}\,F_{xy}\\ \delta\gamma_{xy1} + \delta\gamma_{xy2} &= A_{31}\,F_{yy} + A_{32}\,F_{xx} + A_{33}\,F_{xy}\end{aligned}\right\} \tag{5.4}$$

where

$$\left.\begin{aligned}A_{11} &= \frac{b_{22}\,b_{33} - b^2_{23}}{\Delta}, \quad A_{12} = A_{21} = \frac{b_{13}\,b_{23} - b_{12}\,b_{33}}{\Delta}, \quad A_{13} = -A_{31} = \frac{b_{12}\,b_{23} - b_{13}\,b_{22}}{\Delta},\\ A_{22} &= \frac{b_{11}\,b_{33} - b^2_{13}}{\Delta}, \quad A_{23} = -A_{32} = \frac{b_{12}\,b_{13} - b_{11}\,b_{23}}{\Delta}, \quad A_{33} = \frac{b^2_{12} - b_{11}\,b_{22}}{\Delta},\end{aligned}\right\} \tag{5.5}$$

and

$$\Delta = b_{11}\,b_{22}\,b_{33} - b^2_{12}\,b_{33} - b_{11}\,b^2_{23} + 2b_{12}\,b_{13}\,b_{23} - b^2_{13}\,b_{22}. \tag{5.6}$$

6. Stability Equation

Substitute (4.13) into the third and fourth of equations (5.1) ; (5.3) and the last three relations of (4.11) into the last of equations (5.1) ; relations (5.4) into (5.2). We obtain a set of four equations for the deflection w, the force function F, and relative angular displacements α and β to analyse the stability of an elastic–plastic sandwich shell of arbitrary shape under small deflections :

$$b_{11}\,\alpha_{xx} - 2b_{13}\,\alpha_{xy} + b_{33}\,\alpha_{yy} - b_{13}\,\beta_{xx} + (b_{12} + b_{33})\,\beta_{xy} - b_{32}\,\beta_{yy} - \frac{2}{c}\,G_c\,(\alpha - w_x) = 0,$$

$$b_{22}\,\beta_{yy} - 2b_{23}\,\beta_{xy} + b_{33}\,\beta_{xx} - b_{31}\,\alpha_{xx} + (b_{21} + b_{33})\,\alpha_{xy} - b_{23}\,\alpha_{yy} - \frac{2}{c}\,G_c\,(\beta - w_y) = 0,$$

$$\left.\begin{aligned}
&\frac{t^2}{6}\,[b_{11}\,w_{xxxx} - 4b_{13}\,w_{xxxy} + 2\,(b_{12} + 2b_{33})\,w_{xxyy} - 4b_{23}\,w_{xyyy} + \\
&\quad + b_{22}\,w_{yyyy}] + \frac{(c+t)^2}{2}\,[b_{11}\,\alpha_{xxx} - 3b_{13}\,\alpha_{xxy} + (b_{21} + 2b_{33})\,\alpha_{xyy} - \\
&\quad - b_{23}\,w_{yyy} - b_{13}\,\beta_{xxx} + (b_{12} + 2b_{33})\,\beta_{xxy} - 3b_{23}\,\beta_{xyy} + \\
&\quad + b_{22}\,\beta_{yyy}] - \frac{F_{yy}}{R_1} - \frac{F_{xx}}{R_2} - 2t\sigma_x\,w_{xx} - \\
&\quad - 2t\sigma_y\,w_{yy} - 4t\tau_{xy}\,w_{xy} = 0, \\
&A_{11}\,F_{yyyy} + 2A_{13}\,F_{xyyy} + (2A_{12} - A_{33})\,F_{xxyy} + 2A_{23}\,F_{xyyy} + \\
&\quad + A_{22}\,F_{xxxx} + 2\,\frac{w_{yy}}{R_1} + 2\,\frac{w_{xx}}{R_2} = 0.
\end{aligned}\right\} \tag{6.1}$$

For the elastic problem :

$$b_{11} = b_{22} = B, \qquad b_{12} = b_{21} = \nu\,B, \qquad b_{33} = \tfrac{1}{2}\,(1 - \nu)\,B,$$

$$b_{13} = b_{31} = b_{32} = b_{23} = 0, \qquad B = Et/(1 - \nu^2),$$

and from equations (6.1) we obtain the set of three equations

$$\left.\begin{aligned}
&\nabla^2\,\Phi - \frac{2G_c}{cB}\,(\Phi - \nabla^2 w) = 0 \\
&\nabla^2\,\nabla^2\,F + 2Et\left(\frac{w_{yy}}{R_1} + \frac{w_{xx}}{R_2}\right) = 0 \\
&2D\nabla^2\,\nabla^2\,w + \frac{(c+t)^2}{2}\,B\nabla^2\,\Phi - \frac{F_{yy}}{R_1} - \frac{F_{xx}}{R_2} - 2\sigma_x\,tw_{xx} - 2\sigma_y\,tw_{yy} - 4\tau_{xy}\,tw_{xy} = 0
\end{aligned}\right\} \tag{6.2}$$

where

$$D = \frac{Et^3}{12\,(1 - \nu^2)}, \qquad \Phi = \alpha_x + \beta_y. \tag{6.3}$$

Between the first and the third of equations (6.2) the variable Φ can be eliminated :

$$\left.\begin{aligned} &2D\nabla^2\nabla^2\nabla^2 w - \frac{(c+t)^2}{c} G_c \left[1 + \frac{4D}{(c+t)^2 B}\right] \nabla^2\nabla^2 w - \\ &- \left(\nabla^2 - \frac{2G_c}{cB}\right)\left[\frac{F_{yy}}{R_1} + \frac{F_{xx}}{R_2} + 2\sigma_x t w_{xx} + \right. \\ &\left. + 2\sigma_y t w_{yy} + 4t\tau_{xy} w_{xy}\right] = 0 \end{aligned}\right\} \tag{6.4}$$

and at last from the second of equations (6.2) and equation (6.4):

$$\left.\begin{aligned} &2D\nabla^2\nabla^2\nabla^2 w - \frac{(c+t)^2}{c} G_c \left[1 + \frac{4D}{(c+t)^2 B}\right] \nabla^2\nabla^2 w + \\ &+ \left(\nabla^2 - \frac{2G_c}{cB}\right)\left\{2Et\left[\frac{1}{R_1}\nabla^{-2}\nabla^{-2}\left(\frac{w_{yy}}{R_1} + \frac{w_{xx}}{R_2}\right)_{yy} + \right.\right. \\ &+ \frac{1}{R_2}\nabla^{-2}\nabla^{-2}\left(\frac{w_{yy}}{R_1} + \frac{w_{xx}}{R_2}\right)_{xx} - (2\sigma_x t w_{xx} + \\ &\left.\left. + 2\sigma_y t w_{yy} + 4\tau_{xy} t w_{xy})\right\} = 0. \end{aligned}\right\} \tag{6.5}$$

7. Stability of a Rectangular Plate

Axial compression. Here $\sigma_x = -\sigma$, $\sigma_y = \tau_{xy} = 0$, therefore $b_{13} = b_{23} = 0$ and equations of neutral equilibrium (6.1) become

$$\left.\begin{aligned} &b_{11}\alpha_{xx} + b_{33}\alpha_{yy} + (b_{12} + b_{33})\beta_{xy} - \frac{2}{c} G_c(\alpha - w_x) = 0 \\ &b_{22}\beta_{yy} + b_{33}\beta_{xx} + (b_{12} + b_{33})\alpha_{xy} - \frac{2}{c} G_c(\beta - w_y) = 0 \\ &\frac{t^2}{6}\{b_{11} w_{xxxx} + 2(b_{12} + 2b_{33}) w_{xxyy} + b_{22} w_{yyyy}\} + \\ &+ \frac{(c+t)^2}{2}[b_{11}\alpha_{xxx} + (b_{12} + 2b_{33})\alpha_{xyy} + b_{22}\beta_{yyy} + \\ &+ (b_{12} + 2b_{33})\beta_{xyy}] + 2\sigma t w_{xx} = 0. \end{aligned}\right\} \tag{7.1}$$

Equations (7.1) are satisfied by

$$\left.\begin{aligned} w &= w_0 \sin x\sqrt{\lambda_1}\sin y\sqrt{\lambda_2}, \\ \alpha &= \alpha_0 \cos x\sqrt{\lambda_1}\sin y\sqrt{\lambda_2}, \\ \beta &= \beta_0 \sin x\sqrt{\lambda_1}\cos y\sqrt{\lambda_2}, \end{aligned}\right\} \tag{7.2}$$

where

$$\lambda_1 = \frac{m^2\pi^2}{a^2}, \qquad \lambda_2 = \frac{n^2\pi^2}{b^2}, \tag{7.3}$$

and w_0, α_0, β_0 are constant, a, b are the plate dimensions in its plane, and m and n are the numbers of halfwaves in the buckled plate.

The critical stress is expressed in the following form :

$$\left.\begin{aligned}\sigma = {} & \frac{t}{12\lambda_1}\left[b_{11}\,\lambda^2{}_1 + 2\,(b_{12} + 2b_{33})\,\lambda_1\,\lambda_2 + b_{22}\,\lambda^2{}_2\right] + \\ & + \frac{G_c\,(c+t)^2}{2ct\lambda_1}\left\{b_{11}\,b_{33}\,\lambda^3{}_1 + (b_{11}\,b_{22} - b^2{}_{12} + b_{11}\,b_{33} - 2b_{12}\,b_{33})\,\lambda^2{}_1\,\lambda_2 + \right. \\ & + (b_{11}\,b_{22} - b^2{}_{12} - 2b_{12}\,b_{33} + b_{22}\,b_{33})\,\lambda_1\,\lambda^2{}_2 + b_{22}\,b_{33}\,\lambda^3{}_2 + \\ & \left. + \frac{2G_c}{c}\left[b_{11}\,\lambda^2{}_1 + 2\,(b_{12} + 2b_{33})\,\lambda_1\,\lambda_2 + b_{22}\,\lambda^2{}_2\right]\right\} : \left\{b_{11}\,b_{33}\,\lambda^2{}_1 + \right. \\ & + (b_{11}\,b_{22} - b^2{}_{12} - 2b_{12}\,b_{33})\,\lambda_1\,\lambda_2 + b_{22}\,b_{33}\,\lambda^2{}_2 + \\ & \left. + \frac{2G_c}{c}\left[(b_{11} + b_{33})\,\lambda_1 + (b_{22} + b_{33})\,\lambda_2\right] + \frac{4G^2{}_c}{c^2}\right\}.\end{aligned}\right\} \tag{7.4}$$

The lowest value of σ is when $n = 1$. The first term in the right hand member of equation (7.4) is due to the flexural stiffness of the faces.

In the case of an infinitely wide plate from equation (7.4) :

$$\sigma = \frac{tb_{11}}{12}\,\lambda_1 + \frac{(c+t)^2\,b_{11}}{4t}\,\lambda_1\,\frac{1 + \dfrac{b_{33}\,c}{2G_c}\,\lambda_1}{1 + \dfrac{(b_{11} + b_{33})\,c}{2G_c}\,\lambda_1 + \dfrac{b_{11}\,b_{33}\,c^2}{4G^2{}_c}\,\lambda^2{}_1}. \tag{7.5}$$

If the first term in equation (7.5), due to the flexural stiffness of the faces, is neglected and if b_{33} is taken to be zero, we obtain the BIJLAARD formula for determining the critical stress of an infinitely wide plate under axial compression in the direction of short edges.

The stiffness parameters have the following values :

(a) According to the deformation theory :

$$\left.\begin{aligned} b_{11} &= Et\,\frac{1 + 3\,\dfrac{E'}{E_s}}{2\,(1-2\nu) + 3\,\dfrac{E}{E_s} - \dfrac{(1-2\nu)^2}{E}\,E'}, \\ b_{12} &= 2Et\,\frac{1 - \dfrac{1-2\nu}{E}\,E'}{2\,(1-2\nu) + 3\,\dfrac{E}{E_s} - \dfrac{(1-2\nu)^2}{E}\,E'}, \\ b_{22} &= 4Et\,\frac{1}{2\,(1-2\nu) + 3\,\dfrac{E}{E_s} - \dfrac{(1-2\nu)^2}{E}\,E'}, \\ b_{33} &= \frac{E_s\,t}{3 - \dfrac{1-2\nu}{E}\,E_s}. \end{aligned}\right\} \tag{7.6}$$

(b) **According to the flow theory :**

$$\left.\begin{aligned} b_{11} &= Et\,\frac{1+1/4\,\phi}{1-\nu^2+(5/4-\nu)\,\phi}, \qquad b_{12} = Et\,\frac{\nu+1/2\,\phi}{1-\nu^2+(5/4-\nu)\,\phi}, \\ b_{22} &= Et\,\frac{1+\phi}{1-\nu^2+(5/4-\nu)\,\phi}, \qquad b_{33} = \frac{Et}{2\,(1+\nu)}. \end{aligned}\right\} \tag{7.7}$$

REFERENCES

BIJLAARD, P. P.	1949	*J. Aero. Sci.* **16**, 573.
	1950	*Inst. Aero. Sci.*, Annual Meeting, Preprint No. 259.
	1951	*J. Aero. Sci.* **18**, 339 and 790.
	1952	*Ibid.* **19**, 502.
BOLLER, K. H.	1947	*Forest Products Lab., Rep.* 1525-A.
ERINGEN, A. C.	1951	*J. Appl. Mech.* **18**, 195.
	1956	*Ibid.* **23**, 476.
FLÜGGE, W. F.	1952	*J. Appl. Mech.* **19**, 104.
GRIGOLJUK, E. I.	1957a	*Bull. Acad. Sci. U.S.S.R.* **1**, 77.
	1957b	*Ibid.* **10**, 2.
KUENZI, E. W. and ERICKSEN, W. S.	1951	*Forest Products Lab., Rep.* 1560.
LIBOVE, C. and BATDORF, S. B.	1948	*N.A.C.A. Rep.* 899 and *Tech. Note* 1526.
NORRIS, C. B.	1948	*Inst. Aero. Sci.*, Annual Meeting, Preprint No. 165.
NORRIS, C. B. and KOMMERS, W. J.	1950	*Forest Products Lab., Rep.* 1817.
REISSNER, E.	1948	*J. Aero. Sci.* **15**, 435.
	1950	*Ibid.* **17**, 125.
SEIDE, P.	1949a	*N.A.C.A., Tech. Note* 1910.
	1949b	*N.A.C.A., Tech. Note* 1886.
	1952	*N.A.C.A., Tech. Note* 2637.
SEIDE, P. and STOWELL, E. Z.	1949	*N.A.C.A., Tech. Note* 1822.
	1950	*N.A.C.A., Rep.* 967.
TROXELL, W. W. and ENGEL, H. C.	1947	*J. Aero. Sci.* **14**, 413.

Journal of the Mechanics and Physics of Solids, 1958, Vol. 6, pp. 267 to 275. Pergamon Press Ltd., London

A RECIPROCAL PROPERTY OF THE FINITE PLANE STRAIN EQUATIONS

By J. E. Adkins
Department of Mathematics, University of Nottingham

(*Received 30th October*, 1957)

Summary

A reciprocal property is established for the equations of finite plane strain superposed on uniform extension for isotropic and transversely isotropic, incompressible elastic materials. Given any solution which expreses the displacements as functions of the initial coordinates of any point of the body, it is possible to derive a second solution in which the displacements are corresponding functions of the final coordinates. This result, which is independent of the functional form of the strain–energy function, is illlustrated by examples.

1. Introduction

In recent work on the mechanics of solids and fluids some attention has been focussed on similarities in the solutions of problems which arise from the structure of the field equations. Thus Hill (1955) has established a connexion between different types of boundary value problem in the classical infinitesimal theory of elastic plane strain and Prager (1956) has extended this theory to a wider class of materials. Still further examples of correspondences between solutions have been given by Hill (1956). In the two-dimensional theory of elasticity the writer (1956) has drawn attention to a feature of the equations for infinitesimal deformations which enables the solution of two or more different types of boundary value problem to proceed simultaneously, while the corresponding second-order theory for finite deformations has been formulated by Adkins *et al.* (1954) and by Adkins and Green (1957) in such a manner that a wide range of problems may be solved together.

In the present paper further attention is given from this point of view to the finite plane strain equations for incompressible elastic bodies. It is shown that, if a solution of these equations is derived for an isotropic material, or for a body isotropic in the planes of movement, in which the coordinates of points in the undeformed body are expressed as given functions of those in the deformed body, then a reciprocal solution can be inferred in which the coordinates of points in the deformed body can be expressed as corresponding functions of the initial coordinates. This result is true irrespective of the magnitude of the deformation or the functional form of the strain-energy function. In general, there appears to be no simple relationship between the stress systems required to maintain the two states of deformation.

The theory is illustrated by the problem of simple flexure and by some deformations considered by ADKINS (1955a) for a Mooney material.

2. NOTATION AND FORMULAE

The points of an unstrained and unstressed elastic body of isotropic, incompressible material are referred to a system of rectangular Cartesian coordinates x_i. This body is subjected to a uniform finite extension with constant extension-ratio λ parallel to the x_3-axis, and subsequently receives a finite plane strain parallel to the x_1, x_2-plane; the final coordinates y_i of the point initially at x_i are therefore given by

$$y_\alpha = y_\alpha(x_1, x_2), \qquad y_3 = \lambda x_3, \tag{2.1}$$

where, here and subsequently, greek indices are restricted to take the values 1, 2. The true (i.e. physical) stress components referred to the coordinates y_i in the deformed body are denoted by t_{ij}, and it is assumed that the material is subjected to a body force per unit mass in the x_1, x_2-plane with components F_α. The equations of equilibrium then become

$$\frac{\partial t_{\alpha\beta}}{\partial y_\alpha} + \rho F_\beta = 0, \tag{2.2}$$

ρ being the density of the strained or unstrained body, assumed constant throughout the material, and the summation convention being employed for repeated indices.

As in the classical theory of elasticity it is convenient for two-dimensional problems to introduce complex variables. We write

$$\zeta = x_1 + ix_2, \qquad z = y_1 + iy_2. \tag{2.3}$$

If the body force can be derived from a two-dimensional potential function U such that $F_\alpha = -\partial U/\partial y_\alpha$, the equations of equilibrium may be satisfied by putting

$$t_{11} - t_{22} + 2it_{12} = -4\frac{\partial^2 \phi}{\partial \bar{z}^2}, \qquad t_{11} + t_{22} = 4\frac{\partial^2 \phi}{\partial z\, \partial \bar{z}} + 2\rho U, \tag{2.4}$$

where ϕ is Airy's stress function for the deformed body.

For an isotropic incompressible material subjected to the plane strain (2.1) it has been shown by ADKINS *et al.* (1953) that the strain-energy function W may be expressed as a function of a single strain invariant I given by

$$I = \lambda^2 + \frac{2}{\lambda} + \frac{4}{\lambda^2}\frac{\partial \zeta}{\partial \bar{z}}\frac{\partial \bar{\zeta}}{\partial z}. \tag{2.5}$$

The stress-strain relations, with the first of (2.4), then yield

$$\lambda^2 \frac{\partial^2 \phi}{\partial z^2} = 2\frac{\partial \zeta}{\partial z}\frac{\partial \bar{\zeta}}{\partial z}\frac{dW(I)}{dI}. \tag{2.6}$$

This relation, together with its complex conjugate and the incompressibility condition

$$\frac{\partial(\zeta, \bar{\zeta})}{\partial(z, \bar{z})} = \lambda, \tag{2.7}$$

may be regarded as three equations for the determination of ϕ, ζ and $\bar{\zeta}$ as functions of z, $\bar{z}$.

3. Reciprocal Relations

If ϕ is eliminated from (2.6) and its complex conjugate we obtain

$$\frac{\partial^2}{\partial \bar{z}^2}\left\{\frac{\partial \zeta}{\partial z}\frac{\partial \bar{\zeta}}{\partial z}\frac{dW}{dI}\right\} = \frac{\partial^2}{\partial z^2}\left\{\frac{\partial \bar{\zeta}}{\partial \bar{z}}\frac{\partial \zeta}{\partial \bar{z}}\frac{dW}{dI}\right\},$$

or remembering (2.5),

$$Im\left[\frac{dW}{dI}\frac{\partial^2}{\partial \bar{z}^2}\left(\frac{\partial \zeta}{\partial z}\frac{\partial \bar{\zeta}}{\partial z}\right) + \frac{4}{\lambda^2}\frac{d^2W}{dI^2}\left\{\frac{\partial \zeta}{\partial z}\frac{\partial \bar{\zeta}}{\partial z}\frac{\partial^2}{\partial \bar{z}^2}\left(\frac{\partial \zeta}{\partial \bar{z}}\frac{\partial \bar{\zeta}}{\partial z}\right) + 2\frac{\partial}{\partial \bar{z}}\left(\frac{\partial \zeta}{\partial z}\frac{\partial \bar{\zeta}}{\partial z}\right)\frac{\partial}{\partial \bar{z}}\left(\frac{\partial \zeta}{\partial \bar{z}}\frac{\partial \bar{\zeta}}{\partial z}\right)\right\} + \frac{16}{\lambda^4}\frac{d^3W}{dI^3}\frac{\partial \zeta}{\partial z}\frac{\partial \bar{\zeta}}{\partial z}\left\{\frac{\partial}{\partial \bar{z}}\left(\frac{\partial \zeta}{\partial \bar{z}}\frac{\partial \bar{\zeta}}{\partial z}\right)\right\}^2\right] = 0. \tag{3.1}$$

In the system of equations (2.7), (2·5) and (3·1), which serve to determine ζ, $\bar{\zeta}$ as functions of z, $\bar{z}$, we may change the independent variables by making use of the formulae

$$\left.\begin{aligned} \frac{\partial \zeta}{\partial z} &= \lambda\frac{\partial \bar{z}}{\partial \bar{\zeta}}, \qquad \frac{\partial \zeta}{\partial \bar{z}} = -\lambda\frac{\partial z}{\partial \bar{\zeta}}, \\ \frac{\partial}{\partial z} &= \lambda\left(\frac{\partial \bar{z}}{\partial \bar{\zeta}}\frac{\partial}{\partial \zeta} - \frac{\partial \bar{z}}{\partial \zeta}\frac{\partial}{\partial \bar{\zeta}}\right), \end{aligned}\right\} \tag{3.2}$$

together with their complex conjugates. This process yields

$$\frac{\partial(z, \bar{z})}{\partial(\zeta, \bar{\zeta})} = \frac{1}{\lambda}, \tag{3.3}$$

$$I = \lambda^2 + \frac{2}{\lambda} + 4\frac{\partial z}{\partial \bar{\zeta}}\frac{\partial \bar{z}}{\partial \zeta}, \tag{3.4}$$

$$Im\left[\frac{dW}{dI}\frac{\partial^2}{\partial \bar{\zeta}^2}\left(\frac{\partial z}{\partial \zeta}\frac{\partial \bar{z}}{\partial \zeta}\right) + 4\frac{d^2W}{dI^2}\left\{\frac{\partial z}{\partial \zeta}\frac{\partial \bar{z}}{\partial \zeta}\frac{\partial^2}{\partial \bar{\zeta}^2}\left(\frac{\partial z}{\partial \bar{\zeta}}\frac{\partial \bar{z}}{\partial \zeta}\right) + 2\frac{\partial}{\partial \bar{\zeta}}\left(\frac{\partial z}{\partial \zeta}\frac{\partial \bar{z}}{\partial \zeta}\right)\frac{\partial}{\partial \bar{\zeta}}\left(\frac{\partial z}{\partial \bar{\zeta}}\frac{\partial \bar{z}}{\partial \zeta}\right)\right\} + 16\frac{d^3W}{dI^3}\frac{\partial z}{\partial \zeta}\frac{\partial \bar{z}}{\partial \zeta}\left\{\frac{\partial}{\partial \bar{\zeta}}\left(\frac{\partial z}{\partial \bar{\zeta}}\frac{\partial \bar{z}}{\partial \zeta}\right)\right\}^2\right] = 0. \tag{3.5}$$

The transformation from (3.1) to (3.5) is lengthy, but may be carried out by considering separately the coefficients of the three derivatives of W which occur in the two expressions; these are equivalent to each other apart from the same constant factor. To establish the equivalence of the coefficients of d^2W/dI^2 in the two cases, it is necessary to make use of the equation

$$\frac{\partial z}{\partial \zeta}\frac{\partial^2 \bar{z}}{\partial \bar{\zeta}^2} = \frac{\partial \bar{z}}{\partial \zeta}\frac{\partial^2 z}{\partial \bar{\zeta}^2} + \frac{\partial z}{\partial \bar{\zeta}}\frac{\partial^2 \bar{z}}{\partial \zeta\,\partial \bar{\zeta}} - \frac{\partial \bar{z}}{\partial \bar{\zeta}}\frac{\partial^2 z}{\partial \zeta\,\partial \bar{\zeta}}, \tag{3.6}$$

derived by differentiation of (3·3), while in transforming the coefficient of dW/dI the additional relation obtained from (3·6) by a further differentiation with respect to $\bar{z}$ must be employed to eliminate $\partial^3 \bar{z}/\partial\zeta^3$. Evidently this transformation does not depend upon the form of W as a function of I. The relations (3.3) to (3.5) can be rendered identical in form with (2.7), (2.5) and (3.1) respectively by the substitutions

$$\zeta' = \lambda^n \zeta, \qquad z' = \lambda^{n+1} z, \tag{3.7}$$

where n is a real constant, and ζ' and z' replace z and ζ respectively in the original formulae. It follows that if

$$\zeta = f(z, \bar{z}, \lambda) \tag{3.8}$$

defines a solution of the finite plane strain equations for an isotropic incompressible elastic material with a given form of strain energy function defined by $W = W(I)$ then

$$z' = f(\zeta', \bar{\zeta}', \lambda),$$

or

$$\lambda^{n+1} z = f(\lambda^n \zeta, \lambda^n \bar{\zeta}, \lambda),$$

also represents a possible solution for the same material. By writing the latter relation as

$$kz = \frac{1}{\lambda} f(k\zeta, k\bar{\zeta}, \lambda), \qquad (k = \lambda^n)$$

we see that these reciprocal solutions, for all values of n, are equivalent apart from the constant scaling factor k. Putting $k = 1$ $(n = 0)$ we therefore have

$$z = \frac{1}{\lambda} f(\zeta, \bar{\zeta}, \lambda), \tag{3.9}$$

as the reciprocal solution associated with (3.8). In terms of the real variables x_α, y_α, it follows from (3.8) and (3.9) that a solution

$$x_\alpha = f_\alpha(y_1, y_2, \lambda) \tag{3.10}$$

of the plane strain equations automatically implies a related solution of the type

$$y_\alpha = \frac{1}{\lambda} f_\alpha(x_1, x_2, \lambda). \tag{3.11}$$

For any given deformation defined by one of the relations (3.8) to (3.11) the stress function ϕ may be determined from (2.6), and the corresponding stress system evaluated from (2·4). We observe that (3.8), or its real variable equivalent (3.10), represents a solution of the pair of differential equations (2.7) and (3.1), neither of which contains terms which depend upon the body force system F_α. It therefore continues to represent a solution of the field equations for any physically permissible, but otherwise arbitrary, choice of the potential function U which defines this system. It can be seen without difficulty from the stress–strain relations given by Adkins *et al.* (1953) that a body force system of the type considered merely increases each of the principal stresses t_{ii} by an amount ρU compared with their values for $U = 0$, and in this respect may be regarded as equivalent to an isotropic pressure. Similar remarks apply to the reciprocal solution (3·9) which

has been inferred by the transformation of equations which are unaffected by the function U; this reciprocal deformation may therefore also be maintained in the presence of body forces $F_\alpha = -\partial U/\partial y_\alpha$ derived from an arbitrary potential function $U = U(y_1, y_2)$. In particular, if the deformation (3·10) can be sustained, in the absence of body forces, by surface tractions alone so also can the reciprocal deformation (3.11). Except possibly in special cases, there appears to be no simple relationship between the two systems of surface tractions required.

4. Transversely Isotropic Bodies

It is readily seen that the reciprocal property represented by (3.10) and (3.11) holds for any incompressible body which is isotropic in the plane of movement. For if a body which is transversely isotropic about x_3-axis is subjected to the deformation (2.1), the strain-energy function W may be expressed as a function of I and

$$J = \tfrac{1}{2}\left(\frac{\partial y_r}{\partial x_3}\frac{\partial y_r}{\partial x_3} - 1\right) = \tfrac{1}{2}(\lambda^2 - 1),$$

(for example Green and Wilkes 1954 or Adkins 1955b). The stress–strain relations then yield formulae for $t_{\alpha\beta}$ which are identical in form with those for an isotropic body apart from the replacement of $dW(I)/dI$ by $\partial W(I, J)/\partial I$. Equation (2.6) is modified in the same manner, and the subsequent analysis leading to the reciprocal property is unaffected by the additional quantity J which does not depend upon ζ or z.

5. The Mooney Material

For an isotropic material with the linear form of strain–energy function suggested by Mooney (1940), the first derivative of W takes the constant value

$$\frac{dW(I)}{dI} = C_1 + \lambda^2 C_2 = C \text{ (say)}, \tag{5.1}$$

where C_1 and C_2 are constants independent of λ, and (3.1) and (3.5) reduce to

$$\left.\begin{aligned}\left(\frac{\partial\zeta}{\partial z}\frac{\partial}{\partial\bar{z}} - \frac{\partial\zeta}{\partial\bar{z}}\frac{\partial}{\partial z}\right)\frac{\partial^2\bar{\zeta}}{\partial z\,\partial\bar{z}} + \left(\frac{\partial\bar{\zeta}}{\partial z}\frac{\partial}{\partial\bar{z}} - \frac{\partial\bar{\zeta}}{\partial\bar{z}}\frac{\partial}{\partial z}\right)\frac{\partial^2\zeta}{\partial z\,\partial\bar{z}} = 0,\\ \left(\frac{\partial z}{\partial\zeta}\frac{\partial}{\partial\bar{\zeta}} - \frac{\partial z}{\partial\bar{\zeta}}\frac{\partial}{\partial\zeta}\right)\frac{\partial^2\bar{z}}{\partial\zeta\,\partial\bar{\zeta}} + \left(\frac{\partial\bar{z}}{\partial\zeta}\frac{\partial}{\partial\bar{\zeta}} - \frac{\partial\bar{z}}{\partial\bar{\zeta}}\frac{\partial}{\partial\zeta}\right)\frac{\partial^2 z}{\partial\zeta\,\partial\bar{\zeta}} = 0,\end{aligned}\right\} \tag{5.2}$$

respectively. Real variable forms of these equations have been given by Adkins (1955a). Equations (5.2), with the corresponding forms (2.7) and (3.3) of the incompressibility condition, show that the solution

$$z = f\left(\zeta, \bar{\zeta}, \frac{1}{\lambda}\right) \tag{5.3}$$

may also be deduced from (3.8). This deformation is, however, similar in character to that represented by (3.9). Furthermore, the substitutions

$$\zeta = k\zeta', \qquad z = lz',$$

where k and l are constants, leave the relations (5.2) unchanged, apart from the replacement of ζ, z by ζ', z' respectively, and change the incompressibility condition (2.7) into

$$\frac{\partial(\zeta', \bar{\zeta}')}{\partial(z', \bar{z}')} = \frac{l^2\lambda}{k^2}.$$

Corresponding to (3.8), (3.9) and (5.3) we then have the further solutions

$$\left.\begin{aligned} \zeta &= kf\left(\frac{z}{l}, \frac{\bar{z}}{l}, \frac{l^2\lambda}{k^2}\right), \\ z &= \frac{k^2}{l\lambda} f\left(\frac{\zeta}{k}, \frac{\bar{\zeta}}{k}, \frac{l^2\lambda}{k^2}\right), \\ z &= lf\left(\frac{\zeta}{k}, \frac{\bar{\zeta}}{k}, \frac{k^2}{l^2\lambda}\right). \end{aligned}\right\} \tag{5.4}$$

These results, which merely arise from a uniform magnification of the coordinate systems in the undeformed and the deformed material, are again not essentially different in character from those given in Section 3.

6. ILLUSTRATIONS

The flexure problem considered by RIVLIN (1949 a, b), ADKINS, *et al.* (1953) and other workers provides a convenient illustration of the foregoing theory. If we define systems of polar coordinates (r, θ) in the undeformed body, and (ρ, ϑ) in the deformed body by means of the relations

$$\zeta = x_1 + ix_2 = re^{i\theta}, \qquad z = y_1 + iy_2 = \rho e^{i\vartheta}, \tag{6.1}$$

then the equations

$$\rho = \rho(x_1), \qquad \vartheta = ax_2, \qquad y_3 = \lambda x_3, \tag{6.2}$$

describe a simple flexure combined with inflation and extension, in which the planes $x_1 =$ constant in the undeformed body are deformed into the concentric cylindrical surfaces $\rho =$ constant, the planes $x_2 =$ constant become the radial planes $\vartheta =$ constant and there is a uniform extension of ratio λ in the longitudinal direction. The incompressibility condition is

$$a\lambda\rho\frac{d\rho}{dx_1} = 1,$$

or

$$a\lambda\rho^2 = 2x_1 + K, \tag{6.3}$$

K being an arbitrary constant. Using this condition, with (6.1) and (6.2), we obtain

$$\left.\begin{aligned} x_1 &= \tfrac{1}{2}\{a\lambda(y_1^2 + y_2^2) - K\}, \\ x_2 &= \frac{1}{a}\tan^{-1}\frac{y_2}{y_1}. \end{aligned}\right\} \tag{6.4}$$

From (3.10) and (3.11) we may then infer that the reciprocal deformation

$$\left.\begin{aligned} y_1 &= \frac{1}{2\lambda}\{a\lambda(x_1^2 + x_2^2) - K\}, \\ y_2 &= \frac{1}{a\lambda}\tan^{-1}\frac{x_2}{x_1}, \end{aligned}\right\} \tag{6.5}$$

is also possible for an incompressible material which is isotropic or transversely isotropic with respect to the x_3-direction. Writing these equations in the form

$$a\lambda r^2 = 2\lambda y_1 + K, \qquad \theta = a\lambda y_2, \tag{6.6}$$

we see that the deformation has the effect of changing an initially curved block into a cuboid. Thus, if the undeformed body is bounded by the cylindrical surfaces $r = r_1, r = r_2\,(r_2 > r_1)$ and the planes $\theta = \pm\alpha, x_3 = \pm l$, the deformed body has the plane boundaries

$$\begin{aligned} y_1 &= A_1, \qquad y_1 = A_2, \qquad (A_2 > A_1), \\ y_2 &= \pm B, \qquad y_3 = \pm L, \qquad \text{where} \\ A_\nu &= (a\lambda r_\nu^2 - K)/(2\lambda), \qquad B = \alpha/(a\lambda), \qquad L = \lambda l \qquad (\nu = 1, 2). \end{aligned}$$

The situation in the x_1, x_2-plane is illustrated by the diagram.

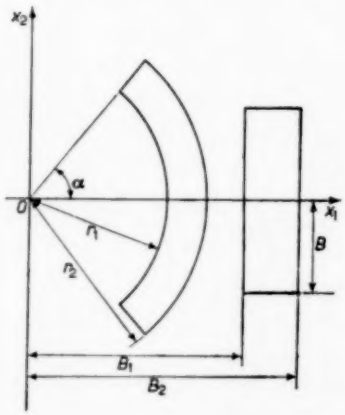

Fig. 1.

The stresses may be evaluated from the formulae of section 2. Solving (6.5) for x_1, x_2 and making use of (2.3) we obtain

$$\zeta\sqrt{(a\lambda)} = \pm e^{\frac{1}{2}a\lambda(z-\bar{z})}\sqrt{\{\lambda(z+\bar{z}) + K\}}, \tag{6.7}$$

and by combining this result with (2.4) and (2.6) we have

$$\begin{aligned} t_{11} - t_{22} + 2it_{12} &= -4\frac{\partial^2\phi}{\partial\bar{z}^2} \\ &= -\frac{2}{\lambda a}\left\{\frac{1}{\lambda(z+\bar{z}) + K} - a^2[\lambda(z+\bar{z}) + K]\right\}\frac{dW}{dI}. \end{aligned} \tag{6.8}$$

The negative sign in (6.7) merely represents a rigid body rotation of the deformed

body through two right angles about the x_3-axis and does not affect the stresses. From (6.7) and (2.5) we infer that I, and hence also W, involves the variables z, $\bar{z}$ in the combination $z + \bar{z}$ only, and (6.8) and 2.4) then yield

$$t_{11} + t_{22} = \frac{2}{\lambda a}\left\{\frac{1}{\lambda(z+\bar{z}) + K} - a^2\left[\lambda(z+\bar{z}) + K\right]\right\}\frac{dW}{dI} + 2(\rho U + K'),$$

K' being a further arbitrary constant. For transversely isotropic bodies these formulae are modified as indicated in Section 4. The real components of stress $t_{\alpha\beta}$ are given by

$$\left.\begin{aligned} t_{11} &= \rho U + K', \qquad t_{12} = 0, \\ t_{22} &= \frac{2}{\lambda a}\left\{\frac{1}{2\lambda y_1 + K} - a^2(2\lambda y_1 + K)\right\}\frac{dW}{dI} + \rho U + K' \\ &= 2\left\{\frac{1}{a^2\lambda^2 r^2} - a^2 r^2\right\}\frac{dW}{dI} + \rho U + K'. \end{aligned}\right\} \tag{6.9}$$

From these results it follows that if the body force system F_α is zero, the deformation can be maintained without applying surface tractions to the initially curved surfaces.

Further examples of the theory are provided by the deformations examined by ADKINS (1955a) for a Mooney material. In these, planes which are initially normal to the x_1-axis remain normal to this axis as a result of the deformation, but are displaced relative to each other through a distance which is a function of their x_1 coordinate. Two typical solutions based on this assumption are

$$\left.\begin{aligned} x_1 &= A \log\tan\left\{\tfrac{1}{2}(ay_1 + b)\right\}, \\ x_2 &= (\lambda y_2/Aa)\sin(ay_1 + b) + B\sin(ay_1 + d), \\ & 2n\pi > ay_1 + b < (2n+1)\pi \end{aligned}\right\} \tag{6.10}$$

and

$$\left.\begin{aligned} x_1 &= e^{ay_1 + b}, \\ x_2 &= (\lambda y_2/a)\, e^{-(ay_1+b)} + e^{ay_1+d}, \end{aligned}\right\} \tag{6.11}$$

where a, b, d, A and B are arbitrary constants and n is an integer. From (3.10) and (3.11) we may again infer that the deformations represented by

$$\left.\begin{aligned} y_1 &= (A/\lambda)\log\tan\left\{\tfrac{1}{2}(ax_1 + b)\right\}, \\ y_2 &= (x_2/Aa)\sin(ax_1 + b) + (B/\lambda)\sin(ax_1 + d), \\ & 2n\pi < ax_1 + b < (2n+1)\pi \end{aligned}\right\} \tag{6.12}$$

and

$$\left.\begin{aligned} \lambda y_1 &= e^{ax_1 + b}, \\ \lambda y_2 &= (\lambda x_2/a)\, e^{-(ax_1+b)} + e^{ax_1+d}, \end{aligned}\right\} \tag{6.13}$$

are also possible for a Mooney material. The systems of stresses required to maintain these deformations may be evaluated from the formulae of Section 2. The additional solutions of Section 5 evidently yield no new results.

References

Adkins, J. E.	1955a	*Proc. Camb. Phil. Soc.* **51**, 363.
	1955b	*Proc. Roy. Soc. A* **229**, 119.
	1956	*J. Mech. Phys. Solids* **4**, 199.
Adkins, J. E. and Green, A. E.	1957	*Proc. Roy. Soc. A* **239**, 557.
Adkins, J. E., Green, A. E. and Nicholas, G. C.	1954	*Phil. Trans. Roy. Soc. A* **247**, 279.
Adkins, J. E., Green, A. E. and Shield, R. T.	1953	*Phil. Trans. Roy. Soc. A* **246**, 181.
Green, A. E. and Wilkes, E. W.	1954	*J. Rat. Mech. Anal.* **3**, 713.
Hill, R.	1955	*J. Mech. Phys. Solids* **4**, 1.
	1956	*J. Mech. Phys. Solids* **5**, 66.
Mooney, M.	1940	*J. Appl. Phys.* **11**, 582.
Prager, W.	1956	*J. Mech. Phys. Solids* **4**, 167.
Rivlin, R. S.	1949a	*Proc. Roy. Soc. A* **195**, 463.
	1949b	*Phil. Trans. Roy. Soc. A* **243**, 173.

Journal of the Mechanics and Physics of Solids, 1958, Vol. 6, pp. 276 to 281. Pergamon Press Ltd., London

AN INVESTIGATION OF PLASTIC STRESS–STRAIN RELATIONSHIPS USING GROOVED TENSILE SPECIMENS

J. P. Ellington
Departments of Civil and Mechanical Engineering, University of Nottingham

(*Received 13th November*, 1957)

Summary

The method suggested by Hill (1953) of straining grooved tensile specimens to investigate the plastic behaviour of ductile metals has been used to find the plastic potentials of thoroughly annealed brass and copper. The brass was found to have a Mises potential (the strain-rate being proportional to the deviatoric stress), while the copper showed a deviation from this potential, presumably due to anisotropy.

1. Introduction

Some of the difficulties and possible inaccuracies attendant on the use of thin-walled tubes in the determination of plastic stress–strain relationships have been emphasized by Hill (1953), who then proposed an alternative method involving the tensile loading of strip specimens. In essence, if deep oblique grooves are machined on opposite sides of a wide plate tensile specimen, plastic deformation is confined to the grooved regions, the constraint of the surrounding material producing a state of biaxial stress. Measurements of load and displacement across the groove, for a range of groove angles, then enable the yield criterion and plastic potential of the material to be calculated.

Alternatively, thin notched specimens may be used, the formation of a straight narrow neck joining the roots of the notches acting effectively as a groove. This method has been used by Hundy and Green (1954) and by Lianis and Ford (1957), the former investigating the properties of rolled copper, zinc and stainless steel, the latter, aluminium rolled at the temperature of liquid nitrogen to obtain a material with a negligible rate of workhardening.

However, notched specimens are not suitable for a material with a high rate of workhardening because of the diffuse zone of deformation between the notches. If the properties of such a material are to be investigated, grooved specimens are necessary. With this in view, the present paper reports experimental results on grooved specimens of thoroughly annealed α–brass and copper.

2. Theory

Full details of the theory for a grooved strip specimen have been given by Hill (1953). For an isotropic ductile material the stress–strain relationships, in terms of Lode's parameters, for stress μ, and for strain ν, are

$$\mu = \frac{2\sigma_2 - \sigma_1 - \sigma_3}{\sigma_1 - \sigma_3} = -\frac{3\cos\theta - \sin(\theta - \psi)}{\cos\theta + \sin(\theta - \psi)} \tag{1}$$

and

$$\nu = \frac{2\dot{\epsilon}_2 - \dot{\epsilon}_1 - \dot{\epsilon}_3}{\dot{\epsilon}_1 - \dot{\epsilon}_3} = -\frac{3(1 - \sin\psi)}{(1 + 3\sin\psi)}. \tag{2}$$

Here σ_i and $\dot{\epsilon}_i$ are the principal stresses and strain-rates in the groove, which is inclined at an angle θ to the tensile axis. The displacements in the groove are such that the rigid sides move apart with a relative velocity inclined at an angle ψ to the groove (Fig. 1).

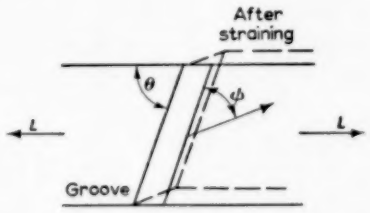

Fig. 1.

If the tensile load L is measured, and h and l are the thickness and length of the grooved portion, then in a principal stress space the length of the reduced stress vector is

$$\bar{\sigma} = \sqrt{(\tfrac{2}{3})}\,(\sigma_1^2 - \sigma_1\sigma_2 + \sigma_2^2)^{\frac{1}{2}}$$

$$= \sqrt{(\tfrac{2}{3})}\,\frac{L}{hl\cos\psi}\,[\sin^2(\theta - \psi) + 3\cos^2\theta]^{\frac{1}{2}}. \tag{3}$$

The inclination of this reduced, or deviatoric, stress vector to the direction of pure shear ($\mu = 0$) is

$$\alpha = \tan^{-1}(-\mu/\sqrt{3}). \tag{4}$$

Provided the material is isotropic and, as is tacitly assumed, yielding is independent of the mean or hydrostatic stress, then the stress state in the groove need only vary between pure tension ($\mu = -1$) and pure shear ($\mu = 0$); i.e., θ need only vary between $\tan^{-1}\sqrt{(2)} = (54^\circ\,44')$ and 90°.

3. Discussion of Errors

The influence of errors in the measured angles θ and ψ is obviously of some importance in assessing the accuracy of the experimental results, and may be discussed as follows.

Suppose that $\delta\theta$ and $\delta\psi$ are the maximum expected small errors in θ and ψ, then from equation (2) the error in the strain-rate parameter ν will be

$$\delta\nu \simeq \frac{\partial\nu}{\partial\psi}\,\delta\psi = \frac{12\cos\psi\,\delta\psi}{(1 + 3\sin\psi)^2} \tag{5}$$

and is not influenced by errors in θ.

Similarly, for the stress parameter μ from equation (1),

$$\delta\mu \simeq \frac{\partial\mu}{\partial\theta}\,\delta\theta + \frac{\partial\mu}{\partial\psi}\,\delta\psi$$

$$= \frac{4\cos\psi\,\delta\theta - 4\cos\theta\cos(\theta-\psi)\,\delta\psi}{[\cos\theta + \sin(\theta-\psi)]^2}.$$

With the exception of mild steel, ductile metals appear to have a plastic potential in the neighbourhood of the Mises potential, or $\mu = \nu$. In this case $\tan\psi = \frac{1}{4}\tan\theta$, the error in μ becoming

$$\delta\mu = \frac{4\cos\psi}{(1+3\sin\psi)^2}\left[(16\tan^2\psi + 1)\,\delta\theta - (4\tan^2\psi + 1)\,\delta\psi\right]. \tag{6}$$

This expression indicates that large errors in μ are possible when θ and ψ are near 90°, or near the region of pure shear. However, as pointed out by HILL, the (μ, ν) curve passes through the origin and thus it is not really necessary to take θ larger than about 80°.

Possible deviations from the true (μ, ν) relationship for a Mises material caused by the most adverse combination of $\frac{1}{2}°$ errors in θ and ψ are shown in Fig. 2, where it can be seen that the estimated (μ, ν) position is within 0·04 of its true position.

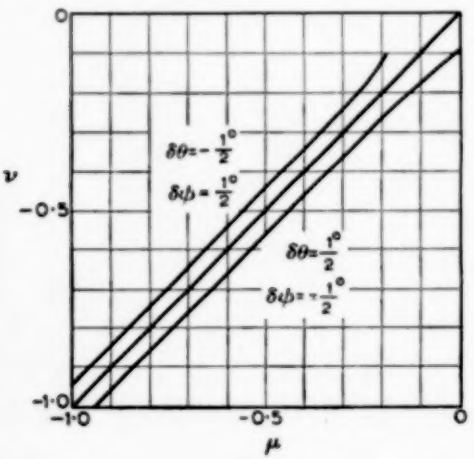

Fig. 2.

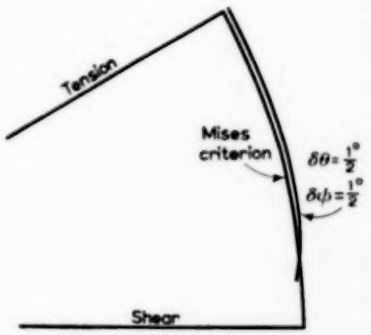

Fig. 3.

In a similar manner, for the same material the error in the length of the reduced stress vector $\bar{\sigma}$ is

$$\delta\bar{\sigma} = -\bar{\sigma}\,\frac{\left[4\tan^2\psi\,(1-\tan\psi)\,\delta\psi + 3\tan\psi\,\delta\theta\right]}{(1+4\tan^2\psi)}, \tag{7}$$

the error in the inclination of this vector in the deviatoric stress plane being

$$\delta\alpha = -\cos^2\alpha\,(\delta\mu/\sqrt{3}). \tag{8}$$

Inspection of these results plotted in Fig. 3 shows that at the most a 1 per cent error in the yield curve arises from errors in the measured angles, and that accuracy of the yield criterion is governed by the accuracy of the load measurements.

In general, these results show that the major part of the above errors arise from the measurement of the groove angle θ, and indicate the superior accuracy of the grooved specimen, the sharp edge at the surface of the specimen allowing a very accurate determination of θ.

4. Details of Specimens

After initial tests for anisotropy, specimens were cut from heat-treated $\frac{1}{4}$in. plate, care being taken to cut each specimen perpendicular to the rolling direction. The overall dimensions of the specimens were as in Fig. 4, preliminary experiments showing that, if ψ was to be measured with reasonable accuracy, two grooves were essential to eliminate relative rotation of the rigid ends. Machining of the grooves was carried out using a box-shaped jig which ensured that the opposite sides of the grooves were correctly positioned. The average difference between the two groove angles on a specimen was about $\frac{1}{4}°$, and if necessary hand-finishing was used to make sure that the grooved portions were centrally spaced and parallel.

Several methods of measuring ψ, the angle of relative motion, were tried, the only successful one being the elegant method of Hundy and Green (1954). Fine lines were scribed at 1° intervals about the expected value of ψ, the lateral displacement of the lines being measured with a microscope and dial gauge.

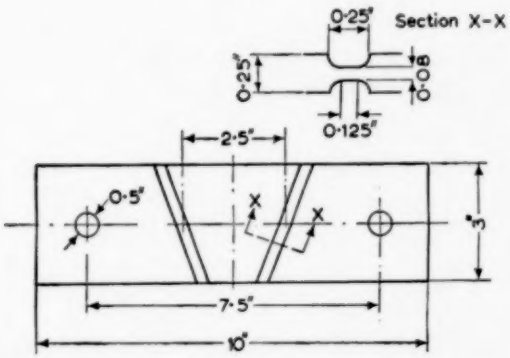

Fig. 4.

Great care was taken to ensure axial loading of the specimens, pairs of Huggenberger extensometers mounted at each end of the grooves showing any bending of the specimens. Load-extension curves were taken by mounting extensometers in the grooves themselves, initially using a small gauge length extensometer, and later using an inductance displacement pick-up to measure the through-strain of the grooved portion. This device showed that the through-strains encountered were about 2-4 per cent.

5. Experimental Results

The brass in the major part of the experiments was obtained in the form of cold-rolled sheet and was annealed twice to remove a small quantity of β-phase.

Microscopic examination revealed no directional properties and showed a grain diameter of about 0·003 in., giving about 20 grains through the thickness of the groove.

Tensile specimens were then cut at 0, 45° and 90° to the rolling direction, the corresponding anisotropy parameters being given in Table 1. Calculations following HILL (1953) showed that the departure from perfect isotropy would produce negligible effect on the (μ, ν) relation.

TABLE 1

	F/H	G/H	N/H
Brass	0·97	1·05	3·08
Copper	0·93	1·08	2·90

The experimental (μ, ν) curve is shown in Fig. 5, the experimental points lying very close to the Mises plastic potential, $\mu = \nu$. This agrees with the results of HUNDY and GREEN, and LIANIS and FORD, for other materials.

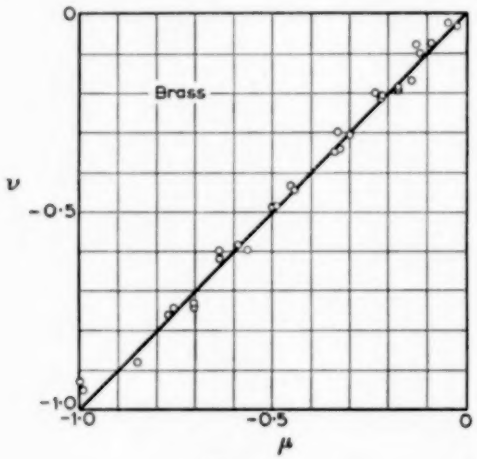

Fig. 5.

No yield criterion was obtained because of the high rate of workhardening, which made it impossible to estimate accurately a yield load. In so far as it was possible to estimate a yield load the results were scattered between the Mises and Tresca criteria. This difficulty is to be encountered with any annealed material and could be easily overcome by giving the material a light rolling or pre-strain before machining.

The copper was supplied as a heavily worked, oxygen-free, high conductivity copper having a yield stress of 20 ton/in^2. After annealing the yield stress was about 3·2 ton/in^2, microscopic examination showing a grain size of about 0·001 in., there being no indication of directional properties. Tensile specimens taken again at 0, 45° and 90° gave the anisotropy parameters in Table I, calculation

showing that this degree of anisotropy would result in an error of 0·01 at most in the (μ, ν) diagram (assuming the plastic potential to be quadratic).

However, the experimental results in Fig. 6 differed considerably from the $\mu = \nu$ line, and are on the opposite side to those of TAYLOR and QUINNEY (1931). It has been pointed out that their results may have been marred by undetected anisotropy, and this may be true also of the present ones, despite the additional precautions. As is well known, it is difficult to remove directional properties from heavily-worked copper, and it is possible that the quadratic stress function assumed for calculating the anisotropy parameters did not sufficiently represent the actual plastic potential.

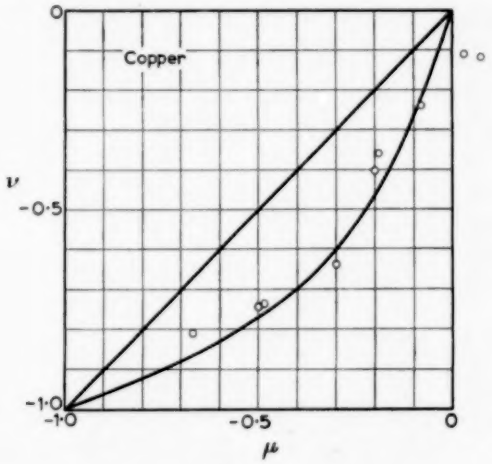

Fig. 6.

The yield criterion was not obtained, although this would have been enlightening since it might be expected to lie outside the Mises criterion.

6. ACKNOWLEDGMENTS

The author would like to thank Messrs. E. OLLERTON, P. A. SIMPSON, N. BREAKWELL for their experimental work, Prof. J. A. POPE for providing the workshop and laboratory facilities and Prof. R. HILL for his advice and guidance.

REFERENCES

HILL, R. 1953 *J. Mech. Phys. Solids* **1**, 271.
HUNDY, B. B. and GREEN, A. P. 1954 *J. Mech. Phys. Solids* **3**, 16.
LIANIS, G. and FORD, H. 1957 *J. Mech. Phys. Solids* **5**, 215.
TAYLOR, G. I. and QUINNEY, H. 1931 *Phil. Trans. Roy. Soc.* A, **230**, 323.

Journal of the Mechanics and Physics of Solids, 1958, Vol. 6, pp. 282 to 300. Pergamon Press Ltd., London

PLASTIC BEHAVIOUR OF COMPRESSION MEMBERS

By J. S. Ellis*
J. D. Lee and Co. Ltd., Consulting Engineers, Kingston, Ontario

(*Received* 17*th October*, 1957)

Summary

This paper describes a theoretical and experimental investigation of the plastic behaviour of mild steel compression members of an annular cross-section when subjected to end loads of equal and unequal end eccentricities. Theoretical collapse curves for a comprehensive range of such members are presented, and it is considered that the experiments support the analysis. From a comparison with the elastic theory it appears that the plastic theory will permit considerable economy in the design of columns of an annular cross-section.

A method of analysing columns in a framework is advanced. This method, which is iterative in character, is considered capable of handling combinations of elastic members, columns stressed in the plastic range, and beams containing plastic hinges.

1. Introduction

The problem was to investigate theoretically and experimentally the plastic behaviour of mild steel compression members of a circular annular cross-section when subjected to end loads of equal and unequal end eccentricities.

The elastic behaviour of eccentrically loaded columns can be represented by a load-deflexion curve which is asymptotic to the critical load (Fig. 1). However, the plastic behaviour of such columns results in a load-deflection curve of a radically different shape (Fig. 2).

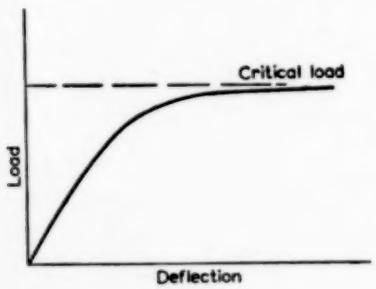

Fig. 1.

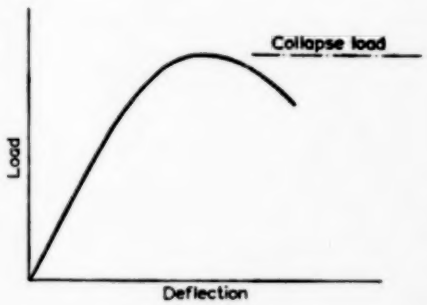

Fig. 2.

Load-deflection curves of the plastic behaviour of eccentrically loaded columns were derived by Baker, Horne and Roderick (1949). Unfortunately, the theory of their method is cumbersome and can only be applied to particular cases by

*Formerly at the Engineering Department, University of Cambridge.

carrying out a lengthy trial-and-error process. Hence the calculation of collapse loads of eccentrically loaded columns by this method appeared most formidable.

More recently HORNE (1956a) developed a convenient method of obtaining collapse loads of columns of a rectangular cross-section loaded symmetrically by equal end eccentricities. EICKHOFF (1955) continued this work by means of extensive calculations by an electronic digital computer.

A comparison between the HORNE collapse curves (rectangular cross-section) and those of this paper (annular cross-section) is given in Fig. 3. Although the general agreement between the two sets of curves is good, there is no constant relationship. BLEICH (1952) intimated that the effects of the cross-sectional form upon the collapse loads of eccentrically loaded columns is liable to be complex, but BIJLAARD (1954) considered that shape factors can cope with differences in cross-section. The writer is of the opinion that no simple factor will enable collapse load data of one cross-section to be adapted to another cross-section. Each cross-section, it is suggested here, requires separate computations.

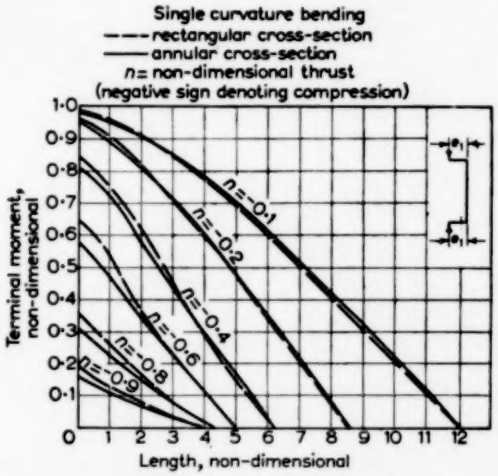

Fig. 3. Collapse loads for eccentrically loaded columns.

It is to be noted that only results applicable to columns loaded symmetrically by equal terminal eccentricities have so far been mentioned. Consideration will now be given to work done on columns subjected to end loads of both equal and unequal end eccentricities. An interesting approach to this problem was advanced by BIJLAARD (1954). Essentially it was an approximate development based on the knowledge of pin-ended struts of rectangular cross-section when stressed in the plastic range. It did not attempt, as the work of this paper does, to compute rigorously the collapse loads of columns subjected to end loads of equal and unequal end eccentricities, but it does outline an approximate method to obtain such data. Unfortunately he did not consider the annular cross-section.

The work of the Building Research Station of Great Britain on the problem of this paper was published in the discussion of the Symposium of the Plastic Theory of Structures (WOOD 1957). It did not contain a general set of collapse curves nor did it treat the case of the annular cross-section. Little similarity exists

between the approach used by the Building Research Station and that of this paper; the former is concerned primarily with a systematic tabulation of column properties and the latter with obtaining a general set of column collapse curves.

2. Theoretical Investigation

It was necessary first to discover a collapse criterion for a compression member under a known thrust and subjected to end loads of unequal eccentricities, and then to make the computations necessary to determine the physical characteristics of compression members on the point of collapse. These computations were

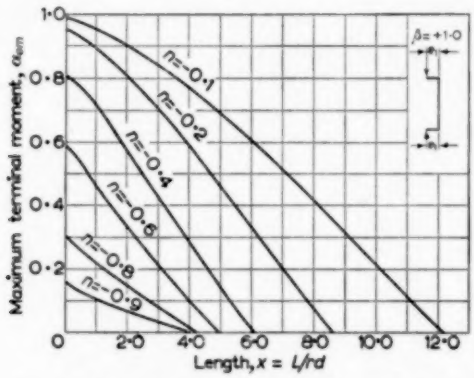

Fig. 4. Collapse loads for eccentrically loaded columns of annular cross-section.

$n = P/P_P$, non-dimensional thrust.
β = Ratio of end eccentricities.
$\alpha = M/M_P$ non-dimensional moment.
α_{em} = Greater numerical α acting at the end of a column.
L = Actual length of a column along its line of thrust.
$r = \sqrt{E/3f_L}$.
E = Young's modulus
f_L = Lower yield stress.
$d = R$ = Actual mean radius of the annulus.
P = Actual thrust.
P_P = Fully plastic actual thrust.
M = Actual moment.
M_P = Fully plastic actual moment.

made for $n = -0{\cdot}1, -0{\cdot}2, -0{\cdot}4, -0{\cdot}6, -0{\cdot}8$ and $-0{\cdot}9$ where n is the ratio of the applied load to the fully plastic thrust (the negative sign denotes compression), and for $\beta = +1{\cdot}0$ to $-1{\cdot}0$ in increments of 0·1 where β is the ratio of the end eccentricities. A positive sign for β indicates that the direction of the eccentricity for both ends is in the same sense and that single curvature bending takes place; a negative sign, of course, indicates double curvature bending. Figs. 4–8 record five of the twenty-one results of these computations for which the electronic digital computer of the University of Cambridge was used. In using these graphs it must be noted that α_{em} is the greater numerical α acting at the

end of a strut, where α is the ratio of the moment to the fully plastic moment under zero axial load. Also, now considering the abscissae of these graphs, L is the actual length of the strut along its line of thrust; $r = \sqrt{E/3f_L}$, where E is

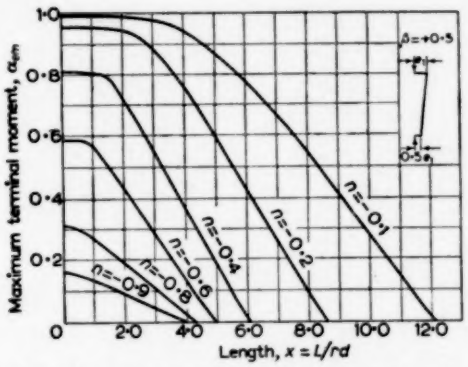

Fig. 5. Collapse loads for eccentrically loaded columns of annular cross-section.

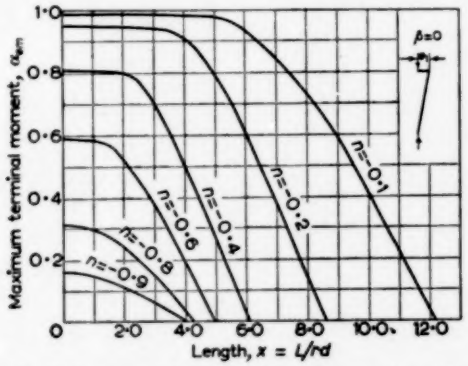

Fig. 6. Collapse loads for eccentrically loaded columns of annular cross-section.

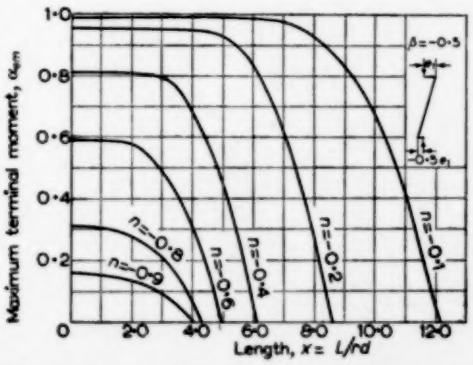

Fig. 7. Collapse loads for eccentrically loaded columns of annular cross-section.

Young's Modulus and f_L is the lower yield stress; and d is a representative dimension of the cross-section which for this problem was taken as the actual mean radius

of the annulus. It should be noted that r is a purely arbitrary relationship and is not to be confused with the radius of gyration.

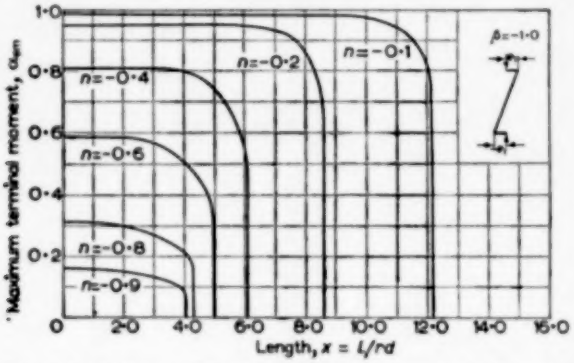

Fig. 8. Collapse loads for eccentrically loaded columns of annular cross-section.

Relation between an actual and a non-dimensional strut

To make the results of this work applicable to the general case of the compression member on the point of collapse, it is necessary to express all the physical data in a non-dimensional form. Figs. 9 and 10 and equations (1) to (6) below relate an actual strut to a non-dimensional one.

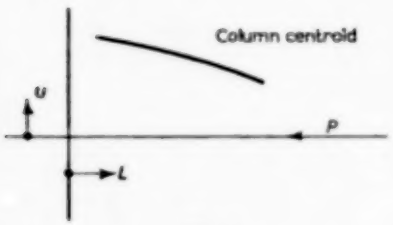

Fig. 9.

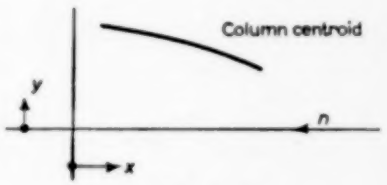

Fig. 10.

$$n = P/P_P \tag{1}$$

$$y = U/d \tag{2}$$

$$x = L/rd \tag{3}$$

$$1/\rho = r^2\, d\,(1/z) \tag{4}$$

$$M = PU \tag{5}$$

$$\alpha = M/M_P \tag{6}$$

In the above equations, n is the ratio of the axial thrust under zero moment to the fully plastic axial thrust, P/P_P. The actual deflection of the centroid of the strut from the thrust line is U. This is translated into a non-dimensional form by dividing it by d, a representative dimension of the cross-section which for this work is taken as the mean radius of the annulus R. The length of the strut measured along the line of thrust is L; its non-dimensional equivalent is x as given by equation

(3) in which r is $\sqrt{E/3f_L}$. The modulus of elasticity is E and the lower yield stress is denoted by f_L. The actual curvature, $1/z$, is changed to the non-dimensional curvature, $1/\rho$, by multiplying by $r^2 d$. Equation (5) expresses the actual moment as the thrust multiplied by the actual deflection (Fig. 9) and equation (6) translates this moment by dividing it by M_P, the fully plastic moment under zero axial thrust, to give α, the non-dimensional expression for the moment. The non-dimensional slope of the centre line of the strut is denoted by ϕ.

The sign convention for Fig. 10 is :

$$x \text{ — positive,} \qquad y \text{ — positive,} \qquad n \text{ — negative,}$$

$$\phi = dy/dx \text{ — negative,} \qquad 1/\rho = d\phi/dx \text{ — negative.}$$

Shape of a strut

The relation of the non-dimensional quantities of moment, thrust and deflexion for a strut having an annular cross-section is given by

$$\alpha = \tfrac{1}{2}\pi ny. \tag{7}$$

The first order differential equations which define the relation of the thrust, moment and length of a strut having an annular cross-section are

$$d\alpha/dx = \tfrac{1}{2}\pi n\phi, \tag{8}$$

$$d\phi/dx = 1/\rho. \tag{9}$$

By integrating (8) and (9), starting from a point where $\phi = 0$ with any given value of α and keeping n constant, the types of curve in Fig. 11 can be obtained.

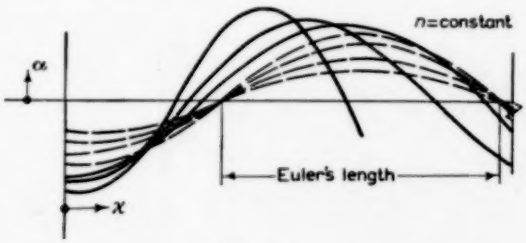

Fig. 11.

When the yield stress is nowhere exceeded, i.e. all stresses are in the elastic range, the integration of (8) and (9) results in the dotted curves which all have the wave length given by Euler's column formula. If, however, the maximum moment just causing yield is reached or exceeded, then stresses in the plastic range are encountered and the integration of (8) and (9) gives the solid curves of Fig. 11. Thus, stresses in the plastic range cause deflexion curves that do *not* have, for a given n, a constant wave length. The fact that such deflexion curves overlap one another at points not on the horizontal axis is the key to the theory of this paper.

Failure criterion A

The writer originally intended to find the shape of a strut and values of $d\alpha/d\phi$, for successive values of x as in Fig. 12. By solving (8) and (9), starting from a

point where ϕ = constant = ϕ_e with any given value of α and keeping n constant, the type of curve shown by the solid line in Fig. 12 can be obtained. If, at the point of maximum moment, stresses exist in the plastic range, then two curves shown by the solid and dotted lines in Fig. 12 can be drawn. Since any strut

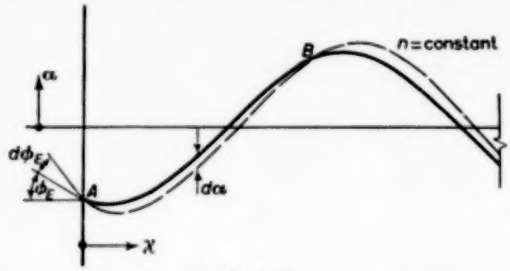

Fig. 12.

having a constant thrust and constant end moments cannot assume more than one shape unless it is collapsing, we have between points *A* and *B* on Fig. 12 a collapse strut.

As mentioned below, this failure criterion *A* was considered less favourable for the present purposes than failure criterion *B*.

Failure criterion B

If, at the point of maximum moment, stresses exist in the plastic range, then two immediately adjacent curves can be drawn as in Fig. 13. A study of Figs. 12 and

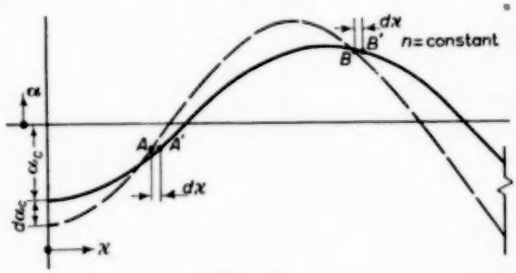

Fig. 13.

13 will reveal that they are similar except that in the latter the vertical axis through the origin has been chosen to intersect with the points of maxima moments of both the solid and the dotted curves.

It must be noted that at points *A* and *B* the horizontal distances between the two curves of Fig. 13 are both the same and equal to dx. Thus the length between *A* and *B* equals the length between *A'* and *B'*. The moments at *A* and *A'* are equal to one another as are the moments at *B* and *B'*. Two different deflexion curves *AB* and *A' B'* exist which are both of the same length ; both are subjected to the same thrust and the same end moments. As any strut having a constant thrust and constant end moments can not assume more than one shape unless it is collapsing, we have between points *A* and *B* a collapse strut.

This failure criterion, which was suggested to the writer by HORNE, was adopted because it promised to reduce the amount of computation by the digital computer which would have been required by the collapse criterion *A*.

Values of $dx/d\alpha_c$ for failure criterion B

The next step was to develop a method of obtaining values of $dx/d\alpha_c$ for successive values of x. Obviously by plotting a number of curves similar to Fig. 13 it would be possible to obtain graphically the required information. Greater accuracy, however, was achieved by following the general method used by EICKHOFF (1955), whereby equations (8) and (9) were differentiated with respect to α_c, the moment at zero slope, giving

$$\frac{d}{dx}\left[\frac{\partial\alpha}{\partial\alpha_c}\right] = \tfrac{1}{2}\,\pi\,n\,\frac{\partial\phi}{\partial\alpha_c}, \tag{10}$$

$$\frac{d}{dx}\left[\frac{\partial\phi}{\partial\alpha_c}\right] = \frac{d\,(1/\rho)}{d\alpha}\left[\frac{\partial\alpha}{\partial\alpha_c}\right]. \tag{11}$$

Before proceeding further it is convenient to collect the differential equations :

$$\frac{d\alpha}{dx} = \tfrac{1}{2}\,\pi\,n\phi, \tag{12}$$

$$\frac{d\phi}{dx} = 1/\rho, \tag{13}$$

$$\frac{d}{dx}\left[\frac{\partial\alpha}{\partial\alpha_c}\right] = \tfrac{1}{2}\,\pi\,n\left[\frac{\partial\phi}{\partial\alpha_c}\right]. \tag{14}$$

$$\frac{d}{dx}\left[\frac{\partial\phi}{\partial\alpha_c}\right] = \frac{d\,(1/\rho)}{d\alpha}\left[\frac{\partial\alpha}{\partial\alpha_c}\right]. \tag{15}$$

The integration of these provided Tables, for a given n, of the following quantities: x, α, ϕ, $\partial\alpha/\partial\alpha_c$ and $\partial\phi/\partial\alpha_c$. From these Tables, $d\alpha/dx = \frac{1}{2}\,\pi\,\phi$ and $\partial\alpha/\partial\alpha_c$ were provided, and $dx/d\alpha_c$ was evaluated using

$$\frac{dx}{d\alpha_c} = \left[\frac{\partial\alpha}{\partial\alpha_c}\right]\frac{1}{(d\alpha/dx)}. \tag{16}$$

This ratio yielded the values of $dx/d\alpha_c$ for successive values of x.

Integration of equations (12) to (15)

The first step to integrate equations (12) to (15) was to obtain, for a constant n, a table relating the moment and the curvature. The algebraic expressions for this relationship for the three stress conditions of elasticity (case 1), plasticity in the compression zone only (case 2), and plasticity in both zones (case 3) are recorded in Appendix A. Only for case 1 was the curvature found to be an explicit function of the moment ; for cases 2 and 3 the numerical values for the moment-curvature tables were computed by a trail process using the E.D.S.A.C. I (WILKES, WHEELER and GILL 1951).

From the moment-curvature table the values of $d\,(1/\rho)$ were obtained in terms of differences by means of the first two terms of the following formula from the *Nautical Almanac* (1937) :

$$d\,(1/\rho) = w\,f_0^{\mathrm{I}} = \Delta_0^{\mathrm{I}} - \frac{1}{6}\,\Delta_0^{\mathrm{III}} + \frac{1}{30}\,\Delta_0^{\mathrm{V}} - \frac{1}{140}\,\Delta_0^{\mathrm{VII}} + \ldots. \tag{17}$$

The interval of tabulation is denoted by w and the notation is given in Table 1.

$$\Delta_0^{\mathrm{I}} = \tfrac{1}{2}\left[\Delta_{-\frac{1}{2}}^{\mathrm{I}} + \Delta_{\frac{1}{2}}^{\mathrm{I}}\right], \qquad \Delta_0^{\mathrm{III}} = \tfrac{1}{2}\left[\Delta_{-\frac{1}{2}}^{\mathrm{III}} + \Delta_{\frac{1}{2}}^{\mathrm{III}}\right]$$

$$\Delta_{\frac{1}{2}}^{\mathrm{II}} = \tfrac{1}{2}\left[\Delta_0^{\mathrm{II}} + \Delta_1^{\mathrm{II}}\right], \qquad \Delta_{\frac{1}{2}}^{\mathrm{IV}} = \tfrac{1}{2}\left[\Delta_0^{\mathrm{IV}} + \Delta_1^{\mathrm{IV}}\right].$$

Two tables were obtained for a constant n, the first relating the moment and the curvature (C Table), and the second relating the moment and $d(1/\rho)$, i.e. relating the moment and the incremental change in the curvature (D Table).

TABLE 1

Function	*1st difference*	*2nd difference*	*3rd difference*
f_{-1}	$\Delta_{-\frac{1}{2}}^{\mathrm{I}}$	$\Delta_{-1}^{\mathrm{II}}$	$\Delta_{-\frac{1}{2}}^{\mathrm{III}}$
f_0	$\Delta_{\frac{1}{2}}^{\mathrm{I}}$	Δ_0^{II}	$\Delta_{\frac{1}{2}}^{\mathrm{III}}$
f_{+1}		$\Delta_{+1}^{\mathrm{II}}$	

Equations (12) to (15) were integrated using these two tables for the plastic zones of a strut. At each value of α the C Table provided a value of $1/\rho$ as required in (13) and the D Table provided a value of $d(1/\rho)$ from which $d(1/\rho)/d\alpha$ was obtained as required in (15). For the elastic zones, of a strut the values of $1/\rho$ and $d(1/\rho)$ were calculated directly without recourse to the tables.

For both plastic and elastic zones the integrations were carried out by means of the Runge-Kutta subroutine of E.D.S.A.C. I (PIAGGIO 1954); U.M.I.L. 1956).

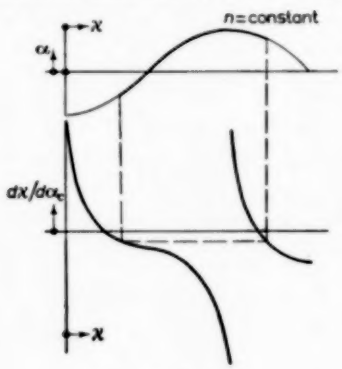

Fig. 14.

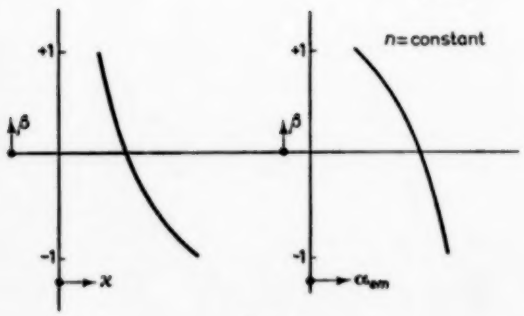

Fig. 15.

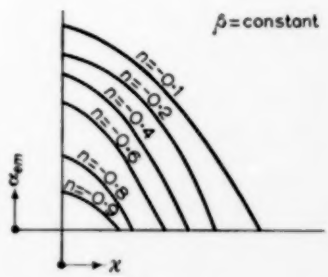

Fig. 16.

Determination of a collapse strut

From one integration result two graphs were plotted (Fig. 14). A failure strut is shown in

heavy outline and the necessary construction lines are shown dotted. This particular failure strut can be represented on Fig. 15 by two points, in which β is the ratio of the terminal moments, and hence by the consideration in Fig. 14 of a number of failure struts the two curves of Fig. 15 can be created.

Fig. 15 was used to obtain one point on a graph for a given value of β such as is shown in Fig. 16. By considering a number of integration results a series of graphs similar to Fig. 16 for different values of β were obtained. These are recorded in Figs. 4–8 which represent examples of the results of this theoretical investigation of the problem.

From these graphs the cross-sectional dimensions of a column namely the mean radius R and the thickness h, can be obtained by trial for given values of P, end moments, and L. Values of R and h are first guessed, and then n is calculated. Knowing n, β and the maximum end moment, one may use the appropriate graph to obtain L, which, if it be less than or equal to the L required, means that the R and h are satisfactory from the stand-point of safety. Further trials would result in the safe and economic dimensions of a collapse strut.

3. Experimental Investigation

A total of 15 column tests, one pure bending test, 14 compression tests, and 10 tensile tests were conducted.

Three sets of column experiments were tested under the following three loading conditions :

(i) Single curvature bending with equal end eccentricities.

(ii) Single curvature bending with eccentricity of load at one end only.

(iii) Double curvature bending with end eccentricities of the same magnitude but of opposite sign.

All the columns were of an annular cross-section with an outside diameter of about 4·5 in. For the first two sets of experiments the tube thickness was about 0·138 in. and the length between the centres of the balls used to transfer the load to the columns was about 61·7 in. For the third set of experiments the tube was about 0·248 in. in thickness and the length between the centres of the balls was about 113·5 in.

The columns tested in double curvature failed at the end which first exhibited marked cracking of the resin with which the member had been coated. The ends remote from the failure ones also exhibited cracking but to a lesser degree. At loads approaching the collapse load the deflected form of the column is shown in an exaggerated manner by Fig. 17. It would appear that a weak section towards the end of a double curvature column could change the type of loading from that of double curvature to one approximating single curvature with no moment at one end. For materials not rigidly inspected the plastic theory of double curvature columns should be based on the single curvature case with no moment at one end.

Fig. 17.

Compression tests of tubing contiguous to each column were implemented to ascertain the yield stress. The load was applied axially through 2 in. diameter balls ; the distance between the centres was 16 in.

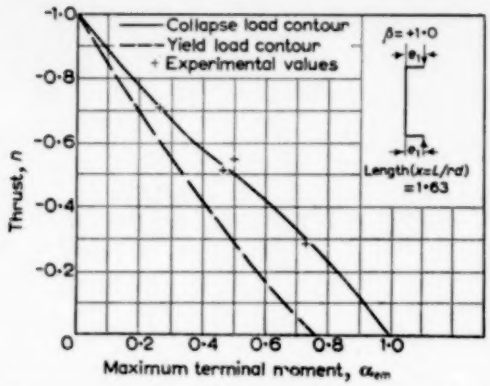

Fig. 18. Comparison between theories and experiments for eccentrically loaded columns of annular cross-section.

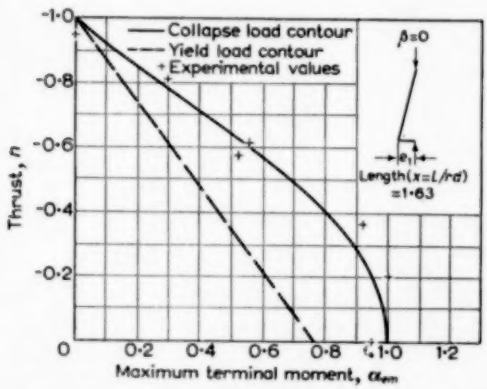

Fig. 19. Comparison between theories and experimenents for eccentrically loaded columns of annular cross-section. *This test was not continued long enough to determine the maximum moment and therefore this point does not include the effect of strain hardening.

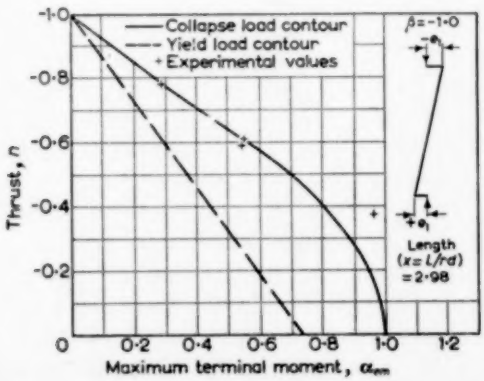

Fig. 20. Comparison between theories and experiments for eccentrically loaded columns of annular cross-section.

Tensile specimens were used to obtain the modulus of elasticity and the ratios between the upper yield stress, the lower yield stress and the ultimate stress.

4. Correlation Between Theory and Experiments

Figs. 18–20 compare the plastic theory, the elastic theory and the experimental results. The reserve of strength, beyond that predicted by the plastic theory, which was exhibited by some of the columns was considered to be due to strain hardening. Strain hardening was only effective where the thrust was relatively low and the length of column subjected to a high bending moment was relatively short and confined to near the end of the member.

It is considered that, if this explanation regarding strain hardening be accepted, these experiments support the plastic theory.

5. Assumptions

In this work the following standard theoretical assumptions of flexure are made:

(i) The material is homogeneous and isotropic in both the elastic and plastic states.

(ii) The moduli of elasticity in tension and compression are equal.

(iii) The yield stresses in tension and compression are equal.

(iv) The material obeys Hooke's law in the elastic range.

(v) There is no significant upper yield stress.

(vi) There is no significant strain hardening.

(vii) In the plastic range the stress remains constant.

(viii) The entire transverse section of the strut, originally plane, remains plane and normal to the longitudinal fibres of the strut after bending.

(ix) Every longitudinal fibre acts separately from every other fibre, i.e. there are no lateral pressures or shearing stresses between the fibres.

(x) The strut is straight and of uniform cross-section.

For this work (i) is the most important of these time-honoured assumptions. The compression yield stresses varied by as much as $\pm$ 4·5 per cent from the average for the material from the same cast. This variation was not considered to be excessive for mild steel.

As the yield stress greatly affects the stength of struts designed by the plastic theory, it is essential that a very thorough knowledge of the minimum value of the yield stress be obtained. As mentioned above an inadequate knowledge of the yield stress is dangerous especially for double curvature loading.

The relationships of the moment-thrust-curvature are derived from algebraic expressions based on the assumption that the cross-section is a thin annulus.

In the analysis of the experiments the effect of the end fittings of the columns was ignored.

In addition the following factors were not taken into account :

(i) Shear acting across a strut weakens the section's resistance to bending.

(ii) A strut is shortened due to strain at the centroid.

(iii) The formula for the curvature is not exact, due to the neglect of a factor equal to the square of the slope of the member which is normally insignificantly small.

(iv) Strain history.

(v) Residual stresses.

(vi) Shakedown.

(vii) Fatigue.

(viii) Local buckling.

6. Analysis of Columns in a Framework

Existing methods of analysis

When the critical loading condition of a framework is an overall collapse mechanism such as that of Fig. 21 then the terminal moments of the columns can be determined by inspection or by the equations of statical equilibrium. Of course the use of the collapse mechanism to analyse a framework is based on the assumption that the terminal moment-end rotation curves of the columns have a long flat peak as shown in Fig. 22 (Horne 1957). Such desirable curves result when the columns have a low slenderness ratio, a low axial stress, and are subjected to double curvature bending or single curvature bending with negligible moment at one end. For columns of high axial stress the curves have a sharp peak; and for columns of symmetrical single curvature bending at both high and moderate axial stress, the fall-off in load is precipitous, although in some cases the extent of end rotation may be sufficient to permit the analysis of frames containing such columns by the basic theorems of collapse mechanisms.

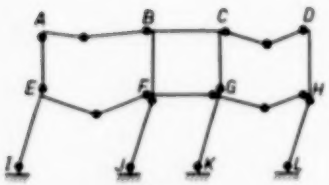

Fig. 21.

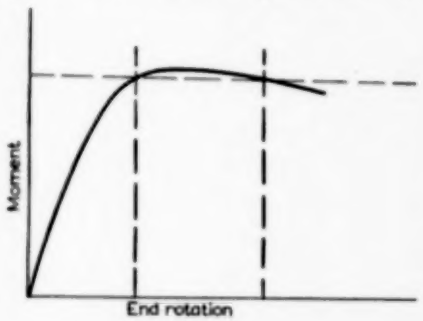

Fig. 22.

For critical loading conditions not specified by overall collapse mechanisms and for columns not having a flat peaked terminal moment-end rotation curve, several methods of analysis have been advanced and are mentioned below.

A theoretically rigorous method for the symmetrical single curvature column of only one storey is outlined towards the end of HORNE's paper (1956a). WOOD (1957) has suggested an extension of this method for the asymmetrical double curvature column of only one storey. Undoubtedly this theoretically rigorous method can cope with the general case of continuous asymmetrical columns attached to elastic-plastic beams, but it is suspected that this method will long remain a research approach.

HORNE (1956b) sets out a method of determining the terminal moments for four values of $\beta = +1{\cdot}0, -1{\cdot}0, 0{\cdot}0$ and $-0{\cdot}5$. This method assumes that the columns would be far removed from their instability load. The results exemplified by Figs. 4–8 of this paper demand a more refined method and one which can deal with columns up to, but not including, their point of collapse.

Another approach is to carry out elastic computations, taking axial thrusts into account and substituting plastic hinges at the points where the moment becomes equal to the plastic one. Of course this assumes that the fully plastic moment at the lower yield stress equals the maximum elastic moment at the higher yield stress, and that the structure is entirely elastic between hinges. This analysis will give the terminal moments and the thrusts for the columns. However, it is illogical because, although the columns are assumed to behave elastically except at the hinges, the resulting terminal moments and thrusts are used to check the safety of these very columns by means of curves (Figs. 4–8) which depend on radically different assumptions.

From this survey of existing methods of analysis, it was considered desirable to attempt to discover an analytical method based on the elastic-plastic behaviour of columns. Such a method should be reasonably straightforward and sufficiently refined to make full use of the extensive data of collapse loads which have been computed for this work.

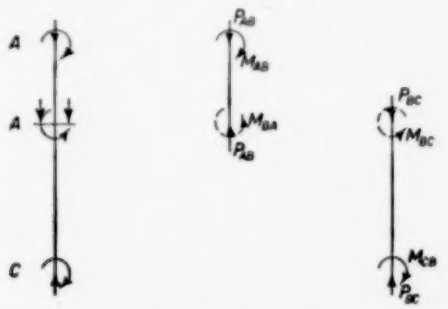

Fig. 23.

An iterative method

This suggestion is best illustrated by the following example in which the problem is to analyse the columns shown in Fig. 23. The joints are assumed to remain in a vertical line.

The external moment at B is distributed into AB according to its elastic stiffness as suggested by HORNE (1956c). Thus, for AB the following quantities are known : n, $\varkappa$, β and α_{em}. From

the appropriate curve of Figs. 4–8 a check is made to determine whether or not this column is safe. If it is safe, its end slopes are obtained by entering Fig. 24. The use of Fig. 24. is unfortunately not straightforward. The upper set of curves is examined until a length is found which suits the column in question. That is, the length of curve equals the column length and its terminal moments are approximately equal to those of the column. The next step is to project vertically from the curve of the upper set to its corresponding curve of the lower set which gives the end slopes.

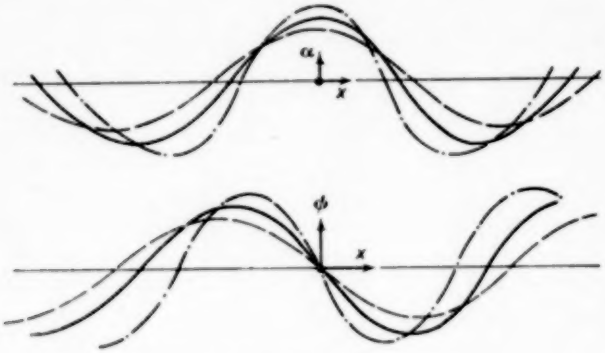

Notes: (1) n is the parameter
(2) Two sets of curves are related by similar dotted lines

Fig. 24.

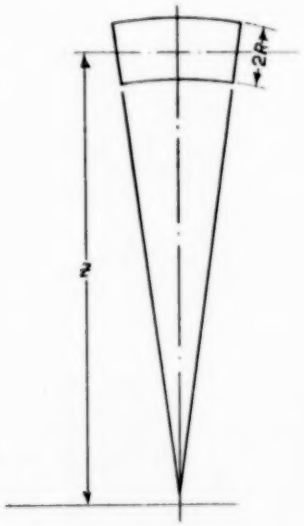

Fig. 25.

Now column BC is considered. Its slope at B is known to equal that of column AB which has just been found; thus for column BC the following quantities are known : ϕ_{BC}, M_{CB}, x and n. From Fig. 24, M_{BC} is determined by a procedure inverse to that described in the preceding paragraph, which gives β. From Figs. 4–8 the safety of the column can be ascertained.

At this stage the safety of both columns has been checked, their slopes at B agree, but the sum of their moments at B does not necessarily equal the external moment at that joint. Only by repeated trials of distributing the moment at B into the columns can the following three requirements be achieved : safety, continuity of slope and equilibrium of moments.

It is true that Fig. 4–8 are in a sense redundant, for if two curves in Fig. 24 were to satisfy the terminal moments and length, the column would be on the point of collapse. However, Figs. 4–8 eliminate the need to check Fig. 24 for this lack of uniqueness.

One point that merits emphasizing is that the column, in this method of analysis, is *not* on the point of collapse. It is safe, i.e. capable of carrying additional load. The margin of safety would be revealed by Figs. 4–8. Obviously, the smaller the margin, the more economic the design.

It will be appreciated that the above method can be extended to a framework of many joints, with or without sidesway, in which the beams either remain completely elastic or have plastic hinges.

The problem of elastic-plastic beams has been explored by EICKHOFF (1955) who considered only a uniform loading of the beams. This question of elastic-plastic beams has also been investigated by PERCY (1956), but design data for different types of loading on beams have been found too complicated to be prepared; therefore the analysis of frameworks having elastic-plastic beams is, as yet, too formidable a task.

A sample calculation of a problem similar to that shown in Fig. 23 was solved by the iterative method to give a numerical answer. The two columns were both bent in asymmetrical double curvature and both had stresses in the plastic range. The solution required four iterations and was straightforward.

The solution of complicated frameworks by the iterative method might prove to be best implemented by digital computers. Of course the extensive series of graphs which are required by this method would have to be replaced by approximate functions (HASTINGS 1955) which could be concisely retained in the store of the computer.

7. CONCLUSIONS

This paper sets forth a theory of predicting the loads at which columns of an annular cross-section will collapse when subjected to end loads of equal and unequal end eccentricities. The results of this theory have been presented in curves, of which Figs. 4–8 are examples. Large scale experiments have been conducted to check this theory and the agreement with the theory is illustrated by Figs. 18–20.

A method of analysing columns in a framework is advanced. This is iterative in character, and is considered capable of handling combinations of elastic members, columns stressed in the plastic range, and beams containing plastic hinges. The analysis of columns in a framework by this iterative approach requires extensive curves which have recently been prepared at Cambridge.

It is now possible to proceed with an examination of the economies that may result from the advances represented by this paper. Work is being started on this at the University of Toronto and the Royal Military College, Kingston, Canada.

8. ACKNOWLEDGMENTS

The writer's chief obligation, which he gratefully acknowledges, is to Dr. M. R. HORNE, Department of Engineering, Cambridge University, for his encouragement and constructive advice. He also wishes to thank Prof. J. F. BAKER and the staff members of the Engineering Laboratory, Cambridge, for their interest and generous co-operation. Dr. M. V. WILKES, Mathematical Laboratory, Cambridge, appointed him a Fully Authorized User of the University's

Electronic Delay Storage Automatic Computer ; he is indebted to him for this, and to the members of his staff for their assistance. Prof. J. W. DOLPHIN of the Royal Military College, Kingston, Canada, gave valuable assistance in the preparation of the paper. The writer received financial support from the Government of the United Kingdom as an Athlone Fellow for two years, and from the National Research Council of Canada for part of one year.

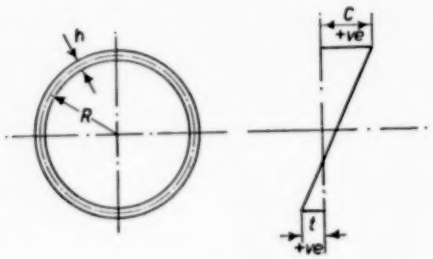

Fig. 26.

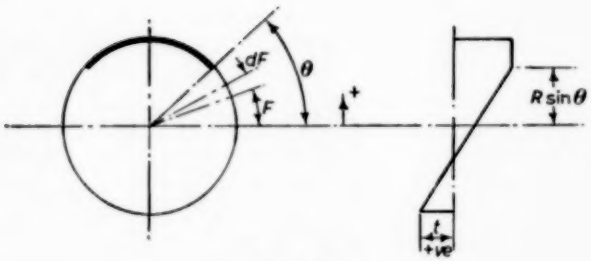

Fig. 27.

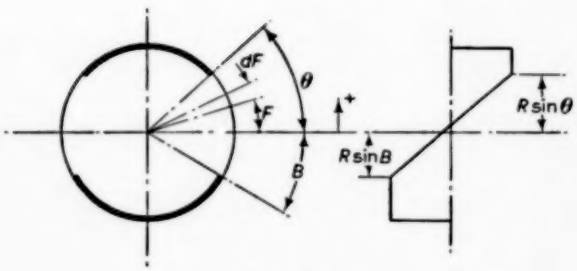

Fig. 28.

APPENDIX A

This appendix records the algebraic expressions relating the moment, thrust and curvature for the three stress conditions : elasticity (case 1), plasticity in the compression zone only (case 2), and plasticity in both zones (case 3). The notation used in this Appendix is illustrated by Figs. 26–28.

Case 1, elasticity (Fig. 26).

$$n = \left(\frac{t-c}{2}\right). \tag{18}$$

$$\alpha = \frac{\pi}{8}(c+t). \tag{19}$$

$$1/\rho = \alpha \times \frac{1}{6} \times \frac{8}{\pi}. \tag{20}$$

Case 2, plasticity in the compression zone only (Fig. 27).

$$n = -\left[1 - \frac{1\,(1+t)}{\pi\,(1+\sin\theta)}\{\sin\theta\,(\theta+\pi/2)+\cos\theta\}\right]. \tag{21}$$

$$\alpha = -\left[\frac{(1+t)}{(1+\sin\theta)}\left\{\frac{\sin\theta\cdot\cos\theta}{4}+\frac{\theta}{4}+\frac{\pi}{8}\right\}\right]. \tag{22}$$

$$1/\rho = \frac{-(1+t)}{3\,(1+\sin\theta)}. \tag{23}$$

Case 3, plasticity in both zones (Fig. 28).

$$n = \frac{2B}{\pi} + \frac{2}{\pi}\left(\frac{\sin\theta}{\sin\theta-\sin B}\right)(\theta - B) + \frac{2\,(\cos\theta-\cos B)}{\pi\,(\sin\theta-\sin B)}. \tag{24}$$

$$\alpha = -\cos B - \frac{\sin\theta\,(\cos\theta-\cos B)}{(\sin\theta-\sin B)} - \frac{(\theta-\sin\theta\cdot\cos\theta-B+\sin B\cdot\cos B)}{2\,(\sin\theta-\sin B)}. \tag{25}$$

$$1/\rho = \frac{-2}{3\,(\sin\theta-\sin B)}. \tag{26}$$

Notation

c = A quantity defining the state of stress across an annular cross-section (Fig. 26).
d = The representative dimension of the cross-section, which for an annulus was taken as R.
e = End eccentricity of the thrust in the experiments.
e_1 = The maximum end eccentricity for the graphs of the collapse loads.
f_L = Lower yield stress.
f_0 = Defined in Section 2.
h = Actual thickness of an annulus.
k = Actual curvature.
n = Mean axial stress divided by f_L.
$r = \sqrt{E/3f_L}$.
t = A quantity defining the state of stress across an annular cross-section (Fig. 26).
w = Defined in Section 2.
x = Non-dimensional length along the line of thrust of the strut.
y = Non-dimension deflection of the centroid of the strut from the line of thrust.
z = Actual radius of curvature (Fig. 25).
B = A quantity defining the state of stress across an annular cross-section (Fig. 28).
E = Young's Modulus.
I = Moment of inertia of the cross-section.
L = Length along the line of thrust of the strut.

M = Bending moment.
M_P = Fully plastic moment under zero axial thrust.
P = Axial thrust.
P_P = Fully plastic axial pull under zero moment.
R = Mean radius of an annulus.
R_0 = Outside radius of an annulus.
R_i = Inside radius of an annulus.
U = Deflexion of the centroid of the strut from the line of thrust.
$\alpha = M/M_P$, non-dimensional moment.
α_c = Non-dimensional moment at zero slope.
α_{em} = The greater numerical α acting at the end of a strut.
β = Ratio of the terminal moments.
Δ_0 = Defined in Section 2.
θ = A quantity defining the state of stress across an annular cross-section (Fig. 27).
$1/\rho$ = Non-dimensional curvature.
$\phi = dy/dx$ Slope.
ϕ_e = Slope at the end of a strut.

REFERENCES

BAKER, J. F., HORNE, M. R. and RODERICK, J. W.	1949	*Proc. Roy. Soc.* A **198**, 493.
BIJLAARD, P. P.	1954	*Proc. Second U.S. Nat. Congr. Appl. Mech.* p. 555.
'LEICH, F.	1952	*Buckling Strength of Metal Structures.* (McGraw-Hill New York).
EICKHOFF, K. G.	1955	Ph.D. Thesis, Cambridge.
HASTINGS, C.	1955	*Approximations for Digital Computers.* (Princeton University Press, Princeton, New Jersey).
HORNE, M. R.	1956*a*	*J. Mech. Phys. Solids* **4**, 104.
	1956*b*	*Brit. Weld. J.* **3**, 336.
	1956*c*	*Proc. Inst. Civ. Engrs.* **5**, 105.
	1957	*Brit. Weld. J.* **4**, 25.
Nautical Almanac	1937	Reprinted from the *Nautical Almanac* for 1937. H.M.S.O.
PERCY, J. H.	1956	Ph.D. Thesis, Cambridge.
PIAGGIO, H. T. H.	1954	*Differential Equations.* (Bell and Sons, London).
U.M.L.	1956	University Mathematical Laboratory, Cambridge.
WILKES, M. V., WHEELER, D. J. and GILL, S.	1951	*The Preparation of Programmes for an Electronic Digital Computer.* (Addison-Wesley, Cambridge, Mass).
WOOD, R. H.	1957	*Brit. Welding. J.* **4**, 9.

Journal of the Mechanics and Physics of Solids, 1958, Vol. 6, pp. 301 to 306. Pergamon Press Ltd., London

SINGLE CRYSTAL LATTICE ROTATION DURING COMPRESSION

By R. L. Fleischer
Massachusetts Institute of Technology

(*Received 22nd September*, 1957)

Summary

It is shown that lattice rotation during compression of a single crystal can be the reverse of that observed in tension rather than the slip-plane rotation predicted and observed by Taylor.

1. Introduction

The currently accepted description of the nature of lattice rotation during the compression of single crystals is that of Taylor (1927). For a crystal deforming on a single slip system, he suggested that the normal to the active slip plane should rotate toward the axis of compression. Taylor demonstrated experimentally that the rotation he predicted did occur in well-lubricated samples with height-to-diameter ratios of approximately 1/6.

This behaviour in compression is not merely in the opposite sense to the predicted and observed tension behaviour, (Taylor 1923), but in general is a rotation about a different axis. The purpose of this discussion is to point out that under suitable stressing conditions the lattice rotation under compression is the reverse of the tension rotation. To determine what these stressing conditions are, one must first examine the nature of the compression considered by Taylor and compare it with conventional tension testing. Slip on a single system is assumed throughout.

Fig. 1 illustrates the distinction between Taylor compression and conventional tension. Taylor considered the compression of a thin disk such as is illustrated in Fig. 1 (a). The compression plates were kept horizontal and the compression force vertical. In order that the crystal deform homogeneously on a single slip system it is necessary for one end of the sample to translate relative to the other, as is illustrated in Fig. 1 (b). To allow this translation careful lubrication of the plates is necessary. The compression axis during deformation is perpendicular to the compression plates and therefore does not remain parallel to the sides of the sample. In tension the stress is parallel to the sides. Figs. 1 (c) and 1 (d) illustrate the change in shape of a portion of a tensile sample which is assumed to be a few sample diameters distant from the grips. This assumption is needed because here the ends of the sample must have freedom to rotate relative to the gripping arrangement.

It can now be seen that the difference in the rotation calculated for tension and for compression arises because of a difference in definition of the stress axis in the two cases. If rotation in the compression case were referred to an axis parallel to the sides of the crystal (C' in Fig. 1 (b)), then lattice rotation as a function of shear strain during compression would be the reverse of that obtained in tension. Similarly, if a crystal is compressed such that the applied stress is always parallel to the sides, its lattice rotations will be the reverse of the tension behaviour (see Fig. 1 (e)).

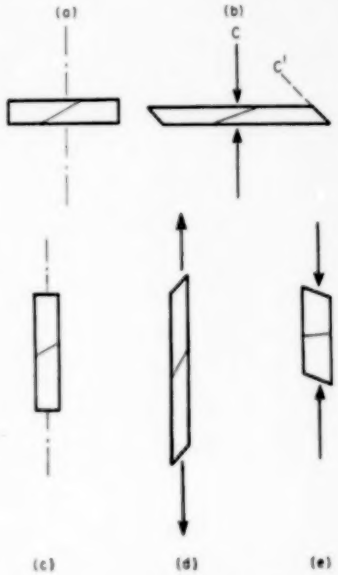

Fig. 1. Compression and tension axes.

In many of the common cases of compression, therefore, the rotation of the sample axis will be away from the slip direction. This should occur on the compression side during bending of a crystal and during the compression in fatigue by bending or push-pull. It follows that in fatigue no net rotation of the average lattice orientation should accumulate; this contrasts with what would be expected if different types of rotation occurred during the two halves of a cycle.

If one were to compress a crystal that is long relative to its thickness, then as long as the sides of the sample remain perpendicular to the compression plates, the slip direction rotates away from the compression axis. The change in shape in a section taken from the middle of such a sample is illustrated in Fig. 1 (c). It can be seen that, if the compression plates are kept horizontal, the rotation observed near the plates (as referred to the normal to the plates) must be different from that far from the plates. The expected rotation near the plates is that observed by TAYLOR for thin samples.

For tension in which the grips remain on a vertical line and do not rotate, KARASHIMA (1955) has pointed out that there exist two types of lattice rotations: (1) far from the grips there is the conventional rotation of the slip direction toward the specimen axis, and (2) near the grips the rotation is away from the slip plane normal. This is the tension analogue of the compression case just described. KARASHIMA showed both theoretically and experimentally that the existence of these two types of rotation could lead to a twisting about the specimen axis. This same effect should occur for cases of compression also.

It should be noted that TAYLOR chose the type of compression he used in order to produce uniform strain in his samples so that the distortion of an originally square grid could be analyzed. This requirement contrasts with the desire here, which, it will be seen, is to demonstrate that more than one type of rotation may exist within a single sample under suitable conditions of stress and lubrication. Needless to say, TAYLOR neither suggested nor implied that the type of compression he considered was of general application to other cases of compression.

2. Procedure and Results

Rotations during compression and bending were examined experimentally, and some fatigue results will be discussed. Lattice rotations were followed by means of the Laue back-reflection X-ray technique (Greninger 1935).

Taylor compression rotations can be distinguished from the reverse of the tension behaviour by (1) the amount of angular rotation for a given change in length along the compression axis and (2) by the direction of rotation. The first method is sensitive for all single slip orientations, while the second becomes more sensitive the further the original specimen axis is distant from the great circle connecting the slip direction and the slip plane normal. The great circle is relevant because rotation on it away from the slip direction and toward the slip plane normal are in the same direction. In Fig. 2 the great circle is drawn. It can be seen that the *direction* of rotation away from the slip direction should be distinct from rotation toward the slip plane normal in the case of samples of orientations *A* and *C* but not for *B*.

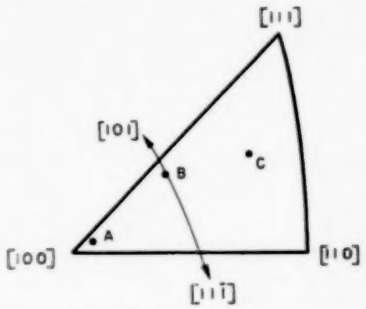

Fig. 2. Orientations of fatigue samples.

(*i*) *Simple compression*

Two single crystals were selected for compression parallel to their sides. The first was a 1·2 cm × 1·2 cm × 18 cm crystal of originally 99·99 per cent Alcoa aluminium, prepared by horizontal growth from the melt under hellium at a furnace motion rate of 1·2 cm/hr. The axial orientation is indicated by the circled dot in Fig. 3; the slip direction for the primary slip system is approximately parallel to one of the lateral faces of the sample. A 40 mm long section was cut from the middle of the original crystal. After etching as described by Barrett (1952), the sample was annealed at 640°C for 24 hr and furnace cooled over an 8 hr period. The sample was again heavily etched. At the start and after compressions of 5·6, 11 and 17 per cent orientations were determined at points 2 mm from one end and midway along the sample on each of two perpendicular lateral faces. After the final compression, orientations were determined at points 6 mm and 11 mm from one end of the sample.

The second crystal was a copper crystal 11 cm long and 1·2 cm in diameter*. The axial orientation is shown by the circled dot in Fig. 4. A 39 mm length was cut from the as-grown sample and etched for 5 min in nitric acid. At the start and after a compression of 6·9 per cent, orientations were determined 2 mm from one end and midway along the sample.

The samples were deformed in compression between accurately aligned steel compression plates. The ends were coated with Molykote M-88, a molybdenum disulphide lubricant. The purpose of the lubrication was to prevent large horizontal stresses such as would cause 'barrelling', but not to allow sufficient freedom that

*Supplied by M. Ebner, this sample was grown vertically from the melt under nitrogen from spectroscopically pure copper at an average growth rate of 1·6 in/hr.

horizontal translation of an end of the sample could occur. In fact after the copper crystal was compressed to strains greater than 6·9 per cent, it was found that horizontal translation had occurred along with some buckling so that only the rotation for 6·9 per cent strain could be measured validly. For the aluminium sample the sides of the sample were perpendicular to the compression plates throughout the deformation.

In Fig. 3 and 4 are indicated the orientations at various stages of the deformation along with the predicted paths of rotation. It was found that better defined X-ray spots could be obtained by reflection from the crystal surface which contained the slip direction, and hence more precise orientation determination was possible. Results from other surfaces are qualitatively identical but display more scatter. Orientations indicated in Fig. 3 and 4 are therefore all determined by X-ray examinations of surfaces oriented parallel to the slip direction.

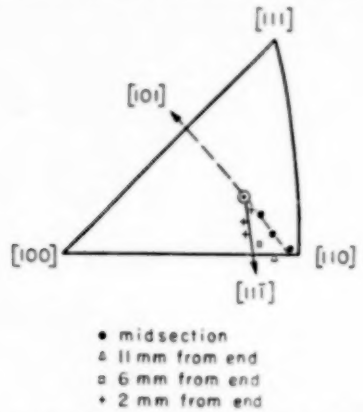

Fig. 3. Lattice rotation during compression of an aluminium crystal.

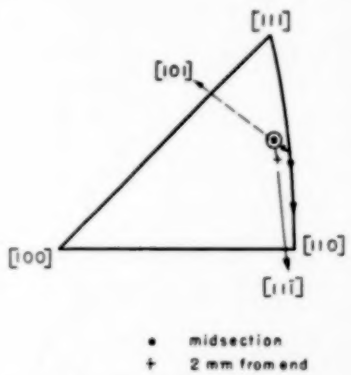

Fig. 4. Lattice rotation during compression of a copper crystal.

It can be seen (1) that the rotation near the end of the sample follows the path corresponding to the rotation of the slip plane toward the compression axis, (2) that the rotation at the centre section corresponds to the slip direction moving away from the axis, and (3) that the nature of the rotation varies gradually from one type to the other. The effects from the ends appear to extend along the length a distance equal to about one sample thickness.

There are three evidences that predominantly single slip did occur in the aluminium sample. The strongest is the nature of the observed lattice rotations, which coincide with what is expected for single slip. Secondly, the sample width perpendicular to the expected slip direction remained essentially constant within 2 per cent during compression. Lastly, some faint slip markings could be observed on two perpendicular surfaces; these markings coincided with the predicted primary slip plane orientation. It could also be seen that the rotation of these markings near the ends (within 6 mm of the ends) was less than nearer the midsection of the sample, agreeing with the X-ray observations.

If it is accepted that rotation at the ends is of the slip plane and at the middle is of the slip direction, the angle (θ) of expected lattice rotations for the two

cases can be computed using the following formulas (SCHMIDT and BOAS 1935):

In the first case $\sin(X - \theta)/\sin X = l_f/l_0$ (slip plane rotation),

and in the second $\sin(\lambda + \theta)/\sin \lambda = l_0/l_f$ (slip direction rotation).

Here X is the original angle between the compressive axis and the slip plane normal, λ is the original angle between the compressive axis and the slip direction, and l_0 and l_f are the original and final sample lengths. The results of such a calculation appear in Table 1. The agreement is good, if it is realized that uniform decrease in length along the sample was assumed for calculating the rotation angles. It seems more likely, however, that less strain occurs near the compression plates where the sample is most constrained, causing the observed rotation to be less than the calculated values at the ends and more at the mid-section.

TABLE 1. *Lattice rotation.*

	Mid-section		*End-section*	
Strain (per cent)	*θ obs.* ± 0·5°	*θ calc.*	*θ obs.* ± 0·5°	*θ calc.*
5·6	4°	3·6°	1°	3·4°
11	9°	7·6°	3·5°	6·2°
17	14°	12·5°	6°	8·9°

The copper sample would be expected to deform on two slip systems once the specimen axis reaches the $[1\bar{1}0]$ zone. The observed rotation at the middle of the sample appears to confirm this prediction.

(ii) Compression in bending

As was outlined earlier the lattice rotation in the compression side of a bent single crystal should be away from the slip direction. This behaviour was confirmed on a second sample cut from the aluminium crystal used for this study. In a previous study YEN and HIBBARD (1949) observed this same rotation.

The observed rotations are indicated in Fig. 5. There being greater difficulty in positioning a bent sample in the X-ray camera, the experimental scatter is considerably greater here than in the previous results.

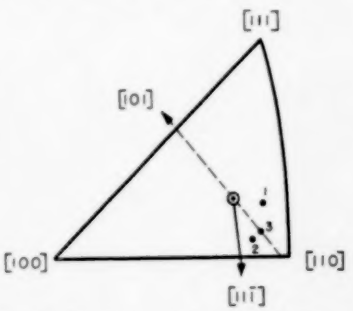

Fig. 5. Lattice rotation during compression in bending of a single crystal of aluminium.

(iii) Lattice rotation in fatigue

It was pointed out in an earlier section that no net lattice rotation should occur during fatigue. EBNER (to be published) has shown the following: In fatigue of copper single crystals (orientations A, B and C in Fig. 2) by plane bending with a surface strain amplitude of approximately 0·2 per cent, Laue back-reflection pictures show that within 2° there are no net lattice rotations. OFHC copper

was used ; growth was from the melt under nitrogen at approximately 1·6 in/hr growth rate. Laue pictures were taken at the start and at varying number of cycles up to 330,000 for sample A, 20,000 for sample B, and 74,000 for sample C.

3. CONCLUSIONS

The conclusions drawn here are these : (1) In many cases involving compression, the lattice rotation is that of the slip direction away from the stress axis ; (2) this is true in the least constrained portion of a single crystal compression sample provided it is long relative to its width ; (3) near the ends of such a sample or for samples short relative to their thickness the effect of the grips causes the rotation of the type predicted and observed by TAYLOR ; (4) the length of the region affected by the grips is of the order of the sample width.

ACKNOWLEDGMENTS

I am grateful to Mr. M. EBNER for permission to quote his unpublished results and for supplying the copper single crystal. Helpful discussions with Mr. M. EBNER and Mr. U. F. KOCKS are appreciated.

The financial assistance of the Atomic Energy Commission is gratefully acknowledged.

REFERENCES

BARRETT, C. S. 1952 *Structure of Metals*, p. 194 (McGraw-Hill, New York).
EBNER, M. (To be published).
GRENINGER, A. B. 1935 *Trans. Amer. Inst. Min. (Metall.) Engrs.* **117**, 61.
KARASHIMA, S. 1955 *Mem. Inst. Sci. Industr. Res.* **12**, 25
SCHMIDT, E. and BOAS, W. 1935 *Kristallplastizität* (Springer, Berlin).
TAYLOR, G. I. 1927 *Proc. Roy. Soc.* A **116**, 16.
TAYLOR, G. I. and ELAM, C. F. 1923 *Proc. Roy. Soc.* A **102**, 643.
YEN, M. K. and HIBBARD, W. A. 1949 *Trans. Amer. Inst. Min. (Metall.) Engrs.* **185**, 710.

Journal of the Mechanics and Physics of Solids, 1958, Vol. 6, pp. 307 to 313. Pergamon Press Ltd., London

GRIP EFFECTS IN THE DEFORMATION OF SINGLE CRYSTALS

By R. L. Fleischer* and B. Chalmers†

(*Received 27th February*, 1957)

Summary

A calculation is made of the average shear stresses caused by the reaction with the grips during a tensile test of a single crystal. By adopting a suitable work-hardening description, effects of changing sample thickness can be understood for face-centred cubic metals.

1. Introduction

The work hardening properties of single crystals vary markedly as a function of the external dimensions of the samples used : see, for instance, Yamaguchi (1927), Gilman (1953), Kitjaima (1954), Kitajima and Shimba (1955), Karashima (1955 and 1956), Suzuki, Ikeda, and Takeuchi (1956), Livingston (1956), Garstone, Honeycombe, and Greetham (1956), Noggle and Koehler (1957), and Fleischer and Chalmers (1958). In some of these cases the observations have been attributed to the bending moment applied by the grips during deformation. By superimposing appropriate bending moments during a tensile test Karashima (1956)showed experimentally that this explanation was consistent with his observations.

In this discussion a model is proposed for calculating the shear stresses caused by reaction with the grips during a tensile test. After assuming a simple qualitative model for workhardening, predictions can be made as to effects of specimen shape on the stress-strain curves. These predictions will be compared to experimental results reported previously for aluminium and copper. The calculation of the grip stress will be applicable to any case of slip, although the detailed description of workhardening will relate to face-centred-cubic lattices primarily.

2. Stress from the Grips

In Fig. 1a is shown a longitudinal cross section of a single crystal tensile sample which has deformed along a crystal plane which is an average distance x from one end and was not restrained by grips. The cross section is taken parallel to the slip direction. If this slip represents a fraction $1/n$ (where n is a large number) of the total elongation ϵL, it will result in a vertical displacement $y = (\epsilon L \tan D)/n$, where D is the angle between the slip direction and the specimen axis.

*Massachusetts Institute of Technology.
†Harvard University

We assume that the tensile machine used has non-rotating grips which require that the two ends of the specimen remain directly in line during the test. It is then necessary to apply a combination of forces and bending moments at the ends of the sample in order that the displacement y and the slope dy/dx be zero at each

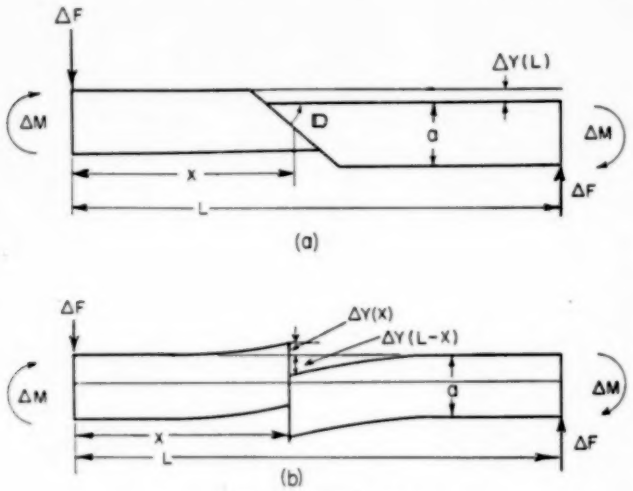

Fig. 1. A grip effect.

end. The specimen will be considered as the beam shown in Fig. 1b with a jog of length $(\epsilon L \tan D)/n$ at a distance x from one end. The force ΔF at the ends is to be found, and from it the total force $F = \int_0^L (n\Delta F)\, dx/L$ is calculated by the superposition of the forces for many such slipped sections distributed uniformly between $x = 0$ and $x = L$. The force F is a shearing force and is equivalent to an average shearing stress $\tau_g = F/S$ perpendicular to the axis of the specimen and in the plane in which y is measured. Here S is the cross sectional area of the sample.

Actually an upper limit will be found for the shearing force, since F will be calculated by assuming the sample is elastic. The general equation for the elastic curve of a beam will be used. The appropriate equation to be solved is

$$EI\,(d^2y/dx^2) = \Sigma M$$

where E is Young's modulus, I is the moment of inertia, and ΣM is the sum of the moments calculated at x. By taking moments about $x = 0$, the bending moment can be found. It then follows that

$$EI\,(d^2y/dx^2) = \tfrac{1}{2}L\Delta F - x\Delta F.$$

The boundary conditions on $y\,(x)$ at $x = 0$ and at the jog are the following:

$$y\,(0) = 0, \qquad dy\,(0)/dx = 0,$$

$$y\,(x) + y\,(L - x) = (\epsilon\, L \tan D)/n,$$

$$\Delta F\,(x) = \Delta F\,(L - x).$$

The third condition arises because the displacement at the jog is $(\epsilon L \tan D)/n$ and the fourth because the forces at the jog from each portion of the beam must be equal and opposite.

Straightforward application of the boundary conditions give

$$\Delta F = 12\,\epsilon E \tan D \left(\frac{I}{L^2}\right) \cdot \frac{1}{n},$$

and, therefore,

$$\tau_g = F/S = 12\,\epsilon E \tan D\,(I/SL^2). \tag{1}$$

In the special case of a rectangular sample with slip direction parallel to a side of width a, equation (1) becomes

$$\tau_g = \epsilon E \tan D\,(a/L)^2. \tag{2}$$

τ_g may be resolved on to the various slip systems by means of geometrical factors r_j so that the contributions to the shear stress on slip system j is $r_j\,\tau_g$, and one finds

$$(r_j/m_j) = 2 \operatorname{ctn} D_p - (\hat{b}_p \cdot \hat{b}_j)/(\sin D_p \cos D_j) - (\hat{b}_p \cdot \hat{N}_j)/(\sin D_p \cos X_j). \tag{3}$$

Here $(\hat{b}_p \cdot \hat{b}_j)$ is the cosine of the angle between the primary slip direction and the jth slip direction, and $(\hat{b}_p \cdot \hat{N}_j)$ is the cosine of the angle between the primary slip direction and the normal of the jth slip plane, D_j = angle between the specimen axis and the jth slip direction, and X_j = angle between the specimen axis and the jth slip plane normal. m_j is the Schmidt factor $\cos X_j \cos D_j$.

In addition to the shear stresses which are created by the shearing force at the ends there are axial tensile and compressive forces caused by the bending moments applied to the sample. Assume an $x - y$ co-ordinate system in the sample of Fig. 1 so that the x axis is along the tension axis, the y axis is perpendicular to it in the plane of the diagram, and the sample extends to $x = \pm \frac{1}{2}L$ and $y = \pm \frac{1}{2}a$. Then by standard methods (SEELY 1935) one finds that the axial stresses are given by

$$\sigma(x, y) = 3\tau_g \left(\frac{L}{a}\right)\left(\frac{2x}{L}\right)\left(\frac{2y}{a}\right).$$

There are then local shear stresses equal to $m_j\,\sigma(x, y)$.

Because of the variation of σ with x the average shear stress resulting from the tensile and compressive stresses is not zero except on a plane normal to the sample axis. By integrating the stress $m_j\,\sigma(x, y)$ over the jth slip plane one finds a shear stress $q_j\,\tau_g$ where q_j is a numerical factor depending on the orientation of the slip plane considered. It can be shown that

$$\frac{q_j}{m_j} = \frac{(b_p \cdot N_j) - \cos X_j \cos D_p}{\cos X_j \sin D_p}. \tag{4}$$

Adding the two contributions to the shear stress one may define a factor n_j where $n_j = r_j + q_j$. From (3) and (4)

$$\frac{n_j}{m_j} = \operatorname{ctn} D_p - \frac{\hat{b}_p \cdot \hat{b}_j}{\sin D_p \cos D_j}$$

$$= -\,(\widehat{A \times b_j}) \cdot (\widehat{A \times b_p}) \tan D_j. \tag{5}$$

where $(\widehat{A \times b_j}) \cdot (\widehat{A \times b_p})$ is the cosine of the angle between the projections of the primary and jth slip directions on the cross section (A is a vector along the sample axis).

In general the resolved shear stress τ_j on the various crystal planes will be the sum of the contributions from the applied stress, σ_a, and the grip stress, τ_g:

$$\tau_j = m_j \sigma_a + \sum_i n_{ij} \tau^i_g \tag{6}$$

where m_j = Schmidt factor for the jth slip system

τ^i_g = grip stress resulting from slip on the ith system

n_{ij} = fraction of the grip stresses arising from slip on system i that is resolved on system j.

Normally only the τ_g resulting from slip on the primary system will be considered, so that (6) reduces to

$$\tau_j = m_j \sigma_a + n_j \tau_g = m_j \left[\sigma_a - \epsilon E \left(\frac{a}{L}\right)^2 (\tan D_p \tan D_j)(\widehat{A \times b_j}) \cdot (\widehat{A \times b_p})\right] \tag{7}$$

where the index i has been dropped.

The resultant stress τ_p on the primary system is therefore

$$m_p \left(\sigma_a - \epsilon E \left(\frac{a}{L}\right)^2 \tan^2 D_p\right).$$

In the case considered here the τ_g term is a maximum on the plane whose normal is the specimen axis and has a direction in the opposite sense to that of the projection of the primary slip direction onto the cross section. It is to be noted that the $n_j \tau_g$ term will increase the stress on some slip systems and decrease it on others.

Once the quantity τ_j has reached a high enough value to produce additional deformation, plastic rather than elastic considerations apply, so that the value of τ_g from (2) would no longer be directly applicable but, as suggested earlier, would provide an upper limit.

3. Relation to the Stress-Strain Properties

To correlate the effect of the grip stress with observed crystal properties it is necessary to assume some model for describing the workhardening processes of single crystals. The model assumed here for face-centred cubic crystals is the following. Slip is very predominantly on the one system which has the highest resolved shear stress. The major source of hardening is slip on other systems, particularly those on other planes. It is primarily because of relatively small amounts of slip on intersecting planes that the slope of the easy glide region is not zero. The easy glide region is assumed to terminate when the stress on a secondary plane produces 'appreciable' slip here. Since secondary slip markings are seldom observed in this region, it would appear that 'appreciable' slip is still considerably less than the slip on the primary plane. The rounding off of the transition in slope from its minimum to its maximum value is evidence that this beginning of

'appreciable' slip is not a sudden process but occurs gradually over a range of stress, as a larger and larger proportion of secondary slip occurs. Following the end of easy glide the same considerations should apply except that larger relative amounts of secondary slip are assumed to occur.

In the light of this viewpoint the grip stress is important in that it alters the stresses on the various systems by amounts that depend on the extent of previous slip.

The effects of varying the sample thickness in a plane containing the slip direction and the tensile axis can now be described. Assume that from (7) it is found that increases in a increase the stress on the second favoured system, which is in a different plane from the primary, and that a decrease in the stress on the primary results. What one expects then is this : (i) The yield stress, since it is developed at small strains, is virtually unaffected. (ii) More slip on secondary systems will occur for the crystals of larger a, and the workhardening rates should consequently be greater. The increase in work hardening rate at the start of the easy glide region should be small (since ϵ is small) ; and after easy glide has ended, it should be larger. (iii) If the end of easy glide occurs when a critical stress τ_c is reached on some secondary system, then the measured stress, computed from (7), is $\tau_c/m - n\tau_g/m$. Hence, where τ_g is larger (for increasing a), the measured stress decreases. (iv) As a result of (ii) and (iii), the strain before easy glide ends would also decrease. (v) Because the ratios of the stresses on the various systems will change more rapidly where τ_g is larger, the wider specimens would have a greater rate of change of workhardening rate.

4. Relation to Experimental Data

To examine predictions of the previous discussion, one needs to know experimentally how the stress-strain curves of single crystals vary as a function of the sample dimensions. One such study has recently been described by the authors (Fleischer and Chalmers 1958). The work included the tension testing of a series

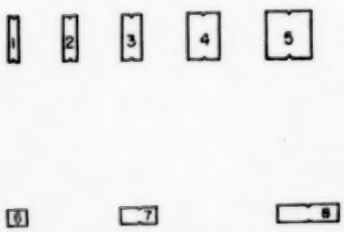

Fig. 2. Cross sections of samples.

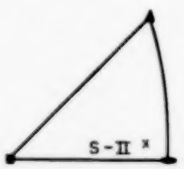

Fig. 3. Axial orientation.

of rectangular single crystals with various exterior dimensions. In one of these series (called S-II) the dimensions were varied in such a way as to vary a (see equation (2)). The proportions of the cross sections are indicated in Fig. 2. The projection of the slip direction would be nearly horizontal in the diagram. Size 5 is approximately 12 mm. by 12 mm. in cross section. The specimen axis orientation is shown in Fig. 3 and is one such that the assumption made in the previous

paragraph applies. Figs. 7, 8 and 9 given by FLEISCHER and CHALMERS indicate that as a is increased the easy glide slope is either constant or increases slightly, the stress and strain at the end of easy glide decrease markedly, the maximum work-hardening slope (after easy glide) increases markedly, and the subsequent rate of change of slope increases in magnitude. All of the preceding are in agreement with the predictions. One exception is to be noted. Although the stress at the end of easy glide decreased markedly for sizes 1 to 5, it remained constant for sizes 6 to 8.

In addition the yield stress varied with the parameter a. This effect, however, was believed to be caused by the oxide coating. As shown by TAKAMURA (1956) this oxide effect should be largest on the yield stress and less for the other parameters used here to describe the stress-strain curve; on the other hand the effect of the grips has been shown to increase the strain.

SUZUKI *et al.* (1956) observed tensile properties of copper single crystals of various diameters. The size effects they observed as a function of crystal diameter are in qualitative agreement with the predictions made here.

It is interesting to calculate values for τ_g from (2) using the strain at the end of easy glide. One finds $\tau_g = 58$ gm/mm^2 for size 3 as compared to an observed applied stress of about 90 gm/mm^2. For sizes 1 and 2 the calculated τ_g is less than 58 gm/mm^2, and for sizes 4 and 5 is greater than 90. The observed strain to the end of easy glide increases rapidly in going from size 3 to 2 to 1, while it is nearly constant from size 3 to size 5. It would therefore appear that, when τ_g is appreciably less than the applied stress, the elastic approximation assumed here is relevant, while when τ_g is of the order of, or larger than, the applied stress plastic considerations must be involved that are not directly calculable by the present arguments. Certainly, if the calculated elastic stress would be greater than the flow stress, some type of plastic deformation must occur. Whether this deformation would be by means of homogeneous slip or by formation of some type of deformation band is best determined by further experimental study.

For the work of SUZUKI *et al.*, a calculation of τ_g reveals that easy glide ended when τ_g was approximately half of the applied tensile stress. It followed that thinner crystals had greater regions of easy glide up to nearly 0·5 shear strain for crystals 0·02 cm. in diameter.

It is interesting to note the thickness-to-length ratio required to ensure that the grip stress be small relative to the flow stress throughout the lattice rotations to the position where duplex slip is expected geometrically. For the extreme case of orientation near a <110> tensile axis, nearly 30° lattice rotation is possible. If easy glide were to occur until the orientations for duplex slip were reached, the a/L value would need to be small relative to 1/100. This value is considerably less than the values usually chosen and seems, therefore, to provide a clue as to why easy glide usually ends well before orientations for duplex slip are reached.

The nature of the effect of length of a crystal on its stress-strain properties may be described as follows. In studies of aluminium and copper no consistent variation of the yield stress or the workhardening rates has been observed (SUZUKI *et al.* 1956, GARSTONE *et al.* 1956, FLEISCHER and CHALMERS 1958). For copper (SUZUKI *et al.*,) no consistent effect of length on the amount of easy glide was observed. For aluminium, results of GARSTONE *et al.* and FLEISCHER and CHALMERS indicate that there is more easy glide for shorter crystals.

The effect of length in the case of aluminium directly contradicts the predictions made here on the basis of elastic considerations. Hence the understanding of this effect must come from plastic rather than elastic arguments.

For hexagonal-close-packed crystals there is little or no slip intersecting the primary. If, as in face-centred-cubic metals, slip on secondary systems is important, these systems must be the other directions in the basal plane. Evaluation of n_j in (7) shows that the stress on the second favoured direction is reduced by the grip stress so that the rate of hardening may be reduced also when τ_g is larger. This effect was observed by GILMAN (1953) in zinc though the effect was not so regular nor consistent as are the effects in face-centred-cubic metals.

CONCLUSIONS

An elastic calculation of average shear stresses arising from reactions with rigid grips are consistent with observed effects of crystal thickness on the stress-strain curves of face-centred cubic metals.

The effects of crystal length must be resolved by further examinations of the plastic properties of metals.

ACKNOWLEDGMENTS

The authors wish to give thanks to Prof. B. BUDIANSKY for helpful discussions and to the Office of Naval Research for financial assistance.

REFERENCES

FLEISCHER, R. L. and CHALMERS, B.	1958	*A.I.M.E.* in course of publication.
GARSTONE, J., HONEYCOMBE, R. W. K. and GREETHAM, G.	1956	*Acta Met.* **4**, 485
GILMAN, J. J.	1953	*A.I.M.E.* **197**, 1217.
KARASHIMA, S.	1955	*Mem. Inst. Sci. Indus. Res.* **12**, 25.
	1956	*Ibid.* **13**, 35.
KITAJIMA, S.	1954	*Bull. Naniwa Univ.* **2**, 71.
KITAJIMA, S and SHIMBA, K.	1955	*Bull Naniwa Univ.* **3**, 159.
LIVINGSTON, J. D.	1956	Harvard University, Ph.D. Thesis.
NOGGLE, T. S. and KOEHLER, J. S.	1957	*J. Appl. Phys.* **28**, 53.
SEELY, F. B.	1935	*Resistance of Materials* (Wiley, N.Y.).
SUZUKI, H., IKEDA, S., and TAKEUCHI, S.	1956	*J. Phys. Soc. Japan* **11**, 382.
TAKAMURA, J.	1956	*Mem. Fac. Eng. Kyoto Univ.* **18**, 255.
YAMAGUCHI, K.	1927	*Sci. Pap. Inst. Phys. Chem. Res.* **6**, 271.

Journal of the Mechanics and Physics of Solids, 1958, Vol. 6, pp. 314 to 320. Pergamon Press Ltd., London

A MODIFICATION OF TAYLOR'S METHOD FOR CALCULATING THE PLASTIC STRESS–STRAIN RELATION IN FACE-CENTRED CUBIC CRYSTALS*

By H. Payne, S. J. Czyzak, J. H. Greiner† and T. H. Lin‡

(*Received 7th December* 1957)

Summary

A method is presented for determining the stress-strain relation in the plastic region for polycrystalline materials from empirical data on slipping in the corresponding single crystal. Results of calculations for uniaxial loading are presented.

1. Introduction

Taylor (1938) has obtained a theoretical stress–strain relation for aluminium in the plastic region, which is in reasonable agreement with experiment, by assuming that the plastic strain is due entirely to slip. This relation for the aggregate is calculated from the single slip data of the single crystal.

For face-centred cubic crystals, slip has been observed in the (111), (11$\bar{1}$), (1$\bar{1}$1) and ($\bar{1}$11) planes. The possible slip directions, of which there are three for each plane, are those joining the nearest neighbours in the lattice. There are thus twelve slip systems. Since the strain can be defined by six components, not all of these systems will be active. If the strain is produced by the slips alone, there will be no change in volume, a condition which will reduce the number of independent components to five.

To determine which five components would be operative Taylor considered all the geometrically-possible combinations and selected that combination which gave the minimum work for a given strain.

Bishop and Hill (1951) have confirmed Taylor's hypothesis that the combination (or combinations) requires minimum work. A physically-possible combination is defined as one which is not only geometrically possible but also satisfies the yield condition, namely, that the critical shear stress, i.e., the resolved stress necessary to induce slip, should not be exceeded in one of the inactive slip systems. Bishop and Hill also advanced the principle of maximum work – that of all the stress states satisfying the yield condition the physically-realizable one is that which maximizes the work for the given plastic strain. Application of this principle enables one to determine the combinations of active systems with fewer computations.

*Research supported by the Solid State Physics Branch of the Office of Scientific Research, Air Research and Development Command, U.S. Air Force, under Contract AF 18 (600)-1466.

†Physics Department, University of Detroit.

‡Engineering Department, University of California, Los Angeles.

In a method developed by LIN (1957) and presented here in modified form and from a different point of view, the physically-realizable combinations are obtained by considering the sequence of slipping following the attainment of the elastic limit by the specimen. This method, in contrast to those of TAYLOR and BISHOP and HILL, incorporates elastic strain.

2. DISCUSSION OF THE METHOD

From uniaxial loading tests on single crystals, it has been found that single slip depends on the resolved stress, τ, which is the shear stress along the direction of slip in the crystal plane. Also, it is independent of the forces normal to the plane, i.e., from this test one obtains the following empirical relation :

$$\tau = f(\gamma),$$

where γ is the plastic shear in the active slip system. Duplex slip occurring in such tests is observed when because of rotation of the crystal axes the resolved stress in a second slip system becomes equal to that in the previously active one. These stresses depend on the sum of the slips in the two active systems in approximately the same manner as the resolved stress depends on the shear in single slipping :

$$\tau_1 = \tau_2 \simeq f(|\gamma^1| + |\gamma^2|).$$

This led TAYLOR to assume that for multiple slip in polycrystals the critical stress is the same for a given crystal in all slip system, active or latent, and is expressible by

$$\tau \simeq f\left(\sum_{\alpha=1}^{n} |\gamma^\alpha|\right), \tag{1}$$

where γ^α is the slip in the αth of the n active systems.

With TAYLOR we assume that the strain in the crystal aggregate is uniform. This is unrealistic since it produces a discontinuity in the force at the grain boundary. However, TAYLOR considered it as providing an upper limit for the calculated stress, which one infers from his result is not too far removed from the correct value. On the other hand BISHOP and HILL have proved the theorem that with certain assumptions the *work* of deformation of a polycrystal for purely plastic strain is the same *as though* it were deformed uniformly. For a combination of elastic and plastic strains, which we consider, the theorem of BISHOP and HILL is no longer valid. We therefore consider the model presented here as an approximation only.

Let us consider a single crystal in an isotropic aggregate subject to an increasing strain in such a way that the ratios of the components of the strain tensor remain constant. As the imposed strain increases, the resolved shear strains in all slip systems in the crystal increase. Slip will first occur in the slip system with the highest resolved shear stress, which is proportional to the resolved elastic strain, as soon as the critical shear stress is reached in that system. Let the system in which slip first occurs be called system 1. Due to workhardening, the resolved shear stress for further slip in the different systems of the crystal increases with the amount of slip, as equation (1) predicts. After system 1 slides, the elastic strain

in the crystal equals the imposed strain on the crystal less the plastic strain due to slip.

Slip in system 1 proceeds with the increase of imposed strain on the crystal until another slip system 2 has the same elastic resolved shear strain as system 1. Then, systems 1 and 2 slide simultaneously. This process continues until still another system 3 has the same resolved elastic shear strain as the two previous ones. In the same way additional slip systems are obtained. Since only five independent components determine the plastic strain tensor, this procedure is continued until the slips in five independent systems are obtained. In this way, the sequence of slip is determined. By a direct approach, then, the five active slip systems are obtained. With the five active slip systems the deviatoric stress tensor is determined with the application of equation (1).

3. Mathematical Formulation of the Theory

To simplify the calculations further elastic strain in a given system is neglected once slipping begins in that system. This can be justified by comparing the modulus of rigidity, for aluminium, with the slope of $f(\gamma)$, as given by TAYLOR.

For the ij component of the strain tensor, e, we write

$$e_{ij} = \zeta\delta_{ij} + \bar{e}_{ij} + \bar{\bar{e}}_{ij}, \tag{2}$$

where $\zeta\delta_{ij}$ accounts for the change in volume due to elastic strain (δ_{ij} = Kronecker delta), $\bar{e}_{ij}$ is the remaining portion of the elastic strain, and $\bar{\bar{e}}_{ij}$ is the plastic strain.

Let the α^{th} of the twelve slip systems be represented by $\mathbf{n}^\alpha$, a unit vector normal to the plane of the α^{th} system, and $\mathbf{l}^\alpha$, a unit vector in the direction of slip. Then, defining

$$S^\alpha_{ij} = \tfrac{1}{2}\,(n^\alpha_i\, l^\alpha_j + n^\alpha_j\, l^\alpha_i)$$

where n^α_i and l^α_i are components of $\mathbf{n}^\alpha$ and $\mathbf{l}^\alpha$ respectively, one can show that the resolved shear strain in the α^{th} system, e^α, is given by

$$e^\alpha = \mathbf{S}^\alpha \cdot \mathbf{e}, \tag{3}$$

where $\mathbf{S}^\alpha$ and $\mathbf{e}$ are six-vectors with components $(S^\alpha_{11}, S^\alpha_{22}, S^\alpha_{33}, S^\alpha_{12}, S^\alpha_{23}, S^\alpha_{31})$ and $(e_{11}, e_{22}, e_{33}, 2e_{12}, 2e_{23}, 2e_{31})$ respectively. Also,

$$\bar{\bar{e}}_{ij} = \sum_{\alpha=1}^{n} S^\alpha_{ij}\,\gamma^\alpha, \tag{4}$$

where it is assumed that values of α are assigned to the n systems attaining the elastic limit according to their order. Then, from equations (2), (3) and (4) and the fact that $\mathbf{n}^\alpha \,.\, \mathbf{l}^\alpha = 0$, we obtain

$$\mathbf{S}^\alpha \cdot \mathbf{e} - \sum_{\beta=1}^{n} (\mathbf{S}^\alpha \cdot \mathbf{S}^\beta)\,\gamma^\beta = \bar{e}^\alpha, \tag{5}$$

where $|\bar{e}^\alpha| = e_0$, the elastic limit, for $\alpha = 1, 2, \cdots\cdots, n$.

Equations (5) for $\alpha = 1, 2, \cdots, n$ represents n equations in n unknowns, $\gamma^1, \gamma^2, \cdots, \gamma^n$, corresponding to the given total strain e_{ij} and elastic limit e_0. Having determined the set γ^β, one then employs equation (5) for $\alpha > n$ to determine the course of the resolved elastic strain in the remaining slip systems with the

increasing values of e_{ij} until in the system to be designated the $(n+1)$ th $|\bar{e}^\alpha| = e_0$. In general a number of systems may reach the elastic limit simultaneously, i.e., a set of values of e_{ij} is reached for which equation (5) gives $|\bar{e}^{n+1}| = |\bar{e}^{n+2}| = \cdots\cdots\cdots = |\bar{e}^m| = e_0$, where $m > n$. Then equation (5), with n replaced by m, gives a new set of γ^β, corresponding to the increased total strain. This procedure, starting in the elastic region, is continued until there are five active systems.

The determinant of the coefficients of the γ^β in equation (5) is not necessarily nonvanishing, i.e., there may exist a set of constants a^α, not all of which can be zero, such that

$$\sum_{\alpha=1}^{m} a^\alpha (\mathbf{S}^\alpha \cdot \mathbf{S}^\beta) = 0, \qquad \beta = 1, 2, \ldots, m. \tag{6}$$

Multiplying both sides of equation (6) by a^β and summing over the m values of β gives

$$\mathbf{S}' \cdot \mathbf{S}' = 0,$$

where

$$\mathbf{S}' = \sum_{\alpha=1}^{m} a^\alpha \mathbf{S}^\alpha.$$

Therefore,

$$\sum_{\alpha=1}^{m} a^\alpha \mathbf{S}^\alpha = 0. \tag{7}$$

From equations (5) (with m replacing n), (6), and (7)

$$\sum_{\alpha=1}^{m} a^\alpha \bar{e}^\alpha = 0, \tag{8}$$

which is the requirement for the existence of the solutions γ^β. Since at the moment the last $(m-n)$ systems attain the elastic limit the $\bar{e}^\alpha$ for $\alpha = 1, 2, \cdots, m$ are equal to $\pm e_0$ and satisfy equation (5) (with the summation over β extending to $\beta = \eta$), one may multiply both sides by a^α, sum over the m values of α, and with the aid of equation (7) obtain the relation (8).

Thus, there exists at least one set of values of γ^β satisfying equation (5). Since, in general, n' $(\leqslant n)$ of the equations corresponding to the first n values of α are independent, it is sufficient to consider only n' nonvanishing values of γ^β (or n' active systems), which has been done in the calculations reported below. Accordingly, there may be more than one set of n' γ^β, chosen from the set of n, satisfying equation (5). This point has been discussed by TAYLOR and BISHOP and HILL for $n' = 5$.

The relation between the deviatoric stress tensor σ and the elastic strain tensor is expressed by

$$\sigma_{ij} = 2\mu \bar{e}_{ij}$$

where μ is the modulus of rigidity. It follows that the yield condition must be satisfied during all stages of loading since

$$|\tau_\alpha| = 2\mu |\bar{e}^\alpha| \leqslant 2\mu e_0 = \tau_0,$$

where τ_0 is the critical shear stress.

4. RESULTS

The method discussed in the previous section has been applied to calculate the successive slip systems for different orientations of the crystals in a cylindrical aggregate loaded in simple tension or compression along the cylindrical axis. In representing the slip systems for a face-centred cubic crystal, we employ the convention of TAYLOR, in which the letters a, b, c and d indicate the slip planes. Each of the subscripts 1, 2, and 3 indicates a slip direction and sense in the given plane. Orientation of the specimen cylindrical axis with respect to the crystal axes is designated in the spherical polar coordinates θ and ϕ. Because of symmetry it is sufficient to consider only a limited range of values of θ and ϕ. Following TAYLOR, we employ forty-four points within the region $0 \leqslant \phi \leqslant \frac{1}{4}\pi$ and $0 \leqslant \cot\theta \leqslant \sin\phi$. Thus, in determining macroscopic characteristics of the specimen, one averages over these forty-four orientations.

Table 1 presents the results of these calculations for the example of the crystal orientation $\theta = 80°$, $\phi = 30°$. The strains are expressed in units of e_0. The diagonal component along the cylindrical axis of the deviatoric strain tensor of the specimen is given under *Tensile strain*. Stage 1 is the state at which the first system (b_2) reaches the elastic limit; stage 2, the state at which the second (a_3) reaches the elastic limit; etc. At stage 5 the elastic limit is reached simultaneously in four systems (a_1, c_1, c_2 and d_2). This gives four possible combinations of slip for loading beyond stage 5, i.e., in the purely plastic region, b_2, d_2, d_1, $\bar{b}_1$, and either a_1, c_1, $\bar{c}_2$, or $\bar{d}_2$. (The line above the symbol for the system signifies that the slip occurs in the negative sense).

The possible combinations of five active slip systems for the forty-four orientations are in essential agreement with those determined by the method described by BISHOP (1953). In order to obtain agreement for orientations $\theta = 75°$, $\phi = 25°$; $\theta = 80°$, $\phi = 15°$; and $\theta = 87°$, $\phi = 45°$, it is necessary to consider combinations which exclude systems active prior to stage 5, i.e., it is necessary for slip to cease in a system attaining the elastic limit at an earlier stage while two of the systems attaining the elastic limit at stage 5 become active. Such a procedure is permissible with the assumption of TAYLOR that all systems, latent or active, harden equally, as is implied in equation (1). Also, for orientation $\theta = 90°$, $\phi = 20°$ it is necessary for the slip in a previously active system to cease in order to prevent a reversal in the sense of the displacement in another active system, i.e., to prevent an elastic strain, which would considerably increase the virtual work.

Table 1 shows that stage 1, or the end of the purely elastic region, occurs for a tensile strain of 1·356 units for this orientation. Of the forty-four orientations the minimum value of the tensile strain for stage 1 is 1·3338 for $\theta = 84°$, $\phi = 25°$. The most favourable of all possible orientations for slip in system b_2 is $\theta = 84{\cdot}735°$, $\phi = 24{\cdot}205°$ with the elastic limit corresponding to a tensile strain of 4/3. The maximum value for the tensile strain at stage 1 among the forty-four orientations was found to be 2·026.

For the tensile strain at stage 5, or the beginning of the purely plastic region, the Table gives the value of 21·8 for the sample orientation. For the forty-four orientations a maximum of 380·9 for $\theta = 75°$, $\phi = 30°$ and a minimum of 1·63 for $\theta = 90°$, $\phi = 0°$ were obtained. This quantity exhibits a decided variation from one orientation to the next. Where the quantity is very high, and there

TABLE 1. *Analysis of strains in crystal of orientation* $\theta = 80°$, $\phi = 30°$

Stage	*Tensile strain*	*Strain*	*Slip systems*											
			a_1	a_2	a_3	b_1	b_2	b_3	c_1	c_2	c_3	d_1	d_2	d_3
		Resolved elastic	− 0·402	0·858	− 0·455	− 0·649	1·00	− 0·351	0·050	0·159	− 0·209	0·296	0·302	− 0·597
1	1·356	*Resolved plastic*	0·000	0·000	0·000	0·000	0·000	0·000	0·000	0·000	0·000	0·000	0·000	0·000
		Slip												
		Resolved elastic	− 0·330	1·00	− 0·670	− 0·760	1·00	− 0·240	0·210	0·030	− 0·240	0·639	0·030	− 0·670
2	2·36	*Resolved plastic*	− 0·372	0·496	− 0·124	− 0·372	0·744	− 0·372	− 0·124	0·248	− 0·124	− 0·124	0·496	− 0·372
		Slip					1·49							
		Resolved elastic	− 0·214	1·00	− 0·786	− 0·828	1·00	− 0·172	0·386	− 0·214	− 0·172	1·00	− 0·214	− 0·786
3	3·38	*Resolved plastic*	− 0·789	1·14	− 0·349	− 0·789	1·49	− 0·703	− 0·263	0·612	− 0·349	− 0·263	0·965	− 0·703
		Slip		0·515			2·64							
		Resolved elastic	− 0·320	1·00	− 0·680	− 1·00	1·00	0·000	0·320	− 0·320	0·000	1·00	− 0·320	− 0·680
4	4·50	*Resolved plastic*	− 1·02	1·85	− 0·831	− 1·15	2·32	1·17	− 0·156	0·849	− 0·694	− 0·018	1·32	− 1·30
		Slip		1·17			4·00					0·825		
		Resolved elastic	− 1·00	1·00	0·000	− 1·00	1·00	0·000	1·00	− 1·00	0·000	1·00	− 1·00	0·000
5	21·8	*Resolved plastic*	− 5·47	12·8	− 7·32	− 9·43	15·1	− 5·64	− 0·204	3·56	− 3·36	3·75	5·85	− 9·60
		Slip		8·94		− 8·23	22·7					15·5		

appears to be no limit on its value in considering all possible orientations, it is indicated that the increment of total strain is very nearly satisfied by slip in less than five systems.

One concludes that according to the model presented here the region where combined elastic and plastic strains occur in the specimen is quite extensive.

The sum of the slips for a unit increment of tensile strain beyond stage 5 was determined for each of the forty-four orientations. For a given orientation this sum is the same for the physically permissible combinations of active systems, in accordance with the theorem of Bishop and Hill. This theorem states that the virtual work, which on the basis of the assumptions presented above is a monotonic function of the sum of slips, is the same for all slip combinations which produce the strain tensor, in purely plastic strain, without violating the yield condition. These sums, with one exception, are equal to or less than those obtained by Taylor The exception is for the orientation $\theta = 87°$, $\phi = 40°$, for which Taylor obtained the value of 3·54 against our value of 3·61. For the orientations $\theta = 87°$, $\phi = 25°$; $\theta = 90°$, $\phi = 30°$; and $\theta = 90°$, $\phi = 20°$, Taylor obtained 2·92, 3·34 and 2·76 respectively as opposed to our 2·81, 3·18 and 2·59. In these three cases the five active slip systems for all combinations are distributed among all four planes. Combinations of this type were not included by Taylor. These occasional differences between Taylor's values and our values for the sums of the slips would produce a negligible effect on the theoretical stress–strain relation. Thus, our load vs. elongation curve for aluminium in the very plastic region would closely approximate that of Taylor.

However, Taylor's method applies only to the plastic region, whereas the method presented here offers a mechanism which provides for the entire stress–strain relation by a suitable choice of ϵ_0.

References

Bishop, J. F. W.	1953	*Phil. Mag.* **43**, 51.
Bishop, J. F. W. and Hill, R.	1951	*Phil. Mag.* **42**, 414 and 1,298.
Lin, T. H.	1957	*J. Mech. Phys. Solids* **5**, 143.
Taylor, G. I.	1938	*J. Inst. Metals* **62**, 307.

Journal of the Mechanics and Physics of Solids, 1958, Vol. 6, pp. 321 to 326. Pergamon Press Ltd., London

FRACTURE MECHANISM OF SEMI-BRITTLE STEELS IN TORSION

By J. B. Hunt
Faculty of Engineering, University of Khartoum

(*Received 6th November*, 1957)

Summary

The petal-shaped pattern noticed on the fracture surface of certain mild steels tested in torsion led the author to investigate the mechanism of a type of fracture hitherto assumed to be a conventional shear separation. It was found that the fracture sequence involved both tensile failure and sliding in shear.

1. Introduction

If test specimens made of a ductile material are subjected to pure torsion, maximum slip occurs in one of the directions of maximum shearing stress, i.e. in a plane at right angles to the axis of the specimen. Separation finally occurs in this plane and it is described as a pure shear fracture across the whole of the cross-section. If the test specimens are made of a brittle material, separation occurs along a helix perpendicular to the direction of the principal tensile stress at an angle of 45° to the axis. It is widely held that if a torsional fracture is not a 45° brittle fracture then it is a pure shear fracture of the type described above. This opinion is usually based on a macroscopic examination of the fracture surface which has the appearance of an apparently pure shear fracture. After performing a large number of tests on specimens of steels usually classified as ductile, the author found that specimens of certain steels when subjected to pure torsion did not fail in either pure shear or tension. The failure mechanism appeared to be a combination of these two methods of separation. This class of steel has been designated here as semi-brittle.

2. Suggested Mechanism

After some twisting a semi-brittle material becomes more brittle in the region where the most severe deformation takes place ; the neighbouring sections remain semi-brittle. After some twisting, therefore, tensile micro-cracks form on the periphery of the specimen but are not propagated to a sufficient extent to cause complete fracture, the propagation being arrested by the less brittle parts of the material. This process was suspected by Nadai (1950). The orientation of these original cracks is shown in Fig. 1a. As twisting proceeds, the angle of orientation of the crack increases until a stage is reached when shearing in the direction of grain flow takes place between adjacent cracks. Separation, however, does not

yet occur as a resisting tensile stress is induced in the more ductile core of the specimen. The angle of strain increases further until separation occurs as a result of one of two sequences. There may be either (i) primary tensile failure at the

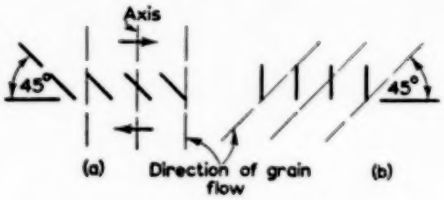

Fig. 1.

surface followed by tensile failure at the core and then separation by shear of the outer annulus, or (ii) primary tensile failure at the surface followed by shear propagated radially inwards, simultaneously with tensile failure at the core propagated radially outwards.

3. METHOD OF TESTING

Solid cylindrical specimens were machined from $\frac{1}{2}$in. square bright drawn bar in the as-received condition, to the dimensions shown in Fig. 2. After machining the surface was found to have a Talysurf C.L.A. of 25 μ. A line was scribed on the surface of the specimen parallel to the axis.

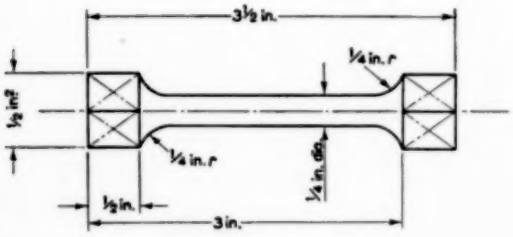

Fig. 2.

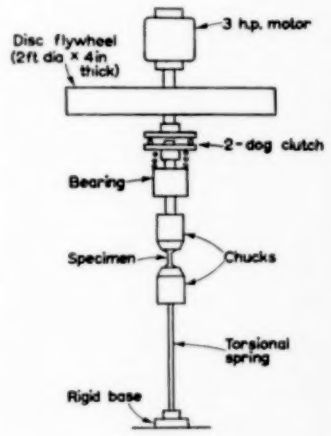

Fig. 3.

Table 1 shows the chemical composition of the steels tested.

The tests were made in a specially designed vertical torsion machine in which, in addition to the normal 'static' test, tests could also be made at very low temperatures and high impact speeds. A simple schematic arrangement of the machine is shown in Fig. 3.

A telescope was converted to a goniometer by attaching to it a circular scale. In this way the deflection of the scribed line could be observed during a test. The surface strain at fracture was checked after a test by means of a tool-room microscope with a × 25 magnification.

Normal tensile tests and Charpy impact tests were also carried out.

TABLE 1

Constituent	1	2	3
C	0·165	0·150	0·140
Si	0·120	0·034	0·050
S	0·043	0·042	0·220
P	0·012	0·012	0·012
M_n	0·690	0·550	0·890

At the start of a test the vertical hair-line of the telescope was focussed on to the scribed line on the specimen. A torque was applied and the twist and surface strain of the specimen were recorded. As the testing proceeded it became evident where separation would occur as the strain rapidly increased in a well-defined locality. The surface strain in this locality was measured with increasing torque and twist until separation occurred.

To make the material more brittle, and to restrict the deformation to a small part of the specimen, tests were also performed at various temperatures within the range + 100°C to − 196°C and at rates of straining from zero to 4·6 per sec. In the dynamic tests and the subnormal temperature tests the goniometer was not used. The fracture strain was measured after the test in the tool room microscope and the torque variation was recorded photographically.

TABLE 2

Steel No.	$\phi_{fract.}$
1	70°
2	69°
3	64·5°

4. RESULTS

For each steel it was found that the surface fracture strain was constant. This was so under all testing conditions – in the most extreme case the yield torque was more than twice that for a normal temperature ' static ' test. The values of surface fracture strain, $\phi_{fract.}$, are given in Table 2.

Torque-twist curves obtained under normal conditions for each of the three steels are shown in Fig. 4.

The normal tensile and Charpy impact characteristics are tabulated in Table 3. The transition temperature is the temperature at which a brittle area was first observed on the fracture face.

TABLE 3

Steel No.	*Yield stress* (lb/in^2)	*UTS* (lb/in^2)	*Impact value at 15°C* (*ft lb*)	*Transition temp.* (°C)
1	61,700	91,200	—	—
2	53,800	85,600	20·5	50
3	67,200	94,400	12	95

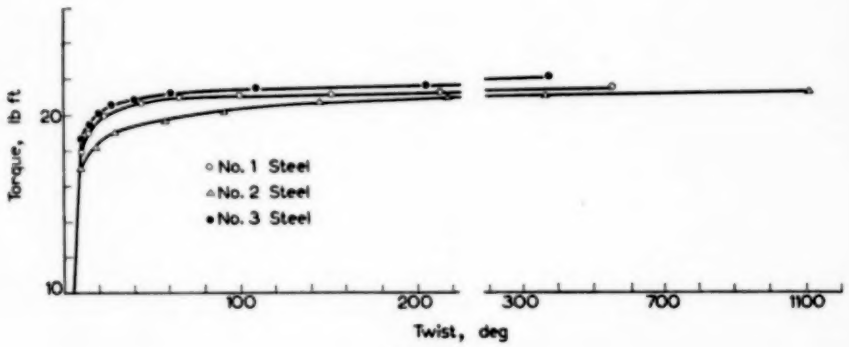

Fig. 4.

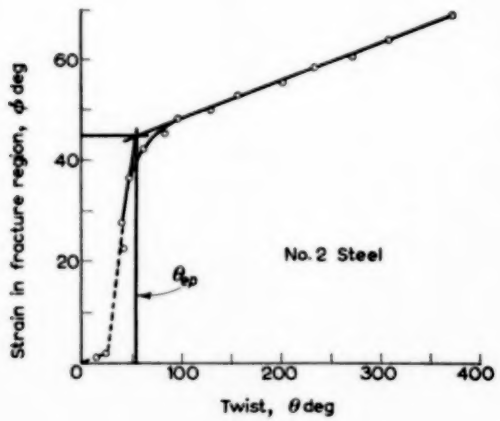

Fig. 5.

The relationship between twist, θ, and strain, ϕ, in the potential fracture region is shown in Fig. 5 for Steel No. 2.

A typical fracture surface is shown in Fig. 6.

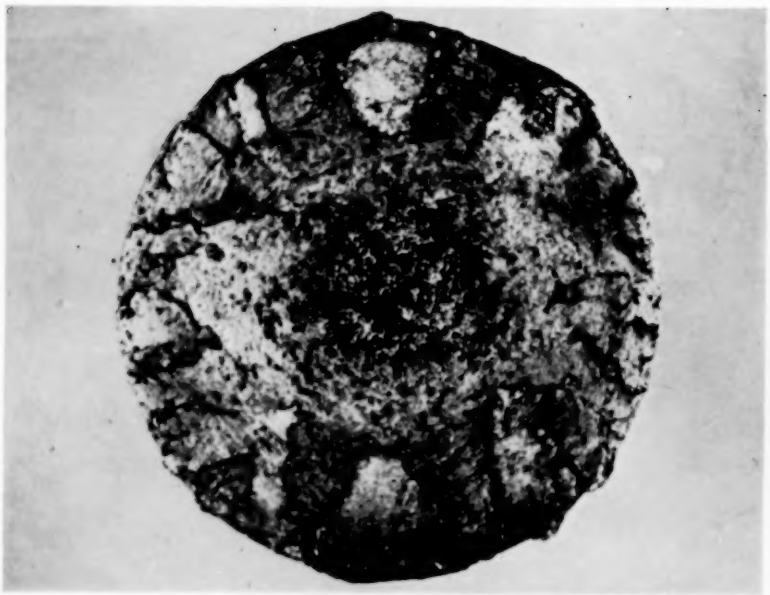

Fig. 6.

5. Discussion

From Fig. 5 it can be seen that in the initial stages of a test the slope of the curve was 16. This would be expected for a $\frac{1}{4}$in. diameter specimen with 2 in. parallel length when the material was wholly elastic. The material then became plastic in a well defined region. The ordinate of Fig. 5 is the strain value in this region. The strain increased almost uniformly with twist until a point was reached when there occurred a sudden change in slope to the original value of 16. While this high local straining was in progress the strain along the remaining length of the specimen was uniform and increased slowly to a maximum value; this is referred to as the elasto–plastic strain, ϕ_{ep}.

If the straight parts of the curve are produced they are found to intersect at a strain value of 45° and a twist of 60° giving a ϕ_{ep} value of 3·75°. This change in slope took place when the shear mechanism began as described (cf. Fig. 1 b). The material could not part in shear at this angle as the core offered too high a resistance. Hence the outer strain increased, at the same time causing a compressive stress to counter-balance the central tensile stress as there was no externally applied axial force. This system of stress propagated radially inwards. Complete separation then started simultaneously from the outer surface (when the strain was 64½° for No. 2 Steel) and the axis of the specimen. By geometric and microscopic analysis of the types of surface shown in Fig. 6 this fracture mechanism was established.

Increases in the length of the specimens averaged 0·01 in. accompanied by a decrease in diameter in the fracture region of 0·005 in.

By reducing the temperature of the test to − 150°C the value of ϕ_{ep} was reduced. At − 196°C ϕ_{ep} became almost zero. The straight line intersection still took place at a strain value of 45°. This is shown in Fig. 7 for No. 2 Steel. The effect of

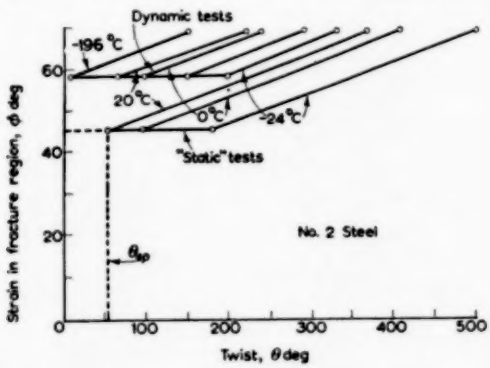

Fig. 7.

testing at a strain rate of 4·6 per sec is also shown in this figure. The effect was to raise the value to 58°; the reason for this is probably associated with high local temperature.

Acknowledgments

The author acknowledges the help given by Dr. A. C. Walshaw, College of

Advanced Technology, Birmingham, where this work was carried out. Thanks are also due to Dr. A. STEVEN, Mond Nickel Research Department, Birmingham, for preparing the Charpy specimens and performing the Charpy tests.

REFERENCES

NADAI, A. 1950 *The Theory of Flow and Fracture of Solids* p. 203. McGraw-Hill, New York.

BOOK REVIEWS

Deformation and Flow of Solids. IUTAM Colloquium, Madrid, 1955. Edited by R. GRAMMEL. Springer-Verlag, Berlin, 1956. 324 pp.

THIS is a compilation of the lectures given at a conference organized by the International Union of Theoretical and Applied Mechanics. The main aim was to bring together two separate types of scientist engaged in research on solids, namely solid-state physicists investigating atomic and microscopic phenomena, and applied mathematicians studying macroscopic behaviour as a branch of mechanics. There are 28 papers, evenly divided between the two groups.

In the first, dislocation theories of flow and fracture are strongly represented by A. H. COTTRELL, F. C. FRANK, G. LIEBFRIED, J. R. LOW, W. P. MASON, N. F. MOTT and A. SEEGER. Recent experimental work on plastic, visco-elastic, and relaxation properties of polycrystals is well covered by H. le BOITEUX, H. G. VAN BUEREN, C. CRUSSARD, B. JAOUL and F. SCHULZ-GRUNOW.

In the second group, which is almost entirely theoretical, there are papers on non-linear elasticity (H. KAUDERER, M. REINER, L. R. G. TRELOAR), visco-elasticity (M. A. BIOT, J. G. OLDROYD), plasticity (P. G. HODGE, H. G. HOPKINS, G. I. TAYLOR), wave propagation (E. H. LEE, E. VOLTERRA).

Whether the assembling of these distinguished, though diverse, elements was a success, scientifically speaking, is difficult for anyone who was not present to say. But it seems certain that the curious location of the conference prevented a really adequate representation of the complementary approaches and of intermediate work tending to bridge the gap. That there is a definite gap is indeed the main overall impression left by this very book; few of the contributors have attempted to foster the declared aim of the conference.

On the other hand, my own feeling is that the actual situation (in this country at least) is a good deal better than the book suggests (though not yet perfect by any means) – it is a well-known feature of international congresses that they invariably elicit an artificial collection of papers. The really worthwhile exchange of views between the two groups continues all the time on a day-by-day basis, through correspondence, circulation of reprints and advance proofs, and by visits when necessary.

R. HILL

I. N. SNEDDON: Elements of Partial Differential Equations. International Series in Pure and Applied Mathematics. McGraw-Hill, 1957. 327 pp., 56s. 6d.

THIS is the book for every research worker who is interested in solving differential equations, be he mathematician, physicist, or engineer. It is shorn of everything that causes so many present-day books on this subject to be drearisome and unrewarding pilgrimages: the tedious minutiae, the academic examples, the compendium of undiscriminating methods – so redolent of the fashion in textbooks fifty years ago. From personal experience in many fields Professor Sneddon knows the best techniques, and he pursues an unswerving path towards them with the minimum of fuss and with perfect clarity. Recent or advanced methods are introduced whenever they justify themselves, and these lend the book a special air of distinction, lifting it well above the usual humdrum primer to a level comparable with that of Courant-Hilbert – less discursive, of course, but for that reason more accessible to those with a modest mathematical equipment. There is, moreover, a very extensive collection of excellent problems for practice; these are interesting in themselves for their varied physical settings and also thoroughly test understanding of the text; this feature of the book makes it admirably suited to the final year in an Honours course.

The following is a typical cross-section of the contents: Pfaffian forms and Carathéodory's axiom in thermodynamics; Cauchy's characteristic strip method for non-linear equations, in

its geometrical context ; solution of linear hyperbolic equations ; integral transforms ; method of the Green's function for the Laplace and diffusion equations, and its connection with conformal transformation ; Riemann-Volterra solution of the two-dimensional wave equation, with application to sound waves of finite amplitude ; Helmholtz, Kirchhoff, and Poisson solutions of the three-dimensional wave equation.

R. HILL

B. G. NEAL : **The Plastic Methods of Structural Analysis.** Chapman and Hall, 1957. 353 pp., 45s.

IN recent years there has been considerable research work on plasticity. Academic texts and accounts of research work exist but the subject is still only in the process of penetrating the undergraduate curriculum. It is in the light of this background that this book, which is the first substantial mainly-undergraduate text on the plastic behaviour of frameworks, is to be considered. The author is well qualified for his task by virtue of his former membership of the Cambridge team and especially because of his outstanding contribution, in conjunction with P.S. Symonds, of the method of combining collapse mechanisms.

The first four Chapters present a straightforward account of the plastic behaviour of plane frames. Much material, usually left for asides by the lecturer in more developed subjects, is given and in the present circumstances this is justifiable although one is reminded of the business man who apologised for writing a ten-page letter because he was too busy to condense his material into two pages. The attribution on p. 38 of catenary effects to a simply supported beam is rather surprising and the load-deflection relation shown in Fig. 2.10 (c) needs further investigation as the formation of hinges cannot be expected to increase the stiffness of a structure.

The remaining Chapters deal in succession with deflection limitations, effects of axial and shear force, minimum weight design and shakedown theory. The subject is growing at such a rate that these Chapters are progress reports rather than accounts of fully developed work.

A fair criticism is that only in a passing reference on one page (p. 217) is it mentioned that all the theory developed neglects instability effects ; a designer is thus given no idea of when simple plastic methods may or may not be applied. In an Appendix it is pointed out that instability effects preclude the application of simple theory to trusses : in fact the theory is easier to extend to cover this case than sway of the rigid frames treated in the book and for which no limitations are given.

The book as a whole is a worthwhile contribution to the job of transforming the results of research into engineering lore and is a welcome addition to one's library.

W. MERCHANT

J. F. NYE : **Physical Properties of Crystals, their Representation by Tensors and Matrices.** Clarendon Press, Oxford, 1957. 322 pp., 50s.

The physics of crystals may be treated in two stages. In the first, the phenomena are described, whereas in the second they are explained in terms of atomic theory and crystal structure. These stages correspond to those in which crystal physics developed first from the times of ERASMUS BARTOLIMUS and HUYGENS to WOLDEMAR VOIGT and then during the last forty-five years since the discovery of X-ray diffraction and the development of the dynamic theory of crystal lattices. The first period ended in 1910 when VOIGT's famous book was published. This was a classic and remained the only book dealing with the phenomenology of crystals with the exception of crystal optics. To many of us it appeared clumsy, as the equations were written using the components of vectors and tensors. However, as VON LAUE pointed out in his note accompanying the reprint in 1928, it would be an impossible task to amend VOIGT's book and introduce vector and tensor notation without destroying the unity and beauty of this masterpiece. An entirely new book had to be written and this is what Dr. NYE has done.

The book is intended as a text book for honours students in physics in their second or later years, and for research workers in solid state physics and metal physics. It starts with a mathe-

matical introduction in which tensors of various ranks, their transformations and the effect of crystal symmetry are discussed. (The essentials of crystallography and of the symmetry of crystals are given in an appendix). The second part, which occupies about half of the book, contains a treatment of those physical properties (magnetic susceptibility, electric polarization, thermal expansion, piezoelectricity, elasticity) which may be measured with the crystal in equilibrium with its surroundings and can be discribed by reference to changes which are thermodynamically reversible. A chapter on the matrix method is included in this part and a unified treatment of the properties is given, which is possible because of their common feature. Such a treatment is not possible with transport properties (thermal and electrical conductivities, thermoelectricity) since they are thermodynamically irreversible. They are discussed in Part III. The final part deals with such optical properties as double refraction, electro-optical and photoelastic effects and optical activity. Each section is concluded by a summary, and there are exercises throughout the book to which the solutions are given in an appendix.

The book is well laid out and clearly written, and it is a pleasure to read the first part with all its fundamental definitions of tensors, matrices, etc., and the methods of operating them. This and the chapter on the matrix method are of importance beyond the scope of this book, as much use is nowadays being made of these notations in treating the crystallography of phase changes, particularly those of the martensite type, and of twinning, and the reviewer is not aware of any other equally lucid and suitable treatment. Another chapter of outstanding value is that on thermodynamics. The treatment of the physical properties is also very clear and satisfactory and the book will certainly be a most useful text. On the other hand, a book of this size can obviously not be a complete treatment of the subject and the research worker will notice gaps which will still induce him to look up details in VOIGT. For instance, the twist accompanying the bending of a crystal is not treated, although it is important in the experimental determination of the elastic constants. However, it is obviously asking too much of a book of 300 pages to be as complete now as VOIGT's was at its time with almost a thousand pages, and the above remark is in no way intended to decry the value and usefulness of the book. We all have to be grateful to Dr. NYE for giving us such a clearly conceived and well written text.

W. BOAS

Surveys in Mechanics: The G. I. Taylor 70th Anniversary Volume. Edited by G. K. BATCHELOR and R. M. DAVIES, Cambridge University Press, 1956. vii + 475 pp., 50s.

THIS volume, made up of a biographical note and ten surveys of the present position in certain branches of mechanics, was published to commemorate the seventieth birthday of SIR GEOFFREY TAYLOR on the 7 March, 1956. Since each survey is concerned with recent developments in fields of considerable current interest in solid or fluid mechanics to which he has made substantial contributions sometime during the last half-century, it is a magnificent tribute to TAYLOR's scientific achievements. It makes us anticipate with pleasure the publication by the Cambridge University Press of his collected papers.

The book opens with a brief biographical note by SIR RICHARD SOUTHWELL. Six pages are far too few to contain all we would know of "G.I." but it is amazing what a wealth of information SOUTHWELL has packed into them and what an endearing portrait he has produced.

Of the ten surveys of the present position of research in certain branches of mechanics (varying in length from about 20 to over 100 pages) the first three are most likely to be of interest to readers of this Journal.

The first of them is *The Mechanics of Quasi-Static Plastic Deformation in Metals* by R. HILL, which contains a discussion of the connexions between single- and poly-crystal behaviour. Beginning with a survey of the relevant mechanical properties of single crystals the author goes on to consider the theory of the plastic behaviour of crystalline aggregates and the relevant experimental data. This leads to the formulation of boundary value problems in the machanics of plastic-elastic continua and the discussion of the plastic-rigid solid. The survey closes with an account of some general theorems relating to the yield point and of the method by which the load intensity at the yield point may be estimated. PROF. HILL's article is one of the shortest in the volume but this is not because he has little to say; rather it shows evidence of careful

rewriting producing a concentrated account of great value. Through it runs the theme of the Principle of Maximum Plastic Work giving unity to the wide variety of topics covered.

While the mechanical properties of single crystals form the starting-point of the theory of plasticity it is the ultimate task of dislocation theory to account for such properties. This topic is covered in the second survey *Dislocations in Crystalline Solids* by N. F. MOTT. In a space of 30 pages, in his usual pellucid style, PROF. MOTT gives a broad general survey of the theory of dislocations and its application to the discussion of problems of solid mechanics—plastic flow, slip-lines, diffusion, creep and recovery.

The third article is on *Stress Waves in Solids* by R. M. DAVIES. This survey begins with a general account of the modern experimental techniques (mechanical, photographic and electrical) whose use has led to some of the more important and interesting features of recent work in this field. This is followed by a discussion of theoretical researches into the three types of stress waves : (a) *elastic waves*, in which the stresses are so low that the behaviour of the solid is elastic ; (b) *visco-elastic waves* in which, in addition to elastic stresses, there are frictional or viscous stresses ; (c) *plastic waves* in which the solid is stressed beyond the elastic limit. The emphasis throughout is on transient rather than on periodic phenomena. PROF. DAVIES gives a clear picture of the major developments in this field in which there has been a great revival of interest in recent years. This survey forms a valuable complement to Kolsky's monograph.

The remaining seven articles are: *Rotating Fluids* by H. B. SQUIRE, *The Mechanics of Drops and Bubbles* by W. R. LANE and H. L. GREEN, *Wave Generation by Wind* by F. URSELL, *Viscosity Effects in Sound Waves of Finite Amplitude* by M. J. LIGHTHILL, *Turbulent Diffusion* by G. K. BATCHELOR and A. A. TOWNSEND, *Atmospheric Turbulence* by T. H. ELLISON, *The Mechanics of Sailing Ships and Yachts* by K. S. M. DAVIDSON. Since the aim of these surveys is to present to a non-specialist audience recent developments in the various branches, the research worker in solid mechanics will get from them a comprehensive view of the present state of fluid mechanics. All of the articles are well written by recognised authorities on the subjects covered but particular mention must be made of the long article (over a hundred pages) by PROF. LIGHTHILL which contains new and interesting material on the properties of shock waves in fluids.

The editors are to be congratulated on the production of a collection of essays on topics in which there is great interest at the present time. Although the individual contributions vary in length and in approach they have one feature in common. They will help the non-specialist (as well as the specialist) to keep pace with the rapid development in mechanics which have taken place since the last war. The publishers have proved worthy of the editors and the individual authors in producing a very fine volume whose purchase is to be recommended to all workers and teachers in the field of mechanics.

I. N. SNEDDON

Rheology. Edited F. R. EIRICH. Vol. I. Academic Press, New York, 1956. xiv + 761 pp. 143s.

THIS is the first volume of three designed to provide an easily accessible and authoritative survey of the broad range of topics falling under the heading of rheology used in its widest sense. The chapters and authors are listed below.

1. Introduction—F. R. EIRICH.
2. Phenomenological Macrorheology—M. REINER.
3. Finite Plastic Deformation—WILLIAM PRAGER.
4. Stress-Strain Relations in the Plastic Range of Metals—Experiments and Basic concepts — D. C. DRUCKER.
5. Mechanical Properties and Imperfections in Crystals—G. J. DIENES.
6. Dislocations in Crystal Lattices—J. M. BURGERS and W. G. BURGERS.
7. Mechanical Properties of Metals—J. FLEEMAN and G. J. DIENES.
8. Some Rheological Properties Under High Pressure—R. B. DOW.
9. Theories of Viscosity—A. BONDI.
10. Large Elastic Deformations—R. S. RIVLIN.
11. Dynamics of Viscoelastic Behaviour—TURNER ALFREY, JR., and E. F. GURNEE.
12. Viscosity Relationships for Polymers in Bulk and in Concentrated Solution—T. G. FOX, SERGE GRATCH and S. LOSHAEK.

13. The Statistical Mechanical Theory of Irreversible Processess in Solutions of Macromolecules—J. RISEMAN and J. G. KIRKWOOD.
14. The Viscosity of Colloidal Suspensions and Macromolecular Solutions—H. L. FRISCH and ROBERT SIMHA.
15. Streaming and Stress Birefringence—A. PETERLIN.
16. Non-Newtonian Flow of Liquids and Solids—J. G. OLDROYD.
17. Acoustics and the Liquid State—R. B. LINDSAY.

A detailed subject index of forty-six pages is given.

Each chapter is a review article by a recognised authority in the relevant field. The number of chapters and the wide field covered precludes detailed comment on each chapter. Attention will be directed to the basic conception of the series, the composition of this first volume and its potential usefulness.

In his preface the Editor notes the broad range of activities touched by rheology. The series is visualised as providing ' the novice with a very general introduction to many topics and the advanced reader a ready means of comparing the viewpoint of the contributing authors and of studying new material in fields related to rheology.' It was hoped originally that a universal nomenclature would be adopted throughout the series but it was concluded in the attempt that the time was not ripe for such an undertaking.

The general field of rheology tends to be fairly sharply divided into separate topics—elasticity, plasticity, etc. This is due to the necessity for simplication to make mathematical problems amenable to solution rather than to a lack of awareness of the complex nature of material behaviour. Moreover the various topics, even within their restricted ranges of validity, are sufficiently involved as to provide more than enough scope for research workers ; they are in fact sub-divided into main lines of attack. In these circumstances there is a strong tendency for compartmentation of techniques as distinct from a failure to appreciate the broad aims and progress of other topics. The present volume in particular should be of considerable value in providing a convenient integrated source book in this context, both in cataloguing methods and in indicating where they may be pursued in greater detail. It is not clear that anything other than a very broad unity of rheology exists and the reviewer finds it difficult to imagine how the Editor expects his hope ' that this book will be instrumental in bringing about a better understanding of the essential unity of rheology ' is to be fulfilled. The experienced worker in some section of the field will be aware of the related topics and the initiate to the field will find it very difficult to prevent the trees obscuring the wood.

The pattern of connexion between the principal topics extant in rheology is too complex to expect a single thread to link the chapters of this book. The Editor has commenced his book with two mathematical introductory chapters covering phenomenological macrorheology and finite plastic deformation followed by a group of contributions on the deformation of solids. The remaining chapters deal with a diversity of topics ranging from finite elastic deformation to acoustics and the liquid state. Alternative arrangements or emphasis could be suggested but with no clear superiority to this present treatment.

The Editor is to be congratulated on persuading his distinguished colleagues to make their contributions to the series. The standards of printing and binding are high and this first volume is a worthwhile addition to the literature in the field.

J. F. W. BISHOP.

La Diffusion dans Les Metaux. Edited by J. D. FAST, H. G. VAN BUEREN and J. PHILIBERT. Bibliotheque Technique Philips (Cleaver-Hume Press, London), 1957. 130 pp., 37s. 6d.

FOR some years a small group of French, Belgian and Dutch metallurgists, together with a few from other countries, have met to discuss problems of metal physics. In 1956 the meeting was held at Eindhoven and the subject discussed was diffusion in metals. The particular importance of diffusion has led the organisers of the conference to break their normal practice by publishing its proceedings in the book reviewed here.

Certainly, the interest and attractiveness of the eleven papers brought together in the book fully justifies this decision. The opening paper, by A. D. LECLAIRE, reviews the thermodynamic and statistical theory underlying the diffusion process, and also outlines interesting recent work

on correlation effects in vacancy diffusion, a subject that is taken up in greater detail in the next paper, by K. COMPAAN and Y. HAVEN. P. LACOMBE surveys in detail theoretical and experimental work on diffusion in grain boundaries, and in the following paper he joins C. LEYMONIE in presenting recent experiments on grain boundary diffusion in α-iron. Four papers, by TH. HEUMANN, J. PHILIBERT, Y. ADDA, A. BOLK, and T. J. TIEPEMA, discuss diffusion in various alloys, and the Kirkendall effect. J. L. MEIJERING gives a useful survey of the interstitial diffusion of hydrogen, carbon, nitrogen, and oxygen, in several metals, and A. VAN WEIRINGEN describes a promising new method for determining the solubility and diffusion of helium in silicon and germanium. Finally C. W. BERGHOUT explains how certain anomalies in the diffusion of vacancies in quenched metals can be understood in terms of the effect of stresses on the mobility of vacancies.

An enjoyable and useful book for those interested in metal-physics.

A. H. COTTRELL

PAPERS TO BE PUBLISHED IN FUTURE ISSUES

B. D. COLEMAN : *On the strength of classical fibres—when broken separately, and when broken in bundles.*

E. T. ONAT : *Analysis of shells of revolution composed of work hardening material.*

F. J. LOCKETT : *Effect of thermal properties of a solid on the velocity of Rayleigh waves.*

G. LIANIS and HUGH FORD : *Plastic yielding of single notched bars due to bending.*

R. SANKARANARAYANAN and P. G. HODGE, JR. : *On the use of linearised yield conditions for combined stresses in beams.*

END OF VOL.